

**Curtin Medical School**

**Design, Synthesis and Biological evaluation of Novel Indole-  
2-carboxamide Derivatives as Anti-tubercular Agents**

**Shahinda Sayed Rabie Alsayed**

**This thesis is presented for the Degree of  
Doctor of Philosophy  
of  
Curtin University**

**September 2021**

## Declaration

To the best of my knowledge and belief, this thesis entitled "**Design, Synthesis and Biological Evaluation of Novel Indole-2-Carboxamide Derivatives as Anti-tubercular Agents**", contains no material previously published by any other person except where due acknowledgement has been made. This thesis contains no material that has been accepted for the award of any other degree or diploma in any university.

Shahinda Sayed Rabie Alsayed



10 / 03 / 2022

## Abstract

A quarter of the human population are estimated to be latently infected with *Mycobacterium tuberculosis* (*M. tb*), the etiologic agent of tuberculosis (TB). The likelihood of developing active TB disease is significantly higher among individuals with compromised immune systems, such as patients co-infected with the human immunodeficiency virus (HIV), which is the major risk factor for TB reactivation in the co-endemic areas. Since the year 2000, around 10 million people fall ill with TB annually with more than 1 million TB fatalities each year. Most of the current anti-tuberculosis (anti-TB) therapies are old (discovered in the last century) and are becoming increasingly ineffective due to the emergence of the drug-resistant (DR) *M. tb* strains. Therefore, novel anti-TB drugs that work through new mode of actions are urgently needed to bypass the resistance mechanisms developed by *M. tb* against the currently used drugs. The difficulty in finding potent anti-TB drugs stems from the thick, waxy outer coating of *M. tb*, that accounts for its impermeability to several therapeutic agents. The hydrophobicity of the cell wall of *M. tb* is predominantly ascribed to the accumulation of long chain fatty acids, called mycolic acids (MAs). Of note, *M. tb* was shown to secrete numerous kinases and phosphatases (virulence factors) that subvert the host immune system and evade phagolysosome fusion, thereby successfully establishing and maintaining an intracellular infection.

The mycobacterial membrane protein large 3 (MmpL3) is a key transporter that is responsible for flipping trehalose monomycolate (TMM), the MAs precursor, from cytoplasm to the periplasm. Thereafter, MAs assemble in the *M. tb* cell wall, forging a protective shield that shelters the mycobacterium from noxious substances, including antibiotics as well as the immune modulators from the host. Numerous MmpL3 inhibitors with diverse chemical structures were uncovered in the past decade, such as the indole-2-carboxamides (I2Cs) and the adamantyl ureas. However, most of the reported MmpL3 inhibitors with potent anti-TB activities developed to date are highly lipophilic, accounting for their poor bioavailabilities. In this thesis, a number of I2C analogues and bioisosteres, with modified lipophilicities, were designed, synthesised, and evaluated for their anti-TB activities against drug-sensitive (DS) *M. tb* H37Rv strain. The top potent compounds were assessed for their growth inhibitory activities against a panel of DR *M. tb* strains. Their cytotoxicities were also evaluated against

healthy Vero cells. *In silico* molecular docking studies were performed to inspect their binding modes within the MmpL3 active site, in comparison to the co-crystallised ligands. In addition, some of the old anti-TB drugs, namely isoniazid (INH), pyrazinamide (PZA), and ciprofloxacin (CPF), were structurally modified in an attempt to improve their anti-TB activities. Some hybrid molecules were also synthesised, conjugating two pharmacophores from various anti-TB agents with diverse mechanisms of action.

On the other hand, since the I2C framework was also demonstrated to have a remarkable activity against cancer cells, numerous novel indoles were designed and synthesised to be tested against paediatric glioblastoma (GBM) tumour cell line KNS42 and other grade IV tumours in addition to the *M. tb* strains. Analysis of gene transcriptional response of KNS42 cells exposed to the most active compounds revealed a significant downregulation of key oncogenes. When the KNS42 cells were found to overexpress cannabinoid receptor 1 (CB<sub>1</sub>R), a rigorous literature search was conducted to scrutinise the antitumour potential of cannabinoids and whether or not their cytotoxic activities are correlated to their cannabinoid (CB) receptor modulation. Within this context, several I2C derivatives were reported in the literature as CB receptor ligands. Accordingly, the most potent antitumour I2C analogues and bioisosteres were assessed for their agonistic and antagonistic activities at both CB<sub>1</sub>R and cannabinoid receptor 2 (CB<sub>2</sub>R). The outcome of this thesis highlights the potential of the I2C architecture as a versatile scaffold that can be fine-tuned for its antimycobacterial and/or antitumour activities.

## Acknowledgements

I would like to express my sincere and heartfelt gratitude to my primary supervisor **Dr Hendra Gunosewoyo** for providing me with this amazing opportunity to do my PhD degree under his exceptional supervision and grow as an independent researcher. I have been immensely fortunate to receive his outstanding guidance, profound support, and invaluable trust. I feel privileged to have had him as a mentor. I also greatly appreciate the advice and feedback I received from my co-supervisor **Dr Alan Payne**. A special thanks to **Professor Mauro Mocerino** for his support and valuable suggestions.

I would like to extend my deepest thanks to **Dr Shichun Lun** and **Professor William Bishai** (Johns Hopkins University) for the *in vitro* testing of compounds against different mycobacterial strains and Vero cells. I am also very grateful to **Amreena Suri**, **Anders Bailey**, and **Associate Professor Simone Treiger Sredni** for the *in vitro* screening of the compounds against different brain tumour cells and non-tumorigenic human fibroblasts in Ann & Robert H. Lurie Children's Hospital of Chicago. I would like to sincerely thank **Samuel Lane**, **Dr Eryn Werry**, and **Professor Michael Kassiou** (Sydney University) for assessing the activity of the top potent compounds for CB<sub>1</sub>R and CB<sub>2</sub>R. I am also thankful to **Professor Chiang-Ching Huang** for converting the raw RNA sequencing data obtained from BGI Americas into a workable worksheet containing the fold changes and statistical significance values for all the expressed genes in KNS42 cells.

I extend my gratitude to **Mr. Giuseppe Luna** in Curtin Medical School for the organisation and provision of necessary solvents and consumables that I needed during my PhD studies. I also appreciate the help and advice I received from **Dr Ching Yong Goh** regarding NMR spectroscopy. My PhD journey has been made more enjoyable by being surrounded by lovely and supportive friends and colleagues at Curtin University. And finally, I would like to express my thanks to my family.

This research has been made possible by the Curtin International Postgraduate Scholarship (CIPRS) gratefully awarded by Curtin University and the funding provided by Curtin Medical School.

## List of Publications

This PhD thesis comprises six peer-reviewed articles (incorporated in Chapters 2 – 7). Copyright permissions for publications were obtained, where necessary, and are encompassed in Appendix II. Author contribution is included prior to each published article in the related chapter.

1. **Alsayed, Shahinda SR**, Chau C. Beh, Neil R. Foster, Alan D. Payne, Yu Yu, and Hendra Gunosewoyo. "Kinase targets for mycolic acid biosynthesis in *Mycobacterium tuberculosis*." *Current Molecular Pharmacology* 12, no. 1 (2019): 27-49. (**Review article**)

(**Impact factor: 3.339**, DOI: [10.2174/1874467211666181025141114](https://doi.org/10.2174/1874467211666181025141114))

2. **Alsayed, Shahinda SR**, Shichun Lun, Giuseppe Luna, Chau Chun Beh, Alan D. Payne, Neil Foster, William R. Bishai, and Hendra Gunosewoyo. "Design, synthesis, and biological evaluation of novel arylcarboxamide derivatives as anti-tubercular agents." *RSC Advances* 10, no. 13 (2020): 7523-7540. (**Research article**)

(**Impact factor: 3.361**, DOI: <https://doi.org/10.1039/C9RA10663D>)

3. **Alsayed, Shahinda SR**, Shichun Lun, Alan Payne, William R. Bishai, and Hendra Gunosewoyo. "Design, synthesis and antimycobacterial evaluation of novel adamantane and adamantanol analogues effective against drug-resistant tuberculosis." *Bioorganic Chemistry* 106 (2021): 104486. (**Research article**)

(**Impact factor: 5.275**, DOI: <https://doi.org/10.1016/j.bioorg.2020.104486>)

4. **Alsayed, Shahinda SR**, Shichun Lun, Alan Payne, William R. Bishai, and Hendra Gunosewoyo. "Facile synthesis and antimycobacterial activity of isoniazid, pyrazinamide and ciprofloxacin derivatives." *Chemical Biology & Drug Design* 97, no. 6 (2021): 1137-1150. (**Research article**)

(**Impact factor: 2.871**, DOI: <https://doi.org/10.1111/cbdd.13836>)

5. **Alsayed, Shahinda SR**, Shichun Lun, Anders W. Bailey, Amreena Suri, Chiang-Ching Huang, Mauro Mocerino, Alan Payne, Simone Treiger Sredni, William R. Bishai, and Hendra Gunosewoyo. "Design, synthesis and evaluation of novel indole-2-

carboxamides for growth inhibition of Mycobacterium tuberculosis and paediatric brain tumour cells." *RSC Advances* 11, no. 26 (2021): 15497-15511. (Research article)

(Impact factor: 3.361, DOI: <https://doi.org/10.1039/D0RA10728J>)

6. **Alsayed, Shahinda SR**, Amreena Suri, Anders W. Bailey, Samuel Lane, Eryn L. Werry, Chiang-Ching Huang, Li-Fang Yu, Michael Kassiou, Simone Treiger Sredni and Hendra Gunosewoyo. "Synthesis and Antitumour Evaluation of Indole-2-Carboxamides against Paediatric Brain Cancer Cells." *RSC Medicinal Chemistry* 12, no. 11 (2021): 1910-1925. (Research article)

(Impact factor: n/a, CiteScore 2020: 5.7,  
DOI: <https://doi.org/10.1039/D1MD00065A>)

### Three review articles are under preparation for submission

1. **Alsayed, Shahinda SR** and Hendra Gunosewoyo. "Tuberculosis: Pathogenesis, Current Treatment Regimens, and Current Hot Targets." (Chapter 1), Intended for submission to *Drug Discovery Today*. (Impact factor: 7.851)

2. **Alsayed, Shahinda SR** and Hendra Gunosewoyo. "*M. tb* Kinases and Phosphatases as Validated Drug Targets to Restore the Host Immune Capacity in Combating TB." (Chapter 2), Intended for submission to *Frontiers in Pharmacology*. (Impact factor: 5.810)

3. **Alsayed, Shahinda SR** and Hendra Gunosewoyo. "Indole-2-carboxamide: A versatile Framework with Diverse Biological Activities and Polypharmacological Profile." (Chapter 6 and 7), Intended for submission to *European Journal of Medicinal Chemistry*. (Impact factor: 6.514)

## List of Abbreviations

|          | Acronym                  | Full name   |
|----------|--------------------------|---|
| <b>A</b> | ABS                      | Androgen binding site   |
|          | ACCases                  | Acetyl-CoA carboxylases   |
|          | ACP                      | Enoyl acyl carrier protein  |
|          | ACPM                     | Mycobacterial acyl carrier protein                                      |
|          | ADME                     | Absorption, distribution, metabolism, and excretion                     |
|          | AG                       | Arabinogalactan   |
|          | AGP                      | Arabinogalactan-peptidoglycan   |
|          | Ag85ABC                  | Antigen 85 complex  |
|          | AMP                      | Adenosine monophosphate   |
|          | ANGPTL4                  | Angiopoietin-related protein 4  |
|          | Anti-TB                  | Anti-tuberculosis   |
|          | APELA                    | Apelin early ligand A <u>or</u> Apelin receptor early endogenous ligand |
|          | APICA                    | <i>N</i> -(1-adamantyl)-1-pentyl-1 <i>H</i> -indole-3-carboxamide       |
|          | AR                       | Androgen receptor   |
|          | ARHGAP9                  | Rho GTPase-activating protein 9   |
|          | AT                       | Acyl transferase  |
| AT/RT    | Teratoid/rhabdoid tumour |   |
| <b>B</b> | BBB                      | Blood brain barrier   |
|          | BCG                      | Bacille Calmette-Guérin   |
|          | Bcl-2                    | B-cell lymphoma 2   |
|          | BDQ                      | Bedaquiline   |
|          | BF3                      | Binding function 3  |
|          | Boc-Gly-OH               | <i>N</i> -( <i>tert</i> -butoxycarbonyl)glycine                         |
|          | (Boc) <sub>2</sub> O     | Di- <i>tert</i> -butyl dicarbonate                                      |
|          | BPaL                     | BDQ, pretomanid, and linezolid regimen                                  |
|          | BTZs                     | 1,3-Benzothiazin-4-ones   |
|          | BZ-IND                   | Benzimidazole-indole hybrid   |
| <b>C</b> | CA9                      | Carbonic anhydrase 9  |
|          | C-ACP                    | The carboxy terminus of ACP domain                                      |



|          |                   |  |
|----------|-------------------|--|
|          | CB                | Cannabinoid  |
|          | CB <sub>1</sub> R | Cannabinoid receptor 1                                     |
|          | CB <sub>2</sub> R | Cannabinoid receptor 2                                     |
|          | CBD               | Cannabidiol  |
|          | CDI               | 1,1'-Carbonyldiimidazole                                   |
|          | CDK1/2            | Cyclin-dependent kinase 1 and 2                            |
|          | CDK9              | Cyclin-dependent kinase 9                                  |
|          | CFU               | Colony forming unit  |
|          | CHO               | Chinese hamster ovary cell                                 |
|          | ClogP             | Octanol-water partition coefficient                        |
|          | cMBT              | Carboxymycobactin  |
|          | CMC               | Carboxymethyl cellulose                                    |
|          | CMC8              | Glyceryl monocaprylate / Lipid Capmul MCM C8               |
|          | CmrA              | Corynebacterineae mycolate reductase A                     |
|          | <i>CNR1</i>       | Cannabinoid receptor 1 gene                                |
|          | CNS               | Central nervous system                                     |
|          | CNS MPO           | Central nervous system multiparameter optimisation         |
|          | COVID-19          | Coronavirus 2019   |
|          | CP1               | Cancer-placenta antigen 1                                  |
|          | CPF               | Ciprofloxacin  |
|          | CRC               | Colorectal cancer  |
|          | CTD               | C-terminal domain  |
|          | CYP               | Cytochrome P450  |
| <b>D</b> | DAT               | Diacyl trehaloses  |
|          | DCC               | <i>N,N'</i> -dicyclohexylcarbodiimide                      |
|          | DCM               | Dichloromethane  |
|          | DCP               | Dihexadecyl hydrogen-Phosphate <b>or</b> Dicetyl Phosphate |
|          | $\Delta^9$ -THC   | Delta-9-tetrahydrocannabinol                               |
|          | DIPEA             | <i>N,N</i> -diisopropylethylamine                          |
|          | DLM               | Delamanid  |
|          | DLV               | Delavirdine  |
|          | DMAP              | 4-Dimethylaminopyridine                                    |

|          |                  |  |
|----------|------------------|--|
|          | DMGs             | Diffuse midline gliomas  |
|          | DMF              | Dimethylformamide  |
|          | DMSO             | Dimethyl sulfoxide   |
|          | DOT              | Directly observed treatment  |
|          | DOTS             | Directly Observed Therapy Short Course   |
|          | DPA              | Decaprenylphosphoryl-D-arabinose   |
|          | DPR              | Decaprenylphosphoryl-D-ribose  |
|          | DprE1            | Decaprenylphosphoryl- $\beta$ -D-ribose 2'-epimerase 1   |
|          | DprE2            | Decaprenylphosphoryl-D-2-keto erythro pentose reductase  |
|          | DPX              | Decaprenylphosphoryl-2'-ketoribose   |
|          | DR               | Drug-resistant   |
|          | DS               | Drug-sensitive   |
|          | DSBs             | Double strand breaks   |
|          | DSPE-PEG<br>2000 | 1, 2-Distearoyl-sn-glycero-3-phosphoethanolamine- <i>N</i> -<br>methoxy (Polyethylene-glycol)-2000 |
| <b>E</b> | EBA              | Early bactericidal activity  |
|          | EDC.HCl          | 1-Ethyl-3-(3-dimethylaminopropyl)carbodiimide<br>hydrochloride                                     |
|          | EEA1             | Early endosome antigen 1   |
|          | eGFP             | Enhanced green fluorescent protein   |
|          | EMA              | European Medicines Agency  |
|          | EMB              | Ethambutol   |
|          | EMME             | 2-(Ethoxymethylene)malonic acid diethyl ester  |
|          | ENR              | Enoyl reductase  |
|          | ETH              | Ethionamide  |
| <b>F</b> | FAAL32           | Fatty acyl-AMP ligase 32   |
|          | FadD32           | Fatty acid degradation protein D32   |
|          | FAD              | Flavin adenine dinucleotide  |
|          | FAS-I            | Fatty acid synthase I  |
|          | FAS-II           | Fatty acid synthase II   |
| <b>G</b> | GBM              | Glioblastoma   |
|          | GI               | Gastrointestinal   |

|                  |                  |   |
|------------------|------------------|---|
|                  | GI <sub>50</sub> | Half-maximal inhibitory concentration of cell growth                      |
|                  | GMM              | Glucose monomycolate  |
|                  | GroMM            | Glycerol monomycolate   |
|                  | GTPase           | Guanosine triphosphatase  |
|                  | GyrA             | DNA gyrase A  |
|                  | GyrB             | DNA gyrase B  |
| <b>H</b>         | HAART            | Highly active antiretroviral therapy                                      |
|                  | HadAB/HadBC      | $\beta$ -hydroxyacyl-AcpM dehydratases                                    |
|                  | HATs             | Histone acetyltransferases  |
|                  | HBA              | Hydrogen-bond acceptors   |
|                  | HBD              | Hydrogen-bond donors  |
|                  | HBTU             | O-(benzotriazol-1-yl)-N,N,N',N'-tetramethyluronium<br>hexafluorophosphate |
|                  | HDAC             | Histone deacetylase   |
|                  | hERG             | Human <i>ether-a-go-go</i> gene   |
|                  | HGGs             | High grade gliomas  |
|                  | His/Asp          | Histidine/aspartate   |
|                  | HIV              | Human immunodeficiency virus  |
|                  | HK               | Histidine kinase  |
|                  | HOBt             | Hydroxybenzotriazole hydrate  |
|                  | HPLC             | High-performance liquid chromatography                                    |
|                  | hPXR             | Human pregnane X receptor   |
|                  | HRZ              | Isoniazid, rifampicin, and pyrazinamide (INH, RIF, and PZA)               |
|                  | HTS              | High throughput screening   |
|                  | <b>I</b>         | I2C   |
| I2C-INH          |                  | Indole-2-carboxamide-isoniazid hybrid                                     |
| I2C-POA          |                  | Indole-2-carboxamide-pyrazinoic acid hybrid                               |
| IC <sub>50</sub> |                  | Half-maximal inhibitory concentration                                     |
| IM               |                  | Inner membrane  |
| INH              |                  | Isoniazid   |
| InhA             |                  | Enoyl-acyl carrier protein reductase                                      |
| INH-POA          |                  | Isoniazid-pyrazinoic acid hybrid  |

|                     |                |  |
|---------------------|----------------|--|
|                     | IPAs           | Imidazopyridine amides                       |
| <b>K</b>            | KAR            | Ketoacyl reductase                           |
|                     | Kas-III/mtFabH | $\beta$ -ketoacyl-AcpM synthase III          |
|                     | KasA/B         | $\beta$ -ketoacyl ACP synthases              |
|                     | KatG           | Mycobacterial catalase-peroxidase            |
|                     | KD             | Kinase domain                                |
|                     | $K_i$          | Inhibition constant                          |
|                     | KS             | Ketoacyl synthase                            |
| <b>L</b>            | LAB            | Labrasol/Caprylocaproyl polyoxyl-8 glyceride |
|                     | LAT1           | L-amino acid transporter 1                   |
|                     | LC-TAG         | Long-chain triacylglycerols                  |
|                     | LGGs           | Low grade gliomas                            |
|                     | Lipoid S-75    | Fat-free soyabean phospholipid               |
|                     | logBB          | log (C brain/C blood)                        |
|                     | logP           | Octanol-water partition coefficient          |
|                     | LPN            | Lipid-polymer hybrid nanoparticles           |
|                     | LTBI           | Latent tuberculosis infection                |
|                     | <b>M</b>       | MABA   |
| MabA/FabG1          |                | $\beta$ -ketoacyl-AcpM reductase             |
| <i>M. abscessus</i> |                | <i>Mycobacterium abscessus</i>               |
| mAGP                |                | Mycolyl-arabinogalactan-peptidoglycan        |
| MAPK4               |                | Mitogen-activated protein kinase 4           |
| MAC                 |                | <i>Mycobacterium avium</i> complex           |
| MAs                 |                | Mycolic acids                                |
| <i>M. avium</i>     |                | <i>Mycobacterium avium</i>                   |
| MBC                 |                | Minimum bactericidal activity                |
| <i>M. bovis</i>     |                | <i>Mycobacterium bovis</i>                   |
| MBT                 |                | Mycobactin                                   |
| MCAT/mtFabD         |                | Malonyl-CoA:AcpM transacylase                |
| <i>M. chelonae</i>  |                | <i>Mycobacterium chelonae</i>                |
| Mcl-1               |                | Myeloid cell leukemia-1                      |
| MCL                 |                | Mantle cell lymphoma                         |

|          |                     |  |
|----------|---------------------|--|
|          | MDR-TB              | Multidrug-resistant tuberculosis                     |
|          | MED                 | Minimum effective dose                               |
|          | MHC                 | Major histocompatibility complex                     |
|          | MIC                 | Minimum inhibitory concentration                     |
|          | <i>M. kansasii</i>  | <i>Mycobacterium kansasii</i>                        |
|          | <i>M. leprae</i>    | <i>Mycobacterium leprae</i>                          |
|          | MM                  | Mycomembrane   |
|          | MmaA4/Hma           | Mycolic acid methyl transferase                      |
|          | <i>M. malmonese</i> | <i>Mycobacterium malmonese</i>                       |
|          | MMDAG               | Monomeromycolyl diacylglycerol                       |
|          | MmpL3               | Mycobacterial membrane protein large 3               |
|          | MOE                 | Molecular Operating Environment                      |
|          | MOM                 | Mycobacterial outer membrane                         |
|          | MPtpA               | Mycobacterial protein tyrosine phosphatase A         |
|          | MPtpB               | Mycobacterial protein tyrosine phosphatase B         |
|          | MPtps               | Mycobacterial protein tyrosine phosphatases          |
|          | <i>M. smegmatis</i> | <i>Mycobacterium smegmatis</i>                       |
|          | <i>M. tb</i>        | <i>Mycobacterium tuberculosis</i>                    |
|          | MTD                 | Maximum tolerated dose                               |
|          | MtF                 | Methyl transferases                                  |
|          | MWE                 | Mycolate wax esters                                  |
|          | MW/MWT              | Molecular weight                                     |
|          | <i>M. xenopi</i>    | <i>Mycobacterium xenopi</i>                          |
|          | mymA                | Mycobacterial monooxygenase                          |
| <b>N</b> | N-ACP               | The amino terminus of the ACP domain                 |
|          | NAD                 | Nicotinamide adenine dinucleotide                    |
|          | NADP                | Nicotinamide adenine dinucleotide phosphate          |
|          | NAI2C               | <i>N</i> -adamantyl-1 <i>H</i> -indole-2-carboxamide |
|          | NALs                | Neutral allosteric ligands                           |
|          | NAMs                | Negative allosteric modulators                       |
|          | NATs                | <i>N</i> -acetyl transferases                        |

|          |                      |   |
|----------|----------------------|---|
|          | NDUFA4L2             | NADH dehydrogenase [ubiquinone] 1 alpha subcomplex subunit 4-like 2 |
|          | NHERF1               | Na <sup>+</sup> /H <sup>+</sup> Exchanger 3 Regulating Factor 1     |
|          | NNRTI                | Non-nucleoside reverse transcriptase inhibitor                      |
|          | NOAEL                | No observed adverse events level                                    |
|          | NRB                  | Number of rotatable bonds   |
|          | NTM                  | Non-tuberculous mycobacteria  |
| <b>O</b> | OL                   | Outer layer   |
|          | OM                   | Outer membrane  |
|          | OtsA                 | Trehalose-6-phosphate synthase                                      |
|          | OtsB                 | Trehalose-6-phosphate phosphatase                                   |
| <b>P</b> | <i>P. aeruginosa</i> | <i>Pseudomonas aeruginosa</i>                                       |
|          | PAMs                 | Positive allosteric modulators                                      |
|          | PanD                 | Aspartate decarboxylase enzyme                                      |
|          | PAS                  | <i>Para</i> -aminosalicylic acid                                    |
|          | PAT                  | Pentaacyl trehaloses  |
|          | PBMC                 | Peripheral blood mononuclear cells                                  |
|          | PBS                  | Phosphate-buffered saline   |
|          | PBTZs                | Piperazinebenzothiazinones  |
|          | PCa                  | Prostate cancer   |
|          | PCaA                 | Cyclopropane synthase A   |
|          | pCD                  | Polymeric β-cyclodextrins   |
|          | PDB                  | Protein data bank   |
|          | PDIM                 | Phthiocerol dimycocerosates   |
|          | PDZ                  | Postsynaptic density 95/discs large/zona occludens 1                |
|          | PEG                  | Poly(ethylene glycol)   |
|          | PG                   | Propylene glycol  |
|          | PI3K                 | Phosphoinositide 3-kinase   |
|          | PI3P                 | Phosphatidylinositol 3-phosphate                                    |
|          | PIs                  | Phosphoinositides   |
|          | PK                   | Pharmacokinetics  |
| PknG     | Protein kinase G     |   |

|          |        |   |
|----------|--------|---|
|          | PKS    | Polyketide synthase                     |
|          | Pks13  | Polyketide synthase 13                  |
|          | PLA    | Polylactic acid                         |
|          | PLAC1  | Placenta specific protein 1             |
|          | PLGA   | Poly(lactic-co-glycolic acid)           |
|          | PMF    | Proton motive force                     |
|          | PMB    | Phagosome maturation block              |
|          | POA    | Pyrazinoic acid                         |
|          | PPA    | Polyphosphoric acid                     |
|          | PSA    | Prostate specific antigen               |
|          | PstP   | Ser/Thr phosphatase                     |
|          | PtkA   | Protein tyrosine kinase                 |
|          | PTM    | Post-translational modification         |
|          | PTPs   | Protein tyrosine phosphatases           |
|          | PVA    | Polyvinyl alcohol                       |
|          | PZA    | Pyrazinamide                            |
|          | PZase  | Pyrazinamidase/nicotinamidase           |
| <b>Q</b> | QcrB   | Cytochrome b subunit                    |
|          | QIDP   | Qualified Infectious Disease Product    |
|          | QRDR   | Quinolone resistance determining region |
| <b>R</b> | RIF    | Rifampicin                              |
|          | RMPI   | Roswell Park Memorial Institute         |
|          | RMSD   | Root mean square deviation              |
|          | RNAPII | RNA polymerase II                       |
|          | RND    | Resistance-nodulation-cell division     |
|          | RO5    | Lipinski's rule of five                 |
|          | RpsA   | Ribosomal protein S1                    |
|          | RR     | Response regulator                      |
|          | rt     | Room temperature                        |
| <b>S</b> | SA     | Stearylamine <u>or</u> Octadecylamine   |
|          | SapM   | Secreted acid phosphatase M             |
|          | SAR    | Structure-activity relationship         |

|          |                   |  |
|----------|-------------------|--|
|          | <i>S. aureus</i>  | <i>Staphylococcus aureus</i>               |
|          | Ser/Thr/Tyr       | Serine/threonine/tyrosine                  |
|          | SI                | Selectivity index                          |
|          | SIT               | Serum inhibition titration                 |
|          | SL-1              | Sulfolipid-1                               |
|          | SCRM <sub>s</sub> | Synthetic cannabinoid receptor modulators  |
|          | Span 60           | Sorbitan monostearate                      |
|          | Span 85           | Sorbitan trioleate                         |
|          | STPK <sub>s</sub> | Serine/threonine protein kinases           |
|          | SYK               | Spleen tyrosine kinase                     |
| <b>T</b> | TAC               | Thioacetazone                              |
|          | TB                | Tuberculosis                               |
|          | TD <sub>50</sub>  | Median toxic dose                          |
|          | TDM               | Trehalose dimycolate                       |
|          | TDR-TB            | Totally-drug resistant tuberculosis        |
|          | TE                | Thioesterase                               |
|          | TFA               | Trifluoroacetic acid                       |
|          | TGI               | Total growth inhibition                    |
|          | THF               | Tetrahydrofuran                            |
|          | TLC               | Thin layer chromatography                  |
|          | TMM               | Trehalose monomycolate                     |
|          | TMMk              | Trehalose monomycolate keto form           |
|          | TP                | Tubulin polymerisation                     |
|          | TPSA              | Topological polar surface area             |
| <b>U</b> | US FDA            | United States Food and Drug Administration |
| <b>V</b> | V-ATPase          | Vacuolar-type adenosine triphosphatase     |
|          | Vps34             | Vacuolar protein sorting 34                |
|          | VPS33B            | Vacuolar protein sorting 33B               |
|          | VPS-C             | Class C vesicular sorting protein          |
| <b>W</b> | WHO               | World Health Organisation                  |
|          | WT                | Wild-type                                  |
| <b>X</b> | XDR-TB            | Extensively drug-resistant tuberculosis    |



# Table of Contents

|   |       |
|---|-------|
| <b>Declaration</b> .....  | i     |
| <b>Abstract</b> .....   | ii    |
| <b>Acknowledgments</b> .....  | iv    |
| <b>List of Publications</b> .....   | v     |
| <b>List of Abbreviations</b> .....  | vii   |
| <b>Table of Contents</b> .....  | xvi   |
| <b>List of Figures</b> .....  | xxiii |
| <br>  |       |
| <b>Chapter 1: General Introduction (Tuberculosis: Pathogenesis, Current Treatment Regimens, and New Drug Targets)</b> ..... | 1     |
| Background .....  | 2     |
| 1.1. Introduction .....   | 3     |
| 1.2. TB Pathogenesis .....  | 5     |
| 1.3. Current Treatment Regimen for Drug-Sensitive (DS) TB .....   | 7     |
| 1.4. Challenges to The Global Control of TB .....   | 9     |
| 1.4.1. Drug-Resistant (DR) TB Crisis .....  | 9     |
| 1.4.2. TB and HIV Co-Infection .....  | 11    |
| 1.4.3. The Coronavirus 2019 (COVID-19) Pandemic and TB .....  | 12    |
| 1.5. TB Drug Targets .....  | 12    |
| 1.5.1. Overview .....   | 12    |
| 1.5.2. Current Hot Targets in <i>M. tb</i> Drug Discovery and Their Corresponding TB Drug Candidates .....                  | 14    |

|  |           |
|--|-----------|
| 1.5.2.1. GyrA/B .....  | 14        |
| 1.5.2.2. ATP Synthase .....  | 16        |
| 1.5.2.3. QcrB .....  | 16        |
| 1.5.2.4. DprE1 .....   | 18        |
| 1.5.2.5. FadD32 and Pks13 .....  | 21        |
| 1.5.2.6. MmpL3 .....   | 24        |
| 1.6. Summary and Concluding Remarks .....  | 27        |
| 1.7. Aims of The Project .....   | 28        |
| 1.7.1. Investigating Kinase Targets Implicated in The Biosynthesis of MAs in <i>M. tb</i> (Chapter 2) .....  | 28        |
| 1.7.2. Design, Synthesis, Purification, and Chemical Characterisation of Various Series of Analogues as Potential Anti-TB Agents .....                   | 29        |
| 1.7.2.1. MmpL3 Inhibitors-Derived New Analogues (Chapters 3 and 4) .....   | 29        |
| 1.7.2.2. INH, PZA, and Ciprofloxacin (CPF) Derivatives (Chapter 5) .....   | 29        |
| 1.7.3. Repurposing The Indole-2-Carboxamide Framework and Its Bioisosteres as Antitumour Agents against Paediatric Brain Gliomas (Chapter 6 and 7) ..... | 30        |
| References .....   | 32        |
| <b>Chapter 2: Protein Phosphorylation and Dephosphorylation in <i>M. tb</i></b> .....  | <b>41</b> |
| Background .....   | 42        |
| 2.1. Introduction .....  | 43        |
| 2.2. <i>M. tb</i> Protein Kinases and Phosphatases Regulate The Host's Immune Response .....   | 44        |
| 2.2.1. The Critical Role of Macrophages in Controlling Infection .....   | 44        |
| 2.2.2. Role of <i>M. tb</i> Kinases and Phosphatases in Warding Off Phagosome Maturation and Preventing Phagosome-Lysosome Fusion .....                  | 46        |

|  |    |
|--|----|
| 2.2.2.1. PknG .....  | 47 |
| 2.2.2.2. <i>M. tb</i> Secreted Phosphatases .....  | 50 |
| 2.3. <i>M. tb</i> Protein Kinases and Phosphatases Regulate The Biosynthesis of Cell Wall Components ..... | 55 |
| References .....   | 57 |
| Statement of contribution to a co-authored published paper .....   | 61 |
| Graphical Abstract .....   | 62 |
| Current Molecular Pharmacology 12, no. 1 (2019): 27-49 .....   | 63 |
| Conclusions .....  | 86 |

**Chapter 3: Bioisosteric Modification of Indole-2-Carboxamides as a Means to Develop Novel Antitubercular Agents .....** 87

|   |     |
|---|-----|
| Background .....  | 88  |
| 3.1. Introduction to Bioisosterism .....  | 89  |
| 3.2. Discovery of The I2Cs as Potent Anti-TB Agents with Exceptional Activity Against DR-TB .....   | 91  |
| 3.3. Targeting Non-Tuberculous Mycobacteria (NTM) by I2Cs .....   | 94  |
| 3.4. Rational Design of Novel Aryl- and Heteroaryl-Carboxamide Derivatives as Novel Antimycobacterial Agents Predicated on The I2C Architecture ..... | 96  |
| References .....  | 97  |
| Statement of contribution to a co-authored published paper .....  | 99  |
| Graphical Abstract .....  | 100 |
| RSC Advances 10, no. 13 (2020): 7523-7540 .....   | 101 |
| Conclusions .....   | 119 |

|   |     |
|---|-----|
| <b>Chapter 4: Design and Synthesis of Indole-2-Carboxamides with Improved Water Solubility as Antimycobacterial Agents</b> .....                | 120 |
| Background .....  | 121 |
| 4.1. Introduction .....   | 122 |
| 4.2. MmpL3: A Crucial Member of The MmpL Transporters Family in <i>M. tb</i> and The Protein Target of The I2Cs .....                           | 123 |
| 4.3. Previous and Current Endeavours to Enhance The Water Solubility of I2Cs .....  | 128 |
| References .....  | 131 |
| Statement of contribution to a co-authored published paper .....  | 134 |
| Graphical Abstract .....  | 135 |
| Bioorganic Chemistry 106 (2021): 104486 .....   | 136 |
| Conclusions .....   | 148 |
| <br>  |     |
| <b>Chapter 5: Design, Synthesis, and Antimycobacterial Evaluation of Isoniazid, Pyrazinamide, and Ciprofloxacin Analogues and Hybrids</b> ..... | 149 |
| Background .....  | 150 |
| 5.1. Introduction .....   | 151 |
| 5.2. INH, PZA, and CPF: Mechanisms of Action and Resistance .....   | 152 |
| 5.2.1. The First-Line Prodrugs INH and PZA .....  | 152 |
| 5.2.2. FQs as Second-Line Anti-TB Drugs .....   | 155 |
| 5.3. 2021 Research Letter "Facile Synthesis and Antimycobacterial Activity of Isoniazid, Pyrazinamide and Ciprofloxacin Derivatives" .....      | 157 |
| References .....  | 160 |
| Statement of contribution to a co-authored published paper .....  | 163 |
| Graphical Abstract .....  | 164 |

|  |     |
|--|-----|
| Chemical Biology & Drug Design 97, no. 6 (2021): 1137-1150 ..... | 165 |
| Conclusions .....  | 179 |

## **Chapter 6: Versatility and Repurposing of the Indole-2-Carboxamide Framework**

|   |     |
|---|-----|
| .....   | 180 |
| Background .....  | 181 |
| 6.1. Introduction .....   | 182 |
| 6.2. I2Cs as Antitumour Agents .....  | 184 |
| 6.2.1. Tubulin Polymerisation (TP) Inhibitors .....   | 184 |
| 6.2.2. Myeloid Cell Leukemia-1 (Mcl-1) Inhibitors .....   | 187 |
| 6.2.3. Na <sup>+</sup> /H <sup>+</sup> Exchanger 3 Regulating Factor 1 (NHERF1) Inhibitors .....    | 188 |
| 6.2.4. Androgen Receptor (AR) Binding Function 3 (BF3) Inhibitors .....                             | 189 |
| 6.2.5. Histone Deacetylase (HDAC) Inhibitors .....  | 190 |
| 6.2.6. DNA Alkylating Agents .....  | 191 |
| 6.2.7. Miscellaneous .....  | 192 |
| 6.3. I2Cs with Dual Anti-TB and Antitumour Activities .....   | 194 |
| 6.4. Design and Synthesis of Novel I2C-Based Small Molecules as Anti-TB and Antitumour Agents ..... | 196 |
| References .....  | 198 |
| Statement of contribution to a co-authored published paper .....                                    | 204 |
| Graphical Abstract .....  | 205 |
| RSC Advances 11, no. 26 (2021): 15497-15511 .....   | 206 |
| Conclusions .....   | 221 |

|  |     |
|--|-----|
| <b>Chapter 7: Correlation Between Modulation of Cannabinoid Receptors and the Antitumour Activity of Indole-2-Carboxamides</b> .....                                 | 222 |
| Background .....   | 223 |
| 7.1. Introduction .....  | 224 |
| 7.2. Indole-Based SCRMs: Transition From the Indole-3-Carboxamide (I3C) Scaffold to The I2C .....  | 227 |
| 7.3. I2Cs with Polypharmacology Profile Resembling Cannabinoids .....  | 231 |
| 7.4. Multimodality of Quinolone-3-Carboxylic Acids/Carboxamides .....  | 232 |
| 7.5. Design/Repurposing, Synthesis, and Biological Evaluation of Novel I2C Derivatives and Bioisosteres against <i>M. tb</i> and Paediatric Brain Tumour Cells ..... | 234 |
| References .....   | 238 |
| Statement of contribution to a co-authored published paper .....   | 246 |
| Graphical Abstract .....   | 247 |
| RSC Medicinal Chemistry 12, no. 11 (2021): 1910-1925 .....   | 248 |
| Conclusions .....  | 264 |
| <br>   |     |
| <b>Chapter 8: Conclusions and Future Directions</b> .....  | 265 |
| 8.1. Conclusions .....   | 266 |
| 8.2. Future Directions .....   | 270 |
| <br>   |     |
| <b>Appendices</b> .....  | 273 |
| Appendix I: Supplementary Information .....  | 274 |
| Supplementary Information – Chapter 3 (RSC Advances 2020 Article) .....  | 275 |
| Supplementary Information – Chapter 4 (Bioorganic Chemistry 2021 Article) .....  | 299 |

|   |     |
|---|-----|
| Supplementary Information – Chapter 5 (Chemical Biology and Drug Design 2021 Article) ..... | 317 |
| Supplementary Information – Chapter 6 (RSC Advances 2021 Article) .....                     | 326 |
| Supplementary Information – Chapter 7 (RSC Medicinal Chemistry 2021 Article) .....          | 342 |
| Appendix II: Copyright Permissions .....  | 358 |
| Current Molecular Pharmacology 2019 Article .....   | 359 |
| RSC Advances 2020 Article .....   | 364 |
| Bioorganic Chemistry 2021 Article .....   | 366 |
| Chemical Biology and Drug Design 2021 Article .....   | 368 |
| RSC Advances 2021 Article .....   | 371 |
| RSC Medicinal Chemistry 2021 Article .....  | 373 |

## List of Figures

|   |     |
|---|-----|
| <b>Figure 1.1.</b> General TB statistics and main symptoms of pulmonary TB .....  | 4   |
| <b>Figure 1.2.</b> Pathophysiology of pulmonary TB .....  | 6   |
| <b>Figure 1.3.</b> The four front-line anti-TB drugs .....  | 8   |
| <b>Figure 1.4.</b> Current second-line anti-TB agents .....   | 10  |
| <b>Figure 1.5.</b> A simplified diagram of target-based and phenotypic TB drug discovery cascade .....  | 13  |
| <b>Figure 1.6.</b> Schematic representation of the site of action of several current promising anti-TB drug candidates and hit/lead compounds .....   | 15  |
| <b>Figure 2.1.</b> Overview of the phagocytosis of microbial invaders and phagosome maturation, showing <i>M. tb</i> secreted kinases and phosphatases interfering with the developmental process of phagosomes ..... | 45  |
| <b>Figure 2.2.</b> Selected PknG, MPtpA, MPtpB, and SapM inhibitors .....   | 50  |
| <b>Figure 3.1.</b> I2Cs <b>1 – 9</b> reported in the literature as potent antimycobacterial agents .....  | 92  |
| <b>Figure 4.1.</b> MmpL1-13 proteins in <i>M. tb</i> .....  | 125 |
| <b>Figure 4.2.</b> Previous attempts to improve the water solubility of the I2C architecture .....  | 129 |
| <b>Figure 5.1.</b> Selected INH, POA, and CPF hybrids/compounds and their anti-TB activity against H37Rv strain .....   | 158 |
| <b>Figure 6.1.</b> Indole-based compounds in biological systems ( <b>1 – 3</b> ) as well as important I2C analogues in pharmaceutical market ( <b>4</b> ) and preclinical studies ( <b>5</b> and <b>6</b> ) .....     | 183 |
| <b>Figure 6.2.</b> Naturally occurring indole-based antitumour drugs .....  | 184 |
| <b>Figure 6.3.</b> TP inhibition and antitumour activities of colchicine and I2C analogues .....  | 185 |



|   |     |
|---|-----|
| <b>Figure 6.4.</b> I2C-based Mcl-1 ( <b>17 – 19</b> ) and NHERF1 ( <b>20 – 22</b> ) inhibitors as antitumour agents .....                                     | 188 |
| <b>Figure 6.5.</b> I2C-based AR-BF3 ( <b>23</b> ) and HDAC ( <b>24</b> ) inhibitors as well as DNA alkylators ( <b>25 – 29</b> ) as antitumour agents .....   | 190 |
| <b>Figure 6.6.</b> Novobiocin and miscellaneous I2C-based antitumour agents .....   | 193 |
| <b>Figure 6.7.</b> Compounds evaluated for their anti-TB and antitumour activities .....  | 196 |
| <b>Figure 7.1.</b> Repurposing of CB receptors ligands rimonabant and cannabidiol against <i>M. tb</i> , <i>M. smegmatis</i> , and various tumour cells ..... | 225 |
| <b>Figure 7.2.</b> Selected I3C and I2C analogues with potent modulatory activities at CB <sub>1</sub> R and/or CB <sub>2</sub> R receptors .....             | 229 |
| <b>Figure 7.3.</b> The <i>N</i> -adamantyl I2C analogue <b>9</b> as a multi-target directed ligand .....  | 232 |
| <b>Figure 7.4.</b> Functional activities at CB receptors and antitumour activities of quinolone-3-carboxamides <b>15 – 17</b> .....                           | 234 |
| <b>Figure 7.5.</b> Design strategies of new and repurposed analogues as antitumour agents .....   | 235 |
| <b>Figure 8.1.</b> Design of new potential anti-TB analogues via conjugating fragments from AX20017 and NAI2C .....   | 271 |

## **Chapter 1: General Introduction**

### **Tuberculosis: Pathogenesis, Current Treatment Regimens, and New Drug Targets**

## Background

Tuberculosis (TB) is a highly communicable airborne disease, claiming the lives of more than 1 million people every year globally at least since 2000. *Mycobacterium tuberculosis* (*M. tb*), the causative agent of TB, is a recalcitrant pathogen which is rife around the world, latently infecting approximately a quarter of the population worldwide. The asymptomatic dormant status of the bacteria escalates to the transmissible active form when the host's immune system becomes debilitated, such as in patients co-afflicted with the human immunodeficiency virus (HIV). The current front-line treatment regimen for drug-sensitive (DS) *M. tb* strains is a 6-months protocol, involving four different drugs, that requires stringent adherence to avoid relapse and resistance. Poverty, difficulty to access proper treatment, and lack of patient compliance contributed to the emergence of more sinister drug-resistant (DR) strains which demand longer duration of treatment (up to two years) with more toxic and more expensive drugs compared to the first-line regimen. Only two new drugs, bedaquiline (BDQ) and delamanid (DLM), were approved in 2013/2014 for treatment of TB—the first anti-TB drugs with novel mode of actions to be introduced to the market in more than 50 years—reflecting the attrition rates in the development and approval of new anti-TB drugs. Therefore, new potent anti-TB agents with novel mechanism of action are urgently required to treat and control the spread of antibiotic resistant *M. tb* strains. In recent years, several small molecules were identified as promising preclinical and clinical anti-TB drug candidates that inhibit new protein targets in *M. tb*. Most of these key targets are implicated in the biogenesis of the thick waxy outer membrane that barricades the *M. tb*, shielding the bacilli against environmental threats, including the host immune system and antibiotics. Accordingly, inhibiting these targets by small molecules can disrupt several critical biosynthetic processes, causing deformations in the intricate protective cell wall of *M. tb*, which eventuates in the death of the mycobacteria.

## 1.1. Introduction

In 1882, Robert Koch identified the tubercle bacillus, also known as *M. tb*, as the etiologic agent of TB (1). Since his discovery, the TB epidemic seems to be unabated, spreading in every corner of the globe. TB is a highly contagious airborne disease and one of the top ten causes of death worldwide (2). Although the disease typically affects the lungs (referred to as pulmonary TB), it can also spread to other parts of the body (known as extrapulmonary TB) (2). *M. tb* can stay dormant for years and persist in the body without any indication of illness, in which many people become asymptomatic carriers (inactive TB) (3). According to the 2020 World Health Organisation (WHO) report (2), around one quarter of the world's population (2 billion) are latently infected with *M. tb* (**Figure 1.1**). In the individuals carrying latent TB infections (LTBI), the estimated lifetime risk for TB reactivation is 5 – 10%. Indeed, the dormant mycobacteria can be awakened (active TB), particularly in the immunocompromised patients, such as those who are co-infected with the human immunodeficiency virus (HIV). Among the 38 million people living with HIV, the risk of developing TB is estimated to be 18 times higher than people without HIV (2). When the stalemate is broken, TB reactivation occurs and the bacterial burden soars, wherefore the disease becomes symptomatic (4).

Although the fraction of people with LTBI predisposed to TB reactivation is seemingly small, roughly 10 million people fall ill with TB annually at least since 2000 (2). In addition, from 2000 to 2019, approximately 1.4 – 2 million people died from TB each year, with the highest mortality rates occurring between 2000 and 2010. The latest 2020 WHO report documented that in 2019 TB claimed the lives of more than one million people worldwide (an estimated 1.2 million and 0.2 million deaths among the HIV-negative and the HIV-positive cohorts, respectively). In fact, TB-related fatalities surpass the deaths toll from any other bacterial pathogen, ranking TB among the 10 leading causes of deaths worldwide (2).

Unfortunately, no effective vaccine is currently available to prevent TB disease in adults, either before or after exposure to *M. tb*. Nonetheless, the only licenced TB vaccine, bacille Calmette-Guérin (BCG), which was developed nearly a century ago, can confer moderate protection in infants and children, especially from severe forms of TB (miliary TB and TB meningitis) (2). Indeed, while anyone anywhere can get

infected with TB, most people (about 90%) who develop active TB are adults, with more incidents among men than women. Therefore, there is a pressing need for a more efficacious vaccine that provides immunity against all forms of TB across all age spectrums.

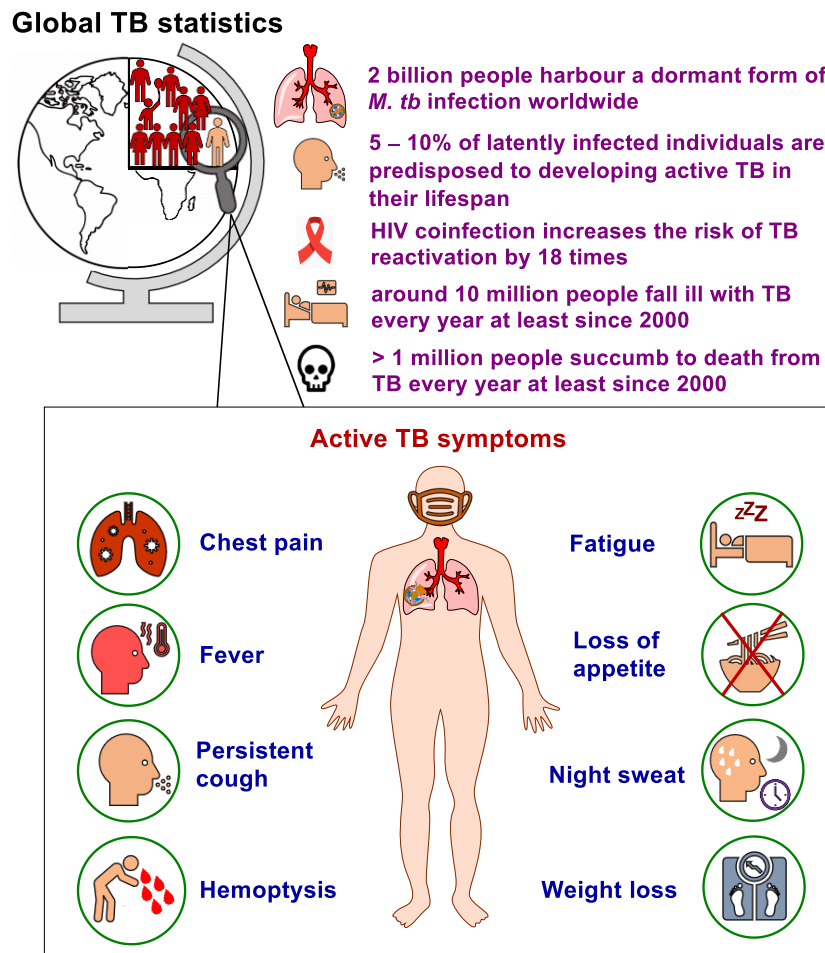


**Figure 1.1. General TB statistics and main symptoms of pulmonary TB.** Data source: latest WHO TB report in 2020.

The clinical manifestations of active pulmonary TB may include pleuritic chest pain, prolonged cough, haemoptysis, fever, fatigue, loss of appetite, night sweat and weight loss (5) (**Figure 1.1**). Geographically, in 2019, the majority of people who developed TB were located in the WHO South-East Asian region (44%), followed by the WHO African region (25%) and the WHO Western Pacific region (18%). Four countries accounted for nearly half of the global TB burden: the two WHO South-East Asian

countries, India (26%) and Indonesia (8.5%), in addition to the two WHO Western Pacific countries, China (8.4%) and the Philippines (6.0%) (2).

## 1.2. TB Pathogenesis

The pathogenic life cycle of *M. tb* is illustrated in **Figure 1.2**. TB is transmitted via *M. tb*-containing aerosol droplets, propelled by active TB patients when they cough, sneeze, or talk (5). After the new host inhale the TB bacteria, they travel through the respiratory tract and reach the lung. At this point, the host's innate immune system comes into play to quell the infection, whereupon the tubercle bacilli are internalised by alveolar macrophages. When the macrophages fail to inhibit or destroy the bacilli, the bacteria multiply within their intracellular environment and then get released and phagocytosed by other alveolar macrophages and the cycle continues (5). Lymphocytes are then recruited to the infection site, initiating a cell-mediated immune response, in which a pile of immune cells arrives, attempting to sequester the bacteria and limit further multiplication (6). At this stage, the host remains asymptomatic, and the TB bacteria may get eliminated completely or step into latency inside the granuloma (7). However, in the setting of impaired immunity, the disease immediately progresses into active TB with clinical symptoms (7).

The granuloma is the cardinal feature of pulmonary TB which is an amorphous collection of macrophages and other immune cells, aimed at restricting the bacterial spread (7). In immunocompetent individuals, although the granuloma is unable to eliminate the pathogen, it restrains the bacilli and halts the progression to active disease (6). However, the bacteria still survive, avoiding death by blocking the phagolysosome fusion and subverting the host's immune response. This process establishes a hospitable niche for *M. tb* where it can survive for decades, outwitting the immune system and persisting in a non-replicating or slowly replicating state (6). In this case, the patient is still non-infectious and asymptomatic (latently infected). Notably, one of the challenges facing the current TB therapy is targeting this tenacious pathogen inside the granuloma.

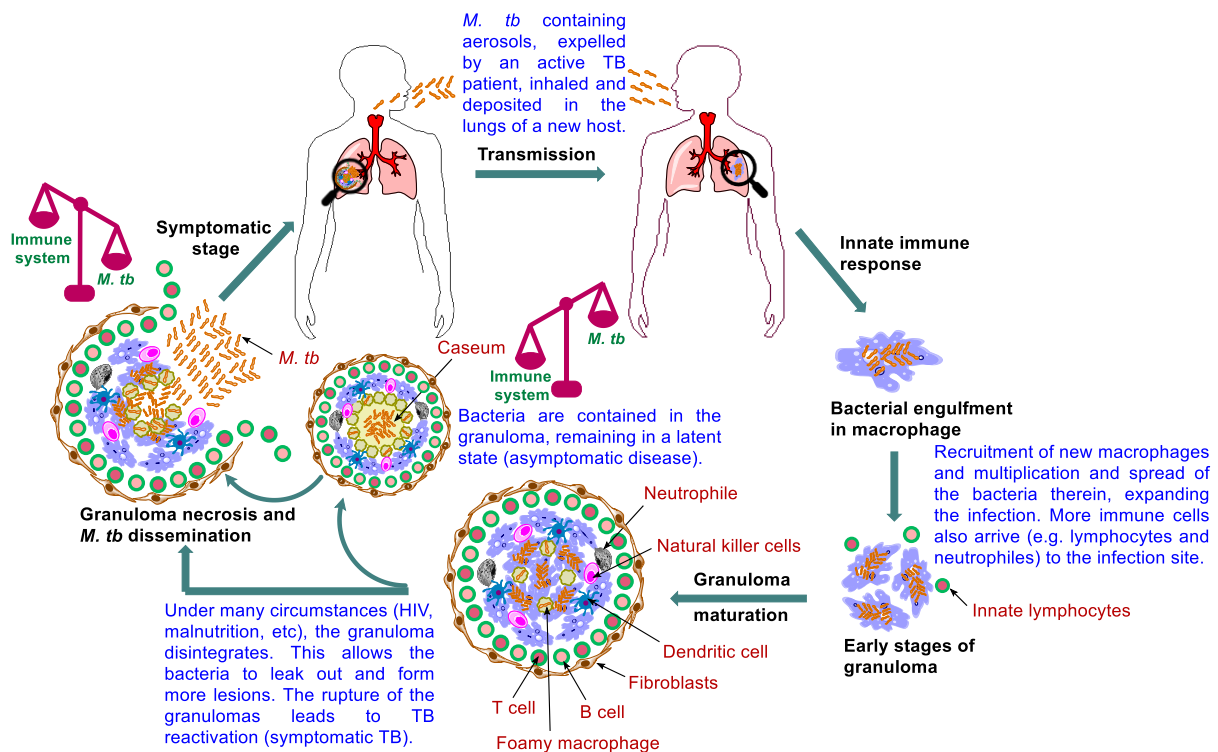


**Figure 1.2. Pathophysiology of pulmonary TB.** Following the *M. tb* transmission to the new host, the bacilli enter the lung and get ingested by macrophages. Further immune cells are recruited to wall off the infected macrophages, leading to the formation of the granuloma, the hallmark of TB. Healthy individuals remain latently infected and the infection is kept at bay at this stage, but prone to the risk of reactivation. Foamy macrophages release their lipid content when they necrotise leading to caseation (cheese-like structure). Caseum is a decay manifested at the core of the granuloma that compromise its rigid integrity. As the granuloma develops, the bacilli commence to seep out of the macrophages into the caseum layer. When the reactivation occurs, *M. tb* proliferates and the bacterial load becomes overwhelmingly high, whereupon the granuloma ruptures, disseminating the bacteria to the airways. The bacilli are then expectorated as contagious aerosol droplets, restarting the cycle, infecting other individuals.

As the granuloma matures, macrophages differentiate into foamy macrophages and other various morphotypes (8). The centre of the granuloma may necrotise as a result of the necrotic lysis of the host immune cells forming what is referred to as caseum (caseous granuloma) (9). Indeed, the accumulating soft necrotic debris, located in the core of the granuloma, resembles cheese (earning it the name caseum). Foamy macrophages, which are characterised by accumulated lipid droplets, distribute around the necrotic foci of the granuloma (10). Importantly, the *M. tb*-induced dysregulation of host lipid metabolism, via disrupting the balance between the influx and efflux of lipid particles from the serum, and sequestration thereof, were found to play a critical role in the disease progression (8). This disturbance in lipid metabolism promotes the formation of foam cells, which support bacterial persistence and eventually result in the accumulation of caseum in the granuloma (8). In addition,

mycolic acids (MAs), which are the major lipid components of the *M. tb* robust cell wall that are essential for the mycobacterial growth and survival, were reported to contribute to the differentiation of macrophages into foam cells (11, 12). The resulting caseous lesions serve as reservoirs, encasing and sheltering the tubercle bacilli which maintain the dormancy of the bacteria (13). However, in the late stage of the disease, the caseous core softens and cavitation takes place, leading to resuscitation of the bacteria, and the patient develops active TB, culminating in transmitting the infectious bacilli into a new host (8, 13). This life-threatening transformation largely relies on the effectiveness of the host's immune response in limiting the bacterial replication (6). Even though the main cause of TB reactivation is ascribed to HIV co-infection, other conditions may also switch the quiescent infection to an active one. These triggering factors include malnutrition, immune suppressive medications, chemotherapy, uncontrolled diabetes mellitus, sepsis, drug or alcohol addiction, chronic renal failure, smoking, and malignancy (6). When the host is immunocompromised, the hibernated bacilli, originally enclosed in the granuloma, will reactivate and replicate, accompanied by the granuloma liquifying and cavitating (10). Accordingly, the structure of the granuloma wanes and the contagious bacteria are released which results in the formation of cavitory lesions, signifying the lung damage observed in TB patients (6, 14). Furthermore, the caseous material serves as a fertile source of nutrients that promotes the growth of the pathogen to an overwhelming burden (14). Finally, the bacilli spread throughout the lung and find their ways to the blood capillaries paving the way not only for transmission to other people but also for dissemination to other organs (14). At this stage, the disease becomes highly infectious and symptomatic (active TB). Lung histology during the active disease indicates the coexistence of granulomas at different stages of development (14).

### **1.3. Current Treatment Regimen for Drug-Sensitive (DS) TB**

The current recommended treatment for DS-TB involves a combination of four antibiotics: isoniazid (INH), rifampicin (RIF), pyrazinamide (PZA) and ethambutol (EMB), which were all discovered nearly 60 years ago (15) (**Figure 1.3**). This four-drug cocktail should be administered for at least 6 months under directly observed treatment (DOT) to ensure high rates of treatment success and cure. The treatment involves two phases: the initial phase which comprises administering the



aforementioned four drugs for two months, and the continuation phase treatment with INH and RIF for the last four months to kill the dormant bacteria (15).

The four drugs target *M. tb* via different mechanisms of action. Briefly, INH is a prodrug that upon activation inhibits the enoyl-acyl carrier protein reductase (InhA) which is a key enzyme in the MAs biosynthetic process (16). MAs are the primary mediators of the hydrophobic attributes and lack of permeability of the mycobacterial outer coating (11). RIF binds to the  $\beta$ -subunit of the bacterial RNA polymerase and exerts its bactericidal activity by inhibiting the early steps of gene transcription (17). Like INH, PZA is a prodrug that gets activated, after diffusing into the TB granuloma, by the pyrazinamidase enzyme to pyrazinoic acid (POA) which subsequently kills the *M. tb* bacillus inside the granuloma (18). However, the mode of action of PZA is still enigmatic. EMB is a bacteriostatic drug that inhibits the synthesis of arabinogalactan and lipoarabinomannan, two essential components of the mycobacterial cell wall, by targeting the three arabinosyltransferases EmbA, EmbB, and EmbC (19).

Despite the effectiveness of the four front-line anti-TB agents against DS-TB, several adverse side effects are associated with this regimen, including liver dysfunction, peripheral neuropathy, erythromelalgia, ocular toxicity, central nervous system (CNS) toxicity, gastrointestinal (GI) intolerance, and skin rash (20-22). Poor patient compliance owing to these unwanted side-effects, high pill count, and protracted duration of therapy in addition to the overuse/misuse of antibiotics contributed to the emergence of DR *M. tb* strains (20).

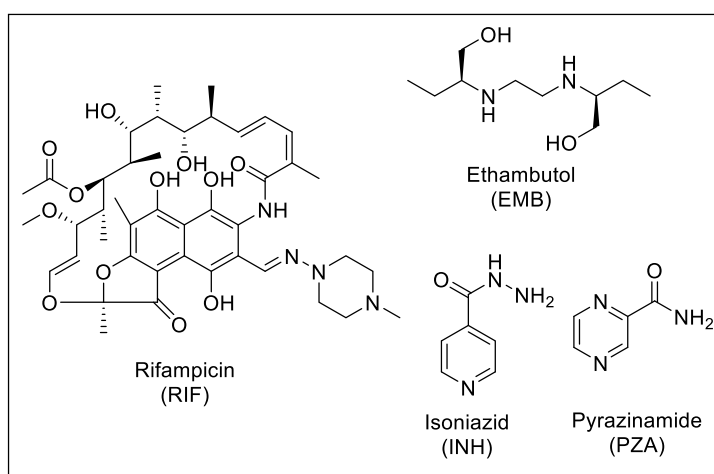


**Figure 1.3. The four front-line anti-TB drugs.**

## 1.4. Challenges to The Global Control of TB

### 1.4.1. Drug-Resistant (DR) TB Crisis

The therapeutic approach for DR-TB and the prognosis thereof is significantly correlated to the resistance pattern, however, the clinical management of DR-TB is generally complicated. Multidrug-resistant TB (MDR-TB) is defined as resistance to INH and RIF, the two most powerful front-line anti-TB drugs (2). In 2019, there were an estimated 465,000 MDR-TB incident cases. The cure rates for MDR-TB are typically lower than DS-TB (2). The 2019 WHO recommended second-line regimen for MDR-TB (**Figure 1.4**) is an 18 – 20 months treatment protocol, contingent on the patient's response to therapy. The MDR-TB medication regimen consists of at least four drugs in the intensive phase: three drugs from group A [linezolid, bedaquiline (BDQ), and moxifloxacin/levofloxacin] and one drug from group B (clofazimine, or terizidone/cycloserine) (23). At least three of these drugs should be prescribed for the rest of the treatment (continuation phase) after BDQ is stopped. Two drugs in group B should be prescribed, if only one or two drugs from group A are used (23). If the *M. tb* strain is resistant to one or more of the preceding drugs, drugs from group C [delamanid (DLM), streptomycin/amikacin, EMB, PZA, 4-aminosalicylic acid, imipenem, meropenem, ethionamide/prothionamide, high dose INH] should be added to the regimen (23, 24). In 2020, the WHO recommended a shorter all-oral regimen for MDR-TB (9 – 11 months) to make it easier for the patients to complete the therapy, in comparison to the aforementioned longer regimen (25). The initial phase of this shorter treatment protocol comprises administering a cocktail of BDQ, moxifloxacin/levofloxacin, clofazimine, ethionamide/prothionamide, INH (high dose), PZA, and EMB for four months (with a possibility of extension for a maximum of six months if the patient's culture or sputum smear remains positive by the end of the fourth month). Regardless, BDQ should be used for 6 months in total. The continuation phase is fixed at 5 months, entailing the administration of moxifloxacin/levofloxacin, clofazimine, PZA, and EMB (25). It is worth noting that BDQ and DLM, which were recently implemented in the second-line regimen, are the first anti-TB drugs with new mechanisms of action to be approved for treatment of TB in more than half a century; RIF was approved for clinical use in Italy in 1968 and in USA in 1971 (26, 27). BDQ was the first to be approved by the United States Food and Drug Administration (US FDA), at the end of 2012, followed by an authorisation granted by the European

Medicines Agency (EMA) for the use of both DLM and BDQ in adults with MDR-TB, in 2013 and 2014, respectively (26).

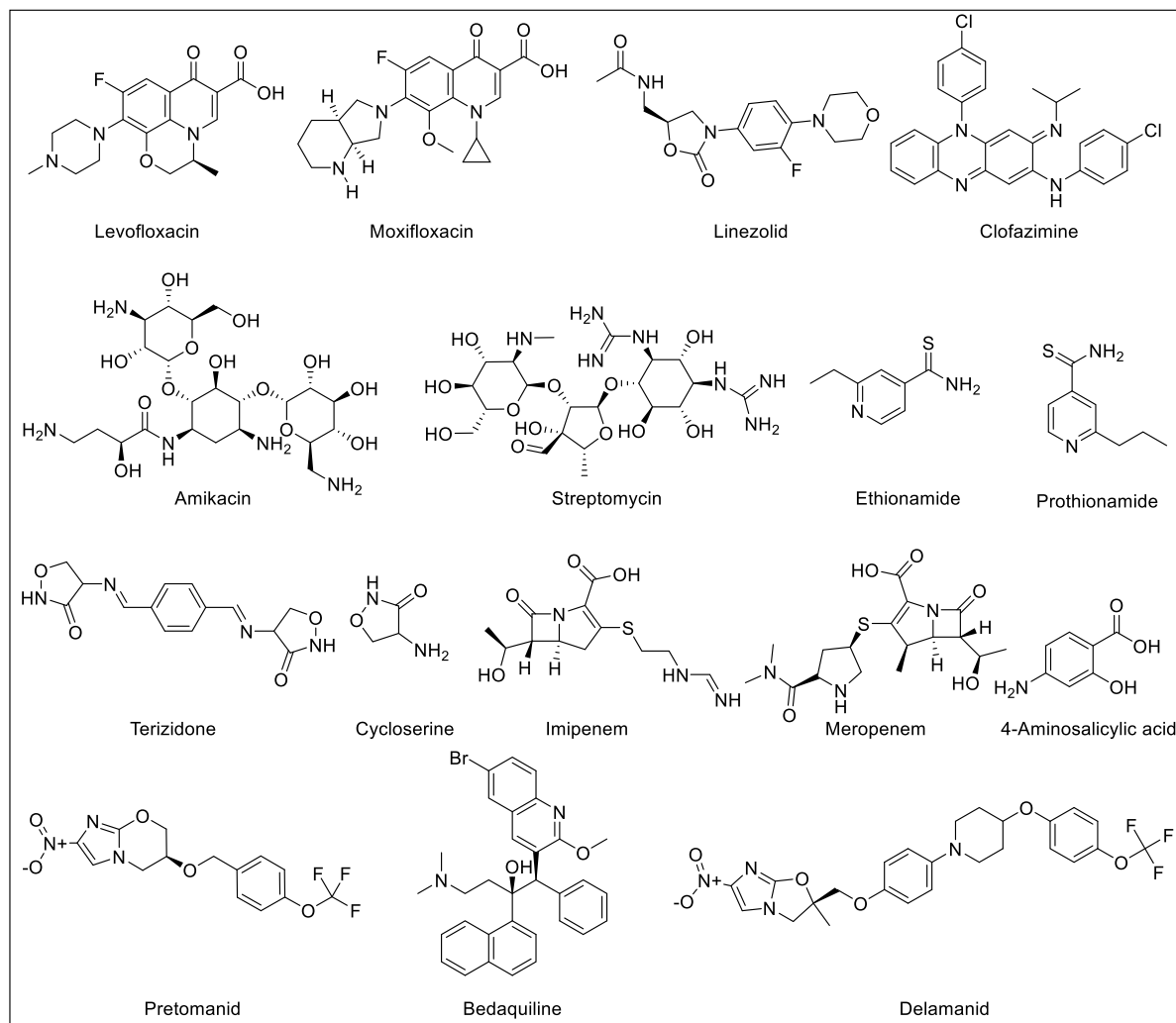


**Figure 1.4. Current second-line anti-TB agents.**

On the other hand, extensively drug-resistant TB (XDR-TB) is a subset of MDR-TB (resistant to INH and RIF) with an additional resistance to at least one fluoroquinolone (such as moxifloxacin or levofloxacin) and any of the injectable second-line TB drugs (such as amikacin) (28). Therefore, very limited treatment options are available for XDR-TB, resulting in extremely high mortality rates and raising the danger of a return to the pre-antibiotic era (29). An intermediate stage between MDR-TB and XDR-TB is called pre-XDR-TB which is an MDR-TB additionally resistant to either a fluoroquinolone or an injectable second-line agent (28). Pre-XDR-TB and XDR-TB treatment duration ranges between 14 – 24 months including also both intensive and

continuation phases with a combination of the second line agents to which the *M. tb* strain is susceptible (28). Recently, a shorter new regimen, comprising BDQ, pretomanid, and linezolid (BPaL regimen), was approved by the US FDA to be administered in patients with XDR-TB (24). However, this regimen should only be administered under operational research conditions and when BDQ and linezolid have not been previously used (24).

People may get MDR-TB or XDR-TB in one of two ways: 1) a primary infection with MDR or XDR bacteria (person-to-person transmission) or 2) resistance may develop when anti-TB drugs are misused or mismanaged in TB patients (23, 24). Overall, MDR-TB and XDR-TB generally require substantially longer duration of treatment (up to two years) compared to the first-line regimen for DS-TB. Moreover, the second-line anti-TB drugs, recommended for MDR- and XDR-TB, are generally more toxic, more expensive, and less efficacious than the front-line drugs (30). All of which exacerbate the patient adherence dilemma and the spread of the disease in the community, perpetuating TB as a global health menace.

#### **1.4.2. TB and HIV Co-Infection**

HIV infection is considered the main predisposing risk factor for patients falling ill with *M. tb*, increasing the likelihood of disease progression into the active stage by 18-fold (2). Similarly, TB is known to exacerbate the HIV infection and is considered the leading cause of death in HIV patients (31). In co-infected individuals, both pathogens have profound effects on the immune system, disarming the host's immune responses, and accelerating the decline of the immunological functions (31). One of the complications of TB and HIV co-infection is devising an appropriate treatment which is attributed to the increased pill burden, overlapping toxic side effects, and drug-drug interactions (29). The main interactions between TB and HIV antibiotics are correlated to RIF-induced elevated expression of hepatic cytochrome P450 (CYP) system. This induction of the CYP enzymes increases the metabolism of several HIV co-medications, such as protease inhibitors, and accordingly decreases their therapeutic concentrations (29). Even the co-administration of CYP inhibitors, such as ritonavir, cannot salvage the normal trough levels of various protease inhibitors. Hence, whether boosted or not, standard protease inhibitors cannot be prescribed with RIF (29). Other rifamycin antibiotic with reduced CYP induction properties is rifabutin, which was identified as an alternative to RIF. However, the co-administration of

ritonavir increases the serum concentration, and accordingly the accompanying toxicity, of rifabutin (29). Taken together, these complications further worsen the clinical management of both infections and the patient adherence to treatment.

### **1.4.3. The Coronavirus 2019 (COVID-19) Pandemic and TB**

TB has long been the world's leading cause of death from a single infectious disease (surpassing HIV/AIDS since 2007) (2). In this context, in 2020 alone, COVID-19 caused the deaths of more than 1.7 million people worldwide according to the WHO (32). Although the 2020 death figures of TB have not been revealed yet, the COVID-19 health crisis is expected to have catastrophic effects on TB. The WHO predicts a 0.2 – 0.4 million increase in the global number of TB deaths in 2020 (2).

## **1.5. TB Drug Targets**

### **1.5.1. Overview**

In 1998, the complete genome sequencing of *M. tb* (approximately 4000 genes) was unveiled which advanced our understanding of the molecular biology of the bacterium (33). Knowledge of the whole-genome *M. tb* sequence enabled researchers to identify a subset of genes that are essential *in vitro* and *in vivo* (34). This revelation in turn contributed to the discovery of new targets for novel compounds via identifying the mutated genes of the strains resistant to these compounds. The gene knockdown techniques, whereby the gene of a specific target is depleted, has also facilitated the validation process of several *M. tb* drug targets (34). The TB drug discovery approaches can be classified into target-based and phenotypic screening (35, 36) (**Figure 1.5**). The genome-derived target-based approach (target-to-drug) involves the identification of a specific cellular target in advance but without giving any information about its druggability (drug penetration or efflux) (35). Indeed, it has been a difficult conundrum to translate a good bacterial enzyme inhibition into a potent whole-cell *M. tb* inhibitory activity because of the difficulty to penetrate the highly impermeable waxy cell wall of *M. tb* (29). In addition, several inhibitors which were identified against essential targets were lacking drug-like properties. Therefore, no anti-TB drug has emerged from this strategy to date (29, 35, 36).

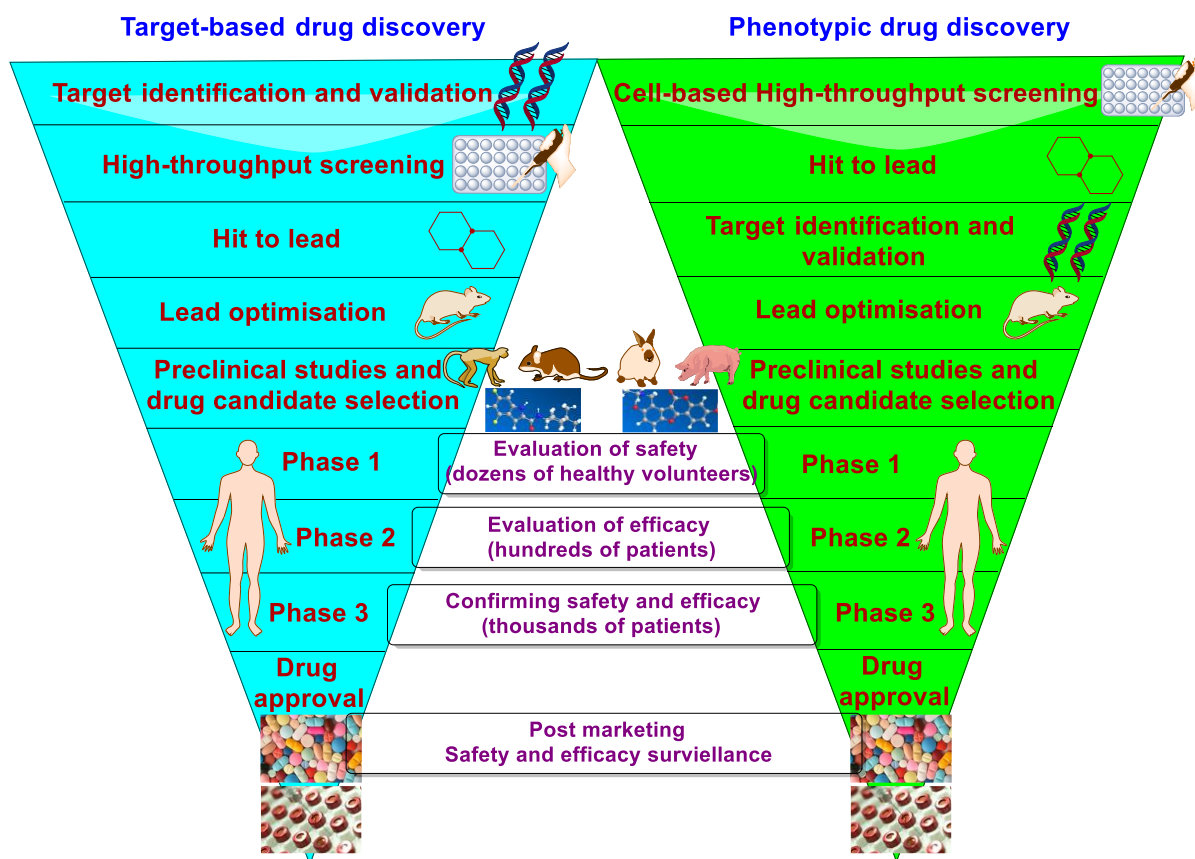


Figure 1.5. A simplified diagram of target-based and phenotypic TB drug discovery cascade.

On the other hand, the cell-based phenotypic screening approach (drug-to-target) is based on a high-throughput screening of compound libraries which proved to be a much more successful strategy (29, 35). In fact, all currently used anti-TB antibiotics were discovered using the phenotypic screening tactic (36). This approach ensures the compounds' capability to inhibit bacterial growth at first, followed by identifying their potential target (29, 35). However, the lack of that upfront knowledge regarding the mechanism of action prevents any structural biology input into the drug design efforts by medicinal chemists (29). Another drawback of the whole-cell screening approach is that although many hits can be delivered, some of them may have detergent effects; they may work through non-specific mechanisms, thereby having toxic effects. Therefore, to circumvent this problem, the cytotoxicity of the hit compounds should be evaluated across several cell lines to obtain "quality hits" with good selectivity and specificity (29). Overall, the identification of targets for compounds with established anti-TB activity (cell-based/phenotypic approach) allows for the rational modification and optimisation, via medicinal chemistry, of the lead candidates

(35). Accordingly, adopting this strategy will ensure that the designed compounds retain activity against their primary target.

## **1.5.2. Current Hot Targets in *M. tb* Drug Discovery and Their Corresponding TB Drug Candidates**

### **1.5.2.1. GyrA/B**

DNA gyrase is a highly conserved type II topoisomerase enzyme which is essential for DNA transcription, replication, and recombination in *M. tb* (37, 38). Therefore, inhibiting DNA gyrase results in impaired DNA replication and permanent double strand breaks which lead to cytotoxic accumulation of cleaved double-strand DNA fragments, inducing bacterial death (9, 39). DNA gyrase is an ATP-dependent tetrameric enzyme (with A<sub>2</sub>B<sub>2</sub> heterotetramers), consisting of GyrA and GyrB subunits (37, 38). The GyrA subunit carries the breakage-reunion active site and is a clinically validated drug target of the fluoroquinolone family of antibiotics, such as moxifloxacin. On the other hand, the GyrB subunit (ATPase) promotes ATP hydrolysis and has been relatively less exploited, thereby representing a new avenue for tackling *M. tb* strains that are resistant to fluoroquinolones (37, 38). Indeed, various chemical entities have been developed as GyrB inhibitors, showing potent activity against DR-TB (37). In particular, a novel class of aminobenzimidazoles was found to target the ATPase subunit, which upon further optimisation led to the discovery of SPR720 (VXc-486) (37) (**Figure 1.6**).

SPR720 was found to inhibit a panel of DS and DR *M. tb* isolates *in vitro* with minimum inhibitory concentrations (MIC) of 0.03 – 0.30 µg/mL and 0.08 – 5.48 µg/mL, respectively (37). It also reduced the *M. tb* burden in the lungs of infected mice *in vivo* and demonstrated bactericidal activity against intracellular and dormant *M. tb* in a low oxygen environment. Interestingly, the phosphate prodrug of SPR720 showed more potent killing of *M. tb* than the parent compound *in vivo*. When combined with other anti-TB drugs, the prodrug sterilised the *M. tb* infection in mice with relapse infection (37). Based on the preclinical efficacy studies of SPR720 *in vitro* and *in vivo* against some important non-tuberculous mycobacterial (NTM) species in addition to the toxicology/safety reports obtained thereof, SPR720 was advanced into human clinical trials (40). Similar to *M. tb*, NTM infections can cause progressive lung disease, especially in patients with structural lung damage or weakened immune systems (41).

Phase I clinical trials of SPR720 were initiated in January 2019, aimed at evaluating its tolerability, safety, and pharmacokinetics (PK) in healthy volunteers (42).

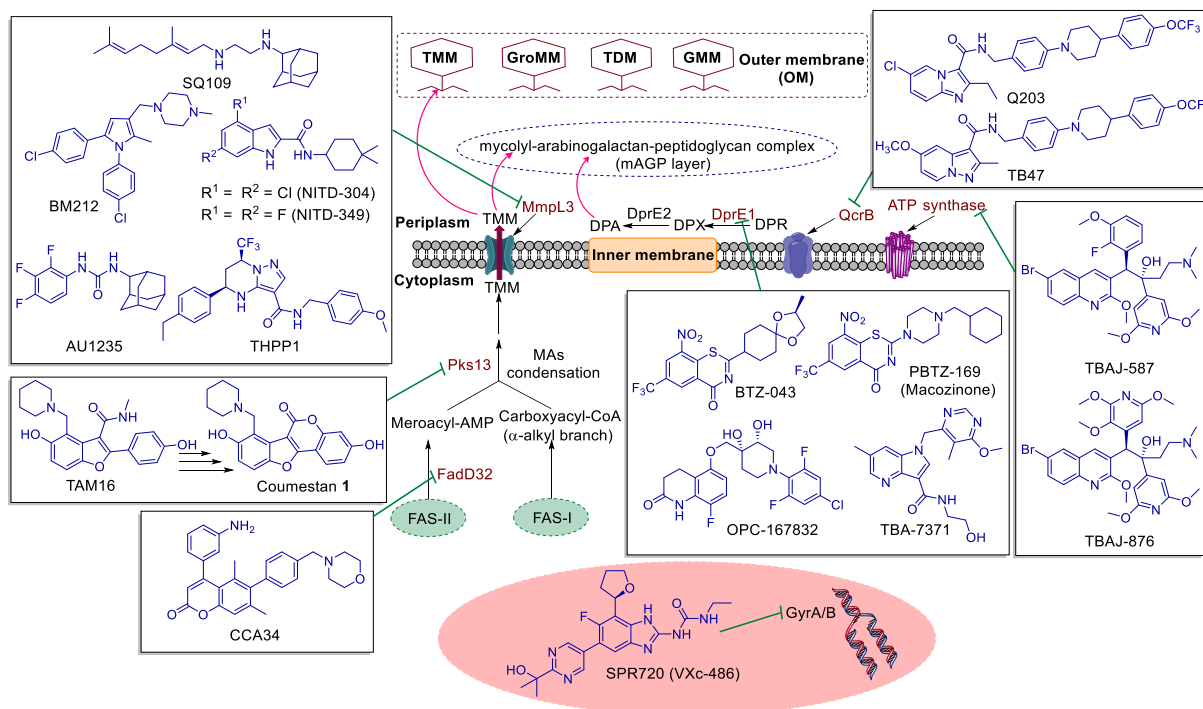


**Figure 1.6. Schematic representation of the site of action of several current promising anti-TB drug candidates and hit/lead compounds.** A simple version of the mycobacterial cell wall and the cytoplasmic membrane is portrayed, showing the current hot targets in TB drug discovery, namely GyrA/B, QcrB, ATP synthase, DprE1, FadD32, Pks13, and MmpL3. TMM: trehalose monomycolate, GroMM: glycerol monomycolate, TDM: trehalose dimycolate, GMM: glucose monomycolate (GMM), DPR: decaprenylphosphoryl-D-ribose, DPX: decaprenylphosphoryl-2'-ketoribose, DPA: decaprenylphosphoryl-D-arabinose, MAs: mycolic acids, FAS-I: fatty acid synthase I, and FAS-II: fatty acid synthase II.

Towards the end of February 2019, SPR720 was designated the Qualified Infectious Disease Product (QIDP) status by the US FDA for the treatment of lung infections caused by *M. tb* and NTM (43). In December 2020, Phase IIa clinical trial of SPR720 started on patients with NTM pulmonary disease caused by *Mycobacterium avium* (*M. avium*) complex (MAC). Shortly Afterwards, a clinical hold has been placed on SPR720 by the US FDA following concerning events correlated with ongoing animal toxicology studies, wherein mortalities in non-human primates were observed, albeit with inconclusive causality to SPR720 (44). It is worth noting that there are no specifically approved oral antibiotics for treatment of pulmonary NTM. Indeed, a prolonged combination therapy with mainly unapproved drugs is recommended (12 –



24 months) and is often complicated by tolerability and/or safety concerns. Therefore, pending trial results, SPR720 could become the first approved oral antibiotic for NTM infections, addressing a crucial unmet need for the treatment of the debilitating pulmonary disease associated therewith (44).

### 1.5.2.2. ATP Synthase

The diarylquinoline BDQ (**Figure 1.4**), the most recently approved anti-TB drug with a novel mechanism of action, was found to elicit its activity via inhibiting the c subunit of the mycobacterial ATP synthase enzyme (45). Accordingly, it disrupts the energy metabolism and decreases intracellular ATP levels in *M. tb* (45, 46). However, some issues were associated with BDQ. First, it has an extremely long *in vivo* elimination half-life and extensive tissue accumulation that could be ascribed to its very high lipophilicity (ClogP = 7.25) (47). It also showed potent inhibition of the human *ether-a-go-go* gene (hERG) cardiac potassium channel (IC<sub>50</sub> = 1.6 μM), which is crucial for the repolarisation of cardiac action potentials. This dysfunction of hERG causes prolonged QT (the time interval between the beginning of the Q wave till the end of the T wave) syndrome, resulting in irregular heart rhythm and potentially sudden death (47). Indeed, BDQ comes with a black box warning for increased risk of arrhythmia and mortality (48). Therefore, next-generation lead optimisation efforts were subsequently initiated, aimed at lowering the lipophilicity and cardiotoxicity of BDQ and improving clearance while maintaining its high anti-TB activity (47). In this respect, two diarylquinolines TBAJ-587 and TBAJ-876 were identified (**Figure 1.6**). Both compounds have anti-TB activity (MIC<sub>90</sub> = 0.006 and 0.004 μM, respectively) superior to BDQ (MIC<sub>90</sub> = 0.03 μM) against H37Rv strain *in vitro* (47). In animal models, TBAJ-587 has better efficacy than BDQ, while the activity of TBAJ-876 was comparable to BDQ. Importantly, the lipophilicities (ClogP = 5.80 and 5.15, respectively) and hERG inhibitory activities (IC<sub>50</sub> = 13 and > 30 μM, respectively) of both compounds are lower than BDQ (47). TBAJ-587 and TBAJ-876 are currently in Phase I clinical trials (49).

### 1.5.2.3. QcrB

The cytochrome b subunit (QcrB) of the cytochrome *bc*<sub>1</sub> complex has recently emerged as an interesting target in *M. tb* (50). The cytochrome *bc*<sub>1</sub> complex is a key component of the respiratory electron transport chain required for ATP synthesis. Therefore, the inhibition of this complex disrupts the *M. tb* ability to generate energy.

A phenotypic screening of a library encompassing more than 100,000 compounds as antimycobacterial agents led to the identification of imidazopyridine amides (IPAs) as a promising class that blocks the *M. tb* growth by targeting QcrB (50). An optimised IPA derivative Q203 (**Figure 1.6**) showed potent growth inhibition against DS *M. tb* H37Rv strain (MIC<sub>50</sub> = 2.7 nM) and numerous MDR and XDR *M. tb* clinical isolates *in vitro* (MIC<sub>90</sub> < 0.43 nM for most DR strains) (50). Q203 was found to trigger a rapid ATP depletion in *M. tb* under both aerobic and anaerobic conditions and when a whole-genome sequencing of resistant mutants was conducted, QcrB was identified as its target. Q203 showed minimal cytotoxicity in different eukaryotic cell lines and was well tolerated in mice when administered as a high single dose (1000 mg/kg) as well as in a long-term administration study in rats (10 mg/kg administered for 20 days) (50). Importantly, Q203 did not inhibit the hERG channel (IC<sub>50</sub> > 30 µM), suggesting its potential low risk of cardiotoxicity. It also did not induce the human pregnane X receptor (hPXR) at 10 µM concentration and did not inhibit any of the CYP450 isoenzymes tested (IC<sub>50</sub> > 10 µM). Q203 was also efficacious at a dose < 1 mg/kg in a mouse model of TB (50). The aforementioned potent anti-TB activities in addition to the promising safety, and PK profiles obtained for Q203 (50) led to its advancement into human clinical trials. Telacebec (Q203) is currently in Phase II clinical trials as an oral antibiotic for treatment of TB. The preliminary results of Phase IIa early bactericidal activity (EBA) demonstrated that Telacebec was well tolerated and safe when administered at different doses to adult patients with pulmonary TB (49).

An analogous pyrazolo[1,5-*a*]pyridine-3-carboxamide derivative TB47 (**Figure 1.6**) was also identified as a preclinical anti-TB candidate that inhibits QcrB (49, 51). TB47 exhibited potent anti-TB activities (MIC = 0.016 – 0.500 µg/mL) against a panel of *M. tb* clinical isolates, including various MDR and XDR strains (51). TB47 also showed promising PK and toxicity profiles, whereby it displayed negligible cytotoxicity (IC<sub>50</sub> > 100 µM against both Vero and HepG2 cell lines), CYP450 interactions (IC<sub>50</sub> > 20 µM), and hERG channel inhibition (IC<sub>50</sub> > 30 µM) (51). In mouse infection models, although TB47 was not bactericidal as a monotherapy, it displayed a strong synergism with PZA and RIF, indicating its potential when combined with other anti-TB drugs (51).

#### 1.5.2.4. DprE1

Decaprenylphosphoryl- $\beta$ -D-ribose 2'-epimerase 1 (DprE1), also called decaprenylphosphoryl- $\beta$ -D-ribose oxidase, is a key enzyme implicated in the mycobacterial cell wall biosynthesis (52, 53). In 2009, a ground-breaking report identified DprE1 as the target of a novel class of inhibitors, namely 1,3-benzothiazin-4-ones (BTZs), that were discovered in a phenotypic screening of a drug library (53). This new class of compounds is endowed with potent antimycobacterial activities, demonstrating bactericidal activities against *M. tb* in the nanomolar range (53). DprE1 is a flavoprotein that works in concert with decaprenylphosphoryl-D-2-keto erythro pentose reductase (DprE2) to generate an arabinose precursor which plays a fundamental role in the synthesis of the mycobacterial cell wall polysaccharides arabinogalactan and lipoarabinomannan (52, 53). In this respect, DprE1 uses flavin adenine dinucleotide (FAD) to oxidise decaprenylphosphoryl-D-ribose (DPR) to a keto intermediate [decaprenylphosphoryl-2'-ketoribose (DPX)], which is subsequently reduced by DprE2 to form decaprenylphosphoryl-D-arabinose (DPA) (54) (**Figure 1.6**). DPA then serve as a sugar donor for the biogenesis of cell wall arabinans. The DPA biosynthesis was recently shown to take place in the periplasmic space of the mycobacterial cell wall, where DprE1 was also found to be located (54). The extracytoplasmic localisation of DprE1 makes it more accessible to drugs which contribute to its vulnerability. It was demonstrated that inhibiting DprE1 abolishes the formation of DPA, thereby provoking cell lysis and mycobacterial death (53). The validity of DprE1 as a drug target was further verified by genetic studies conducted using *M. tb* conditional knock-down mutants (55). Indeed, downregulation of DprE1 therein led to bacterial cell wall damage and lysis. Furthermore, rapid death was manifested in the DprE1-depleted mutants *in vitro* and intracellularly, accentuating its crucial role in bacterial growth and survival (55). In addition to BTZs, several new classes of DprE1 inhibitors effective against *M. tb* have been identified. Four compounds are currently in advanced stages of clinical trials, namely BTZ-043, PBTZ-169 (Macozinone), OPC-167832, and TBA-7371 (**Figure 1.6**).

The benzothiazinone analogue BTZ-043, which is the first identified DprE1 inhibitor, stood out as an exemplar of the BTZs class (53). In fact, BTZ-043 was found to be a suicide inhibitor of the mycobacterial FAD-dependent DprE1 enzyme, irreversibly inactivating the enzyme by forming a covalent adduct (56). BTZ-043 displayed

nanomolar bactericidal activities both *in vitro* and *ex vivo* against *M. tb* (53). Indeed, BTZ-043 exhibited an MIC value of 1 ng/mL (2.3 nM) against DS H37Rv *M. tb* strain and similar activities against a panel of clinical isolates of *M. tb*, including MDR-TB and XDR-TB strains. In the *ex vivo* model, BTZ-043 killed *M. tb* intracellularly (MIC < 10 ng/mL) in *M. tb* infected macrophages, demonstrating higher potency than INH and RIF against intracellular bacteria (53). In murine infection models of TB, the efficacy of BTZ-043 was comparable to INH and RIF although the *in vitro* anti-TB activities of the preceding two front-line drugs were far less than that of BTZ-043 (53, 57). In preclinical toxicology studies, BTZ-043 was well tolerated in minipigs (at 360 mg/kg) and rats (up to 170 mg/kg), showing low toxicological potential (49). BTZ-043 showed limited cytotoxic activities against human cell lines, including monocytic THP-1 cells, two hepatic cells (Huh7 and HepG2), and lung epithelial A549 cells [median toxic doses (TD<sub>50</sub>) = 16 – 77 µg/mL; selectivity indices (SI) = 16000 – 77000] (58). Phase IIa EBA clinical trials of BTZ-043 commenced in November 2020 (49).

Since the exceptional *in vitro* potency of BTZ-043 did not translate to comparably high *in vivo* efficacy in TB mouse models, further optimisations were conducted which led to the development of a new series of enhanced BTZs, namely piperazinebenzothiazinones (PBTZs) (57). This study was aimed at improving the pharmacological properties of the first-generation lead compound BTZ-043, particularly water solubility which was achieved by incorporating a piperazine group into the BTZ scaffold. Indeed, the next generation PBTZ-169 (**Figure 1.6**) displayed superior physicochemical properties and antimycobacterial activity compared to BTZ-043 (57). PBTZ-169 (Macozinone) inhibited DprE1 by forming a covalent bond with the cysteine residue in the active site thereof, demonstrating a mechanism of action identical to BTZ-043. The *in vitro* activity of PBTZ-169 against *M. tb* H37Rv strain (MIC = 0.3 ng/mL) was nearly 3-fold higher than BTZ-043 (57). Importantly, PBTZ-169 retained its potent activity against a panel of MDR and XDR *M. tb* clinical isolates. Besides its improved *in vitro* anti-TB potency, PBTZ-169 showed greater promise than BTZ-043 in the following aspects: 1) the lack of chiral centres in PBTZ-169 made the synthesis, manufacture, and quality control thereof more convenient than BTZ-043, which decreases its production cost; 2) PBTZ-169 was significantly more efficacious than BTZ-043 in murine models of TB which may stem from the fact that PBTZ-169 is a more efficient DprE1 inhibitor than BTZ-043; 3) PBTZ-169 displayed less cytotoxicity

than BTZ-043; 4) PBTZ-169 demonstrated better solubility than BTZ-043 which accounted for its rapid absorption compared to BTZ-043, indicating a better PK profile (57). PBTZ-169 acted synergistically with BDQ, while additive effects were observed when combined with other anti-TB drugs (57). Although PBTZ-169 was developed years after BTZ-043 (53, 57), PBTZ-169 made a remarkable progress in the clinical trials, therefore it is currently on par with BTZ043 as both candidates are in Phase II (49). Phase I studies of PBTZ-169 in healthy male volunteers revealed its favourable safety profile and good tolerability. Phase IIa EBA study of PBTZ-169 was completed early 2018 which established its acceptable safety in DS-TB patients. In addition, a statistically significant bactericidal activity was manifested when PBTZ-169 was administered as a monotherapy in a group of seven patients for 14 days (49).

Another phenotypic screening campaign conducted on a library of carbostyrils has identified and optimised 3,4-dihydrocarbostyril derivatives with potent anti-TB activities (59). Notably, the carbostyril structural core constitutes the backbone of numerous drugs and has been recognised for having favourable PK and safety profiles. These efforts led to the identification of the promising anti-TB drug candidate OPC-167832 (**Figure 1.6**). Whole genome sequencing of OPC-167832 resistant mutants subsequently identified DprE1 as the target of this compound and further studies also demonstrated its inhibition of DprE1 enzymatic activity (59). The MIC values of OPC-167832 against various DS and DR *M. tb* strains ranged from 0.24 – 2 ng/mL. It showed bactericidal activity against both growing and intracellular *M. tb* at concentrations of 0.5 and 4 ng/mL, respectively. Of note, the killing activity of OPC-167832 against growing *M. tb* was superior to BDQ and linezolid, whilst being similar to RIF, moxifloxacin, and levofloxacin (59). This potent bactericidal activity was recapitulated *in vivo* in a mouse model of chronic TB, in which OPC-167832 displayed a very low minimum effective dose (MED = 0.625 mg/kg). OPC-167832 was also evaluated in combination therapies in TB infected mice, in which it was used alongside DLM as the core component of drug-combination regimens comprising 3 or 4 drugs, whereupon the third and/or fourth drug was linezolid, moxifloxacin, or BDQ (59). The observed sterilising activities of five out of six of these regimens was greater than the front-line regimen (INH, RIF, PZA, and EMB). Indeed, the new combinations demonstrated a rapid decrease in the bacterial burden in mice and relapse-preventing

effects superior to the standard treatment cocktail (59). These key attributes resulted in the entry of OPC-167832 into the clinical pipeline (Phase I/II EBA) (49).

A series of 4-azaindoles emerged from a scaffold morphing approach based on the imidazopyridine scaffold, exemplified by Q203 (60). This new class demonstrated excellent *in vitro* and *in vivo* anti-TB activities, with DprE1 being identified as their target. In fact, they were found to be non-covalent inhibitors of DprE1 (60, 61). TBA-7371 (**Figure 1.6**) was the highlight of this class that proceeded to clinical development (60, 62). This compound displayed potent anti-TB activities against DS and DR *M. tb* strains *in vitro* (MIC = 0.4 – 6.25  $\mu$ M). TBA-7371 also showed potent bactericidal activity against *M. tb* with minimum bactericidal activity (MBC) value of 0.78 – 1.56  $\mu$ M and was active against intracellular *M. tb* (60, 62). TBA-7371 was efficacious in a mouse/rat model of chronic TB infection, significantly reducing the bacterial burden in the lungs of infected animals (62). TBA-7371 showed minimal inhibition of the hERG channel (IC<sub>50</sub> > 33  $\mu$ M), suggesting its low risk of cardiotoxicity (62). When TBA-7371 was tested against THP1 cells (human monocytic cell line), it demonstrated no inhibition up to 100  $\mu$ M concentration, indicating its lack of cytotoxicity (60, 62). TBA-7371 did not inhibit any of the CYP450 isoenzymes (IC<sub>50</sub> > 50  $\mu$ M), suggesting its low tendency for drug-drug interactions. In general, when tested against a panel of human targets, TBA-7371 showed no major safety liabilities (60, 62). When its PK properties were assessed in rodents, good oral exposure was observed (60). TBA-7371 is currently in Phase I/IIa EBA clinical trials (49, 63).

#### 1.5.2.5. FadD32 and Pks13

The fatty acyl-AMP ligase 32, which is also called fatty acid degradation protein D32, (FAAL32 or FadD32) and polyketide synthase 13 (Pks13) are crucial enzymes that act in concert with each other, playing pivotal roles in the biosynthetic machinery of MAs (**Figure 1.6**) (64, 65). MAs are the major integral lipid components of the exceptionally fortified waxy cell wall of *M. tb* and the primary mediators of hydrophobicity and impermeability thereof (11). Briefly, in the *M. tb* cytoplasm, the C<sub>24</sub> – C<sub>26</sub>  $\alpha$ -alkyl branch of the MAs and the C<sub>50</sub> – C<sub>60</sub> meromycolate chain are generated from the fatty acid synthase I (FAS-I) and fatty acid synthase II (FAS-II) systems, respectively. These two fatty acids chains get activated before the final condensation takes place (11). FadD32 is an adenylating enzyme that activates and transfers the meromycolyl-AMP

(meroacyl-AMP) onto the terminal condensing enzyme Pks13. In other words, FadD32 serves as a linking enzyme connecting the FAS and PKS biosynthetic pathways (66). Pks13 then catalyses a key Claisen condensation reaction, coupling both of the two loaded fatty acyl chains, the  $\alpha$ -alkyl branch and meromycolate chain, to produce  $\alpha$ -alkyl  $\beta$ -ketoacids (64). The resulting assembled chain attach to trehalose, followed by a final reduction step to form trehalose monomycolate (TMM). The formed TMMs serve as MAs precursors which then get shuttled from cytoplasm to periplasm via the mycobacterial membrane protein large 3 (MmpL3) (64).

The closely partnered triad of FadD32, Pks13, and MmpL3, implicated in the MAs biosynthesis, composes a new territory that has not been fully exploited in *M. tb* (**Figure 1.6**). Therefore, they represent promising drug targets for the development of new anti-TB agents that could be used in tackling DR-TB. Both *fadD32* and *pks13* genes are adjacent on the same operon (the *fadD32-pks13-accD4* cluster) (67). MAs contribute to the intrinsic resistance of *M. tb* and are indispensable to mycobacterial survival, persistence, and virulence. Therefore, inhibiting crucial enzymes that are involved in the MAs biosynthesis is considered a viable approach in the TB drug discovery (68). This notion is substantiated by the currently used drugs that target the MAs biosynthesis, exemplified by the well-established anti-TB drug INH which constitutes the backbone of TB chemotherapy along with RIF. Accordingly, inhibiting FadD32 or Pks13 results in impairment in MAs biosynthesis, compromising the integrity of the *M. tb* outer membrane. Indeed, the deletion of the *fadD32* or *pks13* genes in *Corynebacterium glutamicum* abolished the production of MAs, altering the structure of the cell envelope (69-71). In *Mycobacterium smegmatis* (*M. smegmatis*), both genes were also shown to be essential for the mycobacterial growth and survival (69, 70).

In *M. tb*, depletion of *fadD32* was clearly bactericidal and increased the sensitivity of *fadD32* knockdown strain to several antibiotics (72). A whole-cell phenotypic screening against *M. tb* led to the identification of a series of diarylcoumarins that inhibit FadD32 (73). The most potent coumarin analogue CCA34 (**Figure 1.6**) showed an MIC value of 0.24  $\mu$ M against DS H37Rv *M. tb* strain (74). CCA34 also exhibited potent activity against an *M. tb* isolate with monoresistance to INH (MIC = 0.44  $\mu$ M). In addition, it demonstrated a potent MBC value of 1.9  $\mu$ M, which is comparable to that of INH (MBC = 0.5  $\mu$ M). In macrophages infected with *M. tb*, CCA34 was able to kill the intracellular

bacilli, whilst it had no effect on the macrophage viability (74). Importantly, in the mouse TB infection models, CCA34 was nontoxic and well-tolerated [maximum tolerated dose (MTD) = 100 mg/kg]. It also inhibited the bacterial proliferation, demonstrating 30-fold reduction in bacterial numbers in the lungs of infected mice after 8 days. This efficacy was found to be comparable to that observed for INH (74). These findings established FadD32 as a valuable and validated *in vivo* druggable target for *M. tb*. Since the 4,6-diaryl-5,7-dimethylcoumarins effectively suppress bacterial replication *in vivo* via inhibiting FadD32, CCA34 could be considered a promising lead compound that can be subjected to further optimisations.

On the other hand, Sacchetti group have developed a technique that is based on high throughput screening paired with whole-genome sequencing of resistant mutants and recombineering to validate the functional significance of the mutations (75). This method led to the identification of several whole-cell active compounds and their targets. One of the scaffolds that was identified therein was a benzofuran derivative which was found to target Pks13 (75). Upon conducting further structure-based modifications, the same group then highlighted the benzofuran derivative TAM16 (**Figure 1.6**) as a potent anti-TB lead compound (MIC values  $\leq 0.42 \mu\text{M}$ ). This compound is also endowed with highly potent *in vitro* bactericidal activities against the tested DS and DR clinical isolates of *M. tb* (76). It also exhibited potent *in vivo* efficacy, equal to that of the front-line anti-TB drug INH, in multiple mouse TB infection models. TAM16 demonstrated excellent drug-like properties and favourable safety and PK profiles (76). TAM16 is currently in the lead optimisation stage (49).

Ensuing structure-activity relationship (SAR) optimisation efforts aided by the Pks13 crystal structure led to the identification of several coumestan analogues as potent anti-TB agents *in vitro* and *in vivo* in serum inhibition titration assay (SIT) (77, 78). Pks13 was shown to be the target of these coumestan analogues (77). Coumestan derivative **1** (**Figure 1.6**) was the highlight of these published reports, showing potent activities against several DS- and DR-TB strains (MIC/MBC  $< 0.008 \mu\text{g/mL}$ ) (77). This excellent *in vitro* activity was translated into potent *in vivo* activity in the mouse SIT assay, displaying higher activity than INH and TAM16 (77). In 2021, further *in vitro* and *in vivo* studies were performed on the coumestan analogue **1** (79). It showed potent sterilising capacity at a concentration of  $0.06 \mu\text{g/mL}$  (15 times the MIC) in culture. In addition, it demonstrated favourable PK parameters when orally administered in mice



(10 mg/kg) with a 19.4% relative bioavailability. Importantly, in mouse infection models, coumestan **1** displayed a dose-dependent activity as a monotherapy. It also showed a synergistic effect when combined with RIF (25 mg/kg of **1** and 10 mg/kg of RIF) in reducing the colony forming unit (CFU) in the mouse lungs after 8 weeks of treatment (79). Taken together, both the benzofuran derivative TAM16 and the coumestan analogue **1** represent promising preclinical anti-TB drug candidates that may undergo further developments in the future.

#### 1.5.2.6. MmpL3

After the FadD32 and Pks13 crosstalk takes place which eventually results in the formation of TMM, these MAs precursors then get flipped from cytoplasm to periplasm via the inner membrane protein MmpL3 (67, 80) (**Figure 1.6**). The mycolyl portion then get anchored to arabinogalactan, the major cell wall polysaccharide, which is further linked to peptidoglycan. It also gets attached to other TMM molecules, glucose, and glycerol (80, 81). This anchoring process leads to the formation of the mycolyl-arabinogalactan-peptidoglycan (mAGP) complex, and the outer membrane glycolipids trehalose dimycolate (TDM), glucose monomycolate (GMM), and glycerol monomycolate (GroMM) (80, 81) (**Figure 1.6**). The fundamental role of MmpL3 in shuttling the MAs across the cytoplasmic membrane and accordingly forging the formidable permeability barrier of *M. tb* was verified in different reports (82-86). In this respect, MmpL3 was found to be essential for the replication and viability of *M. tb* (84). Indeed, downregulation of the *mmpL3* gene in *M. tb* was associated with an abrogation in mycobacterial division and rapid cell death (82, 84). Not only did silencing *mmpL3* have a bactericidal effect *in vitro*, but it also reduced the bacterial load in both acute and chronic mouse lung infection models (84). All of which established the MmpL3 transporter as a well-validated target in *M. tb*.

Several small molecules with diverse chemical entities, including SQ109 (87), indole-2-carboxamides (I2Cs) (88-90), AU1235 (83), BM212 (35), and THPP1 (91), have been identified as potent anti-TB agents and MmpL3 was shown to be their target. In fact, the results of one study favoured a direct mechanism of inhibition of MmpL3 by the preceding five classes of compounds (92). In the same report, SQ109, BM212, and AU1235 were additionally found to dissipate the proton motive force (PMF) from which MmpL3 derive its energy (indirect mechanism). In 2019, the crystal structure of

MmpL3 came to light, elucidating the binding modes of SQ109, I2Cs, and AU1235 within the MmpL3 binding pocket (93). Upon binding, these derivatives occupied three subsites in the proton transportation channel, disrupting the key Asp-Tyr pairs implicated in proton relay and blocking the PMF for substrate translocation (93). In general, compounds that are targeting MmpL3 are quite lipophilic which can undermine the water solubility and bioavailability of this class of inhibitors.

Compound SQ109 (**Figure 1.6**) is a 1,2-ethylenediamine that was developed from high-throughput screening of EMB analogues, aimed at identifying an EMB-based drug candidate with a decreased toxicity and an improved anti-TB activity (94). SQ109 is the most advanced MmpL3 inhibitor in the clinical trials (Phase II) (49). Of note, although SQ109 emerged from a combinatorial library based on EMB, both compounds have different structures and SQ109 was found to have an entirely new mode of action which is different from EMB (94). Indeed, a retrospective evaluation of SQ109-resistant mutants divulged a disruption in the assembly of MAs onto the *M. tb* cell wall which was ascribed to inhibiting the MmpL3 transporter (87). SQ109 displayed excellent activity against several DS and DR *M. tb* strains *in vitro* (MIC  $\leq$  0.78  $\mu$ g/mL). It was also efficacious *in vivo* in mouse TB infection models at a dose of 10 mg/kg, which is way below its MTD in mice (600 mg/kg) (94). SQ109 displayed bactericidal activity with an MBC value of 0.64  $\mu$ g/mL. SQ109 killed *M. tb* inside macrophages with activity superior to EMB and equivalent to INH (94). It also reduced the intracellular *M. tb* load by 99% at its MIC and showed synergistic effects when combined with other anti-TB drugs. In preclinical safety studies in dogs, rats, and nonhuman primates, the no observed adverse events level (NOAEL) of SQ109 was 30 – 40 mg/kg/day, depending on the species. SQ109 was safe and well tolerated in Phase I and the preliminary Phase II clinical studies (94). In a Phase II study, SQ109 showed promising efficacy and tolerability results when added to the standard treatment regimen for patients with pulmonary MDR-TB (49).

The whole-cell phenotypic screening technique has also led to the discovery of more classes of MmpL3 inhibitors. In particular, two I2C analogues NITD-304 and NITD-349 (**Figure 1.6**) were previously highlighted as potent anti-TB preclinical candidates for treating MDR-TB (89). Li *et al* employed a combination of *in vitro* and whole-cell-based approaches and revealed that both NITD-304 and NITD-349 inhibit the MmpL3 via a direct mechanism (92). Both lead candidates displayed potent activities against DS

and DR *M. tb* clinical isolates ( $MIC_{99} \leq 0.08 \mu M$ ) (89). They exhibited bactericidal activity against *in vitro* replicating *M. tb* and intramacrophage *M. tb*, in which NITD-304 displayed a bactericidal activity profile similar to isoniazid (INH), rapidly killing *M. tb* at concentrations greater than  $0.2 \mu M$ . Both compounds also showed favourable oral PK properties in dogs and rodents (89). The two advanced lead analogues were also efficacious in treating both acute and chronic *M. tb* infections in murine efficacy models [MED = 37.5 (NITD-304) and 25 (NITD-349) mg/kg]. The *in vivo* activity of both compounds (100 mg/kg each) was comparable to RIF (10 mg/kg) and better than EMB (100 mg/kg). In these mouse infection models, one month of daily dosing (100 mg/kg) of NITD-304 or NITD-349 was well tolerated in all animals (89). Furthermore, *in vitro* and *in vivo* safety assessment of both candidates including exploratory two-week rat toxicology studies revealed their promising safety margin. Indeed, both compounds showed no cytotoxicity towards mammalian cells ( $CC_{50} > 20 \mu M$ ) with a selectivity index  $> 1000$ . They also showed no inhibition/toxicity in nearly 40 biochemical assays including a panel of human G protein-coupled receptors, proteases, phosphodiesterases and ion channels ( $IC_{50} > 30 \mu M$ ) (89). Unlike many anti-TB drugs, for instance, moxifloxacin and BDQ, both NITD-304 and NITD-349 were devoid of the cardiotoxic liability as neither of them inhibited the hERG channel ( $IC_{50} > 30 \mu M$ ). Additionally, both candidates neither inhibited nor stimulated the CYP enzymes at  $10 \mu M$  concentration, except for the CYP2C9 isoform which was inhibited by NITD-349 at  $IC_{50}$  value of  $2.67 \mu M$ . They also did not induce hPXR activation at  $10 \mu M$  concentration. Collectively, these findings suggest the low potential for drug-drug interactions correlated with these two I2C analogues (89). Both compounds are currently in the lead optimisation phase (49).

Three hit compounds, AU1235, BM212, and THPP1 (**Figure 1.6**), were also shown to have potent bactericidal activities against *M. tb* via targeting MmpL3 (83, 91, 95). The adamantyl urea derivative AU1235 demonstrated potent activities against DS and DR *M. tb* strains ( $MIC < 0.12 \mu g/mL$ ), while having negligible cytotoxicity against mammalian Vero cells ( $IC_{50} = 219 \mu g/mL$ ) (83, 96). The diarylpyrrole derivative BM212 (**Figure 1.6**) exhibited strong inhibitory activities against several *M. tb* strains, including MDR-TB ( $MIC = 0.7 - 1.5 \mu g/mL$ ). It also displayed bactericidal activity against intracellular *M. tb* ( $MIC = 0.5 \mu g/mL$ ) with no macrophage loss detected (95). Finally, the tetrahydropyrazolo[1,5-*a*]pyrimidine-3-carboxamide compound (THPP1) showed

potent anti-TB activities against a panel of DS and mono-resistant *M. tb* strains (MIC = 0.16 – 0.6  $\mu$ M) in addition to MDR and XDR *M. tb* strains (MIC = 0.16 – 5  $\mu$ M) (91). THPP1 also demonstrated a potent intracellular anti-TB activity with MIC value of 0.16  $\mu$ M in infected murine macrophages. THPP1 also exhibited minimal cytotoxicity against human HepG2 cells (IC<sub>50</sub> > 25  $\mu$ M) (91).

## 1.6. Summary and Concluding Remarks

Despite the availability of potentially curative antibiotics, TB continues to cause morbidity and mortality at alarming rates worldwide, especially in developing countries. The TB control efforts are generally hampered by the HIV co-infection, poor patient compliance, and suboptimal treatment approaches in different parts of the world. Several initiatives, such as Stop TB Partnership, were launched globally, with the goal of controlling the TB pandemic. In 2014, the WHO adopted the End TB Strategy (2016 – 2035), which is aimed at 90% reduction in TB incidents and 95% reduction in TB deaths by 2035. However, judging by the slow decrease in TB incidence and fatalities in the past two decades in addition to the unfolding crisis of the COVID-19 pandemic, a significant breakthrough is required promptly to accomplish the WHO End TB Strategy objectives.

The tubercle bacilli are typically trammelled by granulomas in immunocompetent individuals, wherein a lifelong standoff between the bacteria and the host's immune system takes place (latent TB infection). This covert (asymptomatic) TB infection can recrudesce when the host immunity is impaired which results in high bacterial burden and the progression of the disease, culminating in developing clinical manifestations and TB transmission. The relentlessness of the TB pandemic evokes some important questions regarding the ability of *M. tb* to establish infection in the host. What are the mechanisms adopted by the *M. tb* to evade immune recognition and elimination? What prompts the balance between the host's immune response and the *M. tb*-mediated immune subversion to shift in favour of the pathogen, leading to bacterial survival? What is the role of epigenetic protein phosphorylation and dephosphorylation signalling machinery in the *M. tb* pathogenesis and virulence?

Regardless of the factors governing the establishment and progression of the TB disease, treating DS *M. tb* infections is usually attainable by the first-line anti-TB drug regimen, whilst managing DR-TB infections is more challenging and less auspicious.

To bypass drug resistance, novel drug targets in *M. tb* have been reported and validated, deflecting from the traditional drug targets of the currently used TB antibiotics. Since the whole genome sequencing of *M. tb* ( $\approx 4000$  genes) was revealed, a multitude of small molecules with potent activities against both DS and DR *M. tb* strains were discovered and their targets were identified and validated. Despite the extensive efforts undertaken to date to introduce more efficacious anti-TB drugs to the market, only two medications, working through new mechanisms, were approved in 2013/2014 in more than 5 decades and are correlated with serious side effects. To this end, feeding the TB drug development pipeline with new highly active drug-like anti-TB molecules may help expedite the discovery of revolutionary TB medications.

## **1.7. Aims of The Project**

### **1.7.1. Investigating Kinase Targets Implicated in The Biosynthesis of MAs in *M. tb* (Chapter 2)**

The adaptation and survival strategies adopted by *M. tb*, which account for its persistence in a non-replicating state for decades, are linked to its unusual cell envelope (97). Nevertheless, little is known regarding the signalling mechanisms, whereby *M. tb* modulates the production of cell wall components to adapt to environmental changes. Phosphorylation and dephosphorylation have emerged as critical epigenetic mechanisms that regulate signal transduction in *M. tb* (97). Indeed, several eukaryotic like mycobacterial serine/threonine (Ser/Thr) protein kinases (STPKs) were found to be connected to the cell wall biosynthesis and cell shape/division of *M. tb* (97). However, there are insufficient literature reports covering the significance of *M. tb* kinases and phosphatases in drug discovery.

Accordingly, in the review article that we published in 2019, the following aspects were comprehensively addressed: 1) the biosynthesis and incorporation of MAs on the *M. tb* cell wall and the enzymes/transporters involved therein; 2) the role of *M. tb* kinases and phosphatases in regulating the activity of several protein targets implicated in MAs biosynthetic machinery; 3) small molecules inhibitors targeting protein kinases and phosphatases in *M. tb*. This review article is included in Chapter 2 herein.

## **1.7.2. Design, Synthesis, Purification, and Chemical Characterisation of Various Series of Analogues as Potential Anti-TB Agents**

### **1.7.2.1. MmpL3 Inhibitors-Derived New Analogues (Chapters 3 and 4)**

The primary focus of this thesis is to develop novel anti-TB agents using the two indole-2-carboxamides NITD-304 and NITD-340 as lead compounds. Towards this objective, two research articles were published so far entailing potential MmpL3 inhibitors and their SAR. Several novel compounds showed potent activities against DS, MDR, and XDR clinical isolates. The most active compounds displayed negligible cytotoxicities against mammalian cells. Docking studies were performed using the MmpL3 crystal structure to shed light on the potential mechanism of action of the most potent compounds. The two research articles are integrated into Chapters 3 and 4 in this thesis.

**Chapter 3** entails exploring the anti-TB activities of the quinolone-2-carboxamide, quinolone-3-carboxamide, naphthamide and 4-arylthiazole-2-carboxamide frameworks as bioisosteric replacements of the I2C counterpart. Two naphthamide derivatives were the most active compounds in our study, displaying anti-TB activities against DS *M. tb* H37Rv strain comparable to EMB. They also retained their high potency against a panel of MDR/XDR strains and showed no cytotoxicity against mammalian Vero cells.

**Chapter 4** main objective is to enhance the physicochemical properties of the I2Cs by integrating water solubilising groups into their framework. Therefore, several novel adamantanol-based I2Cs and their adamantane counterparts were synthesised and evaluated for their anti-TB activity and cytotoxicity. The kinetic water solubilities of selected 3-hydroxyadamantane and bare adamantane derivatives were determined using analytical high-performance liquid chromatography (HPLC).

### **1.7.2.2. INH, PZA, and Ciprofloxacin (CPF) Derivatives (Chapter 5)**

In order to discover novel anti-TB compounds with optimised activity against DS and DR *M. tb* strains, some of the old anti-TB drugs in the market were revisited, namely INH, PZA, and CPF. Several chemical modifications were employed in an attempt to improve the physicochemical properties of the preceding drugs and generate new hybrids linking two different anti-TB entities with distinct biological activities. These

changes were presumed to lead to better anti-TB activity and circumvent the resistance mechanisms of the parent compounds. However, none of these changes resulted in improved anti-TB activities against DS *M. tb* H37Rv strain compared to the parent counterpart. Furthermore, the INH-POA hybrid, which showed the highest anti-TB activity against DS-TB in this set of derivatives, was inactive against our tested DR *M. tb* isolates, similar to INH. We recently published these findings in a research letter which is incorporated in Chapter 5 herein.

### **1.7.3. Repurposing The Indole-2-Carboxamide Framework and Its Bioisosteres as Antitumour Agents against Paediatric Brain Gliomas (Chapter 6 and 7)**

Apart from the outstanding activity of the I2C framework against TB, the antitumour potential of several I2C analogues is well documented in the literature. Since numerous overlapping structural features were discerned between the I2C-containing anti-TB and anti-tumour agents, new I2C analogues were designed, synthesised, and evaluated against DS-TB and paediatric glioblastoma (GBM) KNS42 cell line. The cytotoxic activities of the most active anti-TB and antitumour compounds were evaluated against normal Vero cells or healthy human fibroblast HFF1 cells. The most potent compounds against the viability and proliferation of KNS42 cells were further tested against a panel of grade IV non-GBM paediatric tumour cells, namely teratoid/rhabdoid (BT12 and BT16 cell lines) in addition to medulloblastoma (DAOY cell line). Towards this, two research articles were recently published and are included in Chapter 6 and 7 in this thesis.

**Chapter 6** comprises the strategy of adding more spacers to the amide linker between the indole ring and the amide nitrogen-linked group. In this respect, several novel I2Cs tethered to a rimantadine group, benzylamine, or 1-carbonylphenyl were prepared. In addition, two dicarboxamide derivatives with a phenyl or piperazine group introduced as the middle linker between the indole ring and the adamantane motif were synthesised. All derivatives were evaluated for their anti-TB activities against DS H37Rv *M. tb* strain and KNS42 GBM cell line to verify the polypharmacological profile of the I2C framework. Indeed, several compounds showed potent anti-TB and antitumour activities. A differential gene expression analysis was carried out on the KNS42 cells treated with the top potent antitumour compound in comparison to the corresponding untreated cells.

**Chapter 7** entails the design, synthesis, and SAR of more I2C analogues and other indole bioisosteres as antitumour agents. In addition, selected quinolone-2-carboxamides and their 3-carboxamide counterparts, which were evaluated for their anti-TB activities in our 2020 paper (Chapter 3), were also tested for their antitumour activities against paediatric GBM KNS42 cells. Interestingly, we found that KNS42 cell line overexpresses cannabinoid receptor 1 gene (CNR1). Additionally, some of the evaluated I2Cs and indole bioisostere analogues were previously shown to activate cannabinoid receptor 1 and/or 2 (CB<sub>1</sub>R and CB<sub>2</sub>R). More importantly, the growth/proliferation of tumour cells overexpressing CB<sub>1</sub>R and/or CB<sub>2</sub>R was previously inhibited upon treatment with cannabinoid receptors modulators. Taken together, the functional activities of our top potent compounds were evaluated to preliminary assess the implication of these receptors in the observed antitumour activities. The most active compounds were then tested against BT12, BT16, and DAOY cell lines and their cytotoxicities were assessed against human fibroblasts. Some compounds showed pan-tumour cell inhibition and preliminary safety towards non-tumour cells. When their functional activities were determined at CB<sub>1</sub>R and CB<sub>2</sub>R, mixed results were obtained, which suggested the non-involvement of these receptors in our observed antitumour activities. Therefore, a gene transcriptional analysis was conducted on KNS42 cells untreated and treated with one of the most active compounds.



## References

1. Kaufmann SH, Schaible UE. 100th anniversary of Robert Koch's Nobel Prize for the discovery of the tubercle bacillus. *Trends Microbiol.* 2005;13(10):469-75.
2. World Health Organisation. Global tuberculosis report 2020. Geneva: World Health Organization. 2020; Licence: CC BY-NC-SA 3.0 IGO, Available from: <https://apps.who.int/iris/bitstream/handle/10665/336069/9789240013131-eng.pdf> (Accessed on 10 September 2021).
3. Flynn JL, Chan J. Tuberculosis: latency and reactivation. *Infect Immun.* 2001;69(7):4195-201.
4. Philips JA, Ernst JD. Tuberculosis pathogenesis and immunity. *Annu Rev Pathol.* 2012;7:353-84.
5. Leung AN. Pulmonary tuberculosis: the essentials. *Radiology.* 1999;210(2):307-22.
6. Luies L, du Preez I. The Echo of Pulmonary Tuberculosis: Mechanisms of Clinical Symptoms and Other Disease-Induced Systemic Complications. *Clin Microbiol Rev.* 2020;33(4).
7. Schluger NW. The pathogenesis of tuberculosis: the first one hundred (and twenty-three) years. *Am J Respir Cell Mol Biol.* 2005;32(4):251-6.
8. Russell DG, Cardona PJ, Kim MJ, Allain S, Altare F. Foamy macrophages and the progression of the human tuberculosis granuloma. *Nat Immunol.* 2009;10(9):943-8.
9. Huszar S, Chibale K, Singh V. The quest for the holy grail: new antitubercular chemical entities, targets and strategies. *Drug Discov Today.* 2020;25(4):772-80.
10. Chai Q, Zhang Y, Liu CH. Mycobacterium tuberculosis: An Adaptable Pathogen Associated With Multiple Human Diseases. *Front Cell Infect Microbiol.* 2018;8:158.
11. Marrakchi H, Laneelle MA, Daffe M. Mycolic acids: structures, biosynthesis, and beyond. *Chem Biol.* 2014;21(1):67-85.
12. Peyron P, Vaubourgeix J, Poquet Y, Levillain F, Botanch C, Bardou F, et al. Foamy macrophages from tuberculous patients' granulomas constitute a nutrient-rich reservoir for *M. tuberculosis* persistence. *PLoS Pathog.* 2008;4(11):e1000204.
13. Grosset J. Mycobacterium tuberculosis in the extracellular compartment: an underestimated adversary. *Antimicrob Agents Chemother.* 2003;47(3):833-6.

14. Gengenbacher M, Kaufmann SH. Mycobacterium tuberculosis: success through dormancy. *FEMS Microbiol Rev.* 2012;36(3):514-32.
15. Zumla A, Nahid P, Cole ST. Advances in the development of new tuberculosis drugs and treatment regimens. *Nat Rev Drug Discov.* 2013;12(5):388-404.
16. Vidossich P, Loewen PC, Carpena X, Fiorin G, Fita I, Rovira C. Binding of the antitubercular pro-drug isoniazid in the heme access channel of catalase-peroxidase (KatG). A combined structural and metadynamics investigation. *J Phys Chem B.* 2014;118(11):2924-31.
17. Louw GE, Warren RM, Gey van Pittius NC, Leon R, Jimenez A, Hernandez-Pando R, et al. Rifampicin reduces susceptibility to ofloxacin in rifampicin-resistant Mycobacterium tuberculosis through efflux. *Am J Respir Crit Care Med.* 2011;184(2):269-76.
18. Zhang Y, Mitchison D. The curious characteristics of pyrazinamide: a review. *Int J Tuberc Lung Dis.* 2003;7(1):6-21.
19. Goude R, Amin AG, Chatterjee D, Parish T. The arabinosyltransferase EmbC is inhibited by ethambutol in Mycobacterium tuberculosis. *Antimicrob Agents Chemother.* 2009;53(10):4138-46.
20. Chiang CY, Centis R, Migliori GB. Drug-resistant tuberculosis: past, present, future. *Respirology.* 2010;15(3):413-32.
21. Sotgiu G, Centis R, D'Ambrosio L, Migliori GB. Tuberculosis treatment and drug regimens. *Cold Spring Harb Perspect Med.* 2015;5(5):a017822.
22. Yee D, Valiquette C, Pelletier M, Parisien I, Rocher I, Menzies D. Incidence of serious side effects from first-line antituberculosis drugs among patients treated for active tuberculosis. *Am J Respir Crit Care Med.* 2003;167(11):1472-7.
23. World Health Organisation. WHO consolidated guidelines on drug-resistant tuberculosis treatment. Geneva: World Health Organization. 2019; Licence: CC BY-NC-SA 3.0 IGO, Available from: <https://apps.who.int/iris/bitstream/handle/10665/311389/9789241550529-eng.pdf> (Accessed on 10 September 2021).
24. Migliori GB, Tiberi S, Zumla A, Petersen E, Chakaya JM, Wejse C, et al. MDR/XDR-TB management of patients and contacts: Challenges facing the new decade. The 2020 clinical update by the Global Tuberculosis Network. *Int J Infect Dis.* 2020;92S:S15-S25.

25. World Health Organisation. WHO operational handbook on tuberculosis. Module 4: treatment - drug-resistant tuberculosis treatment. Geneva: World Health Organization; 2020. Licence: CC BY-NC-SA 3.0 IGO., Available from: <https://www.who.int/publications/i/item/9789240006997> (Accessed on 10 September 2021).
26. Zumla A, Chakaya J, Centis R, D'Ambrosio L, Mwaba P, Bates M, et al. Tuberculosis treatment and management--an update on treatment regimens, trials, new drugs, and adjunct therapies. *Lancet Respir Med*. 2015;3(3):220-34.
27. Sensi P. History of the development of rifampin. *Rev Infect Dis*. 1983;5 Suppl 3:S402-6.
28. Nahid P, Mase SR, Migliori GB, Sotgiu G, Bothamley GH, Brozek JL, et al. Treatment of Drug-Resistant Tuberculosis. An Official ATS/CDC/ERS/IDSA Clinical Practice Guideline. *Am J Respir Crit Care Med*. 2019;200(10):e93-e142.
29. Koul A, Arnoult E, Lounis N, Guillemont J, Andries K. The challenge of new drug discovery for tuberculosis. *Nature*. 2011;469(7331):483-90.
30. Ginsberg AM, Spigelman M. Challenges in tuberculosis drug research and development. *Nat Med*. 2007;13(3):290-4.
31. Pawlowski A, Jansson M, Skold M, Rottenberg ME, Kallenius G. Tuberculosis and HIV co-infection. *PLoS Pathog*. 2012;8(2):e1002464.
32. World Health Organisation. COVID-19 Weekly epidemiological update - 29 December 2020. 2020, Available from: <https://www.who.int/publications/m/item/weekly-epidemiological-update---29-december-2020> (Accessed on 10 September 2021).
33. Cole ST, Brosch R, Parkhill J, Garnier T, Churcher C, Harris D, et al. Deciphering the biology of *Mycobacterium tuberculosis* from the complete genome sequence. *Nature*. 1998;393(6685):537-44.
34. Mdluli K, Kaneko T, Upton A. The tuberculosis drug discovery and development pipeline and emerging drug targets. *Cold Spring Harb Perspect Med*. 2015;5(6).
35. La Rosa V, Poce G, Canseco JO, Buroni S, Pasca MR, Biava M, et al. MmpL3 is the cellular target of the antitubercular pyrrole derivative BM212. *Antimicrob Agents Chemother*. 2012;56(1):324-31.
36. Manjunatha UH, Smith PW. Perspective: Challenges and opportunities in TB drug discovery from phenotypic screening. *Bioorg Med Chem*. 2015;23(16):5087-97.

37. Locher CP, Jones SM, Hanzelka BL, Perola E, Shoen CM, Cynamon MH, et al. A novel inhibitor of gyrase B is a potent drug candidate for treatment of tuberculosis and nontuberculosis mycobacterial infections. *Antimicrob Agents Chemother.* 2015;59(3):1455-65.
38. Mdluli K, Ma Z. Mycobacterium tuberculosis DNA gyrase as a target for drug discovery. *Infect Disord Drug Targets.* 2007;7(2):159-68.
39. Bruch EM, Petrella S, Bellinzoni M. Structure-Based Drug Design for Tuberculosis: Challenges Still Ahead. *Appl Sci.* 2020;10(12):4248.
40. Spero Therapeutics Announces Positive Results from SPR720 IND-Enabling Studies and Plans to Initiate a Phase 1 Trial, Available from: <https://investors.sperotherapeutics.com/news-releases/news-release-details/sperotherapeutics-announces-positive-results-spr720-ind> (Accessed on 10 September 2021).
41. Stout JE, Koh WJ, Yew WW. Update on pulmonary disease due to non-tuberculous mycobacteria. *Int J Infect Dis.* 2016;45:123-34.
42. Spero Therapeutics Announces Initiation of SPR720 Phase 1 Clinical Trial, Available from: <https://www.globenewswire.com/en/news-release/2019/01/29/1706794/0/en/Spero-Therapeutics-Announces-Initiation-of-SPR720-Phase-1-Clinical-Trial.html> (Accessed on 10 September 2021).
43. Spero Therapeutics Receives QIDP Designation from the U.S. FDA for the Development of SPR720, Available from: <https://investors.sperotherapeutics.com/news-releases/news-release-details/sperotherapeutics-receives-qidp-designation-us-fda-0> (Accessed on 10 September 2021).
44. Spero Therapeutics Provides Update on SPR720 Phase 2a Clinical Trial, Available from: <https://investors.sperotherapeutics.com/news-releases/news-release-details/sperotherapeutics-provides-update-spr720-phase-2a-clinical> (Accessed on 10 September 2021).
45. Koul A, Dendouga N, Vergauwen K, Molenberghs B, Vranckx L, Willebrords R, et al. Diarylquinolines target subunit c of mycobacterial ATP synthase. *Nat Chem Biol.* 2007;3(6):323-4.
46. Lu P, Lill H, Bald D. ATP synthase in mycobacteria: special features and implications for a function as drug target. *Biochim Biophys Acta.* 2014;1837(7):1208-18.

47. Sutherland HS, Tong AST, Choi PJ, Blaser A, Conole D, Franzblau SG, et al. 3,5-Dialkoxypyridine analogues of bedaquiline are potent antituberculosis agents with minimal inhibition of the hERG channel. *Bioorg Med Chem*. 2019;27(7):1292-307.
48. Chahine EB, Karaoui LR, Mansour H. Bedaquiline: a novel diarylquinoline for multidrug-resistant tuberculosis. *Ann Pharmacother*. 2014;48(1):107-15.
49. 2021 Global New TB Drug Pipeline, Available from: <https://www.newtbdugs.org/pipeline/clinical> and <https://www.newtbdugs.org/pipeline/discovery> (Accessed on 10 September 2021).
50. Pethe K, Bifani P, Jang J, Kang S, Park S, Ahn S, et al. Discovery of Q203, a potent clinical candidate for the treatment of tuberculosis. *Nat Med*. 2013;19(9):1157-60.
51. Lu X, Williams Z, Hards K, Tang J, Cheung CY, Aung HL, et al. Pyrazolo[1,5-a]pyridine Inhibitor of the Respiratory Cytochrome bcc Complex for the Treatment of Drug-Resistant Tuberculosis. *ACS Infect Dis*. 2019;5(2):239-49.
52. Chikhale RV, Barmade MA, Murumkar PR, Yadav MR. Overview of the Development of DprE1 Inhibitors for Combating the Menace of Tuberculosis. *J Med Chem*. 2018;61(19):8563-93.
53. Makarov V, Manina G, Mikusova K, Mollmann U, Ryabova O, Saint-Joanis B, et al. Benzothiazinones kill *Mycobacterium tuberculosis* by blocking arabinan synthesis. *Science*. 2009;324(5928):801-4.
54. Brecik M, Centarova I, Mukherjee R, Kolly GS, Huszar S, Bobovska A, et al. DprE1 Is a Vulnerable Tuberculosis Drug Target Due to Its Cell Wall Localization. *ACS Chem Biol*. 2015;10(7):1631-6.
55. Kolly GS, Boldrin F, Sala C, Dhar N, Hartkoorn RC, Ventura M, et al. Assessing the essentiality of the decaprenyl-phospho-d-arabinofuranose pathway in *Mycobacterium tuberculosis* using conditional mutants. *Mol Microbiol*. 2014;92(1):194-211.
56. Trefzer C, Skovierova H, Buroni S, Bobovska A, Nenci S, Molteni E, et al. Benzothiazinones are suicide inhibitors of mycobacterial decaprenylphosphoryl-beta-D-ribofuranose 2'-oxidase DprE1. *J Am Chem Soc*. 2012;134(2):912-5.
57. Makarov V, Lechartier B, Zhang M, Neres J, van der Sar AM, Raadsen SA, et al. Towards a new combination therapy for tuberculosis with next generation benzothiazinones. *EMBO Mol Med*. 2014;6(3):372-83.

58. Makarov V, Neres J, Hartkoorn RC, Ryabova OB, Kazakova E, Sarkan M, et al. The 8-Pyrrole-Benzothiazinones Are Noncovalent Inhibitors of DprE1 from *Mycobacterium tuberculosis*. *Antimicrob Agents Chemother*. 2015;59(8):4446-52.
59. Hariguchi N, Chen X, Hayashi Y, Kawano Y, Fujiwara M, Matsuba M, et al. OPC-167832, a Novel Carbostyryl Derivative with Potent Antituberculosis Activity as a DprE1 Inhibitor. *Antimicrob Agents Chemother*. 2020;64(6).
60. Shirude PS, Shandil R, Sadler C, Naik M, Hosagrahara V, Hameed S, et al. Azaindoles: noncovalent DprE1 inhibitors from scaffold morphing efforts, kill *Mycobacterium tuberculosis* and are efficacious in vivo. *J Med Chem*. 2013;56(23):9701-8.
61. Shirude PS, Shandil RK, Manjunatha MR, Sadler C, Panda M, Panduga V, et al. Lead optimization of 1,4-azaindoles as antimycobacterial agents. *J Med Chem*. 2014;57(13):5728-37.
62. Chatterji M, Shandil R, Manjunatha MR, Solapure S, Ramachandran V, Kumar N, et al. 1,4-azaindole, a potential drug candidate for treatment of tuberculosis. *Antimicrob Agents Chemother*. 2014;58(9):5325-31.
63. Early Bactericidal Activity of TBA-7371 in Pulmonary Tuberculosis, Available from: <https://clinicaltrials.gov/ct2/show/NCT04176250> (Accessed on 10 September 2021).
64. Gavalda S, Bardou F, Laval F, Bon C, Malaga W, Chalut C, et al. The polyketide synthase Pks13 catalyzes a novel mechanism of lipid transfer in mycobacteria. *Chem Biol*. 2014;21(12):1660-9.
65. Li W, Gu S, Fleming J, Bi L. Crystal structure of FadD32, an enzyme essential for mycolic acid biosynthesis in mycobacteria. *Sci Rep*. 2015;5:15493.
66. Kuhn ML, Alexander E, Minasov G, Page HJ, Warwzrak Z, Shuvalova L, et al. Structure of the Essential *Mtb* FadD32 Enzyme: A Promising Drug Target for Treating Tuberculosis. *ACS Infect Dis*. 2016;2(8):579-91.
67. Gavalda S, Leger M, van der Rest B, Stella A, Bardou F, Montrozier H, et al. The Pks13/FadD32 crosstalk for the biosynthesis of mycolic acids in *Mycobacterium tuberculosis*. *J Biol Chem*. 2009;284(29):19255-64.
68. Bhatt A, Molle V, Besra GS, Jacobs WR, Jr., Kremer L. The *Mycobacterium tuberculosis* FAS-II condensing enzymes: their role in mycolic acid biosynthesis, acid-fastness, pathogenesis and in future drug development. *Mol Microbiol*. 2007;64(6):1442-54.

69. Portevin D, De Sousa-D'Auria C, Houssin C, Grimaldi C, Chami M, Daffe M, et al. A polyketide synthase catalyzes the last condensation step of mycolic acid biosynthesis in mycobacteria and related organisms. *Proc Natl Acad Sci U S A*. 2004;101(1):314-9.
70. Portevin D, de Sousa-D'Auria C, Montrozier H, Houssin C, Stella A, Laneelle MA, et al. The acyl-AMP ligase FadD32 and AccD4-containing acyl-CoA carboxylase are required for the synthesis of mycolic acids and essential for mycobacterial growth: identification of the carboxylation product and determination of the acyl-CoA carboxylase components. *J Biol Chem*. 2005;280(10):8862-74.
71. Gande R, Gibson KJ, Brown AK, Krumbach K, Dover LG, Sahm H, et al. Acyl-CoA carboxylases (accD2 and accD3), together with a unique polyketide synthase (Cg-pks), are key to mycolic acid biosynthesis in Corynebacteriaceae such as *Corynebacterium glutamicum* and *Mycobacterium tuberculosis*. *J Biol Chem*. 2004;279(43):44847-57.
72. Carroll P, Faray-Kele MC, Parish T. Identifying vulnerable pathways in *Mycobacterium tuberculosis* by using a knockdown approach. *Appl Environ Microbiol*. 2011;77(14):5040-3.
73. Kawate T, Iwase N, Shimizu M, Stanley SA, Wellington S, Kazyanskaya E, et al. Synthesis and structure-activity relationships of phenyl-substituted coumarins with anti-tubercular activity that target FadD32. *Bioorg Med Chem Lett*. 2013;23(22):6052-9.
74. Stanley SA, Kawate T, Iwase N, Shimizu M, Clatworthy AE, Kazyanskaya E, et al. Diarylcoumarins inhibit mycolic acid biosynthesis and kill *Mycobacterium tuberculosis* by targeting FadD32. *Proc Natl Acad Sci U S A*. 2013;110(28):11565-70.
75. Ioerger TR, O'Malley T, Liao R, Guinn KM, Hickey MJ, Mohaideen N, et al. Identification of new drug targets and resistance mechanisms in *Mycobacterium tuberculosis*. *PLoS One*. 2013;8(9):e75245.
76. Aggarwal A, Parai MK, Shetty N, Wallis D, Woolhiser L, Hastings C, et al. Development of a Novel Lead that Targets *M. tuberculosis* Polyketide Synthase 13. *Cell*. 2017;170(2):249-59 e25.
77. Zhang W, Lun S, Liu LL, Xiao S, Duan G, Gunosewoyo H, et al. Identification of Novel Coumestan Derivatives as Polyketide Synthase 13 Inhibitors against *Mycobacterium tuberculosis*. Part II. *J Med Chem*. 2019;62(7):3575-89.

78. Zhang W, Lun S, Wang SH, Jiang XW, Yang F, Tang J, et al. Identification of Novel Coumestan Derivatives as Polyketide Synthase 13 Inhibitors against *Mycobacterium tuberculosis*. *J Med Chem*. 2018;61(3):791-803.
79. Lun S, Xiao S, Zhang W, Wang S, Gunosewoyo H, Yu LF, et al. Therapeutic potential of coumestan Pks13 inhibitors for tuberculosis. *Antimicrob Agents Chemother*. 2021.
80. Xu Z, Meshcheryakov VA, Poce G, Chng SS. MmpL3 is the flippase for mycolic acids in mycobacteria. *Proc Natl Acad Sci U S A*. 2017;114(30):7993-8.
81. Tima HG, Al Dulayymi JR, Denis O, Lehebel P, Baols KS, Mohammed MO, et al. Inflammatory Properties and Adjuvant Potential of Synthetic Glycolipids Homologous to Mycolate Esters of the Cell Wall of *Mycobacterium tuberculosis*. *J Innate Immun*. 2017;9(2):162-80.
82. Degiacomi G, Benjak A, Madacki J, Boldrin F, Provvedi R, Palu G, et al. Essentiality of mmpL3 and impact of its silencing on *Mycobacterium tuberculosis* gene expression. *Sci Rep*. 2017;7:43495.
83. Grzegorzewicz AE, Pham H, Gundi VA, Scherman MS, North EJ, Hess T, et al. Inhibition of mycolic acid transport across the *Mycobacterium tuberculosis* plasma membrane. *Nat Chem Biol*. 2012;8(4):334-41.
84. Li W, Obregon-Henao A, Wallach JB, North EJ, Lee RE, Gonzalez-Juarrero M, et al. Therapeutic Potential of the *Mycobacterium tuberculosis* Mycolic Acid Transporter, MmpL3. *Antimicrob Agents Chemother*. 2016;60(9):5198-207.
85. Varela C, Rittmann D, Singh A, Krumbach K, Bhatt K, Eggeling L, et al. MmpL genes are associated with mycolic acid metabolism in mycobacteria and corynebacteria. *Chem Biol*. 2012;19(4):498-506.
86. Su CC, Klenotic PA, Bolla JR, Purdy GE, Robinson CV, Yu EW. MmpL3 is a lipid transporter that binds trehalose monomycolate and phosphatidylethanolamine. *Proc Natl Acad Sci U S A*. 2019;116(23):11241-6.
87. Tahlan K, Wilson R, Kastrinsky DB, Arora K, Nair V, Fischer E, et al. SQ109 targets MmpL3, a membrane transporter of trehalose monomycolate involved in mycolic acid donation to the cell wall core of *Mycobacterium tuberculosis*. *Antimicrob Agents Chemother*. 2012;56(4):1797-809.
88. Lun S, Guo H, Onajole OK, Pieroni M, Gunosewoyo H, Chen G, et al. Indoleamides are active against drug-resistant *Mycobacterium tuberculosis*. *Nat Commun*. 2013;4:2907.



89. Rao SP, Lakshminarayana SB, Kondreddi RR, Herve M, Camacho LR, Bifani P, et al. Indolcarboxamide is a preclinical candidate for treating multidrug-resistant tuberculosis. *Sci Transl Med*. 2013;5(214):214ra168.
90. Stec J, Onajole OK, Lun S, Guo H, Merenbloom B, Vistoli G, et al. Indole-2-carboxamide-based MmpL3 Inhibitors Show Exceptional Antitubercular Activity in an Animal Model of Tuberculosis Infection. *J Med Chem*. 2016;59(13):6232-47.
91. Remuinan MJ, Perez-Herran E, Rullas J, Alemparte C, Martinez-Hoyos M, Dow DJ, et al. Tetrahydropyrazolo[1,5-a]pyrimidine-3-carboxamide and N-benzyl-6',7'-dihydrospiro[piperidine-4,4'-thieno[3,2-c]pyran] analogues with bactericidal efficacy against *Mycobacterium tuberculosis* targeting MmpL3. *PLoS One*. 2013;8(4):e60933.
92. Li W, Stevens CM, Pandya AN, Darzynkiewicz Z, Bhattarai P, Tong W, et al. Direct Inhibition of MmpL3 by Novel Antitubercular Compounds. *ACS Infect Dis*. 2019;5(6):1001-12.
93. Zhang B, Li J, Yang X, Wu L, Zhang J, Yang Y, et al. Crystal Structures of Membrane Transporter MmpL3, an Anti-TB Drug Target. *Cell*. 2019;176(3):636-48 e13.
94. Sacksteder KA, Protopopova M, Barry CE, 3rd, Andries K, Nacy CA. Discovery and development of SQ109: a new antitubercular drug with a novel mechanism of action. *Future Microbiol*. 2012;7(7):823-37.
95. Deidda D, Lampis G, Fioravanti R, Biava M, Porretta GC, Zanetti S, et al. Bactericidal activities of the pyrrole derivative BM212 against multidrug-resistant and intramacrophagic *Mycobacterium tuberculosis* strains. *Antimicrob Agents Chemother*. 1998;42(11):3035-7.
96. Brown JR, North EJ, Hurdle JG, Morisseau C, Scarborough JS, Sun D, et al. The structure-activity relationship of urea derivatives as anti-tuberculosis agents. *Bioorg Med Chem*. 2011;19(18):5585-95.
97. Molle V, Kremer L. Division and cell envelope regulation by Ser/Thr phosphorylation: *Mycobacterium* shows the way. *Mol Microbiol*. 2010;75(5):1064-77.

## **Chapter 2**

### **Protein Phosphorylation and Dephosphorylation in *M. tb***

## Background

*Mycobacterium tuberculosis* (*M. tb*) is a remarkably versatile pathogen that possesses a unique ability to counteract the killing mechanisms generated by the host to control the infection. Several protein kinases and phosphatases were found to play a key role in impeding phagosomes maturation in macrophages and accordingly blocking the phagosome-lysosome fusion, allowing the bacteria to survive. During phagocytosis, both *M. tb* and the host's phagocytic cells develop mechanisms to fight each other, resulting in pathogen elimination or survival. In this respect, *M. tb* uses a phosphorylation-based signal transduction mechanism, whereby it senses extracellular signals from the host and initiates the appropriate adaptation responses. Indeed, the ability of *M. tb* to exist in different states in the host (persistent quiescent state or actively replicating mode) is mainly mediated through protein phosphorylation/dephosphorylation signalling. The *M. tb* regulatory and defensive responses coordinate different aspects of the bacilli's physiology, for instance, cell wall components, metabolic activity, virulence, and growth. In the review article published in 2019, we summarised the role of protein phosphorylation/dephosphorylation in modulating the activity of the enzymes involved in the mycolic acids (MAs) biosynthetic machinery in *M. tb*. Additionally, selected inhibitors of various kinases and phosphatases encoded by *M. tb* and their anti-TB activities were discussed therein.

## 2.1. Introduction

Signal transduction is a cellular mechanism that is critical for adaptation of bacterial pathogens to extracellular environmental changes (1). It involves sensing a signal or input via a sensor protein, followed by generating an intracellular response or output via a transducer protein (1). This process is governed by protein kinases and phosphatases that mediate protein phosphorylation and dephosphorylation, respectively (2). In bacteria, the stimulus-response adjusting mechanism is mainly regulated by a two-component system, comprising histidine kinase sensors and their corresponding response regulators (transducers) (2). In this regard, a histidine kinase is stimulated by a particular intracellular or environmental signal which results in autophosphorylating a key histidine residue (3). This phosphorylated histidine then serves as a substrate to the cognate response regulator, wherein an aspartate residue is autophosphorylated. In response to this phosphorylation cascade, the response regulators, which are mainly DNA binding proteins, trigger the expression of certain genes, bringing forth the requisite response (3). In eukaryotes, the backbone of the signal transduction network consists of serine, threonine, and tyrosine (Ser/Thr/Tyr) protein kinases and their coupled phosphatases (2). The histidine/aspartate (His/Asp) phosphorylation (two-component system) was previously thought to be exclusive to prokaryotes, whereas the Ser/Thr/Tyr phosphorylation was considered a eukaryotic trait. However, both systems were detected in numerous prokaryotic and eukaryotic cells (3).

In *M. tb*, the pathogenic success mostly relies on the ability of the mycobacteria to sense and adjust to the complex and dynamic environmental cues of the host (3). Accordingly, the *M. tb* possesses a wide repertoire of an advanced intracellular signal transduction network encompassing: 1) "eukaryotic-like" eleven serine/threonine protein kinases (STPKs); 2) twelve classic prokaryotic signalling machinery (two-component system protein kinases); 3) a single protein tyrosine kinase (PtkA); 4) two protein tyrosine phosphatases (MPtps); 5) one Ser/Thr phosphatase (PstP) (3, 4). The presence of Ser/Thr/Tyr protein kinases and His/Asp two-component system enables the bacterium to fine-tune its response depending on the cellular environment. Indeed, *M. tb* employs the His/Asp phosphorylation system when a rapid short-term response is required, whilst the Ser/Thr/Tyr phosphorylation comes into play when a stable long-

term response is mandatory (3). The *M. tb* exploitation of the two phosphorylation systems allows for its survival and adaption in complex environments.

## **2.2. *M. tb* Protein Kinases and Phosphatases Regulate The Host's Immune Response**

### **2.2.1. The Critical Role of Macrophages in Controlling Infection**

Macrophages constitute the immune system's first-line of defence against microbial invaders in the human's body and are the connecting link between the innate and adaptive immunity (5). Pathogen invasion sets off a series of macrophages' signalling cascades, rendering a hostile environment that undermines the microbial pathogenesis. Indeed, macrophages orchestrate a panoply of innate immune events, such as phagocytosis, phagosome-lysosome fusion, and autophagy, to ensure the pathogen clearance from the body (5). However, in certain cases macrophages become overpowered by the invading microbes, thereby failing to eliminate them. As a result, these pathogenic intruders manage to form a safe niche within the host which constitutes a ticking time bomb that can ultimately transform into a full-blown disease. Phagocytosis is an essential part of the macrophage killing machinery, whereby microorganisms are captured, engulfed, and destroyed (6, 7). The phagocytic process can be divided into four main phases: 1) microbial recognition; 2) phagosome formation and maturation; 3) phagosome-lysosome fusion (phagolysosome formation); 4) pathogen degradation (6).

Phagocytosis is initiated upon recognition of distinctive molecular patterns associated with pathogens (6, 7). This recognition is accomplished via several specialised receptors on the cell surface of phagocytes which in turn trigger signalling cascades that prompt phagocytosis. In this respect, after receptor engagement, the plasma membrane wall off the microorganism via surrounding it, followed by membrane sealing, forming a vacuole where the microbe is internalised (6, 7) (**Figure 2.1**). This phagocytic vesicle (early phagosome), confining the microorganism, subsequently changes its membrane composition and contents in a process called phagosome maturation through fusion with endosomes and ultimately lysosomes. A "kiss and run" dynamic process between early phagosomes and endocytic vesicles take place, wherein sequential events of fusion and fission lead to the formation of late phagosomes and recycling of endosomes (7). Early phagosomes are characterised

by the presence of Rab5 which is a small membrane-based guanosine triphosphatase (GTPase). Rab5 regulate the fusion between early phagosomes and endosomes via recruiting early endosome antigen 1 (EEA1) (7). It also recruits human vacuolar protein sorting 34 (Vps34) which is a class III phosphoinositide 3-kinase (PI3K) that is responsible for the generation of phosphatidylinositol 3-phosphate (PI3P). This lipid prompts phagosome maturation via recruiting other effector proteins, such as Rab7 which is a small GTPase, signifying late phagosomes (7). In fact, Rab5 is considered the key marker of early phagosome, whereas in mature late phagosomes, Rab7 takes over, mediating the fusion between phagosomes and lysosomes and bringing about the dissociation of Rab5 (6-8).

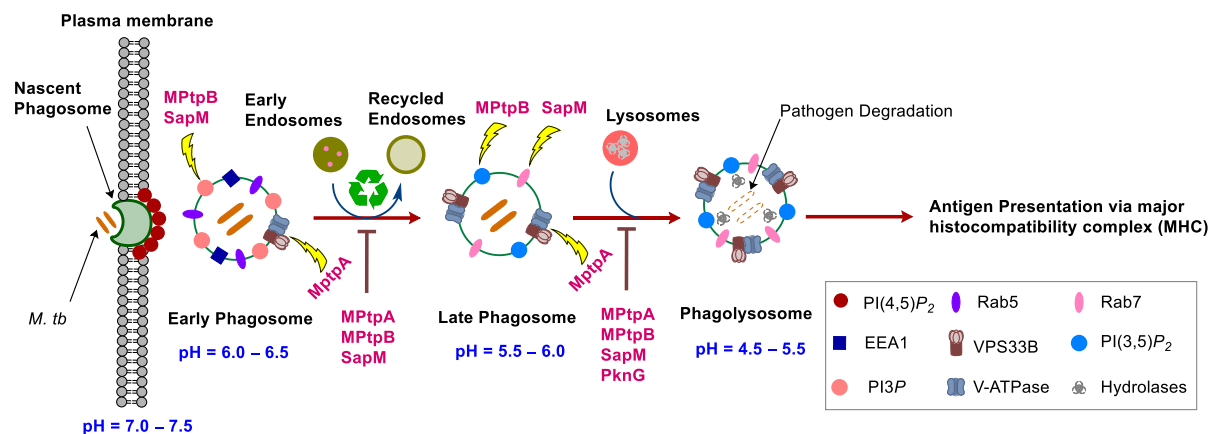


**Figure 2.1. Overview of the phagocytosis of microbial invaders and phagosome maturation, showing *M. tb* secreted kinases and phosphatases interfering with the developmental process of phagosomes.** Generally, once engulfed, the pathogen remains confined within early phagosomes which then undergo a maturation process that involves fusion with endosomes and lysosomes to eventually turn into phagolysosomes, the definitive pathogenicidal vacuoles. Early phagosomes are marked by the presence of EEA1, PI3P, and Rab5, which contribute to the phagosome-endosome fusion. Upon the procession of phagosomal maturation, V-ATPase accumulate on the phagosomal membrane, lowering the pH of phagosomal lumen. The acidic nature of phagolysosomes constitutes a harsh environment for the microbes and is a prerequisite for the activation of several hydrolytic enzymes. Subsequently, the antigen is degraded and presented, alerting the adaptive immune system. *M. tb* secreted virulence factors PknG, MPtpA, MPtpB, and SapM impair the phagolysosome fusion, allowing the bacteria to survive. MPtpA impedes phagosome acidification via hydrolysing VPS33B and inhibiting the trafficking of V-ATPase to late phagosomes. MPtpB hydrolyses PI3P and PI(3,5)P<sub>2</sub> that mediate the transition to late phagosomes and phagolysosome, respectively. Similar to MPtpB, SapM blocks the preceding transition events via hydrolysing PI(4,5)P<sub>2</sub>, PI3P and binding to Rab7.

When the late phagosomes fuse with lysosomes, they evolve into microbicidal vacuoles called phagolysosomes. Importantly, Vacuolar-type adenosine triphosphatase (V-ATPase or V-type H<sup>+</sup>-ATPases) gradually accumulates on the

phagosomal membrane upon maturation (7). Of note, V-ATPases team up with the human vacuolar protein sorting 33B (VPS33B, **Figure 2.1**) which is a crucial component of the phagocytosis process (*vide infra*) (9, 10). V-ATPases use cytosolic ATP as an energy source to translocate protons (H<sup>+</sup>) into the phagosomal lumen leading to progressive acidification of phagosomes, in which the phagosomal pH gradually drop from 6.5 (early phagosomes) to 4.5 (phagolysosomes) (7, 9). Sturgill-Koszycki and collaborators demonstrated that the lack of acidification in mycobacterial containing phagosomes could correlate to the exclusion of V-ATPase from the vesicles (11).

Many sophisticated mechanisms directed towards degrading and eliminating the pathogen take place in phagolysosomes. Indeed, the phagosome-lysosome fusion results in membrane remodelling (alterations in the characteristics of phagosomal membrane) and acquisition of more V-ATPases in addition to lysosomal hydrolases (proteolytic enzymes), such as proteases, cathepsins, lipases, and lysosomes (7, 9). The low luminal pH of the phagolysosomes can be directly toxic to the microorganism in addition to being optimal for the hydrolytic enzymes to carry out the degradation process of the phagocytosed pathogen (6, 7). Furthermore, other microbicidal elements come into the picture, including scavenger molecules and reactive oxygen species. Collectively, the oxidative and degradative milieu of the phagolysosomes render the interior environment inhospitable to the invading microorganisms which ultimately lead to pathogen degradation (7). The protein-based microbial antigen resulting from this process are then presented to T-lymphocytes, whereupon the adaptive immune system gets activated (6). Therefore, the adequate maturation of phagosomes into phagolysosomes (innate immunity) is of paramount importance for the degradation of the pathogen and presenting the degraded antigen to the adaptive immunity which will subsequently result in eliminating the pathogen. In general, this phagocytic process is efficient in removing the invading microorganisms and maintaining homeostasis. However, several microbes, including *M. tb*, have developed tactics to prevent phagosomal ripening and thwart the phagosome-lysosome fusion (7). Accordingly, these microbes survive in the host by escaping the macrophage killing schemes, perpetuating the infection.

### **2.2.2. Role of *M. tb* Kinases and Phosphatases in Warding Off Phagosome Maturation and Preventing Phagosome-Lysosome Fusion**

When the tubercle bacilli are inhaled and enter the lungs, they are faced with various subpopulations of phagocytic cells, such as dendritic cells and alveolar macrophages (6). After the bacilli are phagocytosed, *M. tb* blocks the formation of the final antimicrobial organelles (phagolysosome) via hijacking the killing pathways of the macrophages which precludes the elimination of the bacilli. In fact, *M. tb* turns the table on the host and use the immune cells to shield itself and form a safe harbour where it can survive for the rest of the host's life. Indeed, *M. tb* has developed several strategies to subvert the immune response and prevent phagosome maturation from proceeding in a normal way, thereby inducing chronic infection, and persisting in a latency mode (6). The *M. tb* ability to survive in the macrophages via blocking the phagosome-lysosome fusion was first published by Armstrong and Hart nearly 50 years ago (12). They demonstrated that nearly 70% of phagosomes containing *M. tb* failed to fuse with lysosomes. Since then, numerous virulence factors, produced by *M. tb*, were found to hamper phagosome maturation, and arrest the formation of the ultimate killing organelles (9, 13). In particular, the mycobacterial protein kinase G (PknG) was found to be implicated in the prevention of phagosome-lysosome fusion (14). In addition, three secreted *M. tb* phosphatases, the mycobacterial protein tyrosine phosphatase A and B (MPtpA, MPtpB) in addition to the secreted acid phosphatase M (SapM), coordinately interfere with the stages of development of phagosomes, thereby preventing pathogen destruction (15). Taken together, the *M. tb*-mediated manipulation of host vesicular trafficking processes leads to a malfunction in the process of antigen presentation, causing an ineffective activation of cell populations that contribute to keeping the infection at bay (see Chapter 1, **Figure 1.2**).

### **2.2.2.1. PknG**

Prokaryotes typically use the His/Asp two-component system to regulate their signal transduction, however, when the *M. tb* genome was sequenced, 11 members of the "eukaryotic-like" Ser/Thr kinase family were discovered, namely PknA, PknB, and PknD – PknL (16). Among these STPKs, three kinases PknA, PknB, and PknG were found to be implicated in the mycobacterial intracellular growth and survival. Both PknA and PknB regulate the mycobacterial cell wall synthesis, cell division-associated morphological changes, and cell growth (16). On the other hand, to date, PknG is the only *M. tb* STPK that has been reported to modulate the host's immune system, as a result of which it enhances the *M. tb* survival in macrophages (3). PknG is released by



*M. tb* into the lumen and cytosol of phagosomes and is considered a key player in the prevention of phagosome-lysosome fusion (17). Therefore, PknG expression is believed to be correlated to the pathogenicity of mycobacteria (14, 18). Since phosphorylation is a key mechanism that is required for regulating vesicular trafficking, it is likely that PknG phosphorylates a host protein that is involved in the phagosome-lysosome fusion, thereby inhibiting this crucial step (13). However, after being secreted from *M. tb* in macrophages, the mechanism by which PknG is translocated to the cytosol and its exact action on the host's substrates and vesicular trafficking machinery are yet to be deciphered (13). Several reports have established the importance of PknG for mycobacteria to avoid lysosomal delivery in both macrophages and dendritic cells (14, 18, 19). Inactivation of PknG by chemical inhibition or gene disruption resulted in rapid lysosomal delivery and mycobacterial degradation in infected macrophages (14). Similarly, when dendritic cells were infected with PknG-deleted ( $\Delta pknG$ ) strain, the mycobacterial mutants were largely transferred to lysosomes (19). In fact, in this study, both macrophages and dendritic cells infected with wild-type mycobacteria remained mainly in nonlysosomal phagosomes. Surprisingly, Majlessi *et al* showed that the degree of intracellular trafficking of mycobacteria to lysosomes does not impact the extent to which T cell responses are generated against mycobacterial antigen (19). They conceded that their findings are in marked contrast with other studies that have established that lysosomal delivery, in both dendritic cells and macrophages, is a prerequisite for the processing and presentation of antigens. Indeed, they reported that the wild-type mycobacteria that resisted lysosomal transfer in macrophages and dendritic cells gave rise to efficient antigen presentation and T cell responses identical to the PknG-deficient mycobacterial mutants that were instantly shuttled to lysosomes (19). Interestingly, while PknG was found to be essential for the survival of *M. tb* after the bacterium is phagocytosed inside the macrophage, in *in vitro* cultures both the PknG-deleted mycobacteria and the wild-type counterpart survived equally (20). Other reports unravelled more functional facets of PknG, showing that, in macrophages, PknG promotes latency-like conditions (21, 22). In this respect, PknG mediates persistence via modulating cellular metabolism, resulting in efficient metabolic adaptation under stressful environment, such as hypoxia. In other words, PknG functions as a "stress

regulator" by combating different stressful conditions experienced by mycobacteria. In addition, PknG was shown to play a role in abetting drug tolerance (21).

The critical role of PknG in promoting the survival of mycobacteria inside macrophages has spurred researchers to search for PknG inhibitors. Unlike most of the currently used anti-TB drugs that interfere directly with *M. tb* growth, inhibiting PknG may recondition the macrophages to carry out their innate microbicidal activity, by delivering the bacilli, residing in phagosomes, to lysosomes (13). In other words, inactivating PknG will revert the macrophage to a degradative milieu, in which the bacilli are efficiently destroyed and cleared. As a secreted protein, an additional benefit of targeting PknG is that inhibitors are not required to access the highly impermeable mycobacterial cell membrane (13). Importantly, despite the high homology between the mycobacterial PknG and the eukaryotic Ser/Thr kinases, PknG possesses a unique kinase domain that is distinct from the eukaryotic kinases (23). AX20017 (**1, Figure 2.2**), a highly selective PknG inhibitor ( $IC_{50} = 0.39 \mu\text{M}$ ), was found to bind to this unique domain. Indeed, blocking the activity of PknG by this tetrahydrobenzothiophene led to a rapid mycobacterial transfer to lysosomes, followed by killing the intracellular residing mycobacteria without impacting the viability of the macrophages (14). Similar to the  $\Delta pknG$  mutant in mycobacteria, AX20017 exhibited no inhibitory activity against mycobacterial growth in culture (outside host cells) (14). Although the topology of the kinase domain of PknG is indeed reminiscent of the eukaryotic kinases, AX20017 is harboured in a narrow pocket that is characterised by a unique set of amino acids which are absent in human kinases (23). This finding in turn explains the high specificity of AX20017 towards PknG and demonstrates that targeting this *M. tb*'s secreted virulence factor can be successfully achieved without compromising the host's homologous kinases. NU-6027 (**2, Figure 2.2**) is another PknG inhibitor that was recently identified from a phenotypic screening of a library of pharmacologically active small-molecules, aimed at discovering novel antimycobacterial agents (24). NU-6027 was previously shown to potently inhibit the activity of various kinases, including cyclin-dependent kinase 1 and 2 (CDK1/2) (25). Its antitumour activity was subsequently investigated against numerous human tumour cell lines, in which it displayed potent tumour cell growth inhibition (25). When evaluated against *M. tb* STPKs, NU-6027 inhibited the autophosphorylation activity associated with both PknG and PknD in a dose-dependent manner without affecting

the kinase activity of the other tested STPKs (24). Remarkably, NU-6027 potently induced apoptosis of mycobacteria in THP-1 infected macrophages which was correlated to an upregulation in the expression of proapoptotic genes in the NU-6027-treated macrophages. Of note, no cytotoxicity was observed towards THP-1 cells when treated with NU-6027 at 25  $\mu$ M concentration. In addition to macrophages, NU-6027 inhibited the growth of *M. tb* in mouse tissues (24). Taken together, the preceding findings substantiate the notion that modulating the host/mycobacterial signalling pathways constitutes an attractive approach for the development of novel anti-TB agents.

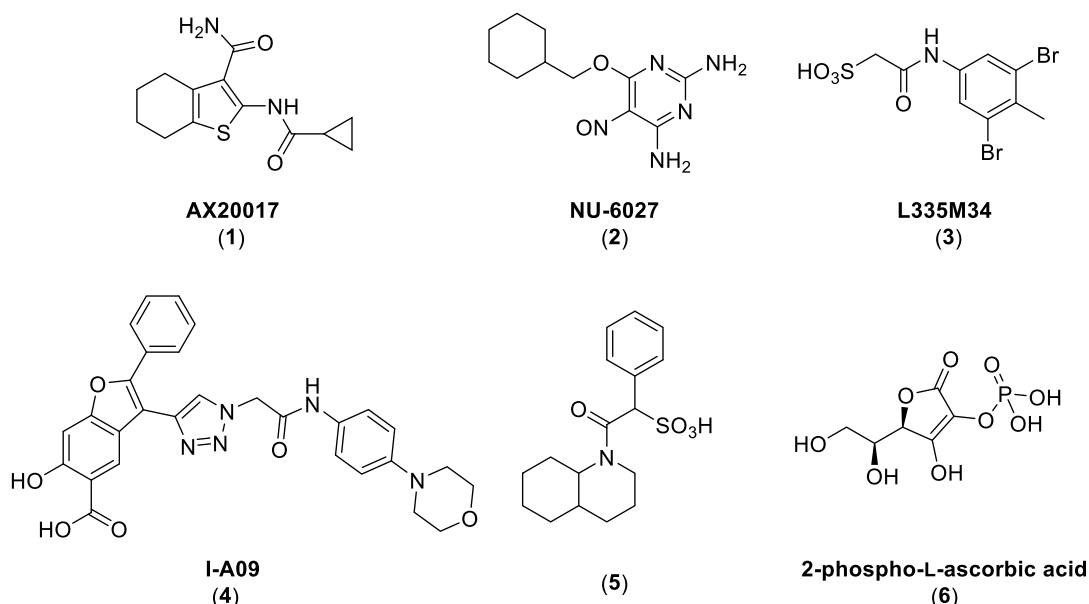


**Figure 2.2. Selected PknG, MPtpA, MPtpB, and SapM inhibitors.** AX20017 and NU-6027 inhibit the kinase activity of PknG. L335M34 is a potent and selective inhibitor of the phosphatase activity of MPtpA. I-A09 and compound **5** potently and specifically inhibit MPtpB. The 2-phospho-L-ascorbic acid (**6**) was recently identified as a competitive inhibitor of SapM.

### 2.2.2.2. *M. tb* Secreted Phosphatases

Among the virulence factors secreted by *M. tb* into the cytoplasm of host macrophages are three phosphatases, denominated MPtpA, MPtpB, and SapM (10). These phosphatases are vital for altering the host's signalling pathways and damping down the immune response, leading to optimal bacillary survival within the host and ultimately pathogenesis. Research efforts from different laboratories led to major leaps in the current understanding of the mechanisms by which these phosphatases

contribute to evading immune detection of *M. tb* (10). Like PknG, these *M. tb*-secreted phosphatases are only required for the *in vivo* growth of the bacteria. Unlike the traditional essential *in vitro* *M. tb* targets which have been the main focus of anti-TB drug discovery to date, these phosphatases are dispensable for the *in vitro* growth of mycobacteria (10). However, targeting these phosphatases could provide a leeway to circumvent the drug delivery issue correlated with the thick hydrophobic cell wall of *M. tb*. In addition, inhibiting their immune-related modulating activity could lead to resetting the macrophage's signalling and restoring the innate host's defence mechanisms.

MPtpA was first identified when the genome of H37Rv *M. tb* strain was sequenced, revealing its homology to eukaryotic protein tyrosine phosphatases (10). *M. tb* secretes MPtpA into the cytosol of host's macrophages, disrupting key elements involved in phagosome maturation (9). In fact, the *mptpA* gene was found to be overexpressed upon the entry of *M. tb* into host macrophages (26). The cognate substrate of MPtpA was found to be VPS33B (**Figure 2.1**), a key player in the process of phagocytosis, functioning as a regulator of vesicle trafficking and membrane fusion (9, 10). Indeed, MPtpA and VPS33B were found to be colocalised in *M. tb*-infected macrophages (27). VPS33B is a protein kinase that is ubiquitously expressed in eukaryotic cells and belongs to class C vesicular sorting protein (VPS-C) complex (9, 10). Dephosphorylating VPS33B by MPtpA inactivates the host protein, resulting in the arrest of phagosome-lysosome fusion (27). In a subsequent study, Wong *et al* identified another key MPtpA target that is partnered with VPS33B, namely V-ATPase (28). Indeed, the lack of phagosome acidification was found to be directly attributed to MPtpA due to its binding to the H subunit of the V-ATPase machinery that drives the low pH of phagosomal lumen. In this regard, they constructed a two-step process model indicating that MPtpA interaction with the V-ATPase machinery is a precondition for the dephosphorylation of VPS33B within the macrophages (28). They proposed that, first, the *M. tb*-secreted MPtpA binds to V-ATPase, resulting in an initial disruption in membrane fusion, while being placed in close proximity to its catalytic substrate VPS33B. Thereafter, MPtpA dephosphorylates VPS33B, leading to inactivating the entire membrane fusion/phagosome maturation machinery and its downstream effectors (28). Consequently, the concerted cancellation of the activity of V-ATPase and VPS33B by MPtpA prevents V-ATPase trafficking to *M. tb* infected phagosomes,

perpetuating the infection in host macrophages. Indeed, genetic deletion of *mptpA* in *M. tb* ( $\Delta mptpA$ ) impaired the bacillary survival within human THP-1 infected macrophages, in which phagosomes harbouring  $\Delta mptpA$  showed enhanced lysosomal fusion, compared to the parental strain (27). In addition, macrophages transfected with  $\Delta mptpA$  knockout strain failed to maintain unacidified phagosomes, therefore the mycobacteria were continually cleared from macrophages (28). Importantly, although a large number of MPtpA inhibitors have been identified, these inhibitors generally tend to suffer from low selectivity due to the fact that MPtpA shares 37% similarity with its human ortholog (10). However, a highly specific MPtpA inhibitor (L335M34, **Figure 2.2**) was reported in 2017 by Dutta *et al*, displaying more than 20-fold selectivity over a panel of tested human protein tyrosine phosphatases (PTPs) (29). Indeed, L335M34 (**3**) showed an IC<sub>50</sub> value of 160 nM against MPtpA, while no significant activity was observed against all examined human PTPs at concentrations less than 3  $\mu$ M. Unsurprisingly, L335M34 was bereft of activity in the standard *M. tb* growth inhibition assays, whilst it markedly suppressed the bacillary load, at low micromolar concentration, in *M. tb*-infected macrophages (IC<sub>50</sub> = 1.38  $\mu$ M) (29).

In contrast to MPtpA, the other secreted *M. tb*'s protein tyrosine phosphatase, namely MPtpB, does not have a human ortholog with only 6% similarity with one human PTP (10). Like MPtpA, MPtpB is released into the cytoplasm of *M. tb*-infected macrophages (30). Beresford *et al* have demonstrated that MPtpB possesses a unique phosphatase activity with triple specificity towards phosphoserine/phosphothreonine, phosphotyrosine, and phosphoinositides (PIs) (31). In particular, manipulating the host phosphoinositide metabolism is a strategy used by pathogenic microbes to promote their colonisation within the infected macrophages (15). Indeed, the alteration of PIs' dynamics by *M. tb* affects the intracellular traffic events correlated with phagosome maturation, enabling the long-term survival of bacteria inside the host. In this regard, PI3P, which is an early phagosomal membrane tag that is critical for the downstream events of the maturation process, was found to be dephosphorylated by MPtpB (**Figure 2.1**) (15). PI3P is an essential membrane trafficking regulatory lipid that is generated by PI3K on the host membranes of early phagosomes and endosomes and represents a docking site for some proteins associated with the maturation of phagosomes into phagolysosomes (13). In addition, MPtpB dephosphorylates PI(3,5)P<sub>2</sub> which is another key lipid component, serving as a marker of late

phagosomes, and is required for the ensuing phagosome-lysosome fusion (15). The importance of MPtpB in the intracellular survival of *M. tb* was experimentally proven by Singh *et al* when they constructed an *mptpB* mutant strain of *M. tb* (32). The authors showed that disrupting the *mptpB* gene impaired the ability of *M. tb* to survive in activated macrophages. However, in resting macrophages, both the mutant strain and the wild-type had similar intracellular growth patterns, suggesting the consequential interplay between the host and *M. tb*. In addition, in guinea pigs, infection with the *mptpB* mutant strain led to a 70-fold inhibition in bacterial burden in the spleens of infected animals, compared to the animals infected with the parental strain (32). Reintroducing the *mptpB* gene to the mutant strain enabled the resulting complemented strain to establish infection and raise the survival rates in guinea pigs to levels on par with the parental strain (32). These findings were further substantiated by other studies, in which selective MPtpB inhibitors were shown to reverse the altered host immune defence reactions and reduce the intracellular growth and survival of *M. tb* in the macrophages (30, 33, 34). For instance, Zhou *et al* identified compound I-A09 (**4**, **Figure 2.2**) as a potent and specific MPtpB inhibitor ( $IC_{50} = 1.26 \mu\text{M}$ ) that was able to overcome the perturbation of host immune surveillance mechanism induced by MPtpB (30). Interestingly, this compound not only recapitulated the phenotype of *mptpB* deleted mutant in active macrophages, but it also inhibited the bacterial load in resting macrophages by 90% relative to the untreated cells, while the viability of macrophages remained unaffected. However, as expected, I-A09 exhibited no activity against *M. tb* in extracellular cultures [minimum inhibitory concentration (MIC) > 100  $\mu\text{M}$ ] (30). A more recent MPtpB inhibitor, compound **5** (**Figure 2.2**), was identified by He *et al* which displayed an outstanding potency and selectivity, with more than 10000-fold preference towards MPtpB ( $K_i = 7.9 \text{ nM}$ ) over a wide panel of 25 phosphatases (34). This compound also showed excellent activity and specificity in averting the MPtpB function in macrophages. Taken together, since both MPtpA and MPtpB are not essential for *M. tb* growth *in vitro*, the phenotypic screening wheel is shifted towards utilising a combination of *ex vivo* macrophage infection models and *in vitro* enzyme inhibition. This unorthodox approach is indeed one of the currently developing trends, aimed at discovering novel anti-TB compounds.

SapM is a "eukaryotic-like" acid phosphatase that is secreted by *M. tb* in the host cell cytosol (35). Recently, SapM was also found to behave as an atypical alkaline

phosphatase (15). Similar to MPtpB, it is believed that SapM functions as a lipid phosphatase, hydrolysing PI3P on the phagosomal membrane, thereby preventing PI3P accumulation on phagosomes and blocking phagosome-lysosome fusion (15). However, how SapM is transferred from the phagosomal lumen, where it is secreted, to the phagosome's cytoplasmic face, where it interacts with PI3P, remains a conundrum (9). While PI3P normally regulates the conveyance of phagocytosed consignments to lysosomes, this trafficking event is pre-empted when the accumulation of PI3P is halted by *M. tb*. In fact, a PI3P-free environment must be maintained by *M. tb* during its occupation in macrophages to accomplish complete phagolysosomal arrest (9). In this respect, SapM promotes the continuous removal of PI3P from phagosomes-containing bacteria, preventing the anchorage of the proteins required for phagosomes to acquire lysosomal components. Indeed, Vergne *et al* demonstrated that dephosphorylation of PI3P mediated by SapM prevented recruitment of the effector protein EEA1 to the phagosomal membrane, thereby inhibiting the phagosomes-late endosomes fusion (36). SapM and MPtpB-induced hydrolysis of PI3P was also shown to prevent Rab5 and Rab7 swapping step that is prerequisite for the transition to late phagosome (15). In addition to PI3P, SapM was found to hydrolyse another PI, namely PI(4,5)P<sub>2</sub>, that is involved in the nascent phagosome formation and its subsequent scission from plasma membrane (15). Therefore, SapM-mediated blocking of this critical step during the mycobacterial invasion facilitates the uptake and colonisation of *M. tb* within the host. Of note, SapM showed a broad PI activity when tested against several PIs; however, it displayed more specificity towards PI(4,5)P<sub>2</sub> and PI3P that are essential in the early stages of phagocytosis of *M. tb* and phagosome maturation (15). In addition, Hu and colleagues supported the SapM's role in the intracellular survival of *M. tb* by showing that it interferes with autophagy (37). Similar to phagocytosis, autophagy is a highly conserved natural process that is operational in numerous immune cells, especially in macrophages (38). They both share common features and serve as host defence mechanisms that are required for fighting infections and maintain proper homeostasis (39). In this regard, pathogenic microorganisms, such as *M. tb*, produce virulence factors to combat these killing machineries. Indeed, SapM was shown to block autophagosome-lysosome fusion and suppress autophagy by binding to Rab7 (37). Taken together, SapM seems to possess a pleiotropic role in the pathogenesis of *M. tb*. Deletion of *sapM* gene in *M. tb* (*M. tb*  $\Delta$ *sapM*) led to phagosomal maturation arrest

and growth inhibition of *M. tb* in human THP-1 macrophages (40). Indeed, upon disrupting *sapM* in *M. tb*, the resulting strain was severely attenuated with impaired ability to grow or cause pathological damage in guinea pig tissues, compared to the parental strain. The importance of SapM in the pathogenesis of *M. tb* was corroborated when the survival of guinea pigs infected with *M. tb*  $\Delta$ *sapM* was compared to *M. tb* infected animals. Indeed, the *M. tb* infected guinea pigs gradually succumbed to death in 4 months, while not even one *M. tb*  $\Delta$ *sapM* infected animal died during the whole duration of the study (7 months) (40). Recently, two SapM inhibitors were identified, namely L-ascorbic acid and 2-phospho-L-ascorbic acid (**6**, **Figure 2.2**) (15). In fact, the latter compound significantly reduced the bacterial load/survival of *M. tb* H37Rv strain in infected THP-1 macrophages, while displaying no detrimental effect on the viability of macrophages. In support of the SapM's function being likely restricted to promoting the intracellular survival of *M. tb*, compound **6** showed no inhibitory effect on the extracellular growth of *M. tb* at 72 hours (15). Overall, contrary to the current antibiotics that are focused on inhibiting traditional essential targets *in vitro*, the intracellular activities of the preceding MPtpA, MPtpB, and SapM inhibitors constitute a proof of concept that reinstating the intrinsic host signalling machinery could be exploited in eradicating the TB infection.

### **2.3. *M. tb* Protein Kinases and Phosphatases Regulate The Biosynthesis of Cell Wall Components**

Contrary to other bacteria, the unusually intricate cell wall of *M. tb* is made up of unique lipid and glycolipid components which are correlated to the virulence and survival of mycobacteria inside the host (13). This fortified cell wall act as a protective shield that insulate the mycobacteria from noxious substances, such as the host's immune killing mechanisms and many antibiotics (3). In addition, the glycolipids of *M. tb* cell wall can impair the normal host trafficking events that is regulated by PI3P, thereby interfering with phagosome-lysosome fusion (13). Apart from modulating the host cell responses, most of the Ser/Thr kinases and phosphatases encoded by *M. tb* appear to be involved in key regulatory processes such as cell wall components synthesis, cell division, and stress responses (3). These manipulations allow the bacterium to enter a state of dormancy, in which protein phosphorylation/dephosphorylation governs translating extracellular signals into adequate responses, such as cell wall remodelling and downregulating the metabolic activity of the bacteria (3). In 2019, we published a



review article covering in detail the biosynthetic machinery of MAs, which are the major constituents of the *M. tb*'s cell wall. This review paper also provides insights into the role of kinases and phosphatases in modulating the activity of several proteins implicated in the MAs synthesis. In addition, several small-molecule inhibitors of mycobacterial kinases and phosphatases were highlighted therein. The review article is subsequently integrated into this Chapter.

## References

1. Prisic S, Husson RN. Mycobacterium tuberculosis Serine/Threonine Protein Kinases. *Microbiol Spectr*. 2014;2(5).
2. Av-Gay Y, Everett M. The eukaryotic-like Ser/Thr protein kinases of Mycobacterium tuberculosis. *Trends Microbiol*. 2000;8(5):238-44.
3. Richard-Greenblatt M, Av-Gay Y. Epigenetic Phosphorylation Control of Mycobacterium tuberculosis Infection and Persistence. *Microbiol Spectr*. 2017;5(2).
4. Chao J, Wong D, Zheng X, Poirier V, Bach H, Hmama Z, et al. Protein kinase and phosphatase signaling in Mycobacterium tuberculosis physiology and pathogenesis. *Biochim Biophys Acta*. 2010;1804(3):620-7.
5. Saha S, Das P, Bose Dasgupta S. "It Takes Two to Tango": Role of Neglected Macrophage Manipulators Coronin 1 and Protein Kinase G in Mycobacterial Pathogenesis. *Front Cell Infect Microbiol*. 2020;10:582563.
6. Carranza C, Chavez-Galan L. Several Routes to the Same Destination: Inhibition of Phagosome-Lysosome Fusion by Mycobacterium tuberculosis. *Am J Med Sci*. 2019;357(3):184-94.
7. Uribe-Querol E, Rosales C. Control of Phagocytosis by Microbial Pathogens. *Front Immunol*. 2017;8:1368.
8. Becken U, Jeschke A, Veltman K, Haas A. Cell-free fusion of bacteria-containing phagosomes with endocytic compartments. *Proc Natl Acad Sci U S A*. 2010;107(48):20726-31.
9. Poirier V, Av-Gay Y. Mycobacterium tuberculosis modulators of the macrophage's cellular events. *Microbes Infect*. 2012;14(13):1211-9.
10. Wong D, Chao JD, Av-Gay Y. Mycobacterium tuberculosis-secreted phosphatases: from pathogenesis to targets for TB drug development. *Trends Microbiol*. 2013;21(2):100-9.
11. Sturgill-Koszycki S, Schlesinger PH, Chakraborty P, Haddix PL, Collins HL, Fok AK, et al. Lack of acidification in Mycobacterium phagosomes produced by exclusion of the vesicular proton-ATPase. *Science*. 1994;263(5147):678-81.
12. Armstrong JA, Hart PD. Response of cultured macrophages to Mycobacterium tuberculosis, with observations on fusion of lysosomes with phagosomes. *J Exp Med*. 1971;134(3 Pt 1):713-40.

13. Pieters J. Mycobacterium tuberculosis and the macrophage: maintaining a balance. *Cell Host Microbe*. 2008;3(6):399-407.
14. Walburger A, Koul A, Ferrari G, Nguyen L, Prescianotto-Baschong C, Huygen K, et al. Protein kinase G from pathogenic mycobacteria promotes survival within macrophages. *Science*. 2004;304(5678):1800-4.
15. Fernandez-Soto P, Bruce AJE, Fielding AJ, Cavet JS, Taberero L. Mechanism of catalysis and inhibition of Mycobacterium tuberculosis SapM, implications for the development of novel antivirulence drugs. *Sci Rep*. 2019;9(1):10315.
16. Khan MZ, Kaur P, Nandicoori VK. Targeting the messengers: Serine/threonine protein kinases as potential targets for antimycobacterial drug development. *IUBMB Life*. 2018;70(9):889-904.
17. Nguyen L, Pieters J. The Trojan horse: survival tactics of pathogenic mycobacteria in macrophages. *Trends Cell Biol*. 2005;15(5):269-76.
18. Tiwari D, Singh RK, Goswami K, Verma SK, Prakash B, Nandicoori VK. Key residues in Mycobacterium tuberculosis protein kinase G play a role in regulating kinase activity and survival in the host. *J Biol Chem*. 2009;284(40):27467-79.
19. Majlessi L, Combaluzier B, Albrecht I, Garcia JE, Nouze C, Pieters J, et al. Inhibition of phagosome maturation by mycobacteria does not interfere with presentation of mycobacterial antigens by MHC molecules. *J Immunol*. 2007;179(3):1825-33.
20. Nguyen L, Walburger A, Houben E, Koul A, Muller S, Morbitzer M, et al. Role of protein kinase G in growth and glutamine metabolism of Mycobacterium bovis BCG. *J Bacteriol*. 2005;187(16):5852-6.
21. Khan MZ, Bhaskar A, Upadhyay S, Kumari P, Rajmani RS, Jain P, et al. Protein kinase G confers survival advantage to Mycobacterium tuberculosis during latency-like conditions. *J Biol Chem*. 2017;292(39):16093-108.
22. Rieck B, Degiacomi G, Zimmermann M, Cascioferro A, Boldrin F, Lazar-Adler NR, et al. PknG senses amino acid availability to control metabolism and virulence of Mycobacterium tuberculosis. *PLoS Pathog*. 2017;13(5):e1006399.
23. Scherr N, Honnappa S, Kunz G, Mueller P, Jayachandran R, Winkler F, et al. Structural basis for the specific inhibition of protein kinase G, a virulence factor of Mycobacterium tuberculosis. *Proc Natl Acad Sci U S A*. 2007;104(29):12151-6.

24. Kidwai S, Bouzeyen R, Chakraborti S, Khare N, Das S, Priya Gosain T, et al. NU-6027 Inhibits Growth of Mycobacterium tuberculosis by Targeting Protein Kinase D and Protein Kinase G. *Antimicrob Agents Chemother.* 2019;63(9).
25. Arris CE, Boyle FT, Calvert AH, Curtin NJ, Endicott JA, Garman EF, et al. Identification of novel purine and pyrimidine cyclin-dependent kinase inhibitors with distinct molecular interactions and tumor cell growth inhibition profiles. *J Med Chem.* 2000;43(15):2797-804.
26. Cowley SC, Babakaiff R, Av-Gay Y. Expression and localization of the Mycobacterium tuberculosis protein tyrosine phosphatase PtpA. *Res Microbiol.* 2002;153(4):233-41.
27. Bach H, Papavinasasundaram KG, Wong D, Hmama Z, Av-Gay Y. Mycobacterium tuberculosis virulence is mediated by PtpA dephosphorylation of human vacuolar protein sorting 33B. *Cell Host Microbe.* 2008;3(5):316-22.
28. Wong D, Bach H, Sun J, Hmama Z, Av-Gay Y. Mycobacterium tuberculosis protein tyrosine phosphatase (PtpA) excludes host vacuolar-H<sup>+</sup>-ATPase to inhibit phagosome acidification. *Proc Natl Acad Sci U S A.* 2011;108(48):19371-6.
29. Dutta NK, He R, Pinn ML, He Y, Burrows F, Zhang ZY, et al. Mycobacterial Protein Tyrosine Phosphatases A and B Inhibitors Augment the Bactericidal Activity of the Standard Anti-tuberculosis Regimen. *ACS Infect Dis.* 2016;2(3):231-9.
30. Zhou B, He Y, Zhang X, Xu J, Luo Y, Wang Y, et al. Targeting mycobacterium protein tyrosine phosphatase B for antituberculosis agents. *Proc Natl Acad Sci U S A.* 2010;107(10):4573-8.
31. Beresford N, Patel S, Armstrong J, Szoor B, Fordham-Skelton AP, Taberero L. MptpB, a virulence factor from Mycobacterium tuberculosis, exhibits triple-specificity phosphatase activity. *Biochem J.* 2007;406(1):13-8.
32. Singh R, Rao V, Shakila H, Gupta R, Khera A, Dhar N, et al. Disruption of mptpB impairs the ability of Mycobacterium tuberculosis to survive in guinea pigs. *Mol Microbiol.* 2003;50(3):751-62.
33. Beresford NJ, Mulhearn D, Szczepankiewicz B, Liu G, Johnson ME, Fordham-Skelton A, et al. Inhibition of MptpB phosphatase from Mycobacterium tuberculosis impairs mycobacterial survival in macrophages. *J Antimicrob Chemother.* 2009;63(5):928-36.

34. He R, Yu ZH, Zhang RY, Wu L, Gunawan AM, Zhang ZY. Cefsulodin Inspired Potent and Selective Inhibitors of mPTPB, a Virulent Phosphatase from *Mycobacterium tuberculosis*. *ACS Med Chem Lett*. 2015;6(12):1231-5.
35. Saleh MT, Belisle JT. Secretion of an acid phosphatase (SapM) by *Mycobacterium tuberculosis* that is similar to eukaryotic acid phosphatases. *J Bacteriol*. 2000;182(23):6850-3.
36. Vergne I, Chua J, Lee HH, Lucas M, Belisle J, Deretic V. Mechanism of phagolysosome biogenesis block by viable *Mycobacterium tuberculosis*. *Proc Natl Acad Sci U S A*. 2005;102(11):4033-8.
37. Hu D, Wu J, Wang W, Mu M, Zhao R, Xu X, et al. Autophagy regulation revealed by SapM-induced block of autophagosome-lysosome fusion via binding RAB7. *Biochem Biophys Res Commun*. 2015;461(2):401-7.
38. Bruns H, Stenger S. New insights into the interaction of *Mycobacterium tuberculosis* and human macrophages. *Future Microbiol*. 2014;9(3):327-41.
39. Gutierrez MG, Master SS, Singh SB, Taylor GA, Colombo MI, Deretic V. Autophagy is a defense mechanism inhibiting BCG and *Mycobacterium tuberculosis* survival in infected macrophages. *Cell*. 2004;119(6):753-66.
40. Puri RV, Reddy PV, Tyagi AK. Secreted acid phosphatase (SapM) of *Mycobacterium tuberculosis* is indispensable for arresting phagosomal maturation and growth of the pathogen in guinea pig tissues. *PLoS One*. 2013;8(7):e70514.

## STATEMENT OF CONTRIBUTION TO A CO-AUTHORED PUBLISHED PAPER

The second half of Chapter 2 includes a co-authored review article that has been published online in the Current Molecular Pharmacology journal (2019)

DOI: [10.2174/1874467211666181025141114](https://doi.org/10.2174/1874467211666181025141114)

Publication link: <https://www.eurekaselect.com/166636/article>

**Title: Kinase Targets for Mycolic Acid Biosynthesis in Mycobacterium Tuberculosis**

**Authors/Co-authors: Shahinda S.R. Alsayed, Chau C. Beh, Neil R. Foster, Alan D. Payne, Yu Yu, Hendra Gunosewoyo**

My contribution to the paper involved: 1) the design of the review article, 2) collecting and organising the information/data/references, 3) preparing and writing up the manuscript (except for Section 6: Formulation of anti-tubercular agents targeting mycolic acid biosynthesis—a brief survey, which was prepared and written up by Chau C. Beh)

(Signed)



(Date)

20/09/2021

Shahinda Sayed Rabie Alsayed

(Countersigned)



(Date)

20/9/21

Corresponding author of the paper: Dr Hendra Gunosewoyo

(Countersigned)

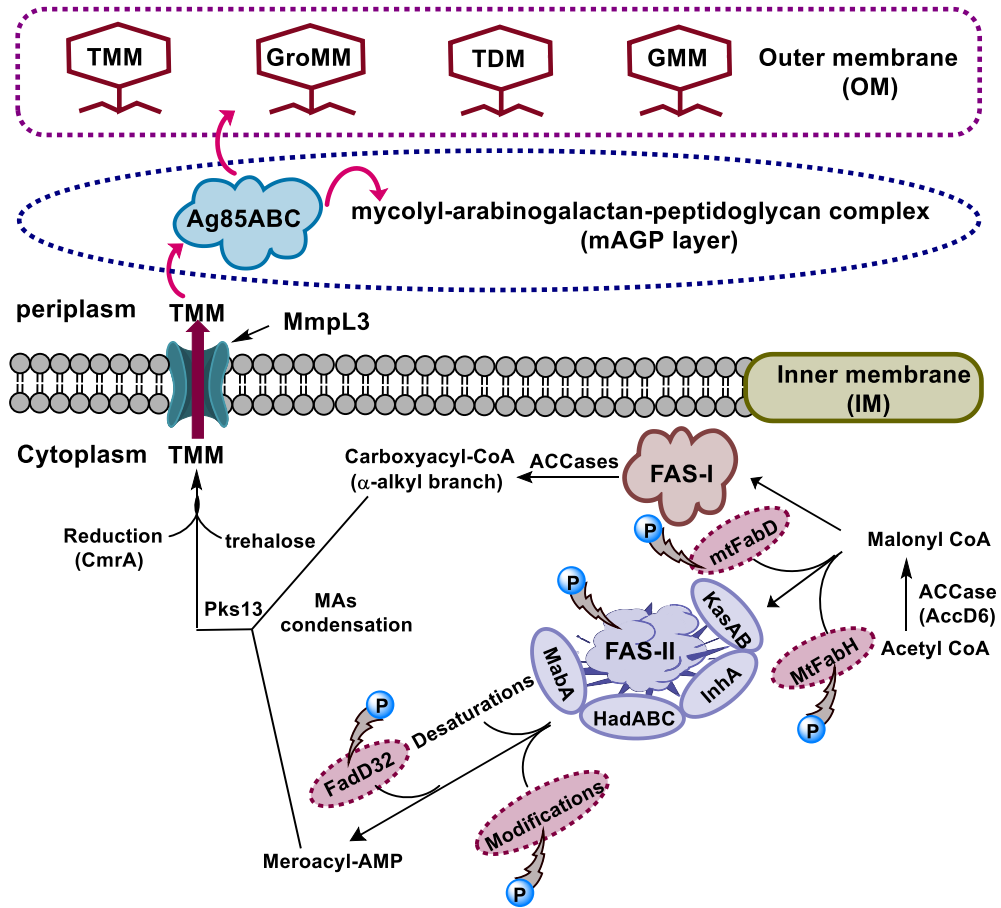


(Date)

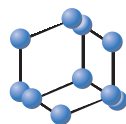
20/9/21

Main supervisor: Dr Hendra Gunosewoyo

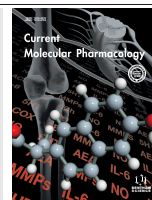
# Graphical Abstract



## REVIEW ARTICLE

BENTHAM  
SCIENCE

# Kinase Targets for Mycolic Acid Biosynthesis in *Mycobacterium tuberculosis*



Shahinda S.R. Alsayed<sup>a</sup>, Chau C. Beh<sup>b,c</sup>, Neil R. Foster<sup>b</sup>, Alan D. Payne<sup>d</sup>, Yu Yu<sup>a</sup> and Hendra Gunosewoyo<sup>a,\*</sup>

<sup>a</sup>School of Pharmacy and Biomedical Sciences, Faculty of Health Sciences, Curtin University, Perth, WA 6102, Australia;

<sup>b</sup>Western Australia School of Mines: Minerals, Energy and Chemical Engineering, Curtin University, Bentley 6102 WA, Australia; <sup>c</sup>David H. Koch Institute for Integrative Cancer Research, Massachusetts Institute of Technology, Cambridge, MA 02142, USA; <sup>d</sup>School of Molecular and Life Sciences, Curtin University, Perth, WA 6102, Australia

**Abstract: Background:** Mycolic acids (MAs) are the characteristic, integral building blocks for the mycomembrane belonging to the insidious bacterial pathogen *Mycobacterium tuberculosis* (*M.tb*). These C<sub>60</sub>-C<sub>90</sub> long  $\alpha$ -alkyl- $\beta$ -hydroxylated fatty acids provide protection to the tubercle bacilli against the outside threats, thus allowing its survival, virulence and resistance to the current antibacterial agents. In the post-genomic era, progress has been made towards understanding the crucial enzymatic machineries involved in the biosynthesis of MAs in *M.tb*. However, gaps still remain in the exact role of the phosphorylation and dephosphorylation of regulatory mechanisms within these systems. To date, a total of 11 serine-threonine protein kinases (STPKs) are found in *M.tb*. Most enzymes implicated in the MAs synthesis were found to be phosphorylated *in vitro* and/or *in vivo*. For instance, phosphorylation of KasA, KasB, mtFabH, InhA, Maba, and FadD32 downregulated their enzymatic activity, while phosphorylation of VirS increased its enzymatic activity. These observations suggest that the kinases and phosphatases system could play a role in *M.tb* adaptive responses and survival mechanisms in the human host. As the mycobacterial STPKs do not share a high sequence homology to the human's, there have been some early drug discovery efforts towards developing potent and selective inhibitors.

**Objective:** Recent updates to the kinases and phosphatases involved in the regulation of MAs biosynthesis will be presented in this mini-review, including their known small molecule inhibitors.

**Conclusion:** Mycobacterial kinases and phosphatases involved in the MAs regulation may serve as a useful avenue for antitubercular therapy.

**Keywords:** Mycobacterium, tuberculosis, kinase, phosphatase, mycolic acids, small molecule inhibitors, formulations.

## 1. INTRODUCTION

The highly contagious tuberculosis (TB) is an airborne disease caused by the microorganism *Mycobacterium tuberculosis* (*M.tb*). It is estimated to latently infect one-quarter of the global population [1]. In particular, co-infection with human immunodeficiency virus (HIV) greatly worsens the scenario with 0.4 million deaths among HIV-positive people [1]. As the ninth overall leading cause of death worldwide, TB surpassed HIV/AIDS as the number one infectious disease killer, making it the major threat to global health. According to the 2017 World Health Organisation report, 10.4 million people suffer from TB in which 1.3 million HIV-negative patients died in 2016 out of 1.7 million total deaths. The treatment option is onerous because *M.tb* persists in the host for extended periods of time, thus requiring a 6-month

minimum treatment with the first-line anti-TB drugs presented in two phases. The intensive phase is two month administration of a cocktail of the four first-line drugs: isoniazid (INH), rifampicin (RIF), pyrazinamide (PZA) and ethambutol (EMB). While the later four months treatment represents the continuation phase which consists of INH and RIF to kill the dormant bacteria [1, 2]. This protracted duration of therapy and high pill count, as well as drug side effects, resulted in poor patient compliance and incomplete eradication of TB, which ultimately lead to the development of drug-resistant TB [3]. The recrudescence of the disease in the form of multi-, extensively- and totally-drug resistant tuberculosis (MDR-, XDR- and TDR-TB, respectively) has left limited drug options available for TB patients [4-9]. Furthermore, the second line anti-TB drugs for MDR-TB and XDR-TB strains should be administered for a longer duration (up to 2 years), even though less effective, more expensive and toxic compared to the first line regimen [10]. Accordingly, anti-TB drugs with a novel mode of action and higher efficacy on the resistant TB strains, and a shorter course of treatment, are urgently needed.

\*Address correspondence to this author at the School of Pharmacy and Biomedical Sciences, Faculty of Health Sciences, Curtin University, Perth, WA 6102, Australia; Tel/Fax: +61-8-9266-3747, +61-8-9266-2769; E-mail: Hendra.Gunosewoyo@curtin.edu.au



The sequencing of *M.tb* genome has uncovered many potential therapeutic targets involved in lipid biosynthesis and metabolism [11]. Of particular interest is the mycolic acids (MAs) which are unique long chain fatty acids (FAs) in *Mycobacterium*. MAs are the major constituents of mycobacterial cell envelope and contribute to the outer membrane permeability and integrity [12]. In addition, MAs biosynthesis can be inhibited by INH and ethionamide (ETH) causing cell viability loss [13]. Recent data on the protein phosphorylation and signal transduction mechanisms in *M.tb* sheds light on the regulatory events in mycobacterial growth, cell wall biosynthesis, cell division and virulence [14]. This review will discuss the role of protein substrates phosphorylation in MAs biosynthesis, as well as small molecules targeting the mycobacterial kinases and phosphatases.

## 2. MYCOLIC ACIDS IN *M.tb*

The thick *M.tb* cell envelope is characterised by tight bundles of complex lipids consisting mainly of three interconnected macromolecules: arabinogalactan, peptidoglycan, and MAs which are key players in the infectious process [15, 16]. MAs are a homologous series of  $\alpha$ -branched  $\beta$ -hydroxylated FAs with an exceptional chain length ( $C_{60}$ - $C_{90}$  in *M.tb*) and the primary mediators of acid-fastness and hydrophobic character of mycobacterial outer coating [17]. They are mainly found as esters of the terminal penta arabinofuranosyl units of the major cell wall polysaccharide, arabinogalactan (AG), which is further covalently linked *via* a phosphodiester bond to the cell wall peptidoglycan to form mycolyl-arabinogalactan-peptidoglycan complex (mAGP); the insoluble cell wall skeleton [18-21]. MAs are also the major lipid components of the outer mycobacterial cell envelope; present as extractable free lipids, such as esters of trehalose, glucose, and possibly glycerol forming trehalose monomycolate (TMM) or trehalose dimycolate (TDM), glucose monomycolate (GMM), and glycerol monomycolate (GroMM), respectively (Fig. 1) [22-28]. TDM, also known as the 'cord factor', accumulates in a cord-like fashion on the surface of the cell, represents the most abundant, granuloma-genic, and significant toxic lipid extractable from the virulent mycobacterial cell surface [29, 30]. This mAGP on the *M.tb* surface with the non-covalently associated glycolipids constitutes a closely packed and formidable bilayer barrier with significantly reduced fluidity and permeability, playing an important role in virulence and immune evasion. Hence, this protective layer insulates the *Tubercle bacillus* against noxious chemicals and the host's immune system, underlining its fundamental role in mycobacterial survival and growth in the host [12]. Being essential for mycobacterial virulence and viability, characterisation of key enzymes involved in the biosynthesis of MAs may lead to the identification of novel targets for drug development.

### 2.1. Mycolic Acid Biosynthesis in *M.tb*

MAs of mycobacteria comprise a very long meromycoloyl chain ( $C_{50}$ - $C_{60}$ ) and a saturated  $\alpha$ -side chain ( $C_{24}$ - $C_{26}$ ) that can be classified according to chain lengths and chemical functions to four distinct structural classes [31]. Firstly,  $\alpha$ -MAs (Fig. 2), are the most abundant form containing two *cis*-cyclopropyl groups attached to the meromycolate chain and they do not contain any oxygen functionality other than

the  $\beta$ -hydroxyl group and therefore are different from the oxygenated MAs such as keto-, methoxy and hydroxyl mycolates. On the other hand, the oxygenated mycolates contain additional oxygen functions in the distal portion of the meromycolate chain and are four to six carbons longer than the  $\alpha$ -MAs [31].

The biosynthesis and incorporation of MAs on the mycobacterial cell wall can be summarised into five distinct steps, which have been illustrated in many excellent reviews [12, 31-33] and are depicted in Fig. (2). The first three steps [34-36] focused on the synthesis of the two chain segments of MAs involve: (i) the synthesis of the  $C_{24}$ - $C_{26}$  saturated  $\alpha$ -alkyl branch of the MAs by the single multi-domain enzyme, FAS-I; (ii) the synthesis of  $C_{50}$ - $C_{60}$  meromycolate chain by FAS-II which includes discrete monofunctional enzymes; (iii) incorporation of double bonds, cyclopropyl, methoxy and keto functionalities to the meromycolic acid backbone by numerous desaturases or dehydratases/isomerases, cyclopropane synthases and methyl transferases (the process that results in the subsequent formation of different MA subclasses). In step (iv), FAS-I derived  $\alpha$ -alkyl branch and meromycolate chain generated from FAS-II are activated and ligated onto the terminal condensing enzyme polyketide synthase (Pks13) which catalyses a Claisen condensation reaction and couples both activated chains together. Trehalose is then attached to the newly formed assembled chain, followed by a final reduction reaction; and step (v) involves shuttling the intact MAs into the periplasm as a trehalose ester by the membrane transporter, mycobacterial membrane protein large 3 (Mmpl3). Thereafter, the antigen 85 complex (Ag85ABC) transfers the MA portion to arabinogalactan, to form mAGP, and other cell wall-associated glycolipids (Fig. 1).

#### Step (i): Biosynthesis of medium-chain FAs precursors *via* fatty acid synthase I system (FAS-I)

In *M.tb*, the multifunctional FAS-I polypeptide encoded by *fas* (*Rv2524c*) possesses all the functional domains corresponding to the *de novo* fatty acid synthesis cycle [37-40]. FAS-I system uses acetyl-CoA and malonyl-CoA as substrates in a cycle of transacylation, condensation,  $\beta$ -ketoacyl reduction, dehydration and enoyl reduction to elongate the acetyl group by two carbon units [12] (Fig. 2, top left). The resulting acyl-CoA produced in each cycle is used as a building block for further extension by two carbon units in another cycle and the elongation will continue until the formation of the medium-chain acyl-CoA primers,  $C_{16}$ - $C_{18}$  and  $C_{24}$ - $C_{26}$  FAs. The former,  $C_{16}$ - $C_{18}$  FAs, is subsequently fed into FAS-II to synthesise the long meromycolic acid segment. While the resulting  $C_{24}$ - $C_{26}$  acyl-CoAs are carboxylated by acetyl-CoA carboxylases (ACCases) prior to the final condensation reaction catalysed by Pks13; accounting for the  $\alpha$ -branch of the final mycolic acid [31] (Fig. 2).

#### Step (ii): Meromycolic backbone biosynthesis *via* type II fatty acid synthase II (FAS-II) and step (iii): incorporation of double bonds, cyclopropyl, methoxy and keto functionalities to the meromycolic acid

In contrast to FAS-I, the FAS-II is composed of four dissociable enzyme components and is incapable of the *de novo*

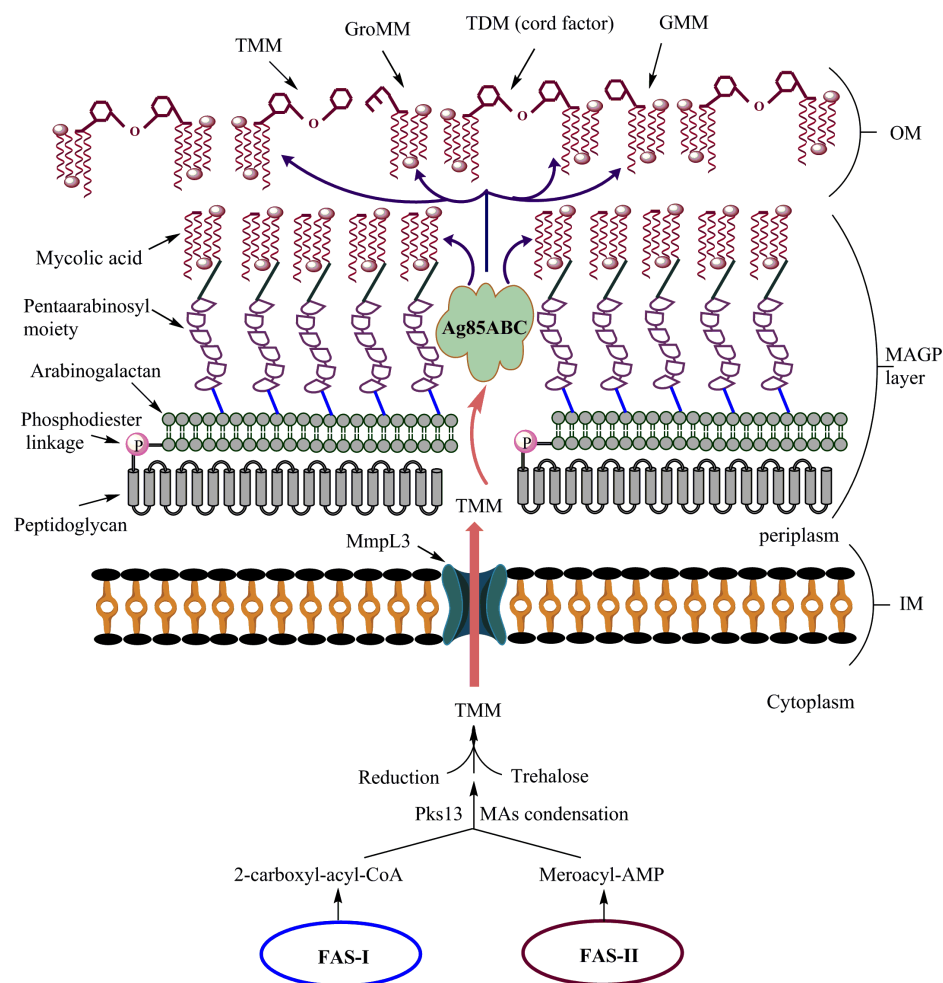


**Fig. (1).** A model depicting the inner membrane (IM) and the cell wall of *M.tb*. Following MAs synthesis in cytoplasm, mycobacterial membrane protein large 3 (MmpL3) acts as a cross gate for the mature MAs in the form of trehalose monomycolate (TMM), commuting them from cytoplasm to periplasm. Next, Ag85ABC complex transfers the MA portion from TMM to: (i) arabinogalactan layer to form mycolyl arabinogalactan peptidoglycan (MAGP) layer, (ii) another TMM to form trehalose dimycolate (TDM), (iii) glucose to form glucose monomycolate (GMM), and (iv) glycerol to form glycerol monomycolate (GroMM). The figure indicates the prevalence of MAs in *M.tb* cell wall, being anchored to arabinogalactan (MAGP) and in the form of glycolipids in the outer membrane (OM).

synthesis of FAs from acetyl-CoA [41, 42]. Instead, mycobacterial FAS-II uses acyl-CoA primers released by FAS-I as a substrate to synthesise the meromycolate chain *via* several iterative cycles; each comprises four steps entailing four enzymes, either mtFabH or KasA/B as well as MabA, HadAB/BC, and InhA [35]. FAS-II enzymes function on mycobacterial acyl carrier protein (AcpM)-bound substrates which necessitate the transfer of the malonate group from malonyl-CoA to the AcpM to form malonyl-S-AcpM, a reaction catalysed by malonyl-CoA:AcpM transacylase (MCAT or mtFabD) enzyme [42]. AcpM function is hypothesised to be shuttling acyl intermediates between enzymes. The FAS-II elongation process is then initiated by  $\beta$ -ketoacyl-AcpM synthase III (Kas-III or mtFabH), the pivotal link between FAS-I and FAS-II, as it catalyses a Claisen condensation between Acyl-CoA primers released from FAS-I and malonyl-AcpM [43] (Fig. 2). The donor malonyl-AcpM is decarboxylated to form the acetyl-AcpM carbanion, a nucleophile which will attack the carbonyl group on the acyl primer to form the elongated  $\beta$ -ketoacyl-AcpM which will be further funneled

into the FAS-II cycle [34]. Next, four enzymes catalyse each cycle of elongation acting successively and repetitively until the required length of meromycolic acid is achieved. Firstly, a nicotinamide adenine dinucleotide phosphate-dependent  $\beta$ -ketoacyl-AcpM reductase (MabA, FabG1) catalyses the reduction of  $\beta$ -keto group in the  $\beta$ -ketoacyl-AcpM precursors [44]. The resulting  $\beta$ -hydroxyacyl-AcpM is dehydrated by  $\beta$ -hydroxyacyl-AcpM dehydratase (HadAB and HadBC) to an enoyl-AcpM. Then, the nicotinamide adenine dinucleotide hydrogen (NADH)-dependent trans-2-enoyl-AcpM reductase (InhA) catalyses the reduction of the resulting enoyl chain to acyl-AcpM [31]. Now the resulting acyl chain is two carbons longer than the starting precursor which will be recycled by  $\beta$ -ketoacyl-AcpM synthases (KasA or KasB) instead of the mtFabH to further elongate the chain length by two carbons forming  $\beta$ -ketoacyl AcpM and the cycle will continue as described until the required meromycolate chain length is obtained [45-49]. Specific modifications are inserted onto the distal and proximal positions of the meromycolic acid chain by eight different methyl transferases (MtF) namely,

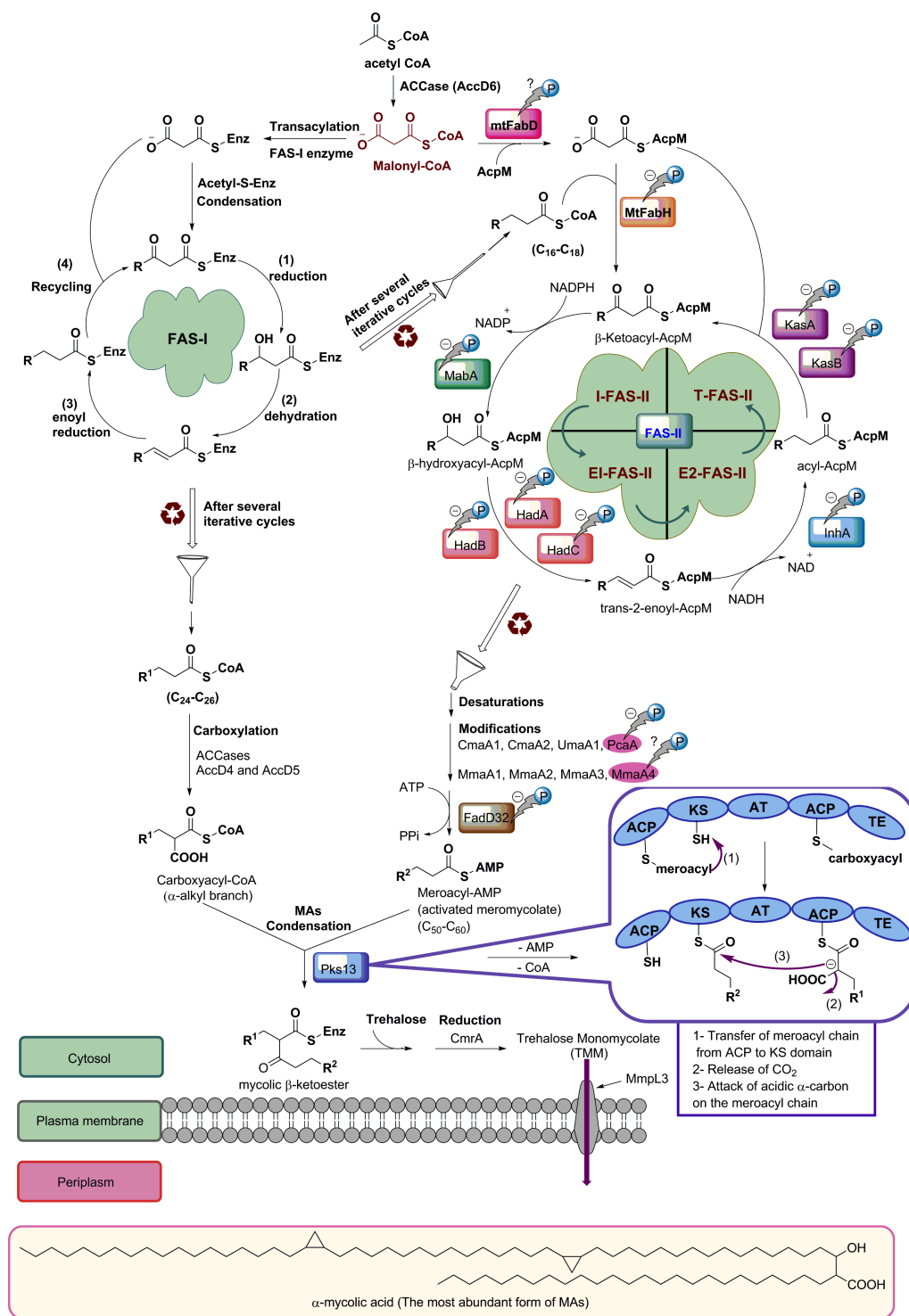


**Fig. (2).** Schematic illustration of MAs biosynthesis and regulation by phosphorylation as well as the proposed four FAS-II complexes and Pks13 domains. MAs biosynthesis starts with the de novo synthesis of two types of medium length acyl-chains by FAS-I in which the relatively shorter one acts as a substrate for further elongation in FAS-II to synthesise meromycolic acids. After modifications on meromycolate chains and FAS-II elongation, Pks13 catalyses Claisen-type condensation of the activated  $\alpha$ -alkyl branch and meromycolic acids. The resulting  $\beta$ -ketoester is then attached to trehalose and then reduced to TMM, which is further shuttled to periplasm by MmpL3.

MmaA1 to MmaA4, CmaA1, CmaA2, PcaA and UmaA [50].

The difference between mtFabH and KasA/KasB is in their acyl substrate preference. The initiation condensing

enzyme, mtFabH, favours acyl-CoA substrates over the acyl-AcpM primers [34]. In addition, mtFabH contains a hydrophobic pocket capped by an  $\alpha$ -helix, which limits the length of the bound acyl chain to C<sub>16</sub>-C<sub>18</sub>; excluding the longer ones (C<sub>24</sub>-C<sub>26</sub>) from chain elongation [34]. While mtFabH initiates

MAs elongation using acyl-CoA as a substrate and malonyl-AcpM as a co-substrate, both KasA and KasB catalyse subsequent rounds of chain extension using acyl-AcpM and malonyl-AcpM. The two distinct elongating condensing enzymes, KasA and KasB, are encoded by two different genes, *kasA* (*Rv2245*) and *kasB* (*Rv2246*), which are present in the same operon and share many similarities, including the specificity for long-chain acyl-AcpM primers [47, 48].

It is also noteworthy that several studies have proposed an attractive model of different specialised interconnected complexes which organise FAS-II system of *M.tb* based on the preferential interaction between the condensing enzymes and dehydratase heterodimers which define the specificity of each elongation complex [50-52]. In this model, three types of specialised FAS-II elongation complexes are interconnected together, all of which contains a 'core' consisting of the reductases (MabA and InhA) and mtFabD: i) the initiation FAS-II (I-FAS-II) comprises in addition to the core, mtFabH and represents the link between FAS-I and FAS-II; ii) two elongation FAS-II complexes (E-FAS-II) consisting of a core and either KasA and HadA/B (E1-FAS-II) or KasB and HadB/C (E2-FAS-II); and iii) the termination FAS-II (T-FAS-II) involving the core and KasB linked to Pks13 which condenses the FAS-I derived  $\alpha$ -branch with the meromycolate branch (Fig. 2). Despite their similar sequence, both KasA and KasB exhibit different chain length specificities in which KasA catalyses the initial elongation of MA chains in E1-FAS-II and KasB extends them to their full length in E2-FAS-II [47-49]. Similar to KasA, HadAB heterodimer is implicated in the initial FA elongation process, whereas the HadBC is involved in the advanced meromycolate extension cycles, in the sense that HadB/C prefers longer substrates than HadA/B. The HadB monomer represents the catalytic subunit, while HadA and HadC control the substrate selectivity for chain extension. This is consistent with the co-existence of KasA and HadA/B in E1-FAS-1 and KasB and HadB/C in E2-FAS-II [53, 54]. The *kasB* mutant strains of *M.tb* were found to produce shorter chain length mycolates and exhibiting impaired growth, increased permeability of cell wall and severe inability to resist the host immune system and antibiotic effect [34, 55]. In addition, enzymes such as isomerases, methyl transferases and cyclopropane synthases are suggested to modify the merochain during these elongation processes [50-52]. These modification enzymes also show a preferential interaction with a particular Had heterodimer and accordingly a specific FAS-II elongation complex. For example, while MmaA3 which incorporates a methoxy group to the distal part of the merochain interacts preferentially with HadA/C, both CmaA2 and PcaA involved in introducing modifications to the proximal part, interact preferentially with HadB/C [50-52].

#### Step (iv): The Claisen condensation mediated by polyketide synthase (Pks13)

After the release of the two MAs segments from FAS-I and FAS-II, they become activated prior to the final assembly step catalysed by Pks13 [12, 56, 57]. In *M.tb*, Pks13 is a member of the type I Pks family, displaying the following distinct domains involved in condensation: (i) two non-equivalent phosphopantetheine binding acyl carrier protein (ACP), (ii) ketoacyl synthase (KS), (iii) acyl transferase

(AT) and (iv) thioesterase (TE) domains [12, 58-60]. The ACP domains are naturally activated by a phosphopantetheinyl arm (P-pant) that carries that growing acyl chains [58-60]. There are also other enzymes implicated in the final condensation reaction apart from Pks13 and they are particularly responsible for the activation of the two condensate substrates. This activation involves both an acyl-AMP ligase (FAAL32 or also named FadD32) which adenylates and ligates the meromycolate chain onto Pks13, and acetyl-CoA carboxylases (ACCases), AccD4 and AccD5, which are responsible for the carboxylation of the  $\alpha$ -branch [56, 58-63]. Interestingly, the *fadD32* gene (*Rv3801c*), *pks13* (*Rv3800*), and *accD4* (*Rv3799c*) are adjacent on the same operon and this genetic organisation suggests the necessity of *fadD32* and *accD4* encoded proteins in the condensation process through acting in concert with Pks13 [57, 63]. FadD32 activates the FAS-II derived meroacyl-S-AcpM *via* its conversion into meroacyl-AMP and subsequently transfer it onto Pks13 [57-60]. On the other hand, the C<sub>24</sub>:C<sub>26</sub>-S-CoA released from FAS-I system is activated *via* carboxylation by the ACCases, AccD4 and AccD5, to yield 2-carboxyl-C<sub>24</sub>:C<sub>26</sub>-S-CoA. The first step is loading both activated acyl segments onto Pks13 in which they covalently attach as thioester [12] (Fig. 1). FAAL32 loads the C<sub>50</sub>:C<sub>60</sub>-meroacyl group onto the amino terminus of the ACP domain (N-ACP) of Pks13, while the AT domain loads the carboxylated alpha acyl chain onto the adjacent carboxy terminus of ACP domain (C-ACP) of Pks13 [12, 58]. The subsequent step entails the meroacyl group transfer from the N-terminus ACP domain to the KS domain catalyzed by AT enzyme at the AT domain. The third step corresponds to Claisen-type condensation of the two fatty acyl groups, catalysed by KS domain in which a nucleophilic attack on the carbonyl group of the meroacyl-S-KS by the acidic  $\alpha$ -carbon of the 2-carboxyl-acyl-S-ACP occurs forming 3-oxo-mycolyl-S-ACP and releasing CO<sub>2</sub> and KS [12]. Upon reaching its full length, the TE domain of Pks13 cleaves the formed thioester bond linking the newly synthesised acyl chain to the P-pant arm of C-ACP domain and most likely forms a transient covalent ester bond between the condensation product and the catalytic Ser1533 in its active site [58]. Then, the TE<sub>Pks13</sub> domain cleaves again this transient ester bond and act as an acyl-transferase, transferring the  $\alpha$ -alkyl  $\beta$ -ketoacyl chain onto trehalose to synthesise TMM keto form (TMMk). The final step is the reduction of the TMMk precursor into secondary alcohol (TMM) catalysed by Corynebacterineae mycolate reductase A (*Rv2509*, CmrA) [58, 64, 65]. Although a full length crystal structure of Pks13 is yet to be determined, the structure of several domains of Pks13 has been reported [66-68]. In particular, the TE domain has been shown to be targeted by several highly potent small molecule inhibitors [66, 69, 70]. It is also reported that disruption of *fadD32* or *pks13* genes in *Corynebacterium glutamicum* leads to severe impairment in MAs synthesis with the accumulation of large amounts of fatty acid precursors [61, 63]. The formed TMM is then shuttled from the cytoplasm to periplasm by MmpL3 membrane transporter.

#### Step (v): Mycobacterial membrane protein large 3 (MmpL3) transporter

The *M.tb* *H37Rv* genome encodes for membrane proteins that belong to the resistance, nodulation, and cell division

(RND) family of membrane transporters, termed mycobacterial membrane proteins large (MmpL) [11, 71]. Located in close proximity to the cell wall-associated glycolipids biosynthesis domains, some of the *M.tb* MmpL encoded proteins have been shown to play a crucial role in transporting the cognate lipids such as TMM [72-75]. Of particular interest, MmpL3 (*Rv0206c*), a fundamental inner membrane protein, is hypothesised to be the MAs flippase at the inner membrane (IM) [76]. In other words, MmpL3 is implicated in the flipping and release of MAs precursor, TMM, after being synthesised in cytoplasm across the IM into periplasm (Fig. 2). Thereafter, TMM serves as both a carrier for the MAs and a substrate to the Ag85ABC mycolyl transferase complex which is tightly associated with the mycomembrane (MM). The Ag85 enzymes then transfer the MA portion from TMM donor onto a polyol core acceptor, mainly arabinogalactan or another TMM and also to glucose and probably glycerol forming mAGP complex, TDM, GMM, and GroMM, respectively [58, 76]. Additionally, MmpL3 was recently proposed in a heme-iron acquisition system and accordingly iron homeostasis along with another family member MmpL11, suggesting their implicated multiple roles in *M.tb* [77, 78]. The role of MmpL3 in TMM translocation across the cytoplasmic membrane was proven in *M. smegmatis* when the conditional depletion of MmpL3 led to the loss of cell wall mycolation and TDM as well as an intracellular accumulation of TMM validating MmpL3 as a promising target for anti-TB drugs [79-81]. In addition, the Ag85-mediated cord factor (TDM) synthesis was found to be blocked with an Ag85C-binding molecule which displays an anti-TB activity both *in vitro* and within macrophages [82].

### 3. PROTEIN KINASE AND PHOSPHATASE SIGNAL TRANSDUCTION IN *M.tb*

Protein phosphorylation/dephosphorylation is a central regulatory mechanism for bacterial signal transduction [83]. It is mediated by protein kinases that transfer a phosphate group from a donor to an acceptor amino acid in a substrate protein, and protein phosphatases mediating protein dephosphorylation. *M.tb* uses several signal transduction mechanisms to modulate the production of cell wall components in response to variable environmental conditions, including growth, differentiation, mobility and expression of virulence factors in pathogenic bacteria during the infection course [84]. Signal transduction is generally achieved *via* sensing of a signal or input typically by a protein that ultimately activates the transducer or the response regulator (RR) [85]. Many of these extracellular stimuli are transduced *via* a sensory kinase protein across the mycobacterial membrane and converted into an intracellular response that alters cell physiology [85].

An extensive intracellular signaling network has been evolved in *M.tb* in which five families of kinases and phosphatases co-mediate signal transduction: (i) twelve paired “prokaryotic” histidine/aspartate two-component system, (ii) eleven “eukaryotic like” serine/threonine protein kinases (STPKs), (iii) a sole protein tyrosine kinase (PtkA), (iv) two protein tyrosine phosphatases (MPtps), and (v) a single serine/threonine phosphatase (PstP) [85, 86]. Many excellent reviews on the description of the *M.tb* kinases and phosphatases and their roles in regulating some of the mycobacterial

substrate proteins are available [14, 84, 86-89]. However, the mechanism by which the MAs biosynthesis is regulated through phosphorylation /dephosphorylation has not been fully addressed.

#### 3.1. The Histidine/Aspartate Two Component System

The two-component signaling systems are the most widely distributed and intensively studied transmembrane signaling systems in bacteria. These systems play an important role in *M.tb* pathogenesis and their adaptation to the hostile host environment and dormancy [85, 90]. The two component systems comprise a sensor histidine kinase (HK) and a transducer (RR) as two separate proteins which are highly selective for each other *via* protein-protein interaction [85]. HKs are usually membrane proteins, composed of two domains: (i) the receiver domain which senses the signal denoting changes in external environment, and (ii) the transmitter or kinase domain which contains both the sites of autophosphorylation and interaction with RR. On the other hand, RRs are cytoplasmic proteins comprising also two different domains: (i) a receiver domain containing a conserved aspartate residue on which a phosphate group is transferred from the cognate phosphorylated HK partner, and (ii) an effector domain with DNA binding site in which transcription of set of genes is subsequently promoted in response to this phosphorylation event, eliciting a specific response.

#### 3.2. The Eukaryotic-Like STPKs

It was assumed that signaling in prokaryotes is generally mediated through the classical two-component system (His/Asp phosphorylation). However, the “eukaryotic-like” serine/threonine and tyrosine kinases and their associated phosphatases have recently emerged from the genome sequencing as critical regulatory mechanisms in bacteria [87-89]. *M.tb* genome encodes for eleven STPKs named PknA, PknB and PknD-PknL described as “eukaryotic-like” protein kinases based on their structural similarity to the eleven sub-domains of Hank’s superfamily of kinases [11, 87]. Nine of the *M.tb* STPKs are classified as receptor type kinases as they are transmembrane proteins with an extracytoplasmic sensor domain and intracellular kinase domain (KD) [84]. The extracellular sensor domain detects the extracytoplasmic signals and transduces the message to the intracellular KD which in turn becomes activated and phosphorylates a specific serine, or threonine on substrate proteins including enzymes, structural proteins and transcription factors [84]. This phosphorylation activates these proteins to perform a special function and/or initiate a signal-response cascade *via* transferring the phosphate group into a downstream effector, establishing interactions between multiple proteins and broadly altering the physiological system in the cell [91]. The other two STPKs, PknG and PknK, are cytoplasmic proteins with regulatory domains that sense intracellular changes [84]. The *M.tb* phosphoproteome includes hundreds of Ser- and Thr-phosphorylated proteins suggesting the crucial influence of these STPKs on a wide range of biological functions in *M.tb* such as cell envelope biosynthesis, cell shape/division, and survival in macrophage which in turn account for its pathogenicity [92, 93]. Yet not all STPKs have been identified in *M.tb* due to the use of the eukaryotic-like biased paradigm

[86]. These kinases and phosphatases act as on/off switch, translating extracellular signals into cellular responses, changing protein expression and/or activity in both eukaryotes and prokaryotes [14, 94]. Generally, at neutral pH, the hydrolytic half-time of phosphoryl-Asp is few hours, whereas Ser/Thr/Tyr phospho-esters are stable for weeks [95]. This, in turn, suggests that the two-component signaling system may be switched on in *M.tb* if rapid, short-term adaptation is needed, while Ser/Thr/Tyr phosphorylation is used in long-term responses that may require phosphatases to be reversed. STPKs and Tyr kinases are ubiquitous in eukaryotes in which more than 500 of protein kinases are encoded in the human genome regulating human substrate proteins by phosphorylation [96, 97]. Hence, these Ser/Thr/Tyr host residues can potentially be targeted by *M.tb* kinases leading to regulation of host signaling pathways. Importantly, *M.tb* kinases show low sequence identity (<30%) to human homologs [89]. Taken together, these observations suggest that inhibition of the mycobacterial kinases or phosphatases may serve as a useful starting point for novel anti-TB drugs.

### 3.3. Mycobacterial Protein Tyrosine Kinases and Phosphatases

*Bach et al.* determined the protein-encoding for PtkA and the autophosphorylation on Tyr residues; however, the exact mode of action of PtkA has not yet been identified [98]. They found that MPtpA, which is located immediately downstream to PtkA in the same operon, is the cognate substrate of PtkA; nevertheless, the role of phosphorylation in regulating the phosphatase activity of MPtpA remains obscure [98, 99]. Additionally, *M.tb* deleted mutant of PtkA ( $\Delta$ ptkA) was found to exhibit impaired intracellular survival in macrophage due to its inability to inhibit phagosome acidification [100].

Phosphorylation of Ser, Thr, or Tyr is a relatively stable modification whose reversal requires phosphatase enzymes that can bind to and dephosphorylate specific phosphorylated residues on proteins, returning them to the unmodified state [101]. In *M.tb* there is one Ser/Thr phosphatase, PstP, encoded by the first gene in the operon that includes *pknA* and *pknB* genes. There are also two Tyr phosphatases, MPtpA and MPtpB [11]. Hence mycobacterial protein kinases significantly outnumber the phosphatases, suggesting possible lack of specificity and selectivity of protein phosphatases. Since PstP is the only Ser/Thr phosphatase, this suggests its critical role in *M.tb* pathophysiology by dephosphorylating all of the STPKs and their substrates. Such idea was further confirmed in many studies in which PstP dephosphorylated PknA and PknB, thereby deactivating them [102, 103]. Importantly, PstP also dephosphorylated Thr residues that had been phosphorylated by STPKs, for instance, the phosphorylated FadD32 (FadD32-P and FadD32\_myc) and the *in vivo* phosphorylated KasA (Kas\_myc) [102, 104]. In addition, PstP was found to play an important role in the cell division and survival of *M.tb*. In other words, depletion of PstP resulted in: (i) elongated multiseptated cells suggesting the occurrence of cell division defects in the absence of PstP mediated-dephosphorylation, and (ii) a detrimental effect on cell survival, leading to cell death in *M. smegmatis* [105]. On the other hand, PstP overexpression led to cell elongation and partially compromised survival, suggesting that fine-

tuning of PstP levels is crucial for the mycobacterial survival. Moreover, depletion of PstP in *M.tb* negatively impacted the pathogen's survival in mice in addition to decreasing the bacillary load even in established infections which emphasizes the critical role of PstP in both establishing and maintaining infection. PstP was also found to be absolutely essential for the *in vitro* mycobacterial growth [105].

MPtpA and MPtpB have attracted a great deal of interest based on data regarding their involvement in virulence factors responsible for hijacking the host signaling pathways. These Tyr phosphatases are secreted cytosol proteins released by *M.tb* of infected macrophage targeting host proteins and disrupting the host signaling machinery [106-108]. This ultimately promotes the mycobacterial intracellular survival *via* attenuating the host immune system, for example, by inhibiting phagosomes maturation and their fusion with lysosomes and accordingly preventing bacterial destruction [106-120]. The importance of tyrosine phosphatases for intracellular bacterial persistence was supported by the deletion strains of *MptpA* or *MptpB* which were found to exhibit impaired *M.tb* growth and survival in human ( $\Delta$ *MptpA*) and murine ( $\Delta$ *MptpB*) macrophages in addition to decreased bacillary load in guinea pig infection model ( $\Delta$ *MptpB*) [110, 116].

## 4. PHOSPHORYLATION CONTROL OF THE ENZYMES INVOLVED IN THE MYCOLIC ACID BIOSYNTHESIS IN *M.TB*

*M.tb* can exist in two distinct states within the infected host: (i) non-replicating dormant form causing asymptomatic latent infection, or (ii) actively replicating organisms producing active TB infection [121]. These pathophysiological stages suggest the existence of special cross-talk signals between the host and the tubercle bacilli in which the bacterium senses a wide range of environmental signals and adjust to new conditions by transcriptomic regulation [122]. The remarkable capacity of this pathogen to evade the host immune system and subsequently survive and persist for several decades stems from its unusual cell wall [22]. The change in the cell wall composition of *M.tb* in response to various environmental stimuli is a critical mechanism of adaptation and survival during disease progression and combating host defenses [22]. Despite the extensive literature, there is still a gap in fully comprehending the mechanisms adopted by the *M.tb* to modulate the expression of its cell wall components in response to environmental changes. MAs are the key virulence factors and the hallmark of the mycobacterial waxy coat playing a crucial role in its intracellular survival and contributing to its physiopathology [55, 123]. Hence, a better understanding of the phosphorylation/dephosphorylation mechanisms in *M.tb*'s MAs biosynthetic pathways could open avenues for novel strategies. STPKs phosphorylation-mediated signaling constitutes a key regulatory mechanism in pathogenic mycobacteria in which introducing negative charges on Ser or Thr residues changes their physiochemical properties and ultimately affect the overall protein activity [14, 89]. Therefore, discerning kinase-substrate cognate pairs in *M.tb*, as well as the phosphorylation effect on each protein substrate *in vivo* is crucial. During the last two decades, a few mycobacterial kinase substrates were identified whose phosphorylation was found to regulate

cell shape/division and cell envelop components biosynthesis [104, 124-145]. Given the critical importance of MAs in *M.tb*, we focus on the enzymes involved in MAs biosynthesis whose regulation rely largely on STPK-dependent mechanisms (Table 1).

#### 4.1. mtFabD or MCAT

Several studies were conducted to investigate the role of phosphorylation of mtFabD (or MCAT) which is responsible for malonyl group transacylation to AcpM forming malonyl-AcpM, the precursor of FAS-II system [42]. Phosphorylation of mtFabD was detected only in growing cultures of *Mycobacterium bovis* Bacille Calmette-Guérin (BCG) and upon cessation of growth, the protein appears to be dephosphorylated [137]. This growth phase dependent phosphorylation pattern suggested that MCAT may be a substrate for *M.tb* kinases and phosphatases [137]. Another study revealed the phosphorylation of mtFabD together with KasA and KasB by different *M.tb* STPKs on threonine residue [129]. It is also noteworthy that all STPKs failed to phosphorylate the crucial FAS-II component, holo-AcpM, which indicates the substrate specificity of these kinases towards mtFabD, KasA, and KasB [129]. Another recent study reported the phosphorylation of mtFabD by PknK both *in vitro* and *in vivo* [128]. In *pknK* silenced cultures, phosphorylation and surprisingly expression levels of mtFabD were low. The effect on MAs synthesis was assessed using a drug susceptibility assay in which both the wild-type and the *pknK* deficient strains of *M. bovis* BCG were subjected to INH. INH showed higher growth inhibitory activity on the *pknK* knockdown mycobacterial culture than the wild-type [128]. This suggests the direct effect of PknK on mtFabD in which MAs biosynthesis was downregulated in PknK silenced cultures due to the low level of mtFabD and/or its decreased phosphorylation level. However, the effect of phosphorylation on mtFabD was not fully investigated. These findings were consistent with the previously confirmed role of PknK in regulating the mycobacterial growth and conferring survival during early persistent infection through affecting the cell size and cell wall composition of *M.tb* [146, 147].

#### 4.2. mtFabH

The mtFabH links FAS-I and FAS-II and represents a potential regulatory key point in MAs biosynthesis. MtFabH was phosphorylated *in vitro* by several mycobacterial STPKs, most efficiently by PknA and PknF, as well as *in vivo* in *M. bovis* BCG [135]. The phosphorylation occurred exclusively on threonine residues, with Thr<sup>45</sup> being the unique phosphoacceptor both *in vitro* and *in vivo*. Adding a phosphate group on Thr<sup>45</sup> which is located at the entrance of the substrate channel suggests an alteration of the substrate accessibility and consequently affecting mtFabH enzymatic activity [135]. Importantly, the phosphomimetic mutant of mtFabH (T45D), designed to mimic constitutive phosphorylation, exhibited significantly decreased malonyl-AcpM decarboxylation, transacylation, and condensing activities compared with the wild-type protein or the phosphoablative (T45A) variant. These findings indicate that phosphorylation of mtFabH inhibits its enzymatic activity which in turn may influence MAs biosynthesis [135].

#### 4.3. MabA

MabA was efficiently phosphorylated *in vitro* by several *M.tb* STPKs as well as *in vivo* in *M. bovis* BCG. Phosphorylation occurred on three threonine residues, with Thr<sup>191</sup> being the predominant phospho-acceptor [136]. The ketoacyl reductase (KAR) activity was markedly decreased in MabA-T191D mutant, designed to mimic constitutive phosphorylation, compared with the wild-type protein (MabA-WT). This is probably related to its impaired binding to the NADPH cofactor necessary for catalysis. In addition, the effect of phosphorylation was further assessed *in vivo* in *M. bovis* BCG strain following conditional expression of the phosphomimetic MabA-T191D. The results demonstrated strongly impaired mycobacterial growth and a significant inhibition of MAs biosynthesis [136].

#### 4.4. HadAb and HadBC

The (3R)-hydroxyacyl-AcpM dehydratases (HadAB and HadBC) are crucial for mycobacterial growth and were found to be downregulated upon phosphorylation by *M.tb* STPKs *in vitro* and *in vivo* in *M. smegmatis* [54, 134, 148]. In addition, phosphorylation of HadAB/BC was increased in the stationary cells growth phase suggesting that mycobacteria might shut down MAs biosynthesis through HadAB and HadBC phosphorylation under non-replicating condition [134].

#### 4.5. InhA

InhA is the primary target of INH, the front-line hallmark anti-TB drug, and a key enzyme in MAs biosynthesis and survival of *M.tb*. Inactivation of InhA severely affect the mycobacteria causing accumulation of saturated FAs, inhibition of MAs biosynthesis and ultimately cell death by lysis [149]. INH is a prodrug that must be activated to the reactive free radical form by the catalase/peroxidase KatG, which then covalently binds to NAD<sup>+</sup> forming the isonicotinyl-NAD complex which is a potent inhibitor of InhA [150]. Mutations in InhA are the dominant phenotype of INH resistance, while other mechanisms of resistance including the activating enzyme KatG are recessive [151]. Since the genes encoding for both MabA and InhA are in the same operon and that the KAR activity of MabA is regulated by STPKs, it was hypothesised that InhA activity may be controlled by post-translational modification (PTM) as well [11, 136, 152]. Two studies in the same year supported this theory by proving that the enzymatic activity of InhA is decreased upon phosphorylation [126, 130]. The two studies showed similar results in which, Thr-266 is the key site of phosphorylation both *in vitro* and *in vivo*, and that the phosphomimetic (InhA-T266E) mutant failed to functionally complement and rescue the *M. smegmatis* conditional *inhA* gene replacement mutant. The first study indicated that the growth dynamics of *M. smegmatis* was severely compromised upon the co-expression of PknA and InhA *in vivo* compared with the cultures expressing PknA alone [126]. This was reminiscent of PknA overexpression cultures which were found to be detrimental to growth, most likely due to hyperphosphorylation of InhA and other substrates [141, 153, 154]. In addition, InhA-T266E phosphomimetic strain exhibited a delayed growth phenotype compared with the wild-type strain [126].

**Table 1.** MAs biosynthesis enzymes biochemically verified as substrates of *M.tb* STPKs.

| Protein Substrate | Cognate Kinase Candidate  | Effect of Phosphorylation | References      |
|-------------------|---|---------------------------|-----------------|
| mtFabD            | PknA (Rv0015c), PknB (Rv0014c), PknD (Rv0931c), PknE (Rv1743), PknF (Rv1746), PknK (Rv3080c) and PknH (Rv1266c) | N/A                       | [128, 129, 137] |
| mtFabH            | PknA (Rv0015c), PknD (Rv0931c), PknE (Rv1743), PknF (Rv1746), and PknH (Rv1266c)                                | Reduced activity          | [135]           |
| MabA              | PknA (Rv0015c), PknB (Rv0014c), PknD (Rv0931c), PknE (Rv1743), and PknL (Rv2176)                                | Reduced activity          | [136]           |
| HadAB/BC          | PknA (Rv0015c), PknB (Rv0014c), PknD (Rv0931c), PknE (Rv1743), PknF (Rv1746), and PknH (Rv1266c)                | Reduced activity          | [134]           |
| InhA              | PknA (Rv0015c), PknB (Rv0014c), PknF (Rv1746), PknH (Rv1266c), PknE (Rv1743), and PknL (Rv2176)                 | Reduced activity          | [126, 130]      |
| KasA              | PknA (Rv0015c), PknB (Rv0014c), PknE (Rv1743), PknF (Rv1746), and PknH (Rv1266c)                                | Reduced activity          | [129]           |
| KasB              | PknA (Rv0015c), PknB (Rv0014c), PknE (Rv1743), PknF (Rv1746), and PknH (Rv1266c)                                | Reduced activity          | [129, 138]      |
| PcA               | PknD (Rv0931c), PknE (Rv1743), PknF (Rv1746), and PknH (Rv1266c)  | Reduced activity          | [124]           |
| MmaA4             | PknJ (Rv2088)   | N/A                       | [125]           |
| FadD32            | PknA (Rv0015c), PknB (Rv0014c), PknD (Rv0931c), and PknF (Rv1746),  | Reduced activity          | [104]           |
| VirS              | PknK (Rv3080c)  | Increased activity        | [127]           |

In line with these results, the second study revealed that the *in vitro* enoyl reductase activity (ENR) was severely impaired in the InhA phosphomimetic mutants (T266D/E) due to their less pronounced binding affinity to NADH compared with the phosphoablative (*inhA-T266A*) allele and wild-type (InhA-WT) strain [130]. In addition, overexpression of (InhA-T266D/E) markedly impaired the growth of both fast and slow growing *M. smegmatis* and *M. bovis* BCG compared with the strains overexpressing InhA-T266A or InhA-WT, presumably due to the impaired ENR activity in both phosphomimetic strains due to inhibition of the activity of FAS-II. Also, the transfer of a single T266D or T266E point mutation within InhA was lethal to *M.tb* [130]. While InhA-T266A or InhA-WT were able to restore both MAs production and growth at 42°C, both InhA-T266D and InhA-T266E exhibited almost complete abrogation of MAs biosynthesis and growth arrest [130]. This MAs biosynthesis cessation profile was analogous to what is observed after INH treatment [149].

#### 4.6. KasA and KasB

KasA and KasB were efficiently phosphorylated *in vitro* by different STPKs with PknA being the most active kinase and both were preferentially phosphorylated at threonine residue *in vitro* and *in vivo* [129]. Of particular note, KasA phosphorylation remained constant regardless of the growth phase, contrasting other reported findings for example in which mtFabD phosphorylation was detected only in growing *M. bovis* BCG cultures [129, 137]. The significance of this finding remains unclear. It was also found that *M.tb* Ser/Thr phosphatase (PstP) dephosphorylate STPK-

phosphorylated KasA (KasA\_myco) suggesting KasA reversible phosphorylation *in vivo* through the regulatory role of PstP. Interestingly, KasA and KasB condensing activities were differentially modulated by phosphorylation [129]. In the presence of either malonyl-AcpM or C<sub>16</sub>-AcpM, the condensation activity of KasA was reduced, while KasB increased, upon phosphorylation. This was surprising given that *kasA* and *kasB* genes are adjacent on the same operon sharing the identical enzymatic activity, strong overall homology, and threonine residues phosphorylation profile *in vivo* [129]. In contrast, more recent findings from the same group have reported an opposite regulation behavior in *M.tb* strains whereby the phosphorylation of KasB at Thr334 and Thr336 located in the vicinity of catalytic triad profoundly decreases its condensing *in vitro* and *in vivo* [138]. This was further supported by observations from isogenic strains of *M.tb* with *kasB* phosphomimetic allele (*T334D/T336D*), *kasB* phosphoablative allele (*T334A/T336A*) and deleted *kasB* gene allele ( $\Delta kasB$ ). Both the phosphomimetic and  $\Delta kasB$  mutant strains produced shorter MAs by 4-6 carbons and lacked trans-cyclopropanation compared to the parental strains. Moreover, both the phosphomimetic and deletion alleles displayed a complete loss of acid-fastness in contrast to the phosphoablative counterparts and parent strains. Importantly, considering the pathogenicity of these strains, KasB phosphomimetic mutant was less virulent and exhibited higher susceptibility to first line anti-TB drugs (INH, ETH and RIF) than the other KasB variants. KasB phosphomimetic mutant also showed severely attenuated growth in both immunodeficient and immunocompetent mice, and failed to affect latent infection, pathophysiological symptoms and mortality in the mice [138]. In line with this observation,



previous work reported that the deletion of *kasB* in *M.tb* ( $\Delta kasB$ ) has led to the loss of acid fastness and longtime persistence in a non-replicating state while failing to produce active infection in immunocompetent mice, the two characteristic features of the *Tubercle bacillus* [45]. Therefore, phosphorylation of KasB represents an interesting mechanism by which *M.tb* regulates these two phenotypes. The long-term persistence of both phosphorylated-KasB and  $\Delta kasB$  *M.tb* strains without causing active disease or mortality might help to understand the mechanism by which *M.tb* enter dormancy and the triggering factors for TB reactivation. In addition, phosphorylation of KasB in *M. bovis* BCG occurred in higher levels in non-replicating bacteria (stationary culture) than in replicating cultures, suggesting a mechanism by which mycobacteria switches on/off MA biosynthesis to assist its survival in human host [138].

#### 4.7. PcaA and MmaA4

Cyclopropane synthase A (PcaA) and MmaA4 are amongst the enzymes involved in the functional modifications of MAs. PcaA, encoded by *pcaA* gene, was identified by previous studies to be required for MAs cyclopropanation in *M.tb* which, in turn, regulates mycobacterial pathogenesis [155]. The inactivated *pcaA* mutants displayed less virulence, less severe granulomatous pathology in mice, and the inability to intertwist into serpentine rope-like structure/cording morphology that is a distinctive feature of pathogenic mycobacteria [155]. Several STPKs were reported to phosphorylate PcaA, but not MmaA2, at Thr-168 and Thr-183 both *in vitro* and in mycobacteria [124]. Consistent with the strategic structural localisation of these two phosphoacceptors, PcaA phosphorylation was associated with a significant decrease in the methyltransferase activity [124]. In contrast to the wild-type *M. bovis* BCG strain and phosphoablative *pcaA* (*T168A/T183A*), both the phosphomimetic *pcaA* (*T168D/T183D*) alleles and  $\Delta pcaA$  mutant featured the following: (i) a significant alteration in MAs profile due to the lack of di-cyclopropanated  $\alpha$ -MA, (ii) inability to form serpentine cords and altered colony morphology, (iii) growth defects, (iv) reduced intramacrophage replication and survival, (v) inability to prevent phagosome maturation and fusion with lysosome [124]. These studies confirmed the crucial role of PcaA and its phosphorylation in the physiology and virulence of mycobacteria through modulating the composition of MAs and phagosome maturation block (PMB) [124, 155]. This, in turn, allows the bacilli to reside in a non-matured phagosome that no longer fuse with lysosomes, underpinning the mycobacterial survival from the cytolytic environment, thus establishing a chronic and lethal infection [156, 157]. On the other hand, mycolic acid methyl transferase (MmaA4/Hma) was found to be phosphorylated *in vitro* by PknJ, yet the effect of this phosphorylation on mycobacterial survival and virulence have not been investigated [125].

#### 4.8. FadD32

FadD32, an adenylating enzyme, belongs to a specific subclass of the FadD (fatty acid degradation) enzymes family establishing the connection between FASs and PKSs [56]. The Fatty acyl-AMP ligase 32 (FAAL32 or FadD32) displays two functions: activating the meromycolate chain

through the formation of fatty acyl-adenylate and channeling this acyl chain onto N-ACP domain of its partner Pks13 [58-60]. A recent study revealed the phosphorylation of MtbFadD32 by multiple mycobacterial STPKs *in vitro* on Thr-552 as a phosphosite. Native, phosphoablative and phosphomimetic FadD32 confirmed the position and the necessity of this residue in negatively regulating FadD32 activity [104]. The co-expression of FadD32 and PknB (FadD32-P) significantly decreased FAAL activity compared to solely expressing FadD32 in E-coli. This impaired activity of FadD32 was recovered when FadD32-P was dephosphorylated by incubation with PstP. Moreover, the native *M.tb* FadD32 protein was phosphorylated when expressed in *M. smegmatis* surrogate host (FadD32\_myc) and showed also a significant and reproducible loss of FAAL activity similar to FadD32-P [104]. This attenuation of activity was again reversed by PstP. Importantly, a decrease in both FadD32 acyl-AMP loading activity on Pks13 and formation of the condensation products were observed in the presence of phosphorylated FadD32\_myc isoform. These results emphasise that both FadD32 acyl-AMP ligase and transferase of meromycolic acid onto Pks13 enzymatic activities are impaired by phosphorylation, leading to a reduction in the entire MAs condensation activity of Pks13 [104].

#### 4.9. VirS

VirS is a transcriptional activator encoded by *virS* gene located divergently from the *mymA* (mycobacterial monooxygenase) operon that regulates its expression [133]. The seven cistrons encoded by the *mymA* operon produce proteins that are involved in the MAs biosynthesis, thus maintaining cell wall integrity [133]. This was further supported when the induction of the wild-type *M.tb*'s *mymA* operon was found to be upregulated in acidic pH, suggesting the significance of the encoded proteins in the pathogen's survival in severely acidic mediums of activated macrophages [133]. Since the transcription of *mymA* operon was shown to be dependent on VirS, disruption of *virS* and *mymA* genes was found to impair the ability of *M.tb* to survive in activated macrophages, but not resting macrophages, implying the role of *mymA* operon in protecting the bacilli against harsher conditions [133, 158]. Interestingly, *pknK* gene encoding for PknK is located in the vicinity of *virS* gene revealing that VirS is the *bona fide* substrate of PknK *in vivo* [127]. Co-expression of VirS and PknK increased its affinity for *mym* promoter DNA, thereby the transcription from *mym* operon under physiological conditions. In addition to VirS, PknK also mediated the phosphorylation of four *mymA* operon-encoded proteins (Mym, LipR, Rv3085, and Rv3088). This indeed further demonstrates the multifaceted complexity of STPKs through phosphorylation of transcriptional regulator and its target genes [127].

### 5. SMALL-MOLECULE INHIBITORS OF THE KINASES/PHOSPHATASES IN MYCOLIC ACID BIOSYNTHESIS

Because of the critical role of human kinases and phosphatases in cell signaling that is dysregulated in diseases such as cancer, many small molecule inhibitors of these enzymes have been developed as potential novel therapeutics [159-165]. The *M.tb* survival and pathogenesis rely largely

upon the critical role of mycobacterial kinases and phosphatases in regulating both their own signaling pathways as well as host signaling networks *via* modulating key processes for *M.tb* viability and virulence as well as cell division and cell wall formation [84, 166]. Hence, there have been literature reports towards the design and development of small molecule inhibitors of STPKs and protein phosphatases that may pave the way to the discovery of new anti-tubercular drugs. This is further supported by the wealth of expertise in targeting human Ser/Thr and Tyr kinases [159-165]. Although a total 11 STPKs have been identified in *M.tb* by genome sequencing, only PknA, PknB and PknG are required for growth *in vitro* and *in vivo* [141, 154, 167-172]. In contrast, none of the other STPKs and PstP appears to be essential for growth *in vitro*; they have more regulatory roles in controlling infection and disease progression *via*, for instance, subverting the host immune response and enabling the bacteria to create permissive niches for their survival [166, 167]. However, MPtpA and MPtpB have been shown to play a crucial role in *M.tb* growth, virulence and survival within animal models of infection and/or in host macrophage cell cultures [110, 116, 171].

PknH; however, is involved in phosphorylating and regulating the activity of the EmbR protein which is a putative transcriptional regulator of the EmbCAB arabinoyltransferases [131]. Activation of EmbR with PknH mediated phosphorylation induces the transcription of *embCAB* operon which encodes for proteins required for arabinosylation of lipoarabinomannan and arabinogalactan [173]. This ultimately leads to a higher lipoarabinomannan/lipomannan ratio, the major cell wall associated lipoglycans, which are important modulators of the immune system [132, 174]. In addition, PknH regulates the synthesis of arabinan, a crucial component of arabinogalactan which is essential for the structural integrity of the cell wall [175]. PknF shows effects on cell division, morphology, glucose transport, and growth rate [176]. PknI is involved in retarding the multiplication of bacteria inside the macrophages [177]. PknJ is responsible for phosphorylating the glycolytic enzyme pyruvate kinase A of *M.tb*; hence regulating the basic fundamental glycolysis pathway [178]. PknK is implicated in mycobacterial growth regulation, immune system modulation (phagocytosis) and the intracellular survival of avirulent mycobacteria [146, 147]. These critical roles of kinases spurred great interest in exploiting the indispensable kinases and phosphatases cunningly used by *M.tb* for its survival as novel drug targets to promote the mycobacterial clearance.

### 5.1. STPKs Inhibitors

Since MAs are essential lipids in *M.tb* virulence and survival, modulating the activity of kinases and phosphatases involved in the regulation of MAs biosynthesis with small molecules might open new perspectives for future anti-TB drug development. Among the mycobacterial STPKs, at least PknA, PknB, and PknG were found to be essential for the mycobacterial growth *in vitro* and survival in the host [141, 154, 167-172]. Both PknA and PknB participate in maintaining cell wall integrity *via* controlling cell morphology, cell wall synthesis, and cell division [141, 154, 167, 169]. The two STPKs PknA and PknB are encoded by adjacent genes

on the same operon together with *pstP* gene and two other proteins implicated in cell wall synthesis and cell shape control [141]. PknB expression predominantly takes place during exponential growth and was found to regulate an oxygen-dependent replication switch [179]. PknG gained much interest as its structure contains an inhibitor-binding pocket which is totally divergent from any human kinase [180]. Additionally, both PknB and PknG are implicated in phosphorylating a protein involved in the regulation of glutamate metabolism, suggesting that inhibition of one or both of them would impact the ability of *M.tb* to regulate this crucial metabolic process [143, 168, 181, 182]. Hence, there has been much interest over the last few years in developing novel kinase inhibitors, especially focused on PknA, PknB, and PknG, as anti-TB drugs. Magnet *et al.* screened a kinase inhibitor library using both whole cell-based assay and target-based assay in which four compounds were identified as inhibitors of PknA with compound **1** (Fig. 3) being the most potent inhibitor exhibiting 86% inhibition against PknA at 100  $\mu\text{M}$  [183]. Several inhibitors targeting PknB or PknG have  $\text{IC}_{50}$  values in the micromolar or even in the nanomolar range [171, 184-188]. For instance, Kéri group identified several potent hit compounds in which the pyridopyrimidine derivative (VI-17494, **2**, Fig. 3) was the most interesting compound, showing good inhibitory activity on PknB and PknG with  $\text{IC}_{50}$  values of 0.129 and 3  $\mu\text{M}$ , respectively [186, 189, 190]. The same group have identified VI-16315 (**3**) as a promising compound since it inhibits both PknG ( $\text{IC}_{50}$  = 0.01  $\mu\text{M}$ ) and *M.tb* NAD synthetase ( $\text{IC}_{50}$  = 55  $\mu\text{M}$ ) and exhibits no significant cellular toxicity in human cells [186, 189, 190]. Moreover, compound **4** (Fig. 3) showed the most potent inhibitory activity against PknB *in vitro* with  $\text{IC}_{50}$  value of 0.023  $\mu\text{M}$  in two studies conducted by another group who investigated the PknB inhibitory activity using several aminopyrimidine derivatives [184, 185]. In addition, the tetrahydrobenzothiophenes, which is an ATP-competitive inhibitor (AX20017, **5**, Fig. 3), was identified as a potent PknG hit compound displaying an  $\text{IC}_{50}$  value of 0.39  $\mu\text{M}$  [171, 180]. Compound **5** also inhibited the growth of *M. bovis* BCG and *M.tb* in macrophages in a dose dependent manner phenocopying the deletion of *pknG* gene [171]. In addition, Anand *et al.* investigated the activity of several triazolymethoxy derivatives in which the most potent PknG inhibitor is a triazolymethoxy aminopyrimidine **6** (Fig. 3), exhibiting 53% inhibition against PknG at 100  $\mu\text{M}$  concentration [188].

Interestingly, a common finding in these studies is the poor minimum inhibitory concentration (MIC) exhibited by the tested compounds against the whole *M.tb* cells in cultures, indicating their lack of bactericidal activity [171, 183-188]. The reasons for low whole cell activities (MICs) and *in vivo* inhibition of PknB ( $\text{IC}_{50}$ s) against the intact pathogen include: (i) poor cell permeability; (ii) possible functional redundancy among kinases; (iii) cross-reactivity of the inhibitors against other proteins or kinases; (iv) the role of efflux pumps [184, 185]. Although PknG may not be essential for *M.tb* growth *in vitro* [171], this still needs to be confirmed as the PknG knockout strain of *M.tb* displayed attenuated *in vitro* growth and reduced virulence, implying that PknG plays an important role in the growing *M.tb* strains in

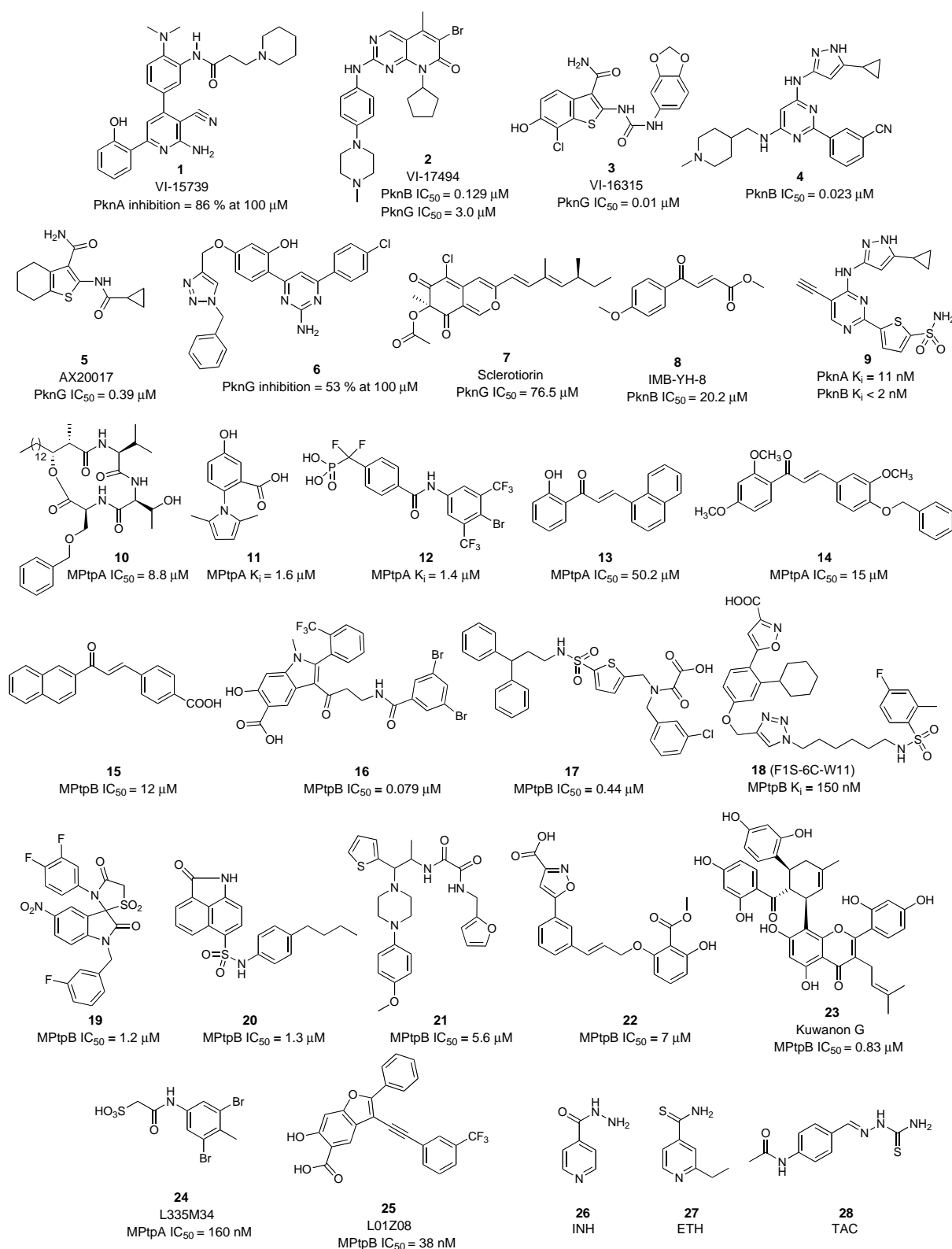


**Fig. (3).** Structures of some selected kinase and phosphatase inhibitors with their reported activity towards their target, in addition to the approved drugs that target MAs biosynthesis machinery, isoniazid (INH), ethionamide (ETH) and thioacetazone (TAC).

culture in the absence of eukaryotic host cells [168]. Chen *et al.* found that sclerotiorin (**7**, Fig. 3) which is derived from marine fungi, exhibited an inhibitory effect on PknG. Sclerotiorin also inhibited the growth of *M. bovis* BCG in murine

macrophages in a dose-dependent manner without affecting the macrophage viability in which the bacterial load is reduced by 81% at 80  $\mu$ M concentration [187]. Moreover, they found that a combination of 0.03  $\mu$ M rifampicin with 40  $\mu$ M

sclerotiorin decreased the bacterial burden within macrophages by 84%, similar to the effect of 0.06  $\mu\text{M}$  rifampicin alone [187].

Recently, Xu *et al.* investigated the role of PknB in sustaining the *M.tb* growth by targeting it with IMB-YH-8 (8, Fig. 3), a compound which showed an inhibitory activity against PknB *in vitro* [191]. Surprisingly, this compound suppressed the growth of drug-sensitive and drug-resistant *M.tb* strains *in vitro* (MIC = 0.25 to 1  $\mu\text{g}/\text{mL}$ ) and inhibited the growth of *M.tb* in human THP-1 macrophages in a dose dependent manner compared to the untreated control cells. Importantly, due to PknB inhibition, IMB-YH-8 deformed the cell wall of *M.tb* after five days incubation at 1  $\mu\text{g}/\text{mL}$  as compared to untreated cells which showed rod-like shape and a smooth cell surface [191]. Similar observations were reported for *pknB* gene depletion or overexpression which resulted in gross morphological changes and also when *M.tb* treated with compounds targeting MAs, such as INH [13, 169]. Despite the promising activities of both sclerotiorin and IMB-YH-8, and their moderate inhibitory activity towards PknG (IC<sub>50</sub> = 76.5  $\mu\text{M}$ ) and PknB (IC<sub>50</sub>=20.2  $\mu\text{M}$ ), respectively, the efficacies of these compounds may still be due to off-target effects on other *M.tb* enzymes [187, 191]. In a recent study, Wang *et al.* screened several compounds as dual PknA and PknB inhibitors with compound 9 (PknA K<sub>i</sub> = 11 nM and PknB K<sub>i</sub> < 2 nM) being the most potent inhibitor displaying MIC value of 4.7  $\mu\text{M}$  against *M.tb* [192].

## 5.2. MPtpA Inhibitors

While MPtpA specifically dephosphorylates tyrosine residues, MPtpB has triple specificity dephosphorylating Ser/Thr and Tyr residues as well as phosphoinositides, suggesting wider signaling network [111, 114, 193]. MPtpA blocks phagosome-lysosome fusion, whereas MPtpB subverts host immune response to infection [109, 110, 116, 120]. Since both MPtpA and MPtpB knockout strains of *M.tb* exhibited severely reduced growth and survival in tested macrophages, inhibition of MPtpA and MPtpB emerges as a highly promising new approach for TB therapy [109, 110, 116, 162]. Importantly, MPtpA structure possesses 37% sequence identity with its human ortholog and a high structural similarity with other mammalian phosphatases, so targeting MPtpA with highly selective inhibitors might be difficult [166]. By contrast, while the phosphatase active site signature sequence is still conserved in MPtpB, it does not have a human ortholog with only 6% similarity with human PTP1B and a distinct structural fold, making it an attractive target for inhibitors because of the minimal side effects on the host [166]. Several groups have identified inhibitors against MPtpA and/or MPtpB having IC<sub>50</sub> values in the low micromolar range; however, some of these compounds exhibited significant activity against one or more human phosphatases [194-205].

Manger *et al.* were the pioneers in identifying MPtpA inhibitors in which the most potent natural compound (10, Fig. 3) tested exhibited IC<sub>50</sub> value of 8.8  $\mu\text{M}$  [198]. In addition, they identified several pyrrol benzoic acid derivatives as potent MPtpA inhibitors with compound 11 (Fig. 3) being the most potent inhibitor with K<sub>i</sub> value of 1.6  $\mu\text{M}$ ; however, these compounds inhibited the human phosphatase PTP1B as

well [198]. Compound 12 (Fig. 3) was identified as the most potent MPtpA inhibitor (K<sub>i</sub> = 1.4  $\mu\text{M}$ ) in a group of aryl difluoromethylphosphonic acid (DFMP) [201]. This compound showed high selectivity against MPtpA compared to the human phosphatases tested [201]. Several chalcones were characterised as MPtpA inhibitors with IC<sub>50</sub> values of 8.4-53.7  $\mu\text{M}$  and the activities of these compounds were elaborated on in another study correlating *in vitro* inhibition of MPtpA and *in vivo* inhibition of mycobacterial survival in human macrophages [195, 206]. The most promising MPtpA inhibitor (13, Fig. 3) exhibited an IC<sub>50</sub> value of 50.2  $\mu\text{M}$  with no toxicity against THP-1 human macrophage and importantly it reduced the bacillary load by 77% at 96 hours post-infection [206]. In a recent study, two chalcones (14 and 15, Fig. 3) showed both promising high inhibitory activity against MPtpA (IC<sub>50</sub> = 15  $\mu\text{M}$ ) and MPtpB (IC<sub>50</sub> = 12  $\mu\text{M}$ ), respectively, as well as selectivity against human PTP1B [194].

Several indole derivatives were developed as MPtpB inhibitors over four studies with compound 16 (Fig. 3) being the most potent inhibitor (IC<sub>50</sub> = 0.079  $\mu\text{M}$ ) [196, 199, 200, 205]. Grunder *et al.* identified compound 17 (Fig. 3) as potent MPtpB inhibitor (IC<sub>50</sub> = 0.44  $\mu\text{M}$ ) with >60 fold specificity towards MPtpB compared to the tested human phosphatases [197]. F1S-6C-W11 (18, Fig. 3) was reported to be the most potent MPtpB isooxazole inhibitor (K<sub>i</sub> = 150 nM) exhibiting as well a good selectivity against a panel of human phosphatases [202, 203]. Vintonyak *et al.* developed several indolin-2-on-3-spirothiazolidinones with compound 19 being the most promising compound in terms of MPtpB inhibition (IC<sub>50</sub> = 1.2  $\mu\text{M}$ ) and showing no activity against other human phosphatases [204]. Chen *et al.* identified two potent MPtpB inhibitors, namely compound 20 (Fig. 3) which is a benzindole derivative (IC<sub>50</sub> = 1.3  $\mu\text{M}$ ), and compound 21 (Fig. 3) which is a piperazinyl-thiophenyl-ethyl-oxalamide derivative (IC<sub>50</sub> = 5.6  $\mu\text{M}$ ) [207]. Additionally, compounds 20 and 21 exhibited almost complete blockage of the intracellular *M.tb* growth in mouse macrophage cell lines [207]. These promising results recapitulated the phenotype of *MptpB* gene deletion which is presumably due to reversing the perturbation of host immune responses induced by MPtpB [116]. Beresford *et al.* developed another potent MPtpB inhibitor which is an isooxazole-salicylate derivative (22, Fig. 3) showing an IC<sub>50</sub> value of 7  $\mu\text{M}$  [208]. In addition, compound 22 also decreased the bacterial burden of *M. bovis* BCG in macrophages in a dose-dependent manner causing >90% reduction at 160  $\mu\text{M}$  [208]. Recently, Mascarello *et al.* investigated the activity of some natural products against MPtpB with Kuwanon G (23, Fig. 3), as the most effective inhibitor having an IC<sub>50</sub> value of 0.83  $\mu\text{M}$ , MIC value of 32  $\mu\text{g}/\text{ml}$  and 61% *M.tb* growth inhibition in THP-1 human macrophage [209]. Dutta *et al.* developed an  $\alpha$ -sulfophenylacetic amide (L335M34, 24) and a benzofuran-salicylate derivative (L01Z08, 25) as two highly potent MPtpA (L335M34) and MPtpB (L01Z08) selective inhibitors, respectively (Fig. 3) [210]. Compounds 24 and 25 displayed IC<sub>50</sub> values of 160 and 38 nM against MPtpA and MPtpB, respectively. Both compounds significantly decreased the bacterial load in *M.tb* infected mouse macrophage and exhibited favorable pharmacokinetics and high selectivity against a panel of human phosphatases [210]. It is

also noteworthy that the potency of compound **25** (L01Z08) far exceeded the potency of the previously reported benzofuran-salicylate derivative with  $IC_{50}$  value at 1.26  $\mu$ M [109]. Interestingly, since each MPtp modulates distinct *M.tb* clearance mechanisms, they found that upon combining either L335M34 or L01Z08 with the standard anti-TB regimen, INH, RIF, and PZA (HRZ), no significant enhancement of bactericidal activity against drug susceptible TB in guinea pigs was observed. In contrast, a combination of HRZ, L335M34, and L01Z08 showed modest synergy with markedly reduced guinea pig lung bacillary burden and improved lung histopathology relative to HRZ alone [210]. Importantly, none of the tested MPtps inhibitors in these studies affected the growth of *M.tb* *in vitro*; they were devoid of activity in the standard MIC assay [109, 206-208, 210]. This suggests the importance of targeting secreted virulence factors such as MPtps in TB treatment rather than *in vitro* growth readout [106-108].

Classical antibiotics possess bactericidal activity against *M.tb* *in vitro* via targeting the intra-bacterial functions such as proteins involved in MAs biosynthetic machinery which are the target of INH (26), Ethionamide (ETH, 27) and thioacetazone (TAC, 28) (Fig. 3) [150]. By contrast, both MPtps are dispensable for *in vitro* growth as they are secretory proteins in the host macrophage's cytosol [106-108]. Hence, several advantages would arise from inhibiting these phosphatases: (i) potentially offsetting the major impediment in developing anti-TB drugs which target proteins in *M.tb* cytoplasm as MPtps inhibitors do not need to be delivered across the poorly permeable mycobacterial cell envelope, (ii) restoration of the host macrophage signaling networks and rebooting host defense mechanisms; therefore enhancing the ability of innate immune response to eradicate the infection. Importantly, using a combination of current anti-TB drugs and MPtps inhibitors may speed up the treatment *via* combating both active and latent TB infection by subduing *M.tb* survival in macrophages' intracellular reservoirs; a hypothesis which was partially supported by Dutta *et al*'s study [210].

## 6. FORMULATION OF ANTI-TUBERCULAR AGENTS TARGETING MYCOLIC ACID BIOSYNTHESIS – A BRIEF SURVEY

Several existing anti-tubercular drugs have been demonstrated to inhibit the mycolic acid biosynthesis of *M.tb*, namely isoniazid, ethambutol, ethionamide, and thiacetazone. Formulations encapsulating these anti-TB drugs in polymeric or similar micro/nano-particles have been under research to control the dissolution rate of drugs, particularly for orally administered drugs. The main objectives of incorporating the drugs in various drug carriers and excipients are: (1) to effectively deliver the drugs to the targeted site, and (2) to prolong the duration of drug efficacy in the body by increasing the circulation time of the drug carriers with drug concentration above the MIC. It is essential to have a high local concentration of these drugs to eliminate *M.tb*, while having a low systemic exposure to decrease the occurrence of drug resistance and toxicity. Formulations generally involve various drug carriers and excipients as controlled-release systems for targeted drug delivery. Drug formulations ensure precise dosage of the drugs used by incorporat-

ing the necessary amount of drugs that are to be released at the targeted site. Therefore, incorrect use of drug dosage intake can be avoided, as well as the adverse effects such as gastrointestinal intolerance that results in hepatotoxicity, vomiting, anorexia, and nausea. The therapeutic effect of the drugs can be enhanced at the targeted site by controlled-released drug delivery systems.

The key elements to produce stable and efficient formulations for the treatment of tuberculosis include the use of excipients to control the adhesion forces between the particles; a considerable drug amount to be loaded and delivered to the lung for local efficacy; and the minimal use of adjuvants to prevent overloading of foreign materials to the lungs [211]. The formulations that have been used in targeting the mycolic acid biosynthesis inhibition in recent years have been summarised in Table 2. The survey was conducted based on their availability for *in vivo* studies. The information of the drug encapsulating carrier materials, encapsulation efficiencies, cell types, and mice efficacy in mice have been tabulated. Thus far, there has not been any *in vivo* study conducted for a formulation of encapsulated thiacetazone.

## CONCLUDING REMARKS AND FUTURE DIRECTIONS

(i) The ability of *M.tb* to modulate the activity of MAs biosynthetic enzymes is one of most intriguing and challenging facets of *M.tb* in which the regulation occurs at a transcriptional level and/or by PTM leading to cell envelope structure/composition modulation [104, 124-130, 134-138].

Therefore, it is hoped that future studies can identify (i) the extracellular cues sensed by the different kinases which result in protein phosphorylation, and (ii) define each substrate/kinase/phosphatase-mediated signaling events which orchestrate adaptive responses to ensure mycobacterial survival. For example, an interesting study reported that in response to glucose inside mammalian host cells, GMM is upregulated in *Mycobacterium avium* on the expense of TDM [227]. This reciprocal regulation and switch from TDM to GMM result from glucose and trehalose substrates competitive selection by AG85A enzyme [227]. These interesting findings represent a significant milestone in understanding the type of environmental stimuli used by *M.tb* for dynamic alteration of cell wall composition. This would also suggest that Ag85A enzyme is a substrate itself to mycobacterial kinases; hence, its phosphorylation may control both the rate and type of glycolipids (glycolipid remodelling) that would possibly constitute the OM. This hypothesis remains to be tested.

(ii) After being released from Pks13, the  $\alpha$ -alkyl  $\beta$ -ketoacyl chain is transferred onto trehalose before being reduced by CmrA to form TMM [58]. *M.tb* was reported to possess three pathways for the synthesis of trehalose [228]. Of particular interest, one of these pathways incorporates trehalose-6-phosphate synthase (OtsA) which catalyses the condensation of glucose 6-phosphate with UDP-glucose to yield trehalose 6-phosphate which is further dephosphorylated by trehalose-6-phosphate phosphatase (OtsB) affording free trehalose [229]. Hence, whether OtsA activity is regulated by *M.tb* kinases and/or phosphatases is yet to be identified.

Table 2. Selected formulations of drugs that inhibit mycolic acid biosynthesis (2011-2018).

| Drug            | Carrier Materials  | Drug Encapsulation % | Cell Study   | <i>In vivo</i> Efficacy   | Note  | Refs. |
|-----------------|--|----------------------|--|---|---|-------|
| Isoniazid (INH) | Chitosan; Sodium alginate; Allylamine; Mannose                                     | 95.58                | THP-1, A549, VERO, HeLa  | -   | INH-loaded micelles had higher inhibitory effect on the bacterial growth than free INH alone  | [212] |
|                 | Lipoid S-75 with 70% phosphatidyl choline; Tween 80; Poloxamer-188; Squalene (SQL) | 71-74                | THP-1  | -   | Lipid nano-formulations were easily engulfed by the human macrophages (for targeted delivery to the intracellular parasite <i>M. tuberculosis</i> ) | [213] |
|                 | Chitosan (50-190 kDa)  | >89                  | J-774.1, AMJ2-C11  | -   | Significant toxicity reduction against peritoneal macrophages; no toxic effect on alveolar macrophages  | [214] |
|                 | Titanium; Alginate; Polydopamine; PEG; PLGA  | 43.8                 | -  | (Rabbit) INH's level remained above its effective MIC (10 µg/mL) @ week 8.  | Continuous release of INH from the Ti rods for 1 week <i>in vitro</i>   | [215] |
|                 | Soy Lecithin; DSPE-PEG 2000; Mannitol  | 64                   | J774A.1  | Male mice (6- 8 weeks old)<br>INH-loaded liposomes are detectable after 24 hr in the plasma, as compared to free INH (12 hr)            | Uptake efficiency of INH-loaded LPN was significantly higher than free INH  | [216] |
|                 | Sodium alginate; mannitol; l-leucine   | 76                   | J774.A1  | Female BALB/c mice (6-8 weeks age) Spray-dried particles showed lower cytotoxicity and good lung uptake up to 8 h.                      | -   | [217] |
|                 | Locust bean gum (polysaccharide with galactose and mannose residues)               | 89                   | A549; THP-1  | -   | INH-loaded microparticles were devoid of cytotoxicity towards A549 cells and THP-1 cells at doses up to 1 mg/mL and 24 h exposure time              | [218] |
|                 | CMC8; LAB; Cremophor® EL   | 94-97                | <i>M. smegmatis</i> cultures (MS-942 and MS-995); <i>M. tb</i>                       | Sprague-Dawley rats:<br>Improved oral absorption  | MIC values were 18.4 and 30.4 µg/ml for CMC8 and LAB against the <i>M. tuberculosis</i> H37 Rv, respectively.                                       | [219] |
|                 | Chitosan; guar gum; mannan; mannitol; leucine                                      | Not Reported         | J-774  | Female BALB/c mice infected with H37Rv strain:<br>ING-loaded microparticles had a prolonged residence time in the lung for at least 8 h | -   | [220] |
| Ethambutol      | Iron oxide magnetite; graphene oxide   | 33.8 (drug loading)  | <i>M. smegmatis</i> using Resazurin Microtiter Assay (REMA) and modified SPOTi assay | -   | Effective MIC 2.1 µg/mL   | [221] |

Table (2) contd....

| Drug              | Carrier Materials                                      | Drug Encapsulation % | Cell Study                               | <i>In vivo</i> Efficacy  | Note   | Refs. |
|-------------------|--|----------------------|--|--|--|-------|
| Ethambutol        | Span 60; Span 85; Cholesterol; DCP; SA                 | 26                   | -  | Swiss Albino mice of average weight 20 g; guinea pigs weighing 300–400 g   | The drug level in mice lungs was higher than that in the group receiving free ethambutol hydrochloride solution by 2.26 (negatively charged niosomes) and 4.47 times (neutral niosomes). These two formulations resulted in targeted, controlled drug release to mice lungs for a prolonged duration over the free ethambutol alone. | [222] |
|                   | Chitosan; L- $\alpha$ phosphatidylcholine; cholesterol | Not Reported         | A549, Calu-3; NR8383                     | -  | Ethambutol dihydrochloride (EDH) formulations showed enhanced MIC values (< 1 $\mu$ g/mL) compared to the free drug alone (MIC of 2 $\mu$ g/mL)  | [223] |
| Ethionamide (ETH) | PLGA; PLA; pCD; PVA (surfactant)                       | 77 $\pm$ 5           | H37Rv (H37Rv-GFP); RAW 267.4 macrophages | 6-week old Balb/C female mice  | The administration of ETH: Booster 3 times/week for 2 weeks via the endotracheal route resulted in a similar therapeutic response to the daily, 6 days/week oral administration of ETH for 3 weeks.  | [224] |
|                   | PLGA; PVA  | 89.0 $\pm$ 0.4       | -  | Wistar rats (4–6 months old & average weight 200–250gm) either sex;<br>A single dose administration of ETH by dry powder inhalation maintained ETH concentration above its MIC value for at least 12 h | -  | [225] |
|                   | PLGA; PVA  | 35.2 $\pm$ 3.1       | -  | Swiss albino mice, 18–22 g and both sexes;<br>ETH-loaded PLGA nanoparticles up to 130 mg/kg produced sustained release <i>in vivo</i> with minimally observed toxicity profile                         | -  | [226] |

## Acronyms:

CMC8: Glyceryl monocaprylate / Lipid Capmul MCM C8;

DCP: Dihexadecyl hydrogen-Phosphate (Dicetyl Phosphate, free acid crystalline);

DSPE-PEG 2000: 1, 2-distearoyl-sn-glycero-3-phosphoethanolamine-N-methoxy (Polyethylene-glycol)-2000);

LAB: Labrasol/Caprylocaproyl polyoxyl-8 glyceride;

Lipoid S-75: Fat-free soyabean phospholipid;

LPN: lipid-polymer hybrid nanoparticles;

pCD: Polymeric  $\beta$ -cyclodextrins;

PEG: Poly(ethylene glycol);

PLA: Poly lactic acid;

PLGA: Poly(lactic-co-glycolic acid);

PVA: Polyvinyl alcohol;

SA: Octadecylamine (Stearylamine);

Span 60: Sorbitan monostearate;

Span 85: Sorbitan trioleate.

(iii) MmpL7, an endogenous substrate of PknD, was found to play a crucial role in *M.tb* virulence, presumably by transporting virulence factors, such as phthiocerol dimycoserolate (PDIM) [230]. These findings suggest that the deposition of cell wall associated virulence factors could be regu-

lated by phosphorylating MmpL7. Of particular interest, MmpL3, the MAs transporter, whose mutations did not cause any cross resistance with current anti-TB drugs, might be a substrate of mycobacterial STPKs [231]. It is therefore tempting to speculate whether *M.tb* is regulating the activity

of MmpL3 via phosphorylation and dephosphorylation, and accordingly the rate by which TMM is transported into the mycobacterial cell wall. In addition, whether the other enzymes involved in MAs synthesis, namely, ACCases, CmaA1, CmaA2, UmaA1, MmaA1, MmaA2, MmaA3, CmrA and most importantly Pks13, are STPKs substrates and the effect of phosphorylation on their activities, are yet to be addressed.

(iv) The enzymatic activity of most MAs biosynthetic enzymes was found to be downregulated via phosphorylation, negatively impacting MAs biosynthesis and/or mycobacterial growth [104, 124, 126, 129, 130, 134-136, 138]. This may suggest that STPKs activators, such as bryostatins [232] may inhibit the mycobacterial growth. This is further supported by the inactivity of the reported STPKs inhibitors against intact TB despite their high inhibitory activity against the respective kinases *in vitro* [184-188]. Their deleted strains, however, *ApknA* and *ApknB* exhibited gross alterations in cell morphology with eventual cell death, while *ApknG* strains exhibited poor *in vitro* growth [154, 168, 169]. Moreover, the apparent lack of substrate specificity of the different kinases due to their overlapping activity *in vitro*, suggests that the activity of one protein could be regulated by multiple extracellular signals. While it remains unclear whether small molecule inhibition, or activation, of mycobacterial STPKs is a validated anti-TB therapeutic strategy, there has been a considerable body of evidence in the literature to support the intricate roles of STPKs in maintaining the bacteria survival and virulence.

## CONSENT FOR PUBLICATION

Not applicable.

## CONFLICT OF INTEREST

The authors declare no conflict of interest, financial or otherwise.

## ACKNOWLEDGEMENTS

HG is the recipient of an Australian Research Council Discovery Early Career Researcher Award (DE160100482) funded by the Australian Government.

## REFERENCES

- [1] WorldHealthOrganization, Global Tuberculosis Report 2017, Geneva. 2017.
- [2] Tiberi, S.; Scardigli, A.; Centis, R.; D'Ambrosio, L.; Munoz-Torrico, M.; Salazar-Lezama, M.A.; Spanevello, A.; Visca, D.; Zumla, A.; Migliori, G.B.; Caminero Luna, J.A. Classifying new anti-tuberculosis drugs: Rationale and future perspectives. *Int. J. Infect. Dis.*, **2017**, *56*, 181-184.
- [3] Al-Humadi, H.W.; Al-Saigh, R.J.; Al-Humadi, A.W. Addressing the challenges of tuberculosis: A brief historical account. *Front. Pharmacol.*, **2017**, *8*, 689, 10.3389/fphar.2017.00689.
- [4] Caminero, J.A.; World Health, O.; American Thoracic, S.; British Thoracic, S. Treatment of multidrug-resistant tuberculosis: Evidence and controversies. *Int. J. Tuberc. Lung Dis.*, **2006**, *10*(8), 829-837.
- [5] Chan, E.D.; Laurel, V.; Strand, M.J.; Chan, J.F.; Huynh, M.L.; Goble, M.; Iseman, M.D. Treatment and outcome analysis of 205 patients with multidrug-resistant tuberculosis. *Am. J. Respir. Crit. Care Med.*, **2004**, *169*(10), 1103-1109.
- [6] Eker, B.; Ortmann, J.; Migliori, G.B.; Sotgiu, G.; Muetterlein, R.; Centis, R.; Hoffmann, H.; Kirsten, D.; Schaberg, T.; Ruesch-Gerdes, S.; Lange, C.; German, T.G. Multidrug- and extensively drug-resistant tuberculosis, Germany. *Emerg. Infect. Dis.*, **2008**, *14*(11), 1700-1706.
- [7] Migliori, G.B.; Lodenkemper, R.; Blasi, F.; Raviglione, M.C. 125 years after Robert Koch's discovery of the *Tubercle bacillus*: The new XDR-TB threat. Is "science" enough to tackle the epidemic? *Eur. Respir. J.*, **2007**, *29*(3), 423-427.
- [8] Mitnick, C.D.; Shin, S.S.; Seung, K.J.; Rich, M.L.; Atwood, S.S.; Furin, J.J.; Fitzmaurice, G.M.; Alcantara Viru, F.A.; Appleton, S.C.; Bayona, J.N.; Bonilla, C.A.; Chalco, K.; Choi, S.; Franke, M.F.; Fraser, H.S.; Guerra, D.; Hurtado, R.M.; Jazayeri, D.; Joseph, K.; Llaro, K.; Mestanza, L.; Mukherjee, J.S.; Munoz, M.; Palacios, E.; Sanchez, E.; Sloutsky, A.; Becerra, M.C. Comprehensive treatment of extensively drug-resistant tuberculosis. *N. Engl. J. Med.*, **2008**, *359*(6), 563-574.
- [9] Velayati, A.A.; Farnia, P.; Masjedi, M.R. The totally drug resistant tuberculosis (TDR-TB). *Int. J. Clin. Exp. Med.*, **2013**, *6*(4), 307-309.
- [10] Sotgiu, G.; Centis, R.; D'Ambrosio, L.; Migliori, G.B. Tuberculosis treatment and drug regimens. *Cold Spring Harb. Perspect. Med.*, **2015**, *5*(5), a017822.
- [11] Cole, S.T.; Brosch, R.; Parkhill, J.; Garnier, T.; Churcher, C.; Harris, D.; Gordon, S.V.; Eiglmeier, K.; Gas, S.; Barry, C.E., 3rd; Tekaiia, F.; Badcock, K.; Basham, D.; Brown, D.; Chillingworth, T.; Connor, R.; Davies, R.; Devlin, K.; Feltwell, T.; Gentles, S.; Hamlin, N.; Holroyd, S.; Hornsby, T.; Jagels, K.; Krogh, A.; McLean, J.; Moule, S.; Murphy, L.; Oliver, K.; Osborne, J.; Quail, M.A.; Rajandream, M.A.; Rogers, J.; Rutter, S.; Seeger, K.; Skelton, J.; Squares, R.; Squares, S.; Sulston, J.E.; Taylor, K.; Whitehead, S.; Barrell, B.G. Deciphering the biology of *Mycobacterium tuberculosis* from the complete genome sequence. *Nature*, **1998**, *393*(6685), 537-544.
- [12] Takayama, K.; Wang, C.; Besra, G.S. Pathway to synthesis and processing of mycolic acids in *Mycobacterium tuberculosis*. *Clin. Microbiol. Rev.*, **2005**, *18*(1), 81-101.
- [13] Takayama, K.; Wang, L.; David, H.L. Effect of isoniazid on the *in vivo* mycolic acid synthesis, cell growth, and viability of *Mycobacterium tuberculosis*. *Antimicrob. Agents Chemother.*, **1972**, *2*(1), 29-35.
- [14] Molle, V.; Kremer, L. Division and cell envelope regulation by Ser/Thr phosphorylation: *Mycobacterium* shows the way. *Mol. Microbiol.*, **2010**, *75*(5), 1064-1077.
- [15] Daffe, M.; Crick, D.C.; Jackson, M. Genetics of *Capsular Polysaccharides* and Cell Envelope (Glyco)lipids. *Microbiol. Spectr.*, **2014**, *2*(4), MGM2-0021-2013.
- [16] Jackson, M.; Stadthagen, G.; Gicquel, B. Long-chain multiple methyl-branched fatty acid-containing lipids of *Mycobacterium tuberculosis*: Biosynthesis, transport, regulation and biological activities. *Tuberculosis (Edinb)*, **2007**, *87*(2), 78-86.
- [17] Nataraj, V.; Varela, C.; Javid, A.; Singh, A.; Besra, G.S.; Bhatt, A. Mycolic acids: Deciphering and targeting the Achilles' heel of the *Tubercle bacillus*. *Mol. Microbiol.*, **2015**, *98*(1), 7-16.
- [18] Lederer, E.; Adam, A.; Ciorbaru, R.; Petit, J.F.; Wietzerbin, J. Cell walls of *Mycobacteria* and related organisms; Chemistry and immunostimulant properties. *Mol. Cell. Biochem.*, **1975**, *7*(2), 87-104.
- [19] Brennan, P.J.; Nikaido, H. The envelope of mycobacteria. *Annu. Rev. Biochem.*, **1995**, *64*, 29-63.
- [20] Misaki, A.; Seto, N.; Azuma, I. Structure and immunological properties of D-arabino-D-galactans isolated from cell walls of *Mycobacterium* species. *J. Biochem.*, **1974**, *76*(1), 15-27.
- [21] Azuma, I.; Yamamura, Y. Studies on the firmly bound lipids of human *Tubercle bacillus*. *J. Biochem.*, **1963**, *53*, 275-281.
- [22] Daffe, M.; Draper, P. The envelope layers of mycobacteria with reference to their pathogenicity. *Adv. Microb. Physiol.*, **1998**, *39*, 131-203.
- [23] Hattori, Y.; Matsunaga, I.; Komori, T.; Urakawa, T.; Nakamura, T.; Fujiwara, N.; Hiromatsu, K.; Harashima, H.; Sugita, M. Glycerol monomycolate, a latent tuberculosis-associated mycobacterial lipid, induces eosinophilic hypersensitivity responses in guinea pigs. *Biochem. Biophys. Res. Commun.*, **2011**, *409*(2), 304-307.
- [24] McNeil, M.R.; Brennan, P.J. Structure, function and biogenesis of the cell envelope of mycobacteria in relation to bacterial physiology, pathogenesis and drug resistance; Some thoughts and possibilities arising from recent structural information. *Res. Microbiol.*, **1991**, *142*(4), 451-463.



- [25] Roura-Mir, C.; Wang, L.; Cheng, T.Y.; Matsunaga, I.; Dascher, C.C.; Peng, S.L.; Fenton, M.J.; Kirschning, C.; Moody, D.B. *Mycobacterium tuberculosis* regulates CD1 antigen presentation pathways through TLR-2. *J. Immunol.*, **2005**, *175*(3), 1758-1766.
- [26] Geisel, R.E.; Sakamoto, K.; Russell, D.G.; Rhoades, E.R. *In vivo* activity of released cell wall lipids of *Mycobacterium bovis* bacillus Calmette-Guerin is due principally to trehalose mycolates. *J. Immunol.*, **2005**, *174*(8), 5007-5015.
- [27] Layre, E.; Collmann, A.; Bastian, M.; Mariotti, S.; Czaplicki, J.; Prandi, J.; Mori, L.; Stenger, S.; De Libero, G.; Puzo, G.; Gilleron, M. Mycolic acids constitute a scaffold for mycobacterial lipid antigens stimulating CD1-restricted T cells. *Chem. Biol.*, **2009**, *16*(1), 82-92.
- [28] Moody, D.B.; Briken, V.; Cheng, T.Y.; Roura-Mir, C.; Guy, M.R.; Geho, D.H.; Tykocinski, M.L.; Besra, G.S.; Porcelli, S.A. Lipid length controls antigen entry into endosomal and nonendosomal pathways for CD1b presentation. *Nat. Immunol.*, **2002**, *3*(5), 435-442.
- [29] Hunter, R.L.; Venkataprasad, N.; Olsen, M.R. The role of trehalose dimycolate (cord factor) on morphology of virulent *M. tuberculosis* *in vitro*. *Tuberculosis (Edinb)*, **2006**, *86*(5), 349-356.
- [30] Hunter, R.L.; Olsen, M.; Jagannath, C.; Actor, J.K. Trehalose 6,6'-dimycolate and lipid in the pathogenesis of caseating granulomas of tuberculosis in mice. *Am. J. Pathol.*, **2006**, *168*(4), 1249-1261.
- [31] Marrakchi, H.; Laneelle, M.A.; Daffe, M. Mycolic acids: Structures, biosynthesis, and beyond. *Chem. Biol.*, **2014**, *21*(1), 67-85.
- [32] Raman, K.; Rajagopalan, P.; Chandra, N. Flux balance analysis of mycolic acid pathway: Targets for anti-tubercular drugs. *PLoS Comput. Biol.*, **2005**, *1*(5), e46.
- [33] Barry, C.E., 3rd; Lee, R.E.; Mdluli, K.; Sampson, A.E.; Schroeder, B.G.; Slayden, R.A.; Yuan, Y. Mycolic acids: Structure, biosynthesis and physiological functions. *Prog. Lipid Res.*, **1998**, *37*, (2-3), 143-179.
- [34] Bhatt, A.; Molle, V.; Besra, G.S.; Jacobs, W.R., Jr.; Kremer, L. The *Mycobacterium tuberculosis* FAS-II condensing enzymes: Their role in mycolic acid biosynthesis, acid-fastness, pathogenesis and in future drug development. *Mol. Microbiol.*, **2007**, *64*(6), 1442-1454.
- [35] Bloch, K. Control mechanisms for fatty acid synthesis in *Mycobacterium smegmatis*. *Adv. Enzymol. Relat. Areas Mol. Biol.*, **1977**, *45*, 1-84.
- [36] Daniel, J.; Oh, T.J.; Lee, C.M.; Kolattukudy, P.E. AccD6, a member of the Fas II locus, is a functional carboxyltransferase subunit of the acyl-coenzyme A carboxylase in *Mycobacterium tuberculosis*. *J. Bacteriol.*, **2007**, *189*(3), 911-917.
- [37] Bloch, K.; Vance, D. Control mechanisms in the synthesis of saturated fatty acids. *Annu. Rev. Biochem.*, **1977**, *46*, 263-298.
- [38] Fernandes, N.D.; Kolattukudy, P.E. Cloning, sequencing and characterization of a fatty acid synthase-encoding gene from *Mycobacterium tuberculosis* var. *bovis* BCG. *Gene*, **1996**, *170*(1), 95-99.
- [39] Zimhony, O.; Vilcheze, C.; Jacobs, W.R., Jr. Characterization of *Mycobacterium smegmatis* expressing the *Mycobacterium tuberculosis* fatty acid synthase I (fasI) gene. *J. Bacteriol.*, **2004**, *186*(13), 4051-4055.
- [40] Smith, S.; Witkowski, A.; Joshi, A.K. Structural and functional organization of the animal fatty acid synthase. *Prog. Lipid Res.*, **2003**, *42*(4), 289-317.
- [41] Odriozola, J.M.; Ramos, J.A.; Bloch, K. Fatty acid synthetase activity in *Mycobacterium smegmatis*. Characterization of the acyl carrier protein-dependent elongating system. *Biochim. Biophys. Acta.*, **1977**, *488*(2), 207-217.
- [42] Kremer, L.; Nampoothiri, K.M.; Lesjean, S.; Dover, L.G.; Graham, S.; Betts, J.; Brennan, P.J.; Minnikin, D.E.; Loch, C.; Besra, G.S. Biochemical characterization of acyl carrier protein (AcpM) and malonyl-CoA:AcpM transacylase (mtFabD), two major components of *Mycobacterium tuberculosis* fatty acid synthase II. *J. Biol. Chem.*, **2001**, *276*(30), 27967-27974.
- [43] Choi, K.H.; Kremer, L.; Besra, G.S.; Rock, C.O. Identification and substrate specificity of beta-ketoacyl (acyl carrier protein) synthase III (mtFabH) from *Mycobacterium tuberculosis*. *J. Biol. Chem.*, **2000**, *275*(36), 28201-28207.
- [44] Marrakchi, H.; Ducasse, S.; Labesse, G.; Montrozier, H.; Margeat, E.; Emorine, L.; Charpentier, X.; Daffe, M.; Quemard, A. MabA (FabG1), a *Mycobacterium tuberculosis* protein involved in the long-chain fatty acid elongation system FAS-II. *Microbiology*, **2002**, *148*(Pt 4), 951-960.
- [45] Bhatt, A.; Fujiwara, N.; Bhatt, K.; Gurucha, S.S.; Kremer, L.; Chen, B.; Chan, J.; Porcelli, S.A.; Kobayashi, K.; Besra, G.S.; Jacobs, W.R., Jr. Deletion of kasB in *Mycobacterium tuberculosis* causes loss of acid-fastness and subclinical latent tuberculosis in immunocompetent mice. *Proc. Natl. Acad. Sci. USA.*, **2007**, *104*(12), 5157-5162.
- [46] Bhatt, A.; Kremer, L.; Dai, A.Z.; Sacchetti, J.C.; Jacobs, W.R., Jr. Conditional depletion of KasA, a key enzyme of mycolic acid biosynthesis, leads to mycobacterial cell lysis. *J. Bacteriol.*, **2005**, *187*(22), 7596-7606.
- [47] Kremer, L.; Dover, L.G.; Carrere, S.; Nampoothiri, K.M.; Lesjean, S.; Brown, A.K.; Brennan, P.J.; Minnikin, D.E.; Loch, C.; Besra, G.S. Mycolic acid biosynthesis and enzymic characterization of the beta-ketoacyl-ACP synthase A-condensing enzyme from *Mycobacterium tuberculosis*. *Biochem. J.*, **2002**, *364*(Pt 2), 423-430.
- [48] Schaeffer, M.L.; Agnihotri, G.; Volker, C.; Kallender, H.; Brennan, P.J.; Lonsdale, J.T. Purification and biochemical characterization of the *Mycobacterium tuberculosis* beta-ketoacyl-acyl carrier protein synthases KasA and KasB. *J. Biol. Chem.*, **2001**, *276*(50), 47029-47037.
- [49] Slayden, R.A.; Barry, C.E. 3rd, The role of KasA and KasB in the biosynthesis of meromycolic acids and isoniazid resistance in *Mycobacterium tuberculosis*. *Tuberculosis (Edinb)*, **2002**, *82*(4-5), 149-160.
- [50] Cantaloube, S.; Veyron-Churlet, R.; Haddache, N.; Daffe, M.; Zerbib, D. The *Mycobacterium tuberculosis* FAS-II dehydratases and methyltransferases define the specificity of the mycolic acid elongation complexes. *PLoS One*, **2011**, *6*(12), e29564.
- [51] Veyron-Churlet, R.; Bigot, S.; Guerrini, O.; Verdoux, S.; Malaga, W.; Daffe, M.; Zerbib, D. The biosynthesis of mycolic acids in *Mycobacterium tuberculosis* relies on multiple specialized elongation complexes interconnected by specific protein-protein interactions. *J. Mol. Biol.*, **2005**, *353*(4), 847-858.
- [52] Veyron-Churlet, R.; Guerrini, O.; Mourey, L.; Daffe, M.; Zerbib, D. Protein-protein interactions within the Fatty Acid Synthase-II system of *Mycobacterium tuberculosis* are essential for mycobacterial viability. *Mol. Microbiol.*, **2004**, *54*(5), 1161-1172.
- [53] Marrakchi, H.; Bardou, F.; Lanéelle, M.-a.; Daffé, M. In The Mycobacterial Cell Envelope; American Society of Microbiology, **2008**.
- [54] Sacco, E.; Covarrubias, A.S.; O'Hare, H.M.; Carroll, P.; Eynard, N.; Jones, T.A.; Parish, T.; Daffe, M.; Backbro, K.; Quemard, A. The missing piece of the type II fatty acid synthase system from *Mycobacterium tuberculosis*. *Proc. Natl. Acad. Sci. USA*, **2007**, *104*(37), 14628-14633.
- [55] Gao, L.Y.; Laval, F.; Lawson, E.H.; Groger, R.K.; Woodruff, A.; Morisaki, J.H.; Cox, J.S.; Daffe, M.; Brown, E.J. Requirement for kasB in *Mycobacterium tuberculosis* mycolic acid biosynthesis, cell wall impermeability and intracellular survival: Implications for therapy. *Mol. Microbiol.*, **2003**, *49*(6), 1547-1563.
- [56] Gokhale, R.S.; Saxena, P.; Chopra, T.; Mohanty, D. Versatile polyketide enzymatic machinery for the biosynthesis of complex mycobacterial lipids. *Nat. Prod. Rep.*, **2007**, *24*(2), 267-277.
- [57] Trivedi, O.A.; Arora, P.; Sridharan, V.; Tickoo, R.; Mohanty, D.; Gokhale, R.S. Enzymic activation and transfer of fatty acids as acyl-adenylates in mycobacteria. *Nature*, **2004**, *428*(6981), 441-445.
- [58] Gavalda, S.; Bardou, F.; Laval, F.; Bon, C.; Malaga, W.; Chalut, C.; Guilhot, C.; Mourey, L.; Daffe, M.; Quemard, A. The polyketide synthase Pks13 catalyzes a novel mechanism of lipid transfer in mycobacteria. *Chem. Biol.*, **2014**, *21*(12), 1660-1669.
- [59] Gavalda, S.; Leger, M.; van der Rest, B.; Stella, A.; Bardou, F.; Montrozier, H.; Chalut, C.; Burlet-Schiltz, O.; Marrakchi, H.; Daffe, M.; Quemard, A. The Pks13/FadD32 crosstalk for the biosynthesis of mycolic acids in *Mycobacterium tuberculosis*. *J. Biol. Chem.*, **2009**, *284*(29), 19255-19264.
- [60] Leger, M.; Gavalda, S.; Guillet, V.; van der Rest, B.; Slama, N.; Montrozier, H.; Mourey, L.; Quemard, A.; Daffe, M.; Marrakchi, H. The dual function of the *Mycobacterium tuberculosis* FadD32 required for mycolic acid biosynthesis. *Chem. Biol.*, **2009**, *16*(5), 510-519.
- [61] Gande, R.; Gibson, K.J.; Brown, A.K.; Krumbach, K.; Dover, L.G.; Sahn, H.; Shioyama, S.; Oikawa, T.; Besra, G.S.; Eggeling, L. Acyl-CoA carboxylases (accD2 and accD3), together with a unique polyketide synthase (Cg-pks), are key to mycolic acid biosynthesis in Corynebacteriaceae such as *Corynebacterium glutamicum* and

- Mycobacterium tuberculosis*. *J. Biol. Chem.*, **2004**, 279(43), 44847-44857.
- [62] Portevin, D.; De Sousa-D'Auria, C.; Houssin, C.; Grimaldi, C.; Chami, M.; Daffe, M.; Guilhot, C. A polyketide synthase catalyzes the last condensation step of mycolic acid biosynthesis in mycobacteria and related organisms. *Proc. Natl. Acad. Sci. USA*, **2004**, 101(1), 314-319.
- [63] Portevin, D.; de Sousa-D'Auria, C.; Montrozier, H.; Houssin, C.; Stella, A.; Laneelle, M.A.; Bardou, F.; Guilhot, C.; Daffe, M. The acyl-AMP ligase FadD32 and AccD4-containing acyl-CoA carboxylase are required for the synthesis of mycolic acids and essential for mycobacterial growth: Identification of the carboxylation product and determination of the acyl-CoA carboxylase components. *J. Biol. Chem.*, **2005**, 280(10), 8862-8874.
- [64] Bhatt, A.; Brown, A.K.; Singh, A.; Minnikin, D.E.; Besra, G.S. Loss of a mycobacterial gene encoding a reductase leads to an altered cell wall containing beta-oxo-mycolic acid analogs and accumulation of ketones. *Chem. Biol.*, **2008**, 15(9), 930-939.
- [65] Lea-Smith, D.J.; Pyke, J.S.; Tull, D.; McConville, M.J.; Coppel, R.L.; Crellin, P.K. The reductase that catalyzes mycolic motif synthesis is required for efficient attachment of mycolic acids to arabinogalactan. *J. Biol. Chem.*, **2007**, 282(15), 11000-11008.
- [66] Aggarwal, A.; Parai, M.K.; Shetty, N.; Wallis, D.; Woolhiser, L.; Hastings, C.; Dutta, N.K.; Galaviz, S.; Dhakal, R.C.; Shrestha, R.; Wakabayashi, S.; Walpole, C.; Matthews, D.; Floyd, D.; Scullion, P.; Riley, J.; Epemolu, O.; Norval, S.; Snavely, T.; Robertson, G.T.; Rubin, E.J.; Ioerger, T.R.; Sirgel, F.A.; van der Merwe, R.; van Helden, P.D.; Keller, P.; Bottger, E.C.; Karakousis, P.C.; Lenaerts, A.J.; Sacchetti, J.C. Development of a Novel Lead that Targets *M. tuberculosis* Polyketide Synthase 13. *Cell*, **2017**, 170(2), 249-259 e225.
- [67] Bergeret, F.; Gavaldà, S.; Chalut, C.; Malaga, W.; Quemard, A.; Pedelacq, J.D.; Daffe, M.; Guilhot, C.; Mourey, L.; Bon, C. Biochemical and structural study of the atypical acyltransferase domain from the mycobacterial polyketide synthase Pks13. *J. Biol. Chem.*, **2012**, 287(40), 33675-33690.
- [68] Yu, M.; Dou, C.; Gu, Y.; Cheng, W. Crystallization and structure analysis of the core motif of the Pks13 acyltransferase domain from *Mycobacterium tuberculosis*. *Peer J.*, **2018**, 6, e4728.
- [69] Thanna, S.; Knudson, S.E.; Grzegorzewicz, A.; Kapil, S.; Goins, C.M.; Ronning, D.R.; Jackson, M.; Slayden, R.A.; Sucheck, S.J. Synthesis and evaluation of new 2-aminothiophenes against *Mycobacterium tuberculosis*. *Org. Biomol. Chem.*, **2016**, 14(25), 6119-6133.
- [70] Zhang, W.; Lun, S.; Wang, S.H.; Jiang, X.W.; Yang, F.; Tang, J.; Manson, A.L.; Earl, A.M.; Gunosewoyo, H.; Bishai, W.R.; Yu, L.F. Identification of Novel Coumestan Derivatives as Polyketide Synthase 13 Inhibitors against *Mycobacterium tuberculosis*. *J. Med. Chem.*, **2018**, 61(3), 791-803.
- [71] Domenech, P.; Reed, M.B.; Barry, C.E. 3rd, Contribution of the *Mycobacterium tuberculosis* MmpL protein family to virulence and drug resistance. *Infect. Immun.*, **2005**, 73(6), 3492-3501.
- [72] Belardinelli, J.M.; Larrouy-Maumus, G.; Jones, V.; Sorio de Carvalho, L.P.; McNeil, M.R.; Jackson, M. Biosynthesis and translocation of unsulfated acyltrehaloses in *Mycobacterium tuberculosis*. *J. Biol. Chem.*, **2014**, 289(40), 27952-27965.
- [73] Converse, S.E.; Mougous, J.D.; Leavell, M.D.; Leary, J.A.; Bertozzi, C.R.; Cox, J.S. MmpL8 is required for sulfolipid-1 biosynthesis and *Mycobacterium tuberculosis* virulence. *Proc. Natl. Acad. Sci. U S A*, **2003**, 100(10), 6121-6126.
- [74] Cox, J.S.; Chen, B.; McNeil, M.; Jacobs, W.R., Jr. Complex lipid determines tissue-specific replication of *Mycobacterium tuberculosis* in mice. *Nature*, **1999**, 402(6757), 79-83.
- [75] Domenech, P.; Reed, M.B.; Dowd, C.S.; Manca, C.; Kaplan, G.; Barry, C.E. 3rd, The role of MmpL8 in sulfatide biogenesis and virulence of *Mycobacterium tuberculosis*. *J. Biol. Chem.*, **2004**, 279(20), 21257-21265.
- [76] Xu, Z.; Meshcheryakov, V.A.; Poce, G.; Chng, S.S. MmpL3 is the flippase for mycolic acids in mycobacteria. *Proc. Natl. Acad. Sci. USA*, **2017**, 114(30), 7993-7998.
- [77] Mdluli, K.; Kaneko, T.; Upton, A. Tuberculosis drug discovery and emerging targets. *Ann. N. Y. Acad. Sci.*, **2014**, 1323, 56-75.
- [78] Owens, C.P.; Chim, N.; Graves, A.B.; Harmston, C.A.; Iniguez, A.; Contreras, H.; Liptak, M.D.; Goulding, C.W. The *Mycobacterium tuberculosis* secreted protein Rv0203 transfers heme to membrane proteins MmpL3 and MmpL11. *J. Biol. Chem.*, **2013**, 288(30), 21714-21728.
- [79] Grzegorzewicz, A.E.; Pham, H.; Gundi, V.A.; Scherman, M.S.; North, E.J.; Hess, T.; Jones, V.; Gruppo, V.; Born, S.E.; Kordulakova, J.; Chavadi, S.S.; Morisseau, C.; Lenaerts, A.J.; Lee, R.E.; McNeil, M.R.; Jackson, M. Inhibition of mycolic acid transport across the *Mycobacterium tuberculosis* plasma membrane. *Nat. Chem. Biol.*, **2012**, 8(4), 334-341.
- [80] Tahlan, K.; Wilson, R.; Kastrinsky, D.B.; Arora, K.; Nair, V.; Fischer, E.; Barnes, S.W.; Walker, J.R.; Alland, D.; Barry, C.E., 3rd; Boshoff, H.I. SQ109 targets MmpL3, a membrane transporter of trehalose monomycolate involved in mycolic acid donation to the cell wall core of *Mycobacterium tuberculosis*. *Antimicrob. Agents Chemother.*, **2012**, 56(4), 1797-1809.
- [81] Varela, C.; Rittmann, D.; Singh, A.; Krumbach, K.; Bhatt, K.; Eggeling, L.; Besra, G.S.; Bhatt, A. MmpL genes are associated with mycolic acid metabolism in mycobacteria and corynebacteria. *Chem. Biol.*, **2012**, 19(4), 498-506.
- [82] Warrior, T.; Tropis, M.; Werngren, J.; Diehl, A.; Gengenbacher, M.; Schlegel, B.; Schade, M.; Oschkinat, H.; Daffe, M.; Hoffner, S.; Eddine, A.N.; Kaufmann, S.H. Antigen 85C inhibition restricts *Mycobacterium tuberculosis* growth through disruption of cord factor biosynthesis. *Antimicrob. Agents Chemother.*, **2012**, 56(4), 1735-1743.
- [83] Stock, J.B.; Ninfa, A.J.; Stock, A.M. Protein phosphorylation and regulation of adaptive responses in bacteria. *Microbiol. Rev.*, **1989**, 53(4), 450-490.
- [84] Prsic, S.; Husson, R.N. *Mycobacterium tuberculosis* Serine/Threonine Protein Kinases. *Microbiol. Spectrum*, **2014**, 2(5), 1-26.
- [85] Parish, T. Two-Component Regulatory Systems of Mycobacteria. *Microbiol. Spectr.*, **2014**, 2(1), MGM2-0010-2013.
- [86] Richard-Greenblatt, M.; Av-Gay, Y. Epigenetic Phosphorylation Control of *Mycobacterium tuberculosis* Infection and Persistence. *Microbiol. Spectr.*, **2017**, 5(2), doi: 10.1128/microbiolspec.TBTB2-0005-2015.
- [87] Av-Gay, Y.; Everett, M. The eukaryotic-like Ser/Thr protein kinases of *Mycobacterium tuberculosis*. *Trends Microbiol.*, **2000**, 8(5), 238-244.
- [88] Greenstein, A.E.; Grundner, C.; Echols, N.; Gay, L.M.; Lombana, T.N.; Miecskowski, C.A.; Pullen, K.E.; Sung, P.Y.; Alber, T. Structure/function studies of Ser/Thr and Tyr protein phosphorylation in *Mycobacterium tuberculosis*. *J. Mol. Microbiol. Biotechnol.*, **2005**, 9(3-4), 167-181.
- [89] Wehenkel, A.; Bellinzoni, M.; Grana, M.; Duran, R.; Villarino, A.; Fernandez, P.; Andre-Leroux, G.; England, P.; Takiff, H.; Cervenansky, C.; Cole, S.T.; Alzari, P.M. Mycobacterial Ser/Thr protein kinases and phosphatases: physiological roles and therapeutic potential. *Biochim. Biophys. Acta.*, **2008**, 1784(1), 193-202.
- [90] Zhou, P.; Long, Q.; Zhou, Y.; Wang, H.; Xie, J. *Mycobacterium tuberculosis* two-component systems and implications in novel vaccines and drugs. *Crit. Rev. Eukaryot. Gene Expr.*, **2012**, 22(1), 37-52.
- [91] Canova, M.J.; Molle, V. Bacterial serine/threonine protein kinases in host-pathogen interactions. *J. Biol. Chem.*, **2014**, 289(14), 9473-9479.
- [92] Narayan, A.; Sachdeva, P.; Sharma, K.; Saini, A.K.; Tyagi, A.K.; Singh, Y. Serine threonine protein kinases of mycobacterial genus: Phylogeny to function. *Physiol. Genomics*, **2007**, 29(1), 66-75.
- [93] Prsic, S.; Dankwa, S.; Schwartz, D.; Chou, M.F.; Locasale, J.W.; Kang, C.M.; Bemis, G.; Church, G.M.; Steen, H.; Husson, R.N. Extensive phosphorylation with overlapping specificity by *Mycobacterium tuberculosis* serine/threonine protein kinases. *Proc. Natl. Acad. Sci. U S A*, **2010**, 107(16), 7521-7526.
- [94] Huse, M.; Kuriyan, J. The conformational plasticity of protein kinases. *Cell*, **2002**, 109(3), 275-282.
- [95] Sickmann, A.; Meyer, H.E. Phosphoamino acid analysis. *Proteomics*, **2001**, 1(2), 200-206.
- [96] Braconi Quintaje, S.; Orchard, S. The annotation of both human and mouse kinomes in UniProtKB/Swiss-Prot: One small step in manual annotation, one giant leap for full comprehension of genomes. *Mol. Cell Proteomics*, **2008**, 7(8), 1409-1419.
- [97] Manning, G.; Whyte, D.B.; Martinez, R.; Hunter, T.; Sudarsanam, S. The protein kinase complement of the human genome. *Science*, **2002**, 298(5600), 1912-1934.

- [98] Bach, H.; Wong, D.; Av-Gay, Y. *Mycobacterium tuberculosis* PtkA is a novel protein tyrosine kinase whose substrate is PtpA. *Biochem. J.*, **2009**, *420*(2), 155-160.
- [99] Zhou, P.; Li, W.; Wong, D.; Xie, J.; Av-Gay, Y. Phosphorylation control of protein tyrosine phosphatase A activity in *Mycobacterium tuberculosis*. *FEBS Lett.*, **2015**, *589*(3), 326-331.
- [100] Wong, D.; Li, W.; Chao, J.D.; Zhou, P.; Narula, G.; Tsui, C.; Ko, M.; Xie, J.; Martinez-Frailes, C.; Av-Gay, Y. Protein tyrosine kinase, PtkA, is required for *Mycobacterium tuberculosis* growth in macrophages. *Sci. Rep.*, **2018**, *8*(1), 155, doi: 10.1038/s41598-017-18547-9.
- [101] Sajid, A.; Arora, G.; Singhal, A.; Kalia, V.C.; Singh, Y. Protein Phosphatases of Pathogenic Bacteria: Role in Physiology and Virulence. *Annu. Rev. Microbiol.*, **2015**, *69*, 527-547.
- [102] Boitel, B.; Ortiz-Lombardia, M.; Duran, R.; Pompeo, F.; Cole, S.T.; Cervenansky, C.; Alzari, P.M. PknB kinase activity is regulated by phosphorylation in two Thr residues and dephosphorylation by PstP, the cognate phospho-Ser/Thr phosphatase, in *Mycobacterium tuberculosis*. *Mol. Microbiol.*, **2003**, *49*(6), 1493-1508.
- [103] Chopra, P.; Singh, B.; Singh, R.; Vohra, R.; Koul, A.; Meena, L.S.; Koduri, H.; Ghildiyal, M.; Deol, P.; Das, T.K.; Tyagi, A.K.; Singh, Y. Phosphoprotein phosphatase of *Mycobacterium tuberculosis* dephosphorylates serine-threonine kinases PknA and PknB. *Biochem. Biophys. Res. Commun.*, **2003**, *311*(1), 112-120.
- [104] Le, N.-H.; Molle, V.; Eynard, N.; Miras, M.; Stella, A.; Bardou, F.; Galandrin, S.; Guillet, V.; Andre-Leroux, G.; Bellinzoni, M.; Alzari, P.; Mourey, L.; Bulet-Schiltz, O.; Daffe, M.; Marrakchi, H. Ser/Thr Phosphorylation Regulates the Fatty Acyl-AMP Ligase Activity of FadD32, an Essential Enzyme in Mycolic Acid Biosynthesis. *J. Biol. Chem.*, **2016**, *291*(43), 22793-22805.
- [105] Sharma, A.K.; Arora, D.; Singh, L.K.; Gangwal, A.; Sajid, A.; Molle, V.; Singh, Y.; Nandicoori, V.K. Serine/Threonine Protein Phosphatase PstP of *Mycobacterium tuberculosis* Is Necessary for Accurate Cell Division and Survival of Pathogen. *J. Biol. Chem.*, **2016**, *291*(46), 24215-24230.
- [106] Chao, J.; Wong, D.; Zheng, X.; Poirier, V.; Bach, H.; Hmama, Z.; Av-Gay, Y. Protein kinase and phosphatase signaling in *Mycobacterium tuberculosis* physiology and pathogenesis. *Biochim. Biophys. Acta*, **2010**, *1804*(3), 620-627.
- [107] Koul, A.; Choidas, A.; Treder, M.; Tyagi, A.K.; Drlica, K.; Singh, Y.; Ullrich, A. Cloning and characterization of secretory tyrosine phosphatases of *Mycobacterium tuberculosis*. *J. Bacteriol.*, **2000**, *182*(19), 5425-5432.
- [108] Koul, A.; Herget, T.; Klebl, B.; Ullrich, A. Interplay between mycobacteria and host signalling pathways. *Nat. Rev. Microbiol.*, **2004**, *2*(3), 189-202.
- [109] Zhou, B.; He, Y.; Zhang, X.; Xu, J.; Luo, Y.; Wang, Y.; Franzblau, S.G.; Yang, Z.; Chan, R.J.; Liu, Y.; Zheng, J.; Zhang, Z.Y. Targeting mycobacterium protein tyrosine phosphatase B for anti-tuberculosis agents. *Proc. Natl. Acad. Sci. USA.*, **2010**, *107*(10), 4573-4578.
- [110] Bach, H.; Papavinasundaram, K.G.; Wong, D.; Hmama, Z.; Av-Gay, Y. *Mycobacterium tuberculosis* virulence is mediated by PtpA dephosphorylation of human vacuolar protein sorting 33B. *Cell Host Microbe.*, **2008**, *3*(5), 316-322.
- [111] Beresford, N.; Patel, S.; Armstrong, J.; Szoor, B.; Fordham-Skelton, A.P.; Taberner, L. MptpB, a virulence factor from *Mycobacterium tuberculosis*, exhibits triple-specificity phosphatase activity. *Biochem. J.*, **2007**, *406*(1), 13-18.
- [112] Castandet, J.; Prost, J.F.; Peyron, P.; Astarie-Dequeker, C.; Anes, E.; Cozzone, A.J.; Griffiths, G.; Maridonneau-Parini, I. Tyrosine phosphatase MptpA of *Mycobacterium tuberculosis* inhibits phagocytosis and increases actin polymerization in macrophages. *Res. Microbiol.*, **2005**, *156*(10), 1005-1013.
- [113] Chauhan, P.; Reddy, P.V.; Singh, R.; Jaisinghani, N.; Gandotra, S.; Tyagi, A.K. Secretory phosphatases deficient mutant of *Mycobacterium tuberculosis* imparts protection at the primary site of infection in guinea pigs. *PLoS One*, **2013**, *8*(10), e77930.
- [114] Cowley, S.C.; Babakaiff, R.; Av-Gay, Y. Expression and localization of the *Mycobacterium tuberculosis* protein tyrosine phosphatase PtpA. *Res. Microbiol.*, **2002**, *153*(4), 233-241.
- [115] Guler, R.; Brombacher, F. Host-directed drug therapy for tuberculosis. *Nat. Chem. Biol.*, **2015**, *11*(10), 748-751.
- [116] Singh, R.; Rao, V.; Shakila, H.; Gupta, R.; Khera, A.; Dhar, N.; Singh, A.; Koul, A.; Singh, Y.; Naseema, M.; Narayanan, P.R.; Paramasivan, C.N.; Ramanathan, V.D.; Tyagi, A.K. Disruption of mptpB impairs the ability of *Mycobacterium tuberculosis* to survive in guinea pigs. *Mol. Microbiol.*, **2003**, *50*(3), 751-762.
- [117] Singh, R.; Singh, A.; Tyagi, A.K. Deciphering the genes involved in pathogenesis of *Mycobacterium tuberculosis*. *Tuberculosis (Edinb)*, **2005**, *85*(5-6), 325-335.
- [118] Wang, J.; Li, B.X.; Ge, P.P.; Li, J.; Wang, Q.; Gao, G.F.; Qiu, X.B.; Liu, C.H. *Mycobacterium tuberculosis* suppresses innate immunity by coopting the host ubiquitin system. *Nat. Immunol.*, **2015**, *16*(3), 237-245.
- [119] Wang, J.; Teng, J.L.; Zhao, D.; Ge, P.; Li, B.; Woo, P.C.; Liu, C.H. The ubiquitin ligase TRIM27 functions as a host restriction factor antagonized by *Mycobacterium tuberculosis* PtpA during mycobacterial infection. *Sci. Rep.*, **2016**, *6*, 34827.
- [120] Wong, D.; Bach, H.; Sun, J.; Hmama, Z.; Av-Gay, Y. *Mycobacterium tuberculosis* protein tyrosine phosphatase (PtpA) excludes host vacuolar-H<sup>+</sup>-ATPase to inhibit phagosome acidification. *Proc. Natl. Acad. Sci. USA.*, **2011**, *108*(48), 19371-19376.
- [121] Parrish, N.M.; Dick, J.D.; Bishai, W.R. Mechanisms of latency in *Mycobacterium tuberculosis*. *Trends Microbiol.*, **1998**, *6*(3), 107-112.
- [122] Schnappinger, D.; Ehr, S.; Voskuil, M.I.; Liu, Y.; Mangan, J.A.; Monahan, I.M.; Dolganov, G.; Efron, B.; Butcher, P.D.; Nathan, C.; Schoolnik, G.K. Transcriptional Adaptation of *Mycobacterium tuberculosis* within Macrophages: Insights into the Phagosomal Environment. *J. Exp. Med.*, **2003**, *198*(5), 693-704.
- [123] Dubnau, E.; Chan, J.; Raynaud, C.; Mohan, V.P.; Laneelle, M.A.; Yu, K.; Quemard, A.; Smith, I.; Daffe, M. Oxygenated mycolic acids are necessary for virulence of *Mycobacterium tuberculosis* in mice. *Mol. Microbiol.*, **2000**, *36*(3), 630-637.
- [124] Corrales, R.M.; Molle, V.; Leiba, J.; Mourey, L.; de Chastellier, C.; Kremer, L. Phosphorylation of mycobacterial PcaA inhibits mycolic acid cyclopropanation. *J. Biol. Chem.*, **2012**, *287*(31), 26187-26199.
- [125] Jang, J.; Stella, A.; Boudou, F.; Levillain, F.; Darthuy, E.; Vaubourgeix, J.; Wang, C.; Bardou, F.; Puzo, G.; Gilleron, M.; Bulet-Schiltz, O.; Monsarrat, B.; Brodin, P.; Gicquel, B.; Neyrolles, O. Functional characterization of the *Mycobacterium tuberculosis* serine/threonine kinase PknJ. *Microbiology (Reading, U.K.)*, **2010**, *156*(6), 1619-1631.
- [126] Khan, S.; Nagarajan, S.N.; Parikh, A.; Samantaray, S.; Singh, A.; Kumar, D.; Roy, R.P.; Bhatt, A.; Nandicoori, V.K. Phosphorylation of enoyl-acyl carrier protein reductase InhA impacts mycobacterial growth and survival. *J. Biol. Chem.*, **2010**, *285*(48), 37860-37871.
- [127] Kumar, P.; Kumar, D.; Parikh, A.; Rananaware, D.; Gupta, M.; Singh, Y.; Nandicoori, V.K. The *Mycobacterium tuberculosis* protein kinase K modulates activation of transcription from the promoter of mycobacterial monoxygenase operon through phosphorylation of the transcriptional regulator VirS. *J. Biol. Chem.*, **2009**, *284*(17), 11090-11099.
- [128] Kumari, R.; Saxena, R.; Tiwari, S.; Tripathi, D.K.; Srivastava, K.K. Rv3080c regulates the rate of inhibition of mycobacteria by isoniazid through FabD. *Mol. Cell Biochem.*, **2013**, *374*(1-2), 149-155.
- [129] Molle, V.; Brown, A.K.; Besra, G.S.; Cozzone, A.J.; Kremer, L. The condensing activities of the *Mycobacterium tuberculosis* type II fatty acid synthase are differentially regulated by phosphorylation. *J. Biol. Chem.*, **2006**, *281*(40), 30094-30103.
- [130] Molle, V.; Gulten, G.; Vilcheze, C.; Veyron-Churlet, R.; Zanella-Cleon, I.; Sacchettini, J.C.; Jacobs, W.R., Jr.; Kremer, L. Phosphorylation of InhA inhibits mycolic acid biosynthesis and growth of *Mycobacterium tuberculosis*. *Mol. Microbiol.*, **2010**, *78*(6), 1591-1605.
- [131] Molle, V.; Kremer, L.; Girard-Blanc, C.; Besra, G.S.; Cozzone, A.J.; Prost, J.F. An FHA phosphoprotein recognition domain mediates protein EmbR phosphorylation by PknH, a Ser/Thr protein kinase from *Mycobacterium tuberculosis*. *Biochemistry*, **2003**, *42*(51), 15300-15309.
- [132] Sharma, K.; Gupta, M.; Pathak, M.; Gupta, N.; Koul, A.; Sarangi, S.; Baweja, R.; Singh, Y. Transcriptional control of the mycobacterial embCAB operon by PknH through a regulatory protein, EmbR, *in vivo*. *J. Bacteriol.*, **2006**, *188*(8), 2936-2944.
- [133] Singh, A.; Gupta, R.; Vishwakarma, R.A.; Narayanan, P.R.; Paramasivan, C.N.; Ramanathan, V.D.; Tyagi, A.K. Requirement of the mymA operon for appropriate cell wall ultrastructure and persistence of *Mycobacterium tuberculosis* in the spleens of guinea pigs. *J. Bacteriol.*, **2005**, *187*(12), 4173-4186.

- [134] Slama, N.; Leiba, J.; Eynard, N.; Daffe, M.; Kremer, L.; Quemard, A.; Molle, V. Negative regulation by Ser/Thr phosphorylation of HadAB and HadBC dehydratases from *Mycobacterium tuberculosis* type II fatty acid synthase system. *Biochem Biophys Res Commun*, **2011**, *412*(3), 401-406.
- [135] Veyron-Churlet, R.; Molle, V.; Taylor, R.C.; Brown, A.K.; Besra, G.S.; Zanella-Cleon, I.; Futterer, K.; Kremer, L. The *Mycobacterium tuberculosis* beta-ketoacyl-acyl carrier protein synthase III activity is inhibited by phosphorylation on a single threonine residue. *J. Biol. Chem.*, **2009**, *284*(10), 6414-6424.
- [136] Veyron-Churlet, R.; Zanella-Cleon, I.; Cohen-Gonsaud, M.; Molle, V.; Kremer, L. Phosphorylation of the *Mycobacterium tuberculosis*  $\beta$ -Ketoacyl-Acyl Carrier Protein Reductase MabA Regulates Mycolic Acid Biosynthesis. *J. Biol. Chem.*, **2010**, *285*(17), 12714-12725.
- [137] Sinha, I.; Boon, C.; Dick, T. Apparent growth phase-dependent phosphorylation of malonyl coenzyme A: Acyl carrier protein transacylase (MCAT), a major fatty acid synthase II component in *Mycobacterium bovis* BCG. *FEMS Microbiol. Lett.*, **2003**, *227*(1), 141-147.
- [138] Vilcheze, C.; Molle, V.; Carrere-Kremer, S.; Leiba, J.; Mourey, L.; Shenai, S.; Baronian, G.; Tufariello, J.; Hartman, T.; Veyron-Churlet, R.; Trivelli, X.; Tiwari, S.; Weinrick, B.; Alland, D.; Guerardel, Y.; Jacobs, W.R., Jr.; Kremer, L. Phosphorylation of KasB regulates virulence and acid-fastness in *Mycobacterium tuberculosis*. *PLoS Pathog.*, **2014**, *10*(5), e1004115.
- [139] Dasgupta, A.; Datta, P.; Kundu, M.; Basu, J. The serine/threonine kinase PknB of *Mycobacterium tuberculosis* phosphorylates PBPA, a penicillin-binding protein required for cell division. *Microbiology*, **2006**, *152*(Pt 2), 493-504.
- [140] Gupta, M.; Sajid, A.; Arora, G.; Tandon, V.; Singh, Y. Forkhead-associated domain-containing protein Rv0019c and polyketide-associated protein PapA5, from substrates of serine/threonine protein kinase PknB to interacting proteins of *Mycobacterium tuberculosis*. *J. Biol. Chem.*, **2009**, *284*(50), 34723-34734.
- [141] Kang, C.M.; Abbott, D.W.; Park, S.T.; Dascher, C.C.; Cantley, L.C.; Husson, R.N. The *Mycobacterium tuberculosis* serine/threonine kinases PknA and PknB: Substrate identification and regulation of cell shape. *Genes Dev.*, **2005**, *19*(14), 1692-1704.
- [142] Kang, C.M.; Nyayapathy, S.; Lee, J.Y.; Suh, J.W.; Husson, R.N. Wag31, a homologue of the cell division protein DivIVA, regulates growth, morphology and polar cell wall synthesis in mycobacteria. *Microbiology*, **2008**, *154*(Pt 3), 725-735.
- [143] Parikh, A.; Verma, S.K.; Khan, S.; Prakash, B.; Nandicoori, V.K. PknB-mediated phosphorylation of a novel substrate, N-acetylglucosamine-1-phosphate uridylyltransferase, modulates its acetyltransferase activity. *J. Mol. Biol.*, **2009**, *386*(2), 451-464.
- [144] Thakur, M.; Chakraborti, P.K. GTPase activity of mycobacterial FtsZ is impaired due to its transphosphorylation by the eukaryotic-type Ser/Thr kinase, PknA. *J. Biol. Chem.*, **2006**, *281*(52), 40107-40113.
- [145] Thakur, M.; Chakraborti, P.K. Ability of PknA, a mycobacterial eukaryotic-type serine/threonine kinase, to transphosphorylate MurD, a ligase involved in the process of peptidoglycan biosynthesis. *Biochem. J.*, **2008**, *415*(1), 27-33.
- [146] Kumari, R.; Singh, S.K.; Singh, D.K.; Singh, P.K.; Chaurasiya, S.K.; Srivastava, K.K. Functional characterization delineates that a *Mycobacterium tuberculosis* specific protein kinase (Rv3080c) is responsible for the growth, phagocytosis and intracellular survival of avirulent mycobacteria. *Mol. Cell Biochem.*, **2012**, *369*(1-2), 67-74.
- [147] Malhotra, V.; Arteaga-Cortes, L.T.; Clay, G.; Clark-Curtiss, J.E. *Mycobacterium tuberculosis* protein kinase K confers survival advantage during early infection in mice and regulates growth in culture and during persistent infection: Implications for immune modulation. *Microbiology*, **2010**, *156*(Pt 9), 2829-2841.
- [148] Brown, A.K.; Bhatt, A.; Singh, A.; Salaria, E.; Evans, A.F.; Besra, G.S. Identification of the dehydratase component of the mycobacterial mycolic acid-synthesizing fatty acid synthase-II complex. *Microbiology*, **2007**, *153*(Pt 12), 4166-4173.
- [149] Vilcheze, C.; Morbidoni, H.R.; Weisbrod, T.R.; Iwamoto, H.; Kuo, M.; Sacchetti, J.C.; Jacobs, W.R., Jr. Inactivation of the inhA-encoded fatty acid synthase II (FASII) enoyl-acyl carrier protein reductase induces accumulation of the FASI end products and cell lysis of *Mycobacterium smegmatis*. *J. Bacteriol.*, **2000**, *182*(14), 4059-4067.
- [150] North, E.J.; Jackson, M.; Lee, R.E. New approaches to target the mycolic acid biosynthesis pathway for the development of tuberculosis therapeutics. *Curr. Pharm. Des.*, **2014**, *20*(27), 4357-4378.
- [151] Vilcheze, C.; Jacobs, W.R., Jr. The mechanism of isoniazid killing: clarity through the scope of genetics. *Annu. Rev. Microbiol.*, **2007**, *61*, 35-50.
- [152] Banerjee, A.; Sugantino, M.; Sacchetti, J.C.; Jacobs, W.R., Jr. The mabA gene from the inhA operon of *Mycobacterium tuberculosis* encodes a 3-ketoacyl reductase that fails to confer isoniazid resistance. *Microbiology*, **1998**, *144*( Pt 10), 2697-2704.
- [153] Chaba, R.; Raje, M.; Chakraborti, P.K. Evidence that a eukaryotic-type serine/threonine protein kinase from *Mycobacterium tuberculosis* regulates morphological changes associated with cell division. *Eur. J. Biochem.*, **2002**, *269*(4), 1078-1085.
- [154] Nagarajan, S.N.; Upadhyay, S.; Chawla, Y.; Khan, S.; Naz, S.; Subramanian, J.; Gandotra, S.; Nandicoori, V.K. Protein kinase A (PknA) of *Mycobacterium tuberculosis* is independently activated and is critical for growth *in vitro* and survival of the pathogen in the host. *J. Biol. Chem.*, **2015**, *290*(15), 9626-9645.
- [155] Glickman, M.S.; Cox, J.S.; Jacobs, W.R., Jr. A novel mycolic acid cyclopropane synthetase is required for cording, persistence, and virulence of *Mycobacterium tuberculosis*. *Mol. Cell*, **2000**, *5*(4), 717-727.
- [156] de Chastellier, C. The many niches and strategies used by pathogenic mycobacteria for survival within host macrophages. *Immunobiology*, **2009**, *214*(7), 526-542.
- [157] de Chastellier, C.; Forquet, F.; Gordon, A.; Thilo, L. Mycobacterium requires an all-around closely apposing phagosome membrane to maintain the maturation block and this apposition is re-established when it rescues itself from phagolysosomes. *Cell Microbiol.*, **2009**, *11*(8), 1190-1207.
- [158] Singh, A.; Jain, S.; Gupta, S.; Das, T.; Tyagi, A.K. mymA operon of *Mycobacterium tuberculosis*: Its regulation and importance in the cell envelope. *FEMS Microbiol. Lett.*, **2003**, *227*(1), 53-63.
- [159] Bialy, L.; Waldmann, H. Inhibitors of protein tyrosine phosphatases: next-generation drugs? *Angew. Chem. Int. Ed. Engl.*, **2005**, *44*(25), 3814-3839.
- [160] Lapenna, S.; Giordano, A. Cell cycle kinases as therapeutic targets for cancer. *Nat. Rev. Drug Discov.*, **2009**, *8*(7), 547-566.
- [161] Taberner, L.; Aricescu, A.R.; Jones, E.Y.; Szedlacsek, S.E. Protein tyrosine phosphatases: Structure-function relationships. *FEBS J.*, **2008**, *275*(5), 867-882.
- [162] Vintonyak, V.V.; Antonchick, A.P.; Rauh, D.; Waldmann, H. The therapeutic potential of phosphatase inhibitors. *Curr. Opin. Chem. Biol.*, **2009**, *13*(3), 272-283.
- [163] Zhang, J.; Yang, P.L.; Gray, N.S. Targeting cancer with small molecule kinase inhibitors. *Nat. Rev. Cancer*, **2009**, *9*(1), 28-39.
- [164] Zhang, Z.Y. Protein tyrosine phosphatases: Prospects for therapeutics. *Curr. Opin. Chem. Biol.*, **2001**, *5*(4), 416-423.
- [165] Wu, P.; Nielsen, T.E.; Clausen, M.H. Small-molecule kinase inhibitors: An analysis of FDA-approved drugs. *Drug Discov. Today*, **2016**, *21*(1), 5-10.
- [166] Wong, D.; Chao, J.D.; Av-Gay, Y. *Mycobacterium tuberculosis*-secreted phosphatases: From pathogenesis to targets for TB drug development. *Trends Microbiol.*, **2013**, *21*(2), 100-109.
- [167] Sasseti, C.M.; Boyd, D.H.; Rubin, E.J. Genes required for mycobacterial growth defined by high density mutagenesis. *Mol. Microbiol.*, **2003**, *48*(1), 77-84.
- [168] Cowley, S.; Ko, M.; Pick, N.; Chow, R.; Downing, K.J.; Gordhan, B.G.; Betts, J.C.; Mizrahi, V.; Smith, D.A.; Stokes, R.W.; Av-Gay, Y. The *Mycobacterium tuberculosis* protein serine/threonine kinase PknG is linked to cellular glutamate/glutamine levels and is important for growth *in vivo*. *Mol. Microbiol.*, **2004**, *52*(6), 1691-1702.
- [169] Chawla, Y.; Upadhyay, S.; Khan, S.; Nagarajan, S.N.; Forti, F.; Nandicoori, V.K. Protein kinase B (PknB) of *Mycobacterium tuberculosis* is essential for growth of the pathogen *in vitro* as well as for survival within the host. *J. Biol. Chem.*, **2014**, *289*(20), 13858-13875.
- [170] Papavinasandaram, K.G.; Chan, B.; Chung, J.H.; Colston, M.J.; Davis, E.O.; Av-Gay, Y. Deletion of the *Mycobacterium tuberculosis* pknH gene confers a higher bacillary load during the chronic phase of infection in BALB/c mice. *J. Bacteriol.*, **2005**, *187*(16), 5751-5760.
- [171] Walburger, A.; Koul, A.; Ferrari, G.; Nguyen, L.; Prescianotto-Baschong, C.; Huygen, K.; Klebl, B.; Thompson, C.; Bacher, G.; Pieters, J. Protein kinase G from pathogenic mycobacteria pro-

- motes survival within macrophages. *Science*, **2004**, *304*(5678), 1800-1804.
- [172] Fernandez, P.; Saint-Joanis, B.; Barilone, N.; Jackson, M.; Gicquel, B.; Cole, S.T.; Alzari, P.M. The Ser/Thr protein kinase PknB is essential for sustaining mycobacterial growth. *J. Bacteriol.*, **2006**, *188*(22), 7778-7784.
- [173] Zhang, N.; Torrelles, J.B.; McNeil, M.R.; Escuyer, V.E.; Khoo, K.H.; Brennan, P.J.; Chatterjee, D. The Emb proteins of mycobacteria direct arabinosylation of lipoarabinomannan and arabinogalactan via an N-terminal recognition region and a C-terminal synthetic region. *Mol. Microbiol.*, **2003**, *50*(1), 69-76.
- [174] Briken, V.; Porcelli, S.A.; Besra, G.S.; Kremer, L. Mycobacterial lipoarabinomannan and related lipoglycans: From biogenesis to modulation of the immune response. *Mol. Microbiol.*, **2004**, *53*(2), 391-403.
- [175] Escuyer, V.E.; Lety, M.A.; Torrelles, J.B.; Khoo, K.H.; Tang, J.B.; Rithner, C.D.; Frehel, C.; McNeil, M.R.; Brennan, P.J.; Chatterjee, D. The role of the embA and embB gene products in the biosynthesis of the terminal hexaarabinofuranosyl motif of *Mycobacterium smegmatis* arabinogalactan. *J. Biol. Chem.*, **2001**, *276*(52), 48854-48862.
- [176] Deol, P.; Vohra, R.; Saini, A.K.; Singh, A.; Chandra, H.; Chopra, P.; Das, T.K.; Tyagi, A.K.; Singh, Y. Role of *Mycobacterium tuberculosis* Ser/Thr kinase PknF: Implications in glucose transport and cell division. *J. Bacteriol.*, **2005**, *187*(10), 3415-3420.
- [177] Gopaldaswamy, R.; Narayanan, S.; Chen, B.; Jacobs, W.R.; Av-Gay, Y. The serine/threonine protein kinase PknI controls the growth of *Mycobacterium tuberculosis* upon infection. *FEMS Microbiol. Lett.*, **2009**, *295*(1), 23-29.
- [178] Arora, G.; Sajid, A.; Gupta, M.; Bhaduri, A.; Kumar, P.; Basu-Modak, S.; Singh, Y. Understanding the role of PknJ in *Mycobacterium tuberculosis*: Biochemical characterization and identification of novel substrate pyruvate kinase A. *PLoS One*, **2010**, *5*(5), e10772.
- [179] Ortega, C.; Liao, R.; Anderson, L.N.; Rustad, T.; Olodart, A.R.; Wright, A.T.; Sherman, D.R.; Grundner, C. *Mycobacterium tuberculosis* Ser/Thr protein kinase B mediates an oxygen-dependent replication switch. *PLoS Biol.*, **2014**, *12*(1), e1001746.
- [180] Scherr, N.; Honnappa, S.; Kunz, G.; Mueller, P.; Jayachandran, R.; Winkler, F.; Pieters, J.; Steinmetz, M.O. Structural basis for the specific inhibition of protein kinase G, a virulence factor of *Mycobacterium tuberculosis*. *Proc. Natl. Acad. Sci. USA.*, **2007**, *104*(29), 12151-12156.
- [181] O'Hare, H.M.; Duran, R.; Cervenansky, C.; Bellinzoni, M.; Wehenkel, A.M.; Pritsch, O.; Obal, G.; Baumgartner, J.; Vialaret, J.; Johnsson, K.; Alzari, P.M. Regulation of glutamate metabolism by protein kinases in mycobacteria. *Mol. Microbiol.*, **2008**, *70*(6), 1408-1423.
- [182] Villarino, A.; Duran, R.; Wehenkel, A.; Fernandez, P.; England, P.; Brodin, P.; Cole, S.T.; Zimny-Arndt, U.; Jungblut, P.R.; Cervenansky, C.; Alzari, P.M. Proteomic identification of *M. tuberculosis* protein kinase substrates: PknB recruits GarA, a FHA domain-containing protein, through activation loop-mediated interactions. *J. Mol. Biol.*, **2005**, *350*(5), 953-963.
- [183] Magnet, S.; Hartkoorn, R.C.; Szekely, R.; Pato, J.; Triccas, J.A.; Schneider, P.; Szantai-Kis, C.; Orfi, L.; Chambon, M.; Banfi, D.; Bueno, M.; Turcatti, G.; Keri, G.; Cole, S.T. Leads for antitubercular compounds from kinase inhibitor library screens. *Tuberculosis (Edinb)*, **2010**, *90*(6), 354-360.
- [184] Chapman, T.M.; Boulloc, N.; Buxton, R.S.; Chugh, J.; Loughheed, K.E.; Osborne, S.A.; Saxty, B.; Smerdon, S.J.; Taylor, D.L.; Whalley, D. Substituted aminopyrimidine protein kinase B (PknB) inhibitors show activity against *Mycobacterium tuberculosis*. *Bioorg. Med. Chem. Lett.*, **2012**, *22*(9), 3349-3353.
- [185] Loughheed, K.E.; Osborne, S.A.; Saxty, B.; Whalley, D.; Chapman, T.; Boulloc, N.; Chugh, J.; Nott, T.J.; Patel, D.; Spivey, V.L.; Kettleborough, C.A.; Bryans, J.S.; Taylor, D.L.; Smerdon, S.J.; Buxton, R.S. Effective inhibitors of the essential kinase PknB and their potential as anti-mycobacterial agents. *Tuberculosis (Edinb)*, **2011**, *91*(4), 277-286.
- [186] Szekely, R.; Waczek, F.; Szabadkai, I.; Nemeth, G.; Hegymegi-Barakonyi, B.; Eros, D.; Szokol, B.; Pato, J.; Hafenbradl, D.; Satchell, J.; Saint-Joanis, B.; Cole, S.T.; Orfi, L.; Klebl, B.M.; Keri, G. A novel drug discovery concept for tuberculosis: Inhibition of bacterial and host cell signalling. *Immunol. Lett.*, **2008**, *116*(2), 225-231.
- [187] Chen, D.; Ma, S.; He, L.; Yuan, P.; She, Z.; Lu, Y. Sclerotiorin inhibits protein kinase G from *Mycobacterium tuberculosis* and impairs mycobacterial growth in macrophages. *Tuberculosis (Edinb)*, **2017**, *103*, 37-43.
- [188] Anand, N.; Singh, P.; Sharma, A.; Tiwari, S.; Singh, V.; Singh, D.K.; Srivastava, K.K.; Singh, B.N.; Tripathi, R.P. Synthesis and evaluation of small libraries of triazolymethoxy chalcones, flavanones and 2-aminopyrimidines as inhibitors of mycobacterial FAS-II and PknG. *Bioorg. Med. Chem.*, **2012**, *20*(17), 5150-5163.
- [189] Hegymegi-Barakonyi, B.; Szekeley, R.; Varga, Z.; Kiss, R.; Borbely, G.; Nemeth, G.; Banhegyi, P.; Pato, J.; Greff, Z.; Horvath, Z.; Meszaros, G.; Marosfalvi, J.; Eros, D.; Szantai-Kis, C.; Breza, N.; Garavaglia, S.; Perozzi, S.; Rizzi, M.; Hafenbradl, D.; Ko, M.; Av-Gay, Y.; Klebl, B.M.; Orfi, L.; Keri, G. Signalling inhibitors against *Mycobacterium tuberculosis*--early days of a new therapeutic concept in tuberculosis. *Curr. Med. Chem.*, **2008**, *15*(26), 2760-2770.
- [190] Sipos, A.; Pato, J.; Szekeley, R.; Hartkoorn, R.C.; Kekesi, L.; Orfi, L.; Szantai-Kis, C.; Mikusova, K.; Svetlikova, Z.; Kordulakova, J.; Nagaraja, V.; Godbole, A.A.; Bush, N.; Collin, F.; Maxwell, A.; Cole, S.T.; Keri, G. Lead selection and characterization of antitubercular compounds using the Nested Chemical Library. *Tuberculosis (Edinb)*, **2015**, *95 Suppl 1*, S200-206.
- [191] Xu, J.; Wang, J.X.; Zhou, J.M.; Xu, C.L.; Huang, B.; Xing, Y.; Wang, B.; Luo, R.; Wang, Y.C.; You, X.F.; Lu, Y.; Yu, L.Y. A novel protein kinase inhibitor IMB-YH-8 with anti-tuberculosis activity. *Sci. Rep.*, **2017**, *7*(1), 5093.
- [192] Wang, T.; Bemis, G.; Hanzelka, B.; Zuccola, H.; Wynn, M.; Moody, C.S.; Green, J.; Locher, C.; Liu, A.; Gao, H.; Xu, Y.; Wang, S.; Wang, J.; Bennani, Y.L.; Thomson, J.A.; Muh, U. Mtb PKNA/PKNB dual inhibition provides selectivity advantages for inhibitor design to minimize host kinase interactions. *ACS Med. Chem. Lett.*, **2017**, *8*(12), 1224-1229.
- [193] Grundner, C.; Ng, H.L.; Alber, T. *Mycobacterium tuberculosis* protein tyrosine phosphatase PtpB structure reveals a diverged fold and a buried active site. *Structure*, **2005**, *13*(11), 1625-1634.
- [194] Chiaradia, L.D.; Martins, P.G.; Cordeiro, M.N.; Guido, R.V.; Ecco, G.; Andricopulo, A.D.; Yunes, R.A.; Vernal, J.; Nunes, R.J.; Terenzi, H. Synthesis, biological evaluation, and molecular modeling of chalcone derivatives as potent inhibitors of *Mycobacterium tuberculosis* protein tyrosine phosphatases (PtpA and PtpB). *J. Med. Chem.*, **2012**, *55*(1), 390-402.
- [195] Chiaradia, L.D.; Mascarello, A.; Purificacao, M.; Vernal, J.; Cordeiro, M.N.; Zenteno, M.E.; Villarino, A.; Nunes, R.J.; Yunes, R.A.; Terenzi, H. Synthetic chalcones as efficient inhibitors of *Mycobacterium tuberculosis* protein tyrosine phosphatase PtpA. *Bioorg. Med. Chem. Lett.*, **2008**, *18*(23), 6227-6230.
- [196] Correa, I.R., Jr.; Noren-Muller, A.; Ambrosi, H.D.; Jakupovic, S.; Saxena, K.; Schwalbe, H.; Kaiser, M.; Waldmann, H. Identification of inhibitors for mycobacterial protein tyrosine phosphatase B (MptpB) by biology-oriented synthesis (BIOS). *Chem. Asian J.*, **2007**, *2*(9), 1109-1126.
- [197] Grundner, C.; Perrin, D.; Hooft van Huijsduijnen, R.; Swinnen, D.; Gonzalez, J.; Gee, C.L.; Wells, T.N.; Alber, T. Structural basis for selective inhibition of *Mycobacterium tuberculosis* protein tyrosine phosphatase PtpB. *Structure*, **2007**, *15*(4), 499-509.
- [198] Manger, M.; Scheck, M.; Prinz, H.; von Kries, J.P.; Langer, T.; Saxena, K.; Schwalbe, H.; Furstner, A.; Rademann, J.; Waldmann, H. Discovery of *Mycobacterium tuberculosis* protein tyrosine phosphatase A (MptpA) inhibitors based on natural products and a fragment-based approach. *Chembiochem*, **2005**, *6*(10), 1749-1753.
- [199] Noren-Muller, A.; Reis-Correa, I., Jr.; Prinz, H.; Rosenbaum, C.; Saxena, K.; Schwalbe, H.J.; Vestweber, D.; Cagna, G.; Schunk, S.; Schwarz, O.; Schiewe, H.; Waldmann, H. Discovery of protein phosphatase inhibitor classes by biology-oriented synthesis. *Proc. Natl. Acad. Sci. U.S.A.*, **2006**, *103*(28), 10606-10611.
- [200] Noren-Muller, A.; Wilk, W.; Saxena, K.; Schwalbe, H.; Kaiser, M.; Waldmann, H. Discovery of a new class of inhibitors of *Mycobacterium tuberculosis* protein tyrosine phosphatase B by biology-oriented synthesis. *Angew. Chem. Int. Ed. Engl.*, **2008**, *47*(32), 5973-5977.
- [201] Rawls, K.A.; Lang, P.T.; Takeuchi, J.; Imamura, S.; Baguley, T.D.; Grundner, C.; Alber, T.; Ellman, J.A. Fragment-based discovery of selective inhibitors of the *Mycobacterium tuberculosis* protein tyrosine phosphatase PtpA. *Bioorg. Med. Chem. Lett.*, **2009**, *19*(24), 6851-6854.

- [202] Soellner, M.B.; Rawls, K.A.; Grundner, C.; Alber, T.; Ellman, J.A. Fragment-based substrate activity screening method for the identification of potent inhibitors of the *Mycobacterium tuberculosis* phosphatase PtpB. *J. Am. Chem. Soc.*, **2007**, *129*(31), 9613-9615.
- [203] Tan, L.P.; Wu, H.; Yang, P.Y.; Kalesh, K.A.; Zhang, X.; Hu, M.; Srinivasan, R.; Yao, S.Q. High-throughput discovery of *Mycobacterium tuberculosis* protein tyrosine phosphatase B (MptpB) inhibitors using click chemistry. *Org. Lett.*, **2009**, *11*(22), 5102-5105.
- [204] Vintonyak, V.V.; Warburg, K.; Kruse, H.; Grimm, S.; Hubel, K.; Rauh, D.; Waldmann, H. Identification of thiazolidinones spirofused to indolin-2-ones as potent and selective inhibitors of the *Mycobacterium tuberculosis* protein tyrosine phosphatase B. *Angew. Chem. Int. Ed. Engl.*, **2010**, *49*(34), 5902-5905.
- [205] Zeng, L.F.; Xu, J.; He, Y.; He, R.; Wu, L.; Gunawan, A.M.; Zhang, Z.Y. A facile hydroxyindole carboxylic acid based focused library approach for potent and selective inhibitors of *Mycobacterium* protein tyrosine phosphatase B. *Chem. Med. Chem.*, **2013**, *8*(6), 904-908.
- [206] Mascarello, A.; Chiaradia, L.D.; Vernal, J.; Villarino, A.; Guido, R.V.; Perizzolo, P.; Poirier, V.; Wong, D.; Martins, P.G.; Nunes, R.J.; Yunes, R.A.; Andricopulo, A.D.; Av-Gay, Y.; Terenzi, H. Inhibition of *Mycobacterium tuberculosis* tyrosine phosphatase PtpA by synthetic chalcones: kinetics, molecular modeling, toxicity and effect on growth. *Bioorg. Med. Chem.*, **2010**, *18*(11), 3783-3789.
- [207] Chen, L.; Zhou, B.; Zhang, S.; Wu, L.; Wang, Y.; Franzblau, S.G.; Zhang, Z.Y. Identification and characterization of novel inhibitors of mPTPB, an essential virulent phosphatase from *Mycobacterium tuberculosis*. *ACS Med. Chem. Lett.*, **2010**, *1*(7), 355-359.
- [208] Beresford, N.J.; Mulhearn, D.; Szczepankiewicz, B.; Liu, G.; Johnson, M.E.; Fordham-Skelton, A.; Abad-Zapatero, C.; Cavet, J.S.; Taberner, L. Inhibition of MptpB phosphatase from *Mycobacterium tuberculosis* impairs mycobacterial survival in macrophages. *J. Antimicrob. Chemother.*, **2009**, *63*(5), 928-936.
- [209] Mascarello, A.; Orbem Menegatti, A.C.; Calcaterra, A.; Martins, P.G.A.; Chiaradia-Delatorre, L.D.; D'Acquarica, I.; Ferrari, F.; Pau, V.; Sanna, A.; De Logu, A.; Botta, M.; Botta, B.; Terenzi, H.; Mori, M. Naturally occurring Diels-Alder-type adducts from *Morus nigra* as potent inhibitors of *Mycobacterium tuberculosis* protein tyrosine phosphatase B. *Eur. J. Med. Chem.*, **2018**, *144*, 277-288.
- [210] Dutta, N.K.; He, R.; Pinn, M.L.; He, Y.; Burrows, F.; Zhang, Z.Y.; Karakousis, P.C. Mycobacterial Protein Tyrosine Phosphatases A and B Inhibitors Augment the Bactericidal Activity of the Standard Anti-tuberculosis Regimen. *ACS Infect. Dis.*, **2016**, *2* (3), 231-239.
- [211] Buttini, F.; Colombo, G. In *Drug Delivery Systems for Tuberculosis Prevention and Treatment*, **2016**.
- [212] Praphakar, R.A.; Shakila, H.; Azger Dusthacker, V.N.; Munusamy, M.A.; Kumar, S.; Rajan, M. A mannose-conjugated multi-layered polymeric nanocarrier system for controlled and targeted release on alveolar macrophages. *Polym. Chem.*, **2018**, *9* (5), 656-667.
- [213] Banerjee, S.; Roy, S.; Nath Bhaumik, K.; Kshetrapal, P.; Pillai, J. Comparative study of oral lipid nanoparticle formulations (LNFs) for chemical stabilization of antitubercular drugs: Physicochemical and cellular evaluation. *Artif. Cells Nanomed. Biotechnol.*, **2018**, *1*-19.
- [214] Oliveira, P.M.; Matos, B.N.; Pereira, P.A.; Gratieri, T.; Faccioli, L.H.; Cunha-Filho, M.S.; Gelfuso, G.M. Microparticles prepared with 50-190 kDa chitosan as promising non-toxic carriers for pulmonary delivery of isoniazid. *Carbohydr. Polym.*, **2017**, *174*, 421-431.
- [215] Li, D.; Li, L.; Ma, Y.; Zhuang, Y.; Li, D.; Shen, H.; Wang, X.; Yang, F.; Ma, Y.; Wu, D. Dopamine-assisted fixation of drug-loaded polymeric multilayers to osteoarticular implants for tuberculosis therapy. *Biomaterials Sci.*, **2017**, *5*(4), 730-740.
- [216] Bhardwaj, A.; Mehta, S.; Yadav, S.; Singh, S.K.; Grobler, A.; Goyal, A.K.; Mehta, A. Pulmonary delivery of antitubercular drugs using spray-dried lipid-polymer hybrid nanoparticles. *Artif. Cells Nanomed. Biotechnol.*, **2016**, *44*(6), 1544-1555.
- [217] Garg, T.; Goyal, A.K.; Rath, G.; Murthy, R. Spray-dried particles as pulmonary delivery system of anti-tubercular drugs: Design, optimization, *in vitro* and *in vivo* evaluation. *Pharm. Develop. Technol.*, **2016**, *21*(8), 951-960.
- [218] Alves, A.D.; Cavaco, J.S.; Guerreiro, F.; Lourenço, J.P.; Rosa da Costa, A.M.; Grenha, A. Inhalable antitubercular therapy mediated by locust bean gum microparticles. *Molecules*, **2016**, *21*(6), 702.
- [219] Hussain, A.; Singh, S.K.; Singh, N.; Verma, P.R.P. *In vitro-in vivo* silico simulation studies of anti-tubercular drugs doped with a self nanoemulsifying drug delivery system. *RSC Adv.*, **2016**, *6*(95), 93147-93161.
- [220] Goyal, A.K.; Garg, T.; Rath, G.; Gupta, U.D.; Gupta, P. Development and characterization of nanoembedded microparticles for pulmonary delivery of antitubercular drugs against experimental tuberculosis. *Mol. Pharm.*, **2015**, *12*(11), 3839-3850.
- [221] Saifullah, B.; Maitra, A.; Chrzastek, A.; Naeemullah, B.; Fakurazi, S.; Bhakta, S.; Hussein, M.Z. Nano-formulation of Ethambutol with multifunctional Graphene Oxide and magnetic nanoparticles retains its anti-tubercular activity with prospects of improving chemotherapeutic efficacy. *Molecules*, **2017**, *22*(10), 1697.
- [222] El-Ridy, M.S.; Yehia, S.A.; Kassem, M.A.-E.-M.; Mostafa, D.M.; Nasr, E.A.; Asfour, M.H. Niosomal encapsulation of ethambutol hydrochloride for increasing its efficacy and safety. *Drug Deliv.*, **2015**, *22*(1), 21-36.
- [223] Ahmad, M.I.; Nakpheng, T.; Srichana, T. The safety of ethambutol dihydrochloride dry powder formulations containing chitosan for the possibility of treating lung tuberculosis. *Inhal. Toxicol.*, **2014**, *26*(14), 908-917.
- [224] Costa-Gouveia, J.; Pancani, E.; Jouny, S.; Machelart, A.; Delorme, V.; Salzano, G.; Iantomasi, R.; Piveteau, C.; Queval, C.J.; Song, O.-R. Combination therapy for tuberculosis treatment: Pulmonary administration of ethionamide and booster co-loaded nanoparticles. *Sci. Rep.*, **2017**, *7*(1), 5390.
- [225] Debnath, S.K.; Saisivam, S.; Omri, A. PLGA Ethionamide Nanoparticles for Pulmonary Delivery: Development and *in vivo* evaluation of dry powder inhaler. *J. Pharm. Biomed. Anal.*, **2017**, *145*, 854-859.
- [226] Kumar, G.; Malhotra, S.; Shafiq, N.; Pandhi, P.; Khuller, G.K.; Sharma, S. *In vitro* physicochemical characterization and short term *in vivo* tolerability study of ethionamide loaded PLGA nanoparticles: potentially effective agent for multidrug resistant tuberculosis. *J. Microencapsul.*, **2011**, *28*(8), 717-728.
- [227] Matsunaga, I.; Naka, T.; Talekar, R.S.; McConnell, M.J.; Katoh, K.; Nakao, H.; Otsuka, A.; Behar, S.M.; Yano, I.; Moody, D.B.; Sugita, M. Mycolyltransferase-mediated glycolipid exchange in *Mycobacteria*. *J. Biol. Chem.*, **2008**, *283*(43), 28835-28841.
- [228] De Smet, K.A.; Weston, A.; Brown, I.N.; Young, D.B.; Robertson, B.D. Three pathways for trehalose biosynthesis in mycobacteria. *Microbiology*, **2000**, *146*( Pt 1), 199-208.
- [229] Woodruff, P.J.; Carlson, B.L.; Siridechadilok, B.; Pratt, M.R.; Senaratne, R.H.; Mougous, J.D.; Riley, L.W.; Williams, S.J.; Bertozzi, C.R. Trehalose is required for growth of *Mycobacterium smegmatis*. *J. Biol. Chem.*, **2004**, *279*(28), 28835-28843.
- [230] Perez, J.; Garcia, R.; Bach, H.; de Waard, J.H.; Jacobs, W.R., Jr.; Av-Gay, Y.; Bubis, J.; Takiff, H.E. *Mycobacterium tuberculosis* transporter MmpL7 is a potential substrate for kinase PknD. *Biochem. Biophys. Res. Commun.*, **2006**, *348*(1), 6-12.
- [231] Lun, S.; Guo, H.; Onajole, O.K.; Pieroni, M.; Gunosewoyo, H.; Chen, G.; Tipparaju, S.K.; Ammerman, N.C.; Kozikowski, A.P.; Bishai, W.R. Indoleamides are active against drug-resistant *Mycobacterium tuberculosis*. *Nat. Commun.*, **2013**, *4*, 2907.
- [232] Shah, I.M.; Laaberki, M.H.; Popham, D.L.; Dworkin, J. A eukaryotic-like Ser/Thr kinase signals bacteria to exit dormancy in response to peptidoglycan fragments. *Cell*, **2008**, *135*(3), 486-496.

## Conclusions

*M. tb* is an extraordinarily resilient microbe that has evolved means to defeat the host's immune system. Several virulence factors secreted by *M. tb* play a crucial role in targeting host signalling pathways. Following the compartmentalisation of the bacteria in macrophages, *M. tb* counteracts the microbicidal mechanisms carried out by the host, taking shelter in intracellular vacuoles. *M. tb*-mediated protein phosphorylation and dephosphorylation were found to be largely implicated in defining the infection status of the macrophages. The *M. tb* manipulating strategies to resist phagosome maturation and lysosomal transfer culminates in evading the host's immune surveillance and successful mycobacterial pathogenesis. Equally important, numerous protein kinases and phosphatases were shown to contribute to the adaptive responses generated by *M. tb* inside the host. Indeed, protein phosphorylation/dephosphorylation represents the main mechanism, whereby *M. tb* regulates the synthesis of its cell wall components, including MAs, which are the primary mediators of the impermeability of the *M. tb*'s outer membrane. Accordingly, exploring the potential of targeting *M. tb*-encoded protein kinases and phosphatases that were proved to be involved in the survival strategies evoked by the pathogen, represents a promising approach in the TB drug discovery that could provide patients with better prognosis. For instance, several PknG, MPtpA, MPtpB, and SapM inhibitors were remarkably efficacious in extricating the macrophages from the *M. tb* subduing tactics, wherefore the intracellular bacteria were trafficked to lysosomes and subsequently eliminated. However, targeting the mycobacterial kinases and phosphatases usually comes at a price owing to the potential off-target effects on the homologous human kinase and phosphatase counterparts, raising multiple concerns about selectivity. Due to the critical role of MAs in many aspects of *M. tb* pathophysiology, including growth, virulence, and survival, a plethora of research efforts have been dedicated to targeting crucial enzymes/proteins that are involved in MAs biosynthesis. In this respect, small molecules that inhibit biological targets in this synthetic machinery compromise the integrity of the mycobacterial outer membrane in view of the defective formation/accumulation of MAs, thereby inhibiting the mycobacterial growth/survival. Ideally, these targets should be different from the ones targeted by the currently used antibiotics with resistance issues in order to ensure that the newly developed compounds are effective against drug-resistant (DR) TB.

## **Chapter 3**

### **Bioisosteric Modification of Indole-2-Carboxamides as a Means to Develop Novel Antitubercular Agents**



## Background

During the laborious process of drug development, medicinal chemists often find themselves faced with the major debacle of converting a biologically active compound *in vitro* into a successful drug. While lead compounds may possess sufficient affinity/potency against certain biological target, most of these candidates fail due to issues related to metabolic stability, pharmacokinetics (PK), toxicity, and/or selectivity. This is well exemplified by the indole-2-carboxamides (I2Cs) which were previously shown to have an outstanding anti-tuberculosis (anti-TB) activity against drug-sensitive (DS) and drug-resistant (DR) *Mycobacterium tuberculosis* (*M. tb*) strains. Indeed, the high lipophilicity of several I2Cs accounted for their reduced bioavailability and accordingly their inactivity *in vivo* (1, 2). Therefore, the I2C chemotype is still in the lead optimisation stage in the TB drug discovery pipeline (3). To overcome the aforementioned issues, a key strategy is usually employed which is based on tactically replacing a specific chemical group in the lead compound with other bioisosteres. In the research article that we published in 2020, the *N*-adamantyl indoleamide framework was used as a template to design several arylcarboxamide analogues. In this respect, several scaffolds were incorporated in place of the indole ring, whilst maintaining the amide linkage and the bulky cycloaliphatic ring. Additionally, a different approach was adopted, in which extra spacers were added to the amide linker while retaining the indole and adamantane motifs. The I2Cs were shown to elicit their anti-TB activities via inhibiting a crucial membrane transporter in *M. tb*, denominated mycobacterial membrane protein large 3 (MmpL3, Chapter 1: section 1.5.2.6). Therefore, molecular docking analysis was performed on the top potent compounds in the MmpL3 active site, utilizing the reported X-ray crystal structure co-crystallised with an I2C derivative.

### 3.1. Introduction to Bioisosterism

The optimisation process of lead compounds into small molecule therapeutics entails several fundamental design principles. The mechanism of action of any identified lead molecule should be well known, ideally at the level of its exact interactions with the target protein and the knowledge of its pharmacophoric groups (4). After correlating a certain lead compound with a desired bioactivity profile, it is usually incumbent upon the medicinal chemistry team to determine potential substituents that would maintain and/or modulate specific desirable and undesirable features. Bioisosterism and scaffold hopping are well-established twin concepts in the drug discovery process which are particularly employed in the lead development stages (5). They are broadly defined as replacing parts of biologically active molecules with other fragments to obtain a new compound with similar biological effects (6). In fact, these strategies are widely employed in the pharmaceutical industry and academia to discover novel analogues while retaining the efficacy/potency of the initial lead compound. The follow-on pharmacologically active molecule is termed "*me-too*" when it is structurally related to the prototype compound in the same therapeutic class (7). The merits of these *me-too* molecules may include enhanced drug-like properties, reduced risk of drug-drug interactions and off-target side effects, and improved target specificity.

The first contemplation of the concept of isosterism is dated back to 1909 and was further refined in 1919, when the word "isostere", derived from the Greek words isos (same) and stereos (solid shape), was first coined by Irving Langmuir (5, 8). Indeed, the idea of isosterism was effectively captured in the experimental observations of Langmuir when he envisaged that the then unknown ketene would possess physical properties similar to diazomethane (8). Later, this term was expanded and given the label bioisosterism instead by Harris Friedman in 1950 (8). Adding the prefix bio- therein clearly indicates the necessity of mimicking the crucial pharmacophoric elements of the original molecule to ensure the new compounds are similarly recognised by the desired biological system. Upon planning a bioisosteric modification, the new substituent should maintain similar shape, size, pharmacophoric characteristics, electronic properties, and chemical reactivity (9). However, since it is nearly impractical to find two groups matching all these properties, assiduously weighing and balancing these parameters is crucial for a successful replacement. Therefore, the strict definition of bioisosterism has transformed into a more

contemporary interpretation that does not obey the electronic and steric requirements necessitated early on (10, 11). The new liberal definition accommodates a broader diversity of bioisosteric structural subunits that are markedly varied in shape and size from the moiety being emulated (10-12). In this context, bioisosteres were divided into classical and nonclassical bioisosteres (8). Classical bioisosteres embody the early definition of bioisosteres, in which structurally equivalent and simple groups, rings, or atoms are used. On the contrary, nonclassical bioisosteres encompass functionalities that are substantially different in steric, electronic, topological and physicochemical properties, extending the concept of bioisosterism to a more sophisticated and subtle manifestation of biochemical emulation (8).

It is important to notice that isosteric compounds may not necessarily be bioisosteric which means that the application of bioisosterism is contextual. In other words, isosteric substitutions can be effective in one biochemical setting and not another, suggesting that isosteres should be tailored to conform with different circumstances (8). To achieve this objective, a detailed insight into the physicochemical characteristics of the exchangeable functional groups, elements or heterocycles complemented by a sufficient level of understanding of the binding pocket of the compound is required (12). For example, the substituted part in the lead molecule could be an insignificant fragment that does not critically interact with the protein/receptor (11). Another scenario is that if the exchangeable motifs are relatively small, the resemblance of the corresponding molecules will amount to similar biological activities (11).

On the other hand, scaffold hopping is regarded as a subclass of the bioisosteric modifications, in which a significantly large part of the lead compound, namely the core scaffold, is exchanged (5, 6). The new core structure is usually preferable to the old one in terms of its improved direct interactions with the target protein and/or providing an optimal scaffolding that would enable the functional groups to be spatially arranged in the apt geometric configuration to engage with the protein (5, 6). The utility of bioisosteres and scaffold hopping is broad, such as improving selected characteristics in the original compound, including potency, selectivity, metabolic stability, and PK as well as modifying or eliminating toxicophores to enhance the compound's safety (8). Other reasons behind generating novel ligands may be correlated to simplifying the synthetic routes or generating new intellectual property to avoid patent related issues

(6, 12). Overall, although the relationship between isosteric replacements and biological activity can be oblique, bioisosterism and scaffold hopping remain the key tactical elements widely utilised during the optimisation process of drug candidates.

### 3.2. Discovery of The I2Cs as Potent Anti-TB Agents with Exceptional Activity Against DR-TB

Over the past decade, multiple research groups have identified numerous I2C analogues as potent anti-TB agents (1, 13, 14). Our team were among the pioneers who uncovered the potential of the I2C framework for developing lead molecules effective against DS and DR *M. tb* strains (1). Indeed, these efforts led to the identification of *N*-cyclooctyl-4,6-dimethyl-indole-2-carboxamide **1** in 2013 [minimum inhibitory concentration (MIC) = 0.0067 – 0.026  $\mu$ M (DS and DR *M. tb* strains)] (**Figure 3.1**). The toxicity profiling of this compound revealed its low cytotoxicity against Vero cells ( $IC_{50}$  = 54  $\mu$ M), thereby displaying high selectivity index value [SI (Vero cells  $IC_{50}$ /H37Rv MIC) = 4100]. In the serum inhibition titration (SIT) assay, compound **1** was found to be orally active, albeit with considerably less potency than the first-line anti-TB agent isoniazid (INH) (1). Later in the same year, our group demonstrated that this compound also kills *M. tb in vitro* with minimum bactericidal concentration (MBC) value of 0.026  $\mu$ M against H37Rv strain (15). In addition, in the *in vivo* murine infection models, compound **1** significantly lowered the colony forming unit (CFU) counts in the lungs of treated mice in comparison to the untreated ones, causing the mycobacterial burden to decline in a dose-dependent manner. In the same report, MmpL3 was identified as the target of the I2C analogues when a single mutation in the *mmpL3* gene was found to confer resistance to this class of compounds. Importantly, this mutant strain remained susceptible to various first and second-line TB antibiotics, indicating the lack of cross-resistance (15).

Around the same time, Rao *et al*, a Novartis research team, accentuated the promising *in vitro* and *in vivo* anti-TB activities, PK properties, and safety margin of the I2Cs (16). They documented that NITD-304 and NITD-349 (**Figure 3.1**) are possible preclinical drug candidates. Both compounds demonstrated bactericidal activity against replicating *M. tb in vitro* and intramacrophage. However, in the non-replicating persistent *M. tb* model, the activity of I2Cs diminished (NITD-304 > 27  $\mu$ M), suggesting that these compounds block a key step in the active metabolism of *M. tb*, similar to

INH (16). Importantly, the minimum inhibitory concentrations of NITD-304 and NITD-349, required to inhibit 99% of bacterial growth of diverse DR *M. tb* clinical isolates (MIC<sub>99</sub> range from < 0.04 to 0.08 μM), were found to be comparable to the wild-type H37Rv counterparts (MIC<sub>99</sub> = 0.02 – 0.04 μM). These results in turn corroborated the new mode of action of these analogues. In the acute murine infection models, the minimum effective doses (MED) of NITD-304 and NITD-349, determined as the lowest dose that significantly prevented the *M. tb* multiplication in the lungs compared to the initial pre-treatment bacterial load, were 37.5 and 25 mg/kg, respectively (16). Both compounds showed acceptable oral bioavailability in preclinical species, namely rodents and dogs, with effective partitioning at the site of *M. tb* infections in the lungs. In addition, in these preclinical species, NITD-304 and NITD-349 displayed favourable PK properties, wherein they showed moderate systemic clearance, large volume of distribution, and long elimination half-lives (16).

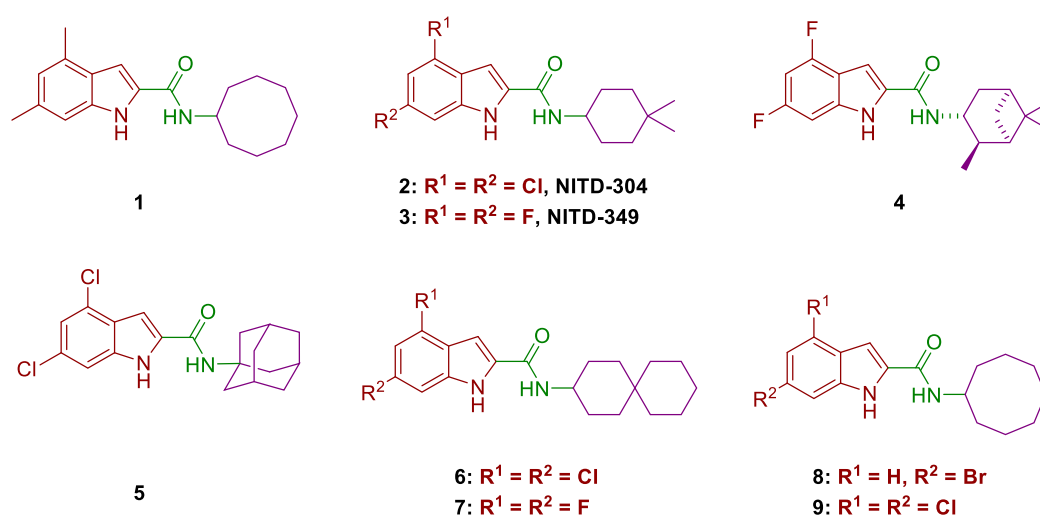


**Figure 3.1.** I2Cs 1 – 9 reported in the literature as potent antimycobacterial agents.

Similar to our group's approach, the Novartis team then conducted a whole-genome sequencing on several *M. tb* mutant strains resistant to the I2Cs which led to the identification of a single nucleotide polymorphism in the *mmpL3* gene. In accordance with our group's findings, Rao and colleagues found that the I2Cs resistance mutations are mapped onto the transmembrane domain of MmpL3 (15, 16). In order to eliminate the possibility that these mutations are ascribed to the ability of MmpL3 to act as a drug efflux pump, they tested the activity of NITD-304 and NITD-349 in the presence

of two broadly active efflux pump inhibitors (16). In this respect, they found that the sensitivity of *M. tb* to these I2Cs was unaltered, indicating that the *mmpL3* mutations-correlated resistance are not derived from drug efflux (i.e. direct inhibition of MmpL3, Chapter 1: section 1.5.2.6).

MmpL3 is an essential membrane protein transporter that is responsible for exporting trehalose monomycolate (TMM), the macromolecule lipid that serves as mycolic acids (MAs) precursor, across the plasma membrane from cytoplasm to periplasm (17). The formed mycolates then gradually accumulate in the mycobacterial outer membrane, thereby contriving a lipid rich matrix that plays a key role in the mycobacterial virulence, growth, and survival. In fact, Rao *et al* performed a lipid profiling analysis on one of the *M. tb* mutants resistant to the I2Cs revealing no discernible changes in the cell wall-anchored mycolates as well as extractable TMM and trehalose dimycolate (TDM) in the presence of the 4 × MIC of one I2C (16). On the contrary, when the wild-type H37Rv was treated with the same I2C analogue, a rapid depletion of cell wall-attached mycolates and accumulation of TMM were observed. The preceding data suggest that the I2Cs inhibition of MmpL3 results in a dearth of the TMM transportation, causing a downward spiral of the MAs' attachment to the mycobacterial cell wall and the subsequent weakening thereof, leading to cell lysis (16).

As a continuation of the work undertaken in 2013, our team reported more I2C derivatives as anti-TB agents in 2016, highlighting compound **4** (**Figure 3.1**) as a potential candidate for advancement to human clinical studies (2). Indeed, using compound **1** and NITD-304 (**2**) as lead compounds, compound **4** was identified as a potent anti-TB agent, displaying excellent activity against DS and DR *M. tb* strains (MIC = 0.006 – 0.047 μM). Compound **4** was also devoid of cytotoxicity against Vero cells (IC<sub>50</sub> > 192 μM, SI > 16000), indicating its improved safety margin compared to lead compound **1** (2). In addition, the *in vivo* bioavailability of compound **4** was found to be superior to that of compound **1** and comparable to INH in the SIT assay. On the contrary, in the same report, the indoleamides **5 – 7** (**Figure 3.1**), which showed high *in vitro* anti-TB activities (MIC = 0.003 – 0.011 μM), turned out to be inactive in the SIT analysis and were dropped from further studies (2). Additionally, compound **4** showed acceptable *in vivo* mouse efficacy and ADME (absorption, distribution, metabolism, and excretion) parameters. However, the observed *in vivo* activity of compounds **2** and **4** in the mouse infection model was significantly less than ethambutol (EMB) (2),

which is already considered a weak anti-TB drug relative to the other front-line TB antibiotics.

However, in a more recent study, when compound **4** was prepared in an optimised formulation [propylene glycol (PG):Tween80], Instead of the carboxymethyl cellulose (CMC) formulation used in the previous report, a significant improvement in the *in vivo* efficacy was observed (18). In fact, in a mouse infection model (4 weeks of treatment), 50 mg/kg of compound **4** in the PG:Tween80 formulation showed lower lung CFU counts compared to EMB (100 mg/kg) and the CMC formulation with 100 mg/kg of compound **4**. Interestingly, in a high-dose aerosol infection model in mice, compound **4** (10 mg/kg) showed superior *in vivo* potency compared to NITD-304 (**2**). In the same study, effects on *M. tb* cell morphology were studied using electron microscopy. In this respect, a significantly high number of the *M. tb* H37Rv cells showed deformations (dimples and wrinkles) when treated with compound **1** at 0.04 µg/mL (10 × its MIC value) (18). Importantly, our group also generated a putative homology model of MmpL3, depicting the main interactions stabilising compound **1** within the MmpL3 binding pocket. This homology model was deemed approximate at the time and suggested the presence of three subpockets; the indole ring and adamantane moiety occupied the first and third hydrophobic subpockets, respectively, whilst the amide linker was stabilised in the central hydrophilic subpocket via H-bonding (2). A few years later, the crystal structure of MmpL3 came to light (19) and the findings therein were in general agreement with the homology model constructed earlier.

### 3.3. Targeting Non-Tuberculous Mycobacteria (NTM) by I2Cs

Mycobacteria are vastly diverse species that can be divided into three categories, tuberculosis-causing mycobacteria, *Mycobacterium leprae* (*M. leprae*; causing leprosy), and NTM (20). To date, around 200 NTM species were identified, with the majority of them being non-pathogenic to animals or humans. Nonetheless, infections with opportunistic pathogenic NTM are correlated with an underappreciated burden of disease worldwide, especially in industrialised countries where these infections are more common than TB (20). More alarmingly, treating NTM infections is notoriously difficult owing to their intrinsic resistance to numerous key antibiotics. The pathogenic NTM strains can cause infections similar to those caused by *M. tb* (both pulmonary and extrapulmonary). Indeed, *Mycobacterium abscessus* (*M. abscessus*),

*Mycobacterium avium* (*M. avium*) complex (MAC), *Mycobacterium kansasii* (*M. kansasii*), *Mycobacterium malmonese* (*M. malmonese*), and *Mycobacterium xenopi* (*M. xenopi*) account for most cases of pulmonary infections among the NTM species (20). *M. abscessus* and *M. avium* complex also cause disseminated and/or systemic infections. One of the most commonly found NTM is *M. abscessus*, a rapidly growing mycobacterium that is responsible for severe mucosal, skin, and pulmonary infections. In addition, *M. abscessus* is mostly resistant to antibiotics, leaving patients with very limited options (20).

In 2017, our group evaluated the activity of numerous I2Cs against *M. abscessus* (21). The potent activities of compounds **8** and **9** (**Figure 3.1**) were highlighted *in vitro* against a wide panel of *M. abscessus* isolates, with an MIC value of 0.125 µg/mL in most strains. Likewise, the earlier reported lead compound **1** (**Figure 3.1**) displayed an MIC value of 0.125 µg/mL against one tested *M. abscessus* strain. The intracellular killing efficacy of compound **9** was also evaluated in infected macrophages, wherein it displayed a significant reduction in the *M. abscessus* load (21). Of note, both compounds **8** and **9** also showed potent anti-TB activity when tested against H37Rv strain (MIC = 0.0313 and 0.0039 µg/mL, respectively). They also displayed minimal cytotoxicities against Vero cells (IC<sub>50</sub> ≥ 64 and 8-16 µg/mL, respectively), resulting in high selectivity indices towards both *M. tb* and *M. abscessus* (21). Similar to *M. tb*, the activity of the I2Cs towards *M. abscessus* was correlated to targeting the MAs transporter MmpL3. Indeed, a single point mutation in *mmpL3*, in a spontaneously resistant *M. abscessus* mutant, was found to be implicated in the high resistance levels observed for the indoleamides **1**, **8** and **9**. In addition, the foregoing I2Cs strongly inhibited the TMM transport from cytoplasm to periplasm, resulting in the abolition of TDM production and abrogation of arabinogalactan mycolation (21). It is important to note that although some parallels were noticed in the structure-activity relationship (SAR) of I2Cs against *M. tb* and *M. abscessus*, this was not the case for many tested analogues. In fact, the *N*-linked cyclooctyl group is superior for activity against *M. abscessus*, whilst the *N*-linked adamantane or isopinocampheyl moieties were preferred for activity against *M. tb* (21). Of note, I2Cs showed no activity against several tested Gram-positive and Gram-negative bacteria, indicating their narrow spectrum of antibacterial activity (13, 16). Conversely, in addition to *M. tb* and *M. abscessus*, I2Cs showed potent activity against *Mycobacterium bovis* (*M. bovis*), *M.*



*xenopi*, and *Mycobacterium smegmatis* (*M. smegmatis*). These findings in turn substantiate the notion that the molecular target of this class is restricted to mycobacteria (13, 16, 21). Overall, the I2Cs appear to be multifaceted biologically active molecules that possess strong potencies against different mycobacterial species via targeting MmpL3.

### **3.4. Rational Design of Novel Aryl- and Heteroaryl-Carboxamide Derivatives as Novel Antimycobacterial Agents Predicated on The I2C Architecture**

The aforementioned favourable activity profiles of the I2Cs indicate that this framework provides a fertile ground for the potential development of novel analogues with promising antimycobacterial activity, including DR-TB. However, in many I2C analogues, the potent *in vitro* anti-TB activity was not mirrored *in vivo* presumably due to their highly lipophilic nature and the low water solubility associated thereupon. As a result, the I2Cs are currently in the lead development stage, wherein extensive modifications are being performed thereon to improve their biological activities, PK properties, and/or toxicity profiles. In congruence with these ongoing efforts, in this Chapter, several structural changes were introduced to the *N*-adamantyl-indole-2-carboxamide architecture. The main body of this work was aimed at steering away from the high lipophilicity correlated with the indole ring, while trying to maintain activity against the primary target MmpL3. Accordingly, the 4-quinolone ring was chosen as a bioisosteric replacement to the indole ring due to its significantly reduced lipophilicity compared to the indole moiety [estimated ClogP (ChemDraw) = 0.28 (quinolone), 2.13 (indole)]. Although high lipophilicity is generally a prerequisite for potent anti-TB activity, this is not a clear-cut phenomenon because of the high efficacy of the first-line anti-TB drugs that have low lipophilicity (22). Therefore, our presumption was that despite the decreased lipophilicity of the designed *N*-cycloaliphatic quinoloneamide derivatives, we may attain improved physicochemical properties in these compounds while retaining anti-TB potency similar to the parent indoleamides. The scaffold hopping approach was also employed by replacing the indole moiety with naphthalene and 4-arylthiazole. Importantly, the quinoloneamide, naphthamide, and 4-arylthiazole-2-amide structural subunits were previously integrated in compounds that showed appreciable anti-TB activities (23, 24). Additionally, we looked into modifying the amide linker connecting the indole moiety and the bulky cycloaliphatic group. Our findings were published in 2020 and the research article is incorporated herein.

## References

1. Onajole OK, Pieroni M, Tipparaju SK, Lun S, Stec J, Chen G, et al. Preliminary structure-activity relationships and biological evaluation of novel antitubercular indolecarboxamide derivatives against drug-susceptible and drug-resistant *Mycobacterium tuberculosis* strains. *J Med Chem*. 2013;56(10):4093-103.
2. Stec J, Onajole OK, Lun S, Guo H, Merenbloom B, Vistoli G, et al. Indole-2-carboxamide-based MmpL3 Inhibitors Show Exceptional Antitubercular Activity in an Animal Model of Tuberculosis Infection. *J Med Chem*. 2016;59(13):6232-47.
3. 2021 Global New TB Drug Pipeline, Available from: <https://www.newtbdrugs.org/pipeline/clinical> and <https://www.newtbdrugs.org/pipeline/discovery> (Accessed on 10 September 2021).
4. Lima LM, Barreiro EJ. Bioisosterism: a useful strategy for molecular modification and drug design. *Curr Med Chem*. 2005;12(1):23-49.
5. Brown N. Bioisosteres and Scaffold Hopping in Medicinal Chemistry. *Mol Inform*. 2014;33(6-7):458-62.
6. Lesnik S, Skrlj B, Erzen N, Bren U, Gobec S, Konc J, et al. BoBER: web interface to the base of bioisosterically exchangeable replacements. *J Cheminform*. 2017;9(1):62.
7. Aronson JK, Green AR. Me-too pharmaceutical products: History, definitions, examples, and relevance to drug shortages and essential medicines lists. *Br J Clin Pharmacol*. 2020;86(11):2114-22.
8. Meanwell NA. Synopsis of some recent tactical application of bioisosteres in drug design. *J Med Chem*. 2011;54(8):2529-91.
9. Wagener M, Lommerse JP. The quest for bioisosteric replacements. *J Chem Inf Model*. 2006;46(2):677-85.
10. Dick A, Cocklin S. Bioisosteric Replacement as a Tool in Anti-HIV Drug Design. *Pharmaceuticals (Basel)*. 2020;13(3).
11. Sheridan RP. The most common chemical replacements in drug-like compounds. *J Chem Inf Comput Sci*. 2002;42(1):103-8.
12. Meanwell NA. Fluorine and Fluorinated Motifs in the Design and Application of Bioisosteres for Drug Design. *J Med Chem*. 2018;61(14):5822-80.

13. Franz ND, Belardinelli JM, Kaminski MA, Dunn LC, Calado Nogueira de Moura V, Blaha MA, et al. Design, synthesis and evaluation of indole-2-carboxamides with pan anti-mycobacterial activity. *Bioorg Med Chem*. 2017;25(14):3746-55.
14. Kondreddi RR, Jiricek J, Rao SP, Lakshminarayana SB, Camacho LR, Rao R, et al. Design, synthesis, and biological evaluation of indole-2-carboxamides: a promising class of antituberculosis agents. *J Med Chem*. 2013;56(21):8849-59.
15. Lun S, Guo H, Onajole OK, Pieroni M, Gunosewoyo H, Chen G, et al. Indoleamides are active against drug-resistant *Mycobacterium tuberculosis*. *Nat Commun*. 2013;4:2907.
16. Rao SP, Lakshminarayana SB, Kondreddi RR, Herve M, Camacho LR, Bifani P, et al. Indolcarboxamide is a preclinical candidate for treating multidrug-resistant tuberculosis. *Sci Transl Med*. 2013;5(214):214ra168.
17. Xu Z, Meshcheryakov VA, Poce G, Chng SS. MmpL3 is the flippase for mycolic acids in mycobacteria. *Proc Natl Acad Sci U S A*. 2017;114(30):7993-8.
18. Lun S, Tasneen R, Chaira T, Stec J, Onajole OK, Yang TJ, et al. Advancing the Therapeutic Potential of Indoleamides for Tuberculosis. *Antimicrob Agents Chemother*. 2019;63(7).
19. Zhang B, Li J, Yang X, Wu L, Zhang J, Yang Y, et al. Crystal Structures of Membrane Transporter MmpL3, an Anti-TB Drug Target. *Cell*. 2019;176(3):636-48 e13.
20. Johansen MD, Herrmann JL, Kremer L. Non-tuberculous mycobacteria and the rise of *Mycobacterium abscessus*. *Nat Rev Microbiol*. 2020;18(7):392-407.
21. Kozikowski AP, Onajole OK, Stec J, Dupont C, Viljoen A, Richard M, et al. Targeting Mycolic Acid Transport by Indole-2-carboxamides for the Treatment of *Mycobacterium abscessus* Infections. *J Med Chem*. 2017;60(13):5876-88.
22. Machado D, Girardini M, Viveiros M, Pieroni M. Challenging the Drug-Likeness Dogma for New Drug Discovery in Tuberculosis. *Front Microbiol*. 2018;9:1367.
23. Gonec T, Bobal P, Suján J, Pesko M, Guo J, Kralova K, et al. Investigating the spectrum of biological activity of substituted quinoline-2-carboxamides and their isosteres. *Molecules*. 2012;17(1):613-44.
24. Lu X, Liu X, Wan B, Franzblau SG, Chen L, Zhou C, et al. Synthesis and evaluation of anti-tubercular and antibacterial activities of new 4-(2,6-dichlorobenzyloxy)phenyl thiazole, oxazole and imidazole derivatives. Part 2. *Eur J Med Chem*. 2012;49:164-71.

## STATEMENT OF CONTRIBUTION TO A CO-AUTHORED PUBLISHED PAPER

Chapter 3 includes a co-authored research article that has been published online in the RSC Advances journal (2020)

DOI: <https://doi.org/10.1039/C9RA10663D>

Publication link: <https://pubs.rsc.org/en/content/articlelanding/2020/ra/c9ra10663d>

Title: **Design, synthesis, and biological evaluation of novel arylcarboxamide derivatives as anti-tubercular agents**

Authors/Co-authors: **Shahinda S. R. Alsayed**, Shichun Lun, Giuseppe Luna, Chau C. Beh, Alan D. Payne, Neil Foster, William R. Bishai and Hendra Gunosewoyo

My contribution to the paper involved: 1) the conception, design, synthesis, purification, and chemical analysis of all the tested molecules, 2) interpreting all the results (chemistry and biology wise), 3) molecular docking of the compounds, 4) collecting and organising the information/data/references, and 5) preparing and writing up the whole manuscript.

(Signed)



(Date)

20/09/2021

Shahinda Sayed Rabie Alsayed

(Countersigned)



(Date)

20/9/21

Corresponding author of the paper: Dr Hendra Gunosewoyo

(Countersigned)

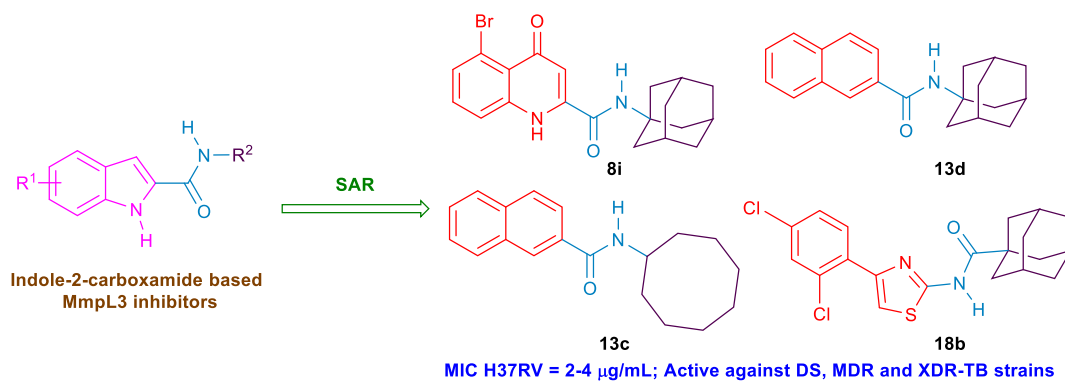


(Date)

20/9/21

Main supervisor: Dr Hendra Gunosewoyo

# Graphical Abstract




 Cite this: *RSC Adv.*, 2020, 10, 7523

# Design, synthesis, and biological evaluation of novel arylcarboxamide derivatives as anti-tubercular agents

 Shahinda S. R. Alsayed,<sup>a</sup> Shichun Lun,<sup>b</sup> Giuseppe Luna,<sup>a</sup> Chau Chun Beh,<sup>c</sup> Alan D. Payne,<sup>d</sup> Neil Foster,<sup>c</sup> William R. Bishai<sup>\*be</sup> and Hendra Gunosewoyo<sup>id\*<sup>a</sup></sup>

Our group has previously reported several indolecarboxamides exhibiting potent antitubercular activity. Herein, we rationally designed several arylcarboxamides based on our previously reported homology model and the recently published crystal structure of the mycobacterial membrane protein large 3 (MmpL3). Many analogues showed considerable anti-TB activity against drug-sensitive (DS) *Mycobacterium tuberculosis* (*M. tb*) strain. Naphthamide derivatives **13c** and **13d** were the most active compounds in our study (MIC: 6.55, 7.11  $\mu$ M, respectively), showing comparable potency to the first line anti-tuberculosis (anti-TB) drug ethambutol (MIC: 4.89  $\mu$ M). In addition to the naphthamide derivatives, we also identified the quinolone-2-carboxamides and 4-arylthiazole-2-carboxamides as potential MmpL3 inhibitors in which compounds **8i** and **18b** had MIC values of 9.97 and 9.82  $\mu$ M, respectively. All four compounds retained their high activity against multidrug-resistant (MDR) and extensively drug-resistant (XDR) *M. tb* strains. It is worth noting that the two most active compounds **13c** and **13d** also exhibited the highest selective activity towards DS, MDR and XDR *M. tb* strains over mammalian cells [IC<sub>50</sub> (Vero cells)  $\geq$  227  $\mu$ M], indicating their potential lack of cytotoxicity. The four compounds were docked into the MmpL3 active site and were studied for their drug-likeness using Lipinski's rule of five.

 Received 18th December 2019  
 Accepted 10th February 2020

DOI: 10.1039/c9ra10663d

[rsc.li/rsc-advances](http://rsc.li/rsc-advances)

## 1. Introduction

Tuberculosis (TB) is an infectious disease with a ubiquitous mortality worldwide caused by *Mycobacterium tuberculosis* (*M. tb*), which predominantly affects the lungs.<sup>1</sup> The 2019 World Health Organisation (WHO) report revealed that approximately one-quarter of the global population are latently infected with *M. tb*. According to the report, 10.0 million people fell ill with TB in 2018, a number that has become relatively stable over the past years. Globally, 1.2 million HIV-negative patients died from TB in 2018 in addition to 0.25 million deaths among HIV-positive people. This inexorable global burden of TB makes it one of the top ten leading causes of death worldwide and number one infectious disease killer, surpassing HIV/AIDS.<sup>1</sup> The onerous current treatment regimen requires 6 months

minimum administration of a cocktail of the first-line anti-TB drugs: isoniazid (INH), rifampicin (RIF), pyrazinamide (PZA) and ethambutol (EMB) for the treatment of drug-sensitive (DS) TB.<sup>1,2</sup> This drawn-out duration of therapy and high pill count in addition to their accompanied side effects, resulted in an incomplete eradication of TB due to the poor patient compliance and ultimately led to the emergence of drug-resistant TB.<sup>3</sup> Notably, the treatment period of the second-line anti-TB drugs used for multi- and extensively-drug resistant TB strains (MDR- and XDR-TB, respectively) may be extended up to two years accompanied with their limited efficacy, drug toxicity and higher price compared to the first line regimen.<sup>4</sup> Accordingly, anti-TB drugs with a novel mode of action to overcome the existing resistance to the current drugs, and shorter course of treatment, are urgently required.

The mycobacterial membrane protein large 3 (MmpL3) which is currently considered as one of the most druggable *M. tb* targets, is responsible for the translocation of mycolic acids (MAs) across the plasma membrane.<sup>5,6</sup> The MAs biosynthesis and incorporation on the mycobacterial cell wall was previously illustrated in our review article.<sup>7</sup> Summarised into five distinct steps, the first four steps of the process entail the biosynthesis of the MAs precursor, trehalose monomycolate (TMM), in the cytoplasm.<sup>7</sup> The last step involves flipping and release of the formed TMM across the inner membrane into the periplasm by the membrane

<sup>a</sup>School of Pharmacy and Biomedical Sciences, Faculty of Health Sciences, Curtin University, Bentley, Perth, WA 6102, Australia. E-mail: Hendra.Gunosewoyo@curtin.edu.au

<sup>b</sup>Center for Tuberculosis Research, Department of Medicine, Division of Infectious Disease, Johns Hopkins School of Medicine, 1550, Orleans Street, Baltimore, Maryland, 21231-1044, USA. E-mail: wbishai1@jhmi.edu

<sup>c</sup>Western Australia School of Mines: Minerals, Energy and Chemical Engineering, Curtin University, Bentley 6102, WA, Australia

<sup>d</sup>School of Molecular and Life Sciences, Curtin University, Perth, WA 6102, Australia

<sup>e</sup>Howard Hughes Medical Institute, 4000 Jones Bridge Road, Chevy Chase, Maryland, 20815-6789, USA



transporter MmpL3.<sup>6</sup> Thereafter, these MAs accumulate in the *M. tb* cell envelope constituting the major lipid component of the outer coating of mycobacteria, rendering an extremely hydrophobic and impermeable bilayer.<sup>8,9</sup> This formidable protective layer insulates the mycobacteria against exogenous compounds, including many antibiotics, and the host's immune system, underpinning its fundamental role in mycobacterial growth and survival in the host.<sup>8–10</sup> Hence, lipophilicity of the anti-TB derivatives (Clog *P*) has been proposed to have positive correlation with their anti-TB activity.<sup>11–16</sup> In other words, anti-TB derivatives with increased lipophilicity (high Clog *P*) are endowed with facilitated diffusion through the lipid-rich cell wall of *M. tb* and thereby enhanced efficacy.<sup>8</sup> The role of MmpL3 in shuttling TMM across the cytoplasmic membrane was proven in *M. smegmatis* when the conditional depletion of MmpL3 led to an intracellular accumulation of TMM and loss of cell wall mycolation.<sup>17–19</sup> In addition, downregulation of MmpL3 expression led to an abolition of cell division and consequently rapid cell death.<sup>20,21</sup> Therefore, inactivation of MmpL3 prohibits this pivotal step in the MAs biosynthesis machinery, collapsing the permeability barrier and validating MmpL3 as a promising target for anti-TB drugs.<sup>22,23</sup> Several MmpL3 inhibitors have been developed, including indolecarboxamides,<sup>14,24–27</sup> benzimidazoles,<sup>28</sup> adamantyl ureas,<sup>17</sup> diamines,<sup>18,29</sup> diphenyl pyrroles,<sup>30</sup> benzothiazoles,<sup>31,32</sup> spirocycles,<sup>33,34</sup> and tetrahydropyrazolopyrimidines.<sup>33,35</sup> Recent literature revealed that some of the well-known MmpL3 inhibitors indeed directly interact with MmpL3, whereas others impact the proton motive force in *M. tb*.<sup>36,37</sup> Our group has previously identified several indolecarboxamides as potent antimycobacterial agents targeting MmpL3.<sup>14,25,27</sup> The preliminary phenotypic screening identified the indole-2-carboxamide **1** (Fig. 1) as a highly potent anti-TB scaffold (MIC = 0.93 μM).<sup>27,38</sup> Further modifications on the indolecarboxamide core were then initiated in which a conspicuous increase in the activity was obtained when the cyclohexyl group was replaced by a cyclooctyl **2**, or an adamantyl ring.<sup>25</sup> More recently, the utmost potency was achieved when the 4,6-dimethyl group on the indole core was replaced with 4,6-dihalo-substituents (compounds **3** and **4**, Fig. 1). The methyl groups present a potential metabolic susceptibility (liable to metabolic oxidation), whereas the

dihalo groups are more resistant while conferring similar lipophilicity.<sup>14</sup>

A putative homology model for the MmpL3 transporter has also been generated to gain an approximate interpretation of the way the indole-2-carboxamides may interact with MmpL3.<sup>14</sup> This homology model proposed the existence of three putative binding subpockets in which our lead compound **3** is stabilised. Despite the high activity of compounds **3** and **4** *in vitro*, unfortunately they turned out to be inactive in the *in vivo* studies.<sup>14</sup> Very recently, the crystal structure of MmpL3 in *M. smegmatis* was reported by two different groups which serves as an excellent paradigm for the *M. tb* counterpart.<sup>39,40</sup> This crystal structure revealed that the MmpL3 inhibitor binding pocket is divided into five subsites (S1–S5) with the S4 subsite being the only hydrophilic one. The indole-2-carboxamides accommodated the S3–S5 subsites, resonating with our previously reported homology model.<sup>14,40</sup>

In this study, we describe the synthesis, *in vitro* biological evaluation and structure–activity relationship (SAR) of a number of arylamides rationally designed as potential anti-tubercular agents using the indole-2-carboxamides **3** and **4** as lead compounds. All the final compounds were screened *in vitro* against *M. tb* H37Rv strain. The top four potent compounds in our study were further evaluated for their antimycobacterial activity against *Mycobacterium abscessus* (*M. abs*), *Mycobacterium avium* (*M. avium*), MDR and XDR *M. tb* strains. In parallel, the cytotoxicity of these four compounds was also tested in Vero cells. Due to the analogy between the indole-2-carboxamides identified as MmpL3 inhibitors and our designed compounds, a docking analysis was performed on the most active compounds using the MmpL3 crystal structure<sup>40</sup> in complex with ICA38 **4**. Their drug-likeness was also assessed to predict their oral bioavailability.

## 2. Results and discussion

### 2.1. Compound design

The general strategy for the chemical modifications of the lead compound **3** is illustrated in Fig. 2 and aimed at enhancing the drug-like properties, particularly the lipophilicity and solubility, while retaining the anti-TB activity. The first approach was to investigate the activity of several heterocyclic and hydrocarbon scaffolds as a replacement of the indole ring, while keeping the important amide linkage that is capable of hydrogen bonding with the side chain of Asp645.<sup>40</sup> It is noteworthy that Asp645 is a crucial component of the two Asp–Tyr pairs which are implicated in the proton relay process.<sup>40</sup> This is consistent with the abrogation of the growth of mycobacteria in culture upon mutation of these two pairs in MmpL3.<sup>41</sup> Therefore, disrupting the two Asp–Tyr pairs blocks the proton motive force for substrate translocation. Towards this, bioisosteric replacements of the indole core by other aromatic moieties<sup>42</sup> have been employed. Hence, several quinolines **8a–k**, **11a–g** and **13a,b** as well as naphthalene derivatives **13c–g** were chosen (Fig. 2). In addition, *o*-hydroxy- and *o*-aminobenzamides **15a–d** were investigated due to their potential in mimicking the NH group of the indole-2-carboxamides. We also scrutinised the activity of

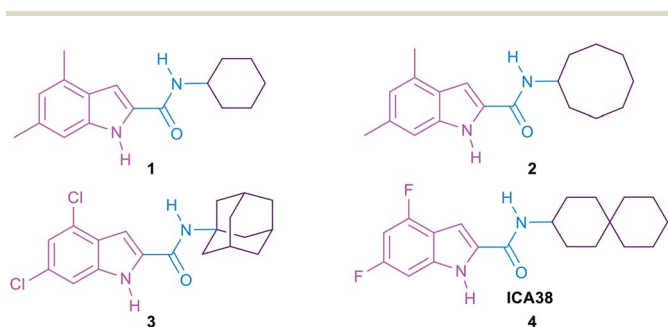


Fig. 1 Hit compound **1**, lead compounds **2**, **3** and **4**.



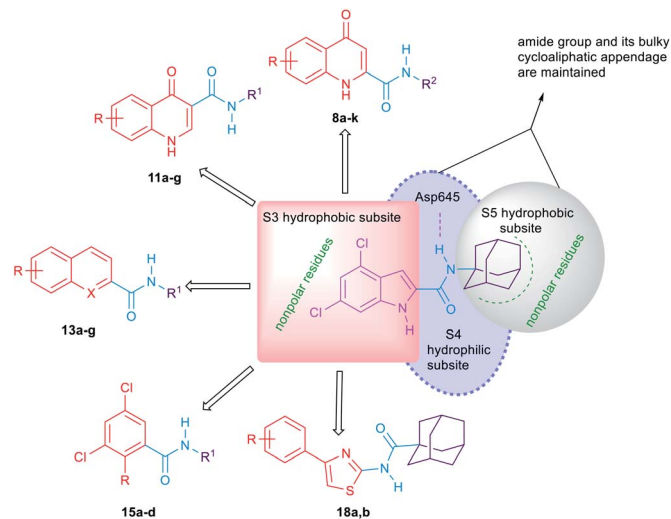


Fig. 2 A diagram indicating the main subpockets of MmpL3 in which the indole-2-carboxamide scaffold is stabilised through hydrophobic interactions and hydrogen bonding, and the strategies adopted for the replacement of the indole ring in lead compound **3**.

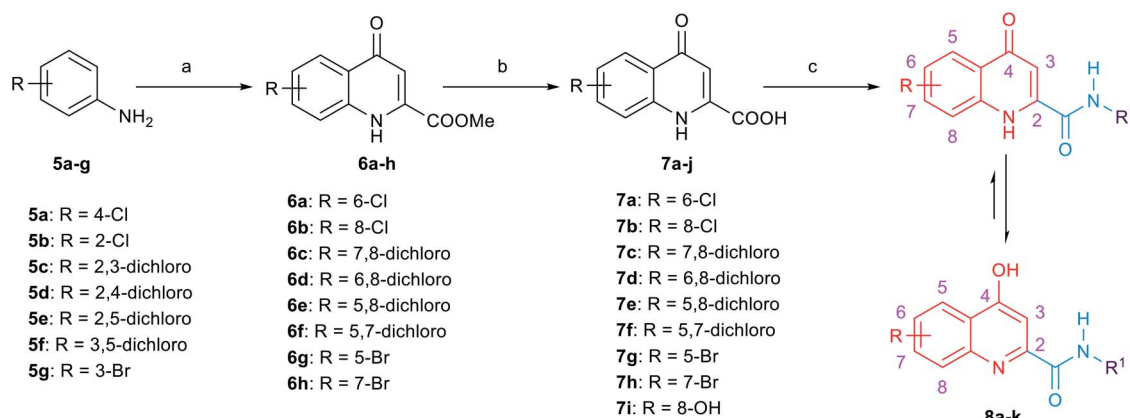
the 4-arylthiazole scaffold **18a,b** in which the substituted benzene ring is oriented in an extended way that could maximise its hydrophobic contacts with the S3 hydrophobic subsite. Throughout the indole replacement investigations, the N-linked hydrophobic moiety containing a lipophilic bulky adamantane or cyclooctane ring was maintained, as they are known to be essential for occupying the S5 hydrophobic subsite.<sup>40</sup>

The second approach was to introduce an extra one, two or three atom spacers to the amide linker while retaining both the 4,6-dihalosubstituted indole ring and the bulky hydrophobic adamantane ring. The reason behind this strategy was to investigate whether these extra atom spacers will participate in forming H-bonds with the hydrophilic residues in the S4 hydrophilic subsite, leading to an improved binding. These

extra spacer/s may also push the N-linked lipophilic moiety deeper to the S5 hydrophobic subsite maximising the hydrophobic interactions with the surrounding residues.

## 2.2. Chemistry

The synthetic routes to obtain the target arylamides **8a-k**, **11a-g**, **13a-g**, **15a-d**, **18a,b**, **21**, **23**, **24** and **27** are depicted in Schemes 1–4. The methyl 4-oxo-1,4-dihydroquinoline-2-carboxylates **6a-h** were obtained through a one-pot solvent-free hydroamination reaction<sup>43</sup> between commercially available anilines **5a-g** and dimethyl acetylenedicarboxylate followed by an intramolecular Friedel–Crafts reaction catalysed by polyphosphoric acid (PPA) (Scheme 1). Subsequent basic hydrolysis afforded the carboxylic acids **7a-h**, which were then coupled with the corresponding amines in the presence of hydroxybenzotriazole hydrate (HOBt) and 1-ethyl-3-(3-dimethylaminopropyl)carbodiimide hydrochloride (EDC·HCl) as coupling agents and *N,N*-diisopropylethylamine (DIPEA) as a base to form final compounds **8a-k**. Anilines **5a-g** were also reacted with 2-(ethoxymethylene)malonic acid diethyl ester (EMME) and the intermediate malonates obtained were cyclised under relatively extreme conditions by heating at 250 °C in diphenyl ether in a one pot reaction according to Gould–Jacobs procedure (Scheme 2). Subsequent basic hydrolysis of the ethyl 4-oxo-1,4-dihydroquinoline-3-carboxylates **9a-g** resulted in the carboxylic acids **10a-g**. These were then coupled with 1-adamantyl amine in the presence of *O*-(benzotriazol-1-yl)-*N,N,N'*-tetramethyluronium hexafluorophosphate (HBTU) as a coupling agent and DIPEA as a base to give the desired compounds **11a-g**. It is noteworthy that as observed by <sup>1</sup>H NMR and <sup>13</sup>C NMR, the 4-hydroxy-quinoline tautomeric form was predominantly manifested in the quinoline-2-carboxamide series (**8a-k**) with only compounds **8a,h-j** appeared in the 4-quinolone form. In the <sup>1</sup>H NMR spectra of the quinoline-2-carboxamides, the signals of the proton at position 3 of the 4-quinolone tautomers appeared at an upper magnetic field than



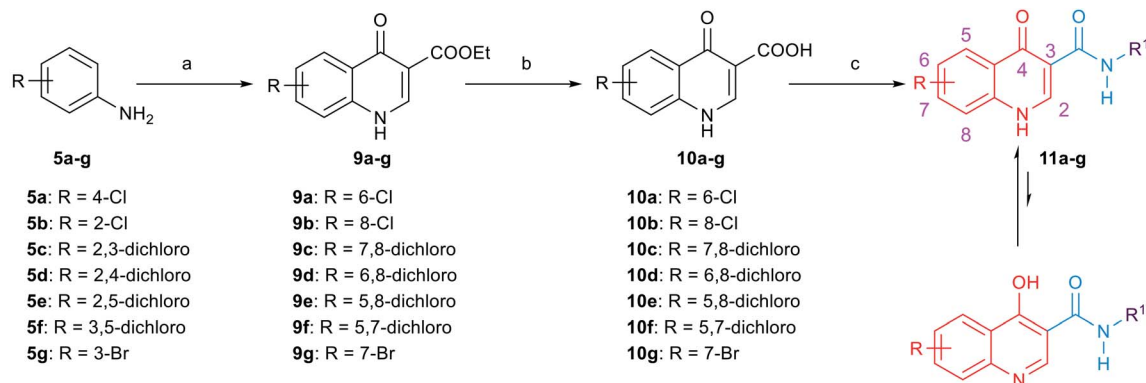
### Reagents and conditions:

(a) (i) dimethyl acetylenedicarboxylate, rt, 24–48 h (ii) polyphosphoric acid, 90 °C, 12 h, 30–92%; (b) 10% NaOH, MeOH, reflux, 4 h, 90–99%; (c) EDC·HCl, HOBt, corresponding amine, DIPEA, DMF, rt, 60–72 h, 25–76%.

Scheme 1 General synthetic procedure for compounds **8a-k**.





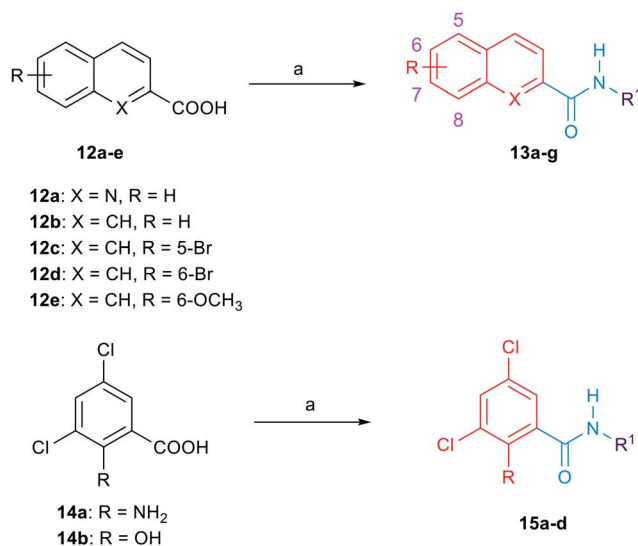
**Reagents and conditions:**

(a) i) 2-(ethoxymethylene)malonic acid diethyl ester, 100 °C, 12-18 h, ii) diphenylether, reflux, 4 h, 37-90%; (b) 10% NaOH, EtOH, reflux, 4 h, 80-90%; (c) HBTU, 1-adamantylamine, DIPEA, DMF, rt, 72 h, 51-89%.

Scheme 2 General synthetic procedure for compounds **11a-g**.

the 4-hydroxyquinoline counterparts. While in the  $^{13}\text{C}$  NMR spectra, the signals of the carbon at position 4 of the 4-quinolones were more deshielded than those of the corresponding 4-hydroxyquinolines. The preponderance of one of these

tautomers was found to be dependent on the NMR solvent used, in which in DMSO, the 4-hydroxy form is predominantly observed for the 2-substituted-quinolines.<sup>44</sup> On the contrary, also in line with another literature report,<sup>45</sup> only the 4-

**Reagents and conditions:**

(a) EDC.HCl, HOBT, corresponding amine, DIPEA, DCM or DMF, rt, 60-72 h, 31-92%; (b) iodine, thiourea, 100 °C, 3-5 h, 54-61%; (c) EDC.HCl, HOBT, 1-adamantanecarboxylic acid, DIPEA, DCM, rt, 72 h, 30-41%.

Scheme 3 General synthetic procedure for compounds **13a-g**, **15a-d** and **18a,b**.

quinolone tautomer was detected in the quinolone-3-carboxamide series **11a-g**.

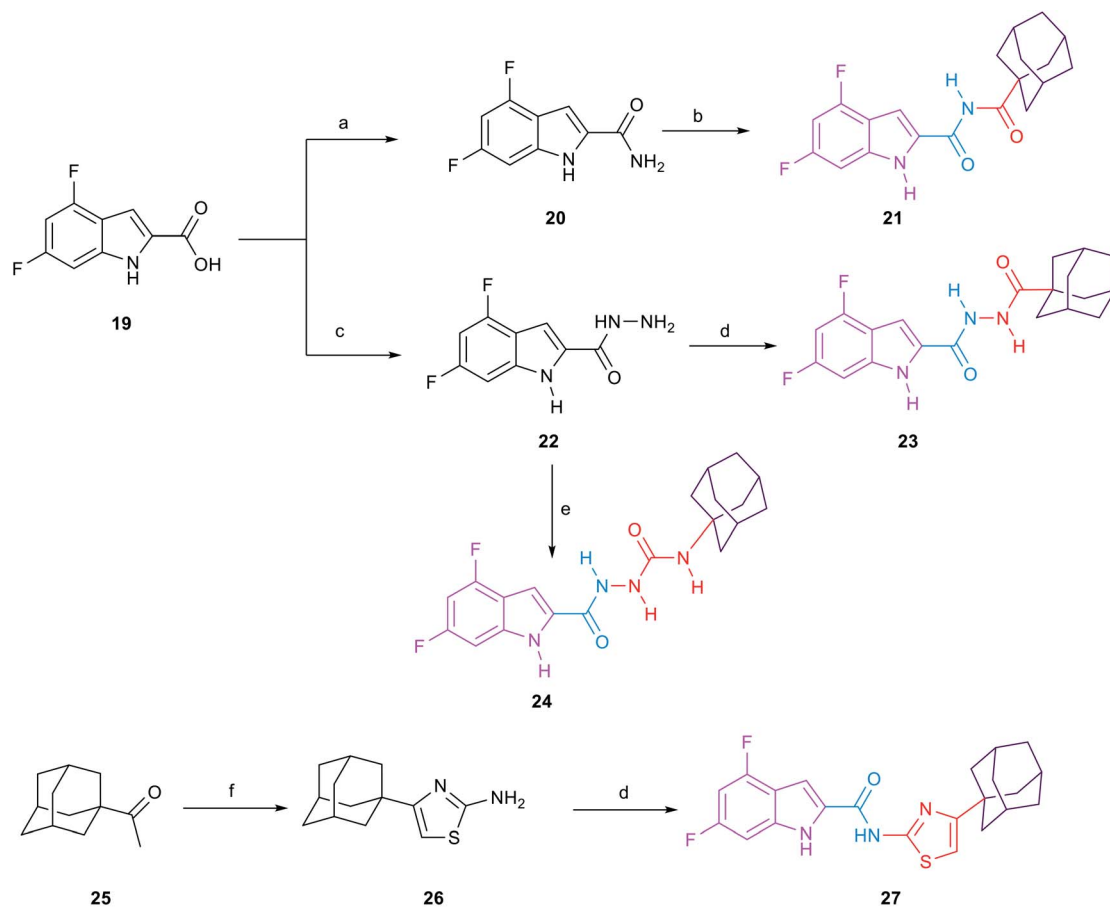
For the preparation of analogues **13a-g** and **15a-d** commercially available carboxylic acids **12a-e** and **14a,b**, respectively, were reacted with their corresponding amines under standard amide coupling conditions (Scheme 3). On the other hand, the aminothiazoles **17a,b** were prepared from the commercially available acetophenone derivatives **16a,b** using iodine and thiourea. Compounds **18a,b** were in turn obtained *via* amide coupling of the aminothiazoles **17a,b** with 1-adamantanecarboxylic acid.

The synthetic route of the novel indole derivatives is outlined in Scheme 4. The synthesis started with 4,6-difluoroindole-2-carboxylic acid (**19**) which was reacted with 1,1'-carbonyldiimidazole (CDI) and either ammonia or hydrazine hydrate to yield the corresponding carboxamide **20** and acetohydrazide **22**, respectively. The corresponding amide **20** was reacted in pyridine with 1-adamantanecarbonyl chloride, which was freshly prepared by treating 1-adamantanecarboxylic acid with oxalyl chloride, to yield the corresponding imide **21**. On the

other hand, the corresponding acetohydrazide **22** underwent two reactions. Firstly, it was reacted with 1-adamantanecarboxylic acid in a standard amide coupling condition forming compound **23**. Secondly, the reaction of **22** with 1-adamantyl isocyanate afforded the corresponding compound **24**. Finally, the 4-(1-adamantyl)-2-aminothiazole **26**, which was prepared by heating 1-acetyladamantane **25** with iodine and thiourea, was subjected to amide coupling conditions with the carboxylic acid derivative **19** to yield compound **27**, incorporating a thiazole ring next to the amide linker.

### 2.3. Biological evaluation and SAR analysis

Target compounds **8a-k**, **11a-g**, **13a-g**, **15a-d**, **18a,b**, **21**, **23**, **24** and **27** were screened *in vitro* against *M. tb* H37Rv strain to obtain the minimum inhibitory concentration (MIC) values using the Microplate Alamar Blue Assay (MABA)<sup>46</sup> as shown in Tables 1 and 2. The calculated Clog *P* values of the designed compounds were estimated using ChemDraw 16.0 to correlate their lipophilicity with the activity displayed. The first round of SAR investigation was focused on the role of the replacement of



#### Reagents and conditions:

a) CDI, NH<sub>4</sub>OH, DMF, rt, 12-16 h, 98%; b) 1-adamantanecarbonyl chloride, pyridine, reflux, 16 h, 42%; c) CDI, NH<sub>2</sub>NH<sub>2</sub>·H<sub>2</sub>O, DMF, rt, 12-16 h, 74%; d) EDC.HCl, HOBT, corresponding carboxylic acid, DIPEA, DCM, rt, 72 h, 30-48%; e) 1-adamantyl isocyanate, ethanol, reflux, 16 h, 54%; f) iodine, thiourea, 100 °C, 3-5 h, 63%.

Scheme 4 General synthetic procedure for compounds **21**, **23**, **24** and **27**.



the indole core with other scaffolds. First, we probed the biological activity of 4-oxoquinoline heterocyclic scaffold as a replacement to the indole core (Table 1). Nevertheless, in the quinoline-2-carboxamide series **8a–k**, the 4-hydroxy-quinoline form was the main tautomer in which compounds **8b–g,k** showed a drastic drop in the activity ( $\text{MIC} \geq 81.78 \mu\text{M}$ ) compared to the lead compound **3** ( $\text{MIC} = 0.011 \mu\text{M}$ ). It is noteworthy that the 8-hydroxy-quinoline derivative **8k** was equally potent to the 8-chloro counterpart **8c** although its  $\text{Clog } P$  is less than half that of **8c**. A similar trend in activity was observed in the 4-quinolone tautomers **8a,h** exhibiting a dramatic attenuation of activity ( $\text{MIC} > 89.67$  and  $40.89 \mu\text{M}$ ,

respectively). However, the bromo-substituted 4-quinolone tautomers **8i** ( $\text{MIC} = 9.97 \mu\text{M}$ ) and **8j** ( $\text{MIC} = 19.93 \mu\text{M}$ ) were the most active compounds in this series, with two-fold and four-fold less activity than the first line anti-TB drug ethambutol ( $\text{MIC} = 4.89 \mu\text{M}$ ), respectively. These data suggest that the 4-quinolone tautomer is likely preferred over the 4-hydroxy-quinoline form for antimycobacterial activity. In addition, the most favourable sites of substitution on the quinolone ring are positions 5 and 7 which resembles the data previously obtained from the indole-2-carboxamides.<sup>14,25</sup> In line with our pursuit of determining the activity of the quinolone scaffold, we scrutinised on shifting the carboxamide moiety to position 3 on the

Table 1 *In vitro* anti-TB activity of compounds **8a–k**, **11a–g**, **13a–g**, **15a–d**, **18a,b**

| Analogue   | R                  | R <sup>1</sup> | X  | MIC <sup>a</sup> ( $\mu\text{g mL}^{-1}$ ) | MIC ( $\mu\text{M}$ ) | $\text{Clog } P^b$ |
|------------|--------------------|----------------|----|--|-----------------------|--------------------|
| <b>8a</b>  | 6-Cl               | 1-Adamantane   | —  | >32  | >89.67                | 2.94               |
| <b>8b</b>  | 8-Cl               | 1-Adamantane   | —  | >32  | >89.67                | 2.94               |
| <b>8c</b>  | 8-Cl               | Cyclooctane    | —  | >32  | >96.14                | 3.43               |
| <b>8d</b>  | 7,8-Dichloro       | 1-Adamantane   | —  | $\geq 32$                                  | $\geq 81.78$          | 3.55               |
| <b>8e</b>  | 7,8-Dichloro       | Cyclooctane    | —  | $\geq 32$                                  | $\geq 87.13$          | 4.04               |
| <b>8f</b>  | 6,8-Dichloro       | Cyclooctane    | —  | $\geq 32$                                  | $\geq 87.13$          | 4.16               |
| <b>8g</b>  | 5,8-Dichloro       | 1-Adamantane   | —  | $\geq 32$                                  | $\geq 81.78$          | 3.67               |
| <b>8h</b>  | 5,7-Dichloro       | 1-Adamantane   | —  | 16   | 40.89                 | 3.67               |
| <b>8i</b>  | 5-Br               | 1-Adamantane   | —  | 4  | <b>9.97</b>           | 3.09               |
| <b>8j</b>  | 7-Br               | 1-Adamantane   | —  | 8  | 19.93                 | 3.09               |
| <b>8k</b>  | 8-OH               | 1-Adamantane   | —  | >32  | >94.56                | 1.60               |
| <b>11a</b> | 6-Cl               | 1-Adamantane   | —  | $\geq 32$                                  | $\geq 89.67$          | 3.20               |
| <b>11b</b> | 8-Cl               | 1-Adamantane   | —  | >32  | >89.67                | 3.20               |
| <b>11c</b> | 7,8-Dichloro       | 1-Adamantane   | —  | >32  | >81.78                | 3.81               |
| <b>11d</b> | 6,8-Dichloro       | 1-Adamantane   | —  | $\geq 32$                                  | $\geq 81.78$          | 3.93               |
| <b>11e</b> | 5,8-Dichloro       | 1-Adamantane   | —  | $\geq 32$                                  | $\geq 81.78$          | 3.93               |
| <b>11f</b> | 5,7-Dichloro       | 1-Adamantane   | —  | >32  | >81.78                | 3.93               |
| <b>11g</b> | 7-Br               | 1-Adamantane   | —  | $\geq 32$                                  | $\geq 79.74$          | 3.09               |
| <b>13a</b> | H                  | Cyclooctane    | N  | 16   | 56.66                 | 4.99               |
| <b>13b</b> | H                  | 1-Adamantane   | N  | 16   | 52.22                 | 4.50               |
| <b>13c</b> | H                  | Cyclooctane    | CH | 2  | <b>7.11</b>           | 5.18               |
| <b>13d</b> | H                  | 1-Adamantane   | CH | 2  | <b>6.55</b>           | 4.69               |
| <b>13e</b> | 5-Br               | 1-Adamantane   | CH | $\geq 32$                                  | $\geq 83.26$          | 5.70               |
| <b>13f</b> | 6-Br               | 1-Adamantane   | CH | $\geq 32$                                  | $\geq 83.26$          | 5.70               |
| <b>13g</b> | 6-OCH <sub>3</sub> | 1-Adamantane   | CH | $\geq 32$                                  | $\geq 95.40$          | 4.82               |
| <b>13h</b> | H                  | Cycloheptane   | N  | —  | <b>111</b> (ref. 47)  | 4.62               |
| <b>15a</b> | NH <sub>2</sub>    | 1-Adamantane   | —  | >32  | >94.32                | 4.85               |
| <b>15b</b> | NH <sub>2</sub>    | Cyclooctane    | —  | >32  | >101                  | 5.34               |
| <b>15c</b> | OH                 | 1-Adamantane   | —  | 32   | 94.05                 | 5.46               |
| <b>15d</b> | OH                 | Cyclooctane    | —  | 32   | 101                   | 5.95               |
| <b>18a</b> | 4-Cl               | —              | —  | 32   | 85.81                 | 5.87               |
| <b>18b</b> | 2,4-Dichloro       | —              | —  | 4  | <b>9.82</b>           | 6.34               |
| Isoniazid  | —                  | —              | —  | 0.04                                       | 0.29                  | −0.66              |
| Ethambutol | —                  | —              | —  | 1  | 4.89                  | 0.11               |

<sup>a</sup> The lowest concentration of drug reducing at least 90% of bacterial growth by the Microplate Alamar Blue Assay (MABA). The reported MIC values are an average of three individual measurements. <sup>b</sup> Calculated using ChemDraw 16.0.



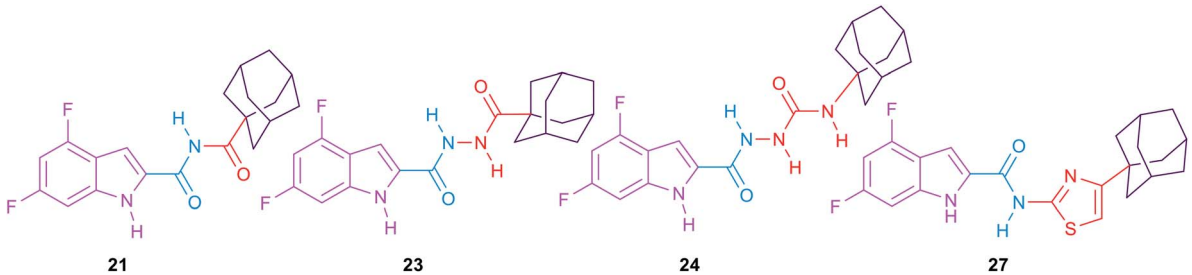
quinolone ring as shown in compounds **11a–g** (Table 1). Despite the sole formation of the 4-quinolone tautomer in this series, all the tested compounds **11a–g** did not show any improved anti-TB activity ( $MIC \geq 79.74 \mu M$ ). The attenuation in the activity of compounds **11f,g** ( $MIC \geq 81.78, \geq 79.74 \mu M$ , respectively) compared to its 2-carboxamide analogues **8h,j** ( $MIC = 40.89, 19.93 \mu M$ , respectively) is also consistent with our previous findings on the indole ring in which positioning the carboxamide group at position 2 was superior to position 3.<sup>14,25</sup> It is noteworthy that all the substituted quinoline derivatives **8a–k** and **11a–g** have lower lipophilicity than the lead indoleamides (compound **3** and **4**) which typically possess  $Clog P$  values of greater than 5. However, the wide gap in the activity between the quinolones and the previously reported indoles suggests that expanding the indole ring with an extra carbonyl group in case of the 4-quinolone ring is not favourable for their anti-TB activities.

Aiming to improve the water solubility by introducing an ionisable nitrogen atom and to extend our investigation on the effect of replacing the indole ring with a quinoline nucleus, we synthesised two quinoline-2-carboxamide derivatives **13a,b**. The *N*-cyclooctylquinoline-2-carboxamide **13a** was equipotent to the adamantane counterpart ( $MIC = 56.66$  and  $52.22 \mu M$ , respectively). Goncec *et al.* have previously investigated the anti-TB activity of similar quinoline derivatives.<sup>47</sup> Their cycloheptyl derivative **13h**, which showed the highest activity in their series of compounds, is two-fold less potent than our cyclooctyl counterpart **13a** ( $MIC = 111$  and  $56.66 \mu M$ , respectively). The authors hypothesised that increasing the bulkiness of the substituent on the amide nitrogen is directly related to the increase of the anti-TB activity, consistent with our previous

findings on the indole ring.<sup>25,47</sup> Surprisingly, however, they encountered a solubility issue when increasing the bulkiness of the amide *N*-cycloaliphatic ring in which they reported the cyclooctyl derivative to be devoid of anti-TB activity. The authors linked its lack of activity to its precipitation in the test media.<sup>47</sup> They also reported several unsubstituted-naphthalene-2-carboxamides in which the derivatives bearing a cycloheptyl or cyclooctyl ring were bereft of anti-TB activity. Contrary to their report, re-evaluation of the *N*-cyclooctyl-2-naphthamide **13c** led us to the identification of the most active compounds in the current series, together with its adamantyl derivative **13d**, with  $MIC$  values of  $7.11$  and  $6.55 \mu M$ , respectively (Table 1), which are very similar to the activity of ethambutol. The higher anti-TB activity of the naphthalene-2-carboxamide derivatives **13c,d** compared to the quinoline-2-carboxamide counterparts **13a,b** contradicts the previous findings reported by Goncec *et al.* The activity of several substituted naphthamides was further investigated in which the increase in lipophilicity in the various tested naphthamides was not accompanied by a rise of activity (**13a,b** vs. **13e–g**).

Further attempts to replace the indole core included the evaluation of the 2-substituted-3,5-dichlorobenzene ring in which we preserved the dichloro substitution besides introducing either a hydroxyl group or an amino group oriented in a way similar to the NH group of the indole-2-carboxamide **3**. Unfortunately, these modifications resulted in a drastic decrease in activity in compounds **15a–d**, with  $MIC$  value of  $\geq 94.05 \mu M$ , despite their high lipophilicity ( $Clog P = 4.85–5.95$ ). These data further highlight the necessity of the 4,6-disubstituted-indole ring in its entirety to elicit a strong anti-TB activity. Moreover, we probed the activity of two 4-arylthiazole

Table 2 *In vitro* anti-TB activity of the linker analogues, compounds **2** and **3**, isoniazid and ethambutol



| Analogue   | $MIC^a$ ( $\mu g mL^{-1}$ ) | $MIC$ ( $\mu M$ ) | $Clog P^b$ |
|------------|-----------------------------|-------------------|------------|
| <b>21</b>  | 8                           | 22.32             | 4.34       |
| <b>23</b>  | >32                         | >85.70            | 3.98       |
| <b>24</b>  | 32                          | 82.38             | 3.13       |
| <b>27</b>  | >32                         | >77.39            | 7.13       |
| <b>2</b>   | 0.004                       | 0.013             | 5.59       |
| <b>3</b>   | 0.004                       | 0.011             | 5.67       |
| Isoniazid  | 0.04                        | 0.29              | -0.66      |
| Ethambutol | 1                           | 4.89              | 0.11       |

<sup>a</sup> The lowest concentration of drug reducing at least 90% of bacterial growth by the microplate alamarBlue assay (MABA). The reported  $MIC$  values are an average of three individual measurements. <sup>b</sup> Calculated using ChemDraw 16.0.



Table 3 Activity [MIC ( $\mu\text{M}$ )] of the top four active compounds on selected clinical isolates of *M. tb* and toxicity on Vero cells [IC<sub>50</sub> ( $\mu\text{M}$ )]

|            | <i>M. abs</i><br>( $\mu\text{M}$ ) | <i>M. avium</i><br>( $\mu\text{M}$ ) | <i>M. tb</i> MIC ( $\mu\text{M}$ ) |                        |                         |                       |                        | IC <sub>50</sub> ( $\mu\text{M}$ ) |                 |
|------------|------------------------------------|--------------------------------------|------------------------------------|------------------------|-------------------------|-----------------------|------------------------|------------------------------------|-----------------|
|            |                                    |                                      | V4207/DS                           | V2475/MDR <sup>a</sup> | KZN494/MDR <sup>a</sup> | R506/XDR <sup>b</sup> | TF274/XDR <sup>b</sup> | Vero cells                         | SI <sup>c</sup> |
| <b>8i</b>  | >159                               | >159                                 | 9.97                               | 9.97                   | 9.97                    | 4.98                  | 4.98                   | 39.87                              | 4               |
| <b>13c</b> | >227                               | >227                                 | 7.11                               | 7.11                   | 7.11                    | 3.55                  | 3.55                   | $\geq 227$                         | $\geq 32$       |
| <b>13d</b> | >209                               | >209                                 | 6.55–13.10                         | 6.55                   | 6.55–13.10              | 3.27                  | 3.27                   | $\geq 419$                         | $\geq 64$       |
| <b>18b</b> | >157                               | >157                                 | 9.82                               | 19.64                  | 9.82                    | 4.91–9.82             | 4.91                   | 9.82                               | 1               |

<sup>a</sup> Resistant to isoniazid and rifampin. <sup>b</sup> Resistant to isoniazid, rifampin, levofloxacin, ofloxacin, and kanamycin. <sup>c</sup> Selectivity index (SI) = IC<sub>50</sub>(Vero)/MIC.

derivatives **18a,b** in which the aryl group is oriented in an extended way that might maximise its hydrophobic interactions with the S3 hydrophobic subsite. The 4-(2,4-dichlorophenyl)thiazole **18b** derivative was two-fold less active than ethambutol, while the 4-chloro counterpart **18a** showed a dramatic loss of activity (MIC = 9.82, 85.81  $\mu\text{M}$ , respectively). Of note is the fact that compound **18b** is more lipophilic than **18a**.

The second round of SAR investigation was focused on keeping the dihalosubstituted-indole nucleus intact as it was proven to be superior in terms of anti-TB activity. We examined the effect of varying the chain length connecting the indole core and the adamantane ring as shown in compounds **21**, **23**, **24** and **27**. The biological activities of these analogues were found to be independent of their lipophilicity (Table 2). The imide derivative **21** showed the highest activity (MIC = 22.32  $\mu\text{M}$ ) in this series compared to the 4 and 5 atom linker derivatives **23** and **24** which exhibited MIC values of >85.70 and 82.38, respectively. Additionally, introducing a thiazole ring next to the amide linker in compound **27** resulted in an inferior activity (MIC > 77.39  $\mu\text{M}$ ) compared to the imide derivative **21**, although its Clog *P* is higher than that of **21**.

Overall, although lipophilicity (high Clog *P*) of some of the designed compounds was correlated with high anti-TB activity, other lipophilic analogues did not display such a positive trend. Accordingly, it seems that lipophilicity is not the sole parameter influencing the anti-TB activity in our series of compounds. The four most active derivatives **8i**, **13c**, **13d** and **18b** (MIC  $\leq 4 \mu\text{g mL}^{-1}$ ) were chosen for further anti-mycobacterial studies, cytotoxicity evaluation and docking analysis.

#### 2.4. *In vitro* activity of the most active compounds against *M. abs*, *M. avium* and clinical isolates of *M. tb* as well as their cytotoxicity evaluation

The most active compounds in our study, namely **8i**, **13c**, **13d** and **18b** were further evaluated for their *in vitro* activity against *M. abs*, *M. avium* and a panel of clinical isolates of *M. tb* (Table 3). All four compounds were inactive against *M. abs* and *M. avium* strains (MIC > 157  $\mu\text{M}$ ), suggesting their selective activity against *M. tb*. On the other hand, within the tested panel of *M. tb* strains, originally obtained from pulmonary TB patients, one was drug sensitive (DS) (V4207), two were MDR *M. tb* (V2475, KZN494), and two were XDR *M. tb* (R506, TF274). To our delight, all four compounds maintained their high activity against the susceptible *M. tb* strain H37Rv in all the tested drug resistant strains. Of note is the fact that all four compounds showed a two-fold increase in activity against the XDR *M. tb* strains (R506, TF274) (Table 3). These high activities against the MDR and XDR TB highlight the potential use of these compounds to treat drug-resistant *M. tb* and the likelihood that they will not exhibit cross resistance with currently used medications. In addition, Vero cells were used to assess the cytotoxicity of the most active compounds against mammalian cells, and a selectivity index (SI) was subsequently calculated (Table 3). Compounds **13c** and **13d** exhibited higher IC<sub>50</sub> values (IC<sub>50</sub>  $\geq 227 \mu\text{M}$ , respectively) against Vero cells than compounds **8i** and **18b** (IC<sub>50</sub> = 9.82–39.87  $\mu\text{M}$ , respectively), resulting in high SI index values (Table 3). The aforementioned results accordingly indicate the potent antitubercular activity of compounds **13c**

Table 4 Docking score and H-bond interactions of lead compound **3**, ICA38 and synthesized compounds **8i**, **13c**, **13d** and **18b** in the MmpL3 binding pocket

| Compounds  | Docking score (kcal mol <sup>-1</sup> ) | No. of H-bonds | Distance | Amino acids | Ligand atom     |
|------------|---|----------------|----------|-------------|-----------------|
| <b>8i</b>  | -14.05                                  | 2              | 2.48     | Asp645      | NH of amide     |
|            |   |                | 2.68     | Asp645      | NH of quinolone |
| <b>13c</b> | -11.97                                  | 1              | 2.49     | Asp645      | NH of amide     |
| <b>13d</b> | -12.01                                  | 1              | 2.39     | Asp645      | NH of amide     |
| <b>18b</b> | -13.99                                  | 1              | 2.39     | Asp645      | NH of amide     |
| <b>3</b>   | -13.16                                  | 2              | 2.39     | Asp645      | NH of amide     |
|            |   |                | 2.75     | Asp645      | NH of indole    |
| ICA38      | -22.71                                  | 1              | 2.54     | Asp645      | NH of amide     |



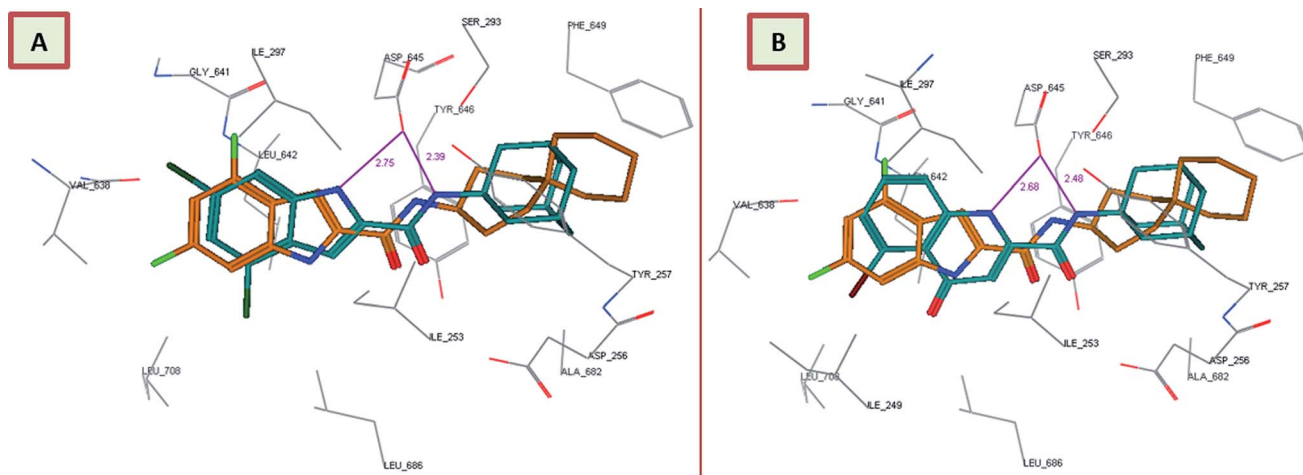


Fig. 3 Lead compound **3** and compound **8i** adopt a similar binding mode, overlaid onto the active site of MmpL3 together with ICA38. (A) Superposition of lead compound **3** (dark cyan), and ICA38 (light brown) in the MmpL3 binding pocket. (B) Superposition of **8i** (dark cyan) onto ICA38 (light brown) in the MmpL3 binding pocket.

and **13d** towards *M. tb* DS, MDR and XDR strains and their potential lack of toxicity toward mammalian cells.

### 2.5. Molecular docking of the most active compounds into MmpL3

In order to gain insight into whether the top-ranked active compounds ( $\text{MIC} \leq 4 \mu\text{g mL}^{-1}$ ) have the potential to fit in the MmpL3 binding site and compare their binding mode to the indoleamides binding profile, a molecular modeling study was performed using the crystal structure of MmpL3 in complex with ICA38 **4** (6AJJ).<sup>40</sup> Docking of compounds **8i**, **13c**, **13d** and **18b** as well as lead compound **3** and ICA38 **4** as reference ligands into the crystal structure of MmpL3 was carried out using MOE 2008.10 modeling software (Molecular Operating Environment).<sup>48</sup> The evaluation of each docking simulation was based on the London dG scores of the generated poses after molecular mechanics refinement indicating the interaction energy between the ligand and the MmpL3 binding site. The

docking scores for the top ranked poses of the aforementioned compounds are presented in Table 4. In order to validate the docking protocol, the co-crystallised ICA38 ligand **4** was redocked into MmpL3 active site and the docking pose was compared with the initial pose using root mean square deviation (RMSD). ICA38 docked almost at the same position ( $\text{RMSD} = 0.477 \text{ \AA}$ ) with docking score of  $-22.71 \text{ kcal mol}^{-1}$  (Table 4). The 4,6-dichloroindole nucleus is positioned in the S3 hydrophobic subsite, forming hydrophobic interactions with the surrounding residues. The amide linker is inserted in the S4 hydrophilic subsite in which the amide nitrogen hydrogen bonds to the side chain of Asp645 (distance =  $2.54 \text{ \AA}$ ). The S5 hydrophobic subsite accommodates the spirocarbocyclic group, forming hydrophobic contacts with the surrounding residues. In addition, lead compound **3** adopted a similar binding mode to ICA38 in the MmpL3 active site (Fig. 3A). An additional H-bond between the indole NH of lead compound **3** and Asp645 is formed (distance =  $2.75 \text{ \AA}$ ), Fig. 3A. Consequently, both

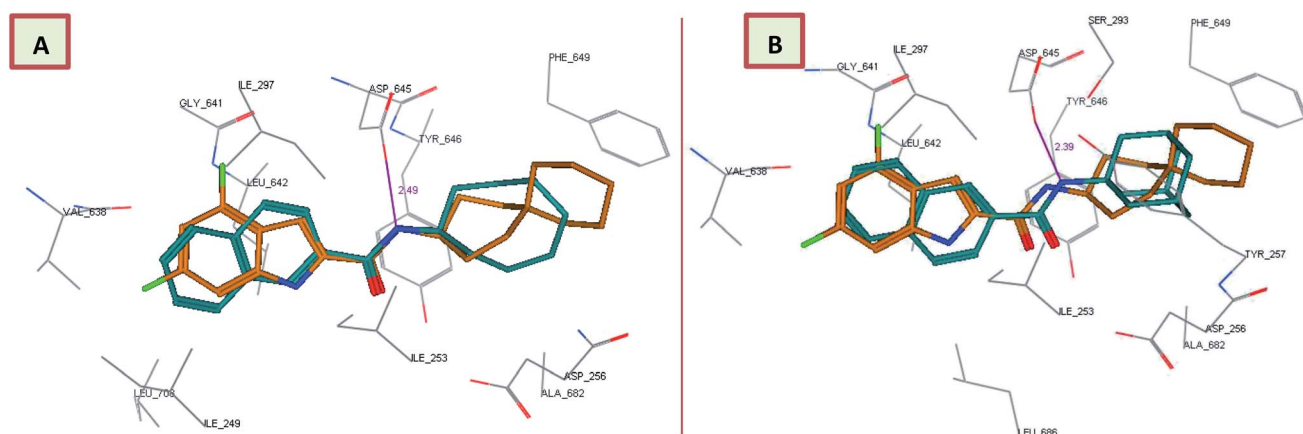


Fig. 4 Superposition of **13c** (A), **13d** (B) (dark cyan), and ICA38 (light brown) in the MmpL3 binding pocket, showing the inhibitors all have similar binding positions.



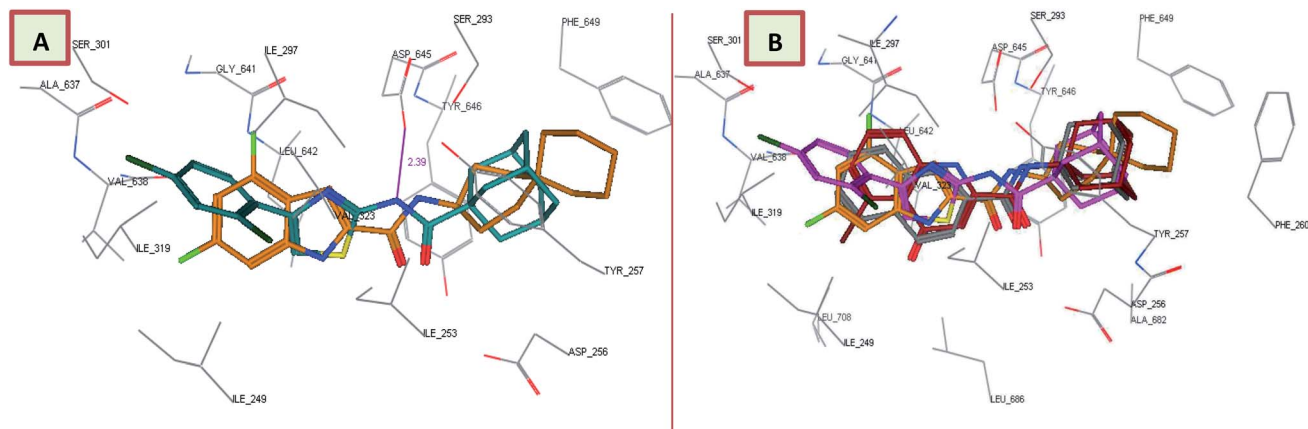


Fig. 5 **18b** binding mode and overlay of **8i**, **13d** and **18b** in the MmpL3 binding pocket. (A) Superimposition of **18b** (dark cyan), and ICA38 (light brown) in the MmpL3 active site, oriented in a similar way and having a similar binding mode as ICA38. (B) Superimposition of new classes of inhibitors in the MmpL3 active site with similar binding positions as ICA38. ICA38 (light brown), **8i** (dark red), **13d** (dark grey), and **18b** (magenta).

compound **3** and ICA38 inhibit the MmpL3 by occupying the proton translocation channel and blocking the proton motive force for substrate translocation by disrupting the two Asp–Tyr pairs for proton relay.<sup>40</sup> Docking of the 4-quinolone derivative **8i** pictured the MmpL3 active site overlaid with both **8i** and ICA38 (Fig. 3B). In addition to the H-bond formed between the amide NH and Asp645, the quinolone NH in compound **8i** H-bonds to Asp645 (distance = 2.48, 2.68 Å, respectively), in a similar manner to lead compound **3**.

Interestingly, the orientation of the most active compounds in our study **13c** and **13d** inside the active site resembled the ICA38 one. They also exhibited a docking score of  $-11.97$  and  $-12.01$  kcal mol<sup>-1</sup>, respectively. The naphthalene moiety occupies the S3 hydrophobic subsite, overlapping with the indole moiety of ICA38. Meanwhile, the amide NH H-bonds with Asp645 in the S4 hydrophilic subsite (distance = 2.49 and 2.39 Å, respectively), Fig. 4. Hence, similar to ICA38, these compounds likely disrupt the two Asp–Tyr pairs that play pivotal roles in proton transportation.

Surprisingly, the thiazole derivative **18b** recognised and showed high binding affinity to the same binding pocket of ICA38 (docking score =  $-13.99$  kcal mol<sup>-1</sup>). In addition, it is oriented in an extended conformation in the active site, adopting a nearly superimposed orientation with ICA38

(Fig. 5A). The 2,4-dichlorophenyl moiety of **18b** is embedded in the S3 hydrophobic subsite occupied by the indole ring of ICA38 and the amide NH H-bonds to Asp645 (distance = 2.39 Å). Again, this might explain its *in vitro* anti-TB activity due to occupying the proton translocation channel similar to ICA38. It is also noteworthy that the eight-fold improvement of the activity of the dichlorophenyl derivative **18b** compared with the monochlorophenyl counterpart **18a** might be attributed to the increase in the electron-withdrawing substituents. Accordingly, the phenyl  $\pi$ -electron density in the former one is less than the latter and the electronic repulsion is reduced, possibly favoring the hydrophobic interactions with the surrounding residues.

Overall, the tested novel classes of compounds show a similar binding mode and orientation as lead compound **3** and ICA38 in the same binding pocket (Fig. 5B). In addition, the *N*-linked hydrophobic moiety in these four compounds, is lodged in the S5 hydrophobic subsite overlapping with the spirocarbocyclic group of ICA38 (Fig. 3–5).

## 2.6. ADME profiling

The bioavailability of the most active compounds **8i**, **13c**, **13d** and **18b** as well as lead compound **3** and ICA38 **4** was predicted using ACD/Labs Percepta 2016 Build 2911 (13 Jul 2016) (Table 5). We particularly evaluated the drug-likeness of the

Table 5 Bioavailability of ICA38 and synthesized compounds **8i**, **13c**, **13d** and **18b** using ACD/Labs Percepta 2016 Build 2911 (13 Jul 2016). MW: molecular weight, HBD: H-bond donors, HBA: H-bond acceptors, log *P*: octanol–water partition coefficient, NRB: number of rotatable bonds, TPSA: topological polar surface area, PPB: plasma protein binding

| Analogues  | MW    | HBD | HBA | Clog <i>P</i><br>(Chemdraw) | log <i>P</i> | NRB | TPSA  | Solubility<br>(mg mL <sup>-1</sup> ) | Caco-2<br>( $\times 10^{-6}$ cm s <sup>-1</sup> ) | PPB (%) |
|------------|-------|-----|-----|-----------------------------|--------------|-----|-------|--------------------------------------|---|---------|
| <b>8i</b>  | 401.3 | 2   | 4   | 3.09                        | 4.66         | 2   | 58.20 | 0.007                                | 186   | 98      |
| <b>13c</b> | 281.4 | 1   | 2   | 5.18                        | 5.13         | 2   | 29.10 | 0.002                                | 190   | 95      |
| <b>13d</b> | 305.4 | 1   | 2   | 4.69                        | 4.91         | 2   | 29.10 | 0.007                                | 207   | 97      |
| <b>18b</b> | 407.4 | 1   | 3   | 6.34                        | 5.99         | 3   | 70.23 | 0.008                                | 77  | 99      |
| <b>3</b>   | 363.3 | 2   | 3   | 5.67                        | 5.49         | 2   | 44.89 | 0.001                                | 91  | 96      |
| ICA38      | 346.4 | 2   | 3   | 5.89                        | 5.17         | 2   | 44.89 | 0.0007                               | 132   | 96      |



compounds *via* assessing their compliance to Lipinski's "rule of five".<sup>49,50</sup> It is important to note, however, that although both lead compounds **3** and ICA38 **4** fulfilled all these rules, these compounds were reported to have poor *in vivo* bioavailability and therefore were not pursued for further studies.<sup>14,51</sup>

The four compounds that showed the highest *in vitro* anti-TB activity in our study **8i**, **13c**, **13d** and **18b** are lipophilic, exhibiting high Clog *P* values (Clog *P* = 4.66–5.99 in ACD Percepta). In addition, their Caco-2 permeability values ranged from 77–207 cm s<sup>-1</sup>, so they all are expected to permeate the cell membrane. Hence, the *in vitro* anti-TB activity of these compounds might be related to their high lipophilicity, and therefore their ability to cross the notoriously known hydrophobic outer membrane. In addition, all the compounds are predicted to have higher solubility than the lead compounds **3** and ICA38 (Table 5). Further studies are needed to ensure the *in vivo* bioavailability and anti-TB activity of these compounds.

### 3. Conclusion

In the present work we rationally designed and evaluated the anti-TB activity of a set of arylcarboxamide derivatives **8a–k**, **11a–g**, **13a–g**, **15a–d** and **18a,b**. Firstly, we replaced the indole ring in lead compound **3** with quinoline, naphthalene, 3,5-dichlorophenyl and 4-arylthiazole. The SAR of these analogues led us to infer that: (a) the 4,6-disubstituted-indole ring is the most beneficial moiety for potent anti-TB activity in which replacing it with 4-quinolone ring **8a–k** and **11a–g**, or *o*-hydroxy- and *o*-aminobenzamides **15a–d** led to a remarkable decrease of activity; (b) the 4-quinolone tautomers exhibited higher anti-TB activities compared to their 4-hydroxy-quinoline counterparts, with compound **8i** showing the highest activity in this series; (c) the carboxamide substitution at position 2 of the 4-quinolone ring is superior to position 3; (d) replacing the indole nucleus in lead compound **3** with naphthalene **13c,d** or 4-arylthiazole **18b** scaffolds was tolerated. Four compounds **8i**, **13c**, **13d** and **18b** exhibited decent *in vitro* anti-TB activities against DS *M. tb* strains, comparable to the activity of ethambutol. The antimycobacterial activity of these four compounds remained the same or two-fold increased when tested against MDR and XDR *M. tb* strains, respectively. However, none of these four compounds was active against *M. abs* or *M. avium* strains, corroborating their distinct activity against *M. tb*. In addition, compounds **13c** and **13d** showed higher IC<sub>50</sub> values against Vero cells than **8i** and **18b** and thus exhibiting high selectivity indices (SI), suggesting their potential lack of cytotoxicity. Taking into account that MmpL3 is the most relevant potential enzymatic target of our compounds, molecular docking simulations were conducted. Compounds **8i**, **13c**, **13d** and **18b** accommodated the MmpL3 active site that was previously reported to harbour the indoleamides, displaying a binding mode similar to ICA38 and lead compound **3**. In addition, we investigated the effect of extending the length of the linker connecting the 4,6-dihalosubstituted-indole and the adamantane ring. The three-atom linker derivative **21** was the most tolerated extension in this set of compounds (**21**, **23**, **24** and **27**).

Overall, the superimposed orientation of the quinolone-2-carboxamides, naphthamides, and 4-arylthiazole-2-carboxamides with ICA38 **4** in the same MmpL3 binding pocket supported their good *in vitro* potency against tested *M. tb* strains. These findings establish the quinolone, naphthalene, and 4-arylthiazole derivatives as promising novel classes of anti-TB compounds that potentially target MmpL3 and can be further evaluated *in vivo*.

## 4. Experimental section

### 4.1. Chemistry

**4.1.1. General information.** The following carboxylic acids, xanthurenic acid (**7i**), quinoline-2-carboxylic acid (**12a**), and 2-naphthoic acid (**12b**) were purchased from Sigma-Aldrich, while 5-bromo-2-naphthoic acid (**12c**), 6-bromo-2-naphthoic acid (**12d**), 6-methoxy-2-naphthoic acid (**12e**), 2-amino-3,5-dichlorobenzoic acid (**14a**), 3,5-dichloro-2-hydroxybenzoic acid (**14b**), 4,6-difluoroindole-2-carboxylic acid (**19**), and 1-acetylamantane (**25**) were purchased from FluoroChem. <sup>1</sup>H NMR and <sup>13</sup>C NMR spectra were recorded on a Bruker Avance III spectrometer at 400 and 100 MHz, respectively, with TMS as an internal standard. Standard abbreviations indicating multiplicity were as follows: s = singlet, d = doublet, dd = doublet of doublets, t = triplet, q = quadruplet, m = multiplet and br = broad. HRMS experiments were performed on a Thermo Scientific Q-Exactive Orbitrap mass spectrometer. TLC was performed with Analtech silica gel F TLC plates (200 microns, 20 × 20 cm). Flash chromatography was performed using a Teledyne Isco CombiFlash Rf system with RediSep columns or manually using SiliCycle UltraPure Silica Gels [40–63 μm (230–400 mesh)]. Final compounds were purified by preparative HPLC unless otherwise stated. The preparative HPLC employed an Omega 5 μm Polar C18 (21.2 mm × 150 mm) column, with detection at 254 and 280 nm on a Shimadzu SPD-20A detector, flow rate = 25.0 mL min<sup>-1</sup>. Method 1: 40–100% acetonitrile/H<sub>2</sub>O in 10 min; 100% acetonitrile in 10 min; 100–40% acetonitrile/H<sub>2</sub>O in 10 min. Method 2: 50–100% acetonitrile/H<sub>2</sub>O in 10 min; 100% acetonitrile in 10 min; 100–50% acetonitrile/H<sub>2</sub>O in 10 min. Method 3: 60–100% acetonitrile/H<sub>2</sub>O in 10 min; 100% acetonitrile in 10 min; 100–60% acetonitrile/H<sub>2</sub>O in 10 min. Both solvents contained 0.05 vol% of trifluoroacetic acid (TFA). Purities of final compounds were established by analytical HPLC, which was carried out using the Waters 1525 HPLC system with a Phenomenex 5 μm C18 (2) (150 × 4.6 mm), on a Waters 2487 dual wavelength detector. Analytical HPLC method: flow rate = 1 mL min; gradient elution over 30 min, from 100% H<sub>2</sub>O to 100% acetonitrile with 0.05% TFA. The purity of all tested compounds was >95% as determined by the method described above.

**4.1.2. General procedure for the synthesis of 6a–h.** A mixture of the appropriate aromatic amine **5a–g** (1 mmol) and diethylacetylenedicarboxylate (1.5 mmol) was stirred at room temperature until completion of the reaction as monitored by TLC (usually 24–48 h). PPA (2 mL) was then added to the reaction mixture and heated at 90 °C for 12 h. The reaction mixture was cooled, and 10 mL of water was added to it with stirring and





the resulting precipitate was collected by filtration, washed with water (3 × 20 mL) and dried. The crude product was purified by flash column chromatography on SiO<sub>2</sub> with CH<sub>2</sub>Cl<sub>2</sub>/MeOH gradient as the eluent to obtain the quinoline-2-carboxylic acid methyl ester derivatives **6a–h** in yields ranging from 30% to 92%. <sup>1</sup>H NMR data of compounds **6a–c** matched those reported previously in the literature.<sup>52,53</sup> A mixture of the 5-bromo and 7-bromo isomers **6g,h** were obtained in 1 : 1 ratio from 3-bromoaniline as a starting material and they were separated *via* recrystallization from dichloromethane (DCM).

*Methyl 6-chloro-4-oxo-1,4-dihydroquinoline-2-carboxylate (6a).*<sup>52</sup> Buff solid, yield: 76%. <sup>1</sup>H NMR (DMSO-*d*<sub>6</sub>) δ 3.97 (s, 3H), 6.65 (s, 1H), 7.76 (dd, *J* = 9.0, 2.4 Hz, 1H), 7.97–8.00 (m, 2H), 12.26 (s, 1H).

*Methyl 8-chloro-4-hydroxyquinoline-2-carboxylate (6b).*<sup>53</sup> Buff solid, yield: 70%. <sup>1</sup>H NMR (DMSO-*d*<sub>6</sub>) δ 3.95 (s, 3H), 7.19–7.78 (m, 2H), 7.98 (dd, *J* = 7.5, 1.3 Hz, 1H), 8.14 (d, *J* = 8.1 Hz, 1H), 12.25 (br s, 1H).

*Methyl 7,8-dichloro-4-hydroxyquinoline-2-carboxylate (6c).*<sup>53</sup> Buff solid, yield: 50%. <sup>1</sup>H NMR (DMSO-*d*<sub>6</sub>) δ 3.94 (s, 3H), 7.48 (s, 1H), 7.70 (d, *J* = 8.3 Hz, 1H), 8.07 (d, *J* = 8.9 Hz, 1H), 12.35 (br s, 1H).

*Methyl 6,8-dichloro-4-hydroxyquinoline-2-carboxylate (6d).* Buff solid, yield: 73%. <sup>1</sup>H NMR (DMSO-*d*<sub>6</sub>) δ 3.94 (s, 3H), 7.47 (br s, 1H), 8.12 (s, 2H), 12.36 (br s, 1H); <sup>13</sup>C NMR (DMSO-*d*<sub>6</sub>) δ 53.4, 106.5, 121.2, 124.1, 131.1, 131.5, 134.9, 143.5, 149.9, 162.9, 165.3.

*Methyl 5,8-dichloro-4-hydroxyquinoline-2-carboxylate (6e).* Buff solid, yield: 85%. <sup>1</sup>H NMR (DMSO-*d*<sub>6</sub>) δ 3.95 (s, 3H), 7.54 (br s, 2H), 7.86 (d, *J* = 8.2 Hz, 1H), 12.32 (br s, 1H); <sup>13</sup>C NMR (DMSO-*d*<sub>6</sub>) δ 53.4, 107.7, 120.7, 128.3, 129.6, 130.6, 133.1, 146.7, 149.5, 164.2, 165.4.

*Methyl 5,7-dichloro-4-oxo-1,4-dihydroquinoline-2-carboxylate (6f).* Buff solid, yield: 92%. <sup>1</sup>H NMR (DMSO-*d*<sub>6</sub>) δ 3.95 (s, 3H), 6.54 (s, 1H), 7.37 (s, 1H), 7.93 (d, *J* = 1.2 Hz, 1H), 12.00 (s, 1H); <sup>13</sup>C NMR (DMSO-*d*<sub>6</sub>) δ 54.1, 113.4, 118.4, 121.0, 126.2, 134.0, 136.5, 137.2, 143.4, 162.6, 176.7.

*Methyl 5-bromo-4-oxo-1,4-dihydroquinoline-2-carboxylate (6g).* The title compound was obtained by following the general procedure using 3-bromoaniline as a starting material. The crude product was purified by flash column chromatography with CH<sub>2</sub>Cl<sub>2</sub>/MeOH gradient as the eluent to obtain a mixture of compounds **6g** and **6h**, followed by crystallisation from DCM to give **6g** as an off white solid; yield: 30%. <sup>1</sup>H NMR (DMSO-*d*<sub>6</sub>) δ 3.96 (s, 3H), 6.59 (s, 1H), 7.41–7.61 (m, 2H), 7.95 (dd, *J* = 8.2, 1.3 Hz, 1H), 12.02 (s, 1H); <sup>13</sup>C NMR (DMSO-*d*<sub>6</sub>) δ 54.0, 112.4, 119.7, 120.1, 122.9, 130.8, 133.0, 137.2, 143.1, 162.6, 177.1.

*Methyl 7-bromo-4-oxo-1,4-dihydroquinoline-2-carboxylate (6h).* As previously mentioned, after obtaining a mixture of **6g** and **6h**, they were separated *via* crystallisation from DCM, affording **6h** as a light brown solid; yield: 30%. It was difficult to characterise its chemical structure by <sup>13</sup>C NMR due its very poor solubility even in DMSO-*d*<sub>6</sub>. <sup>1</sup>H NMR (DMSO-*d*<sub>6</sub>) δ 3.97 (s, 3H), 6.64 (s, 1H), 7.52 (dd, *J* = 8.6, 1.6 Hz, 1H), 7.99 (d, *J* = 8.6 Hz, 1H), 8.17 (d, *J* = 1.4 Hz, 1H), 12.10 (s, 1H).

**4.1.3. General procedure for the synthesis of 7a–h.** The appropriate ester **6a–h** (1 mmol) was refluxed for 4 h in

a mixture of 10% sodium hydroxide (5 mL) and methanol (5 mL). After cooling, the mixture was acidified by adding 2 M HCl and the solid obtained was collected by filtration, excessively washed with water and dried to obtain the quinoline-2-carboxylic acid derivatives in yields ranging from 90% to 99%. The crude product was used for next reaction without further purification.

**4.1.4. General procedure for the synthesis of 8a–k.** To a solution of the appropriate carboxylic acid **7a–i** (1 mmol) in anhydrous dichloromethane (DCM) or dimethylformamide (DMF, 10 mL), hydroxybenzotriazole hydrate (HOBt, 1.2 mmol) and 1-ethyl-3-(3-dimethylaminopropyl)carbodiimide hydrochloride (EDC·HCl, 1.2 mmol) were added at room temperature (rt) under an argon atmosphere. After stirring for 10 min, the corresponding amine (1.2 mmol) and *N,N*-diisopropylethylamine (DIPEA, 1.5 equiv.) were added, and the reaction mixture was stirred at room temperature until disappearance of the starting material (usually 60–72 h). After this time water (10 mL) was added, and the mixture was extracted with EtOAc (3 × 25 mL). The organic layers were separated, washed with water (5 × 25 mL), brine (1 × 25 mL), dried over anhydrous Na<sub>2</sub>SO<sub>4</sub>, filtered, and concentrated under reduced pressure. The crude product was purified by flash chromatography using CH<sub>2</sub>Cl<sub>2</sub>/MeOH gradient to obtain the quinoline-2-carboxamides **8a–k** in yields ranging from 25% to 76%, which were further purified by preparative HPLC.

*N-(1-Adamantanyl)-6-chloro-4-oxo-1,4-dihydroquinoline-2-carboxamide (8a).* White solid, yield: 56%. <sup>1</sup>H NMR (DMSO-*d*<sub>6</sub>) δ 1.66 (s, 6H), 2.08 (s, 9H), 6.91 (s, 1H), 7.72 (dd, *J* = 8.9, 2.4 Hz, 1H), 7.95 (d, *J* = 9.0 Hz, 1H), 8.01 (d, *J* = 2.1 Hz, 1H), 8.18 (s, 1H); <sup>13</sup>C NMR (DMSO-*d*<sub>6</sub>) δ 29.3, 36.4, 41.0, 52.7, 107.0, 123.5, 126.0, 129.3, 132.6, 140.1, 145.1, 158.4, 161.7, 174.7; HRMS (ESI) *m/z* calcd for C<sub>20</sub>H<sub>21</sub>ClN<sub>2</sub>O<sub>2</sub> ([M + H]<sup>+</sup>) *m/z* 357.1364; found 357.1356.

*N-(1-Adamantanyl)-8-chloro-4-hydroxyquinoline-2-carboxamide (8b).* White solid, yield: 70%. <sup>1</sup>H NMR (DMSO-*d*<sub>6</sub>) δ 1.69 (s, 6H), 2.10 (s, 9H), 7.54 (s, 2H), 7.97 (d, *J* = 7.5 Hz, 1H), 8.14 (d, *J* = 8.3 Hz, 1H), 8.20 (s, 1H), 12.20 (s, 1H); <sup>13</sup>C NMR (DMSO-*d*<sub>6</sub>) δ 29.3, 36.3, 41.3, 51.2, 102.3, 122.1, 123.3, 126.8, 131.1, 132.5, 143.8, 152.2, 162.5, 163.8; HRMS (ESI) *m/z* calcd for C<sub>20</sub>H<sub>21</sub>ClN<sub>2</sub>O<sub>2</sub> ([M + H]<sup>+</sup>) *m/z* 357.1364; found 357.1357.

*8-Chloro-N-cyclooctyl-4-hydroxyquinoline-2-carboxamide (8c).* White solid, yield: 66%. <sup>1</sup>H NMR (DMSO-*d*<sub>6</sub>) δ 1.44–1.91 (m, 14H), 3.93–4.14 (m, 1H), 7.52 (br s, 2H), 7.95 (d, *J* = 7.3 Hz, 1H), 8.12 (d, *J* = 7.2 Hz, 1H), 8.38 (br s, 1H), 12.21 (br s, 1H); <sup>13</sup>C NMR (DMSO-*d*<sub>6</sub>) δ 23.7, 25.5, 27.2, 32.0, 49.5, 102.8, 122.1, 123.4, 126.8, 131.2, 132.7, 144.1, 152.0, 162.7, 163.7; HRMS (ESI) *m/z* calcd for C<sub>18</sub>H<sub>21</sub>ClN<sub>2</sub>O<sub>2</sub> ([M + H]<sup>+</sup>) *m/z* 333.1364; found 333.1364.

*N-(1-Adamantanyl)-7,8-dichloro-4-hydroxyquinoline-2-carboxamide (8d).* White solid, yield: 74%. <sup>1</sup>H NMR (DMSO-*d*<sub>6</sub>) δ 1.68 (s, 6H), 2.09 (s, 9H), 7.56 (br s, 1H), 7.70 (d, *J* = 8.9 Hz, 1H), 8.10 (d, *J* = 9.0 Hz, 1H), 8.15 (s, 1H), 12.40 (s, 1H); <sup>13</sup>C NMR (DMSO-*d*<sub>6</sub>) δ 29.3, 36.3, 41.3, 51.3, 102.7, 121.7, 122.8, 127.6, 130.4, 134.5, 144.8, 153.2, 162.2, 164.1; HRMS (ESI) *m/z* calcd for C<sub>20</sub>H<sub>20</sub>Cl<sub>2</sub>N<sub>2</sub>O<sub>2</sub> ([M + H]<sup>+</sup>) *m/z* 391.0975; found 391.0964.



**7,8-Dichloro-*N*-cyclooctyl-4-hydroxyquinoline-2-carboxamide (8e).** White solid, yield: 76%.  $^1\text{H NMR}$  (DMSO- $d_6$ )  $\delta$  1.39–1.92 (m, 14H), 3.90–4.15 (m, 1H), 7.55 (br s, 1H), 7.70 (d,  $J = 7.8$  Hz, 1H), 8.10 (d,  $J = 8.8$  Hz, 1H), 8.36 (br s, 1H), 12.25 (br s, 1H);  $^{13}\text{C NMR}$  (DMSO- $d_6$ )  $\delta$  23.8, 25.5, 27.2, 32.1, 49.6, 103.2, 121.7, 122.9, 127.6, 130.4, 134.6, 145.0, 153.0, 162.5, 163.9; HRMS (ESI)  $m/z$  calcd for  $\text{C}_{18}\text{H}_{20}\text{Cl}_2\text{N}_2\text{O}_2$  ( $[\text{M} + \text{H}]^+$ )  $m/z$  367.0975; found 367.0967.

**6,8-Dichloro-*N*-cyclooctyl-4-hydroxyquinoline-2-carboxamide (8f).** White solid, yield: 50%.  $^1\text{H NMR}$  (DMSO- $d_6$ )  $\delta$  1.36–1.91 (m, 14H), 3.94–4.12 (m, 1H), 7.55 (br s, 1H), 8.08 (s, 2H), 8.36 (br s, 1H), 12.44 (br s, 1H);  $^{13}\text{C NMR}$  (DMSO- $d_6$ )  $\delta$  23.7, 25.5, 27.2, 32.0, 49.5, 103.6, 121.1, 123.6, 130.5, 131.2, 134.3, 142.7, 152.3, 162.4, 163.0; HRMS (ESI)  $m/z$  calcd for  $\text{C}_{18}\text{H}_{20}\text{Cl}_2\text{N}_2\text{O}_2$  ( $[\text{M} + \text{H}]^+$ )  $m/z$  367.0975; found 367.0966.

***N*-(1-Adamantanyl)-5,8-dichloro-4-hydroxyquinoline-2-carboxamide (8g).** White solid, yield: 38%.  $^1\text{H NMR}$  (DMSO- $d_6$ )  $\delta$  1.69 (s, 6H), 2.09 (s, 9H), 7.47–7.74 (m, 2H), 7.91 (d,  $J = 7.8$  Hz, 1H), 8.13 (s, 1H), 12.40 (s, 1H);  $^{13}\text{C NMR}$  (DMSO- $d_6$ )  $\delta$  29.3, 36.4, 41.4, 51.2, 104.5, 120.3, 128.6, 128.9, 130.2, 132.1, 145.5, 152.0, 162.1, 164.9; HRMS (ESI)  $m/z$  calcd for  $\text{C}_{20}\text{H}_{20}\text{Cl}_2\text{N}_2\text{O}_2$  ( $[\text{M} + \text{H}]^+$ )  $m/z$  391.0975; found 391.0971.

***N*-(1-Adamantanyl)-5,7-dichloro-4-oxo-1,4-dihydroquinoline-2-carboxamide (8h).** White solid, yield: 32%.  $^1\text{H NMR}$  (DMSO- $d_6$ )  $\delta$  1.65 (s, 6H), 2.07 (s, 9H), 6.77 (s, 1H), 7.37 (s, 1H), 7.96 (s, 1H), 8.18 (s, 1H), 11.73 (s, 1H);  $^{13}\text{C NMR}$  (DMSO- $d_6$ )  $\delta$  29.3, 36.4, 41.0, 53.0, 110.5, 118.4, 120.4, 125.9, 134.0, 136.1, 141.7, 143.5, 161.1, 177.1; HRMS (ESI)  $m/z$  calcd for  $\text{C}_{20}\text{H}_{20}\text{Cl}_2\text{N}_2\text{O}_2$  ( $[\text{M} + \text{H}]^+$ )  $m/z$  391.0975; found 391.0965.

***N*-(1-Adamantanyl)-5-bromo-4-oxo-1,4-dihydroquinoline-2-carboxamide (8i).** White solid, yield: 25%.  $^1\text{H NMR}$  (DMSO- $d_6$ )  $\delta$  1.67 (s, 6H), 2.09 (s, 9H), 6.74 (br s, 1H), 7.45–7.52 (m, 2H), 7.93 (dd,  $J = 8.4, 1.0$  Hz, 1H), 8.18 (s, 1H), 11.69 (s, 1H);  $^{13}\text{C NMR}$  (DMSO- $d_6$ )  $\delta$  29.3, 36.4, 41.0, 52.8, 109.3, 119.4, 120.1, 122.2, 130.5, 132.5, 141.6, 143.0, 161.5, 177.3; HRMS (ESI)  $m/z$  calcd for  $\text{C}_{20}\text{H}_{21}\text{BrN}_2\text{O}_2$  ( $[\text{M} + \text{H}]^+$ )  $m/z$  401.0859; found 401.0849.

***N*-(1-Adamantanyl)-7-bromo-4-oxo-1,4-dihydroquinoline-2-carboxamide (8j).** White solid, yield: 32%.  $^1\text{H NMR}$  (DMSO- $d_6$ )  $\delta$  1.67 (s, 6H), 2.09 (s, 9H), 6.81 (br s, 1H), 7.51 (s, 1H), 7.99 (d,  $J = 8.4$  Hz, 1H), 8.11–8.25 (m, 2H), 11.80 (br s, 1H);  $^{13}\text{C NMR}$  (DMSO- $d_6$ )  $\delta$  29.3, 36.4, 41.0, 52.8, 108.3, 122.1, 124.6, 126.0, 127.2, 127.3, 141.4, 143.0, 161.6, 177.9; HRMS (ESI)  $m/z$  calcd for  $\text{C}_{20}\text{H}_{21}\text{BrN}_2\text{O}_2$  ( $[\text{M} + \text{H}]^+$ )  $m/z$  401.0859; found 401.0848.

***N*-(1-Adamantanyl)-4,8-dihydroxyquinoline-2-carboxamide (8k).** White solid, yield: 42%.  $^1\text{H NMR}$  (DMSO- $d_6$ )  $\delta$  1.68 (s, 6H), 2.08 (s, 3H), 2.14 (s, 6H), 7.09 (dd,  $J = 7.6, 0.9$  Hz, 1H), 7.37 (s, 1H), 7.45–7.68 (m, 2H), 8.68 (br s, 1H), 10.10 (br s, 1H);  $^{13}\text{C NMR}$  (DMSO- $d_6$ )  $\delta$  29.4, 36.5, 41.4, 51.9, 102.4, 112.3, 122.6, 127.5, 138.4, 138.8, 150.3, 153.9, 162.8, 163.4; HRMS (ESI)  $m/z$  calcd for  $\text{C}_{20}\text{H}_{21}\text{BrN}_2\text{O}_2$  ( $[\text{M} + \text{H}]^+$ )  $m/z$  339.1703; found 339.1693.

**4.1.5. General procedure for the synthesis of 9a–g.** A mixture of the appropriate aromatic amine **5a–g** (1 mmol) and 2-ethoxymethylene-malonic acid diethyl ester (2 mmol) was heated at 100 °C until completion of the reaction as monitored by TLC (usually 12–18 h). Diphenyl ether (3 mL) was then added to the reaction mixture and heated at 250 °C for 4 h. After the

reaction mixture was cooled at room temperature, 10 mL of hexane was added to it with stirring and the formed precipitate was collected by filtration, washed with hexane (3 × 10 mL), recrystallized from DMF to provide the quinoline-3-carboxylic acid ethyl ester derivatives in yields ranging from 37% to 90%.  $^1\text{H NMR}$  data of compounds **9a–f** matched those which were reported in the literature.<sup>54–56</sup> The 7-bromo derivative **9g** was the only isomer that could be isolated as a product from the starting material 3-bromoaniline and it was difficult to characterise its chemical structure by  $^1\text{H NMR}$  due its poor solubility even in DMSO- $d_6$  as previously reported.<sup>57</sup>

**6-Chloro-4-oxo-1,4-dihydroquinoline-3-carboxylic acid ethyl ester (9a).**<sup>56</sup> Buff solid, yield: 64%.  $^1\text{H NMR}$  (DMSO- $d_6$ )  $\delta$  1.28 (t,  $J = 7.1$  Hz, 3H), 4.22 (q,  $J = 7.1$  Hz, 2H), 7.66 (d,  $J = 8.8$  Hz, 1H), 7.74 (dd,  $J = 8.8, 2.5$  Hz, 1H), 8.08 (d,  $J = 2.2$  Hz, 1H), 8.58 (s, 1H), 12.39 (br s, 1H).

**8-Chloro-4-oxo-1,4-dihydroquinoline-3-carboxylic acid ethyl ester (9b).**<sup>56</sup> Buff solid, yield: 60%.  $^1\text{H NMR}$  (DMSO- $d_6$ )  $\delta$  1.28 (t,  $J = 7.1$  Hz, 3H), 4.23 (q,  $J = 7.1$  Hz, 2H), 7.42 (t,  $J = 7.9$  Hz, 1H), 7.89 (dd,  $J = 7.7, 1.3$  Hz, 1H), 8.13 (dd,  $J = 8.1, 1.3$  Hz, 1H), 8.43 (s, 1H), 11.92 (br s, 1H).

**7,8-Dichloro-4-oxo-1,4-dihydroquinoline-3-carboxylic acid ethyl ester (9c).**<sup>55</sup> Buff solid, yield: 86%.  $^1\text{H NMR}$  (DMSO- $d_6$ )  $\delta$  1.28 (t,  $J = 7.1$  Hz, 3H), 4.23 (q,  $J = 7.1$  Hz, 2H), 7.64 (d,  $J = 8.7$  Hz, 1H), 8.11 (d,  $J = 8.7$  Hz, 1H), 8.42 (s, 1H), 11.99 (br s, 1H).

**6,8-Dichloro-4-oxo-1,4-dihydroquinoline-3-carboxylic acid ethyl ester (9d).**<sup>55</sup> Buff solid, yield: 90%.  $^1\text{H NMR}$  (DMSO- $d_6$ )  $\delta$  1.28 (t,  $J = 7.1$  Hz, 3H), 4.23 (q,  $J = 7.1$  Hz, 2H), 8.06 (d,  $J = 2.4$  Hz, 1H), 8.08 (d,  $J = 2.4$  Hz, 1H), 8.43 (s, 1H), 12.11 (s, 1H).

**5,8-Dichloro-4-oxo-1,4-dihydroquinoline-3-carboxylic acid ethyl ester (9e).**<sup>55</sup> Buff solid, yield: 37%.  $^1\text{H NMR}$  (DMSO- $d_6$ )  $\delta$  1.27 (t,  $J = 7.0$  Hz, 3H), 4.22 (q,  $J = 7.0$  Hz, 2H), 7.38 (d,  $J = 8.4$  Hz, 1H), 7.81 (d,  $J = 8.4$  Hz, 1H), 8.32 (s, 1H), 11.73 (s, 1H).

**5,7-Dichloro-4-oxo-1,4-dihydroquinoline-3-carboxylic acid ethyl ester (9f).**<sup>54,55</sup> Buff solid, yield: 37%.  $^1\text{H NMR}$  (DMSO- $d_6$ )  $\delta$  1.28 (t,  $J = 7.1$  Hz, 3H), 4.21 (q,  $J = 7.1$  Hz, 2H), 7.30 (d,  $J = 2.0$  Hz, 1H), 7.53 (d,  $J = 2.0$  Hz, 1H), 8.43 (s, 1H).

**7-Bromo-4-oxo-1,4-dihydroquinoline-3-carboxylic acid ethyl ester (9g).**<sup>57</sup> Buff solid, yield: 75%.

**4.1.6. General procedure for the synthesis of 10a–g.** The quinoline-3-carboxylic acid ethyl esters **9a–g** (1 mmol) were refluxed for 4 h in a mixture of 10% sodium hydroxide (5 mL) and ethanol (5 mL). After cooling, the mixture was acidified by adding 2 M HCl and the solid obtained was collected by filtration, excessively washed with water and dried to obtain the quinoline-3-carboxylic acid derivatives **10a–g** in yields ranging from 80% to 99%. The crude product was used for next reaction without further purification.

**4.1.7. General procedure for the synthesis of 11a–g.** To a solution of the appropriate carboxylic acid **10a–g** (1 mmol) in anhydrous DMF (10 mL), *O*-(benzotriazol-1-yl)-*N,N,N',N'*-tetramethyluronium hexafluorophosphate (HBTU, 2 mmol), 1-aminoadamantane (1.2 mmol), and DIPEA (3 mmol) were added and the reaction mixture was stirred at rt for 72 h. Water (10 mL) was then added to the reaction mixture and extracted with EtOAc (3 × 25 mL). The organic layers were separated, washed with water (5 × 25 mL), brine (1 × 25 mL), dried over anhydrous



Na<sub>2</sub>SO<sub>4</sub>, filtered, and concentrated under reduced pressure. The crude product was purified by manual column chromatography using CH<sub>2</sub>Cl<sub>2</sub>/MeOH gradient to obtain the quinoline-3-carboxamides **11a–g** in yields ranging from 51% to 89% and further purified by recrystallisation from DCM.

*N*-(1-Adamantanyl)-6-chloro-4-oxo-1,4-dihydroquinoline-3-carboxamide (**11a**). White solid, yield: 84%. <sup>1</sup>H NMR (DMSO-d<sub>6</sub>) δ 1.67 (s, 6H), 2.06 (s, 9H), 7.72 (d, *J* = 8.8 Hz, 1H), 7.79 (dd, *J* = 8.8, 2.4 Hz, 1H), 8.17 (d, *J* = 2.4 Hz, 1H), 8.71 (s, 1H), 9.85 (s, 1H), 12.76 (s, 1H); <sup>13</sup>C NMR (DMSO-d<sub>6</sub>) δ 29.3, 36.5, 41.9, 51.0, 112.5, 121.9, 124.8, 127.7, 129.9, 133.1, 138.2, 144.1, 163.2, 175.4; HRMS (ESI) *m/z* calcd for C<sub>20</sub>H<sub>21</sub>ClN<sub>2</sub>O<sub>2</sub> ([M + H]<sup>+</sup>) *m/z* 357.1364; found 357.1362.

*N*-(1-Adamantanyl)-8-chloro-4-oxo-1,4-dihydroquinoline-3-carboxamide (**11b**). White solid, yield: 56%. <sup>1</sup>H NMR (DMSO-d<sub>6</sub>) δ 1.67 (s, 6H), 2.06 (s, 9H), 7.47 (t, *J* = 7.9 Hz, 1H), 7.95 (dd, *J* = 7.7, 1.3 Hz, 1H), 8.22 (dd, *J* = 8.2, 1.3 Hz, 1H), 8.64 (s, 1H), 9.80 (s, 1H), 12.24 (s, 1H); <sup>13</sup>C NMR (DMSO-d<sub>6</sub>) δ 29.4, 36.5, 41.9, 51.1, 112.9, 122.7, 125.3, 125.4, 128.2, 132.9, 136.1, 144.4, 162.9, 176.3; HRMS (ESI) *m/z* calcd for C<sub>20</sub>H<sub>21</sub>ClN<sub>2</sub>O<sub>2</sub> ([M + H]<sup>+</sup>) *m/z* 357.1364; found 357.1359.

*N*-(1-Adamantanyl)-7,8-dichloro-4-oxo-1,4-dihydroquinoline-3-carboxamide (**11c**). White solid, yield: 68%. <sup>1</sup>H NMR (DMSO-d<sub>6</sub>) δ 1.69 (s, 6H), 2.08 (s, 9H), 7.62 (d, *J* = 8.7 Hz, 1H), 8.21 (d, *J* = 9.0 Hz, 1H), 8.66 (s, 1H), 9.72 (s, 1H), 12.29 (s, 1H); <sup>13</sup>C NMR (DMSO-d<sub>6</sub>) δ 29.4, 36.5, 41.9, 51.1, 113.2, 121.4, 125.9, 126.0, 126.5, 136.3, 137.8, 145.1, 162.8, 175.9; HRMS (ESI) *m/z* calcd for C<sub>20</sub>H<sub>20</sub>Cl<sub>2</sub>N<sub>2</sub>O<sub>2</sub> ([M + H]<sup>+</sup>) *m/z* 391.0975; found 391.0971.

*N*-(1-Adamantanyl)-6,8-dichloro-4-oxo-1,4-dihydroquinoline-3-carboxamide (**11d**). White solid, yield: 89%. <sup>1</sup>H NMR (DMSO-d<sub>6</sub>) δ 1.67 (s, 6H), 2.06 (s, 9H), 8.05–8.22 (m, 2H), 8.63 (s, 1H), 9.70 (s, 1H), 12.41 (s, 1H); <sup>13</sup>C NMR (DMSO-d<sub>6</sub>) δ 29.4, 36.5, 41.8, 51.2, 113.2, 124.2, 124.5, 128.7, 129.6, 132.4, 135.1, 144.6, 162.6, 175.2; HRMS (ESI) *m/z* calcd for C<sub>20</sub>H<sub>20</sub>Cl<sub>2</sub>N<sub>2</sub>O<sub>2</sub> ([M + H]<sup>+</sup>) *m/z* 391.0975; found 391.0973.

*N*-(1-Adamantanyl)-5,8-chloro-4-oxo-1,4-dihydroquinoline-3-carboxamide (**11e**). White solid, yield: 51%. <sup>1</sup>H NMR (DMSO-d<sub>6</sub>) δ 1.67 (s, 6H), 2.05 (s, 9H), 7.43 (d, *J* = 8.4 Hz, 1H), 7.86 (d, *J* = 8.4 Hz, 1H), 8.58 (s, 1H), 9.67 (s, 1H), 12.07 (s, 1H); <sup>13</sup>C NMR (DMSO-d<sub>6</sub>) δ 29.3, 36.5, 41.8, 51.1, 114.2, 121.9, 123.9, 128.0, 132.5, 132.7, 138.5, 144.1, 162.6, 176.3; HRMS (ESI) *m/z* calcd for C<sub>20</sub>H<sub>20</sub>Cl<sub>2</sub>N<sub>2</sub>O<sub>2</sub> ([M + H]<sup>+</sup>) *m/z* 391.0975; found 391.0976.

*N*-(1-Adamantanyl)-5,7-dichloro-4-oxo-1,4-dihydroquinoline-3-carboxamide (**11f**). White solid, yield: 64%. <sup>1</sup>H NMR (DMSO-d<sub>6</sub>) δ 1.67 (s, 6H), 2.05 (s, 9H), 7.53 (d, *J* = 2.0 Hz, 1H), 7.65 (d, *J* = 2.1 Hz, 1H), 8.66 (s, 1H), 9.74 (s, 1H), 12.66 (s, 1H); <sup>13</sup>C NMR (DMSO-d<sub>6</sub>) δ 29.3, 36.5, 41.8, 51.0, 114.1, 118.1, 121.5, 127.4, 134.9, 136.5, 142.6, 143.9, 162.9, 176.0; HRMS (ESI) *m/z* calcd for C<sub>20</sub>H<sub>20</sub>Cl<sub>2</sub>N<sub>2</sub>O<sub>2</sub> ([M + H]<sup>+</sup>) *m/z* 391.0975; found 391.0974.

*N*-(1-Adamantanyl)-7-bromo-4-oxo-1,4-dihydroquinoline-3-carboxamide (**11g**). White solid, yield: 75%. <sup>1</sup>H NMR (DMSO-d<sub>6</sub>) δ 1.67 (s, 6H), 2.06 (s, 9H), 7.61 (dd, *J* = 8.7, 1.6 Hz, 1H), 7.88 (d, *J* = 1.8 Hz, 1H), 8.14 (d, *J* = 8.7 Hz, 1H), 8.70 (s, 1H), 9.86 (s, 1H), 12.59 (s, 1H); <sup>13</sup>C NMR (DMSO-d<sub>6</sub>) δ 29.3, 36.5, 41.9, 51.0, 112.7, 121.6, 125.5, 126.4, 128.2, 128.3, 140.5, 144.3, 163.2, 176.2; HRMS (ESI) *m/z* calcd for C<sub>20</sub>H<sub>21</sub>BrN<sub>2</sub>O<sub>2</sub> ([M + H]<sup>+</sup>) *m/z* 401.0859; found 401.0859.

**4.1.8. General procedure for the synthesis of 13a–g and 15a–d.** Title compounds were prepared following the general amide coupling protocol used for obtaining compounds **8a–k**. The crude product was purified by flash column chromatography using CH<sub>2</sub>Cl<sub>2</sub>/MeOH gradient to obtain the title compounds in yields ranging from 31% to 92%. Compounds **13a–d** were further purified by recrystallisation from acetone. Compounds **13e,f** and **15a,c,d** were already >95% pure after flash chromatography, while compounds **13g** and **15b** were further purified by preparative HPLC. <sup>1</sup>H NMR data of compounds **13a–c** matched those which were reported in the literature.<sup>47,58</sup>

*N*-Cyclooctylquinoline-2-carboxamide (**13a**).<sup>47</sup> White solid, yield: 46%. <sup>1</sup>H NMR (DMSO-d<sub>6</sub>) δ 1.41–1.98 (m, 14H), 3.96–4.21 (m, 1H), 7.72 (dd, *J* = 8.1, 7.0 Hz, 1H), 7.87 (dd, *J* = 8.3, 7.0 Hz, 1H), 8.08 (d, *J* = 8.1 Hz, 1H), 8.16 (dd, *J* = 8.4, 6.1 Hz, 2H), 8.56 (d, *J* = 8.5 Hz, 1H), 8.60 (d, *J* = 8.3 Hz, 1H).

*N*-(1-Adamantanyl)-2-quinoline-2-carboxamide (**13b**).<sup>58</sup> White solid, yield: 65%. <sup>1</sup>H NMR (DMSO-d<sub>6</sub>) δ 1.69 (s, 6H), 2.10 (s, 3H), 2.13 (s, 6H), 7.71 (ddd, *J* = 8.1, 6.9, 1.2 Hz, 1H), 7.86 (ddd, *J* = 8.4, 6.9, 1.4 Hz, 1H), 8.05–8.16 (m, 4H), 8.56 (d, *J* = 8.4 Hz, 1H).

*N*-Cyclooctyl-2-naphthamide (**13c**).<sup>47</sup> White solid, yield: 56%. <sup>1</sup>H NMR (DMSO-d<sub>6</sub>) δ 1.42–1.89 (m, 14H), 3.94–4.21 (m, 1H), 7.54–7.63 (m, 2H), 7.89–8.04 (m, 4H), 8.38 (d, *J* = 7.8 Hz, 1H), 8.42 (s, 1H).

*N*-(1-Adamantanyl)-2-naphthamide (**13d**). White solid, yield: 60%. <sup>1</sup>H NMR (DMSO-d<sub>6</sub>) δ 1.68 (s, 6H), 2.07 (s, 3H), 2.12 (s, 6H), 7.62–7.53 (m, 2H), 7.76 (s, 1H), 7.85 (dd, *J* = 8.6, 1.6 Hz, 1H), 7.93–8.01 (m, 3H), 8.36 (s, 1H); <sup>13</sup>C NMR (DMSO-d<sub>6</sub>) δ 29.4, 36.6, 41.4, 52.1, 125.1, 127.0, 127.71, 127.74, 128.0 (2C), 129.2, 132.6, 133.8, 134.4, 166.6; HRMS (ESI) *m/z* calcd for C<sub>21</sub>H<sub>23</sub>NO ([M + H]<sup>+</sup>) *m/z* 306.1852; found 306.1844.

*N*-(1-Adamantanyl)-5-bromo-2-naphthamide (**13e**). White solid, yield: 52%. <sup>1</sup>H NMR (DMSO-d<sub>6</sub>) δ 1.69 (s, 6H), 2.09 (s, 3H), 2.14 (s, 6H), 7.50 (dd, *J* = 8.5, 7.5 Hz, 1H), 7.58 (dd, *J* = 7.0, 1.0 Hz, 1H), 7.69 (dd, *J* = 8.5, 7.1 Hz, 1H), 7.93 (dd, *J* = 7.4, 0.9 Hz, 1H), 8.05–8.14 (m, 2H), 8.21 (d, *J* = 8.5 Hz, 1H); <sup>13</sup>C NMR (DMSO-d<sub>6</sub>) δ 29.4, 36.6, 41.4, 52.3, 122.5, 126.0, 126.1, 127.5, 127.7 (2C), 130.8, 131.5, 131.6, 137.6, 168.2; HRMS (ESI) *m/z* calcd for C<sub>21</sub>H<sub>22</sub>BrNO ([M + H]<sup>+</sup>) *m/z* 384.0958; found 384.0956.

*N*-(1-Adamantanyl)-6-bromo-2-naphthamide (**13f**). White solid, yield: 31%. <sup>1</sup>H NMR (DMSO-d<sub>6</sub>) δ 1.68 (s, 6H), 2.07 (s, 3H), 2.11 (s, 6H), 7.69 (dd, *J* = 8.7, 1.9 Hz, 1H), 7.80 (s, 1H), 7.88–7.99 (m, 3H), 8.25 (s, 1H), 8.37 (s, 1H); <sup>13</sup>C NMR (DMSO-d<sub>6</sub>) δ 29.4, 36.6, 41.4, 52.1, 121.1, 126.2, 127.3, 127.7, 130.0, 130.1, 131.1, 131.4, 134.4, 135.5, 166.4; HRMS (ESI) *m/z* calcd for C<sub>21</sub>H<sub>22</sub>BrNO ([M + H]<sup>+</sup>) *m/z* 384.0958; found 384.0960.

*N*-(1-Adamantanyl)-6-methoxy-2-naphthamide (**13g**). White solid, yield: 52%. <sup>1</sup>H NMR (DMSO-d<sub>6</sub>) δ 1.67 (s, 6H), 2.07 (s, 3H), 2.11 (s, 6H), 3.89 (s, 3H), 7.21 (dd, *J* = 9.0, 2.5 Hz, 1H), 7.35 (d, *J* = 2.4 Hz, 1H), 7.66 (s, 1H), 7.83 (s, 2H), 7.90 (d, *J* = 9.0 Hz, 1H), 8.30 (s, 1H); <sup>13</sup>C NMR (DMSO-d<sub>6</sub>) δ 29.4, 36.6, 41.4, 52.0, 55.7, 106.3, 119.6, 125.5, 126.8, 127.6, 127.9, 130.8, 131.5, 136.0, 158.8, 166.6; HRMS (ESI) *m/z* calcd for C<sub>22</sub>H<sub>25</sub>NO ([M + H]<sup>+</sup>) *m/z* 336.1958; found 336.1951.



*N*-(1-Adamantanyl)-2-amino-3,5-dichlorobenzamide (**15a**). White solid, yield: 86%. <sup>1</sup>H NMR (DMSO-*d*<sub>6</sub>) δ 1.65 (s, 6H), 2.05 (s, 9H), 6.30 (s, 2H), 7.46 (s, 2H), 7.78 (s, 1H); <sup>13</sup>C NMR (DMSO-*d*<sub>6</sub>) δ 29.4, 36.5, 41.1, 52.4, 118.3, 119.7, 120.0, 127.8, 130.7, 144.1, 167.2; HRMS (ESI) *m/z* calcd for C<sub>17</sub>H<sub>20</sub>Cl<sub>2</sub>N<sub>2</sub>O ([M + H]<sup>+</sup>) *m/z* 339.1025; found 339.1022.

2-Amino-3,5-dichloro-*N*-cyclooctylbenzamide (**15b**). White solid, yield: 92%. <sup>1</sup>H NMR (DMSO-*d*<sub>6</sub>) δ 1.49–1.77 (m, 14H), 3.88–4.04 (m, 1H), 6.52 (s, 2H), 7.49 (d, *J* = 2.4 Hz, 1H), 7.55 (d, *J* = 2.4 Hz, 1H), 8.33 (d, *J* = 7.7 Hz, 1H); <sup>13</sup>C NMR (DMSO-*d*<sub>6</sub>) δ 24.0, 25.6, 27.3, 31.9, 49.7, 118.3, 118.4, 119.9, 127.4, 131.0, 144.5, 166.2; HRMS (ESI) *m/z* calcd for C<sub>15</sub>H<sub>20</sub>Cl<sub>2</sub>N<sub>2</sub>O ([M + H]<sup>+</sup>) *m/z* 315.1025; found 315.1020.

*N*-(1-Adamantanyl)-3,5-dichloro-2-hydroxybenzamide (**15c**). White solid, yield: 50%. <sup>1</sup>H NMR (DMSO-*d*<sub>6</sub>) δ 1.66 (s, 6H), 2.08 (s, 9H), 7.67 (d, *J* = 2.3 Hz, 1H), 8.04 (d, *J* = 2.4 Hz, 1H), 8.51 (s, 2H), 13.59 (br s, 1H); <sup>13</sup>C NMR (DMSO-*d*<sub>6</sub>) δ 29.3, 36.3, 40.9, 53.5, 118.0, 121.9, 122.8, 126.8, 133.1, 156.4, 168.2; HRMS (ESI) *m/z* calcd for C<sub>17</sub>H<sub>19</sub>Cl<sub>2</sub>NO<sub>2</sub> ([M + H]<sup>+</sup>) *m/z* 340.0866; found 340.0864.

3,5-Dichloro-*N*-cyclooctyl-2-hydroxybenzamide (**15d**). White solid, yield: 63%. <sup>1</sup>H NMR (DMSO-*d*<sub>6</sub>) δ 1.42–1.79 (m, 14H), 4.02–4.08 (m, 1H), 7.68 (d, *J* = 1.2 Hz, 1H), 8.03 (d, *J* = 1.6 Hz, 1H), 9.19 (s, 1H), 13.87 (br s, 1H); <sup>13</sup>C NMR (DMSO-*d*<sub>6</sub>) δ 23.9, 25.6, 27.1, 31.8, 50.2, 117.0, 122.1, 122.7, 126.2, 133.3, 156.5, 167.3; HRMS (ESI) *m/z* calcd for C<sub>15</sub>H<sub>19</sub>Cl<sub>2</sub>NO<sub>2</sub> ([M + H]<sup>+</sup>) *m/z* 316.0866; found 316.0861.

**4.1.9. General procedure for the synthesis of 17a,b.** A mixture of the corresponding acetophenone **16a,b** (1 mmol), thiourea (2 mmol) and iodine (1 mmol) was heated at 100 °C for 3–5 h. Then the reaction mixture was cooled, washed with diethyl ether to remove the unreacted acetophenone and iodine. The residue was dissolved in hot water, filtered to remove sulphone, and the filtrate was basified with aqueous NH<sub>4</sub>OH to yield the corresponding 2-amino-4-(substituted-phenyl)-1,3-thiazoles **17a,b**. The crude product was purified by flash column chromatography on SiO<sub>2</sub> with CH<sub>2</sub>Cl<sub>2</sub>/MeOH gradient as the eluent to obtain the title compounds **17a,b** in yields 61% and 54%, respectively. <sup>1</sup>H NMR data of compounds **17a,b** matched the ones reported in the literature.<sup>59,60</sup>

2-Amino-4-(4-chlorophenyl)-1,3-thiazole (**17a**). Yellowish white solid, yield: 61%. <sup>1</sup>H NMR (DMSO-*d*<sub>6</sub>) δ 7.06 (s, 1H), 7.07 (s, 2H), 7.41 (d, *J* = 8.6 Hz, 2H), 7.80 (d, *J* = 8.6 Hz, 2H).<sup>59</sup>

2-Amino-4-(2,4-dichlorophenyl)-1,3-thiazole (**17b**). Yellowish white solid, yield: 54%. <sup>1</sup>H NMR (DMSO-*d*<sub>6</sub>) δ 7.09 (s, 2H), 7.10 (s, 1H), 7.45 (dd, *J* = 8.5, 2.2 Hz, 1H), 7.64 (d, *J* = 2.1 Hz, 1H), 7.87 (d, *J* = 8.5 Hz, 1H).<sup>60</sup>

**4.1.10. General procedure for the synthesis of 18a,b.** Title compounds were prepared following the general amide coupling procedure used for preparing compounds **8a–k**. The crude product was purified by flash chromatography using CH<sub>2</sub>Cl<sub>2</sub>/MeOH gradient to obtain the thiazole-2-carboxamides **18a,b** in yields 41% and 30%, respectively, and were further purified by preparative HPLC.

*N*-(4-(4-Chlorophenyl)thiazol-2-yl)adamantane-1-carboxamide (**18a**). White solid, yield: 41%. <sup>1</sup>H NMR (DMSO-*d*<sub>6</sub>) δ 1.69 (s, 6H),

1.95 (s, 6H), 2.01 (s, 3H), 7.48 (d, *J* = 8.6 Hz, 2H), 7.63 (s, 1H), 7.92 (d, *J* = 8.6 Hz, 2H), 11.83 (s, 1H); <sup>13</sup>C NMR (DMSO-*d*<sub>6</sub>) δ 28.0, 36.3, 38.0, 41.1, 109.2, 127.9, 129.2, 132.6, 133.8, 148.0, 159.2, 176.8; HRMS (ESI) *m/z* calcd for C<sub>20</sub>H<sub>21</sub>ClN<sub>2</sub>OS ([M + H]<sup>+</sup>) *m/z* 373.1136; found 373.1127.

*N*-(4-(2,4-Dichlorophenyl)thiazol-2-yl)adamantane-1-carboxamide (**18b**). White solid, yield: 30%. <sup>1</sup>H NMR (DMSO-*d*<sub>6</sub>) δ 1.69 (s, 6H), 1.95 (s, 6H), 2.01 (s, 3H), 7.52 (dd, *J* = 8.5, 2.2 Hz, 1H), 7.62 (s, 1H), 7.70 (d, *J* = 2.2 Hz, 1H), 7.89 (d, *J* = 8.5 Hz, 1H), 11.90 (s, 1H); <sup>13</sup>C NMR (DMSO-*d*<sub>6</sub>) δ 28.0, 36.3, 38.0, 41.1, 113.7, 128.0, 130.2, 132.3, 132.7, 132.8, 133.2, 144.7, 158.4, 176.8; HRMS (ESI) *m/z* calcd for C<sub>20</sub>H<sub>20</sub>Cl<sub>2</sub>N<sub>2</sub>OS ([M + H]<sup>+</sup>) *m/z* 407.0746; found 407.0737.

**4.1.11. General procedure for the synthesis of 20 and 22.** A mixture of 4,6-difluoro-1*H*-indole-2-carboxylic acid (**19**, 1 mmol) and 1,1'-carbonyldiimidazole (CDI) (1.5 mmol) in anhydrous DMF (10 mL) was stirred at rt for two hours, followed by the addition of aqueous NH<sub>4</sub>OH or hydrazine hydrate solution (5 mmol) and stirring was continued for 12–16 h at rt. Water (25 mL) was then added to the reaction mixture and extracted with EtOAc (3 × 25 mL). The organic layers were separated, washed with water (5 × 25 mL), brine (1 × 25 mL), dried over anhydrous Na<sub>2</sub>SO<sub>4</sub>, filtered, and concentrated under reduced pressure. The crude product was purified by flash column chromatography on SiO<sub>2</sub> with CH<sub>2</sub>Cl<sub>2</sub>/MeOH gradient as the eluent to obtain the title compounds in yields 98% and 74%, respectively.

4,6-Difluoro-1*H*-indole-2-carboxamide (**20**). Buff solid, yield: 98%. <sup>1</sup>H NMR (400 MHz, DMSO) δ 6.86 (td, *J* = 10.5, 2.0 Hz, 1H), 7.01 (dd, *J* = 9.4, 1.9 Hz, 1H), 7.22 (s, 1H), 7.44 (s, 1H), 8.03 (s, 1H), 11.97 (s, 1H); <sup>13</sup>C NMR δ 95.0 (dd, *J* = 25.8, 4.5 Hz), 95.6 (dd, *J* = 29.7, 23.3 Hz), 99.3, 113.6 (d, *J* = 21.8 Hz), 133.3 (d, *J* = 3.2 Hz), 138.1 (dd, *J* = 15.2, 13.2 Hz), 156.2 (dd, *J* = 248.6, 15.6 Hz), 159.6 (dd, *J* = 238.4, 12.1 Hz), 162.5.

4,6-Difluoro-1*H*-indole-2-carbohydrazide (**22**). Buff solid, yield: 74%. <sup>1</sup>H NMR (400 MHz, DMSO) δ 4.52 (s, 2H), 6.87 (td, *J* = 10.4, 1.9 Hz, 1H), 7.02 (d, *J* = 9.4 Hz, 1H), 7.16 (s, 1H), 9.86 (s, 1H), 12.04 (s, 1H); <sup>13</sup>C NMR δ 95.0 (dd, *J* = 25.9, 4.5 Hz), 95.6 (dd, *J* = 29.7, 23.3 Hz), 98.0, 113.6 (d, *J* = 22.5 Hz), 132.0 (d, *J* = 3.3 Hz), 138.0 (dd, *J* = 15.2, 13.2 Hz), 156.1 (dd, *J* = 248.5, 15.5 Hz), 159.5 (dd, *J* = 238.4, 12.3 Hz), 160.8.

*N*-Adamantane-1-carbonyl-4,6-difluoro-1*H*-indole-2-carboxamide (**21**). To a solution of 1-adamantanecarboxylic acid (1.5 mmol) in DCM (10 mL), DMF (0.1 mL) and oxalyl chloride (3 mmol) were added. After stirring for 2 h at rt, the mixture was concentrated under vacuum. The residue was dissolved in pyridine (5 mL), followed by addition of compound **20** (1 mmol) and the reaction mixture was refluxed for 16 h. After cooling, 2 M HCl (25 mL) was added to the reaction mixture and extracted with EtOAc (3 × 25 mL). The organic layers were separated, washed with brine (1 × 25 mL), dried over anhydrous Na<sub>2</sub>SO<sub>4</sub>, filtered, and concentrated under reduced pressure. The crude product was purified by flash chromatography on SiO<sub>2</sub> using CH<sub>2</sub>Cl<sub>2</sub>/MeOH gradient to obtain the title compound and was further purified by preparative HPLC. White solid, yield: 42%. <sup>1</sup>H NMR (400 MHz, DMSO) δ 1.71 (s, 6H), 1.95 (s, 6H), 2.02 (s, 3H), 6.95 (t, *J* = 10.3 Hz, 1H), 7.05 (d, *J* = 8.6 Hz, 1H), 7.52 (s, 1H), 10.01 (s, 1H), 12.26 (s, 1H); <sup>13</sup>C NMR δ 28.0, 36.2, 37.7, 42.5,



95.2 (dd,  $J = 26.0, 4.5$  Hz), 96.3 (dd,  $J = 30.0, 23.1$  Hz), 103.2, 113.3 (d,  $J = 22.0$  Hz), 131.7 (d,  $J = 3.2$  Hz), 139.0 (dd,  $J = 15.3, 12.6$  Hz), 156.7 (dd,  $J = 250.2, 15.7$  Hz), 160.0, 160.5 (dd,  $J = 240.3, 12.1$  Hz), 176.4; HRMS (ESI)  $m/z$  calcd for  $C_{20}H_{20}F_2N_2O_2$  ( $[M + H]^+$ )  $m/z$  359.1566; found 359.1559.

*N*-Adamantane-1-carbonyl-4,6-difluoro-1H-indole-2-carbohydrazide (**23**). Title compound was prepared following the standard amide coupling procedure used for preparing compounds **8a–k**. The crude product was purified by flash chromatography on  $SiO_2$  using  $CH_2Cl_2/MeOH$  gradient and was further purified by preparative HPLC. White solid, yield: 48%.  $^1H$  NMR (400 MHz, DMSO)  $\delta$  1.69 (s, 6H), 1.88 (s, 6H), 1.99 (s, 3H), 6.89 (td,  $J = 10.4, 1.6$  Hz, 1H), 7.06 (d,  $J = 9.2$  Hz, 1H), 7.29 (s, 1H), 9.50 (s, 1H), 10.28 (s, 1H), 12.05 (s, 1H);  $^{13}C$  NMR  $\delta$  28.0, 36.5, 39.0, 40.1, 95.1 (dd,  $J = 25.9, 4.2$  Hz), 95.9 (dd,  $J = 29.5, 23.5$  Hz), 99.4, 113.6 (d,  $J = 21.9$  Hz), 131.3 (d,  $J = 3.2$  Hz), 138.2 (dd,  $J = 15.3, 13.1$  Hz), 156.2 (dd,  $J = 249.0, 15.6$  Hz), 159.8 (dd,  $J = 238.7, 12.1$  Hz), 160.2, 176.9; HRMS (ESI)  $m/z$  calcd for  $C_{20}H_{21}F_2N_3O_2$  ( $[M + H]^+$ )  $m/z$  374.1675; found 374.1665.

*N*-(1-Adamantanyl)-2-(4,6-difluoro-1H-indole-2-carbonyl)hydrazine-1-carboxamide (**24**). A mixture of compound **22** and 1-adamantylisocyanate in ethanol was refluxed for 16 h. The reaction mixture was then concentrated under vacuum, and water (50 mL) was added to the residue. The formed precipitate was filtered off, dried, purified by flash chromatography on  $SiO_2$  using  $CH_2Cl_2/MeOH$  gradient and was further purified by preparative HPLC. White solid, yield: 54%.  $^1H$  NMR (400 MHz, DMSO)  $\delta$  1.61 (s, 6H), 1.91 (s, 6H), 2.00 (s, 3H), 5.96 (s, 1H), 6.89 (td,  $J = 10.4, 1.7$  Hz, 1H), 7.03 (dd,  $J = 9.3, 1.5$  Hz, 1H), 7.27 (d,  $J = 1.5$  Hz, 1H), 7.72 (s, 1H), 10.18 (s, 1H), 12.09 (s, 1H);  $^{13}C$  NMR  $\delta$  29.4, 36.5, 42.2, 50.4, 95.1 (dd,  $J = 25.9, 4.3$  Hz), 95.8 (dd,  $J = 29.8, 23.2$  Hz), 99.3, 113.6 (d,  $J = 21.8$  Hz), 131.3 (d,  $J = 3.2$  Hz), 138.2 (dd,  $J = 15.2, 13.2$  Hz), 156.2 (dd,  $J = 248.8, 15.5$  Hz), 157.1, 159.9 (dd,  $J = 238.7, 11.5$  Hz), 160.9; HRMS (ESI)  $m/z$  calcd for  $C_{20}H_{22}F_2N_4O_2$  ( $[M + H]^+$ )  $m/z$  389.1784; found 389.1772.

4-(1-Adamantanyl)-2-amino-1,3-thiazole (**26**). The title compound was prepared following the general procedure used for preparing compounds **17a,b**. The crude product was purified by flash column chromatography on  $SiO_2$  with  $CH_2Cl_2/MeOH$  gradient as the eluent.  $^1H$  NMR data of compound **26** matched the reported one in the literature.<sup>61</sup> White solid, yield: 63%.  $^1H$  NMR (DMSO- $d_6$ )  $\delta$  1.55–1.75 (m, 6H), 1.80 (s, 6H), 1.98 (s, 3H), 5.99 (s, 1H), 6.74 (s, 2H).

*N*-(4-(1-Adamantanyl)thiazol-2-yl)-4,6-difluoro-1H-indole-2-carboxamide (**27**). A mixture of compound **26** and 4,6-difluoro-1H-indole-2-carboxylic acid (**19**) were then reacted following the general amide coupling protocol used in preparing compounds **8a–k**. The crude product was purified by flash chromatography on  $SiO_2$  using  $CH_2Cl_2/MeOH$  gradient to obtain the title compound and was further purified by recrystallization from diethyl ether. Yellowish white solid, yield: 30%.  $^1H$  NMR (400 MHz, DMSO)  $\delta$  1.82–1.62 (m, 6H), 1.93 (s, 6H), 2.05 (s, 3H), 6.73 (s, 1H), 6.93 (td,  $J = 10.3, 1.7$  Hz, 1H), 7.07 (dd,  $J = 9.3, 1.2$  Hz, 1H), 7.73 (s, 1H), 12.29 (br s, 1H);  $^{13}C$  NMR  $\delta$  28.4, 36.3, 36.8, 42.1, 95.2 (dd,  $J = 26.1, 4.3$  Hz), 96.1 (dd,  $J = 29.8, 23.1$  Hz), 101.9, 105.5, 113.8 (d,  $J = 21.8$  Hz), 131.0,

138.8 (dd,  $J = 15.4, 12.7$  Hz), 156.5 (dd,  $J = 249.8, 15.7$  Hz), 157.9, 159.0, 160.3 (dd,  $J = 239.9, 12.2$  Hz), 161.2; HRMS (ESI)  $m/z$  calcd for  $C_{22}H_{21}F_2N_3OS$  ( $[M + H]^+$ )  $m/z$  414.1446; found 414.1434.

## 4.2. Biology

MIC was determined using the MABA assay as previously reported in the literature.<sup>38,46</sup> MABA format was also used in the cytotoxicity evaluation on Vero Cells.<sup>38</sup>

## 4.3. Molecular modeling studies

All the molecular modeling and docking simulations were done on Molecular Operating Environment MOE software version 2008.10.<sup>48</sup> The structures of compounds **8i**, **13c**, **13d** and **18b** were drawn in ChemDraw Ultra 16.0 and saved as .mol file, then opened inside the MOE program. They were then 3D protonated and geometrically optimised using MMFF94  $\times$  forcefield with gradient 0.05. The X-ray crystal structure of MmpL3 bound to the ICA38 (PDB: 6AJJ) was obtained from the protein data bank. The target binding pocket was prepared for docking by: (1) removing co-crystallised ligand molecules and (2) 3D protonating the enzyme, in which hydrogens and partial charges were added to the system for optimisation. In order to validate the docking protocol, ICA38 was docked into the active site of 6AJJ. The generated conformers were docked into the same binding pocket of ICA38 with MOE-DOCK using Triangle Matcher placement method and scored using London dG scoring function. A molecular mechanics force field refinement was applied on the generated top 30 poses. For each ligand–enzyme complex, the top-ranked pose with the best docking score (*i.e.* the lowest binding free energy) was selected.

## Conflicts of interest

There are no conflicts to declare.

## Acknowledgements

We gratefully acknowledge Curtin University for the funding of Curtin International Postgraduate Research Scholarship (CIPRS) for SSRA. We thank the support of NIH grants AI 27856 and HL 133190 for WRB. We also acknowledge ARC Discovery Early Career Researcher Award DE160100482 for HG.

## References

- 1 World Health Organization, *Global Tuberculosis Report*, Geneva, 2019.
- 2 S. Tiberi, A. Scardigli, R. Centis, L. D'Ambrosio, M. Munoz-Torrico, M. A. Salazar-Lezama, A. Spanevello, D. Visca, A. Zumla, G. B. Migliori and J. A. Caminero Luna, *Int. J. Infect. Dis.*, 2017, **56**, 181–184.
- 3 H. W. Al-Humadi, R. J. Al-Saigh and A. W. Al-Humadi, *Front. Pharmacol.*, 2017, **8**, 689.
- 4 G. Sotgiu, R. Centis, L. D'Ambrosio and G. B. Migliori, *Cold Spring Harbor Perspect. Med.*, 2015, **5**, a017822.



- 5 W. Li, A. Upadhyay, F. L. Fontes, E. J. North, Y. Wang, D. C. Crans, A. E. Grzegorzewicz, V. Jones, S. G. Franzblau, R. E. Lee, D. C. Crick and M. Jackson, *Antimicrob. Agents Chemother.*, 2014, **58**, 6413–6423.
- 6 Z. Xu, V. A. Meshcheryakov, G. Poce and S. S. Chng, *Proc. Natl. Acad. Sci. U. S. A.*, 2017, **114**, 7993–7998.
- 7 S. S. R. Alsayed, C. C. Beh, N. R. Foster, A. D. Payne, Y. Yu and H. Gunosewoyo, *Curr. Mol. Pharmacol.*, 2019, **12**, 27–49.
- 8 P. J. Brennan and H. Nikaido, *Annu. Rev. Biochem.*, 1995, **64**, 29–63.
- 9 V. Nataraj, C. Varela, A. Javid, A. Singh, G. S. Besra and A. Bhatt, *Mol. Microbiol.*, 2015, **98**, 7–16.
- 10 K. Takayama, C. Wang and G. S. Besra, *Clin. Microbiol. Rev.*, 2005, **18**, 81–101.
- 11 M. V. de Almeida, M. F. Saraiva, M. V. de Souza, C. F. da Costa, F. R. Vicente and M. C. Lourenco, *Bioorg. Med. Chem. Lett.*, 2007, **17**, 5661–5664.
- 12 Y. Q. Hu, S. Zhang, F. Zhao, C. Gao, L. S. Feng, Z. S. Lv, Z. Xu and X. Wu, *Eur. J. Med. Chem.*, 2017, **133**, 255–267.
- 13 B. D. Palmer, A. M. Thompson, H. S. Sutherland, A. Blaser, I. Kmentova, S. G. Franzblau, B. Wan, Y. Wang, Z. Ma and W. A. Denny, *J. Med. Chem.*, 2010, **53**, 282–294.
- 14 J. Stec, O. K. Onajole, S. Lun, H. Guo, B. Merenbloom, G. Vistoli, W. R. Bishai and A. P. Kozikowski, *J. Med. Chem.*, 2016, **59**, 6232–6247.
- 15 A. S. T. Tong, P. J. Choi, A. Blaser, H. S. Sutherland, S. K. Y. Tsang, J. Guillemont, M. Motte, C. B. Cooper, K. Andries, W. Van den Broeck, S. G. Franzblau, A. M. Upton, W. A. Denny, B. D. Palmer and D. Conole, *ACS Med. Chem. Lett.*, 2017, **8**, 1019–1024.
- 16 E. Uh, E. R. Jackson, G. San Jose, M. Maddox, R. E. Lee, R. E. Lee, H. I. Boshoff and C. S. Dowd, *Bioorg. Med. Chem. Lett.*, 2011, **21**, 6973–6976.
- 17 A. E. Grzegorzewicz, H. Pham, V. A. Gundi, M. S. Scherman, E. J. North, T. Hess, V. Jones, V. Gruppo, S. E. Born, J. Kordulakova, S. S. Chavadi, C. Morisseau, A. J. Lenaerts, R. E. Lee, M. R. McNeil and M. Jackson, *Nat. Chem. Biol.*, 2012, **8**, 334–341.
- 18 K. Tahlan, R. Wilson, D. B. Kastrinsky, K. Arora, V. Nair, E. Fischer, S. W. Barnes, J. R. Walker, D. Alland, C. E. Barry 3rd and H. I. Boshoff, *Antimicrob. Agents Chemother.*, 2012, **56**, 1797–1809.
- 19 C. Varela, D. Rittmann, A. Singh, K. Krumbach, K. Bhatt, L. Eggeling, G. S. Besra and A. Bhatt, *Chem. Biol.*, 2012, **19**, 498–506.
- 20 G. Degiacomi, A. Benjak, J. Madacki, F. Boldrin, R. Proveddi, G. Palu, J. Kordulakova, S. T. Cole and R. Manganello, *Sci. Rep.*, 2017, **7**, 43495.
- 21 W. Li, A. Obregon-Henao, J. B. Wallach, E. J. North, R. E. Lee, M. Gonzalez-Juarrero, D. Schnappinger and M. Jackson, *Antimicrob. Agents Chemother.*, 2016, **60**, 5198–5207.
- 22 M. Jackson, M. R. McNeil and P. J. Brennan, *Future Microbiol.*, 2013, **8**, 855–875.
- 23 E. J. North, M. Jackson and R. E. Lee, *Curr. Pharm. Des.*, 2014, **20**, 4357–4378.
- 24 R. R. Kondreddi, J. Jiricek, S. P. Rao, S. B. Lakshminarayana, L. R. Camacho, R. Rao, M. Herve, P. Bifani, N. L. Ma, K. Kuhen, A. Goh, A. K. Chatterjee, T. Dick, T. T. Diagana, U. H. Manjunatha and P. W. Smith, *J. Med. Chem.*, 2013, **56**, 8849–8859.
- 25 O. K. Onajole, M. Pieroni, S. K. Tipparaju, S. Lun, J. Stec, G. Chen, H. Gunosewoyo, H. Guo, N. C. Ammerman, W. R. Bishai and A. P. Kozikowski, *J. Med. Chem.*, 2013, **56**, 4093–4103.
- 26 S. P. Rao, S. B. Lakshminarayana, R. R. Kondreddi, M. Herve, L. R. Camacho, P. Bifani, S. K. Kalapala, J. Jiricek, N. L. Ma, B. H. Tan, S. H. Ng, M. Nanjundappa, S. Ravindran, P. G. Seah, P. Thayalan, S. H. Lim, B. H. Lee, A. Goh, W. S. Barnes, Z. Chen, K. Gagaring, A. K. Chatterjee, K. Pethe, K. Kuhen, J. Walker, G. Feng, S. Babu, L. Zhang, F. Blasco, D. Beer, M. Weaver, V. Dartois, R. Glynne, T. Dick, P. W. Smith, T. T. Diagana and U. H. Manjunatha, *Sci. Transl. Med.*, 2013, **5**, 214ra168.
- 27 S. Lun, H. Guo, O. K. Onajole, M. Pieroni, H. Gunosewoyo, G. Chen, S. K. Tipparaju, N. C. Ammerman, A. P. Kozikowski and W. R. Bishai, *Nat. Commun.*, 2013, **4**, 2907.
- 28 S. A. Stanley, S. S. Grant, T. Kawate, N. Iwase, M. Shimizu, C. Wivagg, M. Silvis, E. Kazyskaya, J. Aquadro, A. Golas, M. Fitzgerald, H. Dai, L. Zhang and D. T. Hung, *ACS Chem. Biol.*, 2012, **7**, 1377–1384.
- 29 K. A. Sacksteder, M. Protopopova, C. E. Barry 3rd, K. Andries and C. A. Nacy, *Future Microbiol.*, 2012, **7**, 823–837.
- 30 V. La Rosa, G. Poce, J. O. Canseco, S. Buroni, M. R. Pasca, M. Biava, R. M. Raju, G. C. Porretta, S. Alfonso, C. Battilocchio, B. Javid, F. Sorrentino, T. R. Ioerger, J. C. Sacchetti, F. Manetti, M. Botta, A. De Logu, E. J. Rubin and E. De Rossi, *Antimicrob. Agents Chemother.*, 2012, **56**, 324–331.
- 31 M. A. De Groote, M. Jackson, M. Gonzalez-Juarrero, W. Li, C. L. Young, C. Wong, J. Graham, J. Day, T. Hoang, T. C. Jarvis, W. Ribble, X. Sun and U. A. Ochsner, *Front. Microbiol.*, 2018, **9**, 2231.
- 32 G. Poce, M. Cocozza, S. Alfonso, S. Consalvi, G. Venditti, R. Fernandez-Menendez, R. H. Bates, D. Barros Aguirre, L. Ballell, A. De Logu, G. Vistoli and M. Biava, *Eur. J. Med. Chem.*, 2018, **145**, 539–550.
- 33 M. J. Remuinan, E. Perez-Herran, J. Rullas, C. Alemparte, M. Martinez-Hoyos, D. J. Dow, J. Afari, N. Mehta, J. Esquivias, E. Jimenez, F. Ortega-Muro, M. T. Fraile-Gabaldon, V. L. Spivey, N. J. Loman, M. J. Pallen, C. Constantinidou, D. J. Minick, M. Cacho, M. J. Rebollo-Lopez, C. Gonzalez, V. Sousa, I. Angulo-Barturen, A. Mendoza-Losana, D. Barros, G. S. Besra, L. Ballell and N. Cammack, *PLoS One*, 2013, **8**, e60933.
- 34 L. Ballell, R. H. Bates, R. J. Young, D. Alvarez-Gomez, E. Alvarez-Ruiz, V. Barroso, D. Blanco, B. Crespo, J. Escribano, R. Gonzalez, S. Lozano, S. Huss, A. Santos-Villarejo, J. J. Martin-Plaza, A. Mendoza, M. J. Rebollo-Lopez, M. Remuinan-Blanco, J. L. Lavandera, E. Perez-Herran, F. J. Gamio-Benito, J. F. Garcia-Bustos, D. Barros, J. P. Castro and N. Cammack, *ChemMedChem*, 2013, **8**, 313–321.



- 35 T. R. Ioerger, T. O'Malley, R. Liao, K. M. Guinn, M. J. Hickey, N. Mohaideen, K. C. Murphy, H. I. Boshoff, V. Mizrahi, E. J. Rubin, C. M. Sasseti, C. E. Barry 3rd, D. R. Sherman, T. Parish and J. C. Sacchettini, *PLoS One*, 2013, **8**, e75245.
- 36 J. M. Belardinelli, A. Yazidi, L. Yang, L. Fabre, W. Li, B. Jacques, S. K. Angala, I. Rouiller, H. I. Zgurskaya, J. Sygusch and M. Jackson, *ACS Infect. Dis.*, 2016, **2**, 702–713.
- 37 W. Li, C. M. Stevens, A. N. Pandya, Z. Darzynkiewicz, P. Bhattarai, W. Tong, M. Gonzalez-Juarrero, E. J. North, H. I. Zgurskaya and M. Jackson, *ACS Infect. Dis.*, 2019, **5**, 1001–1012.
- 38 M. Pieroni, S. K. Tipparaju, S. Lun, Y. Song, A. W. Sturm, W. R. Bishai and A. P. Kozikowski, *ChemMedChem*, 2011, **6**, 334–342.
- 39 C. C. Su, P. A. Klenotic, J. R. Bolla, G. E. Purdy, C. V. Robinson and E. W. Yu, *Proc. Natl. Acad. Sci. U. S. A.*, 2019, **116**, 11241–11246.
- 40 B. Zhang, J. Li, X. Yang, L. Wu, J. Zhang, Y. Yang, Y. Zhao, L. Zhang, X. Yang, X. Yang, X. Cheng, Z. Liu, B. Jiang, H. Jiang, L. W. Guddat, H. Yang and Z. Rao, *Cell*, 2019, **176**, 636–648.
- 41 A. Bernut, A. Viljoen, C. Dupont, G. Sapriel, M. Blaise, C. Bouchier, R. Brosch, C. de Chastellier, J. L. Herrmann and L. Kremer, *Mol. Microbiol.*, 2016, **99**, 866–883.
- 42 S. Ancizu, N. Castrillo, S. Pérez-Silanes, I. Aldana, A. Monge, P. Delagrangé, D.-H. Caignard and S. Galiano, *Molecules*, 2012, **17**(7), 7737–7757.
- 43 C. Huang, J.-H. Guo, H.-M. Fu, M.-L. Yuan and L.-J. Yang, *Tetrahedron Lett.*, 2015, **56**, 3777–3781.
- 44 Y. Kurasawa, K. Yoshida, N. Yamazaki, K. Iwamoto, Y. Hamamoto, E. Kaji, K. Sasaki and Y. Zamami, *J. Heterocycl. Chem.*, 2012, **49**, 1323–1331.
- 45 E. Stern, G. G. Muccioli, R. Millet, J. F. Goossens, A. Farce, P. Chavatte, J. H. Poupaert, D. M. Lambert, P. Depreux and J. P. Henichart, *J. Med. Chem.*, 2006, **49**, 70–79.
- 46 L. Collins and S. G. Franzblau, *Antimicrob. Agents Chemother.*, 1997, **41**, 1004–1009.
- 47 T. Gonec, P. Bobal, J. Suján, M. Pesko, J. Guo, K. Kralova, L. Pavlacka, L. Vesely, E. Kreckova, J. Kos, A. Coffey, P. Kollar, A. Imramovsky, L. Placek and J. Jampilek, *Molecules*, 2012, **17**, 613–644.
- 48 MOE, Chemical Computing Group, Inc., Montreal, <http://www.chemcomp.com>.
- 49 C. A. Lipinski, F. Lombardo, B. W. Dominy and P. J. Feeney, *Adv. Drug Deliv. Rev.*, 2001, **46**, 3–26.
- 50 C. A. Lipinski, *Drug Discovery Today: Technol.*, 2004, **1**, 337–341.
- 51 J. H. McKerrow and C. A. Lipinski, *Int. J. Parasitol.: Drugs Drug Resist.*, 2017, **7**, 248–249.
- 52 K. Yoshikawa, A. Yokomizo, H. Naito, N. Haginoya, S. Kobayashi, T. Yoshino, T. Nagata, A. Mochizuki, K. Osanai, K. Watanabe, H. Kanno and T. Ohta, *Bioorg. Med. Chem.*, 2009, **17**, 8206–8220.
- 53 D. Zewge, C. Y. Chen, C. Deer, P. G. Dormer and D. L. Hughes, *J. Org. Chem.*, 2007, **72**, 4276–4279.
- 54 M. J. López Rivilli, E. L. Moyano and G. I. Yranzo, *Tetrahedron Lett.*, 2010, **51**, 478–481.
- 55 B. Podányi, G. Keresztúri, L. Vasvári-Debreczy, I. Hermeecz and G. Tóth, *Magn. Reson. Chem.*, 1996, **34**, 972–978.
- 56 E. Stern, G. G. Muccioli, B. Bosier, L. Hamtiaux, R. Millet, J. H. Poupaert, J. P. Henichart, P. Depreux, J. F. Goossens and D. M. Lambert, *J. Med. Chem.*, 2007, **50**, 5471–5484.
- 57 Z. Zhang, X. Xiao, T. Su, J. Wu, J. Ren, J. Zhu, X. Zhang, R. Cao and R. Du, *Eur. J. Med. Chem.*, 2017, **140**, 239–251.
- 58 M. Vanejevs, C. Jatzke, S. Renner, S. Muller, M. Hechenberger, T. Bauer, A. Klochkova, I. Pyatkin, D. Kazyulkin, E. Aksenova, S. Shulepin, O. Timonina, A. Haasis, A. Gutcaits, C. G. Parsons, V. Kaus and T. Weil, *J. Med. Chem.*, 2008, **51**, 634–647.
- 59 D. Vogt, J. Weber, K. Ihlefeld, A. Bruggerhoff, E. Proschak and H. Stark, *Bioorg. Med. Chem.*, 2014, **22**, 5354–5367.
- 60 T. Hanke, F. Dehm, S. Liening, S. D. Popella, J. Maczewsky, M. Pillong, J. Kunze, C. Weinigel, D. Barz, A. Kaiser, M. Wurglics, M. Lammerhofer, G. Schneider, L. Sautebin, M. Schubert-Zsilavec and O. Werz, *J. Med. Chem.*, 2013, **56**, 9031–9044.
- 61 O. Kouatly, A. Geronikaki, C. Kamoutsis, D. Hadjipavlou-Litina and P. Eleftheriou, *Eur. J. Med. Chem.*, 2009, **44**, 1198–1204.



## Conclusions

Rational modifications were performed on the I2C framework, employing bioisosterism and scaffold hopping strategies, to obtain novel molecules with favourable physicochemical properties. Two naphthamide derivatives stood out as moderately potent anti-TB agents, effective against DS and DR *M. tb* strains, while exhibiting negligible cytotoxicity towards Vero cells. Although the *N*-cyclooctyl indoleamide architecture showed excellent potency against *M. abscessus* in previous work, our most active *N*-cyclooctyl naphthamide anti-TB analogue was bereft of activity against *M. abscessus* and *M. avium*. Importantly, the majority of the evaluated quinoloneamides were inactive against *M. tb*, suggesting that the cut back on lipophilicity may have detrimentally influenced the anti-TB activity of these analogues. Overall, it seems like I2C is the most favourable structural core for eliciting potent anti-TB activity. Therefore, in the subsequent Chapter, the I2C scaffold was preserved while subtle changes were implemented therein in order to increase the aqueous solubility, while maintaining optimum lipophilicity to elicit adequate anti-TB potency.



## **Chapter 4**

### **Design and Synthesis of Indole-2-Carboxamides with Improved Water Solubility as Antimycobacterial Agents**

## Background

The indole-2-carboxamide (I2C) architecture, integrated with a cycloaliphatic group, has been proven to possess superior anti-TB efficacy compared to the other similar structural subunits. Equally important, the mode of action of the I2Cs as inhibitors of the mycobacterial membrane protein large 3 (MmpL3) transporter is well established in the literature. Indeed, the recently published crystal structure of MmpL3 provided much insight into the interactions that take place between the I2Cs and the MmpL3 active site. Our group and others have attempted to enhance the aqueous solubility of the I2Cs in order to improve drug-likeness. However, increasing the water solubility is often accompanied with decreased lipophilicity and accordingly reduced compound permeation into the thick waxy outer membrane of *Mycobacterium tuberculosis* (*M. tb*). Therefore, despite the industrious efforts that were previously undertaken to improve the water solubility of the I2Cs, the resulting compounds generally failed to potently inhibit the growth of *M. tb*. In fact, the relationship between water solubility, lipophilicity, and anti-TB activity is a convoluted one. While high lipophilicity is generally correlated with higher anti-TB activity, the concomitant low water solubility often precludes the oral bioavailability of the compound in question. Accordingly, these two parameters should be optimised in parallel to obtain potent anti-TB agents with enhanced drug-like profiles. In this respect, we published a research article in 2021, entailing the incorporation of a hydroxy group into the adamantane moiety *N*-linked to the I2C scaffold. The resulting adamantanol analogues displayed improved kinetic water solubility (determined experimentally) compared to the adamantane counterparts. Pleasingly, this improvement in water solubility was complemented by potent anti-TB activity against both drug-sensitive (DS) and drug-resistant (DR) *M. tb* clinical isolates in several I2C derivatives [minimum inhibitory concentration (MIC) = 0.66 – 5.77  $\mu$ M]. Overall, fine-tuning both lipophilicity and aqueous solubility in newly designed anti-TB compounds is imperative to procuring drug-like molecules. Introducing a hydroxy group to the adamantane moiety in the *N*-adamantyl I2C framework resulted in compounds with optimum lipophilicity, enhanced water solubility, and potent anti-TB activities.

## 4.1. Introduction

Apart from the *in vitro* potency against *M. tb* isolates, it is widely recognised that pharmacokinetics (PK) and physicochemical properties need to be taken into consideration before the compound could be advanced in the drug development pipeline. Indeed, assessment of physicochemical parameters in addition to *in vitro* toxicity assays should be integrated in the early stages of drug discovery to minimise the attrition rate correlated with insufficient drug exposure and safety concerns. Computational and experimental analyses of physicochemical properties are commonly used to predict/determine the oral bioavailability and the ADME (absorption, distribution, metabolism, and excretion) profile of compounds. Within this context, Lipinski's rule of five (RO5) has been widely applied to evaluate drug-likeness and predict if a certain pharmacologically active compound possesses appropriate physicochemical properties that would qualify it to be an orally active drug candidate (1). This rule of thumb was formulated, more than two decades ago, by Christopher A. Lipinski and is still employed to date to assess the drug-like properties.

Lipinski's filter encompasses the following physicochemical parameters' limits: 1) molecular weight (MWT)  $\leq 500$ ; 2) H-bond donors (HBD)  $\leq 5$ , derived from the sum of NHs and OHs; 3) H-bond acceptors (HBA)  $\leq 10$ , derived from the sum of Os and Ns; 4) ClogP  $\leq 5$  (1, 2). Compounds conforming with these parameters are likely to be imparted with acceptable water solubility and intestinal permeability, which are prerequisites for oral bioavailability. Indeed, according to this rule, if a compound exhibits one violation or more of the foregoing four parameter cut-offs, it is highly likely that poor permeation and/or absorption (oral activity problems) will be encountered (1, 2). In resonance with Lipinski's rule, Gleeson's analysis demonstrated that molecules with MWT  $< 400$  and ClogP  $< 4$  are classified as desirable, while ADME issues generally start to arise should either parameter or both exceed the cut-offs (3). Indeed, Gleeson revealed that these two parameters are often sufficient to predict the ADME profile of a compound, wherein a deterioration in almost all ADME properties were observed upon increasing MWT and ClogP values. Therefore, Gleeson's filter can be regarded as a downsized or simplified version of the RO5. Importantly, passing the RO5 does not guarantee the procession of the compound in the drug development pipeline. Relatedly, many orally administered drugs in the market fall outside the preceding parameter cut-offs, defying the RO5 premise (1, 2). Many of these outliers

are natural products and they are often described as beyond rule of five (bRo5) drugs (4-7). However, the attrition rates of drug-like molecules, conforming to the RO5, tend to be low during clinical trials, increasing the compound's chance of reaching the market (8). In fact, the RO5 was established based on the physicochemical profiles of drug candidates in Phase II clinical trials (1).

The RO5, which was developed by a Pfizer team, has spawned some suggestions for adjustments, aimed at improving the prediction of drug-likeness. Veber's rule, which was generated after analysing the molecular properties of more than 1000 drug candidates in GlaxoSmithKline and their influence on the oral bioavailability in rats, stands out as an important variant of the RO5 (9). Veber *et al* brought into question the importance of the MWT parameter cut-off in discriminating compounds with good oral bioavailability from those with poor values. They, alternatively, proposed that if a compound meets only two criteria, namely number of rotatable bonds (NRB)  $\leq 10$  and topological polar surface area (TPSA)  $\leq 140 \text{ \AA}^2$  [or hydrogen bond count (sum of HBD and HBA)  $\leq 12$ ], it tends to have a high chance of acceptable oral bioavailability in rats ( $\geq 20\%$ ), independent of its MWT (9). In fact, they revealed that low TPSA generally correlates better with enhanced permeation than does reduced lipophilicity (ClogP), while the increased rotatable bond count negatively affected the permeation rate. In resonance with Veber's *et al* findings, Egan *et al* dismissed the MWT parameter as superfluous, while showing that both logP (AlogP98) and TPSA can be used as a predictive tool for passive intestinal absorption (referred to as the Egan egg model) (10, 11). Overall, while the RO5 laid the primary foundation for the design and development of orally bioavailable drug-like candidates, other researchers elaborated on Lipinski's original framework to provide more insights into successful ADME predictions. This is particularly important as all these factors/parameters were carefully considered in the design stage of our *N*-adamantanol indole-2-carboxamides which subsequently showed superior water solubility values compared to the adamantane counterparts (results published in our 2021 article, *vide infra*).

#### **4.2. MmpL3: A Crucial Member of The MmpL Transporters Family in *M. tb* and The Protein Target of The I2Cs**

The *M. tb* cell wall has a complex structure, comprising a broad range of glycolipids and other distinctive lipids, some of which act as virulence determinants or immuno-

modulators in addition to playing a key role in the *M. tb* pathophysiology (12). The unique architecture of the *M. tb* cell envelope consists of four sectors that define the border separating the *M. tb* cytoplasm from the extracellular environment (13). These regions are the following: 1) the capsule or outer layer (OL), 2) the mycomembrane or mycobacterial outer membrane (MOM), 3) the arabinogalactan-peptidoglycan (AGP) cell wall core, and 4) the plasma membrane (13). Collectively, they constitute a robust physical barrier that limits the ingress of therapeutic agents into the *M. tb* cytoplasm. In addition, some components of the *M. tb* cell envelope directly interfere with essential events of the host immune defences, potentiating the survival and persistence of *M. tb* (13). Therefore, targeting the enzymes involved in the *M. tb* cell wall biosynthetic machinery has long been a successful strategy to defeat TB (14). However, DR-TB is still incorrigible, running rampant in every corner of the globe, which mandates the search for new druggable targets in *M. tb* to circumvent this dilemma.

The past two decades have witnessed multiple breakthroughs in the quest for viable novel *M. tb* drug targets (15). One of the recently identified promising druggable targets is the crucial mycolic acids (MAs) transporter MmpL3. Numerous small molecules that were proven to target MmpL3 were found to have exquisite anti-TB activities against both DS and DR *M. tb* clinical isolates (16-19). MmpL3 is a member of the mycobacterial membrane protein large (MmpL) family which is a subclass of the resistance-nodulation-cell division (RND) superfamily transport system. *M. tb* encodes 13 MmpL transporters (MmpL1-13) which are transmembrane proteins that contribute to the transport of lipid components across the inner membrane (12, 13, 20) (**Figure 4.1**). These transportations are mediated by the proton motive force (PMF) of the transmembrane electrochemical proton gradient. Besides their important role in the substrate transport across the cytoplasmic membrane, MmpL proteins are generally responsible for the efflux of antibiotics from periplasm in *M. tb* and NTM, culminating in drug resistance (12, 13, 20).

Among the MmpL transporters, MmpL3 governs the export of trehalose monomycolate (TMM), synthesised in the cytoplasm, to periplasm where it gets assembled, forging the thick waxy mycobacterial cell wall (21). It is encoded by the *mmpL3* gene which is the only *mmpL* gene that Domenech *et al* could not knock out in the H37Rv strain, inferring its involvement in important physiological processes in *M. tb* (22). Therefore, *mmpL3* is known to be the sole *mmpL* gene that is essential for the viability and *in vitro*

growth of *M. tb*. No difference in the *in vitro* mycobacterial growth was observed in the rest of the generated *mmpL* mutants when compared to the wild-type H37Rv *M. tb* strain, corroborating other similar findings published around the same time (22, 23). On the contrary, in the *in vivo* studies, disruptions in six *mmpL* genes, namely *mmpL4*, *mmpL5*, *mmpL7*, *mmpL8*, *mmpL10*, and *mmpL11*, severely attenuated the ability of *M. tb* mutants to replicate in the lungs of infected mice (23). On the other hand, mutations in *mmpL1*, *mmpL2*, *mmpL6*, *mmpL9*, and *mmpL12* did not correlate to any *in vivo* survival defect (23). In fact, the substrates and functions of the five MmpL transporters encoded by the foregoing five genes as well as MmpL13 have not been definitively characterised yet; they are not as critical as the remaining MmpL transporters (13) (Figure 4.1).

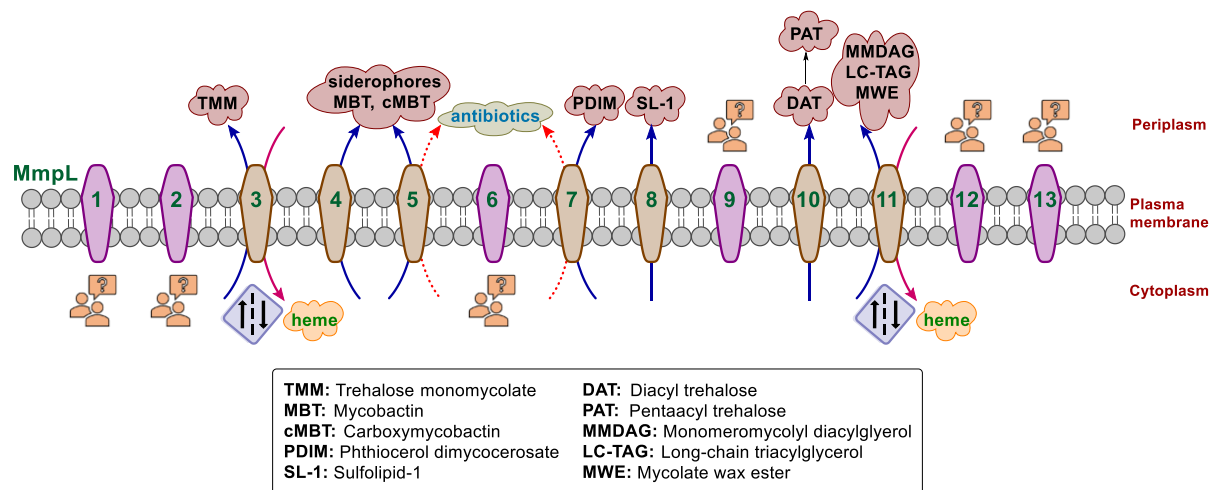


**Figure 4.1. MmpL1-13 proteins in *M. tb*.** While a number of substrates have been identified for seven MmpL transporters, the functions of the remaining six MmpL proteins have not yet been conclusively determined.

In addition to exporting MAs from cytoplasm to periplasm, MmpL3 is also responsible for importing heme into cytoplasm (24, 25). In fact, to date, three *M. tb* proteins are known to be implicated in the mycobacterial heme acquisition system, namely Rv0203, MmpL3, and MmpL11. While Rv0203 scavenges heme from the host and transports it across the mycobacterial periplasm, both MmpL3 and MmpL11 shuttle it to cytoplasm, wherein the sequestered iron can be used in promoting mycobacterial survival and pathogenicity (24, 25). Interestingly, *mmpL3* is located in close proximity to *mmpL11* and both transporters are homologous to each other, bearing 24% amino

acid sequence identity (24). Of note, the *mmp3/mmp11* chromosomal locus, encoding both MmpL3 and MmpL11, is conserved across the mycobacterium genus (pathogenic and non-pathogenic) (26). Similar to MmpL3, MmpL11 serves as a two-way traffic tunnel. Indeed, in addition to its role as a heme importer, MmpL11 coordinates the conveyance of monomeromycolyl diacylglycerol (MMDAG), long-chain triacylglycerols (LC-TAG), and mycolate wax esters (MWE) in *M. tb* (27). These lipids are crucially required for the formation of biofilms in *M. tb* and mycobacterial persistence (27). Bacterial biofilms possess the ability to tolerate host defence systems, antibiotics, and other environmental stressors, thereby contributing to chronic persistent infections (28). It was also suggested that MAs play a pivotal role in the development and modulation of *M. tb* biofilms (28). Accordingly, these findings hint at the implication of MmpL3 and MmpL11 in the phenotypic drug tolerance of *M. tb* which in turn prompts the administration of extensive drug treatment regimens.

On the other hand, both MmpL4 and MmpL5 are considered unique redundant transporters that do not transport lipid to the cell envelope, but instead they are responsible for the export of siderophores (29). *M. tb* generates two siderophores, namely mycobactin (MBT) and carboxymycobactin (cMBT). The former molecule is hydrophobic, while the latter is its more water-soluble cousin; both chelate iron from the human host environment. Therefore, both transporters are critically required for siderophore-mediated iron uptake in *M. tb* (29). MmpL7 and MmpL8 coordinate the translocation of phthiocerol dimycocerosates (PDIM) and sulfolipid-1 (SL-1), respectively, from their production site in cytoplasm to periplasm (13). Both lipids contribute to *M. tb* virulence by masking/impairing the recognition of pathogen by host immune receptors, thereby restricting the innate immune response to *M. tb*. Due to the high lipophilicity of PDIM, it also limits the fluidity of the *M. tb* cell envelope, contributing to the intrinsic resistance against antibiotics (13). Of note, MmpL5 and MmpL7 were the only MmpL transporters that were shown to be involved in drug efflux. Finally, MmpL10 was found to be implicated in the transfer of diacyl trehaloses (DAT) from cytoplasm, where they are synthesised, to the periplasm (13). DAT is subsequently acylated to generate pentaacyl trehaloses (PAT). However, the role of DAT/PAT in *M. tb* virulence is still perplexing (13). Taken together, while MmpL3 was found to be indispensable to the growth and survival of *M. tb*, six other MmpL transporters were shown to be required for full mycobacterial virulence.

Due to the salient attributes of MmpL3 that made it critical to the *M. tb* virulence and pathogenicity (*vide supra*), this MAs transporter remains the principal MmpL protein that drug discovery research efforts have been focused on. Indeed, different groups have documented the necessity of the *mmpL3* gene for the multiplication and viability of *M. tb* *in vitro*, intramacrophage, and *in vivo* (30, 31). Within this context, silencing the *mmpL3* gene halted bacterial cell division and elicited a rapid bactericidal effect on *M. tb* in axenic cultures. Additionally, significant changes in the *M. tb* cell envelope were observed upon depleting the *mmpL3* gene, wherein TMM accumulated in the cytoplasm, resulting in a shortage of cell wall bound mycolates, in comparison with the wild-type strain (30, 31). These findings clearly corroborate the critical role of MmpL3 in flipping the TMMs from cytoplasm to periplasm, an indispensable step in the construction of a properly functioning *M. tb* cell wall. MmpL3 was also demonstrated to be essential for the *M. tb* growth in macrophages (30). In addition, knocking down the *mmpL3* gene was correlated with a significant reduction in the bacterial burden in the lungs of acutely and chronically infected mice, compared to the wild-type H37Rv-infected mice (31). Additionally, MmpL3 was found to be essential for the growth and viability of other mycobacterial species (16, 32). I2Cs are probably the most prominent MmpL3 inhibitors in the literature. In 2019, two groups made a huge progress in the MmpL3 research area (33, 34). First, Zhang *et al* reported the crystal structure of MmpL3 and the interactions that take place between different MmpL3 inhibitors and the binding site therein (33). They highlighted two Asp-Tyr pairs, which are located in the transmembrane domain of MmpL3, as the key facilitators of proton transportation. They found that ICA38, AU1235, SQ109, and rimonabant bind inside the transmembrane region, whereupon they disrupt these critical Asp-Tyr pairs required for proton relay, blocking the PMF for substrate translocation. Interestingly, their findings suggested that MmpL3 is unlikely to act as a drug efflux pump, in contrast to previous reports (33).

Shortly afterwards, the second landmark study, conducted by Li *et al*, entailed *in vitro* and whole-cell-based investigations to unveil whether the identified drug candidates/lead compounds inhibit MmpL3 via a direct mechanism or an indirect one (through dissipating the PMF) (34). Their results evidently pointed to a direct mode of inhibition displayed by all compound series analysed therein, including the I2Cs, regardless of their impact on the PMF, which they considered an auxiliary role that



augments the inhibitory activities of the compounds. The preceding two studies underpinned the predilection for lipophilic compounds to inhibit MmpL3 as they will be more predisposed to traverse the exterior hydrophobic matrix of *M. tb*, whereupon they interact with MmpL3 whose active site is mainly hydrophobic. However, this prerequisite lipophilicity condition renders the compound lacking sufficient water solubility which is mandatory for achieving adequate bioavailability. This is well typified by a number of I2Cs reported to date that displayed exceptional *in vitro* activities, yet they failed in the *in vivo* studies (18). Overall, while MmpL3 undoubtedly represents a promising target, a judicious modulation of the lipophilicity of its inhibitors is highly coveted.

#### 4.3. Previous and Current Endeavours to Enhance The Water Solubility of I2Cs

Several groups, including ours, have attempted to improve the water solubility of the I2Cs without incurring a serious decline in the *in vitro* anti-TB activity (18, 35-37). However, most of these efforts, reported thus far, led to a substantial decrease in the activity due to the positive correlation between lipophilicity and anti-TB potency observed in MmpL3 inhibitors. Indeed, our group and Kondreddi *et al* have investigated the impact of introducing a basic nitrogen to the indole ring and the *N*-linked cycloaliphatic group (18, 35, 36). While the two 5-aza-6-methoxyindoles **1** and **2** (**Figure 4.2**) showed considerable *in vitro* anti-TB activities (MIC = 6.6 and 1.5  $\mu$ M, respectively), the nitrogen-containing *N*-linked aromatic/cycloaliphatic analogues **3 – 6** (**Figure 4.2**) demonstrated a massive loss in the anti-TB activity (MIC > 200  $\mu$ M) (35, 36). However, when an azabicyclo motif was used in compound **7** (**Figure 4.2**) instead of the comparably hydrophobic cycloaliphatic moieties, the resulting anti-TB activity was modest (MIC = 10.9  $\mu$ M) (18). Similar to compounds **3 – 6**, when a polar tetrahydropyran motif was *N*-tethered to the indole ring **8** (**Figure 4.2**), the anti-TB activity drastically decreased (MIC > 20  $\mu$ M) (35). Nonetheless, when Kondreddi *et al* introduced a hydroxyl group to the *N*-attached cyclohexyl group **9** (**Figure 4.2**), a moderate activity was observed (MIC = 8.9  $\mu$ M) (35).

Accordingly, with the goal of uncovering drug-like candidates with enhanced water solubility, in the study that we published in 2021, a hydroxyl group was incorporated to the adamantane moiety linked to the I2C framework. Some of the adamantanol derivatives therein displayed potent anti-TB activity against DS and DR *M. tb* clinical

isolates. Compound **10** (Figure 4.2) was the most active *N*-adamantanol analogue in our study with MIC values of 0.66 – 2.64  $\mu\text{M}$  against DS, multi-drug resistant (MDR), and extensively drug-resistant (XDR) *M. tb* strains. Of note, the measured kinetic water solubility of two representative adamantanol analogues was approximately 2 and 3-fold higher than their adamantane counterparts, suggesting their likely improved PK profile. Equally important, the most potent adamantanol analogue **10** showed minimal cytotoxicity against healthy Vero cells ( $\text{IC}_{50} \geq 169 \mu\text{M}$ ).

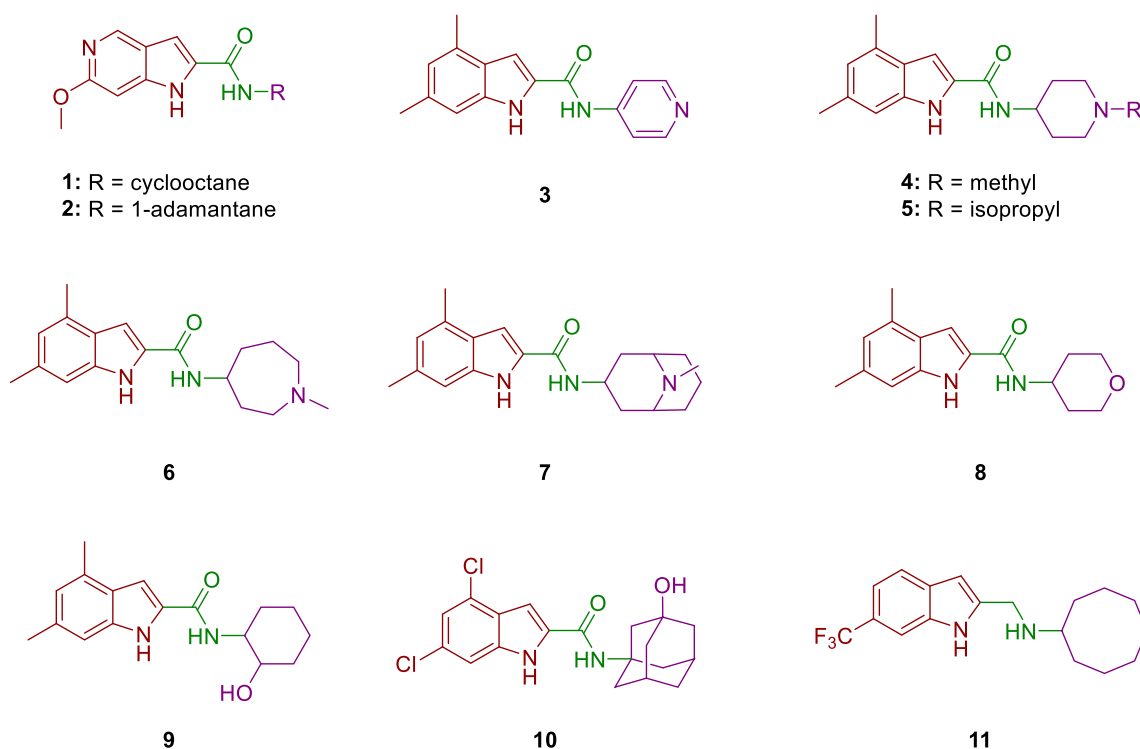


**Figure 4.2. Previous attempts to improve the water solubility of the I2C architecture.**

Due to the strong resemblance between our compounds and the previously reported MmpL3 inhibitors, the top potent analogues in our study were also docked into the MmpL3 active site in order to assess their mode of action. Our compounds were oriented in a fashion similar to the co-crystallised ligands; most of the interactions that took place between the original ligands and the surrounding amino acids were recapitulated upon docking the new compounds. These molecular modelling findings in turn indicate that our compounds elicit their anti-TB activity presumably by inhibiting MmpL3. Of note, around the same time, another laboratory disclosed the potent anti-

TB activity of the indolemethylamine analogue **11** (MIC = 0.13  $\mu$ M, **Figure 4.2**) which also displayed improved aqueous solubility (37). However, this compound demonstrated moderate cytotoxicity against Vero cells (IC<sub>50</sub> = 22  $\mu$ M) (37). Taken together, while improving the water solubility of the I2C architecture, in several previous reports, was synchronised with undermined anti-TB activity or safety, some of our recently published adamantanol analogues exhibited potent anti-TB activities, enhanced aqueous solubilities, and negligible cytotoxicities. The corresponding research article, published in *Bioorganic Chemistry*, is included herein.

## References

1. Lipinski CA, Lombardo F, Dominy BW, Feeney PJ. Experimental and computational approaches to estimate solubility and permeability in drug discovery and development settings. *Adv Drug Deliv Rev.* 2001;46(1-3):3-26.
2. Lipinski CA. Lead- and drug-like compounds: the rule-of-five revolution. *Drug Discov Today Technol.* 2004;1(4):337-41.
3. Gleeson MP. Generation of a set of simple, interpretable ADMET rules of thumb. *J Med Chem.* 2008;51(4):817-34.
4. Doak BC, Kihlberg J. Drug discovery beyond the rule of 5 - Opportunities and challenges. *Expert Opin Drug Discov.* 2017;12(2):115-9.
5. Doak BC, Over B, Giordanetto F, Kihlberg J. Oral druggable space beyond the rule of 5: insights from drugs and clinical candidates. *Chem Biol.* 2014;21(9):1115-42.
6. Doak BC, Zheng J, Dobritzsch D, Kihlberg J. How Beyond Rule of 5 Drugs and Clinical Candidates Bind to Their Targets. *J Med Chem.* 2016;59(6):2312-27.
7. S OH, Swainston N, Handl J, Kell DB. A 'rule of 0.5' for the metabolite-likeness of approved pharmaceutical drugs. *Metabolomics.* 2015;11(2):323-39.
8. Leeson PD, Springthorpe B. The influence of drug-like concepts on decision-making in medicinal chemistry. *Nat Rev Drug Discov.* 2007;6(11):881-90.
9. Veber DF, Johnson SR, Cheng HY, Smith BR, Ward KW, Kopple KD. Molecular properties that influence the oral bioavailability of drug candidates. *J Med Chem.* 2002;45(12):2615-23.
10. Egan WJ, Lauri G. Prediction of intestinal permeability. *Adv Drug Deliv Rev.* 2002;54(3):273-89.
11. Egan WJ, Merz KM, Jr., Baldwin JJ. Prediction of drug absorption using multivariate statistics. *J Med Chem.* 2000;43(21):3867-77.
12. Szekely R, Cole ST. Mechanistic insight into mycobacterial MmpL protein function. *Mol Microbiol.* 2016;99(5):831-4.
13. Melly G, Purdy GE. MmpL Proteins in Physiology and Pathogenesis of *M. tuberculosis*. *Microorganisms.* 2019;7(3).
14. Abrahams KA, Besra GS. Mycobacterial cell wall biosynthesis: a multifaceted antibiotic target. *Parasitology.* 2018;145(2):116-33.
15. Shetye GS, Franzblau SG, Cho S. New tuberculosis drug targets, their inhibitors, and potential therapeutic impact. *Transl Res.* 2020;220:68-97.

16. Grzegorzewicz AE, Pham H, Gundi VA, Scherman MS, North EJ, Hess T, et al. Inhibition of mycolic acid transport across the *Mycobacterium tuberculosis* plasma membrane. *Nat Chem Biol.* 2012;8(4):334-41.
17. Lun S, Guo H, Onajole OK, Pieroni M, Gunosewoyo H, Chen G, et al. Indoleamides are active against drug-resistant *Mycobacterium tuberculosis*. *Nat Commun.* 2013;4:2907.
18. Stec J, Onajole OK, Lun S, Guo H, Merenbloom B, Vistoli G, et al. Indole-2-carboxamide-based MmpL3 Inhibitors Show Exceptional Antitubercular Activity in an Animal Model of Tuberculosis Infection. *J Med Chem.* 2016;59(13):6232-47.
19. Rao SP, Lakshminarayana SB, Kondreddi RR, Herve M, Camacho LR, Bifani P, et al. Indolcarboxamide is a preclinical candidate for treating multidrug-resistant tuberculosis. *Sci Transl Med.* 2013;5(214):214ra168.
20. Viljoen A, Dubois V, Girard-Misguich F, Blaise M, Herrmann JL, Kremer L. The diverse family of MmpL transporters in mycobacteria: from regulation to antimicrobial developments. *Mol Microbiol.* 2017;104(6):889-904.
21. Xu Z, Meshcheryakov VA, Poce G, Chng SS. MmpL3 is the flippase for mycolic acids in mycobacteria. *Proc Natl Acad Sci U S A.* 2017;114(30):7993-8.
22. Domenech P, Reed MB, Barry CE, 3rd. Contribution of the *Mycobacterium tuberculosis* MmpL protein family to virulence and drug resistance. *Infect Immun.* 2005;73(6):3492-501.
23. Lamichhane G, Tyagi S, Bishai WR. Designer arrays for defined mutant analysis to detect genes essential for survival of *Mycobacterium tuberculosis* in mouse lungs. *Infect Immun.* 2005;73(4):2533-40.
24. Owens CP, Chim N, Graves AB, Harmston CA, Iniguez A, Contreras H, et al. The *Mycobacterium tuberculosis* secreted protein Rv0203 transfers heme to membrane proteins MmpL3 and MmpL11. *J Biol Chem.* 2013;288(30):21714-28.
25. Tullius MV, Harmston CA, Owens CP, Chim N, Morse RP, McMath LM, et al. Discovery and characterization of a unique mycobacterial heme acquisition system. *Proc Natl Acad Sci U S A.* 2011;108(12):5051-6.
26. Pacheco SA, Hsu FF, Powers KM, Purdy GE. MmpL11 protein transports mycolic acid-containing lipids to the mycobacterial cell wall and contributes to biofilm formation in *Mycobacterium smegmatis*. *J Biol Chem.* 2013;288(33):24213-22.
27. Melly GC, Stokas H, Davidson PM, Roma JS, Rhodes HL, Purdy GE. Identification of residues important for *M. tuberculosis* MmpL11 function reveals that

function is modulated by phosphorylation in the C-terminal domain. *Mol Microbiol.* 2021;115(2):208-21.

28. Sharma D, Misba L, Khan AU. Antibiotics versus biofilm: an emerging battleground in microbial communities. *Antimicrob Resist Infect Control.* 2019;8:76.

29. Wells RM, Jones CM, Xi Z, Speer A, Danilchanka O, Doornbos KS, et al. Discovery of a siderophore export system essential for virulence of *Mycobacterium tuberculosis*. *PLoS Pathog.* 2013;9(1):e1003120.

30. Degiacomi G, Benjak A, Madacki J, Boldrin F, Provvedi R, Palu G, et al. Essentiality of mmpL3 and impact of its silencing on *Mycobacterium tuberculosis* gene expression. *Sci Rep.* 2017;7:43495.

31. Li W, Obregon-Henao A, Wallach JB, North EJ, Lee RE, Gonzalez-Juarrero M, et al. Therapeutic Potential of the *Mycobacterium tuberculosis* Mycolic Acid Transporter, MmpL3. *Antimicrob Agents Chemother.* 2016;60(9):5198-207.

32. Varela C, Rittmann D, Singh A, Krumbach K, Bhatt K, Eggeling L, et al. MmpL genes are associated with mycolic acid metabolism in mycobacteria and corynebacteria. *Chem Biol.* 2012;19(4):498-506.

33. Zhang B, Li J, Yang X, Wu L, Zhang J, Yang Y, et al. Crystal Structures of Membrane Transporter MmpL3, an Anti-TB Drug Target. *Cell.* 2019;176(3):636-48 e13.

34. Li W, Stevens CM, Pandya AN, Darzynkiewicz Z, Bhattarai P, Tong W, et al. Direct Inhibition of MmpL3 by Novel Antitubercular Compounds. *ACS Infect Dis.* 2019;5(6):1001-12.

35. Kondreddi RR, Jiricek J, Rao SP, Lakshminarayana SB, Camacho LR, Rao R, et al. Design, synthesis, and biological evaluation of indole-2-carboxamides: a promising class of antituberculosis agents. *J Med Chem.* 2013;56(21):8849-59.

36. Onajole OK, Pieroni M, Tipparaju SK, Lun S, Stec J, Chen G, et al. Preliminary structure-activity relationships and biological evaluation of novel antitubercular indolecarboxamide derivatives against drug-susceptible and drug-resistant *Mycobacterium tuberculosis* strains. *J Med Chem.* 2013;56(10):4093-103.

37. Tan YJ, Li M, Gunawan GA, Nyantakyi SA, Dick T, Go M-L, et al. Amide–Amine Replacement in Indole-2-carboxamides Yields Potent Mycobactericidal Agents with Improved Water Solubility. *ACS Med Chem Lett.* 2021;12(5):704-12.

## STATEMENT OF CONTRIBUTION TO A CO-AUTHORED PUBLISHED PAPER

Chapter 4 includes a co-authored research article that has been published online in the Bioorganic Chemistry journal (2021)

DOI: <https://doi.org/10.1016/j.bioorg.2020.104486>

Publication link:

<https://www.sciencedirect.com/science/article/abs/pii/S0045206820317843>

Title: **Design, synthesis and antimycobacterial evaluation of novel adamantane and adamantanol analogues effective against drug-resistant tuberculosis**

Authors/Co-authors: **Shahinda S. R. Alsayed**, Shichun Lun, Alan Payne, William R. Bishai and Hendra Gunosewoyo

My contribution to the paper involved: 1) the conception, design, synthesis, purification, and chemical analysis of all the tested molecules, 2) determining the kinetic water solubility of the synthesised molecules, 3) interpreting all the results (chemistry and biology wise), 4) molecular docking of the compounds, 5) collecting and organising the information/data/references, and 6) preparing and writing up the whole manuscript.

(Signed)  (Date) 20/09/2021

Shahinda Sayed Rabie Alsayed

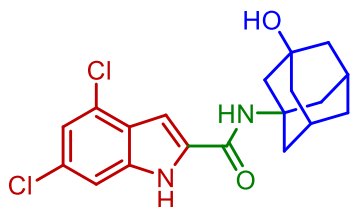
(Countersigned)  (Date) 20/9/21

Corresponding author of the paper: Dr Hendra Gunosewoyo

(Countersigned)  (Date) 20/9/21

Main supervisor: Dr Hendra Gunosewoyo

## Graphical Abstract



**8j**

**DS *M. tb* (H37Rv & V4207)**

MIC = 1.32  $\mu$ M

**MDR *M. tb* (V2475 & KZN494)**

MIC = 1.32 – 2.64  $\mu$ M

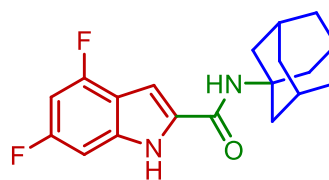
**XDR *M. tb* (R506 & TF274)**

MIC = 0.66  $\mu$ M

**Cytotoxicity (Vero cells)**

IC<sub>50</sub>  $\geq$  169  $\mu$ M

SI  $\geq$  128



**8k**

**DS *M. tb* (H37Rv & V4207)**

MIC = 0.024  $\mu$ M

**MDR *M. tb* (V2475 & KZN494)**

MIC = 0.024  $\mu$ M

**XDR *M. tb* (R506 & TF274)**

MIC = 0.012  $\mu$ M

**Cytotoxicity (Vero cells)**

IC<sub>50</sub>  $\geq$  194  $\mu$ M

SI  $\geq$  8205





# Design, synthesis and antimycobacterial evaluation of novel adamantane and adamantanol analogues effective against drug-resistant tuberculosis

Shahinda S.R. Alsayed<sup>a</sup>, Shichun Lun<sup>b</sup>, Alan Payne<sup>c</sup>, William R. Bishai<sup>b,d,\*</sup>,  
Hendra Gunosewoyo<sup>a,\*</sup>

<sup>a</sup> School of Pharmacy and Biomedical Sciences, Faculty of Health Sciences, Curtin University, Bentley, Perth, WA 6102, Australia

<sup>b</sup> Center for Tuberculosis Research, Department of Medicine, Division of Infectious Disease, Johns Hopkins School of Medicine, 1550, Orleans Street, Baltimore, MD 21231-1044, United States

<sup>c</sup> School of Molecular and Life Sciences, Curtin University, Perth, WA 6102, Australia

<sup>d</sup> Howard Hughes Medical Institute, 4000 Jones Bridge Road, Chevy Chase, Maryland 20815-6789, United States

## ARTICLE INFO

### Keywords:

Tuberculosis  
MmpL3  
Indoleamides  
Adamantane  
Adamantanol  
MDR-TB  
XDR-TB  
Cytotoxicity  
Water solubility

## ABSTRACT

The treacherous nature of tuberculosis (TB) combined with the ubiquitous presence of the drug-resistant (DR) forms pose this disease as a growing public health menace. Therefore, it is imperative to develop new chemotherapeutic agents with a novel mechanism of action to circumvent the cross-resistance problems. The unique architecture of the *Mycobacterium tuberculosis* (*M. tb*) outer envelope plays a predominant role in its pathogenesis, contributing to its intrinsic resistance against available therapeutic agents. The mycobacterial membrane protein large 3 (MmpL3), which is a key player in forging the *M. tb* rigid cell wall, represents an emerging target for TB drug development. Several indole-2-carboxamides were previously identified in our group as potent anti-TB agents that act as inhibitor of MmpL3 transporter protein. Despite their highly potent in vitro activities, the lingering Achilles heel of these indoleamides can be ascribed to their high lipophilicity as well as low water solubility. In this study, we report our attempt to improve the aqueous solubility of these indole-2-carboxamides while maintaining an adequate lipophilicity to allow effective *M. tb* cell wall penetration. A more polar adamantanol moiety was incorporated into the framework of several indole-2-carboxamides, whereupon the corresponding analogues were tested for their anti-TB activity against drug-sensitive (DS) *M. tb* H37Rv strain. Three adamantanol derivatives **8i**, **8j** and **8l** showed nearly 2- and 4-fold higher activity (MIC = 1.32 – 2.89  $\mu$ M) than ethambutol (MIC = 4.89  $\mu$ M). Remarkably, the most potent adamantanol analogue **8j** demonstrated high selectivity towards DS and DR *M. tb* strains over mammalian cells [IC<sub>50</sub> (Vero cells)  $\geq$  169  $\mu$ M], evincing its lack of cytotoxicity. The top eight active compounds **8b**, **8d**, **8f**, **8i**, **8j**, **8k**, **8l** and **10a** retained their in vitro potency against DR *M. tb* strains and were docked into the MmpL3 active site. The most potent adamantanol/adamantane-based indoleamides **8j/8k** displayed a two-fold surge in potency against extensively DR (XDR) *M. tb* strains with MIC values of 0.66 and 0.012  $\mu$ M, respectively. The adamantanol-containing indole-2-carboxamides exhibited improved water solubility both *in silico* and experimentally, relative to the adamantane counterparts. Overall, the observed antimycobacterial and physicochemical profiles support the notion that adamantanol moiety is a suitable replacement to the adamantane scaffold within the series of indole-2-carboxamide-based MmpL3 inhibitors.

## 1. Introduction

Tuberculosis (TB) is a life-threatening insidious disease that has afflicted humanity for millennia, taking a heavy toll on human life and health [1]. *Mycobacterium tuberculosis* (*M. tb*), the etiologic agent of TB, is a highly communicable airborne pathogen. It mainly affects the lungs

and is capable of hijacking the host immune system, often persisting for years without causing any symptoms (termed latent TB) [2–6]. The status of bacteria switches from being dormant to active mode, when the host immune system becomes compromised, allowing the bacteria to invade the host and causing the disease to be symptomatic and contagious [7–9]. Globally, in 2018, TB was contracted by 10 million people;

\* Corresponding authors.

E-mail addresses: [wbishai1@jhmi.edu](mailto:wbishai1@jhmi.edu) (W.R. Bishai), [Hendra.Gunosewoyo@curtin.edu.au](mailto:Hendra.Gunosewoyo@curtin.edu.au) (H. Gunosewoyo).

<https://doi.org/10.1016/j.bioorg.2020.104486>

Received 3 October 2020; Received in revised form 11 November 2020; Accepted 16 November 2020

Available online 19 November 2020

0045-2068/© 2020 Elsevier Inc. All rights reserved.

an infection rate that remained steady for the past few years, and claimed the lives of an estimated 1.5 million people, including around 0.25 million in the HIV-positive cohort [10]. The World Health Organisation (WHO) also declared that one quarter of the human population are latently infected with TB [10]. This relentless burden places TB as the number one infectious disease killer (outranking HIV/AIDS) and one of the top 10 causes of death worldwide [10]. Due to the complexity and heterogeneity of the *M. tb* infection, the treatment protocol is protracted and burdensome [11,12]. The directly observed TB treatment, short course (TB-DOTS) comprises an initial 2-months intensive therapy with a cocktail of the first-line drugs: isoniazid (INH), rifampicin (RIF), pyrazinamide (PZA) and ethambutol (EMB), followed by a 4-months continuation phase with INH and RIF [10,13]. Poor patient compliance to this multi-drug regimen (due to side effects, high pill count and lengthy duration of therapy) together with HIV co-epidemic have fuelled the emergence of drug-resistant TB (DR-TB) [12]. Hence, new labels were assigned to the disease, namely multi-, extensively and totally drug-resistant TB (MDR-, XDR-, TDR-TB, respectively), perpetuating TB as a global health threat [14–20]. Besides the increasing prevalence of these refractory strains, the TB resistance crisis is further exacerbated by the limited drug options thereof which require administration for a longer duration (up to 2 years) and are less efficacious, more expensive and cytotoxic compared to the front-line regimen [10,21]. Accordingly, there is an urgent need to identify novel anti-TB agents directed against new cellular targets, different from the ones targeted by the current anti-TB drugs, in order for them to be effective against drug-sensitive TB (DS-TB) and DR-TB.

Genetic and lipid profiling studies identified a membrane transporter, the mycobacterial membrane protein large 3 (MmpL3) as a promising antimycobacterial target [22–25]. MmpL3 plays an important role in the heme uptake into the bacterial cell. More importantly, it is responsible for the translocation of mycolic acids (MAs) precursors, trehalose monomycolates (TMMs), across the plasma membrane [26–30]. MAs are the major lipid components of the mycobacterial outer membrane, which are responsible for its hydrophobicity and impermeability to a range of therapeutic agents [31–33]. We previously detailed the MAs biosynthetic machinery and their assembly into the mycobacterial cell envelope [34]. Not only is this intricate protective lipid coating impervious to exogenous substances, including many antibiotics, it also insulates the mycobacteria against the host's immune system, accentuating its importance in the mycobacterial growth and survival in host [35–37]. Conditional depletion of MmpL3 in *Mycobacterium smegmatis* (*M. smegmatis*) led to the loss of cell wall mycolation concomitant with intracellular accumulation of TMM, verifying the role of MmpL3 in shuttling TMM across the cytoplasmic membrane [24,26,38]. A downregulation of *mmpL3* expression was in fact followed by an abrogation in cell division and rapid cell death [39,40]. Several MmpL3 inhibitors with varied chemical entities have been reported to date by various high throughput screening (HTS) campaigns, further validating MmpL3 as a viable target for anti-TB drugs. Five structurally

distinct analogues, including the indole-2-carboxamides and adamantyl ureas, were recently found to directly inhibit MmpL3 [41–43]. NITD-304 (**1**, Fig. 1) was previously identified as a preclinical agent for treating MDR-TB [23]. In our previous work, the lead indoleamide **2** and ICA38 **3** were also highlighted as highly potent anti-TB agents [44,45]. Unfortunately, both compounds were found to be inactive in vivo, likely due to their poor bioavailability [44,45].

Very recently, the crystal structure of MmpL3 in *M. smegmatis* was disclosed, serving as an excellent paradigm for the *M. tb* counterpart due to the high homology between these two mycobacteria [25]. The MmpL3 binding site therein is divided into five subsites (S1-S5) with S4 being the only hydrophilic one. Upon binding, both the indole-2-carboxamides and adamantyl ureas occupy the S3-S5 subsites in the proton translocation channel, elaborating a common inhibitory mechanism (Fig. 2) [25]. These findings were in harmony with the homology model previously constructed by our group [45]. These compounds were found to be likely disrupting the key components of the S4 subsite (the two Asp-Tyr pairs) implicated in the proton relay, thereby blocking the proton motive force (PMF) for substrate translocation. Indeed, this was further substantiated by another study that employed in vitro and whole-cell-based approaches where they found that the adamantyl urea AU1235 **4** dissipates the PMF in *M. tb* from which the MmpL3 transporter derives its energy (indirect mechanism) [42]. Nevertheless, the same group provided evidence that the indole-2-carboxamide derivatives, NITD-304 **1** and its analogous difluoro compound NITD-349, in addition to AU1235 **4**, are able to inhibit MmpL3 via a direct mechanism and that whether or not dissipation of PMF is observed, can be regarded as an additional quality that potentiates the overall activity [42].

The valuable insights brought forth by this crystal structure prompted us to reinvigorate our efforts to develop new anti-TB agents that could be endowed with better lead-like properties than the current lead candidates. Therefore, herein, we describe the design, synthesis, and in vitro biological evaluation of adamantane and adamantanol analogues tethered to the framework of various indole-2-carboxamides, phenylureas and benzimidazoles, aspiring to improve water solubility while retaining potent antitubercular activity. All final compounds were screened in vitro against DS *M. tb* H37Rv strain. The top potent compounds in our study were further evaluated against two nontuberculous mycobacterial (NTM) strains as well as one DS and four DR *M. tb* strains. In parallel, we tested their cytotoxicity in Vero cells and assessed their drug-likeness *in silico* to predict their oral bioavailability. We also measured the kinetic water solubility for two pairs of analogues **8b/8c** and **8k/8l**, as representatives of the adamantane/adamantanol counterparts. Molecular docking analysis was also performed on the top active compounds using the MmpL3 crystal structure.

## 2. Design

Lipophilicity is an important parameter in the design of novel anti-TB

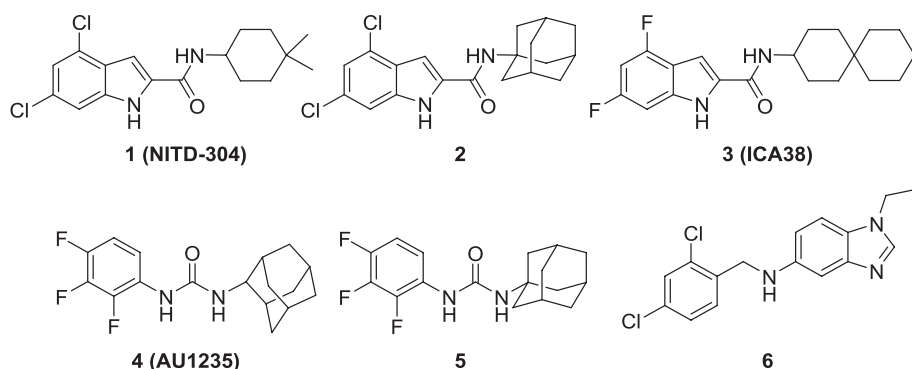
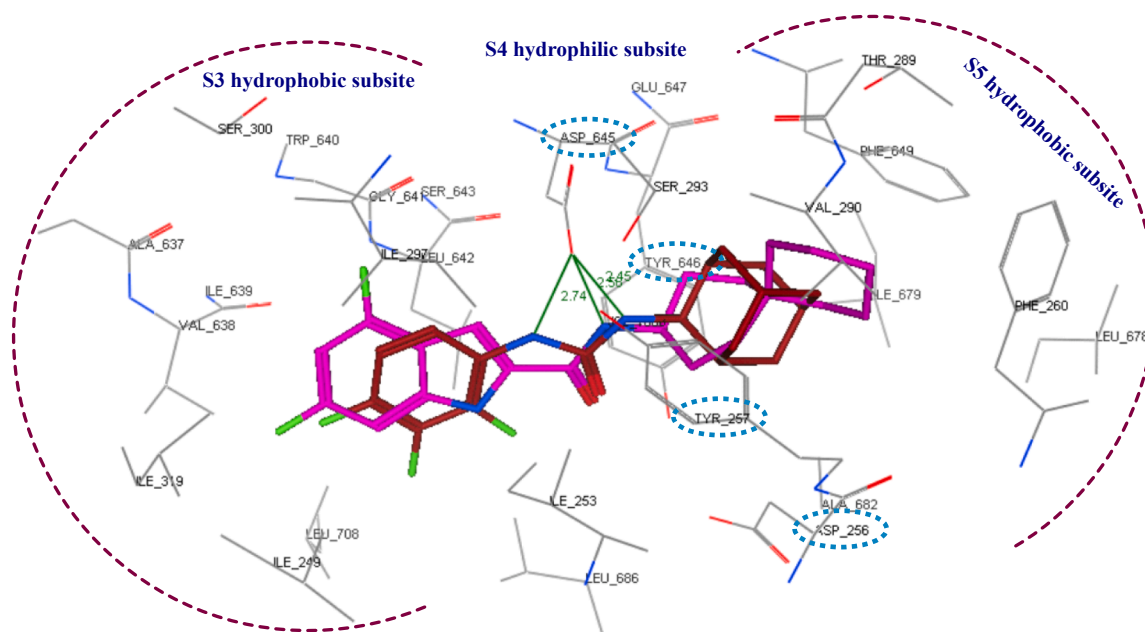


Fig. 1. Anti-TB derivatives: Indole-2-carboxamides **1**, **2** and **3**, adamantyl ureas **4** and **5**, and benzimidazole **6**.



**Fig. 2.** Close-up view of the MmpL3 binding site showing the S3-S5 subsites in which the indole-2-carboxamide ICA38 (magenta) and the adamantyl urea AU1235 (maroon) are stabilised by a set of hydrophobic interactions and hydrogen bonding. The two key Asp-Tyr pairs implicated in the proton relay in the S4 subpocket are marked in cyan hashed ovals. (For interpretation of the references to colour in this figure legend, the reader is referred to the web version of this article.)

analogues to ensure their permeation through the capsular lipids of *M. tb*. Unfortunately, high lipophilicity can also be detrimental especially when accompanied with low water solubility and subsequently poor bioavailability. For instance, the bioavailability of the highly lipophilic lead indole-2-carboxamide derivatives **2** and **3** (ClogP = 5.67 and 5.89, respectively) was associated with low water solubility [45]. Their limited aqueous solubility stems from the high lipophilicity of the indole and carbocyclic rings, fulfilling the requisite requirements for the hydrophobic binding pockets of MmpL3 (S3 and S5). Although compounds with high lipophilicity may have improved cellular permeability through the lipid rich mycobacterial cell wall, they need to be sufficiently water soluble at the site of absorption (the aqueous gastrointestinal fluids) in order to traverse through membranes. In other words, both water solubility and lipophilicity are intertwined limiting factors that are crucial for achieving the desired bioavailability and cellular diffusion. In light of these data, the general strategy for the chemical modifications in the present work is mainly aimed at improving the drug-like physicochemical properties of the indole-2-carboxamides by enhancing the water solubility while retaining sufficient lipophilicity to elicit high anti-TB activity. This was attained by integrating water solubilising groups as outlined below.

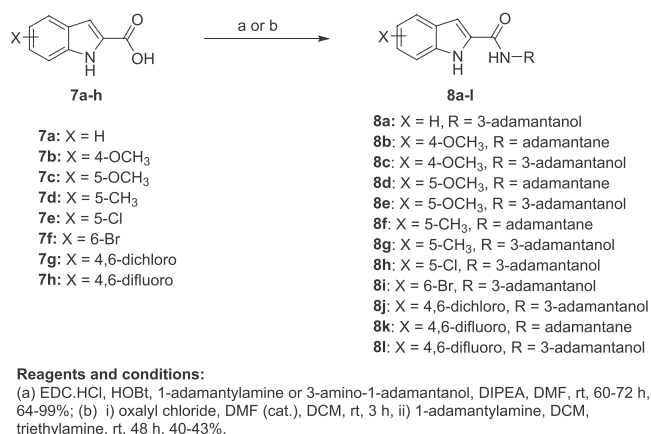
First, in an unprecedented approach, we appended a 3-adamantanol moiety to the indole-2-carboxamides. We reasoned that the insertion of a polar functional substituent (OH group) on the adamantane moiety could be tolerated in terms of steric hindrance while potentially providing the new compounds with improved water solubility. The anti-TB activities of the new 3-hydroxyadamantane analogues were compared to the previously reported and current study's novel bare adamantane counterparts (**8a-l**). It is worth noting that adamantane is a privileged scaffold in medicinal chemistry that is considered a "lipophilic bullet", functioning as an add-on used in the modification of known pharmacophores to provide the needed lipophilicity and enhance the stability of the drugs [46]. On the other hand, adamantyl ureas **4** and **5** were also identified as potent anti-TB compounds (Fig. 1) [43]. As the adamantyl urea AU1235 **4** was proven to target MmpL3 [25,26,42], we scrutinised the activity of two novel 3,5-dichlorophenyl urea analogues bearing an adamantane moiety **10a,b**. Similar to the indolecarboxamides, we also assessed the influence of introducing a polar OH group

on the adamantane moiety in the urea derivative **10b** in comparison to the plain adamantane analogue counterpart **10a**.

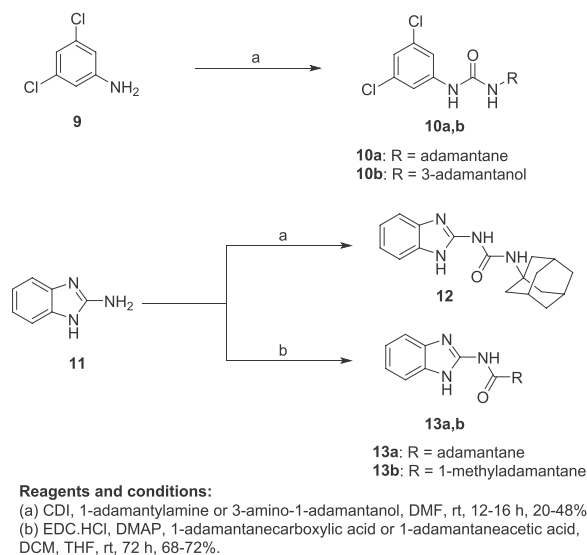
Additionally, benzimidazole urea analogue **12** was prepared to explore the activity of the benzimidazole scaffold (containing an extra ionisable nitrogen) as a replacement to the phenyl core in the adamantyl ureas. It is noteworthy that benzimidazole derivative **6** (Fig. 1) was previously reported to inhibit MmpL3, exhibiting an IC<sub>90</sub> value of 16 μM against *M. tb* H37Rv strain [47]. Besides lowering the lipophilicity, we explored whether the extra NH spacer in the urea analogue **12** would lead to an improved binding with the hydrophilic residues in the S4 subsite, similar to AU1235, thereby exhibiting an enhanced biological activity. We also investigated the activity of the benzimidazole nucleus as a bioisosteric replacement to the indole core to improve the water solubility. Towards this, two benzimidazole amides **13a,b** were synthesised and evaluated for their anti-TB activity.

### 3. Chemistry

The synthetic routes for the preparation of target compounds **8a-l**, **10a,b**, **12** and **13a,b** are delineated in Scheme 1 and 2. The synthesis of



**Scheme 1.** Synthetic conditions for compounds **8a-l**.



**Scheme 2.** Synthetic conditions for compounds **10a,b**, **12**, and **13a,b**.

the indole-2-carboxamide derivatives **8a-l** was accomplished in a one-step amide coupling reaction in which commercially available indole-2-carboxylic acids **7a-h** were coupled with 1-adamantylamine or 3-amino-1-adamantanol (Scheme 1) following either amide coupling conditions A or B. 1-Ethyl-3-(3-dimethylaminopropyl)carbodiimide hydrochloride (EDC.HCl), hydroxybenzotriazole hydrate (HOBt) and *N,N*-diisopropylethylamine (DIPEA) were the coupling reagents used to get most of our carboxamide analogues (Method A). Alternatively, we also treated carboxylic acid derivatives **7b** and **7d** with oxalyl chloride to generate the acid chloride which was subsequently reacted in situ with 1-adamantylamine in the presence of triethylamine to provide the final amides **8b** and **8f** (Method B). To afford the urea analogues **10a,b**, a one pot reaction was carried out in which imidazocarbonylation of 3,5-dichloroaniline (**9**) was initially conducted under anhydrous conditions at an elevated temperature. The 1,1'-carbonyldiimidazole (CDI)-mediated amidation protocol is a modified approach from the one described by Padiya and co-workers [48]. The resulting carbonylimidazolides were subsequently subjected to a nucleophilic substitution reaction with the corresponding 1-adamantylamine or 3-amino-1-adamantanol in situ to provide the asymmetrical urea analogues **10a,b**, respectively (Scheme 2). Padiya *et al* used water as a solvent and reported that under their conditions neither aromatic amines with a deactivated ring (due to their low nucleophilicity) nor adamantylamine reacted with CDI to yield any product. Hence, we employed more extreme conditions (i.e. heated at 90 °C) and anhydrous dimethylformamide (DMF) as a solvent to render the desired ureas with poor to moderate yields (20–48%).

On the other hand, analogous to **10a,b**, the benzimidazole urea derivative **12** was obtained by treating 2-aminobenzimidazole **11** and 1-adamantylamine with CDI as a crosslinking agent (Scheme 2). Finally, 2-aminobenzimidazole was subjected to amide coupling conditions C [EDC.HCl and 4-dimethylaminopyridine (DMAP)] with 1-adamantane-carboxylic acid and 1-adamantaneacetic acid to deliver the requisite amides **13a,b**, respectively.

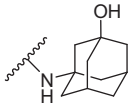
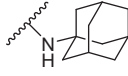
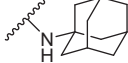
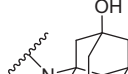
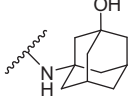
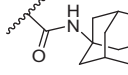
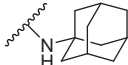
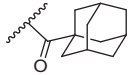
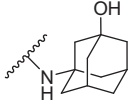
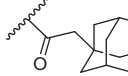
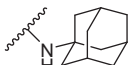
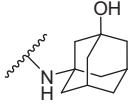
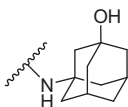
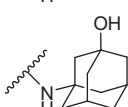
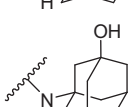
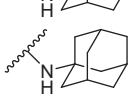
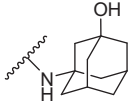
## 4. Results and discussion

### 4.1. Biological evaluation (*DS M. tb* H37Rv) and SAR analysis

The synthesised seventeen compounds **8a-l**, **10a,b**, **12** and **13a,b** were screened in vitro against *M. tb* H37Rv strain. The obtained activities, determined as the minimum inhibitory concentration of the drug (MIC) inhibiting the growth of *M. tb* by at least 90% using the microplate alamarBlue assay (MABA), are summarised in Table 1. The first round of

investigation, intended for increasing the polarity and accordingly the water solubility, entailed tethering a 3-hydroxyadamantane moiety to several indole-2-carboxamides and comparing the anti-TB activities between the adamantane and adamantanol analogues. The unsubstituted indole-2-carboxamide attached to 3-adamantanol moiety **8a** showed a drastic drop in activity (MIC = 51.5 μM) compared to the previously reported adamantane analogue counterpart (MIC = 0.68 μM [49]). However, the 4-methoxyindole derivative **8b** possessing an unsubstituted adamantane moiety exhibited an excellent anti-TB activity (MIC = 0.096 μM). Compound **8b** is approximately 3-fold more active than the standard first-line anti-TB drug INH (MIC = 0.29 μM). In contrast, its hydroxyadamantane analogue **8c** showed a modest anti-TB activity (MIC = 11.7 μM). Shifting the methoxy group to position 5 of the indole ring **8d** led to an approximately 8-fold loss of activity (MIC = 0.77 μM) compared to compound **8b** (MIC = 0.096 μM). Again, the less lipophilic 3-adamantanol analogue **8e** (MIC = 47.0 μM, ClogP = 2.73) was nearly 61-fold less active than the adamantane counterpart **8d** (MIC = 0.77 μM, ClogP = 4.12). Similar to compounds pair **8d/8e**, the 5-methylindole derivative containing an adamantanol moiety **8g** displayed a dramatic attenuation of activity compared to compound **8f** (MIC = 24.7 and 0.20 μM, respectively). Of particular note, compound **8f** is approximately 1.5- and 4-fold more potent than INH and **8d**, respectively. This signifies that methyl substituents are generally more favourable than the more polar methoxy groups due to their enhanced lipophilicity (**8d**: ClogP = 4.12, **8f**: ClogP = 4.60). However, the nearly 8- and 2-fold increase in activity manifested in the 4-methoxyindole analogue **8b** compared to the 5-methoxyindole **8d** and 5-methylindole **8f** counterparts, respectively, epitomises the consequential role of the substitution pattern in the indole ring on the activity. The 5-chloroindole derivative **8h** bearing a 3-adamantanol moiety was bereft of anti-TB activity (MIC > 93 μM), as opposed to the previously observed high potency of the *N*-adamantane-5-chloroindole analogue (MIC = 0.38 μM [44]). This is a noteworthy result because the lipophilicity of compound **8h** (ClogP = 3.53) is more than that of the above-mentioned adamantanol **8a**, **8c**, **8e** and **8g**, yet **8h** displayed lower potency than the foregoing analogues. Intriguingly, compound **8i**, a 6-bromoindole carrying a 3-adamantanol moiety, was approximately 2-fold more active than the first line anti-TB drug EMB (MIC = 2.57, 4.89 μM, respectively). Despite the gap in the activity between **8i** and its previously reported adamantane counterpart (MIC = 0.042 μM [45,50]), the satisfactory activity of **8i** establishes it as a promising anti-TB compound. In this case, **8i** still retained a decent anti-TB activity while being significantly less lipophilic than its adamantane analogue (ClogP = 3.68 and 5.07, respectively). Next, we explored the effect of disubstitution with chloro and fluoro groups on the indole ring. Indoleamides bearing the 4,6-dihalogen groups, for instance compounds **2** and **3**, were previously deemed more advantageous than the 4,6-dimethyl counterpart as the methyl groups presented metabolic liability (prone to metabolic oxidation) [45]. In this regard, the dihalogen groups circumvent this metabolism issue while equipping the indole ring with similar lipophilicity. It was pleasing to find that the dichloro analogue **8j** (MIC = 1.32 μM) bearing an adamantanol moiety is about 4- and 2-fold more active than EMB and compound **8i**, respectively. Importantly, the dichloroindole **8j**, which is the most lipophilic derivative in the *N*-(3-hydroxyadamantane) indole-2-carboxamide series (ClogP = 4.27), proved to be the most active compound in this set of adamantanol derivatives. These findings in turn clearly reflect the positive correlation between lipophilicity and anti-TB activity. A similar trend in activity was observed for compounds **8k** and **8l** with 4,6-difluoro substitution on the indole ring. The bare adamantane analogue of the 4,6-difluoroindole **8k** (MIC = 0.024 μM) was the most active compound in our study, displaying more potency than the adamantanol counterpart **8l** (MIC = 2.89 μM). It is important to note, however, that the activity of the adamantanol analogue **8l** is still high, possessing nearly a 2-fold improvement in activity compared to EMB and about a 2-fold inferior activity compared to **8j**. Interestingly, compound **8l** is less lipophilic than **8i** (ClogP = 3.13, 3.68, respectively)

**Table 1**In vitro anti-TB activity of target compounds **8a-l**, **10a,b**, **12**, and **13a,b** as well as reference standards INH, EMB, **1**, **2**, **4**, **5**, and **6**.

| Comp      | X                  | R   | MIC <sup>a</sup> $\mu$ M | ClogP <sup>b</sup> | Comp       | X | R   | MIC <sup>a</sup> $\mu$ M | ClogP <sup>b</sup> |
|-----------|--------------------|---|--------------------------|--------------------|------------|---|---|--------------------------|--------------------|
| <b>8a</b> | H                  |    | 51.5                     | 2.71               | <b>10a</b> | - |  | 1.47                     | 5.59               |
| <b>8b</b> | 4-OCH <sub>3</sub> |    | <b>0.096</b>             | 4.12               | <b>10b</b> | - |  | > 90                     | 4.15               |
| <b>8c</b> | 4-OCH <sub>3</sub> |    | 11.7                     | 2.73               | <b>12</b>  | - |  | 25.8                     | 4.15               |
| <b>8d</b> | 5-OCH <sub>3</sub> |    | <b>0.77</b>              | 4.12               | <b>13a</b> | - |  | 13.5                     | 4.07               |
| <b>8e</b> | 5-OCH <sub>3</sub> |    | 47.0                     | 2.73               | <b>13b</b> | - |  | > 103                    | 5.73               |
| <b>8f</b> | 5-CH <sub>3</sub>  |   | <b>0.20</b>              | 4.60               | <b>INH</b> | - | -   | 0.29 [22]                | -0.67              |
| <b>8g</b> | 5-CH <sub>3</sub>  |  | 24.7                     | 3.21               | <b>EMB</b> | - | -   | 4.89 [22]                | 0.12               |
| <b>8h</b> | 5-Cl               |  | > 93                     | 3.53               | <b>1</b>   | - | -   | 0.015 [23]               | 6.08               |
| <b>8i</b> | 6-Br               |  | <b>2.57</b>              | 3.68               | <b>2</b>   | - | -   | 0.011 [45]               | 5.67               |
| <b>8j</b> | 4,6-dichloro       |  | <b>1.32</b>              | 4.27               | <b>4</b>   | - | -   | 0.03–0.3 [26,43]         | 5.08               |
| <b>8k</b> | 4,6-difluoro       |  | <b>0.024</b>             | 4.53               | <b>5</b>   | - | -   | 1.23 [43]                | 4.04               |
| <b>8l</b> | 4,6-difluoro       |  | <b>2.89</b>              | 3.13               | <b>6</b>   | - | -   | 16 [47]                  | 5.76               |

<sup>a</sup> The lowest concentration of drug diminishing at least 90% of bacterial growth by the microplate alamarBlue assay (MABA). The reported MIC values are an average of three individual measurements.

<sup>b</sup> Estimated using ChemDraw 16.0.

and yet both molecules displayed comparable potencies with MIC values of 2.89 and 2.57  $\mu$ M, respectively. In addition, while compound **8k** showed a 2-fold decrease in activity when compared to the previously reported dichloroindole counterpart (MIC = 0.011  $\mu$ M [45]), its lipophilicity was more optimal than the 4,6-dichloroindole analogue (ClogP = 4.53 and 5.67, respectively). Thus far, these findings support

the notion that the anti-TB activity is lipophilicity-driven in these indole-2-carboxamides. A polar hydroxy group placed at the adamantane moiety impacted the MIC values, but substituting the indole ring at position 4 and/or 6 appeared to salvage the anti-TB activity, in agreement with our previous findings on the indole-2-carboxamides [45].

In line with the activity and framework of the dichloroindole

derivative **8j**, we were interested in evaluating the 3,5-dichlorophenyl urea derivative bearing either adamantane **10a** or adamantanol **10b**. Our attention was drawn to the adamantyl urea skeleton because they are well-known MmpL3 inhibitors with potent anti-TB activity, wherein the halogenated derivative AU1235 (**4**) stands out as an exemplar of this class [25,42,43,51]. The 3,5-dichloro analogue **10a** exhibited potent anti-TB activity (MIC = 1.47  $\mu\text{M}$ ) which is approximately 3-fold more than EMB and around 5-fold less than AU1235. It is worth mentioning that AU1235 was initially reported to have an MIC value of 0.03  $\mu\text{M}$  and in the subsequent reports of the same group they identified its MIC to be 0.3  $\mu\text{M}$  [26,43,52]. Indeed, in our previous evaluation of AU1235, the observed MIC was 0.096 – 0.19  $\mu\text{M}$  [22]. Although compound **10a** was less active than the *N*-(2-adamantyl)urea analogue AU1235, it exhibited similar activity to the more homologous *N*-(1-adamantyl)urea analogue **5** (MIC = 1.23  $\mu\text{M}$  [43]). The discrepancies in the activities of compound **10a** and **5** in comparison to AU1235 is ostensibly correlated to the preference for the 2-adamantyl urea scaffold over the 1-adamantyl counterpart. This was further supported by the fact that despite the higher lipophilicity of compound **10a** compared to AU1235 (ClogP = 5.59 and 5.08, respectively), **10a** was less potent than AU1235. Unfortunately, the adamantanol counterpart **10b** was devoid of anti-TB activity (MIC > 90  $\mu\text{M}$ ), featuring once again the apparent impact of lipophilicity on activity (ClogP = 5.59 and 4.15 corresponding to compounds **10a** and **10b**, respectively).

On the other hand, replacing the phenyl core in the urea analogue **10a** with a benzimidazole nucleus (entailing an ionisable nitrogen) yielded the urea derivative **12** (MIC = 25.8  $\mu\text{M}$ ) which showed more activity than **10b**, despite their similar lipophilicity (ClogP = 4.15). Additionally, our group previously reported some benzimidazole-2-carboxamides as potent anti-TB compounds [44]. Therefore, in consonance with our endeavour to achieve more water-soluble compounds, we further examined the benzimidazole scaffold as a replacement to the indole core. We were particularly interested in probing the influence of reversing the amide linker in the benzimidazoleamide derivatives. The reversed amide compound **13a** showed moderate activity with an MIC value of 13.5  $\mu\text{M}$  which is 2-fold higher than that of compound **12**. This activity was significantly lower than the evaluated *N*-adamantyl benzimidazole-2-carboxamide derivatives in our previous study (MIC = 0.39 and 1.5  $\mu\text{M}$  [44]), suggesting that reversing the amide linker in this framework is unfavourable. Nevertheless, **13a** was more potent than the most active benzimidazole derivative **6** in Stanley *et al* study (MIC = 16  $\mu\text{M}$  [47]). Finally, the influence of extending the length between the benzimidazole nucleus and the adamantane ring was further scrutinised. In this respect, a methylene spacer was inserted between the carboxamide linker and the adamantane moiety, yielding the highly lipophilic compound **13b** (ClogP = 5.73), which surprisingly showed a large loss of activity (MIC > 103  $\mu\text{M}$ ) compared to **13a**. This finding is discrepant with our previous results on the indole-2-carboxamides, in which the

addition of a methylene spacer next to the cycloaliphatic ring was tolerated [44]. These data suggest that lipophilicity seems to not be the main factor driving the anti-TB potency in these benzimidazoles.

#### 4.2. In vitro activity of the most potent compounds against NTM strains and clinical isolates of *M. tb* along with their cytotoxicity evaluation

Based on their satisfactory results in vitro against the wild-type *M. tb* H37Rv strain, the most promising eight compounds, namely **8b**, **8d**, **8f**, **8i**, **8j**, **8k**, **8l** and **10a** were selected for further in vitro studies against two NTM strains and a panel of clinical isolates of *M. tb* (Table 2). Ciprofloxacin (CPF), one of the second-line anti-TB drugs (used in the treatment of MDR-TB), was simultaneously evaluated against the same mycobacterial strains, serving as a positive control. Interestingly, *N*-adamantyl-4-methoxyindole-2-carboxamide (**8b**) exhibited a decent activity against *Mycobacterium abscessus* (*M. abs*) which is 2-fold higher than that of CPF (MIC = 12.3 and 24.1  $\mu\text{M}$ , respectively). However, compound **8b** was devoid of activity against *Mycobacterium avium* (*M. avium*) in comparison to CPF (MIC > 197 and 0.75  $\mu\text{M}$ , respectively). Conversely, the adamantyl urea derivative **10a** exhibited more potency against *M. avium* than *M. abs* (MIC = 47.2 and > 189  $\mu\text{M}$ , respectively). Meanwhile, the rest of the compounds were bereft of activity in the *M. abs* and *M. avium* assays (MIC > 164  $\mu\text{M}$ ), suggesting the selective activity of these compounds against *M. tb*. On the other hand, pleasingly, all eight compounds retained their high activity against a panel of DS and DR *M. tb* strains, originally procured from pulmonary TB patients. The *M. tb* clinical isolates comprise one DS (V4207), two MDR (V2475, KZN494), and two XDR (R506, TF274) strains. Three derivatives **8b**, **8f**, and **8k** were more potent than CPF when tested against DS *M. tb* H37Rv and V4207 strains (CPF MIC = 0.75  $\mu\text{M}$ ) and the preceding MDR *M. tb* isolates, whilst the activity of compound **8d** against these strains was comparable to CPF. Notably, the most active adamantanol and adamantane-based indoleamides **8j** and **8k** fortuitously displayed a 2-fold increase in activity against the forenamed XDR *M. tb* strains (MIC = 0.66 and 0.012  $\mu\text{M}$ , respectively). In fact, all eight compounds showed significantly higher activities against XDR-strains compared to CPF. The remarkable potencies of these compounds spotlight not only their potential to treat DS- and DR-TB, but also the prospective lack of cross resistance between these derivatives and the currently used medications. We also further evaluated the toxicity of the top potent compounds against Vero cells, expressed as IC<sub>50</sub> values, and their selectivity index (SI) were subsequently calculated. All compounds, except for **10a**, exhibited high SI values, demonstrating the potential lack of cytotoxicity of these analogues against mammalian cells (Table 2). In particular, compound **8j** (IC<sub>50</sub>  $\geq$  169  $\mu\text{M}$ ), the most active compound in the 3-adamantanol set of derivatives, displayed higher IC<sub>50</sub> value than the other two analogous compounds **8i** and **8l** in the same series (IC<sub>50</sub> = 82.2 and 92.4  $\mu\text{M}$ , respectively). Similar to **8j**, the tested *N*-(1-adamantyl)-indole-

**Table 2**

In vitro activities of the top eight potent compounds and CPF against *M. abs*, *M. avium* and selected clinical isolates of *M. tb* [MIC ( $\mu\text{M}$ )] as well as their cytotoxicity against Vero cells [IC<sub>50</sub> ( $\mu\text{M}$ )].

| Comp       | <i>M. abs</i> ( $\mu\text{M}$ ) | <i>M. avium</i> ( $\mu\text{M}$ ) | <i>M. tb</i> MIC ( $\mu\text{M}$ ) |                        |                         |                       |                        | IC <sub>50</sub> ( $\mu\text{M}$ ) |                 |
|------------|---------------------------------|-----------------------------------|------------------------------------|------------------------|-------------------------|-----------------------|------------------------|------------------------------------|-----------------|
|            |                                 |                                   | V4207/DS                           | V2475/MDR <sup>a</sup> | KZN494/MDR <sup>a</sup> | R506/XDR <sup>b</sup> | TF274/XDR <sup>b</sup> | Vero cells                         | SI <sup>c</sup> |
| <b>8b</b>  | 12.3                            | >197                              | 0.096                              | 0.096                  | 0.048                   | 0.024–0.048           | 0.024–0.048            | $\geq$ 197                         | $\geq$ 2048     |
| <b>8d</b>  | >197                            | >197                              | 0.39–0.77                          | 0.39–0.77              | 0.39                    | 0.39                  | 0.39                   | $\geq$ 197                         | $\geq$ 256      |
| <b>8f</b>  | >207                            | >207                              | 0.20                               | 0.20                   | 0.20                    | 0.10–0.20             | 0.10–0.20              | $\geq$ 207                         | $\geq$ 1024     |
| <b>8i</b>  | >164                            | >164                              | 5.14                               | 5.14                   | 2.57–5.14               | 2.57                  | 2.57                   | 82.2                               | 32              |
| <b>8j</b>  | >169                            | >169                              | 1.32                               | 2.64                   | 1.32                    | 0.66                  | 0.66                   | $\geq$ 169                         | $\geq$ 128      |
| <b>8k</b>  | >194                            | >194                              | 0.024                              | 0.024                  | 0.024                   | 0.012                 | 0.012                  | $\geq$ 194                         | $\geq$ 8205     |
| <b>8l</b>  | >185                            | >185                              | 2.89                               | 5.77                   | 2.89                    | 2.89                  | 1.44                   | 92.4                               | 32              |
| <b>10a</b> | >189                            | 47.2                              | 1.47                               | 1.47–2.95              | 1.47                    | 0.74                  | 0.74                   | 5.9                                | 4.0             |
| CPF        | 24.1                            | 0.75                              | 0.75                               | 0.75                   | 0.75                    | 6.04                  | 6.04                   | $\geq$ 193                         | $\geq$ 256      |

<sup>a</sup> Resistant to INH and rifampin (RIF).

<sup>b</sup> Resistant to INH, RIF, levofloxacin, ofloxacin, and kanamycin.

<sup>c</sup> Selectivity index (SI) = IC<sub>50</sub>(Vero)/MIC(H37Rv).

2-carboxamides exhibited high selectivity against DS and DR *M. tb* strains over mammalian cells ( $IC_{50} \geq 194 \mu\text{M}$ ,  $SI \geq 256$ ). Meanwhile, the urea analogue **10a** showed some toxicity against Vero cells with  $IC_{50}$  of  $5.9 \mu\text{M}$  ( $SI = 4.0$ ). This result was in fact counterintuitive due to the previously reported limited cytotoxicity of the analogous adamantyl urea AU1235 **4** and compound **5** ( $IC_{50} = 675$  and  $2238 \mu\text{M}$ , respectively [43]).

#### 4.3. Molecular docking

Considering that MmpL3 is most likely the target of our compounds, a molecular modelling study was performed on the most active derivatives ( $MIC \leq 3 \mu\text{M}$ ) to gain some perspectives on their binding mechanism within the active site of this membrane transporter (PDB ID: 6AJJ). Initially, reference ligands ICA38 **3** and AU1235 **4** were redocked into the MmpL3 binding pocket to validate the docking protocol, using MOE 2008.10 modelling software (Molecular Operating Environment), as published previously [53,54]. The bulky S3 and S5 hydrophobic subsites harboured the 4,6-dichloroindole/trifluorophenyl scaffolds and the spirocyclic/adamantane groups, respectively, with regard to ligands **3/4**, forming extensive set of hydrophobic contacts with the surrounding residues (Fig. 2). The amide and urea linkers, meanwhile, were positioned in the S4 hydrophilic subsite, whereupon the amide NH of the spirocyclic ligand ICA38 formed only one hydrogen bond with Asp645, whereas two hydrogen bonds connected Asp645 and the NH groups of the urea motif in AU1235, in accordance with Zhang *et al* crystal structure report [25]. Notably, Asp645 is an integral piece of the two Asp-Tyr pairs, the key elements of the S4 subsite, implicated in proton relay. Upon binding, ICA38 and AU1235 were found to inhibit MmpL3 by occupying S3-S5 subsites in the proton translocation channel, disrupting the two Asp-Tyr pairs, wherefore they dissipate the PMF for substrate transport [25]. The binding mode of lead compound **2** in the MmpL3 receptor was similar to ICA38 and AU1235 [54].

Next, the most active compounds in our study **8b**, **8d**, **8f**, **8i**, **8j**, **8k**, **8l** and **10a** were docked into the MmpL3 active site. London dG scoring was used to rank the generated poses after the forcefield refinement stage, in which lower scores designate more favourable ligand configurations. As expected, all eight compounds were oriented inside the MmpL3 binding pocket in a manner resembling that of ICA38 and AU1235, whereby they all showed high binding affinities (docking score  $-12.5 - -13.6$  kcal/mol). The docking poses of the indole-2-carboxamides, showing the lowest binding energy (most favourable poses), retained the main interactions discerned in ICA38. In the S4 hydrophilic subsite, in addition to the hydrogen bond formed between the amide NH and Asp645 (distance =  $2.37-2.43 \text{ \AA}$ ), another one took place between Asp645 and the indole NH in the adamantane and adamantanol-based indoleamide analogues (distance =  $2.64-2.77 \text{ \AA}$ ), similar to lead compound **2**. Meanwhile, the indole ring and the

adamantane/adamantanol moiety were embedded in the S3 and S5 hydrophobic subsites, respectively. The binding fashion and overlapping of compounds **8j** and **8k** with ICA38 are illustrated in Fig. 3, respectively, exemplifying the 3-adamantanol and adamantane series, respectively. Compound **10a** adopted nearly a superimposed orientation with both ICA38 and AU1235 **4** as depicted in Fig. 4. Akin to AU1235 **4**, the dichlorophenyl group and adamantane moiety of **10a** were lodged in the S3 and S5 hydrophobic subsites, respectively, whilst the urea linker occupied the S4 hydrophilic subsite forming two hydrogen bonds with Asp645 (distance =  $2.61$  and  $2.36 \text{ \AA}$ ). The binding mode and superimposed orientation between the most active compounds in the current study and MmpL3 inhibitors ICA38 and AU1235 suggest that our analogues presumably inhibit the same target, likely by disrupting the two Asp-Tyr pairs involved in the proton relay. The results from another study also favoured a direct mechanism of MmpL3 inhibition by the indole-2-carboxamides and adamantyl ureas [42].

#### 4.4. In silico ADME profiling

The physicochemical properties of adamantane/adamantanol-based derivatives **8a-l** and **10a,b** as well as lead compounds **2** and **4** were predicted using ACD/Labs Percepta 2016 Build 2911 (13 Jul 2016) (Table 3). We particularly assessed the compliance of these compounds with Lipinski's rule of five (RO5) in order to evaluate their drug-likeness [55]. All compounds showed zero violation to the RO5, except for **10a** and lead compound **2**. The one violation observed in lead compound **2**, related to its high lipophilicity, may also explain the lack of in vivo activity of this derivative. Importantly, the most active indoleamides **8b**, **8d**, **8f**, **8i**, **8j**, **8k**, and **8l** conform to the RO5, suggesting the drug-like attributes of these compounds, including their prospective in vivo drug absorption and permeation. In fact, all the indoleamides derivatives evaluated in our study exhibited desirable lipophilicities [55] ( $\log P = 2.94-4.57$ ). In general, ClogP values obtained from Chemdraw resembled those from ACD/Labs Percepta. Indeed, all the adamantanol-derived compounds in our study were predicted to have higher hydrophilicity/lower lipophilicity than their bare adamantane counterparts. It is noteworthy that the lipophilicity of the most active compound in our study **8k** ( $\log P = 4.32$ ) is significantly less than that of bedaquiline ( $\log P > 7$  [56]). In 2012, bedaquiline was approved by the United States Food and Drug Administration (FDA), representing the first anti-TB medication with a novel mechanism of action approved by the FDA since 1971 [57]. Several adverse effects correlated with bedaquiline are likely ascribed to its high lipophilicity, therefore it is provisionally recommended for people with pulmonary MDR-TB when no other effective treatment regimen can be designed [56,57]. Importantly, compound **8k** ( $MIC = 0.012-0.024 \mu\text{M}$ ) displayed higher potency than bedaquiline ( $MIC = 0.11 \mu\text{M}$  [58]) against both DS- and DR-TB. On the other hand, the Caco-2 permeability values of **8a-l** and **10a,b** fluctuated between 94

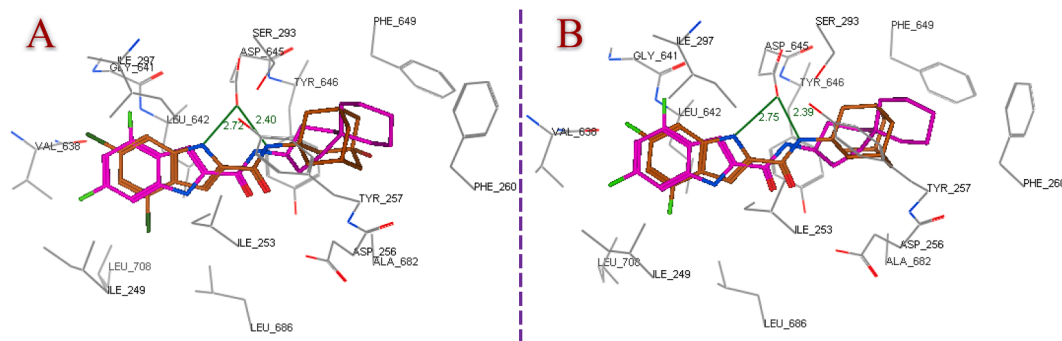
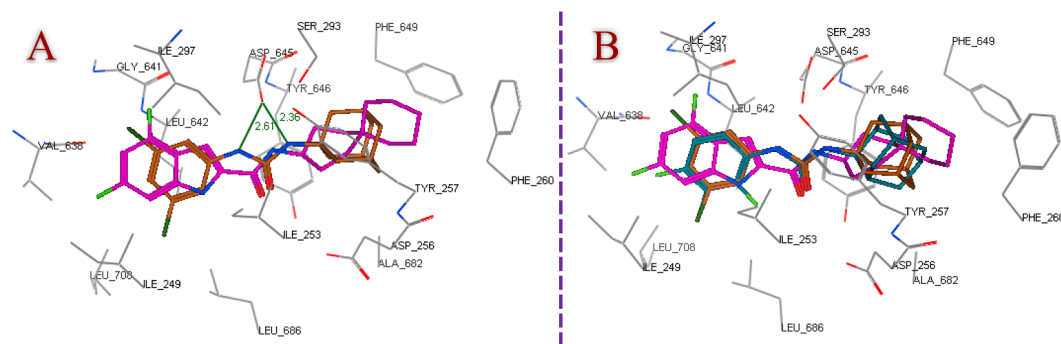


Fig. 3. Superposition of the top ranked docking pose of **8j** (A) and **8k** (B) (brown) and co-crystallised ligand ICA38 (magenta) in the MmpL3 binding pocket, portraying both compounds having similar binding pattern as ICA38. (For interpretation of the references to colour in this figure legend, the reader is referred to the web version of this article.)



**Fig. 4.** Putative binding mode of compound **10a** (brown) superpositioned with ICA38 (magenta) (A) and their overlay with AU1235 (dark cyan) (B) in the MmpL3 active site. (For interpretation of the references to colour in this figure legend, the reader is referred to the web version of this article.)

**Table 3**

*In silico* physicochemical and pharmacokinetic parameters of the adamantane/adamantanol-based analogues **8a–l** and **10a,b** in addition to reference compounds **2** and **4** as per ACD/Labs Percepta 2016 Build 2911 (13 Jul 2016).

| Comp | MW     | HBD | HBA | NRB | ClogP (Chemdraw) | logP | TPSA  | Solubility (mg/L) | Caco-2 (x 10 <sup>-6</sup> cm/s) | PPB (%) |
|------|--------|-----|-----|-----|------------------|------|-------|-------------------|----------------------------------|---------|
| 8a   | 310.39 | 3   | 4   | 2   | 2.71             | 2.94 | 65.12 | 60                | 151                              | 91      |
| 8b   | 324.42 | 2   | 4   | 3   | 4.12             | 4.04 | 54.12 | 20                | 214                              | 93      |
| 8c   | 340.42 | 3   | 5   | 3   | 2.73             | 3.03 | 74.35 | 40                | 155                              | 92      |
| 8d   | 324.42 | 2   | 4   | 3   | 4.12             | 4.07 | 54.12 | 20                | 214                              | 93      |
| 8e   | 340.42 | 3   | 5   | 3   | 2.73             | 3.02 | 74.35 | 40                | 155                              | 92      |
| 8f   | 308.42 | 2   | 3   | 2   | 4.60             | 4.57 | 44.89 | 20                | 194                              | 92      |
| 8g   | 324.42 | 3   | 4   | 2   | 3.21             | 3.26 | 65.12 | 30                | 168                              | 92      |
| 8h   | 344.84 | 3   | 4   | 2   | 3.53             | 3.51 | 65.12 | 30                | 177                              | 97      |
| 8i   | 389.29 | 3   | 4   | 2   | 3.68             | 3.83 | 65.12 | 20                | 180                              | 93      |
| 8j   | 379.28 | 3   | 4   | 2   | 4.27             | 4.26 | 65.12 | 5                 | 167                              | 95      |
| 8k   | 330.37 | 2   | 3   | 2   | 4.53             | 4.32 | 44.89 | 20                | 207                              | 91      |
| 8l   | 346.37 | 3   | 4   | 2   | 3.13             | 3.10 | 65.12 | 60                | 161                              | 87      |
| 10a  | 339.26 | 2   | 3   | 2   | 5.59             | 5.47 | 41.13 | 1                 | 94                               | 98      |
| 10b  | 355.26 | 3   | 4   | 2   | 4.15             | 4.57 | 61.36 | 4                 | 144                              | 98      |
| 2    | 363.28 | 2   | 3   | 2   | 5.67             | 5.49 | 44.89 | 1                 | 91                               | 96      |
| 4    | 324.34 | 2   | 3   | 2   | 5.08             | 4.59 | 41.13 | 10                | 194                              | 92      |

MW: molecular weight, HBD: H-bond donors, HBA: H-bond acceptors, NRB: number of rotatable bonds, logP: octanol–water partition coefficient, TPSA: topological polar surface area, PPB: plasma protein binding.

and  $214 \times 10^{-6}$  cm/s, therefore they all are expected to traverse the cell membrane. The plasma protein binding (PPB) degree of the preceding compounds was also estimated to range from 87 to 98%, suggesting their long plasma half-life ( $T_{1/2}$ ), low volume of distribution and low clearance.

#### 4.5. Kinetic water solubility

Aqueous solubility is a critical parameter for the absorption and oral bioavailability of compounds, in which derivatives equipped with good water solubility are often better qualified for clinical advancement. MmpL3 inhibitors are generally lipophilic due to the hydrophobic nature of the binding site, thereby having an intrinsic poor aqueous solubility which can hamper their drug-like properties as seen in Table 3. This interplay between water solubility and lipophilicity govern the bioavailability of these inhibitors and their ability to penetrate the hydrophobic cell wall of *M. tb* to elicit anti-TB activity. This was further corroborated by the fact that despite the high activity of the previously evaluated *N*-(1-adamantyl)-4,6-dichloroindole-2-carboxamide **2** (MIC = 0.011  $\mu$ M, logP > 5), it turned out to be inactive *in vivo* due to its poor bioavailability and was not pursued for further studies [45]. The kinetic water solubility assessment using high performance liquid chromatography (HPLC), entailing the solution-precipitation technique using DMSO stock solutions is well established in the literature [59]. Water solubility (mg/L) was measured using analytical HPLC for the *N*-adamantanol-derived indoles **8c** and **8l**, serving as representatives of this class, in addition to their bare adamantane counterparts **8b** and **8k**, respectively. The adamantanol derivatives **8c** and **8l** showed a

conspicuous improvement in water solubility in comparison to their homologous more lipophilic adamantane analogues **8b** and **8k**. The *N*-adamantanol-4-methoxy indole **8c** was 6-fold more soluble than the corresponding adamantane analogue **8b** with aqueous solubility values of 30 and 5 mg/L, respectively. Likewise, the *N*-adamantanol-4,6-difluoro indole **8l** possessed a moderate water solubility (19 mg/L) which is approximately 3-fold better than the respective adamantane derivative **8k** (7 mg/L). It is important to note that the ACD/Lab Percepta solubility values of the adamantanol analogues **8c** and **8l** were predicted to be 40 and 60 mg/L, respectively, compared to 20 mg/L for both adamantane counterparts **8b** and **8k**, amounting to 2- and 3-fold increase in solubility in compounds pairs **8b/8c** and **8k/8l**, respectively. Hence, it seems that the computationally estimated water solubility data of our analogues are in harmony with the HPLC-based aqueous solubility experimental values.

## 5. Conclusions

A series of adamantane and adamantanol analogues were designed and synthesised geared toward identifying potent anti-TB compounds possessing optimal lipophilicity and improved water solubility. All the *N*-(1-adamantyl)indole-2-carboxamide analogues evaluated in this study were highly potent (MIC = 0.024 – 0.77  $\mu$ M) when tested against the *M. tb* H37Rv strain. In case of the analogous 3-adamantanol counterparts, mixed results were obtained. In general, indoles bearing an adamantane moiety were more potent than their corresponding 3-adamantanol derivatives. However, three of these relatively polar adamantanol analogues **8i**, **8j** and **8l** displayed promising activities (MIC =



1.32 – 2.89  $\mu\text{M}$ ), higher than the activity of EMB (MIC = 4.89  $\mu\text{M}$ ). Evidently, substitutions at position 4 and/or 6, especially with halogens, on the indole ring are optimal for activity. On the other hand, the adamantylurea derivative **10a** (MIC = 1.47  $\mu\text{M}$ ) exhibited higher potency than EMB, whereas its adamantanol counterpart **10b** was inactive. The benzimidazole derivatives **12** and **13a,b** in which the extra ionisable nitrogen is expected to confer higher aqueous solubility, showed moderate or negligible activities. The excellent activities displayed by our eight most active compounds **8b**, **8d**, **8f**, **8i**, **8j**, **8k**, **8l**, and **10a** were not duplicated against *M. abs* and *M. avium*. However, compound **8b** still managed to elicit better activity against *M. avium* than CPF. To our delight, all eight compounds maintained the same high activities against MDR and XDR *M. tb* strains. In particular, **8j** and **8k** stood out as the most potent compounds in the adamantanol and adamantane set of derivatives, respectively, in addition to exhibiting high selectivity against the tested *M. tb* strains over mammalian cells, denoting their potential lack of cytotoxicity. The top potent eight derivatives were also docked into the MmpL3 active site, in which they were accommodated in the S3-S5 subsites, recapitulating the binding modes and alignment of ICA38 and AU1235. Importantly, the enhanced kinetic aqueous solubility of **8c** and **8l**, typifying the 3-adamantanol class, compared to the bare more lipophilic adamantane counterparts **8b** and **8k**, respectively, is in agreement with the predicted figures obtained *in silico*. These findings foreground the *N*-(3-adamantanol)-indole-2-carboxamides as good anti-TB candidates with improved water solubility while maintaining potency against both DS and DR *M. tb* strains.

## 6. Experimental section

### 6.1. Chemistry

#### General information

All indole-2-carboxylic acids, 1-adamantylamine, 3-amino-1-adamantanol, 1-adamantaneacetic acid were purchased from Fluorochem, while 1-adamantanecarboxylic acid was purchased from Sigma-Aldrich. 2-Aminobenzimidazole and 3,5-dichloroaniline were obtained from AlfaAesar.  $^1\text{H}$  NMR and  $^{13}\text{C}$  NMR spectra were recorded on a Bruker Avance III spectrometer at 400 and 100 MHz, respectively, with TMS as an internal standard. Standard abbreviations indicating multiplicity were as follows: s = singlet, d = doublet, dd = doublet of doublets, t = triplet, td = triplet of doublets, q = quadruplet, m = multiplet and br = broad. HRMS experiments were done on a Thermo Scientific Q-Exactive Orbitrap mass spectrometer. TLC was carried out on SiliCycle SiliaPlate TLC plates (200  $\mu\text{m}$ , 20 X 20 cm). Flash chromatography was performed using a Teledyne Isco CombiFlash Rf system with RediSep columns or manually using SiliCycle SiliaFlash® P60 Silica Gels [40–63  $\mu\text{m}$  (230–400 mesh)]. Final compounds were purified by preparative HPLC unless otherwise stated. The preparative HPLC (Shimadzu) employed a Phenomenex Luna® Omega 5  $\mu\text{m}$  Polar C18 100A (150 × 21.2 mm) column, with detection at 254 and 280 nm on a Shimadzu SPD-20A detector, flow rate = 25.0 mL/min. Method 1: 40–100% acetonitrile/Milli-Q water ( $\text{CH}_3\text{CN}/\text{H}_2\text{O}$ ) in 15 min; 100%  $\text{CH}_3\text{CN}$  in 10 min; 100–40%  $\text{CH}_3\text{CN}/\text{H}_2\text{O}$  in 10 min. Method 2: 60–100%  $\text{CH}_3\text{CN}/\text{H}_2\text{O}$  in 10 min; 100%  $\text{CH}_3\text{CN}$  in 15 min; 100–60%  $\text{CH}_3\text{CN}/\text{H}_2\text{O}$  in 10 min. Both solvents contained 0.05% of trifluoroacetic acid (TFA). Purities of final compounds were established by analytical HPLC, which was conducted using Waters HPLC system (1525 binary pump, 2487 dual wavelength absorbance detector, and 717 plus autosampler) with a Phenomenex Luna® 5  $\mu\text{m}$  C18(2) 100 Å (150 X 4.6 mm) column. Analytical HPLC method: flow rate = 1 mL/min; gradient elution over 30 min. Gradient: 20–100%  $\text{CH}_3\text{CN}/\text{H}_2\text{O}$  in 10 min; 100%  $\text{CH}_3\text{CN}$  in 10 min; 100–20%  $\text{CH}_3\text{CN}/\text{H}_2\text{O}$  in 10 min. 0.05% of TFA was incorporated in both solvents. The purity of all tested compounds was > 95% as determined by the method described above.

#### 6.1.1. General procedure for amide coupling (Method A)

To a solution of the appropriate carboxylic acid (1 mmol) in anhydrous dimethylformamide (DMF, 10 mL), 1-ethyl-3-(3-(dimethylamino)propyl)carbodiimide hydrochloride (EDC-HCl, 1.2 mmol), hydroxybenzotriazole hydrate (HOBT, 1.2 mmol) and the corresponding amine (1.2 mmol) were added at room temperature (rt). The reaction was then basified with *N,N*-Diisopropylethylamine (DIPEA, 1.5 equiv) and the mixture was stirred at room temperature (rt) until the disappearance of the starting material (usually 60–72 h). After this time water (50 mL) was added, and the mixture was extracted with EtOAc (3 × 50 mL). The combined organic layers were washed with water (5 × 25 mL), brine (1 × 25 mL), dried over anhydrous  $\text{Na}_2\text{SO}_4$ , filtered, and concentrated under reduced pressure. The residue was initially purified by flash chromatography using dichloromethane/methanol (DCM/MeOH) gradient prior to further preparative HPLC purification unless otherwise stated.

#### 6.1.2. General procedure for amide coupling (Method B)

To a solution of the indole-2-carboxylic acid derivative (1 mmol) in anhydrous dichloromethane (DCM, 10 mL), DMF (0.1 mL) and oxalyl chloride (2 mmol) were added. After stirring for 3 h at rt, the mixture was concentrated under vacuum and the residue was dissolved in anhydrous DCM. Thereafter, 1-adamantylamine (1.5 mmol) and triethylamine (2 mmol) were added and the mixture was stirred at rt for 48 h and filtered off. The precipitate was washed with DCM (2 × 25 mL) and the collected 50 mL DCM combined with the filtrate were evaporated *in vacuo* and the crude residue was purified by flash chromatography using DCM/MeOH gradient. The obtained compounds were already > 95% pure after flash chromatography.

#### 6.1.3. General procedure for amide coupling (Method C)

To a stirred solution of 2-aminobenzimidazole (1 mmol) in a 1:1 mixture of tetrahydrofuran (THF) and DCM, EDC.HCl (1.2 mmol), the corresponding carboxylic acid (1.2 mmol), and 4-dimethylaminopyridine (DMAP, 1.2 mmol) were added and the reaction mixture was stirred at room temperature for 72 h. The solvent was then removed under vacuum and the residue was purified by flash or manual chromatography using DCM/MeOH gradient prior to further HPLC purification unless otherwise stated.

#### 6.1.4. General procedure for urea formation (Method D)

A mixture of the aromatic amine (1 mmol) and 1,1'-carbonyldiimidazole (CDI) (1.2 mmol) in anhydrous DMF (10 mL) was stirred at 90 °C for two hours, followed by the addition of 1-adamantylamine or 3-amino-1-adamantanol (1.1 mmol) and stirring was continued for 48 h at 90 °C. Water (50 mL) was then added to the reaction mixture, followed by extraction with EtOAc (3 × 50 mL). The organic layers were separated, washed with water (5 × 25 mL), brine (1 × 25 mL), dried over anhydrous  $\text{Na}_2\text{SO}_4$ , filtered, and concentrated under reduced pressure. The crude was then purified by flash chromatography using DCM/MeOH gradient prior to HPLC purification.

##### 6.1.4.1. *N*-(3-hydroxyadamantan-1-yl)-1*H*-indole-2-carboxamide (8a).

The title compound was synthesised from indole-2-carboxylic acid (**7a**) and 3-amino-1-adamantanol following general procedure A. Off white solid, yield: 97%.  $^1\text{H}$  NMR ( $\text{DMSO}-d_6$ )  $\delta$  11.41 (s, 1H), 7.63 (s, 1H), 7.58 (d,  $J$  = 7.9 Hz, 1H), 7.42 (dd,  $J$  = 8.2, 0.8 Hz, 1H), 7.20–7.13 (m, 2H), 7.02 (ddd,  $J$  = 8.0, 7.1, 0.9 Hz, 1H), 4.56 (s, 1H), 2.19 (s, 2H), 2.06–1.90 (m, 6H), 1.64–1.43 (m, 6H);  $^{13}\text{C}$  NMR ( $\text{DMSO}-d_6$ )  $\delta$  161.0, 136.7, 133.0, 127.6, 123.6, 121.8, 120.0, 112.6, 103.4, 67.8, 54.5, 49.6, 44.7, 35.4, 30.6; HRMS (ESI)  $m/z$  calcd for  $\text{C}_{19}\text{H}_{22}\text{N}_2\text{O}_2$  ( $[\text{M}+\text{H}]^+$ )  $m/z$  311.1754; found 311.1748.

##### 6.1.4.2. *N*-(1-Adamantyl)-4-methoxy-1*H*-indole-2-carboxamide (8b).

The title compound was obtained from 4-methoxyindole-2-carboxylic

acid (**7b**) and 1-adamantylamine employing method B. Yellow solid, yield: 40%.  $^1\text{H}$  NMR (DMSO- $d_6$ )  $\delta$  11.40 (s, 1H), 7.52 (s, 1H), 7.25 (dd,  $J = 2.2, 0.7$  Hz, 1H), 7.07 (t,  $J = 7.9$  Hz, 1H), 7.00 (d,  $J = 8.2$  Hz, 1H), 6.49 (dd,  $J = 7.6, 0.5$  Hz, 1H), 3.87 (s, 3H), 2.09 (s, 6H), 2.06 (s, 3H), 1.67 (s, 6H);  $^{13}\text{C}$  NMR (DMSO- $d_6$ )  $\delta$  160.9, 154.0, 138.1, 131.7, 124.5, 118.5, 105.8, 100.9, 99.6, 55.4, 52.0, 41.6, 36.6, 29.4; HRMS (ESI)  $m/z$  calcd for  $\text{C}_{20}\text{H}_{24}\text{N}_2\text{O}_2$  ( $[\text{M}+\text{H}]^+$ )  $m/z$  325.1911; found 325.1903.

6.1.4.3. *N*-(3-hydroxyadamantan-1-yl)-4-methoxy-1H-indole-2-carboxamide (**8c**). This compound was synthesised from 4-methoxyindole-2-carboxylic acid (**7b**) and 3-amino-1-adamantanol according to method A. White solid, yield: 90%.  $^1\text{H}$  NMR (DMSO- $d_6$ )  $\delta$  11.39 (d,  $J = 1.4$  Hz, 1H), 7.61 (s, 1H), 7.26 (d,  $J = 1.7$  Hz, 1H), 7.08 (t,  $J = 7.9$  Hz, 1H), 7.00 (d,  $J = 8.2$  Hz, 1H), 6.49 (d,  $J = 7.5$  Hz, 1H), 4.55 (s, 1H), 3.87 (s, 3H), 2.18 (s, 2H), 2.03–1.90 (m, 6H), 1.65–1.41 (m, 6H);  $^{13}\text{C}$  NMR (DMSO- $d_6$ )  $\delta$  160.9, 154.0, 138.1, 131.6, 124.6, 118.5, 105.8, 100.9, 99.6, 67.9, 55.4, 54.5, 49.5, 44.7, 35.4, 30.6; HRMS (ESI)  $m/z$  calcd for  $\text{C}_{20}\text{H}_{24}\text{N}_2\text{O}_3$  ( $[\text{M}+\text{H}]^+$ )  $m/z$  341.1860; found 341.1858.

6.1.4.4. *N*-(1-Adamantyl)-5-methoxy-1H-indole-2-carboxamide (**8d**). The title compound was obtained from 5-methoxyindole-2-carboxylic acid (**7c**) and 1-adamantylamine employing method A. It was > 95% pure after flash chromatography. White solid, yield: 98%.  $^1\text{H}$  NMR (DMSO- $d_6$ )  $\delta$  11.26 (s, 1H), 7.49 (s, 1H), 7.30 (d,  $J = 8.9$  Hz, 1H), 7.04 (d,  $J = 1.4$  Hz, 1H), 7.03 (d,  $J = 2.4$  Hz, 1H), 6.81 (dd,  $J = 8.9, 2.5$  Hz, 1H), 3.75 (s, 3H), 2.09 (s, 6H), 2.06 (s, 3H), 1.67 (s, 6H);  $^{13}\text{C}$  NMR (DMSO- $d_6$ )  $\delta$  160.9, 154.1, 133.5, 132.0, 127.9, 114.6, 113.4, 103.1, 102.4, 55.7, 52.0, 41.5, 36.5, 29.4; HRMS (ESI)  $m/z$  calcd for  $\text{C}_{20}\text{H}_{24}\text{N}_2\text{O}_2$  ( $[\text{M}+\text{H}]^+$ )  $m/z$  325.1911; found 325.1908.

6.1.4.5. *N*-(3-hydroxyadamantan-1-yl)-5-methoxy-1H-indole-2-carboxamide (**8e**). This compound was synthesised from 5-methoxyindole-2-carboxylic acid (**7c**) and 3-amino-1-adamantanol following method A. Dusty pink solid, yield: 96%.  $^1\text{H}$  NMR (DMSO- $d_6$ )  $\delta$  11.28 (s, 1H), 7.58 (s, 1H), 7.32 (d,  $J = 8.9$  Hz, 1H), 7.07 (d,  $J = 1.5$  Hz, 1H), 7.04 (d,  $J = 2.3$  Hz, 1H), 6.83 (dd,  $J = 8.9, 2.4$  Hz, 1H), 4.55 (s, 1H), 3.76 (s, 3H), 2.19 (s, 2H), 2.06–1.91 (m, 6H), 1.67–1.43 (m, 6H);  $^{13}\text{C}$  NMR (DMSO- $d_6$ )  $\delta$  160.9, 154.1, 133.4, 132.0, 127.8, 114.6, 113.4, 103.1, 102.5, 67.8, 55.7, 54.5, 49.6, 44.7, 35.4, 30.6; HRMS (ESI)  $m/z$  calcd for  $\text{C}_{20}\text{H}_{24}\text{N}_2\text{O}_3$  ( $[\text{M}+\text{H}]^+$ )  $m/z$  341.1860; found 341.1852.

6.1.4.6. *N*-(1-Adamantyl)-5-methyl-1H-indole-2-carboxamide (**8f**). This compound was obtained from 5-methylindole-2-carboxylic acid (**7d**) and 1-adamantylamine according to method B. White solid, yield: 43%.  $^1\text{H}$  NMR (DMSO- $d_6$ )  $\delta$  11.28 (s, 1H), 7.49 (s, 1H), 7.34 (s, 1H), 7.30 (d,  $J = 8.4$  Hz, 1H), 7.05 (d,  $J = 1.8$  Hz, 1H), 6.98 (dd,  $J = 8.4, 1.2$  Hz, 1H), 2.36 (s, 3H), 2.10 (s, 6H), 2.07 (s, 3H), 1.67 (s, 6H);  $^{13}\text{C}$  NMR (DMSO- $d_6$ )  $\delta$  161.0, 135.1, 133.1, 128.5, 127.8, 125.4, 121.1, 112.3, 102.8, 52.0, 41.6, 36.5, 29.4, 21.6; HRMS (ESI)  $m/z$  calcd for  $\text{C}_{20}\text{H}_{24}\text{N}_2\text{O}$  ( $[\text{M}+\text{H}]^+$ )  $m/z$  309.1961; found 309.1953.

6.1.4.7. *N*-(3-hydroxyadamantan-1-yl)-5-methyl-1H-indole-2-carboxamide (**8g**). This compound was synthesised from 5-methylindole-2-carboxylic acid (**7d**) and 3-amino-1-adamantanol following method A. White solid, yield: 65%.  $^1\text{H}$  NMR (DMSO- $d_6$ )  $\delta$  11.27 (s, 1H), 7.58 (s, 1H), 7.34 (s, 1H), 7.29 (d,  $J = 8.4$  Hz, 1H), 7.05 (d,  $J = 1.4$  Hz, 1H), 6.98 (dd,  $J = 8.4, 1.1$  Hz, 1H), 4.53 (s, 1H), 2.35 (s, 3H), 2.18 (s, 2H), 2.05–1.88 (m, 6H), 1.67–1.41 (m, 6H);  $^{13}\text{C}$  NMR (DMSO- $d_6$ )  $\delta$  161.0, 135.1, 133.0, 128.5, 127.8, 125.4, 121.1, 112.3, 102.9, 67.8, 54.5, 49.6, 44.7, 35.4, 30.6, 21.6; HRMS (ESI)  $m/z$  calcd for  $\text{C}_{20}\text{H}_{24}\text{N}_2\text{O}_2$  ( $[\text{M}+\text{H}]^+$ )  $m/z$  325.1911; found 325.1914.

6.1.4.8. *5*-chloro-*N*-(3-hydroxyadamantan-1-yl)-1H-indole-2-carboxamide (**8h**). The title compound was obtained from 5-chloroindole-2-carboxylic acid (**7e**) and 3-amino-1-adamantanol employing method

A. White solid, yield: 64%.  $^1\text{H}$  NMR (DMSO- $d_6$ )  $\delta$  11.63 (s, 1H), 7.74 (s, 1H), 7.66 (d,  $J = 2.0$  Hz, 1H), 7.42 (d,  $J = 8.7$  Hz, 1H), 7.20–7.13 (m, 2H), 4.56 (s, 1H), 2.18 (s, 2H), 2.03–1.90 (m, 6H), 1.64–1.43 (m, 6H);  $^{13}\text{C}$  NMR (DMSO- $d_6$ )  $\delta$  160.6, 135.1, 134.5, 128.6, 124.5, 123.6, 120.9, 114.2, 102.9, 67.8, 54.6, 49.5, 44.7, 35.3, 30.6; HRMS (ESI)  $m/z$  calcd for  $\text{C}_{19}\text{H}_{21}\text{ClN}_2\text{O}_2$  ( $[\text{M}+\text{H}]^+$ )  $m/z$  345.1364; found 345.1364.

6.1.4.9. *6*-bromo-*N*-(3-hydroxyadamantan-1-yl)-1H-indole-2-carboxamide (**8i**). This compound was synthesised from 6-bromoindole-2-carboxylic acid (**7f**) and 3-amino-1-adamantanol according to method A. White solid, yield: 93%.  $^1\text{H}$  NMR (DMSO- $d_6$ )  $\delta$  11.57 (s, 1H), 7.72 (s, 1H), 7.57 (s, 1H), 7.55 (s, 1H), 7.20 (d,  $J = 0.9$  Hz, 1H), 7.15 (dd,  $J = 8.5, 1.8$  Hz, 1H), 4.54 (s, 1H), 2.18 (s, 2H), 2.04–1.88 (m, 6H), 1.64–1.43 (m, 6H);  $^{13}\text{C}$  NMR (DMSO- $d_6$ )  $\delta$  160.6, 137.5, 133.9, 126.6, 123.7, 123.1, 116.3, 115.1, 103.4, 67.8, 54.6, 49.5, 44.7, 35.3, 30.6; HRMS (ESI)  $m/z$  calcd for  $\text{C}_{19}\text{H}_{21}\text{BrN}_2\text{O}_2$  ( $[\text{M}+\text{H}]^+$ )  $m/z$  389.0859; found 389.0866.

6.1.4.10. *4,6*-dichloro-*N*-(3-hydroxyadamantan-1-yl)-1H-indole-2-carboxamide (**8j**). This compound was obtained from 4,6-dichloroindole-2-carboxylic acid (**7g**) and 3-amino-1-adamantanol employing method A. It was > 95% pure after flash chromatography. Buff solid, yield: 99%.  $^1\text{H}$  NMR (DMSO- $d_6$ )  $\delta$  11.93 (d,  $J = 1.5$  Hz, 1H), 7.92 (s, 1H), 7.41 (dd,  $J = 1.6, 0.8$  Hz, 1H), 7.35 (dd,  $J = 2.2, 0.8$  Hz, 1H), 7.20 (d,  $J = 1.7$  Hz, 1H), 4.55 (s, 1H), 2.18 (s, 2H), 2.05–1.90 (m, 6H), 1.64–1.42 (m, 6H);  $^{13}\text{C}$  NMR (DMSO- $d_6$ )  $\delta$  160.1, 137.1, 134.7, 128.0, 126.7, 125.3, 119.7, 111.5, 101.5, 67.8, 54.8, 49.4, 44.6, 35.3, 30.6; HRMS (ESI)  $m/z$  calcd for  $\text{C}_{19}\text{H}_{20}\text{Cl}_2\text{N}_2\text{O}_2$  ( $[\text{M}+\text{H}]^+$ )  $m/z$  379.0975; found 379.0977.

6.1.4.11. *N*-(1-Adamantyl)-4,6-difluoro-1H-indole-2-carboxamide (**8k**). This compound was obtained from 4,6-difluoroindole-2-carboxylic acid (**7h**) and 1-adamantylamine following method A. It was > 95% pure after flash chromatography. Off white solid, yield: 94%.  $^1\text{H}$  NMR (DMSO- $d_6$ )  $\delta$  11.83 (s, 1H), 7.67 (s, 1H), 7.30 (d,  $J = 0.5$  Hz, 1H), 7.02 (dd,  $J = 9.5, 1.4$  Hz, 1H), 6.85 (td,  $J = 10.4, 2.1$  Hz, 1H), 2.08 (s, 6H), 2.07 (s, 3H), 1.67 (s, 6H);  $^{13}\text{C}$  NMR (DMSO- $d_6$ )  $\delta$  160.1, 159.5 (dd,  $J = 238.1, 12.1$  Hz), 156.1 (dd,  $J = 248.4, 15.6$  Hz), 137.9 (dd,  $J = 15.2, 13.4$  Hz), 134.0 (d,  $J = 3.3$  Hz), 113.5 (dd,  $J = 21.9, 0.6$  Hz), 99.0, 95.4 (dd,  $J = 29.6, 23.3$  Hz), 95.0 (dd,  $J = 25.9, 4.4$  Hz), 52.2, 41.4, 36.5, 29.4; HRMS (ESI)  $m/z$  calcd for  $\text{C}_{19}\text{H}_{20}\text{F}_2\text{N}_2\text{O}$  ( $[\text{M}+\text{H}]^+$ )  $m/z$  331.1610; found 331.1610.

6.1.4.12. *4,6*-difluoro-*N*-(3-hydroxyadamantan-1-yl)-1H-indole-2-carboxamide (**8l**). This compound was synthesised from 4,6-difluoroindole-2-carboxylic acid (**7h**) and 3-amino-1-adamantanol employing method A. It was > 95% pure after flash chromatography. Light buff solid, yield: 87%.  $^1\text{H}$  NMR (DMSO- $d_6$ )  $\delta$  11.83 (s, 1H), 7.75 (s, 1H), 7.30 (d,  $J = 1.5$  Hz, 1H), 7.02 (dd,  $J = 9.5, 1.5$  Hz, 1H), 6.85 (td,  $J = 10.4, 2.0$  Hz, 1H), 4.54 (s, 1H), 2.18 (s, 2H), 2.06–1.87 (m, 6H), 1.66–1.41 (m, 6H);  $^{13}\text{C}$  NMR (DMSO- $d_6$ )  $\delta$  160.2, 159.5 (dd,  $J = 238.1, 12.1$  Hz), 156.1 (dd,  $J = 248.4, 15.6$  Hz), 137.9 (dd,  $J = 15.2, 13.4$  Hz), 134.0 (d,  $J = 3.3$  Hz), 113.5 (d,  $J = 21.8$  Hz), 99.1, 95.5 (dd,  $J = 29.6, 23.3$  Hz), 95.0 (dd,  $J = 25.8, 4.4$  Hz), 67.8, 54.7, 49.5, 44.7, 35.3, 30.6; HRMS (ESI)  $m/z$  calcd for  $\text{C}_{19}\text{H}_{20}\text{F}_2\text{N}_2\text{O}_2$  ( $[\text{M}+\text{H}]^+$ )  $m/z$  347.1566; found 347.1559.

6.1.4.13. *1*-(1-Adamantyl)-3-(3,5-dichlorophenyl)urea (**10a**). The title compound was obtained from 3,5-dichloroaniline (**9**) and 1-adamantylamine following method D. White solid, yield: 48%.  $^1\text{H}$  NMR (DMSO- $d_6$ )  $\delta$  8.67 (s, 1H), 7.39 (d,  $J = 1.8$  Hz, 2H), 7.02 (t,  $J = 1.8$  Hz, 1H), 6.04 (s, 1H), 2.02 (s, 3H), 1.92 (s, 6H), 1.62 (s, 6H);  $^{13}\text{C}$  NMR (DMSO- $d_6$ )  $\delta$  153.8, 143.5, 134.4, 120.2, 115.8, 50.6, 41.9, 36.4, 29.3; HRMS (ESI)  $m/z$  calcd for  $\text{C}_{17}\text{H}_{20}\text{Cl}_2\text{N}_2\text{O}$  ( $[\text{M}+\text{H}]^+$ )  $m/z$  339.1025; found 339.1030.

6.1.4.14. *1*-(3,5-dichlorophenyl)-3-(3-hydroxyadamantan-1-yl)urea (**10b**). This compound was obtained from 3,5-dichloroaniline (**9**) and 3-amino-1-adamantanol employing method D. White solid, yield: 20%.  $^1\text{H}$

NMR (DMSO- $d_6$ )  $\delta$  8.64 (s, 1H), 7.40 (d,  $J$  = 1.9 Hz, 2H), 7.04 (t,  $J$  = 1.9 Hz, 1H), 6.14 (s, 1H), 4.51 (s, 1H), 2.14 (s, 2H), 1.92–1.71 (m, 6H), 1.61–1.35 (m, 6H);  $^{13}\text{C}$  NMR (DMSO- $d_6$ )  $\delta$  153.9, 143.5, 134.4, 120.3, 115.8, 67.8, 53.2, 49.9, 44.6, 35.2, 30.6; HRMS (ESI)  $m/z$  calcd for  $\text{C}_{17}\text{H}_{20}\text{Cl}_2\text{N}_2\text{O}_2$  ( $[\text{M}+\text{H}]^+$ )  $m/z$  355.0975; found 355.0980.

6.1.4.15. 1-(1-adamantyl)-3-(1H-benzo[d]imidazol-2-yl)urea (12). This compound was obtained from 2-aminobenzimidazole (11) and 1-adamantylamine employing method D. White solid, yield: 36%.  $^1\text{H}$  NMR (DMSO- $d_6$ )  $\delta$  7.64–7.57 (m, 2H), 7.40 (s, 1H), 7.39–7.34 (m, 2H), 2.14 (s, 3H), 2.08 (s, 6H), 1.73 (s, 6H);  $^{13}\text{C}$  NMR (DMSO- $d_6$ )  $\delta$  151.4, 145.6, 130.4, 124.0, 113.3, 51.5, 41.5, 36.3, 29.3; HRMS (ESI)  $m/z$  calcd for  $\text{C}_{18}\text{H}_{22}\text{N}_4\text{O}$  ( $[\text{M}+\text{H}]^+$ )  $m/z$  311.1866; found 311.1865.

6.1.4.16. *N*-(1H-benzo[d]imidazol-2-yl)adamantane-1-carboxamide (13a). The title compound was synthesised from 2-aminobenzimidazole (11) and 1-adamantanecarboxylic acid according to method C. White solid, yield: 68%.  $^1\text{H}$  NMR (DMSO- $d_6$ )  $\delta$  7.61 (s, 2H), 7.32 (s, 2H), 2.05 (s, 3H), 1.97 (s, 6H), 1.72 (s, 6H);  $^{13}\text{C}$  NMR (DMSO- $d_6$ )  $\delta$  177.6, 145.3, 131.1, 124.2, 114.0, 41.9, 37.9, 36.1, 27.8; HRMS (ESI)  $m/z$  calcd for  $\text{C}_{18}\text{H}_{21}\text{N}_3\text{O}$  ( $[\text{M}+\text{H}]^+$ )  $m/z$  296.1756; found 296.1755.

6.1.4.17. 2-(1-Adamantyl)-*N*-(1H-benzo[d]imidazol-2-yl)acetamide (13b). This compound was obtained from 2-aminobenzimidazole (11) and 1-adamantanecarboxylic acid following method C. It was > 95% pure after flash chromatography. White solid, yield: 72%.  $^1\text{H}$  NMR (DMSO- $d_6$ )  $\delta$  12.05 (s, 1H), 11.41 (s, 1H), 7.43 (s, 2H), 7.15–6.95 (m, 2H), 2.19 (s, 2H), 1.91 (s, 3H), 1.74–1.49 (m, 12H);  $^{13}\text{C}$  NMR (DMSO- $d_6$ )  $\delta$  170.9, 147.0, 140.8, 133.0, 121.5, 121.4, 117.3, 112.0, 50.0, 42.4, 36.8, 33.3, 28.5; HRMS (ESI)  $m/z$  calcd for  $\text{C}_{19}\text{H}_{23}\text{N}_3\text{O}$  ( $[\text{M}+\text{H}]^+$ )  $m/z$  310.1914; found 310.1911.

## 6.2. Biology

Microplate alamarBlue assay (MABA) was used in the MIC evaluation against the tested mycobacteria as previously reported [60,61]. MABA format was also used in the cytotoxicity assessment on Vero cells and the corresponding IC<sub>50</sub> values were subsequently determined [22].

## 6.3. Molecular modelling

Computational docking analysis was performed using the Molecular Operating Environment MOE software version 2008.10. The MmpL3 crystal structure in complex with ICA38 (6AJJ) was downloaded from the protein data bank (PDB), implementing the same docking protocol in our previous report [54]. In brief, the most potent compounds were docked into the binding pocket of ICA38 using MOE-DOCK function. Triangle Matcher placement method was applied, and the generated poses were rescored according to London dG methodology. The same scoring function was also used to then rank the poses output after being relaxed (energy minimised) through the conventional molecular mechanics forcefield refinement setup. The top 30 poses were retained and the highest-ranked pose with the best docking score (i.e. the lowest binding energy) pertaining to each ligand was selected. It is noteworthy that when Pharmacophore placement method, in lieu of Triangle Matcher, was used to filter the ligand poses while docking, identical results were produced. In this context, final poses that do not satisfy the pharmacophore model were automatically eliminated.

## 6.4. Water solubility measurement

Kinetic water solubility was experimentally determined utilising analytical HPLC [Waters HPLC system (1525 Binary pump, 2487 dual wavelength absorbance detector, and 717 plus Autosampler) with a Phenomenex Luna® 5 $\mu$  C18(2) 100 Å (150 X 4.6 mm) column]. The

following gradient was operated: 20–100% CH<sub>3</sub>CN/water over 15 min, maintained at 100% CH<sub>3</sub>CN for 10 min, and finally returned to 20% CH<sub>3</sub>CN in water over 5 min. Both CH<sub>3</sub>CN and Milli-Q water solvents used were containing 0.05% TFA and the flow rate was set at 1.0 mL/min. First, 4000 mg/L stock solutions in DMSO were created for compounds 8b, 8c, 8k, and 8l, followed by serial dilutions using CH<sub>3</sub>CN/H<sub>2</sub>O (9:1) to create a calibration curve for each compound by plotting absorbance versus concentrations of 200 mg/L, 400 mg/L, 600 mg/L, 800 mg/L and 1000 mg/L. The absorbance values of each concentration are an average of two individual measurements. Next, from the 4000 mg/L stock solution in DMSO, three samples of each compound were diluted 1:20 (200 mg/L) in deionised water and centrifuged. A 100  $\mu\text{L}$  sample from the supernatant was diluted 1:1 with 100  $\mu\text{L}$  neat CH<sub>3</sub>CN, mixed, filtered using a 0.45  $\mu\text{m}$  filter, and 100  $\mu\text{L}$  sample was taken for analytical HPLC testing. Two absorbance values of each sample were measured and averaged, followed by appropriate calculation and extrapolation to the established calibration curve.

## Declaration of Competing Interest

The authors declare that they have no known competing financial interests or personal relationships that could have appeared to influence the work reported in this paper.

## Acknowledgments

SSRA is thankful for the support of Curtin International Postgraduate Research Scholarship (CIPRS). WRB acknowledges the support of NIH grants AI 37856 and HL 133190. HG is the recipient of an Australian Research Council Discovery Early Career Researcher Award (DE160100482) funded by the Australian Government.

## References

- [1] I. Barberis, N.L. Bragazzi, L. Galluzzo, M. Martini, The history of tuberculosis: from the first historical records to the isolation of Koch's bacillus, *J. Prev. Med. Hyg.* 58 (1) (2017) E9–E12.
- [2] R. Blomgran, L. Desvignes, V. Briken, J.D. Ernst, Mycobacterium tuberculosis inhibits neutrophil apoptosis, leading to delayed activation of naive CD4 T cells, *Cell Host Microbe.* 11 (1) (2012) 81–90.
- [3] C.J. Cambier, S. Falkow, L. Ramakrishnan, Host evasion and exploitation schemes of Mycobacterium tuberculosis, *Cell* 159 (7) (2014) 1497–1509.
- [4] A.A. Chackerian, J.M. Alt, T.V. Perera, C.C. Dascher, S.M. Behar, Dissemination of Mycobacterium tuberculosis is influenced by host factors and precedes the initiation of T-cell immunity, *Infect. Immun.* 70 (8) (2002) 4501–4509.
- [5] S.A. Khader, S. Partida-Sanchez, G. Bell, D.M. Jolley-Gibbs, S. Swain, J.E. Pearl, N. Ghilardi, F.J. Desauvage, F.E. Lund, A.M. Cooper, Interleukin 12p40 is required for dendritic cell migration and T cell priming after Mycobacterium tuberculosis infection, *J. Exp. Med.* 203 (7) (2006) 1805–1815.
- [6] L.G. Wayne, Dormancy of Mycobacterium tuberculosis and latency of disease, *Eur. J. Clin. Microbiol. Infect. Dis.* 13 (11) (1994) 908–914.
- [7] M.J. Blaser, D. Kirschner, The equilibria that allow bacterial persistence in human hosts, *Nature* 449 (7164) (2007) 843–849.
- [8] S.H. Kaufmann, A.J. McMichael, Annulling a dangerous liaison: vaccination strategies against AIDS and tuberculosis, *Nat. Med.* 11 (4 Suppl) (2005) S33–S44.
- [9] A. Pawlowski, M. Jansson, M. Skold, M.E. Rottenberg, G. Kallenius, Tuberculosis and HIV co-infection, *PLoS Pathog.* 8 (2) (2012).
- [10] World Health Organization Global Tuberculosis Report, Geneva, 2019.
- [11] H.M. Blumberg, W.J. Burman, R.E. Chaisson, C.L. Daley, S.C. Etkind, L. N. Friedman, P. Fujiwara, M. Grzemska, P.C. Hopewell, M.D. Iseman, R.M. Jasmer, V. Koppaka, R.I. Menzies, R.J. O'Brien, R.R. Reves, L.B. Reichman, P.M. Simone, J. R. Starke, A.A. Vernon, C.F.D.C. American Thoracic Society, Prevention, S. the Infectious Diseases, American Thoracic Society/Centers for Disease Control and Prevention/Infectious Diseases Society of America: treatment of tuberculosis, *Am. J. Respir. Crit. Care Med.* 167 (4) (2003) 603–662.
- [12] S. Keshavjee, P.E. Farmer, Tuberculosis, drug resistance, and the history of modern medicine, *N. Engl. J. Med.* 367 (10) (2012) 931–936.
- [13] K. Dheda, C.E. Barry 3rd, G. Maartens, Tuberculosis, *Lancet* 387 (10024) (2016) 1211–1226.
- [14] J.A. Caminero, O. World Health S. American Thoracic S. British Thoracic, Treatment of multidrug-resistant tuberculosis: evidence and controversies, *Int. J. Tuberc. Lung Dis.* 10 (8) (2006) 829–837.
- [15] E.D. Chan, V. Laurel, M.J. Strand, J.F. Chan, M.L. Huynh, M. Goble, M.D. Iseman, Treatment and outcome analysis of 205 patients with multidrug-resistant tuberculosis, *Am. J. Respir. Crit. Care Med.* 169 (10) (2004) 1103–1109.

- [16] B. Eker, J. Ortmann, G.B. Migliori, G. Sotgiu, R. Muetterlein, R. Centis, H. Hoffmann, D. Kirsten, T. Schaberg, S. Ruesch-Gerdes, C. Lange, T.G. German, Multidrug- and extensively drug-resistant tuberculosis, Germany, *Emerg. Infect. Dis.* 14 (11) (2008) 1700–1706.
- [17] G.B. Migliori, R. Loddenkemper, F. Blasi, M.C. Raviglione, 125 years after Robert Koch's discovery of the tubercle bacillus: the new XDR-TB threat. Is "science" enough to tackle the epidemic? *Eur. Respir. J.* 29 (3) (2007) 423–427.
- [18] C.D. Mitnick, S.S. Shin, K.J. Seung, M.L. Rich, S.S. Atwood, J.J. Furin, G. M. Fitzmaurice, F.A. Alcantara Viru, S.C. Appleton, J.N. Bayona, C.A. Bonilla, K. Chalco, S. Choi, M.F. Franke, H.S. Fraser, D. Guerra, R.M. Hurtado, D. Jazayeri, K. Joseph, K. Llaro, L. Mestanza, J.S. Mukherjee, M. Munoz, E. Palacios, E. Sanchez, A. Sloutsky, M.C. Becerra, Comprehensive treatment of extensively drug-resistant tuberculosis, *N. Engl. J. Med.* 359 (6) (2008) 563–574.
- [19] A.A. Velayati, P. Farnia, M.R. Masjedi, The totally drug resistant tuberculosis (TDR-TB), *Int. J. Clin. Exp. Med.* 6 (4) (2013) 307–309.
- [20] S.K. Parida, R. Axelsson-Robertson, M.V. Rao, N. Singh, I. Master, A. Lutckii, S. Keshavjee, J. Andersson, A. Zumla, M. Mauerer, Totally drug-resistant tuberculosis and adjunct therapies, *J. Intern. Med.* 277 (4) (2015) 388–405.
- [21] J.A. Caminero, G. Sotgiu, A. Zumla, G.B. Migliori, Best drug treatment for multidrug-resistant and extensively drug-resistant tuberculosis, *Lancet Infect. Dis.* 10 (9) (2010) 621–629.
- [22] S. Lun, H. Guo, O.K. Onajole, M. Pieroni, H. Gunosewoyo, G. Chen, S.K. Tipparaju, N.C. Ammerman, A.P. Kozikowski, W.R. Bishai, Indoleamides are active against drug-resistant Mycobacterium tuberculosis, *Nat. Commun.* 4 (2013) 2907.
- [23] S.P. Rao, S.B. Lakshminarayana, R.R. Kondreddi, M. Herve, L.R. Camacho, P. Bifani, S.K. Kalapala, J. Jiricek, N.L. Ma, B.H. Tan, S.H. Ng, M. Nanjundappa, S. Ravindran, P.G. Seah, P. Thayalan, S.H. Lim, B.H. Lee, A. Goh, W.S. Barnes, Z. Chen, K. Gagaring, A.K. Chatterjee, K. Pethe, K. Kuhlen, J. Walker, G. Feng, S. Babu, L. Zhang, F. Blasco, D. Beer, M. Weaver, V. Dartois, R. Glynn, T. Dick, P. W. Smith, T.T. Diagan, U.H. Manjunatha, Indolcarboxamide is a preclinical candidate for treating multidrug-resistant tuberculosis, *Sci. Transl. Med.* 5 (214) (2013) 214ra168.
- [24] K. Tahlán, R. Wilson, D.B. Kastinsky, K. Arora, V. Nair, E. Fischer, S.W. Barnes, J. R. Walker, D. Alland, C.E. Barry 3rd, H.I. Boshoff, SQ109 targets MmpL3, a membrane transporter of trehalose monomycolate involved in mycolic acid donation to the cell wall core of Mycobacterium tuberculosis, *Antimicrob. Agents Chemother.* 56 (4) (2012) 1797–1809.
- [25] B. Zhang, J. Li, X. Yang, L. Wu, J. Zhang, Y. Yang, Y. Zhao, L. Zhang, X. Yang, X. Yang, X. Cheng, Z. Liu, B. Jiang, H. Jiang, L.W. Guddat, H. Yang, Z. Rao, Crystal Structures of Membrane Transporter MmpL3, an Anti-TB Drug Target, *Cell* 176 (3) (2019) 636–648 e13.
- [26] A.E. Grzegorzewicz, H. Pham, V.A. Gundi, M.S. Scherman, E.J. North, T. Hess, V. Jones, V. Gruppo, S.E. Born, J. Kordulakova, S.S. Chavadi, C. Morisseau, A. J. Lenaerts, R.E. Lee, M.R. McNeil, M. Jackson, Inhibition of mycolic acid transport across the Mycobacterium tuberculosis plasma membrane, *Nat. Chem. Biol.* 8 (4) (2012) 334–341.
- [27] C.P. Owens, N. Chim, C.W. Goulding, Insights on how the Mycobacterium tuberculosis heme uptake pathway can be used as a drug target, *Future Med. Chem.* 5 (12) (2013) 1391–1403.
- [28] C.P. Owens, N. Chim, A.B. Graves, C.A. Harmston, A. Iniguez, H. Contreras, M. D. Liptak, C.W. Goulding, The Mycobacterium tuberculosis secreted protein Rv0203 transfers heme to membrane proteins MmpL3 and MmpL11, *J. Biol. Chem.* 288 (30) (2013) 21714–21728.
- [29] M.V. Tullius, C.A. Harmston, C.P. Owens, N. Chim, R.P. Morse, L.M. McMath, A. Iniguez, J.M. Kimmey, M.R. Sawaya, J.P. Whitelegge, M.A. Horwitz, C. W. Goulding, Discovery and characterization of a unique mycobacterial heme acquisition system, *Proc. Natl. Acad. Sci. U S A* 108 (12) (2011) 5051–5056.
- [30] Z. Xu, V.A. Meshcheryakov, G. Poce, S.S. Chng, MmpL3 is the flippase for mycolic acids in mycobacteria, *Proc. Natl. Acad. Sci. U S A* 114 (30) (2017) 7993–7998.
- [31] P.J. Brennan, Structure, function, and biogenesis of the cell wall of Mycobacterium tuberculosis, *Tuberculosis (Edinb)* 83 (1–3) (2003) 91–97.
- [32] C. Hoffmann, A. Leis, M. Niederweis, J.M. Plietzko, H. Engelhardt, Disclosure of the mycobacterial outer membrane: cryo-electron tomography and vitreous sections reveal the lipid bilayer structure, *Proc. Natl. Acad. Sci. U S A* 105 (10) (2008) 3963–3967.
- [33] J. Liu, C.E. Barry 3rd, G.S. Besra, H. Nikaido, Mycolic acid structure determines the fluidity of the mycobacterial cell wall, *J. Biol. Chem.* 271 (47) (1996) 29545–29551.
- [34] S.S.R. Alsayed, C.C. Beh, N.R. Foster, A.D. Payne, Y. Yu, H. Gunosewoyo, Kinase Targets for Mycolic Acid Biosynthesis in Mycobacterium tuberculosis, *Curr. Mol. Pharmacol.* 12 (1) (2019) 27–49.
- [35] P.J. Brennan, H. Nikaido, The envelope of mycobacteria, *Annu. Rev. Biochem.* 64 (1995) 29–63.
- [36] V. Nataraj, C. Varela, A. Javid, A. Singh, G.S. Besra, A. Bhatt, Mycolic acids: deciphering and targeting the Achilles' heel of the tubercle bacillus, *Mol. Microbiol.* 98 (1) (2015) 7–16.
- [37] K. Takayama, C. Wang, G.S. Besra, Pathway to synthesis and processing of mycolic acids in Mycobacterium tuberculosis, *Clin. Microbiol. Rev.* 18 (1) (2005) 81–101.
- [38] C. Varela, D. Rittmann, A. Singh, K. Krumbach, K. Bhatt, L. Eggeling, G.S. Besra, A. Bhatt, MmpL genes are associated with mycolic acid metabolism in mycobacteria and corynebacteria, *Chem. Biol.* 19 (4) (2012) 498–506.
- [39] G. Degiacomi, A. Benjak, J. Madacki, F. Boldrin, R. Provvedi, G. Palu, J. Kordulakova, S.T. Cole, R. Manganeli, Essentiality of mmpL3 and impact of its silencing on Mycobacterium tuberculosis gene expression, *Sci. Rep.* 7 (2017) 43495.
- [40] W. Li, A. Obregon-Henao, J.B. Wallach, E.J. North, R.E. Lee, M. Gonzalez-Juarrero, D. Schnappinger, M. Jackson, Therapeutic Potential of the Mycobacterium tuberculosis Mycolic Acid Transporter, MmpL3, *Antimicrob. Agents Chemother.* 60 (9) (2016) 5198–5207.
- [41] A. Campanico, R. Moreira, F. Lopes, Drug discovery in tuberculosis. New drug targets and antimycobacterial agents, *Eur. J. Med. Chem.* 150 (2018) 525–545.
- [42] W. Li, C.M. Stevens, A.N. Pandya, Z. Darzynkiewicz, P. Bhattarai, W. Tong, M. Gonzalez-Juarrero, E.J. North, H.I. Zgurskaya, M. Jackson, Direct Inhibition of MmpL3 by Novel Antitubercular Compounds, *ACS Infect. Dis.* 5 (6) (2019) 1001–1012.
- [43] J.R. Brown, E.J. North, J.G. Hurdle, C. Morisseau, J.S. Scarborough, D. Sun, J. Kordulakova, M.S. Scherman, V. Jones, A. Grzegorzewicz, R.M. Crew, M. Jackson, M.R. McNeil, R.E. Lee, The structure-activity relationship of urea derivatives as anti-tuberculosis agents, *Bioorg. Med. Chem.* 19 (18) (2011) 5585–5595.
- [44] O.K. Onajole, M. Pieroni, S.K. Tipparaju, S. Lun, J. Stec, G. Chen, H. Gunosewoyo, H. Guo, N.C. Ammerman, W.R. Bishai, A.P. Kozikowski, Preliminary structure-activity relationships and biological evaluation of novel antitubercular indolecarboxamide derivatives against drug-susceptible and drug-resistant Mycobacterium tuberculosis strains, *J. Med. Chem.* 56 (10) (2013) 4093–4103.
- [45] J. Stec, O.K. Onajole, S. Lun, H. Guo, B. Merenbloom, G. Vistoli, W.R. Bishai, A. P. Kozikowski, Indole-2-carboxamide-based MmpL3 Inhibitors Show Exceptional Antitubercular Activity in an Animal Model of Tuberculosis Infection, *J. Med. Chem.* 59 (13) (2016) 6232–6247.
- [46] L. Wanka, K. Iqbal, P.R. Schreiner, The lipophilic bullet hits the targets: medicinal chemistry of adamantane derivatives, *Chem. Rev.* 113 (5) (2013) 3516–3604.
- [47] S.A. Stanley, S.S. Grant, T. Kawate, N. Iwase, M. Shimizu, C. Wivagg, M. Silvis, E. Kazynskaya, J. Aquadro, A. Golas, M. Fitzgerald, H. Dai, L. Zhang, D.T. Hung, Identification of novel inhibitors of M. tuberculosis growth using whole cell based high-throughput screening, *ACS Chem. Biol.* 7 (8) (2012) 1377–1384.
- [48] K.J. Padiya, S. Gavade, B. Kardile, M. Tiwari, S. Bajare, M. Mane, V. Gaware, S. Varghese, D. Harel, S. Kurhade, Unprecedented "In Water" imidazole carbonylation: paradigm shift for preparation of urea and carbamate, *Org. Lett.* 14 (11) (2012) 2814–2817.
- [49] N.D. Franz, J.M. Belardinelli, M.A. Kaminski, L.C. Dunn, V. Calado Nogueira de Moura, M.A. Blaha, D.D. Truong, W. Li, M. Jackson, E.J. North, Design, synthesis and evaluation of indole-2-carboxamides with pan anti-mycobacterial activity, *Bioorg. Med. Chem.* 25 (14) (2017) 3746–3755.
- [50] A.P. Kozikowski, O.K. Onajole, J. Stec, C. Dupont, A. Viljoen, M. Richard, T. Chaira, S. Lun, W. Bishai, V.S. Raj, D. Ordway, L. Kremer, Targeting Mycolic Acid Transport by Indole-2-carboxamides for the Treatment of Mycobacterium abscessus Infections, *J. Med. Chem.* 60 (13) (2017) 5876–5888.
- [51] M.S. Scherman, E.J. North, V. Jones, T.N. Hess, A.E. Grzegorzewicz, T. Kasagami, I. H. Kim, O. Merzlikin, A.J. Lenaerts, R.E. Lee, M. Jackson, C. Morisseau, M. R. McNeil, Screening a library of 1600 adamantyl ureas for anti-Mycobacterium tuberculosis activity in vitro and for better physical chemical properties for bioavailability, *Bioorg. Med. Chem.* 20 (10) (2012) 3255–3262.
- [52] W. Li, A. Upadhyay, F.L. Fontes, E.J. North, Y. Wang, D.C. Crans, A. E. Grzegorzewicz, V. Jones, S.G. Franzblau, R.E. Lee, D.C. Crick, M. Jackson, Novel insights into the mechanism of inhibition of MmpL3, a target of multiple pharmacophores in Mycobacterium tuberculosis, *Antimicrob. Agents Chemother.* 58 (11) (2014) 6413–6423.
- [53] MOE, Chemical Computing Group, Inc., Montreal, <http://www.chemcomp.com>.
- [54] S.S.R. Alsayed, S. Lun, G. Luna, C.C. Beh, A.D. Payne, N. Foster, W.R. Bishai, H. Gunosewoyo, Design, synthesis, and biological evaluation of novel arylcarboxamide derivatives as anti-tubercular agents, *RSC Advances* 10 (13) (2020) 7523–7540.
- [55] C.A. Lipinski, F. Lombardo, B.W. Dominy, P.J. Feeney, Experimental and computational approaches to estimate solubility and permeability in drug discovery and development settings, *Adv. Drug Deliv. Rev.* 46 (1–3) (2001) 3–26.
- [56] H.S. Sutherland, A.S.T. Tong, P.J. Choi, D. Conole, A. Blaser, S.G. Franzblau, C. B. Cooper, A.M. Upton, M.U. Lotlikar, W.A. Denny, B.D. Palmer, Structure-activity relationships for analogs of the tuberculosis drug bedaquiline with the naphthalene unit replaced by bicyclic heterocycles, *Bioorg. Med. Chem.* 26 (8) (2018) 1797–1809.
- [57] M.V. Worley, S.J. Estrada, Bedaquiline: a novel antitubercular agent for the treatment of multidrug-resistant tuberculosis, *Pharmacotherapy* 34 (11) (2014) 1187–1197.
- [58] K. Andries, P. Verhasselt, J. Guillemont, H.W. Gohlmann, J.M. Neefs, H. Winkler, J. Van Gestel, P. Timmerman, M. Zhu, E. Lee, P. Williams, D. de Chaffoy, E. Huitric, S. Hoffner, E. Cambau, C. Truffot-Pernot, N. Lounis, V. Jarlier, A diarylquinoline drug active on the ATP synthase of Mycobacterium tuberculosis, *Science* 307 (5707) (2005) 223–227.
- [59] K. Yamamoto, Y. Ikeda, Kinetic solubility and lipophilicity evaluation connecting formulation technology strategy perspective, *J. Drug Deliv. Sci. Technol.* 33 (2016) 13–18.
- [60] L. Collins, S.G. Franzblau, Microplate alamar blue assay versus BACTEC 460 system for high-throughput screening of compounds against Mycobacterium tuberculosis and Mycobacterium avium, *Antimicrob. Agents Chemother.* 41 (5) (1997) 1004–1009.
- [61] M. Pieroni, S.K. Tipparaju, S. Lun, Y. Song, A.W. Sturm, W.R. Bishai, A. P. Kozikowski, Pyrido[1,2-a]benzimidazole-based agents active against tuberculosis (TB), multidrug-resistant (MDR) TB and extensively drug-resistant (XDR) TB, *ChemMedChem* 6 (2) (2011) 334–342.

## Conclusions

Following the cumulative data that proved MmpL3 as the protein target of the I2Cs using genetic approaches and lipid profiling, in 2019 the crystal structure of MmpL3 came to light, revealing the interactions of an I2C analogue within its active site. This study was hailed as a significant milestone that could expedite the discovery of novel MmpL3 inhibitors. However, high lipophilicity, synchronised with low water solubility, is the earmark of the compounds targeting MmpL3, including the I2Cs, forestalling their advancement to clinical trials. Previous research efforts, poised to overcome the shortfall in water solubility, entailed implementing subtle structural changes to the *N*-linked cycloaliphatic group. Nevertheless, for the most part, these modifications were deleterious to the anti-TB activity. Therefore, a balance between water solubility and lipophilicity is mandated to increase the chances of procuring a potent anti-TB compound with the potential to evolve into an orally active drug. In our 2021 published article, a hydroxyl group was introduced to the *N*-attached adamantane moiety, which enhanced the aqueous solubility of the corresponding I2Cs while maintaining adequate lipophilicity. Although the cut back on lipophilicity led to a decrease in the anti-TB activities in the *N*-adamantanol I2Cs, some of these analogues still displayed potent activities against DS and DR *M. tb* clinical isolates (MIC = 0.66 – 5.77  $\mu$ M). These analogues showed minimal cytotoxicities against healthy Vero cells, highlighting their promising preliminary safety profiles compared to numerous highly potent I2Cs documented in earlier reports. The empirical kinetic water solubility values of these adamantanol derivatives were superior to their homologous adamantane counterparts. The most active compounds in our study were also docked into the MmpL3 active site, wherein they were oriented in a manner similar to the co-crystallised ligands. Overall, introducing a polar OH group to the adamantane moiety linked to the I2C scaffold proved to be a successful approach in improving the water solubility of the *N*-adamantane I2Cs, while maintaining adequate lipophilicity. Indeed, the optimum balance between lipophilicity and aqueous solubility of some *N*-adamantanol I2C analogues was accompanied by potent anti-TB activities against DS and DR *M. tb* strains.

## **Chapter 5**

### **Design, Synthesis, and Antimycobacterial Evaluation of Isoniazid, Pyrazinamide, and Ciprofloxacin Analogues and Hybrids**

## Background

In pursuit of discovering new anti-TB agents with potent activities against drug-sensitive and drug-resistant tuberculosis (DS-TB and DR-TB), we revisited drugs that already exist in the market but are associated with resistance issues. In this respect, implementing subtle modifications to these marketed drugs can lead to novel molecules that will likely engage with the target of the parent drug. More importantly, these new compounds can elude the resistance mechanism developed by *Mycobacterium tuberculosis* (*M. tb*) against the original antibiotic. In addition, the introduced structural changes may transform the problematic drug into another active molecule with better drug-like and safety profiles. Indeed, numerous research efforts have been geared towards improving the anti-TB activity and/or the physicochemical and toxicological properties of several anti-TB drugs. For instance, the first line anti-TB drugs, isoniazid (INH) and pyrazinamide (PZA), in addition to the second-line antibiotic previously recommended for treatment of multidrug-resistant TB (MDR-TB), ciprofloxacin (CPF), have negative ClogP values. The diminished lipophilicities of these drugs in turn allude to room for improvement which may conduce to better anti-TB activity. In fact, the study that we published in 2021 was premised on increasing the lipophilicity of the preceding three drugs in addition to forming hybrids conjugating different pharmacophores. Disappointingly, most of the compounds evaluated therein were devoid of anti-TB activity. However, one hybrid molecule, linking INH with pyrazinoic acid (POA), exhibited good anti-TB activity against DS *M. tb* strains [minimum inhibitory concentration (MIC) = 2 – 4 µg/mL], whilst the tested MDR and extensively drug-resistant (XDR) clinical isolates as well as non-tuberculous mycobacterial (NTM) strains were refractory to this compound. Furthermore, this hybrid displayed negligible cytotoxicity against Vero cells ( $IC_{50} \geq 64$  µg/mL). Overall, although none of our evaluated compounds displayed better activity profile than INH, the primary efficacy and safety data of the INH-POA hybrid warrant further improvements.

## 5.1. Introduction

The history of TB drug discovery recounts streptomycin as the first effective anti-TB drug developed (1). This breakthrough achievement in 1944 was followed by a setback in its efficacy which was later ascribed to the evolution of DR *M. tb* strains that rendered streptomycin ineffective. To address this liability, in 1950, a combination therapy of streptomycin and *para*-aminosalicylic acid (PAS) was pioneered by the British Medical Research Council for treatment of pulmonary TB (1). The following years witnessed the introduction of an array of various anti-TB drugs in succession. Amongst these drugs is INH, which was first synthesised in 1912. However, the anti-TB activity of INH was later discovered in the 1950s and was found to be superior to other anti-TB agents tested around the same time *in vitro* and *in vivo* (2). More importantly, INH exhibited an exquisite selectivity against mycobacteria, including strains that are resistant to streptomycin and PAS (2). Similar to INH, PZA was first synthetically prepared in 1936, but its anti-TB activity was only recognised in 1952 (3). The subsequent discovery of RIF in 1965 and its inclusion in the TB drug therapy together with PZA was considered a game changer (1). Indeed, the use of either RIF or PZA was found to shorten the duration of TB treatment from 12 months or more to 9 months, while integrating both of them to the regimen truncated it to 6 months (3). In fact, the current Directly Observed Therapy Short Course (DOTS), which is a standard 6-month treatment regimen, was introduced by the WHO in the 1990s (1). It consists of 2 months treatment with INH, RIF, PZA, and EMB, followed by 4 months administration of INH and RIF.

Despite the early success of this combination therapy showing low relapse and high cure rates, DR *M. tb* strains unfortunately continued to evolve. Fluoroquinolones (FQs), which are broad spectrum antibiotics, were first shown to be efficacious against TB in 1984 (4, 5). Since then, FQs gained much interest in the TB control efforts and are currently considered an essential backbone component of MDR-TB therapy. However, *M. tb* strains resistant to FQs started to arise (5). Of note, poor patient adherence to therapy and disparities in the quality of public health systems around the globe contributed to the emergence and spread of the *M. tb* superbugs (1). In the absence of effective vaccine, restocking the TB medicine chest has been the focus of researchers throughout the world in order to halt the evolution and transmission of *M. tb* resistant variants, in addition to ameliorating the treatment outcome of MDR and



XDR-TB. Despite the exhaustive efforts undertaken to date to develop novel anti-TB drugs, only two antibiotics, bedaquiline (BDQ) and delamanid (DLM), were approved in the last decade for treatment of DR-TB (second line regimen) and are unfortunately associated with multiple adverse effects (6-8). Importantly, no novel front-line anti-TB medicine has been developed since RIF was introduced in the 1960s (9), indicating that the early fruitfulness that yielded the current anti-TB drugs has waned in the subsequent decades. This slump could be ascribed to the fact that the earlier paradigm fortuitously dissociated the process of developing an active antibiotic from understanding its mechanism of action (2). INH and PZA, whose exact mechanisms as anti-TB agents are still not fully understood, conspicuously embody this early strategy (3, 10). Altogether, the current use of the first-line anti-TB drugs that were developed in the last century indicates their indispensability in the treatment of DS-TB. However, their therapeutic success can be further exploited via optimising their chemical structure to attain novel drug-like molecules that could be imparted with efficacy against DR-TB.

## **5.2. INH, PZA, and CPF: Mechanisms of Action and Resistance**

### **5.2.1. The First-Line Prodrugs INH and PZA**

Approximately 70 years after the discovery of its anti-TB potential (11), INH remains a centrepiece of the TB therapy. The low cost, high bioavailability, excellent bactericidal activity against *M. tb*, and narrow spectrum of action/selectivity marked INH as an ideal anti-TB agent (10). INH has not only been used as a front-line treatment of active TB but also it is the core prophylactic agent prescribed for latent *M. tb* infections to prevent TB reactivation (10). Despite its small and simple structure, chemically known as pyridine-4-carbohydrazide or isonicotinic acid hydrazide, the mode of action of INH is multifaceted and contentious (10, 12). In brief, INH infiltrates into the *M. tb* cytoplasm by passive diffusion, whereupon it kills actively dividing mycobacteria, while no bactericidal effects are exerted on stationary-phase or anaerobic mycobacteria (10). INH behaves as a prodrug that gets activated by the mycobacterial catalase-peroxidase enzyme (KatG) (10, 12). Subsequently, INH-derived reactive radical species are generated, especially the isonicotinic acyl radical (also termed isonicotinoyl radical) which is the key active metabolite that is believed to couple with

NAD<sup>+</sup> and NADP<sup>+</sup>, forming adducts that are capable of disabling mycobacterial cellular processes (10, 12).

The best-known targets of the activated INH derivatives are two crucial enzymes that are implicated in the mycolic acids (MAs) biosynthetic machinery, namely *InhA* which is an enoyl acyl carrier protein (ACP) reductase in addition to the  $\beta$ -ketoacyl ACP synthase (*KasA*, Chapter 2: Current Molecular Pharmacology 2019 article) (10). Therefore, one of the distinctive features of the mycobacterial cells treated with INH is the loss of acid fastness, which is attributed to inhibiting the MAs synthesis. Conversely, INH is deactivated by arylamine *N*-acetyl transferases (NATs) which play important role in the MAs biosynthesis (10). Of note, *InhA*, *KasA*, and NATs are all considered efficient anti-TB targets. A vast array of other crucial mycobacterial enzymes was also found to be influenced by INH (10). In fact, the concerted inhibitory effects of INH against the mycobacterial cell wall lipid biosynthesis, metabolic enzymes, and nucleic acid biosynthetic enzymes, that were shown to date, likely account for the exceptional potency of this drug (12). However, due to the multitude of these effects, the precise mechanism of INH that results in cell death of the tubercle bacillus is still debatable (10, 12). Expectedly, numerous genes were found to be involved in the resistance mechanisms, evolved by *M. tb*, against INH (10). In this regard, the major cause for INH resistance was correlated to mutations in the *katG* gene (the most commonly found INH resistance mechanism), followed by *inhA*, *kasA*, and other important genes (10, 12). Of note, Pasca *et al* found that overexpressing *M. tb mmp17* gene (discussed in Chapter 4: section 4.2) in *Mycobacterium smegmatis* (*M. smegmatis*), confers a high resistance level to INH, suggesting its implication in INH extrusion (13). This finding was further corroborated when the mycobacterial resistance level dropped upon exposure to efflux pump inhibitors (13).

Similar to INH, since the second half of the 20<sup>th</sup> century, PZA has been a cornerstone of TB chemotherapy (14). PZA is a paradoxical drug that plays a critical role in shortening the duration of TB treatment from 9 months or more to 6 months (15). The necessity of PZA stems from its ability to kill the semi-dormant or non-replicating tubercle bacilli (also known as persisters) that elude other anti-TB drugs (3, 15). In fact, multiple research efforts geared towards finding more optimal drug combinations in mouse models to shorten the TB treatment indicated that PZA is the only medicine that is irreplaceable as eliminating it compromises the treatment efficacy (3). Of note,

PZA is nearly equipotent to RIF as a sterilising agent and synergism is observed upon combining both drugs. In addition to its indispensable role as a first-line anti-TB agent, PZA is an integral ingredient of MDR-TB treatment regimen and any newly constructed combination therapies containing clinical drug candidates (3). Indeed, even the highly potent new drugs BDQ and DLM are recommended to be prescribed with PZA, since PZA-lacking drug combinations have been shown to be invariably subpar in animal studies. Despite its exceptional sterilising activity *in vivo*, PZA is devoid of activity against *M. tb* under standard culture conditions (neutral pH) (3). Fortunately, the activity of PZA was first evaluated in infected animal models, otherwise its inactivity in traditional culture media would have presumably excluded it from additional biological tests (16). Due to its unconventional and remarkable activity against both DS- and DR-TB, PZA is projected to remain a mainstay in future anti-TB combination therapies (3). Notably, the mode of action of PZA has been puzzling researchers since its anti-TB activity was uncovered in the 1950s. The perplexity of PZA could be attributed to the great discrepancy between it and typical antibiotics, which are mainly active against growing bacteria, whilst showing no or limited activity against non-replicating persisters (3). While its *in vitro* activity is diminished at neutral pH, PZA slowly kills *M. tb* in culture media at acidic pH of 5.5. Indeed, this is consistent with the high sterilising activity of PZA against non-growing persisters *in vivo*, wherein an acidic environment is generated during the active inflammation induced by the TB infection. The unparalleled ability of PZA to kill *M. tb* persisters is responsible for reducing relapse and shortening the TB therapy (3).

Based on numerous studies, a plausible model interpreting the mechanism of action of PZA was proposed (3). Like INH, PZA enters the tubercle bacilli via passive diffusion and acts as a prodrug. It gets subsequently transformed in the mycobacterial cytoplasm into the active form POA by nicotinamidase/pyrazinamidase (PZase) which is encoded by the *pncA* gene in *M. tb* (3). POA is then extruded from the cell by an efflux mechanism in *M. tb*. If the extracellular environment is acidic (pH = 5.5), POA becomes protonated (HPOA) and readily re-enters the mycobacterial cell (3). Of note, the POA extrusion route in *M. tb* is deficient as the efflux pump requires energy to function, therefore it is unable to counteract the acid-facilitated passive influx of POA, accounting for the unique susceptibility of *M. tb* to PZA. In contrast, *M. smegmatis* is

naturally resistant to PZA due to its highly active POA efflux mechanism, which quickly expels POA from the cell (3).

In *M. tb*, after POA fetches protons from the outer acidic environment, HPOA permeates back to the cell and gradually accumulates in the cytoplasm, lowering the pH therein. This cytoplasmic acidification can in turn inhibit the activity of critical mycobacterial enzymes (3). Furthermore, this process can lead to the collapse of proton motive force (PMF) in *M. tb* and accordingly the de-energisation/depletion of membrane potential. On the contrary, at neutral or basic pH, POA fails to pass through the *M. tb* membrane as it remains in its charged/anionic form which cannot easily get into the cell. These findings explain the anomalies of the MIC values of PZA in different pH settings (3). Indeed, some studies demonstrated that PZA fails to sterilise *M. tb* in caseous granulomas under neutral pH conditions (17, 18). Paradoxically, it was shown that PZA susceptibility can be attained at neutral pH under specific *in vitro* conditions, such as nutrient starvation in stationary cultures and hypoxia; both of which are present in necrotic lesions (17). Therefore, it is unclear if other host stress factors contribute to the activity of PZA. In general, PZA is believed to be involved in the inhibition of different targets, including: 1) ribosomal protein S1 (RpsA), implicated in the trans-translation process, and 2) aspartate decarboxylase enzyme (PanD), involved in the biosynthesis of  $\beta$ -alanine, which is the precursor of pantothenate/coenzyme A; the latter downstream products are thought to be critical for the survival of persisters (3). PZA resistance is predominantly caused by mutations in *pncA* gene, encoding for the PZase enzyme. Mutations in *rpsA* and *panD* genes were also found in PZA-resistant strains (3). Thus far, despite the plethora of studies carried out after the discovery of INH and PZA, the exact mechanism of action of both drugs is still elusive. Within this context, the mode of action of PZA is considered the least understood amongst all the anti-TB drugs due to its peculiar properties.

### **5.2.2. FQs as Second-Line Anti-TB Drugs**

FQs are quinolone-based antibiotics that are widely used to treat various bacterial infections in the urinary, gastrointestinal, and respiratory tract in addition to osteomyelitis and sexually transmitted diseases (19). In 1984, FQs were shown, for the first time, to be useful in TB treatment (4). FQs demonstrated excellent *in vitro* and *in vivo* activities against *M. tb* and have become a fundamental part of the bedrock of

MDR-TB therapy since the late 1980s (19, 20). FQs are also used in patients experiencing serious adverse effects to the front-line anti-TB agents (19). In addition, they are recommended as a prophylactic therapy in individuals exposed to MDR-TB (21). FQs encompass different generations of antibiotics (22). The newer FQs generations have supplanted the older ones in treatment of MDR-TB owing to their high efficacy and the development of resistance against the earlier generations. Indeed, although CPF and norfloxacin, the second generation FQs, were the first FQs to show potent activities against *M. tb* (4), the third generation FQs, including moxifloxacin and levofloxacin, are the currently used second-line anti-TB agents (23).

FQs act by inhibiting an ATP-dependent enzyme, namely DNA gyrase, in addition to topoisomerase IV (19). DNA gyrase is a heterodimer, comprising two subunits GyrA and GyrB, encoded by *gyrA* and *gyrB*, respectively. Similarly, two subunits constitute the topoisomerase IV enzyme, denominated ParC and ParE, encoded by *parC* and *parE*, respectively (19). DNA gyrase is responsible for cleaving and resealing double stranded DNA, wherefore it incorporates negative supercoils into the DNA. This process is of paramount importance to DNA transcription, replication, and recombination. On the other hand, topoisomerase IV primarily relaxes (or untangle/unknott) positive supercoils in DNA in addition to decatenating DNA after replication, enabling the separation of two daughter chromosomes (19). Although most bacterial species entail both gyrase and topoisomerase IV, *M. tb* lacks the topoisomerase IV homologues *parC* and *parE*. Indeed, in *M. tb*, DNA gyrase appears to be additionally displaying the functional properties of topoisomerase IV. Therefore, DNA gyrase is likely the sole target for the FQs in *M. tb* (19, 24). The FQs-bound (poisoned) gyrases block DNA synthesis and cause DNA double strand breaks (DSBs) either via serving as "roadblocks" for DNA replication forks or independently of these replication forks (25).

Despite their remarkable bactericidal activity against *M. tb*, resistant strains have emerged against FQs (5, 19, 21). In fact, resistance to FQs is a hallmark in XDR-TB. FQs resistance in *M. tb* is mainly attributed to mutations in the quinolone resistance determining region (QRDR) in *gyrA* (19). Mutations in this region were shown to be correlated with 42 – 100% of FQs resistance in *M. tb*. In addition, mutations in *gyrB* were found in several *M. tb* clinical isolates resistant to FQs (19). However, FQs resistance due to mutations in *gyrB* are markedly less frequent than mutations in *gyrA*

loci (5, 19, 21). In our 2021 study, the second generation FQ antibiotic CPF was of choice due to its safety profile. Although CPF (MIC = 0.5 – 4.0 µg/mL) is less potent than the ensuing generation of FQs, including levofloxacin (MIC = 1 µg/mL) and moxifloxacin (MIC = 0.12 – 0.5 µg/mL), CPF has the lowest risk to cause serious hepatotoxicity and cardiovascular-related morbidity (26). In fact, CPF has minimal adverse drug reactions ( $\leq 5\%$ ) and they are mostly gastrointestinal in nature (abdominal pain, diarrhea, nausea, and vomiting). In addition, the clearance rate of CPF is the highest in all FQs which makes it ideally suited for the treatment of *M. tb* patients with renal impairment (26). Despite its impressive bactericidal, safety, and pharmacokinetic (PK) profile, resistance to CPF developed rapidly in *M. tb* (27). Therefore, it is no longer recommended for TB treatment. Overall, CPF constitutes a fertile ground for structural modifications that could lead to new FQ derivatives with limited adverse side effects and improved activity against DR *M. tb* strains.

### **5.3. 2021 Research Letter "Facile Synthesis and Antimycobacterial Activity of Isoniazid, Pyrazinamide and Ciprofloxacin Derivatives"**

Two design strategies were used in our recently published article: 1) increasing the lipophilicity of INH, PZA, and CPF, which was attained by attaching an adamantane moiety to each of these drugs via amide coupling, and 2) creating hybrid compounds that not only merge two different anti-TB pharmacophores together, but also exhibit higher lipophilicity than INH and PZA. The most active compound in our study is an INH-POA hybrid **1** (**Figure 5.1**; DS *M. tb* MIC = 2 – 4 µg/mL). This activity is likely ascribed to the INH fragment in this hybrid due to the unwonted behaviour of PZA/POA that necessitates an acidic media to bring about growth inhibition in *M. tb*. However, since we did not evaluate the activity of this hybrid in acidic media or *in vivo*, the activity of this compound could still be higher than our identified MIC value due to the POA segment. Importantly, this hybrid was devoid of activity when evaluated against different MDR and XDR strains, suggesting that the mechanism of action/resistance of this compound resembles that of INH or PZA/POA. These results are in consonance with many previously reported INH-containing hybrids which showed potent anti-TB activity against sensitive strains, while they were stripped of potency when evaluated against DR strains (28).

Although the observed inactivity against DR-TB is seemingly expected, some previously reported hybrids entailing INH showed potent activity against DR *M. tb* strains. In this regard, since many pyrazoline derivatives showed potent activity against multiple pathogenic mycobacteria, Shaharyar *et al* conjugated INH with the pyrazoline nucleus (29). Most of their evaluated compounds displayed excellent activity against DS *M. tb*, with some hybrids surpassing INH in activity. More importantly, all of their compounds retained their potent activities against INH-resistant *M. tb*. For instance, the INH-pyrazoline hybrid **2** (**Figure 5.1**), which is the most active compound in their study, displayed an MIC value of 0.26  $\mu\text{M}$  against both H37Rv and INH-resistant *M. tb* strains (29). Their findings in turn suggest that the mechanistic pathway of these compounds as anti-TB agents is distinct from that of INH.

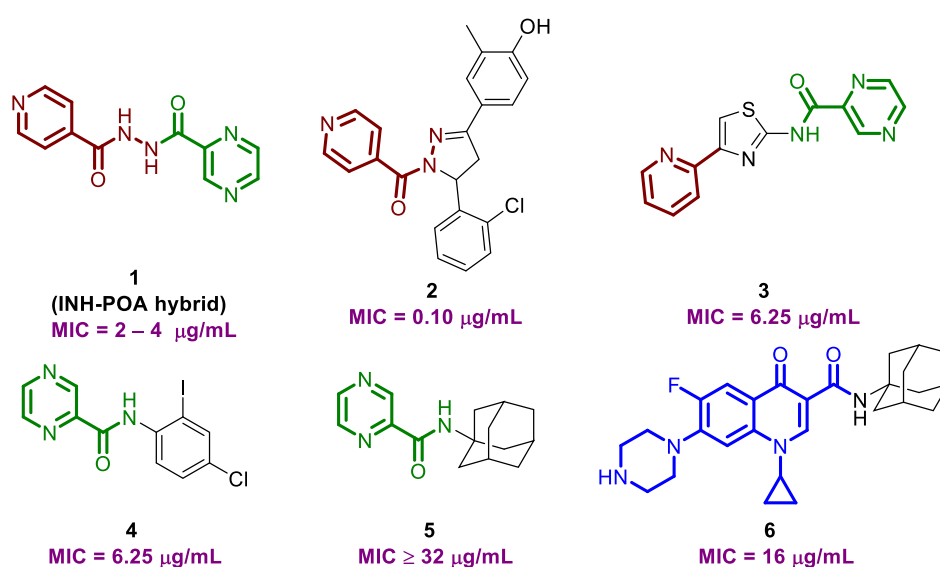


**Figure 5.1. Selected INH, POA, and CPF hybrids/compounds and their anti-TB activity against H37Rv strain.** Compounds **1**, **5**, and **6** were evaluated in our 2021 article, while analogues **2 – 4** were previously assessed by other research groups.

On the other hand, Zitko *et al* investigated the anti-TB activity of several PZA-based hybrids (30, 31). They conjugated POA with the 4-(2-pyridinyl)thiazole-2-amine scaffold which demonstrated potent anti-TB activity in earlier studies, resulting in compound **3** (**Figure 5.1**) (30). This conjugate was less potent than our INH-POA hybrid (H37Rv MIC = 6.25 and 2  $\mu\text{g/mL}$ , respectively). Of note, the two compounds feature some structural similarities as they both entail pyridine ring and PZA core. In

addition, both compounds **1** and **3** were bereft of activity when evaluated against *Mycobacterium avium* (*M. avium*) (30). However, Zitko and collaborators did not assess the anti-TB activity of their compounds against DR-TB. While our compound showed no cytotoxicity against Vero cells ( $IC_{50} \geq 64 \mu\text{g/mL}$ ), the cytotoxicity of compound **3** was inconclusive due to its precipitation in culture media at more than 25  $\mu\text{M}$  concentration (30). In terms of increasing the lipophilicity, Zitko *et al* synthesised and evaluated the anti-TB activity of several *N*-phenyl PZA derivatives (31), in which the anilide **4** exhibited an MIC value of 6.25  $\mu\text{g/mL}$  ( $\text{ClogP} = 2.3$ ). Contrary to compound **4**, in our study, the analogous *N*-adamantyl PZA **5** failed to display an improvement in the anti-TB activity despite having  $\text{ClogP}$  value similar to **4** (**Figure 5.1**;  $\text{MIC} \geq 32 \mu\text{g/mL}$ ,  $\text{ClogP} = 2.3$ ).

Finally, aiming for increasing the lipophilicity and accordingly the anti-TB activity of CPF, the *N*-adamantyl CPF analogue **6** was prepared and evaluated against H37Rv *M. tb* strain in our study (**Figure 5.1**;  $\text{MIC} = 16 \mu\text{g/mL}$ ). Although this compound was less potent than CPF, its activity is higher than the analogous CPF-3-carboxamides which were previously assessed against the same *M. tb* strain ( $\text{MIC} > 125 \mu\text{M}$ ) (32). Indeed, although the carboxylic acid group in position 3 of the FQ scaffold is amenable to numerous modifications, the anti-TB activity usually takes a nosedive when other moieties are introduced into this functional group. In contrast, most of the successful attempts to improve the activity of CPF were carried out on the piperazine ring at position 7 of the fluoroquinolone core (33, 34). The moderate activity displayed by compound **6** suggest that modifying the carboxylic acid group is not a dead-end strategy. Our 2021 research letter published in Chemical Biology and Drug Design journal is included herein.



## References

1. Gygli SM, Borrell S, Trauner A, Gagneux S. Antimicrobial resistance in *Mycobacterium tuberculosis*: mechanistic and evolutionary perspectives. *FEMS Microbiol Rev.* 2017;41(3):354-73.
2. Chakraborty S, Rhee KY. Tuberculosis Drug Development: History and Evolution of the Mechanism-Based Paradigm. *Cold Spring Harb Perspect Med.* 2015;5(8):a021147.
3. Zhang Y, Shi W, Zhang W, Mitchison D. Mechanisms of Pyrazinamide Action and Resistance. *Microbiol Spectr.* 2013;2(4):1-12.
4. Gay JD, DeYoung DR, Roberts GD. In vitro activities of norfloxacin and ciprofloxacin against *Mycobacterium tuberculosis*, *M. avium* complex, *M. chelonae*, *M. fortuitum*, and *M. kansasii*. *Antimicrob Agents Chemother.* 1984;26(1):94-6.
5. Jabeen K, Shakoor S, Hasan R. Fluoroquinolone-resistant tuberculosis: implications in settings with weak healthcare systems. *Int J Infect Dis.* 2015;32:118-23.
6. Brigden G, Hewison C, Varaine F. New developments in the treatment of drug-resistant tuberculosis: clinical utility of bedaquiline and delamanid. *Infect Drug Resist.* 2015;8:367-78.
7. Esposito S, Bianchini S, Blasi F. Bedaquiline and delamanid in tuberculosis. *Expert Opin Pharmacother.* 2015;16(15):2319-30.
8. Mohr E, Ferlazzo G, Hewison C, De Azevedo V, Isaakidis P. Bedaquiline and delamanid in combination for treatment of drug-resistant tuberculosis. *Lancet Infect Dis.* 2019;19(5):470.
9. Sloan DJ, Davies GR, Khoo SH. Recent advances in tuberculosis: New drugs and treatment regimens. *Curr Respir Med Rev.* 2013;9(3):200-10.
10. Unissa AN, Subbian S, Hanna LE, Selvakumar N. Overview on mechanisms of isoniazid action and resistance in *Mycobacterium tuberculosis*. *Infect Genet Evol.* 2016;45:474-92.
11. Robitzek EH, Selikoff IJ. Hydrazine derivatives of isonicotinic acid (rimifon marsilid) in the treatment of active progressive caseous-pneumonic tuberculosis; a preliminary report. *Am Rev Tuberc.* 1952;65(4):402-28.
12. Timmins GS, Deretic V. Mechanisms of action of isoniazid. *Mol Microbiol.* 2006;62(5):1220-7.

13. Pasca MR, Gugliera P, De Rossi E, Zara F, Riccardi G. mmpL7 gene of *Mycobacterium tuberculosis* is responsible for isoniazid efflux in *Mycobacterium smegmatis*. *Antimicrob Agents Chemother*. 2005;49(11):4775-7.
14. Yeager RL, Munroe WG, Dessau FI. Pyrazinamide (aldinamide) in the treatment of pulmonary tuberculosis. *Am Rev Tuberc*. 1952;65(5):523-46.
15. Zhang Y, Wade MM, Scorpio A, Zhang H, Sun Z. Mode of action of pyrazinamide: disruption of *Mycobacterium tuberculosis* membrane transport and energetics by pyrazinoic acid. *J Antimicrob Chemother*. 2003;52(5):790-5.
16. Lamont EA, Baughn AD. Impact of the host environment on the antitubercular action of pyrazinamide. *EBioMedicine*. 2019;49:374-80.
17. Irwin SM, Prideaux B, Lyon ER, Zimmerman MD, Brooks EJ, Schrupp CA, et al. Bedaquiline and Pyrazinamide Treatment Responses Are Affected by Pulmonary Lesion Heterogeneity in *Mycobacterium tuberculosis* Infected C3HeB/FeJ Mice. *ACS Infect Dis*. 2016;2(4):251-67.
18. Lanoix JP, Lenaerts AJ, Nuermberger EL. Heterogeneous disease progression and treatment response in a C3HeB/FeJ mouse model of tuberculosis. *Dis Model Mech*. 2015;8(6):603-10.
19. Malik S, Willby M, Sikes D, Tsodikov OV, Posey JE. New insights into fluoroquinolone resistance in *Mycobacterium tuberculosis*: functional genetic analysis of *gyrA* and *gyrB* mutations. *PLoS One*. 2012;7(6):e39754.
20. Leibert E, Rom WN. New drugs and regimens for treatment of TB. *Expert Rev Anti-Infect Ther*. 2010;8(7):801-13.
21. Wang JY, Lee LN, Lai HC, Wang SK, Jan IS, Yu CJ, et al. Fluoroquinolone resistance in *Mycobacterium tuberculosis* isolates: associated genetic mutations and relationship to antimicrobial exposure. *J Antimicrob Chemother*. 2007;59(5):860-5.
22. King DE, Malone R, Lilley SH. New classification and update on the quinolone antibiotics. *Am Fam Physician*. 2000;61(9):2741-8.
23. World Health Organisation. WHO operational handbook on tuberculosis. Module 4: treatment - drug-resistant tuberculosis treatment. Geneva: World Health Organization; 2020. Licence: CC BY-NC-SA 3.0 IGO., Available from: <https://www.who.int/publications/i/item/9789240006997> (Accessed on 10 September 2021).

24. Aldred KJ, Blower TR, Kerns RJ, Berger JM, Osheroff N. Fluoroquinolone interactions with Mycobacterium tuberculosis gyrase: Enhancing drug activity against wild-type and resistant gyrase. *Proc Natl Acad Sci U S A*. 2016;113(7):E839-46.
25. Ojkic N, Lilja E, Direito S, Dawson A, Allen RJ, Waclaw B. A Roadblock-and-Kill Mechanism of Action Model for the DNA-Targeting Antibiotic Ciprofloxacin. *Antimicrob Agents Chemother*. 2020;64(9).
26. Knoll KE, Lindeque Z, Adeniji AA, Oosthuizen CB, Lall N, Loots DT. Elucidating the Antimycobacterial Mechanism of Action of Ciprofloxacin Using Metabolomics. *Microorganisms*. 2021;9(6).
27. Gumbo T, Louie A, Deziel MR, Drusano GL. Pharmacodynamic evidence that ciprofloxacin failure against tuberculosis is not due to poor microbial kill but to rapid emergence of resistance. *Antimicrob Agents Chemother*. 2005;49(8):3178-81.
28. Hu YQ, Zhang S, Zhao F, Gao C, Feng LS, Lv ZS, et al. Isoniazid derivatives and their anti-tubercular activity. *Eur J Med Chem*. 2017;133:255-67.
29. Shaharyar M, Siddiqui AA, Ali MA, Sriram D, Yogeewari P. Synthesis and in vitro antimycobacterial activity of N1-nicotinoyl-3-(4'-hydroxy-3'-methyl phenyl)-5-[(sub)phenyl]-2-pyrazolines. *Bioorg Med Chem Lett*. 2006;16(15):3947-9.
30. Zitko J, Jand'ourek O, Paterova P, Navratilova L, Kunes J, Vinsova J, et al. Design, synthesis and antimycobacterial activity of hybrid molecules combining pyrazinamide with a 4-phenylthiazol-2-amine scaffold. *Medchemcomm*. 2018;9(4):685-96.
31. Zitko J, Servusová-Vaňásková B, Paterová P, Navrátilová L, Trejtnar F, Kuneš J, et al. Design, synthesis and anti-mycobacterial evaluation of some new N-phenylpyrazine-2-carboxamides. *Chem Pap*. 2016;70(5):649-57.
32. Cilliers P, Seldon R, Smit FJ, Aucamp J, Jordaan A, Warner DF, et al. Design, synthesis, and antimycobacterial activity of novel ciprofloxacin derivatives. *Chem Biol Drug Des*. 2019;94(2):1518-36.
33. Sharma PC, Jain A, Jain S, Pahwa R, Yar MS. Ciprofloxacin: review on developments in synthetic, analytical, and medicinal aspects. *J Enzyme Inhib Med Chem*. 2010;25(4):577-89.
34. Zhang GF, Liu X, Zhang S, Pan B, Liu ML. Ciprofloxacin derivatives and their antibacterial activities. *Eur J Med Chem*. 2018;146:599-612.

## STATEMENT OF CONTRIBUTION TO A CO-AUTHORED PUBLISHED PAPER

Chapter 5 includes a co-authored research article that has been published online in the Chemical Biology and Drug Design journal (2021)

DOI: <https://doi.org/10.1111/cbdd.13836>

Publication link: <https://onlinelibrary.wiley.com/doi/abs/10.1111/cbdd.13836>

**Title: Facile synthesis and antimycobacterial activity of isoniazid, pyrazinamide and ciprofloxacin derivatives**

**Authors/Co-authors: Shahinda S. R. Alsayed, Shichun Lun, Alan Payne, William R. Bishai and Hendra Gunosewoyo**

My contribution to the paper involved: 1) the conception, design, synthesis, purification, and chemical analysis of all of the tested molecules, 2) interpreting all the results (chemistry and biology wise), 3) molecular docking of the compounds, 4) collecting and organising the information/data/references, and 5) preparing and writing up the whole manuscript.

(Signed)



(Date)

20/09/2021

Shahinda Sayed Rabie Alsayed

(Countersigned)



(Date)

20/9/21

Corresponding author of the paper: Dr Hendra Gunosewoyo

(Countersigned)

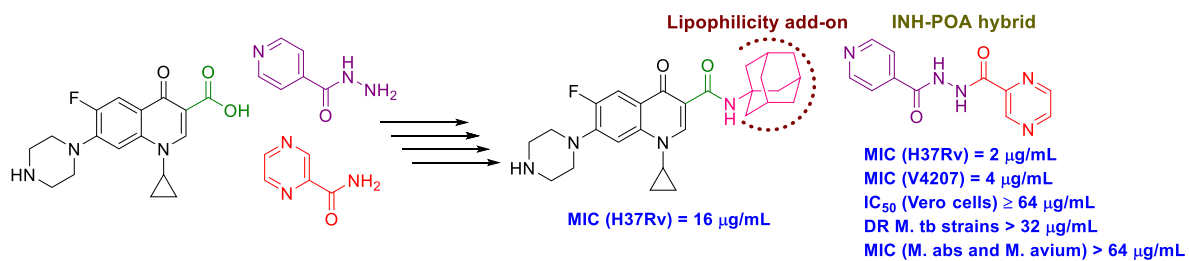


(Date)

20/9/21

Main supervisor: Dr Hendra Gunosewoyo

# Graphical Abstract



# Facile synthesis and antimycobacterial activity of isoniazid, pyrazinamide and ciprofloxacin derivatives

Shahinda S. R. Alsayed<sup>1</sup> | Shichun Lun<sup>2</sup> | Alan Payne<sup>3</sup> | William R. Bishai<sup>2,4</sup> | Hendra Gunosewoyo<sup>1</sup>

<sup>1</sup>School of Pharmacy and Biomedical Sciences, Faculty of Health Sciences, Curtin University, Perth, WA, Australia

<sup>2</sup>Division of Infectious Disease, Department of Medicine, Center for Tuberculosis Research, Johns Hopkins School of Medicine, Baltimore, MD, USA

<sup>3</sup>School of Molecular and Life Sciences, Curtin University, Perth, WA, Australia

<sup>4</sup>Howard Hughes Medical Institute, Chevy Chase, MD, USA

## Correspondence

Hendra Gunosewoyo, School of Pharmacy and Biomedical Sciences, Faculty of Health Sciences, Curtin University, Perth, WA, Australia.  
Email: Hendra.Gunosewoyo@curtin.edu.au

William R. Bishai, Division of Infectious Disease, Department of Medicine, Center for Tuberculosis Research, Johns Hopkins School of Medicine, Baltimore, MD, USA  
Email: wbishai1@jhmi.edu

## Funding information

Australian Research Council; National Institutes of Health

## Abstract

Several rationally designed isoniazid (INH), pyrazinamide (PZA) and ciprofloxacin (CPF) derivatives were conveniently synthesized and evaluated in vitro against H37Rv *Mycobacterium tuberculosis* (*M. tb*) strain. CPF derivative **16** displayed a modest activity (MIC = 16 µg/ml) and was docked into the *M. tb* DNA gyrase. Isoniazid-pyrazinoic acid (INH-POA) hybrid **21a** showed the highest potency in our study (MIC = 2 µg/ml). It also retained its high activity against the other tested *M. tb* drug-sensitive strain (DS) V4207 (MIC = 4 µg/ml) and demonstrated negligible cytotoxicity against Vero cells (IC<sub>50</sub> ≥ 64 µg/ml). Four tested drug-resistant (DR) *M. tb* strains were refractory to **21a**, similar to INH, whilst being sensitive to CPF. Compound **21a** was also inactive against two non-tuberculous mycobacterial (NTM) strains, suggesting its selective activity against *M. tb*. The noteworthy activity of **21a** against DS strains and its low cytotoxicity highlight its potential to treat DS *M. tb*.

## KEYWORDS

ciprofloxacin, hybrid molecules, indoleamides, isoniazid, pyrazinamide, tuberculosis

## 1 | INTRODUCTION

Tuberculosis (TB) is a highly contagious airborne disease that has existed for millennia and continues to pose a major threat to human health. It is one of the oldest life-threatening and leading deadliest diseases known to mankind, claiming more than 1 million lives annually throughout the world (Barberis et al., 2017; WHO, 2020). TB is caused by *Mycobacterium tuberculosis* (*M. tb*) organism that has the ability to stay dormant for years, persisting in the host body without any indication of disease, causing many people to become symptom-free carriers (inactive TB; Boon

& Dick, 2012). Once the immune system of these latently infected people become compromised due to, for instance, co-infection with HIV, this silent warfare of the bacteria will ultimately transform into the active form of TB (Pawlowski et al., 2012; Shankar et al., 2014). According to the World Health Organisation (WHO), one quarter of the human population harbour a latent *M. tb* infection with around 10 million people falling ill with TB every year. In 2018, TB caused an estimated 1.2 million deaths among HIV-negative people in addition to 0.25 million deaths among HIV-positive patients. This inexorable burden ranks TB as the number one cause of mortality/morbidity from a single infectious agent

(surpassing HIV/AIDS; WHO, 2020). The WHO directly observed treatment, and short course (TB-DOTS) requires a 6-month minimum treatment for drug-sensitive (DS) TB with the first-line anti-TB drugs divided into two phases. The first 2 months are the intensive phase treatment with a cocktail of four drugs (Figure 1), including isoniazid (INH, **1**), rifampin (RIF), pyrazinamide (PZA, **3**) and ethambutol (EMB). The subsequent 4 months represent the continuation phase treatment with INH and RIF to kill the dormant bacteria (Tiberi et al., 2017; WHO, 2020). Poor patient compliance to the lengthy duration of therapy, high pill count and drug side-effects contributed to the emergence of drug-resistant (DR) TB (Dheda et al., 2014; Lange et al., 2018; Seung et al., 2015; Sotgiu & Migliori, 2015; Velayati et al., 2013). Hydrophilic properties, charge, size and/or stability under physiological conditions account for inefficient cellular penetration of many anti-TB drugs and sub-optimal treatment. Accordingly, high drug doses are prescribed to compensate for the reduced penetration and bioavailability, taking its toll on the host's vital organs, causing strong adverse effects. Therefore, highly efficacious anti-TB drugs are urgently needed. A common design tactic is to modify old drugs or existing compounds with an established bioactivity in order to attain, ideally, an enhanced anti-TB potency, efficacy against DR strains and short duration of treatment.

Among the front-line TB antibiotics for treatment of DS strains, INH **1** is a prodrug that requires activation by the mycobacterial catalase-peroxidase enzyme (KatG) to the reactive free radical form which then gets implicated in a series of reactions, forming the isonicotinyl-NAD complex **2**. This complex is a potent inhibitor to the enoyl-acyl carrier protein reductase InhA, a key enzyme in the biosynthesis of mycolic acids (MAs; Vidossich et al., 2014). MAs are the integral building blocks of the mycobacterial cell wall and the primary mediators of the notorious impermeability

and hydrophobic characters of the outer coating (Alsayed et al., 2019). Therefore, inhibiting InhA eventually leads to collapsing of the mycobacterial outer coating that serves as a protective permeability barrier from many antibiotics (Vilcheze & Jacobs, 2019). However, serum concentration of INH is greatly influenced by its acetylation *via* *N*-acetyltransferase enzyme (NAT) which constitutes the main metabolic pathway of INH in humans (Erwin et al., 2019). The generated *N*-acetylisoniazid metabolite is devoid of anti-TB activity, leading to a significant decrease in the INH bioavailability. Additionally, in *M. tb*, NAT is implicated in the resistance mechanism to INH (Unissa et al., 2016). For these reasons, chemically modifying the hydrazine unit in INH *via* incorporating a functional group is commonly used to avoid the *N*-acetylation process and thereupon improve the drug bioavailability and the curative outcomes (Hu, Zhang, et al., 2017). Moreover, appending lipophilic moieties to the INH core can impart enhanced cell wall permeation to the drug. Hence, INH analogues with greater lipophilicity have emerged as potential anti-TB agents (Hu, Zhang, et al., 2017).

Like INH (Figure 1), PZA **3** is a prodrug which diffuses into the *M. tb* granuloma, where it gets activated by the pyrazinamidase enzyme to the active form of the drug pyrazinoic acid (POA, **4**; Miotto et al., 2014). However, the exact mechanism of PZA is still ambiguous. After penetrating the TB lesion, the active form of the drug POA accumulates inside the bacillus and kills the bacterial cell in the acidic environment of the TB granuloma (Njire et al., 2016). On the other hand, fluoroquinolones, such as ciprofloxacin (CPF, **5**), have become a mainstay in treating multi-drug-resistant (MDR) TB. The mechanism of action of this class of antibiotics is distinct from the first-line drugs in which they inhibit DNA gyrases and in turn prevent bacterial DNA synthesis (Aldred et al., 2016; Schluger, 2013). When CPF **5** was rendered more hydrophobic by attaching alkyl substituents to the piperazine

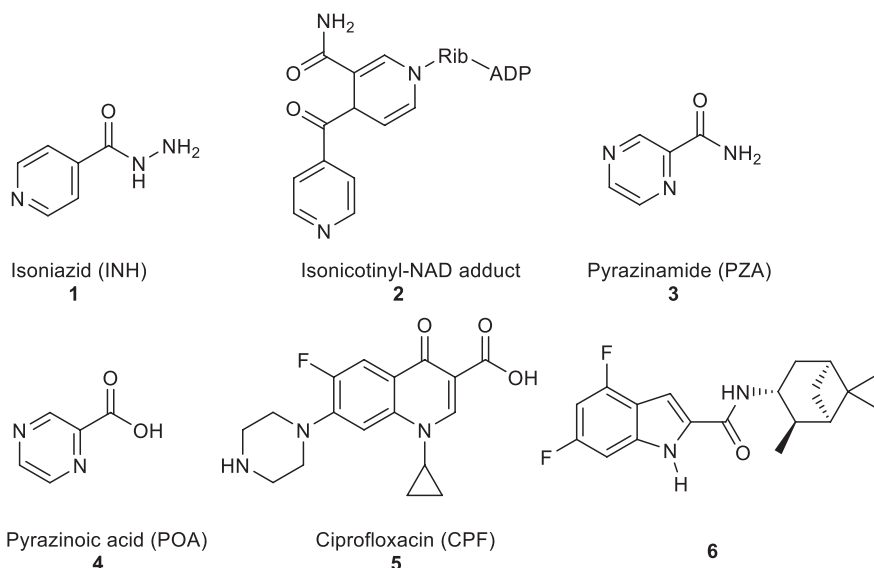


**FIGURE 1** Structures of INH, isonicotinyl-NAD complex, POA, PZA and ciprofloxacin

NH, the resulting *N*-alkylated ciprofloxacin derivatives were more active against *M. tb* than CPF **5** (Haemers et al., 1990).

The present study entails a simple and efficient synthesis of a number of INH, POA and CPF derivatives as well as their in vitro anti-TB activity. All final compounds were screened in vitro against *M. tb* H37Rv strain. The most potent compound **21a** in our study was further evaluated for its antimycobacterial activity against another DS strain and four DR *M. tb* strains in addition to *Mycobacterium abscessus* (*M. abs*) and *Mycobacterium avium* (*M. avium*). In parallel, this compound was also tested in Vero cells for cytotoxicity evaluation.

## 2 | DESIGN

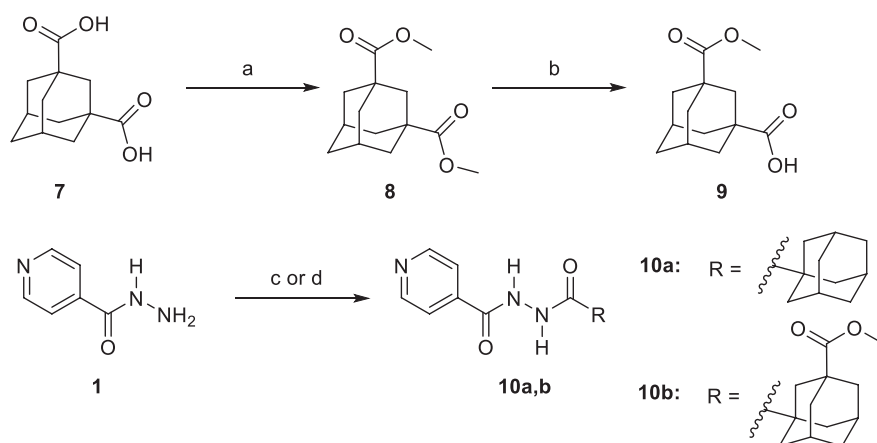
The first design strategy was to incorporate an adamantane ring as a hydrophobic moiety into the framework of INH, POA and CPF. Adamantane is considered an add-on ‘lipophilic bullet’ that has a multifaceted value in medicinal chemistry (Wanka et al., 2013). The hydrophobic substituent constant of this carbocyclic group is estimated as  $\pi_{\text{adamantyl}} = 3.1$ ; therefore integrating an adamantane motif into the structure of highly water-soluble molecules can shift their ClogP to a region that is more clinically useful (Liu et al., 2011). Hence, our first approach is based on endowing the aforementioned drugs with increased lipophilicity which in turn may enhance their penetration through the mammalian host tissues and the lipid-rich mycobacterial cell wall. Beyond enhancing the partition coefficient, the adamantyl group may also improve the stability of drugs and their pharmacokinetics and modulate their therapeutic index (Liu et al., 2011; Wanka et al., 2013). For instance, an inserted adamantane to the INH skeleton might serve as a protecting group, chemically modifying the hydrazine unit and blocking the *N*-acetylation process (Hu, Zhang, et al., 2017). Towards this, five derivatives **10a,b**,

**13a,b** and **16** were synthesized to investigate the effect of these modifications on the in vitro biological activity compared to the parent drug.

Our group has previously reported several indole-2-carboxamides, such as **6**, as potent anti-TB agents targeting the mycobacterial membrane protein large 3 (MmpL3; Lun et al., 2013; Onajole et al., 2013; Stec et al., 2016). MmpL3 is a crucial transporter implicated in the flipping and release of the MAs precursors across the plasma membrane (Xu et al., 2017). Thereafter, MAs get accumulated in the *M. tb* cell envelope, forming a bilayer barrier, standing out as key players in the infection process. Accordingly, we synthesized and scrutinized the biological activity of two conjugates **18** and **20** in which we integrated INH and POA, respectively, into the indoleamide architecture. Another hybrid conjugating both INH and POA **21a** was also evaluated. The foregoing compounds design strategy is based on conjugating two different pharmacophore moieties of diverse bioactive substances known to inhibit different targets in *M. tb* to develop a new chemical entity. The new molecule might be capable of simultaneously hitting different targets, exerting multiple drug actions or one part can offset the adverse effects caused by the other part. The aforementioned approach of forming hybrids of bioactive molecules via conjugating efficacious drug fragments is well-known in drug design (Panda et al., 2016, 2019). Finally, we replaced the pyridine ring in **21a** with a benzene ring, forming the analogous derivative **21b** which is more lipophilic than INH-POA hybrid **21a** to compare their activities.

## 3 | CHEMISTRY

The synthesis of target compounds **10a,b**, **13a,b**, **16**, **18**, **20** and **21a,b** was accomplished as depicted in Schemes 1–4



### Reagents and conditions:

(a) MeOH, conc. H<sub>2</sub>SO<sub>4</sub>, reflux, 16 h, 98%; (b) NaOH (1.1 equiv.), THF, MeOH, rt, 24 h, 70%; (c) EDC.HCl, HOBT, 1-adamantanecarboxylic acid or **9**, DIPEA, DMF, 50 °C, 18 h, 30–87%; (d) EDC.HCl, DMAP, **9**, THF, DCM, rt, 72 h, 45%.

**SCHEME 1** Synthetic pathway for compounds **10a,b**



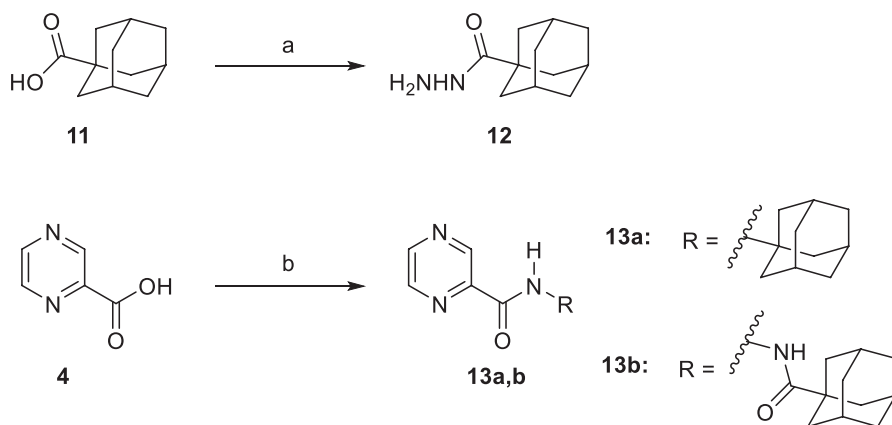
using commercially available INH (**1**), POA (**4**), CPF (**5**) and 4,6-difluoroindole-2-carboxylic acid (**17**). Adamantane derivative **7** was esterified with methanol to give the diester derivative **8**. Subsequent mono hydrolysis with sodium hydroxide of the diester **8** yielded the carboxylic acid **9**. INH **1** was then coupled with either 1-adamantanecarboxylic acid or **9**, following either amide coupling procedure A [1-ethyl-3-(3-dimethylaminopropyl)carbodiimide hydrochloride (EDC.HCl), hydroxybenzotriazole hydrate (HOBt) and *N,N*-diisopropylethylamine (DIPEA)] or coupling conditions B [EDC.HCl and 4-dimethylaminopyridine (DMAP)] to give the requisite final compounds **10a,b** (Scheme 1). Although EDC.HCl/HOBt-mediated coupling is typically conducted at room temperature (rt) in the literature (Onajole et al., 2013), even after 48 hr of stirring, very low yields were obtained. Hence, we applied relatively harsh conditions via heating EDC.HCl/HOBt amide coupling reactions at 50°C for 18 hr which resulted in improved yield. Similar EDC-coupling protocol was previously adopted in which the reaction was heated at 45°C in a microwave (Bahde et al., 2011). Alternatively, EDC.HCl/DMAP was also used as coupling reagents which generally provided better yield than EDC.HCl/HOBt in the derivatives in which both methods were employed. In Scheme 2, 1-adamantanecarboxylic acid **11** was treated with hydrazine hydrate in the presence of 1,1'-carbonyldiimidazole (CDI) to render the hydrazide intermediate **12**. Then, similar to **10a,b**, under standard amide coupling conditions A, compounds **13a,b** were obtained via reacting POA **4** with 1-adamantylamine and **12**, respectively. Both compounds **10a** and **13a** were previously reported, but their synthetic protocols were different from ours and they have never been evaluated against *M. tb* (Harikishore et al., 2013; Naredla et al., 2013). On the other hand, the synthesis of *N*-adamantyl CPF derivative **16** is delineated in Scheme 3, accomplished in three steps. The pyrazine *NH* of CPF **5** was initially protected using di-*tert*-butyl dicarbonate (Boc)<sub>2</sub>O to form the *N*-Boc derivative **14** which was then

subjected to coupling procedure A with 1-adamantylamine to provide the amide **15**. The Boc group in the crude amide **15** was then cleaved using trifluoroacetic acid (TFA) to afford the desired amine **16**.

In the second part of our study, various conjugates were synthesized as described in Scheme 4. For the preparation of hybrid **18**, amide coupling of 4,6-difluoroindole-2-carboxylic acid **17** with INH **1** was conducted under coupling conditions A. Compound **17** was initially converted into the hydrazide derivative **19** using CDI and hydrazine hydrate, and was followed by amide coupling of **19** with POA **4** to furnish conjugate **20**. Treatment of INH **1** with POA **4** using coupling method B delivered the desired hybrid **21a**. This INH-POA conjugate was previously prepared using different synthetic strategies (Miniyar & Bhat, 1999; Panda et al., 2019). It was evaluated against H37Rv *M. tb* strain, albeit without specifying its exact minimum inhibitory concentration (MIC) (Miniyar & Bhat, 1999). Finally, analogue **21b** was obtained via reacting INH **1** with benzohydrazide following coupling conditions A.

## 4 | RESULTS AND DISCUSSION

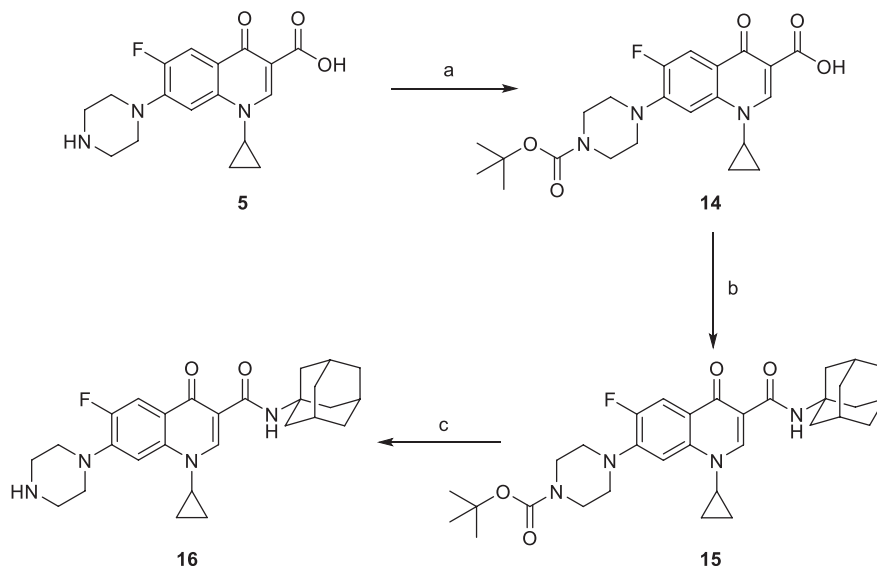
Final compounds **10a,b**, **13a,b**, **16**, **18**, **20** and **21a,b** were evaluated for their antimycobacterial activity in vitro against *M. tb* H37Rv strain using the microplate alamarBlue assay (MABA) to obtain their corresponding MIC values as shown in Table 1. First, with the aim of increasing lipophilicity, an adamantyl group was appended to INH, PZA and CPF, whereupon five compounds **10a,b**, **13a,b** and **16** were evaluated. Both adamantane-based INH derivatives **10a,b** were less active (MIC > 64 and = 32 µg/ml, respectively) than INH (MIC = 0.04 µg/ml) although they exhibited ClogP values of 2.22 and 1.84, respectively, higher than that of INH (ClogP = -0.67). It is noteworthy that the methyl ester adamantane derivative **10b** was more potent than



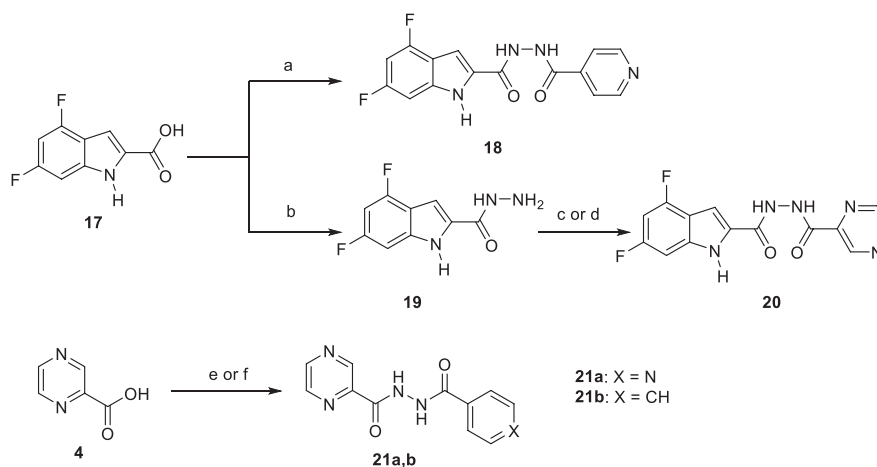
### Reagents and conditions:

(a) CDI, NH<sub>2</sub>NH<sub>2</sub>.H<sub>2</sub>O, DMF, rt, 12-16 h, 78%; (b) EDC.HCl, HOBt, 1-adamantylamine or **12**, DIPEA, DMF, 50 °C, 18 h, 50-76%.

**SCHEME 2** Synthetic pathway for compounds **13a,b**

**SCHEME 3** Synthetic pathway for compound **16****Reagents and conditions:**

(a) Di-*tert*-butyl dicarbonate, 2.0 M aqueous NaOH, dioxane, H<sub>2</sub>O, rt, 48 h, 99%; (b) EDC.HCl, HOBT, 1-adamantylamine, DIPEA, DMF, 50 °C, 18 h; (c) TFA, DCM, rt, 12 h, 40% (over two steps).

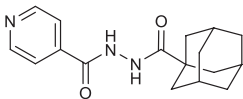
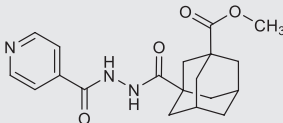
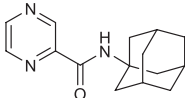
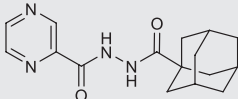
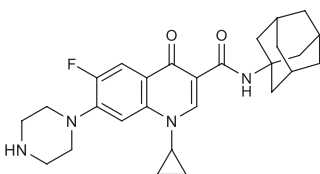
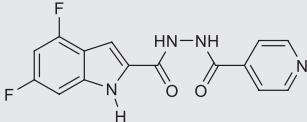
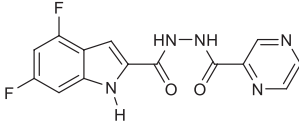
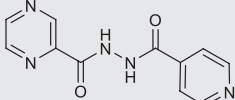
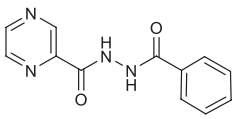
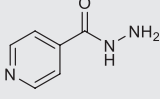
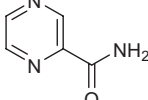
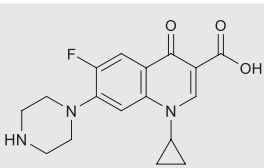
**SCHEME 4** Synthetic pathway for compounds **18**, **20** and **21a,b****Reagents and conditions:**

(a) EDC.HCl, HOBT, INH, DIPEA, DMF, 50 °C, 18 h, 64%; (b) CDI, NH<sub>2</sub>NH<sub>2</sub>·H<sub>2</sub>O, DMF, rt, 16 h, 74%; (c) EDC.HCl, HOBT, POA, DIPEA, DMF, 50 °C, 18 h, 32%; (d) EDC.HCl, DMAP, POA, THF, DCM, rt, 72 h, 70%; (e) EDC.HCl, DMAP, INH, THF, DCM, rt, 72 h, 66%; (f) EDC.HCl, HOBT, benzohydrazide, DIPEA, DMF, 50 °C, 18 h, 41%.

PZA (MIC = 200 µg/ml [Hu, Wu, et al., 2017; Werngren et al., 2012; Zhang et al., 2002]) and the unsubstituted adamantane derivative **10a**. PZA derivatives **13a** (MIC = 32 µg/ml) and **13b** (MIC ≥ 32 µg/ml) were more potent compared to PZA. The higher lipophilicity of **13a,b** (ClogP = 2.33 and 1.78, respectively), emanated from the adamantyl motif, compared to PZA (ClogP = -0.68) appeared to positively modulate the activity of this lead. It is also conceded that PZA displays poor activity against *M. tb* in vitro, notwithstanding its potent effect in vivo (Gopal et al., 2019). Additionally, our attempt to enhance the lipophilicity of CPF resulted in compound **16** which exhibited moderate anti-TB activity (MIC = 16 µg/ml) in comparison to its precursor CPF (MIC = 0.25 µg/ml). Importantly, when docked into *M.*

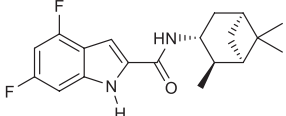
*tb* DNA gyrase (PDB ID: 5BTC; Blower et al., 2016), the keto-amide moiety of **16** was anchored in the gyrase binding pocket via hydrated magnesium ion bridge (Figure 2). Several studies substantiated the importance of this bridge in connecting the fluoroquinolones to the DNA gyrase enzyme, foregrounding it as the primary conduit for the enzyme-drug interactions (Aldred et al., 2013, 2014; Wohlkonig et al., 2010). Two crucial amino acids Ser90 and Asp94 were found to interact with this bridge, providing further support to the hydrogen-bonding network (Figure 3; Aldred et al., 2016; Blower et al., 2016; Wohlkonig et al., 2010). When **16** was docked to the gyrase active site, the hydroxyl group of Ser90 was directly linked to the magnesium ion associated waters, similar to CPF. Because of the absence of Ser90 in the wild

**TABLE 1** In vitro anti-TB activity of target compounds **10a,b**, **13a,b**, **16**, **18**, **20** and **21a,b** as well as reference compounds INH, PZA, CPF and **6**

| Analogue     | Structure   | MIC <sup>a</sup> (µg/ml) | ClogP <sup>b</sup> |
|--------------|---|--------------------------|--------------------|
| <b>10a</b>   |    | >64                      | 2.22               |
| <b>10b</b>   |    | 32                       | 1.84               |
| <b>13a</b>   |    | ≥32                      | 2.33               |
| <b>13b</b>   |    | 32                       | 1.78               |
| <b>16</b>    |    | 16                       | 2.99               |
| <b>18</b>    |   | >64                      | 2.37               |
| <b>20</b>    |  | >64                      | 1.96               |
| <b>21a</b>   |  | 2                        | -0.32              |
| <b>21b</b>   |  | >64                      | 1.03               |
| <b>INH 1</b> |  | 0.04                     | -0.67              |
| <b>PZA 3</b> |  | 200                      | -0.68              |
| <b>CPF 5</b> |  | 0.25                     | -0.72              |

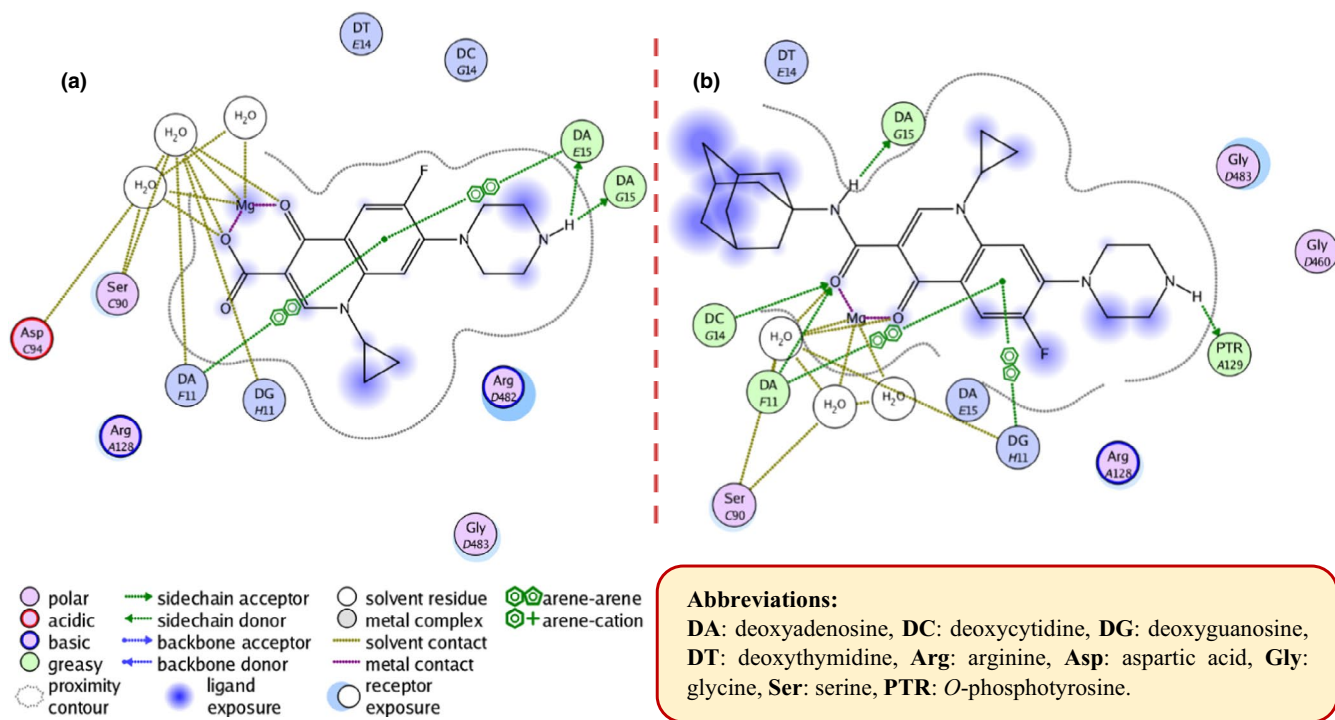
(Continues)

TABLE 1 (Continued)

| Analogue | Structure   | MIC <sup>a</sup> (µg/ml) | ClogP <sup>b</sup> |
|----------|---|--------------------------|--------------------|
| 6        |  | 0.004                    | 5.74               |

<sup>a</sup>The lowest concentration of drug causing at least 90% reduction of bacterial growth by the Microplate alamarBlue assay (MABA). The reported MIC values are an average of three individual measurements.

<sup>b</sup>Calculated using ChemDraw 16.0.



**FIGURE 2** 2D representation of the putative binding interactions of ciprofloxacin (a) and compound **16** (b) with DNA gyrase [Colour figure can be viewed at [wileyonlinelibrary.com](http://wileyonlinelibrary.com)]

type (WT) *M. tb* gyrase, it was proved that the critical water-metal ion bridge that govern the interaction between the fluoroquinolones and the enzyme is primarily anchored by one amino acid Asp94 (Aldred et al., 2016). This is in accordance with previous results showing fluoroquinolone resistance in *M. tb* brought forth by various mutations at Asp94 in GyrA which could be attributed to the disrupted bridge function (Aldred et al., 2016; Maruri et al., 2012). Unlike CPF, the water-mediated magnesium ion network that bridges the quinolone core of **16** to the enzyme did not seem to interact with Asp94 (Figure 2). Compound **16** was also aligned in a slightly different fashion from CPF in the gyrase binding pocket as portrayed in Figure 3. All of these may contribute to the reduced activity of **16** compared to CPF.

Next, we conjugated pharmacophoric units of different anti-TB substances with distinct mechanism of actions.

The first two hybrids, comprising the 4,6-difluoroindole nucleus linked to INH or POA to give **18** and **20**, respectively, showed a dramatic loss of activity (MIC > 64 µg/ml) compared to the original agents. The inactivity of **18** and **20** relative to the 4,6-difluoroindoleamide **6** (MIC = 0.004 µg/ml) is likely ascribed to the diminished lipophilicity of these two analogues (ClogP = 2.37 and 1.96, respectively) compared to **6** (ClogP = 5.74). In addition, extending the amide linker of the indoleamide analogues in our previous study was unfavourable (Alsayed et al., 2020), resonating with the reduced activities of **18** and **20**. On the other hand, tethering INH with POA, which generated conjugate **21a**, led to the most active compound in our current study (MIC = 2 µg/ml). In fact, this hybrid was previously reported to exhibit >70% growth inhibition at 3 µg/ml against the highly virulent *M. tb* Erdman strain (Panda et al., 2019). Evidently, this

hybrid exhibited higher anti-TB activity than PZA but less than INH. Meanwhile, the homologous derivative **21b**, in which we replaced the pyridine moiety with benzoic acid, was bereft of anti-TB activity (MIC > 64 µg/ml) despite its increased lipophilicity compared to **21a** (ClogP = 1.03 and -0.32). The discrepancy between the activities of **21a** and **21b** could be attributed to the presence/lack of the INH produg moiety, respectively. In other words, removal of the INH pharmacophore in **21b** likely accounted for its attenuated activity compared to **21a**, as both compounds retained PZA which displayed poor in vitro activity (MIC = 200 µg/ml [Hu, Wu, et al., 2017; Werngren et al., 2012; Zhang et al., 2002]). Indeed, this was further corroborated by the previous findings of Judge *et al* in which when they coupled INH with

benzoic acid, the resulting *N'*-benzoylisonicotinohydrazide compound showed some potency against the H37Rv strain (Judge et al., 2013). Overall, it seems that lipophilicity is not the sole driving force for anti-TB activity in our study. The higher anti-TB activity demonstrated by the more hydrophilic anti-TB drugs, currently in the market, compared to our relatively lipophilic analogues, gives validity to the notion that the positive correlation between lipophilicity and anti-TB activity is not a clear-cut phenomenon (Machado et al., 2018; Piccaro et al., 2015; Tong et al., 2017).

The most potent INH-POA hybrid **21a**, together with CPF as a positive control, were further evaluated for their cytotoxicity against mammalian cells. In addition, these two compounds were tested for their antimycobacterial activity against another DS and four DR *M. tb* strains, as well as *M. abs* and *M. avium* (Table 2). Both **21a** and CPF exhibited the same high IC<sub>50</sub> against Vero cells (IC<sub>50</sub> ≥ 64 µg/ml), indicating their limited cytotoxicity. We further assessed **21a** and CPF against a panel of clinical isolates of *M. tb*, originally procured from TB patients. Compound **21a** retained its activity against DS *M. tb* strain (V4207), albeit less active than CPF (MIC = 4 and 0.25 µg/ml, respectively). This hybrid was stripped of its potency when tested against two multi-drug-resistant (MDR) *M. tb* strains (V2475, KZN494) and two extensively drug-resistant (XDR) *M. tb* strains (R506, TF274). Notably, the anti-TB activity of CPF against the tested MDR strains was 8-fold higher than the XDR ones (MIC = 0.25 and 2 µg/ml, respectively). Panda *et al* evaluated hybrid **21a** against tuberculous and non-tuberculous mycobacterial (NTM) strains, wherein it exhibited activity at 20 µg/ml concentration against *Mycobacterium bovis* (*M. bovis*) and at 10 µg/ml against *Mycobacterium marinum* (*M. marinum*) and *Mycobacterium fortuitum* (*M. fortuitum*; Panda et al., 2019). Hence, in line with our pursuit to scrutinize the antimycobacterial activity of **21a**, we further evaluated both **21a** and CPF against another two NTM strains, namely *M. abs* and *M. avium*. Surprisingly, compound **21a** was devoid of activity against both strains (MIC > 64 µg/ml). CPF, however, displayed a 32-fold surge in potency against *M. avium* compared to *M. abs* (MIC = 0.25 and 8, respectively). This in turn suggests the selective activity of **21a** against DS *M. tb*.

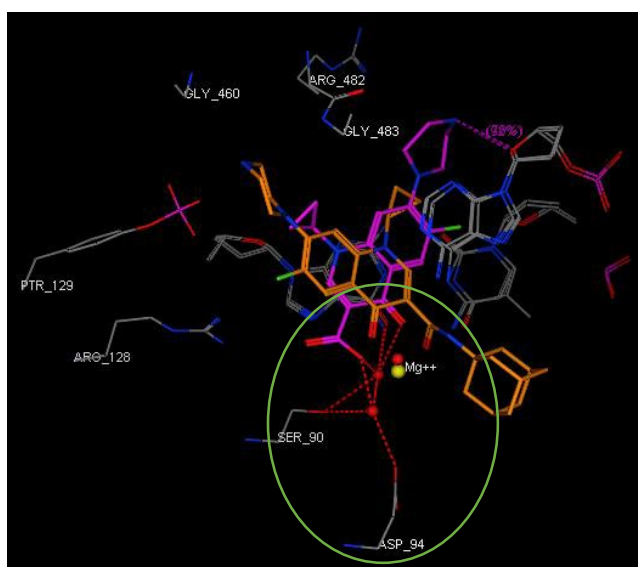


**FIGURE 3** Close-up view of the DNA gyrase active site (retrieved from PDB ID: 5BTC) in complex with CPF (magenta) and compound **16** (light brown, docked in silico in the active site), showing their overlay and different alignment. Green circled is the chelation/hydrogen-bonding network, designating the water/magnesium ion bridge (red/yellow spheres) coordinating the keto acid in CPF. The putative binding profile of CPF also shows an increased support of the hydrogen bond interactions by Ser90 and Asp94 [Colour figure can be viewed at [wileyonlinelibrary.com](http://wileyonlinelibrary.com)]

**TABLE 2** Cytotoxicity [IC<sub>50</sub> (µg/ml)] against Vero cells of **21a** and CPF (positive control) and their activity [MIC (µg/ml)] on selected clinical isolates of *M. tb* and two NTM strains

|            | IC <sub>50</sub> |                 | <i>M. tb</i> |                            |                             |                           |                            | <i>M. abs</i> | <i>M. avium</i> |
|------------|------------------|-----------------|--------------|----------------------------|-----------------------------|---------------------------|----------------------------|---------------|-----------------|
|            | Vero cells       | SI <sup>a</sup> | V4207/<br>DS | V2475/<br>MDR <sup>b</sup> | KZN494/<br>MDR <sup>b</sup> | R506/<br>XDR <sup>c</sup> | TF274/<br>XDR <sup>c</sup> |               |                 |
| <b>21a</b> | ≥64              | ≥32             | 4            | >32                        | >32                         | >32                       | >32                        | >64           | >64             |
| <b>CPF</b> | ≥64              | ≥256            | 0.25         | 0.25                       | 0.25                        | 2                         | 2                          | 8             | 0.25            |

<sup>a</sup>Selectivity index (SI) = IC<sub>50</sub> (Vero)/MIC(H37Rv).

<sup>b</sup>Resistant to INH and rifampin (RIF).

<sup>c</sup>Resistant to INH, RIF, levofloxacin, ofloxacin and kanamycin.

## 5 | CONCLUSION

In summary, we rationally designed, concisely synthesized and evaluated the anti-TB activity of several INH, PZA and CPF derivatives against H37Rv DS *M. tb* strain. The adamantane-dependent modulation of the preceding drugs resulted in enhanced lipophilicity (higher ClogP) in compounds **10a,b**, **13a,b**, and **16**. The noteworthy activity of the adamantane-derived INH compound **10b** set this derivative forth for future modifications in which the integrated methyl ester functional group can serve as a building block amenable to further structure changes. The higher lipophilicity of **13a,b**, with respect to the reference standard PZA was likely responsible for their improved potency. CPF derivative **16** manifested modest activity and was docked into *M. tb* DNA gyrase enzyme. In derivatives **18**, **20** and **21a**, pharmacophores from various anti-TB ligands working through different mechanisms were conjugated. INH-POA hybrid **21a** displayed the most potent activity in our study which was replicated against V4207 DS *M. tb* strain. Compound **21a** and CPF showed low cytotoxicity in mammalian cells (Vero Cells). Unlike CPF, when tested against four MDR- and XDR-TB strains and two NTM strains, **21a** was devoid of activity. This in turn suggests the selective activity of **21a** against DS *M. tb* without any significant effects on the tested DR *M. tb* strains and the NTM strains *M. abs* and *M. avium*. These findings provide valuable information for future elaboration on the adamantane-based compounds, especially the methyl ester derivative **10b**, to attain higher potency and drug-like molecules. Additionally, the low cytotoxicity of hybrid **21a** and its high in vitro potency merit further studies on its in vivo anti-TB activity against DS strains.

## 6 | EXPERIMENTAL DETAILS

### 6.1 | Chemistry

#### 6.1.1 | General information

<sup>1</sup>H NMR and <sup>13</sup>C NMR spectra were recorded on a Bruker Avance III spectrometer at 400 and 100 MHz, respectively, with TMS as an internal standard. Standard abbreviations indicating multiplicity were as follows: s = singlet, d = doublet, dd = doublet of doublets, t = triplet, td = triplet of doublets, q = quadruplet, m = multiplet and br = broad. HRMS experiments were performed on a Thermo Scientific Q-Exactive Orbitrap mass spectrometer. TLC was carried out on Analtech silica gel TLC plates (200 μm, 20 × 20 cm). Flash chromatography was performed using a Teledyne Isco CombiFlash Rf system with RediSep columns or manually using SiliCycle SiliaFlash® P60 Silica Gels [40–63 μm (230–400 mesh)]. Final compounds were purified by preparative HPLC unless otherwise stated. The preparative HPLC employed a Phenomenex Luna® Omega 5 μm Polar

C18 100A (21.2 mm × 150 mm) column, with detection at 254 and 280 nm on a Shimadzu SPD-20A detector, flow rate = 25.0 ml/min. Method 1: 5–50% acetonitrile/H<sub>2</sub>O in 15 min; 50–50% acetonitrile/H<sub>2</sub>O in 10 min; 50–5% acetonitrile/H<sub>2</sub>O in 10 min. Method 2: 20–50% acetonitrile/H<sub>2</sub>O in 15 min; 50–70% acetonitrile/H<sub>2</sub>O in 10 min; 70–20% acetonitrile/H<sub>2</sub>O in 10 min. Both solvents contained 0.05 vol% of trifluoroacetic acid (TFA). Purities of final compounds were established by analytical HPLC, which was carried out using Waters 1525 binary pump, 717 plus autosampler, and 2487 dual wavelength absorbance detector, with a Phenomenex Luna® 5 μm C18(2) 100 Å (150 × 4.6 mm) column. Analytical HPLC method: flow rate = 1 ml/min; gradient elution over 30 min. Gradient: 100% H<sub>2</sub>O to 100% acetonitrile in 10 min; 100% acetonitrile in 10 min; 100% acetonitrile to 100% H<sub>2</sub>O in 10 min. Both solvents again incorporated 0.05% TFA. The purity of all tested compounds was >95% as determined by the HPLC method described above.

#### 6.1.2 | General procedure for amide coupling (Method A)

To a solution of the appropriate carboxylic acid (1 equiv.) in anhydrous dimethylformamide (DMF, 10 ml/mmol), hydroxybenzotriazole hydrate (HOBt, 2 equiv.) and 1-ethyl-3-(3-(dimethylaminopropyl)carbodiimide hydrochloride (EDC·HCl, 2 equiv.) were added at room temperature (rt). After stirring for 10 min, the corresponding amine (1.5 equiv.) and *N,N*-diisopropylethylamine (DIPEA, 3 equiv.) were added, and the reaction mixture was stirred at 50°C for 18 hr. After this time, NaHCO<sub>3</sub> solution (25 ml) was added, and the mixture was extracted with EtOAc (3 × 25 ml). The combined organic layers were washed with NaHCO<sub>3</sub> solution (5 × 25 ml), brine (1 × 25 ml), dried over anhydrous Na<sub>2</sub>SO<sub>4</sub>, filtered and concentrated under reduced pressure. The residue was purified by flash chromatography using dichloromethane/methanol (DCM/MeOH) gradient prior to further preparative HPLC purification unless otherwise stated.

#### 6.1.3 | General procedure for amide coupling (Method B)

To a stirred solution of carboxylic acid (1 mmol) in a 1:1 mixture of tetrahydrofuran (THF) and DCM, EDC.HCl (1.2 mmol), the corresponding amine (1.2 mmol) and 4-dimethylaminopyridine (DMAP, 0.3 mmol) were added and the reaction mixture was stirred at room temperature for 72 hr. The solvent was then removed under vacuum, and the residue was purified by flash chromatography using DCM/MeOH gradient prior to further HPLC purification unless otherwise stated.

### 6.1.4 | General procedure for amide coupling (Method C)

A mixture of carboxylic acid (1 mmol) and 1,1'-carbonyldiimidazole (CDI) (1.5 mmol) in anhydrous DMF (10 ml) was stirred at rt for 2 hr, followed by the addition of hydrazine hydrate solution (5 mmol) and stirring was continued for 16 hr at rt. Water (25 ml) was then added to the reaction mixture and the formed precipitate was filtered off, washed with water (4 × 25 ml) and dried. The crude product was used directly in the next step without additional purification as they were already pure according to the crude <sup>1</sup>H/<sup>13</sup>C NMR spectra.

### 6.1.5 | Preparation of intermediates and final compounds **8**, **9**, **10a,b**, **12**, **13a,b**, **14**, **16**, **18–20** and **21a,b**

#### *Dimethyl adamantane-1,3-dicarboxylate (8)*

To a solution of 1,3-adamantanedicarboxylic acid in methanol, 0.5 ml of conc. H<sub>2</sub>SO<sub>4</sub> was added and the reaction mixture was refluxed for 16 hr and then concentrated in vacuo. The residue was slowly quenched with saturated NaHCO<sub>3</sub> solution, followed by extraction with DCM (3 × 25 ml). The combined organic layers were washed with brine (1 × 25 ml), dried over anhydrous Na<sub>2</sub>SO<sub>4</sub>, filtered and evaporated under vacuum. <sup>1</sup>H NMR data of **8** matched that reported in the literature (Averina et al., 2014). White solid, yield: 98%. <sup>1</sup>H NMR (DMSO-*d*<sub>6</sub>) δ 3.59 (s, 6H), 2.12–2.03 (m, 2H), 1.90 (s, 2H), 1.84–1.70 (m, 8H), 1.63 (s, 2H).

#### *3-(Methoxycarbonyl)adamantane-1-carboxylic acid (9)*

To a solution of compound **8** (1 mmol) in dry THF, a solution of NaOH (1.1 mmol) in dry methanol was added dropwise under an argon atmosphere. After 24 hr of stirring at rt, the reaction mixture was concentrated in vacuo, diluted with water (1 × 25 ml) and washed with DCM (1 × 25 ml). The aqueous layer was subsequently acidified with HCl until the pH value dropped to 1–2 and extracted with DCM (4 × 25 ml). The combined organic layers were dried over anhydrous Na<sub>2</sub>SO<sub>4</sub> filtered and evaporated under reduced pressure. The crude product was used for the next reaction without further purification. White solid, yield: 70%. <sup>1</sup>H NMR (CDCl<sub>3</sub>) δ 3.67 (s, 3H), 2.17 (s, 2H), 2.06 (s, 2H), 1.88 (s, 8H), 1.69 (s, 2H); <sup>13</sup>C NMR (CDCl<sub>3</sub>) δ 183.3, 177.2, 51.8, 40.9, 40.8, 39.5, 37.9, 37.7, 35.3, 27.7.

#### *N'-(adamantane-1-carbonyl)isonicotinohydrazide (10a)*

The title compound was synthesized from INH and 1-adamantanecarboxylic acid according to general procedure A. White solid, yield: 87%. <sup>1</sup>H NMR (DMSO-*d*<sub>6</sub>) δ 10.57 (s, 1H), 9.59 (s, 1H), 8.82 (s, 2H), 7.86 (d, *J* = 5.8 Hz, 2H), 2.01

(s, 3H), 1.88 (d, *J* = 2.6 Hz, 6H), 1.70 (d, *J* = 2.2 Hz, 6H); <sup>13</sup>C NMR (DMSO-*d*<sub>6</sub>) δ 176.7, 164.0, 149.6, 141.5, 122.5, 40.1, 39.0, 36.5, 28.0; HRMS (ESI) *m/z* calcd for C<sub>17</sub>H<sub>21</sub>N<sub>3</sub>O<sub>2</sub> (*[M + H]*<sup>+</sup>) *m/z* 300.1707; found 300.1700.

#### *Methyl-3-(2-isonicotinoylhydrazine-1-carbonyl)adamantane-1-carboxylate (10b)*

The title compound was obtained from reacting INH and compound **9** following method A or B. After flash chromatography, the product was further purified via crystallization from diethyl ether. White solid, yield: 30% (method A) and 45% (method B). <sup>1</sup>H NMR (DMSO-*d*<sub>6</sub>) δ 10.52 (s, 1H), 9.67 (s, 1H), 8.76 (dd, *J* = 4.6, 1.3 Hz, 2H), 7.77 (dd, *J* = 4.5, 1.5 Hz, 2H), 3.61 (s, 3H), 2.11 (s, 2H), 1.96 (s, 2H), 1.91–1.73 (m, 8H), 1.65 (s, 2H); <sup>13</sup>C NMR (DMSO-*d*<sub>6</sub>) δ 177.0, 176.0, 164.4, 150.9, 140.1, 121.7, 52.0, 41.0, 40.3, 38.04, 37.99, 35.3, 27.9; HRMS (ESI) *m/z* calcd for C<sub>19</sub>H<sub>23</sub>N<sub>3</sub>O<sub>4</sub> (*[M + H]*<sup>+</sup>) *m/z* 358.1761; found 358.1754.

#### *Adamantane-1-carbohydrazide (12)*

This compound was obtained from 1-adamantanecarboxylic acid employing method C and its <sup>1</sup>H NMR data matched that reported in the literature (Seliverstova et al., 2018). White solid, yield: 78%. <sup>1</sup>H NMR (DMSO-*d*<sub>6</sub>) δ 8.67 (s, 1H), 4.10 (s, 2H), 1.94 (s, 3H), 1.75 (d, *J* = 2.7 Hz, 6H), 1.71–1.58 (m, 6H).

#### *N-(1-adamantyl)pyrazine-2-carboxamide (13a)*

The title compound was synthesized from POA and 1-adamantylamine according to general procedure A and its <sup>1</sup>H NMR data matched that reported in the literature (Naredla et al., 2013). The purity of the compound was >95% after flash chromatography. White solid, yield: 76%. <sup>1</sup>H NMR (DMSO-*d*<sub>6</sub>) δ 9.16 (s, 1H), 8.81 (s, 1H), 8.63 (s, 1H), 7.74 (s, 1H), 2.08 (s, 9H), 1.67 (s, 6H).

#### *N'-(adamantane-1-carbonyl)pyrazine-2-carbohydrazide (13b)*

The title compound was obtained from POA and compound **12** employing method A and further purified via crystallization from ethanol after flash chromatography. Buff solid, yield: 50%. <sup>1</sup>H NMR (DMSO-*d*<sub>6</sub>) δ 10.48 (s, 1H), 9.54 (s, 1H), 9.16 (d, *J* = 1.3 Hz, 1H), 8.91 (d, *J* = 2.4 Hz, 1H), 8.77 (dd, *J* = 2.3, 1.5 Hz, 1H), 2.00 (s, 3H), 1.88 (d, *J* = 2.1 Hz, 6H), 1.70 (s, 6H); <sup>13</sup>C NMR (DMSO-*d*<sub>6</sub>) δ 176.5, 162.5, 148.3, 144.9, 144.1, 144.0, 40.1, 39.0, 36.5, 28.0; HRMS (ESI) *m/z* calcd for C<sub>16</sub>H<sub>20</sub>N<sub>4</sub>O<sub>2</sub> (*[M + H]*<sup>+</sup>) *m/z* 301.1659; found 301.1651.

#### *7-(4-(tert-butoxycarbonyl)piperazin-1-yl)-1-cyclopropyl-6-fluoro-4-oxo-1,4-dihydroquinoline-3-carboxylic acid (14)*

Commercially available CPF (2 mmol) was dissolved in 20 ml of water:dioxane (1:1) containing 4 ml of 2.0 M

aqueous NaOH solution. Di-*tert*-butyl dicarbonate (Boc<sub>2</sub>O, 3 mmol) was then added, and the reaction mixture was stirred at rt until completion (48 hr). Three quarters of the solvent was evaporated in vacuo, followed by acidification with aqueous 2.0 M HCl solution and the formed precipitate was filtered off, extensively washed with water (2 × 50 ml) and dried. <sup>1</sup>H NMR data of the product matched that reported in the literature (Tehler et al., 2013). White solid, yield: 99%. <sup>1</sup>H NMR (CDCl<sub>3</sub>) δ 8.78 (s, 1H), 8.05 (d, *J* = 12.9 Hz, 1H), 7.37 (d, *J* = 7.1 Hz, 1H), 3.67 (t, *J* = 5.0 Hz, 4H), 3.60–3.43 (m, 1H), 3.29 (t, *J* = 5.1 Hz, 4H), 1.50 (s, 9H), 1.43–1.36 (m, 2H), 1.24–1.18 (m, 2H).

*N*-(1-adamantyl)-1-cyclopropyl-6-fluoro-4-oxo-7-(piperazin-1-yl)-1,4-dihydroquinoline-3-carboxamide (16)

Compound **14** and 1-adamantylamine were reacted following general procedure A. The residue obtained after evaporating the EtOAc extract in vacuo was dissolved in 20 ml DCM, followed by the addition of 4 ml TFA. The reaction mixture was stirred for 12 hr and concentrated in vacuo. NaHCO<sub>3</sub> solution was then added to the residue, followed by extraction with DCM (3 × 50 ml). The combined organic phases were washed with brine (1 × 25 ml), dried over anhydrous Na<sub>2</sub>SO<sub>4</sub>, filtered and concentrated under reduced pressure. The residue was purified by flash chromatography using DCM/MeOH gradient prior to further HPLC purification. White solid, yield: 40%. <sup>1</sup>H NMR (DMSO-*d*<sub>6</sub>) δ 9.89 (s, 1H), 8.59 (s, 1H), 7.82 (d, *J* = 13.6 Hz, 1H), 7.45 (d, *J* = 7.5 Hz, 1H), 3.80–3.61 (m, 1H), 3.18 (t, *J* = 4.4 Hz, 4H), 2.90 (s, 4H), 2.04 (s, 9H), 1.66 (s, 6H), 1.32–1.24 (m, 2H), 1.14–1.03 (m, 2H); <sup>13</sup>C NMR (DMSO-*d*<sub>6</sub>) δ 174.8, 163.0, 152.9 (d, *J* = 247.0 Hz), 147.1, 143.5 (d, *J* = 10.6 Hz), 138.8, 121.9 (d, *J* = 6.9 Hz), 111.9 (d, *J* = 22.6 Hz), 111.4, 107.0, 51.0, 47.0 (d, *J* = 4.2 Hz), 43.2, 41.9, 36.5, 35.5, 29.3, 8.0; HRMS (ESI) *m/z* calcd for C<sub>27</sub>H<sub>33</sub>FN<sub>4</sub>O<sub>2</sub> ([*M* + H]<sup>+</sup>) *m/z* 465.2660; found 465.2659.

4,6-difluoro-*N'*-isonicotinoyl-1H-indole-2-carbohydrazide (18)

The title compound was obtained from commercially available 4,6-difluoroindole-2-carboxylic acid (**17**) and INH employing method A. White solid, yield: 64%. <sup>1</sup>H NMR (DMSO-*d*<sub>6</sub>) δ 12.22 (s, 1H), 10.95 (s, 1H), 10.77 (s, 1H), 8.87 (s, 2H), 7.92 (d, *J* = 4.9 Hz, 2H), 7.39 (d, *J* = 2.0 Hz, 1H), 7.07 (dd, *J* = 9.3, 1.7 Hz, 1H), 6.95 (td, *J* = 10.4, 1.9 Hz, 1H); <sup>13</sup>C NMR (DMSO-*d*<sub>6</sub>) δ 164.5, 160.4, 160.0 (dd, *J* = 239.3, 12.1 Hz), 156.3 (dd, *J* = 249.2, 15.6 Hz), 149.9, 140.9, 138.4 (dd, *J* = 15.2, 12.9 Hz), 130.8 (d, *J* = 3.2 Hz), 122.5, 113.6 (d, *J* = 21.7 Hz), 99.9, 96.0 (dd, *J* = 29.7, 23.2 Hz), 95.2 (dd,

*J* = 25.9, 4.4 Hz); HRMS (ESI) *m/z* calcd for C<sub>15</sub>H<sub>10</sub>F<sub>2</sub>N<sub>4</sub>O<sub>2</sub> ([*M* + H]<sup>+</sup>) *m/z* 317.0845; found 317.0839.

4,6-difluoro-1H-indole-2-carbohydrazide (19)

This compound was synthesized from 4,6-difluoroindole-2-carboxylic acid (**17**) according to method C. Buff solid, yield: 74%. <sup>1</sup>H NMR (DMSO-*d*<sub>6</sub>) δ 12.04 (s, 1H), 9.86 (s, 1H), 7.16 (s, 1H), 7.01 (dd, *J* = 9.4, 1.4 Hz, 1H), 6.87 (td, *J* = 10.4, 1.9 Hz, 1H), 4.52 (s, 2H); <sup>13</sup>C NMR (DMSO-*d*<sub>6</sub>) δ 160.8, 159.5 (dd, *J* = 238.4, 12.3 Hz), 156.1 (dd, *J* = 248.5, 15.5 Hz), 138.0 (dd, *J* = 15.2, 13.2 Hz), 132.0 (d, *J* = 3.3 Hz), 113.6 (dd, *J* = 21.8, 0.7 Hz), 98.0, 95.6 (dd, *J* = 29.7, 23.3 Hz), 95.0 (dd, *J* = 25.9, 4.5 Hz).

4,6-difluoro-*N'*-(pyrazine-2-carbonyl)-1H-indole-2-carbohydrazide (20)

The title compound was obtained from POA and intermediate **19** employing method A or B. The product was further crystallized from DCM to attain >95% purity. Light buff solid, yield: 32% (method A) and 70% (method B). <sup>1</sup>H NMR (DMSO-*d*<sub>6</sub>) δ 12.22 (br s, 1H), 10.72 (br s, 2H), 9.23 (s, 1H), 8.94 (d, *J* = 1.8 Hz, 1H), 8.81 (s, 1H), 7.41 (s, 1H), 7.07 (d, *J* = 9.0 Hz, 1H), 6.92 (t, *J* = 10.1 Hz, 1H); <sup>13</sup>C NMR (DMSO-*d*<sub>6</sub>) δ 162.9, 160.1, 159.9 (dd, *J* = 239.1, 12.1 Hz), 156.3 (dd, *J* = 249.2, 15.6 Hz), 148.6, 144.6, 144.2, 144.1, 138.3 (dd, *J* = 15.2, 13.0 Hz), 131.0 (d, *J* = 3.2 Hz), 113.6 (d, *J* = 21.8 Hz), 99.9, 96.0 (dd, *J* = 29.7, 23.3 Hz), 95.2 (dd, *J* = 25.9, 4.3 Hz); HRMS (ESI) *m/z* calcd for C<sub>14</sub>H<sub>9</sub>F<sub>2</sub>N<sub>5</sub>O<sub>2</sub> ([*M* + H]<sup>+</sup>) *m/z* 318.0797; found 318.0793.

*N'*-isonicotinoylpyrazine-2-carbohydrazide (21a)

The title compound was prepared from POA and INH employing method B and further purified via recrystallization from diethyl ether after flash chromatography. White solid, yield: 66%. <sup>1</sup>H NMR (DMSO-*d*<sub>6</sub>) δ 10.96 (s, 2H), 9.22 (s, 1H), 8.94 (d, *J* = 2.3 Hz, 1H), 8.79 (d, *J* = 6.0 Hz, 3H), 7.82 (d, *J* = 5.8 Hz, 2H); <sup>13</sup>C NMR (DMSO-*d*<sub>6</sub>) δ 164.7, 162.8, 150.9, 148.6, 144.5, 144.2, 144.1, 140.0, 121.9; HRMS (ESI) *m/z* calcd for C<sub>11</sub>H<sub>9</sub>N<sub>5</sub>O<sub>2</sub> ([*M* + H]<sup>+</sup>) *m/z* 244.0829; found 244.0824.

*N'*-benzoylpyrazine-2-carbohydrazide (21b)

The title compound was obtained from benzohydrazide and POA employing method A. White solid, yield: 41%. <sup>1</sup>H NMR (DMSO-*d*<sub>6</sub>) δ 10.85 (s, 1H), 10.60 (s, 1H), 9.22 (d, *J* = 1.2 Hz, 1H), 8.94 (d, *J* = 2.4 Hz, 1H), 8.80 (dd, *J* = 2.4, 1.5 Hz, 1H), 7.93 (d, *J* = 7.1 Hz, 2H), 7.61 (t, *J* = 7.3 Hz, 1H), 7.53 (t, *J* = 7.4 Hz, 2H); <sup>13</sup>C NMR (DMSO-*d*<sub>6</sub>) δ 167.2, 163.3, 148.3, 144.4, 144.3, 143.7, 132.8, 132.2, 129.2, 127.9; HRMS (ESI) *m/z* calcd for C<sub>12</sub>H<sub>10</sub>N<sub>4</sub>O<sub>2</sub> ([*M* + H]<sup>+</sup>) *m/z* 243.0877; found 243.0870.



## 6.2 | Biology

MIC was determined using Microplate alamarBlue assay (MABA) as previously reported (Collins & Franzblau, 1997; Pieroni et al., 2011). Modified MABA was used to determine the MIC of PZA. Briefly, 7H9 (Difco™ Middlebrook 7H9 Broth, BD) without Tween 80 but containing 10% OADC (BBL™ Middlebrook OADC Enrichment, BD) was prepared fresh with the pH value was adjusted to 5.45. Assay was set up as previously reported (Collins & Franzblau, 1997; Pieroni et al., 2011). After 15 days of incubation, 15 µl of 7H9 (pH = 10.75) was added to each well and immediately followed by addition of 32.5 µl of alamar blue. Plate was incubated overnight before reading. MABA format was also used in the cytotoxicity evaluation on Vero Cells (Lun et al., 2013).

## 6.3 | Molecular docking protocol

In silico molecular modelling analysis was undertaken using the Molecular Operating Environment MOE software version 2008.10 (Chemical Computing Group, Montreal, Canada). The X-ray crystal structure of *M. tb* DNA gyrase in complex with CPF (5BTC; Blower et al., 2016) was retrieved from the protein data bank (PDB). The binding pocket was ready for docking after 3D protonating the enzyme, whereby hydrogens and partial charges were added to the system for optimization. In order to validate the docking protocol, the co-crystallized CPF was docked into the active site. Next, the structure of **16** was drawn in ChemDraw Ultra 16.0, saved as.mol file, opened inside the MOE program, 3D protonated and geometrically optimized using MMFF94x forcefield with gradient 0.05. Compound **16** was then docked into the same binding site of CPF using MOE-DOCK function, employing Triangle Matcher placement method and scored using London dG scoring methodology. Then, molecular mechanics forcefield was applied to relax the generated poses which were further ranked using London dG scoring function and the top 30 poses were retained. The best-ranked pose with the lowest binding free energy (i.e. the smallest docking score) was selected.

## ACKNOWLEDGMENTS

SSRA is grateful for the support of Curtin International Postgraduate Research Scholarship (CIPRS). WRB is thankful for the support of NIH grants AI 37856 and HL 133190. HG acknowledges the ARC Discovery Early Career Researcher Award DE160100482.

## REFERENCES

Aldred, K. J., Blower, T. R., Kerns, R. J., Berger, J. M., & Osheroff, N. (2016). Fluoroquinolone interactions with *Mycobacterium tuberculosis* gyrase: Enhancing drug activity against wild-type and resistant gyrase. *Proceedings of the National Academy of Sciences of the United States of America*, *113*(7), E839–E846. <https://doi.org/10.1073/pnas.1525055113>

- Aldred, K. J., Breland, E. J., Vlckova, V., Strub, M. P., Neuman, K. C., Kerns, R. J., & Osheroff, N. (2014). Role of the water-metal ion bridge in mediating interactions between quinolones and *Escherichia coli* topoisomerase IV. *Biochemistry*, *53*(34), 5558–5567. <https://doi.org/10.1021/bi500682e>
- Aldred, K. J., McPherson, S. A., Turnbough, C. L. Jr., Kerns, R. J., & Osheroff, N. (2013). Topoisomerase IV-quinolone interactions are mediated through a water-metal ion bridge: Mechanistic basis of quinolone resistance. *Nucleic Acids Research*, *41*(8), 4628–4639. <https://doi.org/10.1093/nar/gkt124>
- Alsayed, S. S. R., Beh, C. C., Foster, N. R., Payne, A. D., Yu, Y., & Gunosewoyo, H. (2019). Kinase targets for mycolic acid biosynthesis in *Mycobacterium tuberculosis*. *Current Molecular Pharmacology*, *12*(1), 27–49. <https://doi.org/10.2174/1874467211666181025141114>
- Alsayed, S. S. R., Lun, S., Luna, G., Beh, C. C., Payne, A. D., Foster, N., Bishai, W. R., & Gunosewoyo, H. (2020). Design, synthesis, and biological evaluation of novel arylcarboxamide derivatives as anti-tubercular agents. *RSC Advances*, *10*(13), 7523–7540. <https://doi.org/10.1039/C9RA10663D>
- Averina, E. B., Sedenkova, K. N., Bakhtin, S. G., Grishin, Y. K., Kutateladze, A. G., Roznyatovsky, V. A., Rybakov, V. B., Butov, G. M., Kuznetsova, T. S., & Zefirov, N. S. (2014). symm-Tetramethylenecyclooctane: En route to polyspirocycles. *Journal of Organic Chemistry*, *79*(17), 8163–8170. <https://doi.org/10.1021/jo501380y>
- Bahde, R. J., Appella, D. H., & Trenkle, W. C. (2011). A one-pot preparation of N-2-mercaptobenzoyl-amino amides. *Tetrahedron Letters*, *52*(32), 4103–4105. <https://doi.org/10.1016/j.tetlet.2011.05.115>
- Barberis, I., Bragazzi, N. L., Galluzzo, L., & Martini, M. (2017). The history of tuberculosis: From the first historical records to the isolation of Koch's bacillus. *Journal of Preventive Medicine and Hygiene*, *58*(1), E9–E12.
- Blower, T. R., Williamson, B. H., Kerns, R. J., & Berger, J. M. (2016). Crystal structure and stability of gyrase-fluoroquinolone cleaved complexes from *Mycobacterium tuberculosis*. *Proceedings of the National Academy of Sciences of the United States of America*, *113*(7), 1706–1713. <https://doi.org/10.1073/pnas.1525047113>
- Boon, C., & Dick, T. (2012). How *Mycobacterium tuberculosis* goes to sleep: The dormancy survival regulator DosR a decade later. *Future Microbiology*, *7*(4), 513–518. <https://doi.org/10.2217/fmb.12.14>
- Collins, L., & Franzblau, S. G. (1997). Microplate alamar blue assay versus BACTEC 460 system for high-throughput screening of compounds against *Mycobacterium tuberculosis* and *Mycobacterium avium*. *Antimicrobial Agents and Chemotherapy*, *41*(5), 1004–1009. <https://doi.org/10.1128/aac.41.5.1004>
- Dheda, K., Gumbo, T., Gandhi, N. R., Murray, M., Theron, G., Udawadia, Z., Migliori, G. B., & Warren, R. (2014). Global control of tuberculosis: From extensively drug-resistant to untreatable tuberculosis. *The Lancet Respiratory Medicine*, *2*(4), 321–338. [https://doi.org/10.1016/S2213-2600\(14\)70031-1](https://doi.org/10.1016/S2213-2600(14)70031-1)
- Erwin, E. R., Addison, A. P., John, S. F., Olaleye, O. A., & Rosell, R. C. (2019). Pharmacokinetics of isoniazid: The good, the bad, and the alternatives. *Tuberculosis (Edinb)*, *116S*, S66–S70. <https://doi.org/10.1016/j.tube.2019.04.012>
- Gopal, P., Gruber, G., Dartois, V., & Dick, T. (2019). Pharmacological and molecular mechanisms behind the sterilizing activity of

- pyrazinamide. *Trends in Pharmacological Sciences*, 40(12), 930–940. <https://doi.org/10.1016/j.tips.2019.10.005>
- Haemers, A., Leysen, D. C., Bollaert, W., Zhang, M. Q., & Pattyn, S. R. (1990). Influence of N substitution on antimycobacterial activity of ciprofloxacin. *Antimicrobial Agents and Chemotherapy*, 34(3), 496–497. <https://doi.org/10.1128/aac.34.3.496>
- Harikishore, A., Leow, M. L., Niang, M., Rajan, S., Pasunooti, K. K., Preiser, P. R., Liu, X., & Yoon, H. S. (2013). Adamantyl derivative as a potent inhibitor of Plasmodium FK506 binding protein 35. *ACS Medicinal Chemistry Letters*, 4(11), 1097–1101. <https://doi.org/10.1021/ml400306r>
- Hu, Y., Wu, X., Luo, J., Fu, Y., Zhao, L., Ma, Y., Li, Y., Liang, Q., Shang, Y., & Huang, H. (2017). Detection of pyrazinamide resistance of *Mycobacterium tuberculosis* using nicotinamide as a surrogate. *Clinical Microbiology & Infection*, 23(11), 835–838. <https://doi.org/10.1016/j.cmi.2017.03.028>
- Hu, Y. Q., Zhang, S., Zhao, F., Gao, C., Feng, L. S., Lv, Z. S., Xu, Z., & Wu, X. (2017). Isoniazid derivatives and their anti-tubercular activity. *European Journal of Medicinal Chemistry*, 133, 255–267. <https://doi.org/10.1016/j.ejmech.2017.04.002>
- Judge, V., Narasimhan, B., Ahuja, M., Sriram, D., Yogeewari, P., De Clercq, E., Pannecouque, C., & Balzarini, J. (2013). Synthesis, antimycobacterial, antiviral, antimicrobial activity and QSAR studies of N(2)-acyl isonicotinic acid hydrazide derivatives. *Medicinal Chemistry*, 9(1), 53–76. <https://doi.org/10.2174/157340613804488404>
- Lange, C., Chesov, D., Heyckendorf, J., Leung, C. C., Udawadia, Z., & Dheda, K. (2018). Drug-resistant tuberculosis: An update on disease burden, diagnosis and treatment. *Respirology*, 23(7), 656–673. <https://doi.org/10.1111/resp.13304>
- Liu, J., Obando, D., Liao, V., Lifa, T., & Codd, R. (2011). The many faces of the adamantyl group in drug design. *European Journal of Medicinal Chemistry*, 46(6), 1949–1963. <https://doi.org/10.1016/j.ejmech.2011.01.047>
- Lun, S., Guo, H., Onajole, O. K., Pieroni, M., Gunosewoyo, H., Chen, G., Tipparaju, S. K., Ammerman, N. C., Kozikowski, A. P., & Bishai, W. R. (2013). Indoleamides are active against drug-resistant *Mycobacterium tuberculosis*. *Nature Communications*, 4, 2907. <https://doi.org/10.1038/ncomms3907>
- Machado, D., Girardini, M., Viveiros, M., & Pieroni, M. (2018). Challenging the drug-likeness dogma for new drug discovery in tuberculosis. *Frontiers in Microbiology*, 9, 1367. <https://doi.org/10.3389/fmicb.2018.01367>
- Maruri, F., Sterling, T. R., Kaiga, A. W., Blackman, A., van der Heijden, Y. F., Mayer, C., Cambau, E., & Aubry, A. (2012). A systematic review of gyrase mutations associated with fluoroquinolone-resistant *Mycobacterium tuberculosis* and a proposed gyrase numbering system. *Journal of Antimicrobial Chemotherapy*, 67(4), 819–831. <https://doi.org/10.1093/jac/dkr566>
- Miniyar, P., & Bhat, A. (1999). Pyrazinoic acid hydrazide derivatives: Synthesis and antimycobacterial activities. *Indian Journal of Heterocyclic Chemistry*, 9(2), 155–156.
- Miotto, P., Cabibbe, A. M., Feuerriegel, S., Casali, N., Drobniewski, F., Rodionova, Y., Bakonyte, D., Stakenas, P., Pimkina, E., Augustynowicz-Kopec, E., Degano, M., Ambrosi, A., Hoffner, S., Mansjo, M., Werngren, J., Rusch-Gerdes, S., Niemann, S., & Cirillo, D. M. (2014). *Mycobacterium tuberculosis* pyrazinamide resistance determinants: A multicenter study. *MBio*, 5(5), e01819–e1814. <https://doi.org/10.1128/mBio.01819-14>
- Naredla, R. R., Dash, B. P., & Klumpp, D. A. (2013). Preparation of pyrazine carboxamides: A reaction involving N-heterocyclic carbene (NHC) intermediates. *Organic Letters*, 15(18), 4806–4809. <https://doi.org/10.1021/ol402200x>
- Njire, M., Tan, Y., Mugweru, J., Wang, C., Guo, J., Yew, W., Tan, S., & Zhang, T. (2016). Pyrazinamide resistance in *Mycobacterium tuberculosis*: Review and update. *Advances in Medical Sciences*, 61(1), 63–71. <https://doi.org/10.1016/j.advms.2015.09.007>
- Onajole, O. K., Pieroni, M., Tipparaju, S. K., Lun, S., Stec, J., Chen, G., Gunosewoyo, H., Guo, H., Ammerman, N. C., Bishai, W. R., & Kozikowski, A. P. (2013). Preliminary structure-activity relationships and biological evaluation of novel antitubercular indolecarboxamide derivatives against drug-susceptible and drug-resistant *Mycobacterium tuberculosis* strains. *Journal of Medicinal Chemistry*, 56(10), 4093–4103. <https://doi.org/10.1021/jm4003878>
- Panda, S. S., Detistov, O. S., Girgis, A. S., Mohapatra, P. P., Samir, A., & Katritzky, A. R. (2016). Synthesis and molecular modeling of antimicrobial active fluoroquinolone-pyrazine conjugates with amino acid linkers. *Bioorganic & Medicinal Chemistry Letters*, 26(9), 2198–2205. <https://doi.org/10.1016/j.bmcl.2016.03.062>
- Panda, S. S., Girgis, A. S., Mishra, B. B., Elagawany, M., Devarapalli, V., Littlefield, W. F., Samir, A., Fayad, W., Fawzy, N. G., Srour, A. M., & Bokhtia, R. M. (2019). Synthesis, computational studies, antimycobacterial and antibacterial properties of pyrazinoic acid-isoniazid hybrid conjugates. *RSC Advances*, 9(35), 20450–20462. <https://doi.org/10.1039/C9RA03380G>
- Pawlowski, A., Jansson, M., Skold, M., Rottenberg, M. E., & Kallenius, G. (2012). Tuberculosis and HIV co-infection. *PLoS Path*, 8(2), e1002464. <https://doi.org/10.1371/journal.ppat.1002464>
- Piccaro, G., Poce, G., Biava, M., Giannoni, F., & Fattorini, L. (2015). Activity of lipophilic and hydrophilic drugs against dormant and replicating *Mycobacterium tuberculosis*. *The Journal of Antibiotics*, 68(11), 711–714. <https://doi.org/10.1038/ja.2015.52>
- Pieroni, M., Tipparaju, S. K., Lun, S., Song, Y., Sturm, A. W., Bishai, W. R., & Kozikowski, A. P. (2011). Pyrido[1,2-a]benzimidazole-based agents active against tuberculosis (TB), multidrug-resistant (MDR) TB and extensively drug-resistant (XDR) TB. *ChemMedChem*, 6(2), 334–342. <https://doi.org/10.1002/cmdc.201000490>
- Schluger, N. W. (2013). Fluoroquinolones in the treatment of tuberculosis: Which is best? *American Journal of Respiratory and Critical Care Medicine*, 188(7), 768–769. <https://doi.org/10.1164/rccm.201308-1446ED>
- Seliverstova, D. V., Suslonov, V. V., Zarubaev, V. V., & Trifonov, R. E. (2018). Synthesis, structure, and anti-influenza activity of 2-(Adamantan-1-yl)-5-aryl-1,3,4-oxadiazoles and 2-(Adamantan-1-yl)-5-aryl tetrazoles. *Russian Journal of Organic Chemistry*, 54(4), 633–638. <https://doi.org/10.1134/s107042801804019x>
- Seung, K. J., Keshavjee, S., & Rich, M. L. (2015). Multidrug-resistant tuberculosis and extensively drug-resistant tuberculosis. *Cold Spring Harbor Perspectives in Medicine*, 5(9), a017863. <https://doi.org/10.1101/cshperspect.a017863>
- Shankar, E. M., Vignesh, R., Ellegard, R., Barathan, M., Chong, Y. K., Bador, M. K., Rukamani, D. V., Sabet, N. S., Kamarulzaman, A., Velu, V., & Larsson, M. (2014). HIV-*Mycobacterium tuberculosis* co-infection: A 'danger-couple model' of disease pathogenesis. *Pathogens and Disease*, 70(2), 110–118. <https://doi.org/10.1111/2049-632X.12108>
- Sotgiu, G., & Migliori, G. B. (2015). Facing multi-drug resistant tuberculosis. *Pulmonary Pharmacology & Therapeutics*, 32, 144–148. <https://doi.org/10.1016/j.pupt.2014.04.006>
- Stec, J., Onajole, O. K., Lun, S., Guo, H., Merenbloom, B., Vistoli, G., Bishai, W. R., & Kozikowski, A. P. (2016).

- Indole-2-carboxamide-based MmpL3 inhibitors show exceptional antitubercular activity in an animal model of tuberculosis infection. *Journal of Medicinal Chemistry*, 59(13), 6232–6247. <https://doi.org/10.1021/acs.jmedchem.6b00415>
- Tehler, U., Fagerberg, J. H., Svensson, R., Larhed, M., Artursson, P., & Bergstrom, C. A. (2013). Optimizing solubility and permeability of a biopharmaceutics classification system (BCS) class 4 antibiotic drug using lipophilic fragments disturbing the crystal lattice. *Journal of Medicinal Chemistry*, 56(6), 2690–2694. <https://doi.org/10.1021/jm301721e>
- Tiberi, S., Scardigli, A., Centis, R., D'Ambrosio, L., Munoz-Torrico, M., Salazar-Lezama, M. A., Spanevello, A., Visca, D., Zumla, A., Migliori, G. B., & Caminero Luna, J. A. (2017). Classifying new anti-tuberculosis drugs: Rationale and future perspectives. *International Journal of Infectious Diseases*, 56, 181–184. <https://doi.org/10.1016/j.ijid.2016.10.026>
- Tong, A. S. T., Choi, P. J., Blaser, A., Sutherland, H. S., Tsang, S. K. Y., Guillemont, J., Motte, M., Cooper, C. B., Andries, K., Van den Broeck, W., Franzblau, S. G., Upton, A. M., Denny, W. A., Palmer, B. D., & Conole, D. (2017). 6-Cyano analogues of bedaquiline as less lipophilic and potentially safer diarylquinolines for tuberculosis. *ACS Medicinal Chemistry Letters*, 8(10), 1019–1024. <https://doi.org/10.1021/acsmedchemlett.7b00196>
- Unissa, A. N., Subbian, S., Hanna, L. E., & Selvakumar, N. (2016). Overview on mechanisms of isoniazid action and resistance in *Mycobacterium tuberculosis*. *Infection, Genetics and Evolution*, 45, 474–492. <https://doi.org/10.1016/j.meegid.2016.09.004>
- Velayati, A. A., Farnia, P., & Masjedi, M. R. (2013). The totally drug resistant tuberculosis (TDR-TB). *International Journal of Clinical and Experimental Medicine*, 6(4), 307–309.
- Vidossich, P., Loewen, P. C., Carpena, X., Fiorin, G., Fita, I., & Rovira, C. (2014). Binding of the antitubercular pro-drug isoniazid in the heme access channel of catalase-peroxidase (KatG). A combined structural and metadynamics investigation. *The Journal of Physical Chemistry B*, 118(11), 2924–2931. <https://doi.org/10.1021/jp4123425>
- Vilcheze, C., & Jacobs, W. R. Jr (2019). The isoniazid paradigm of killing, resistance, and persistence in *Mycobacterium tuberculosis*. *Journal of Molecular Biology*, 431(18), 3450–3461. <https://doi.org/10.1016/j.jmb.2019.02.016>
- Wanka, L., Iqbal, K., & Schreiner, P. R. (2013). The lipophilic bullet hits the targets: Medicinal chemistry of adamantane derivatives. *Chemical Reviews*, 113(5), 3516–3604. <https://doi.org/10.1021/cr100264t>
- Werngren, J., Sturegard, E., Jureen, P., Angeby, K., Hoffner, S., & Schon, T. (2012). Reevaluation of the critical concentration for drug susceptibility testing of *Mycobacterium tuberculosis* against pyrazinamide using wild-type MIC distributions and pncA gene sequencing. *Antimicrobial Agents and Chemotherapy*, 56(3), 1253–1257. <https://doi.org/10.1128/AAC.05894-11>
- WHO. (2020). *World Health Organisation Global Tuberculosis Report, Geneva*. Retrieved from <https://apps.who.int/iris/bitstream/handle/10665/336069/9789240013131-eng.pdf>
- Wohlkonig, A., Chan, P. F., Fosberry, A. P., Homes, P., Huang, J., Kranz, M., Leydon, V. R., Miles, T. J., Pearson, N. D., Perera, R. L., Shillings, A. J., Gwynn, M. N., & Bax, B. D. (2010). Structural basis of quinolone inhibition of type IIA topoisomerases and target-mediated resistance. *Nature Structural & Molecular Biology*, 17(9), 1152–1153. <https://doi.org/10.1038/nsmb.1892>
- Xu, Z., Meshcheryakov, V. A., Poce, G., & Chng, S. S. (2017). MmpL3 is the flippase for mycolic acids in mycobacteria. *Proceedings of the National Academy of Sciences of the United States of America*, 114(30), 7993–7998. <https://doi.org/10.1073/pnas.1700062114>
- Zhang, Y., Permar, S., & Sun, Z. (2002). Conditions that may affect the results of susceptibility testing of *Mycobacterium tuberculosis* to pyrazinamide. *Journal of Medical Microbiology*, 51(1), 42–49. <https://doi.org/10.1099/0022-1317-51-1-42>

**How to cite this article:** Alsayed SSR, Lun S, Payne A, Bishai WR, Gunosewoyo H. Facile synthesis and antimycobacterial activity of isoniazid, pyrazinamide and ciprofloxacin derivatives. *Chem Biol Drug Des*. 2021;97:1137–1150. <https://doi.org/10.1111/cbdd.13836>

## Conclusions

In line with the previous endeavours to enhance the anti-TB activity of INH, PZA, and CPF, several compounds/hybrids incorporating the preceding drugs were designed, synthesised, and evaluated for their anti-TB activity. The most active compound was an INH-POA hybrid which displayed potent activity against DS *M. tb* strains, while the resistant strains remained refractory to this conjugate. This disparity in potency against DS and DR *M. tb* strains suggest that the mechanism of action/resistance of the INH-POA hybrid mimics that of INH or PZA/POA; however, more studies are needed to confirm that presumption. The second most potent compound in our study was an *N*-adamantyl CPF derivative, which showed moderate anti-TB activity and was docked into the *M. tb* DNA gyrase. Although this compound is less active than the parent CPF drug, it was found to be more potent than the previously evaluated CPF analogues that were modified at the carboxylic acid group at position 3 of the FQ core. The rest of the tested compounds showed weak or no anti-TB activity. Based on lipophilicity alone, these findings were counterintuitive due to the increased ClogP values of these compounds (adamantane-derived INH or PZA) compared to the parent drugs. In addition to the INH-POA hybrid, two other hybrids I2C-INH and I2C-PZA were evaluated and shown to be bereft of activity. Overall, our succinct compilation of INH, PZA, and CPF analogues provided a rudimentary SAR information that highlights the impact of increasing the lipophilicity of these compounds. These findings bring to light the preliminary safety data and potential of INH-POA hybrid for further development. In addition, the appreciable activity of the *N*-adamantyl CPF alludes to the possibility of future adjustments to the carboxylic acid moiety in CPF.

## **Chapter 6**

### **Versatility and Repurposing of the Indole-2-Carboxamide Framework**

## Background

The indole-2-carboxamide (I2C) scaffold represents an important pharmacophore in the design and discovery of novel biologically active agents. Apart from their exceptional activities against drug-sensitive and drug-resistant tuberculosis (DS-TB and DR-TB), numerous I2C analogues were proven to have potent antitumour activities against a vast array of tumour cell lines in a multitude of reports. Accordingly, the antitumour profiles of manifold I2C derivatives with assorted mechanisms of action were collated herein to elucidate the I2C-linked diverse structural earmarks that elicit potent antitumour activities. Notably, the succinct literature review, provided in this Chapter, indicate that I2Cs were scarcely tested against grade IV brain tumour cells. To this end, a small library of new I2C analogues were designed, synthesised, and biologically evaluated against the growth of *Mycobacterium tuberculosis* (*M. tb*) H37Rv strain as well as paediatric glioblastoma (GBM) tumour cell line KNS42. The most active compounds were evaluated against a panel of grade IV brain tumour cell lines and non-tumourigenic cells. A piperazine-linked I2C analogue with potent activity against KNS42 cells was further studied for its antitumour mechanism. Indeed, KNS42 cells treated with this I2C derivative were subjected to DNBSEQ Eukaryotic Stranded Transcriptome Resequencing. The differential gene expression between KNS42 cells exposed to this compound and the untreated (control) cells was analysed, wherein all the significantly downregulated and upregulated genes were studied. Two oncogenes were found to be significantly downregulated in the treated KNS42 cells, suggesting their involvement in the antitumour mechanism of the tested piperazine-containing I2C analogue.

## 6.1. Introduction

The indole moiety is an important building block that was first discovered in 1866, when von Adolf Baeyer showed that the indole nucleus is the parent substance of the indigo structure (1). The chemistry of this bicyclic heteroaromatic ring is well established and detailed in different review articles (2-5). The indole ring is described as a "privileged" structural subunit, a term first coined by Evans *et al* to describe scaffolds that can serve as ligands for a different array of receptors (6-8). In addition, the indole skeleton is presumably the most ubiquitous biologically active heterocycle in nature and is largely present in many pharmaceutical drugs in the market (9, 10). Indole-based molecules are also produced by a variety of microorganisms and are widely distributed in biological systems and biologically active natural products, such as plants (11-15). For instance, tryptophan **1** (**Figure 6.1**) is an essential amino acid and an integral component of many proteins. Tryptophan serves as a precursor to the neurotransmitter serotonin **2** which is the precursor for the melatonin hormone **3** (16, 17).

The synthesis and biological activities of numerous indoles are summarised in multiple reviews (4, 18-23). Due to the large number of indole-containing compounds, some reviews were only focused on covering a particular biological activity. In this respect, the antibacterial, antitumour, and antiviral activities were the most reviewed biological attributes of the indole framework (24-30). Delavirdine **4** (DLV, **Figure 6.1**) is a prominent example of the I2C-containing medicine in the market. DLV is a non-nucleoside reverse transcriptase inhibitor (NNRTI) that is used in the treatment of HIV as a part of the highly active antiretroviral therapy (HAART) (31). In addition, as mentioned in the previous Chapters, several I2Cs have also demonstrated a great potential for advancement as anti-TB agents, exemplified by the two preclinical agents NITD-304 (**5**) and NITD-349 (**6**), **Figure 6.1**. Since this thesis revolves around the I2C pharmacophore, a comprehensive literature search was conducted in this Chapter to identify the antitumour potential of the I2Cs and their associated mechanism of action.

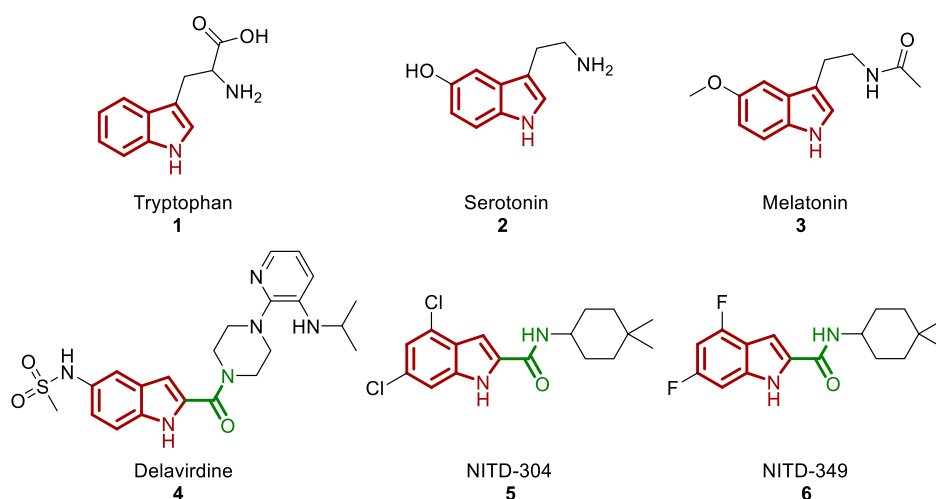


**Figure 6.1. Indole-based compounds in biological systems (1 – 3) as well as important I2C analogues in pharmaceutical market (4) and preclinical studies (5 and 6).**

To the best of my knowledge, no I2C-based antitumour agent is currently available in the market. However, many naturally occurring indoles, such as vinblastine **7** and vincristine **8** (**Figure 6.2**), have been clinically approved for treatment of various kinds of tumours (32). Vinblastine and vincristine are Vinca alkaloids that are primarily isolated from the *Vinca rosea* plant (also referred to as *Catharanthus roseus*). Both plant-derived alkaloids in addition to vindesine **9**, vinorelbine **10**, and vinflunine **11** (**Figure 6.2**), which are semisynthetic derivatives of vinblastine, act as antitumour agents via occupying the vinca-binding domain on tubulin, resulting in destabilisation and suppression of microtubule dynamics (32, 33). Microtubules are key components of the cytoskeleton and contribute to a variety of important cellular functions, such as mitosis, cell signalling, intracellular transport, polarity, and maintenance of cell shape. The essential role of microtubules in cell division explains the potent activity of the aforementioned microtubules-targeting alkaloids against rapidly dividing cancer cells, wherein they interfere with cell cycle progression, thereby inducing apoptosis (32). Of note, vincristine exhibits the highest affinity to tubulin, followed by vindesine, vinblastine, vinorelbine, and vinflunine (vincristine > vindesine > vinblastine > vinorelbine > vinflunine) (34-36). The five alkaloids are currently important chemotherapeutic drugs that are widely administered in the treatment of different types of cancers.



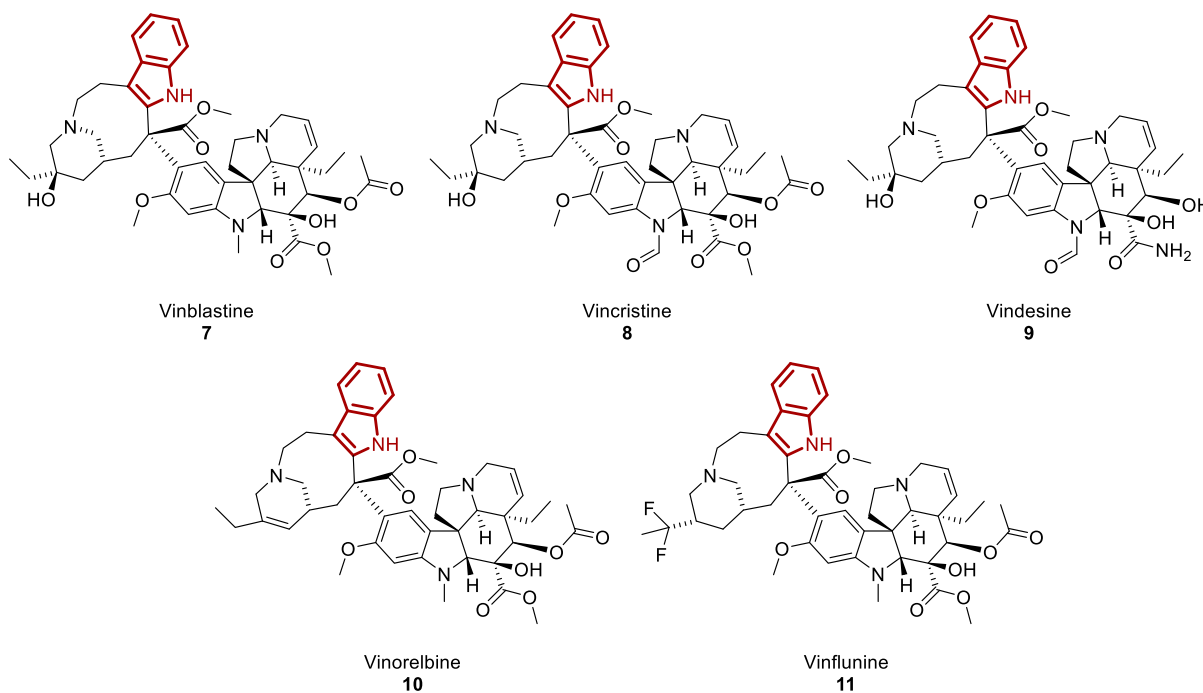


**Figure 6.2. Naturally occurring indole-based antitumour drugs.**

## 6.2. I2Cs as Antitumour Agents

### 6.2.1. Tubulin Polymerisation (TP) Inhibitors

Microtubules are imperative for the formation of mitotic spindles which constitute the key machinery required for successful mitosis (37). As mentioned above, they play a major role in maintaining the division, growth, and functioning of cells. Microtubules consist of two closely related heterodimers constituted of  $\alpha$ - and  $\beta$ -tubulin subunits. Perturbing the dynamics of the tubulin polymerisation into microtubules or, conversely, the depolymerisation of microtubules into tubulin, results in arrested cell division, followed by apoptosis (37). Inhibiting tubulin assembly or disassembly has proven to be clinically useful in suppressing the growth of different tumours. Within this context, inhibitors targeting either of the preceding key processes are referred to as antimetotics or spindle poisons (38). The most salient TP inhibitors are the Vinca alkaloids which are currently used in clinical settings as antitumour drugs (37).

Apart from the Vinca-derived TP inhibitors, colchicine **12** (Figure 6.3), another natural product, was also found to inhibit TP via binding to the  $\beta$ -tubulin at a site different from the Vinca alkaloids (38). Towards this, Keller *et al* investigated the activity of several I2C derivatives, combining some of the structural features of colchicine and Vinca

alkaloids (38). The I2C analogue **13** (**Figure 6.3**) was the highlight of their work which exhibited an  $IC_{50}$  value of  $1.9 \mu M$  against TP. This compound displayed potent antiproliferative activities, with cellular  $IC_{50}$  values ranging from  $30 - 70 \text{ nM}$ , against a wide variety of tumour cell lines, namely cervical carcinoma (KB), breast cancer (MDA-MB231, MDA-MB435, and MCF7), human non-small cell lung cancer (A549), skin melanoma (B16F10), leukemia (L1210, K562), and human colon cancer (HCT116 and HT29) (38). Notably, the growth inhibition exhibited by this compound was comparable to colchicine in the tumour cells in which both compounds were tested. Compound **13** impacted cell morphology in a way consistent with TP inhibition and induced apoptosis in three tumour cell lines in a dose-dependent manner. Additionally, it significantly reduced tumour progression in a human glioma graft model of U87 cells (38).

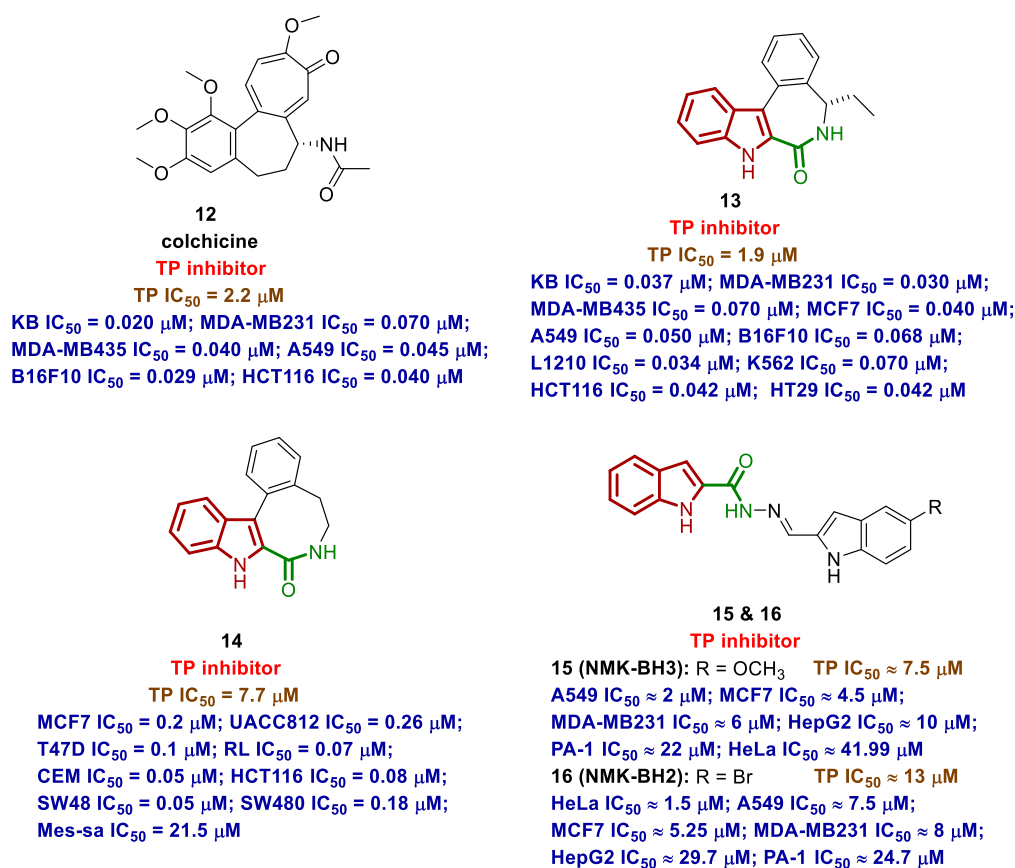


**Figure 6.3.** TP inhibition and antitumour activities of colchicine and I2C analogues.

A follow-on work was published a year later by Putey *et al*, wherein they replaced the indolobenzazepine core with indolobenzazocine (39). Expectedly, the I2C derivative **14** (**Figure 6.3**) in their study showed a potent inhibitory profile similar to compound **13**. It showed IC<sub>50</sub> value of 7.7 µM against TP. When tested against different tumour cells, namely breast cancer (MCF7, UACC812, and T47D), lymphoma (RL), T-cell acute lymphoblastic leukemia (CEM), and human colon cancer (HCT116, SW48, SW480), it displayed potent antiproliferative activities (IC<sub>50</sub> = 0.05 – 0.26 µM) (39). Only one cell line, denominated Mes-sa (uterine sarcoma), was less sensitive to **14** (IC<sub>50</sub> = 21.5 µM). The authors also performed a molecular modelling analysis, in which they docked compound **14** in the binding site of colchicine in tubulin. Their docking studies suggested that the indole ring of **14** is presumably overlaid with the trimethoxyphenyl moiety of colchicine **12** (39).

Similar to compound **14**, Das Mukherjee *et al* found that the hydrazone-derived I2C analogue **15** (NMK-BH3, **Figure 6.3**) has a specific and strong binding to tubulin, in a site very close to that of colchicine, in the molecular docking and tubulin-ligand fluorescence spectroscopy studies (40). In the *in vitro* assay, this compound potently inhibited the assembly of microtubules (IC<sub>50</sub> ≈ 7.5 µM). In the proliferation assay, compound **15** inhibited the growth of various tumour cell lines (IC<sub>50</sub> ≈ 2 – 22 µM) (40). The highest cytotoxic activity was displayed in the human lung adenocarcinoma cells (A549), followed by MCF7, MDA-MB231, human hepatocellular carcinoma (HepG2), and human ovarian carcinoma (PA-1). They also found that compound **15** induced cell cycle block, resulting in apoptosis, by depolymerising the microtubules of A549 cells. Importantly, this compound displayed limited cytotoxicity against healthy human cells, namely lung fibroblasts (WI38; IC<sub>50</sub> ≈ 48.5 µM) and peripheral blood mononuclear cells (PBMC; IC<sub>50</sub> ≈ 62 µM), suggesting its selectivity towards cancer cells (40).

A follow-up study, published by the same group in 2020, documented the activity profile of the bis (indolyl)-hydrazide-hydrazone analogue **16** (NMK-BH2, **Figure 6.3**), in which the methoxy group in **15** was replaced with a bromo group (41). This compound inhibited the TP in a concentration-dependent manner with IC<sub>50</sub> value of ≈ 13 µM. The I2C derivative **16** displayed a potent and selective antiproliferative activity towards cervical cancer cells (HeLa) compared to the other tested human tumour cells and non-cancerous cells (41). Of note, compound **15** demonstrated weak antiproliferative activity against HeLa cells (IC<sub>50</sub> ≈ 41.99 µM). The unique activity of

compound **16** against HeLa cells was attributed to its ability to target the tubulin-microtubule system via strong and rapid binding to tubulin at the binding site of colchicine (41). In fact, they found that this compound perturbed and disorganised the integrity of microtubules of HeLa cells, resulting in mitotic block and induction of cell death through both apoptosis and autophagy. Similar to compound **15**, the bromo analogue **16** showed moderate growth inhibition against A549, MCF7, and MDA-MB231 ( $IC_{50} \approx 7.5, 5.25, \text{ and } 8 \mu\text{M}$ , respectively), while it was marginally effective against HepG2 and PA-1 cancer cell lines ( $IC_{50} \approx 29.7 \text{ and } 24.7 \mu\text{M}$ , respectively) (40, 41). Additionally, when tested against normal cell lines, this compound exhibited negligible cytotoxicity against WI38 ( $IC_{50} \approx 41.5 \mu\text{M}$ ), PBMC ( $IC_{50} \approx 50 \mu\text{M}$ ), and human embryonic kidney cells (HEK;  $IC_{50} \approx 46.5 \mu\text{M}$ ) (41). Overall, the preceding colchicine-mimicking I2C analogues embody the significance of the I2C structure core in inhibiting the polymerisation of tubulin and the growth of a vast array of tumour cells.

### 6.2.2. Myeloid Cell Leukemia-1 (Mcl-1) Inhibitors

Mcl-1 is an antiapoptotic member of the B-cell lymphoma 2 (Bcl-2) family of proteins which are the main regulators of apoptosis, a programmed cell death responsible for the elimination of unwanted tumour cells (42, 43). Abnormal cells enhance their survival by breaking down the balance between the antiapoptotic and proapoptotic proteins in the Bcl-2 family. The resulting imbalance leads to disruptions in the normal apoptotic pathways which contribute to carcinogenesis (42, 43). One of the ways that tumour cells use to subvert apoptosis is by upregulating the antiapoptotic Mcl-1 protein. Indeed, amplification of Mcl-1 gene is one of the most commonly found genetic aberrations in human cancers. In addition, several reports have shown that downregulating the expression of Mcl-1 gene suppresses the growth of various cancer cell types (42, 43). Therefore, inhibiting the activity of Mcl-1 protein is considered an effective approach for the development of new chemotherapeutic agents. Several I2Cs were shown to potently inhibit the activity of Mcl-1 (42, 43). In the Mcl-1 binding assay, compounds **17 – 19 (Figure 6.4)** demonstrated a single-digit nanomolar (nM)  $K_i$  values [ $K_i = 2.1 \text{ nM}$  (**17**) and  $< 1.0 \text{ nM}$  (**18** and **19**)] (42). When tested against the Mcl-1 sensitive multiple myeloma cell line H929, the three I2Cs **17 – 19** displayed growth inhibitory concentrations against cell proliferation in the low-micromolar range ( $GI_{50} = 6.4, 1.4, \text{ and } 2.0 \mu\text{M}$ , respectively). On the contrary, when tested against myelogenous leukemia K562 cell line, which is resistant to Mcl-1 inhibitors, the preceding

compounds showed a markedly lower antitumour activities (42). These results in turn substantiate the Mcl-1-mediated antitumour activity of these compounds.

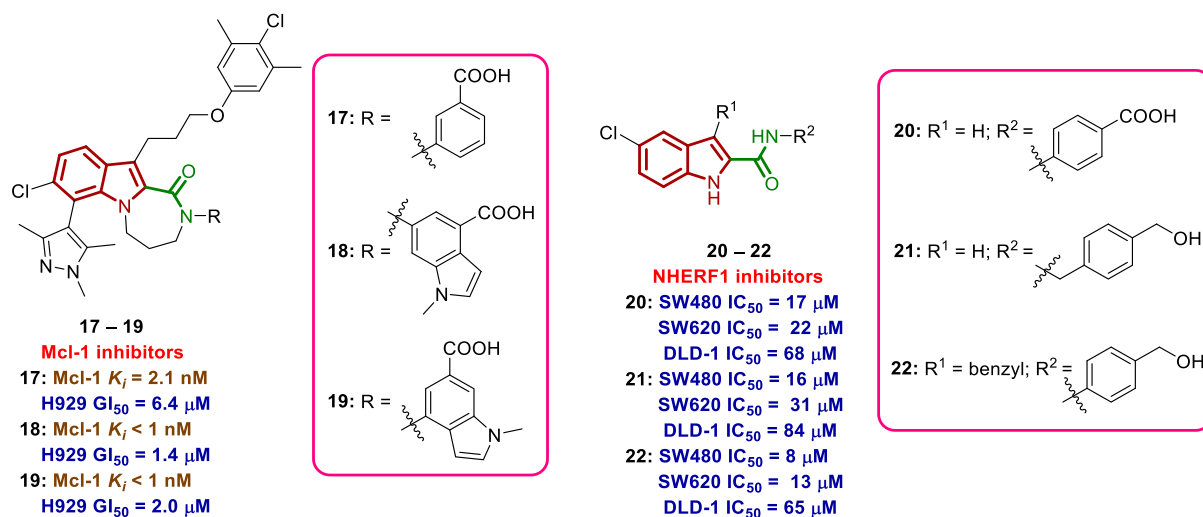


Figure 6.4. I2C-based Mcl-1 (17 – 19) and NHERF1 (20 – 22) inhibitors as antitumour agents.

### 6.2.3. Na<sup>+</sup>/H<sup>+</sup> Exchanger 3 Regulating Factor 1 (NHERF1) Inhibitors

NHERF1 is a scaffolding "Janus like" protein that can behave as a tumour suppressor and as an oncogene (44). Scaffold proteins bring together two or more protein entities, such as cytoplasmic signalling molecules and membrane transporters/receptors, allowing the formation of macromolecular complexes. Accordingly, these scaffolds partake in coordinating and positively or negatively regulating key signalling pathways (44). Indeed, the protein-protein interactions between NHERF1 and different molecules were found to be involved in cancer signalling. The interplay between NHERF1 and various prominent signalling pathways as well as the implication/relevance thereof in tumourigenesis and cancer progression was previously reviewed (44). Recently, Coluccia *et al* performed molecular modelling studies on numerous I2Cs within the postsynaptic density 95/discs large/zona occludens 1 (PDZ1) domain of NHERF1 (45). They identified several NHERF1 inhibitors with antitumour activities against three colorectal cancer (CRC) cell lines, namely SW480, SW620, and DLD-1. Three I2C analogues **20 – 22** displayed  $IC_{50}$  values ranging from 8 – 84  $\mu$ M against the foregoing tumour cells (**Figure 6.4**). Upon combining compound **22** with other antagonists of  $\beta$ -catenin, a CRC triggering protein,

they observed synergistic cell growth inhibition against the same CRC cell lines (45). Taken together, the aforementioned findings indicate the I2Cs potential in inhibiting the growth of different colorectal tumours.

#### 6.2.4. Androgen Receptor (AR) Binding Function 3 (BF3) Inhibitors

Since the discovery of the role of androgens in promoting the growth of prostate cancer (PCa) in the early 1940s, antiandrogens have been a vital component in the standard therapeutic care for PCa (46). Indeed, the first-generation antiandrogens flutamide, nilutamide, and bicalutamide in addition to the second-generation drug enzalutamide can efficiently block AR signalling pathways. In this respect, antiandrogens serve as competitive inhibitors/antagonists of the AR via binding to the androgen binding site (ABS), thereby blocking the binding of endogenous androgens and subsequently preventing receptor activation. However, after the initial success of antiandrogen therapy in PCa patients, many of them acquire resistance to treatment. Mutations in ABS (which switch AR antagonists to agonists) were found to be correlated with antiandrogens resistance (46). In fact, all current antiandrogens, even including the newly approved enzalutamide, interact with the same ABS location of the AR. The likelihood of cross resistance between these compounds is also high when mutations in the ABS arise, owing to their similar structural features. Therefore, alternative AR binding sites have been explored to overcome the antiandrogen resistance. One of these sites is BF3 of the ligand binding domain (LBD) of the AR, which was first identified by Estebanez-Perpina *et al* (47). BF3 is implicated in the recruitment of coregulators of AR which are important for AR-dependent gene expression (46).

Ban *et al* identified several I2C-based furan derivatives as selective and potent AR-BF3 inhibitors (46). Most of their I2C analogues demonstrated strong antitumour activities, in the low micromolar range, against both wild-type and drug-resistant PCa cells. Upon performing structure-based pharmacophore modelling, they discovered that these I2Cs target BF3. Compound **23** (**Figure 6.5**) was the highlight of their work which exhibited an IC<sub>50</sub> value of 0.70 µM against AR transcription in the cell-based enhanced green fluorescent protein (eGFP) assay, indicating its potent BF3 inhibition. Compound **23** was also evaluated for its capacity to reduce the expression of prostate specific antigen (PSA) in the prostatic cancer LNCaP cell line and enzalutamide-resistant MR49F cells (46). Remarkably, this compound potently inhibited the

expression of PSA in both cell lines with  $IC_{50}$  values of 0.84 and 2.18  $\mu\text{M}$ , respectively. Of note, the expression of PSA is dependent on the activity of AR in prostate epithelial cells. More importantly, this compound was highly efficacious in inhibiting the growth/proliferation of both LNCaP and MR49F cells ( $IC_{50}$  = 0.55 and 1.31  $\mu\text{M}$ , respectively) (46). The lack of cross resistance between the I2C **23** and enzalutamide suggests that both compounds target different binding sites in the AR. As expected, compound **23** showed no activity when tested against AR-independent PCa cells (46). Overall, these findings validate the I2Cs as viable antitumour agents against PCa cells, wherein they exert their activity via targeting AR-BF3.

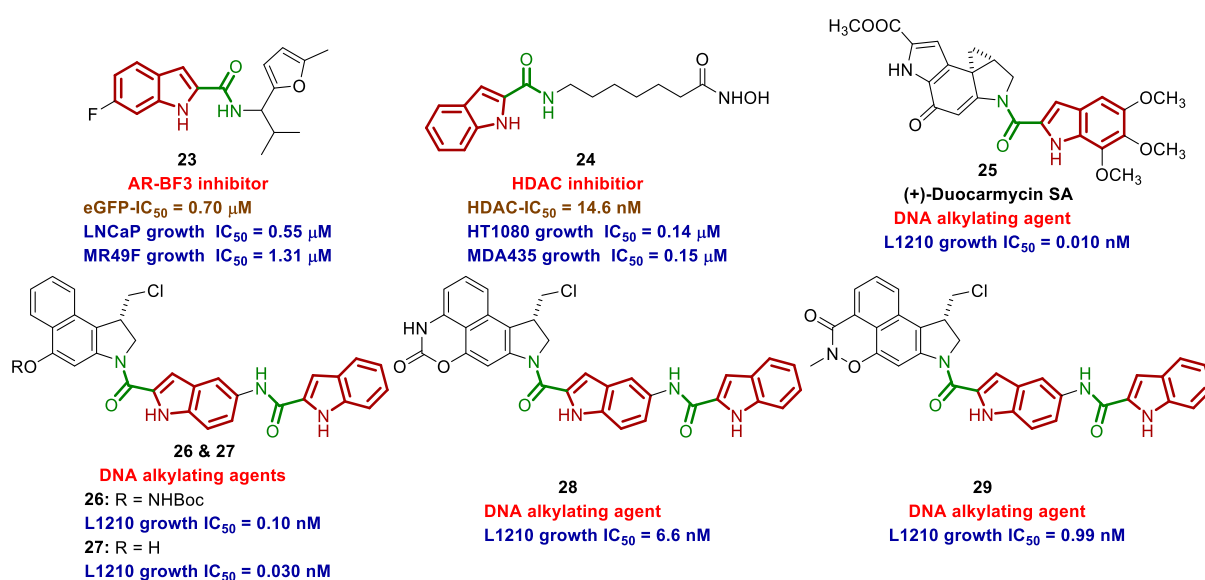


**Figure 6.5.** I2C-based AR-BF3 (**23**) and HDAC (**24**) inhibitors as well as DNA alkylators (**25 – 29**) as antitumour agents.

### 6.2.5. Histone Deacetylase (HDAC) Inhibitors

During the process of DNA packaging, histone proteins serve as key building blocks that contribute to several elaborate post-translational modifications, including acetylation (48). Two families of enzymes regulate the status of acetylation, namely histone acetyltransferases (HATs) and HDACs (48). In particular, HDACs were previously correlated with tumorigenesis, metastasis, and tumour angiogenesis (49). Indeed, improper recruitment of HDACs can result in excessive proliferation and malignancy due to the repression of a specific set of key genes (48). A series of hydroxamate-based I2C derivatives, with various substitutions at positions 4, 5, and 6

on the indole ring, were shown to potently inhibit the HDAC activity in the nanomolar range. In addition, these I2C analogues displayed potent antiproliferative activities, in the submicromolar range, when evaluated against human fibrosarcoma HT1080 and breast carcinoma MDA435 cell lines (48). The authors in this paper used the I2C analogue **24** [Figure 6.5; IC<sub>50</sub> = 14.6 nM (HDAC), 0.14 μM (HT1080), and 0.15 μM (MDA435)] as a representative of this class for further *in vivo* tests. Notably, this compound was found to be orally active in cancer animal model (HT1080 mouse xenograft), in which it displayed a significant tumour growth inhibition (48). These results suggest the prospects of I2Cs as orally active antitumour agents.

#### 6.2.6. DNA Alkylating Agents

Duocarmycin SA **25** (Figure 6.5) is one of the parent members of a class of molecules that mediate their antitumour activity via selectively alkylating the DNA duplex (50). Many DNA alkylating I2C-based duocarmycin analogues **26** – **29** (Figure 6.5) were identified as potent antitumour agents, both *in vitro* and *in vivo*, against murine L1210 leukemia cells (50-52). In 2010, Boger group investigated the antitumour activity of several I2C-derived prodrugs containing a tunable/weak N–O bond that is subjective to nucleophilic cleavage (reductive activation) (50). All of their prodrugs efficiently released the free drug *in vitro* (functional cellular assays) and in antitumour models *in vivo*. Compound **26** was the most potent prodrug therein, inhibiting the growth of L1210 cells (IC<sub>50</sub> = 0.10 nM), while the free analogue **27** and duocarmycin SA **25** displayed IC<sub>50</sub> values of 0.030 and 0.010 nM, respectively, against the same cell line. Interestingly, compound **26** surpassed the activity of the free drug **27** in an *in vivo* antitumour model of L1210 cells implanted into mice (50).

In a subsequent study conducted by the same group, another prodrug **28** was developed which showed an IC<sub>50</sub> value of 6.6 nM against L1210 tumour cells (51). Although this compound was less active than the corresponding free drug **27** *in vitro* (IC<sub>50</sub> = 0.030 nM), compound **28** was more efficacious and substantially safer/more tolerable in the L1210 tumour-bearing mice model than the parent drug **27**. In this regard, compound **28** was superior in extending the life expectancy of mice, wherein it displayed improved safety margin and was tolerated at doses 150-fold higher than the free drug **27** (51). Importantly, the cyclic carbamate ring in **28** provided more stability over the acyclic counterparts identified earlier by this group. This superior



stability in turn allowed a sustained, slow release of the free drug, permitting larger doses to be used safely which can attain more efficacious antitumour activity (51). The following year, a follow-up study was published in which the I2C-containing prodrug **29** was identified which displayed a similar behaviour as compounds **26** and **28** (52). The *in vitro* IC<sub>50</sub> of **29** against L1210 cells was 0.99 nM, which is less than the free drug **27** and higher than the analogous prodrug **28**. This compound also showed extraordinary activity in leukemia mouse models, substantially exceeding the efficacy of the parent drug **27** (52). Indeed, like compound **28**, the I2C analogue **29** exhibited larger therapeutic window of efficacy compared to **27**, wherein it did not suffer from the characteristic toxicity correlated with the free drug even at 40-fold higher doses. In addition, similar to the prodrug **26**, compound **29** entails a weak N–O bond that is amenable to reductive cleavage, permitting a controlled release of the free active analogue (52). The remarkable antitumour activities of the preceding DNA alkylating agents *in vivo* indicate the great potential of the duocarmycin-mimicking I2C analogues for further advancements.

### 6.2.7. Miscellaneous

Several research groups reported potent growth inhibition of different tumour cell lines treated with various I2Cs; however, the exact antitumour mechanism of these analogues was not fully defined. First, Burlison *et al* investigated the structure-activity relationship (SAR) of numerous novobiocin **30** (**Figure 6.6**) analogues as antitumour agents (53). Novobiocin is an aminocoumarin natural product that inhibits DNA gyrase and has potent antibacterial activity against different microbial strain, including *M. tb* [minimum inhibitory concentration (MIC) against H37Rv = 2 µg/mL (54)]. The antitumour activity of novobiocin was previously evaluated in several studies, wherein it failed to exhibit considerable antiproliferative activity against different tested tumour cells (55, 56). When Burlison and colleagues replaced the prenylated benzamide side chain in novobiocin **30** with the indole nucleus in compound **31** (**Figure 6.6**), a remarkable improvement in the antiproliferative activity against a wide range of tumour cells was observed (IC<sub>50</sub> = 0.17 – 22.3 µM) (53). The tested tumour cell lines comprised breast cancer (SkBr3 and MCF7), colon cancer (HCT116), pancreatic cancer (PL45), and prostate cancer (LNCaP and PC-3). Notably, the I2C-derived novobiocin analogue **31** displayed an exquisite antiproliferative activity against PL45 (IC<sub>50</sub> = 0.47 µM), a very aggressive pancreatic ductal adenocarcinoma that is resistant

to chemotherapies and is associated with high mortality rates (53). Although the antimicrobial activity of compound **31** was not explored therein, it would be intriguing to uncover the anti-TB activity of this compound as well as its efficacy against other bacterial species.

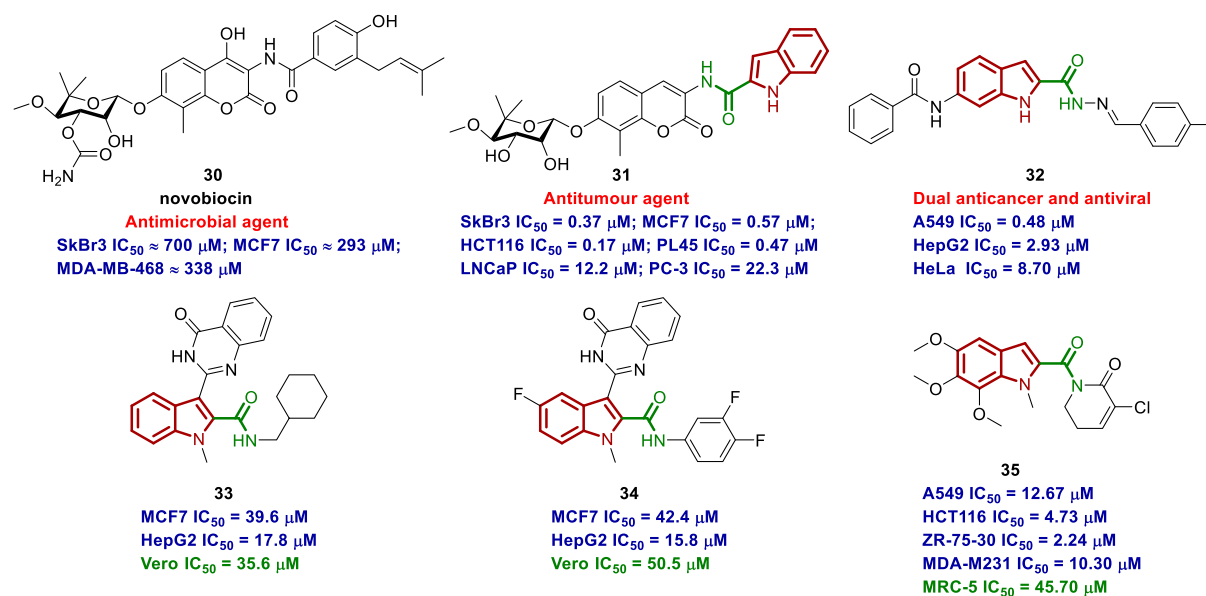


**Figure 6.6. Novobiocin and miscellaneous I2C-based antitumour agents.**

On the other hand, Hu *et al* showed the dual pharmacology profile of compound **32** (Figure 6.6) as potent antitumour and anti-HIV agent (57). This compound structurally resembled the hydrazone-derived I2C analogues **15** and **16** (Figure 6.3) which were shown to exert their antitumour activity via inhibiting TP, eliciting apoptosis in A549 and HeLa tumour cells, respectively (40, 41). Relatedly, the antitumour activity of compound **32** against A549 was found to be likely attributed to induction of cell apoptosis via inhibiting Ser2 phosphorylation in the C-terminal domain (CTD) of RNA polymerase II (RNAPII) (57). Of note, cyclin-dependent kinase 9 (CDK9) was found to promote RNA synthesis via phosphorylating Ser2 in the CTD of RNAPII (58). In addition, CDK9 was also found to play a vital role in the replication of HIV-1 (59). Therefore, CDK9 constitutes an important target for the development of novel anticancer and anti-HIV agents. Indeed, various CDK9 inhibitors, such as flavopiridol and seliciclib, have been reported to have dual anticancer and anti-HIV activities (57). Similarly, the benzylidene-linked I2C analogue **32** showed potent antiproliferative

activity against A549, HepG2, and HeLa tumour cells ( $IC_{50} = 0.48 - 8.70 \mu M$ ). This compound also demonstrated an excellent inhibitory activity against HIV-1 (57).

In 2016, Gokhale *et al* reported the antiproliferative activity of multiple I2C derivatives bearing a quinazolinone moiety at position 3 of the indole ring (60). Two compounds **33** and **34** (**Figure 6.6**) showed the highest cytotoxic activities therein against the tumour cell lines MCF7 and HepG2. Both compounds showed weak cytotoxic activities against non-tumourigenic Vero cells ( $IC_{50} = 35.6$  and  $50.5 \mu M$ , respectively), reflecting the modest selectivity of these compounds towards HepG2 (60). Finally, in 2019, Lu *et al* investigated the activity of several trimethoxy I2C analogues based on piperlongumine, a natural product that was reported to have multiple biological activities, including anticancer (61). Compound **35** (**Figure 6.6**) was the most active antiproliferative agent in their study, displaying good activity against four tumour cell lines ( $IC_{50} = 2.24 - 12.67 \mu M$ ), namely A549, HCT116, human breast ductal carcinoma (ZR-75-30), and MDA-MB231. While the anticancer mechanism of piperlongumine was attributed to increasing the level of reactive oxygen species (ROS), leading to apoptotic cell death, compound **35** exhibited no effect on the ROS level (61). However, this I2C-derived piperlongumine analogue showed more potent apoptotic effect in A549 cells (92.6%) at  $10 \mu M$  concentration, compared to piperlongumine (77.7%), indicating that both compounds induce apoptosis via different mechanisms of action. Importantly, compound **35** showed negligible cytotoxicity towards normal human lung fibroblast cell line MRC-5 ( $IC_{50} = 45.70 \mu M$ ), indicating its moderate selective activity towards cancer cells. This compound significantly inhibited the tumour growth of A549 lung cancer xenograft (54.6%), showing a comparable activity to the antitumour drug doxorubicin (53.3%) and exceeding the activity of piperlongumine (38.3%) (61). Overall, although the mechanisms of action of the preceding I2Cs were not precisely characterised, the activity profiles of some of these analogues suggest their low cytotoxicity towards healthy cells compared to cancer cells. Additionally, it can be inferred that the I2C-based derivatives could be repurposed against various diseases (polypharmacological agents).

### 6.3. I2Cs with Dual Anti-TB and Antitumour Activities

In addition to the antitumour profile previously reported for the hydrazone-derived I2C analogues (*vide supra*), Cihan-Üstündağ *et al* identified the indole-2-carbohydrazide

analogue **36** (**Figure 6.7**) which possessed dual antitumour and anti-TB activities. This compound inhibited the growth of *M. tb* H37Rv strain by 58% at 6.25 µg/mL concentration (62). It was also tested against 60 tumour cell lines, encompassing leukemia, melanoma, breast cancer, ovarian cancer, prostate cancer, renal cancer, colon cancer, CNS cancer, and non-small cell lung cancer. The antitumour activities were represented in the form of  $\log_{10}GI_{50}$ ,  $\log_{10}TGI$ , and  $\log_{10}LC_{50}$ , in which  $GI_{50}$  is the concentration eliciting 50% inhibition of cell growth, TGI is the concentration causing total growth inhibition, and  $LC_{50}$  is the concentration evoking 50% of cell death. The cut-off value for activity from the standpoint of the authors was -4, whereupon compounds with  $\log_{10}GI_{50} = -4$  and  $< -4$  were declared active (62).

Compound **36** exhibited  $\log_{10}GI_{50} = -5.23 - -4.01$  in 57 tumour cell lines and  $\log_{10}GI_{50} > -4$  in the remaining three cell lines. However, this compound was not the highlight of their study. The I2C-based spirothiazolidinone **37** (**Figure 6.7**) was the most potent dual anti-TB and antitumour compound identified therein (62). It showed 82% inhibition towards *M. tb* H37Rv strain at 6.25 µg/mL concentration. This I2C derivative was the most potent antitumour compound in their study, demonstrating  $\log_{10}GI_{50}$  values ranging from -6.09 to -4.26 against all tested tumour cell lines, with the highest activity manifested in leukemia cell lines (62). In 2016, the same group reported the antiproliferative activity of the I2C hydrazone analogue **38** (**Figure 6.7**) against 60 tumour cell lines, similar to their previously used panel (63). Unlike the homologous derivative **36**, compound **38** was inactive against H37Rv *M. tb* strain (MIC > 25 µg/mL); however, it displayed remarkable inhibitory activities against the proliferation of 57 different tumour cell lines ( $GI_{50} = 13 - 74$  nM) (63). Taken together, the I2C-based agents seem to have the ability to potently interact with multiple targets and impact key pathways in various diseases. In addition, the dual anti-TB and anti-tumour activities of **36** versus the selective antitumour activity of the analogous derivative **38** indicate the possibility of customising the I2C framework to attain a particular biological activity.

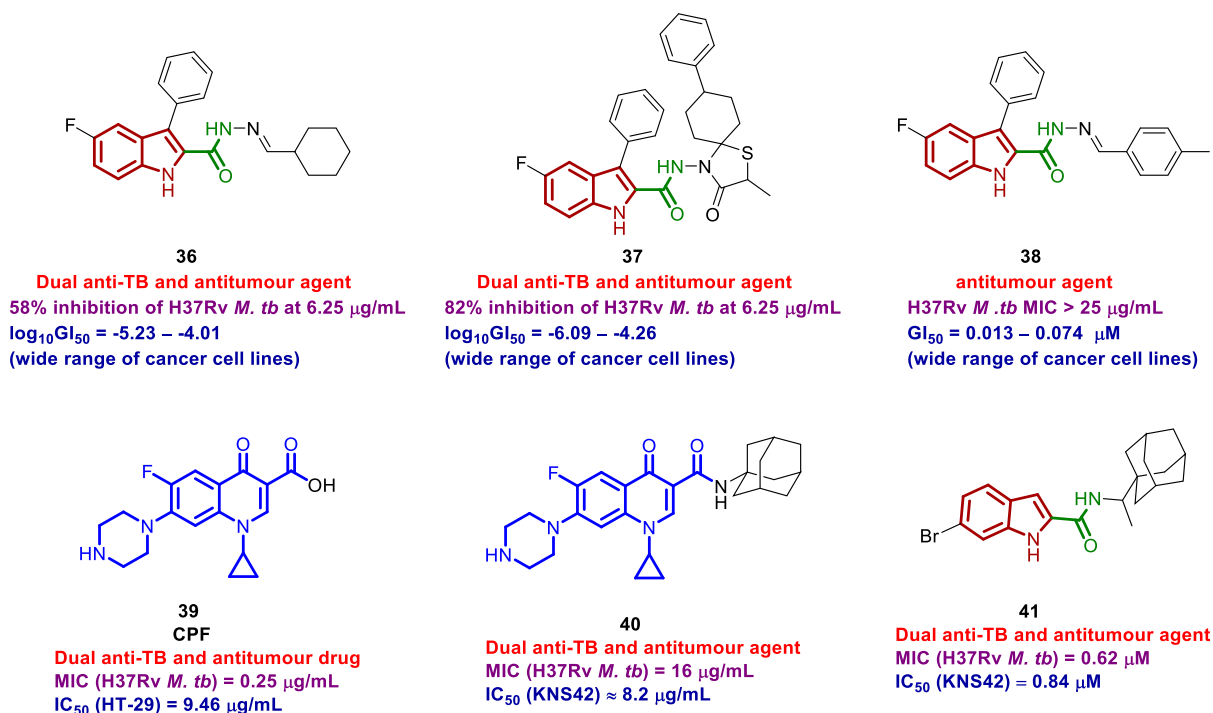


**Figure 6.7. Compounds evaluated for their anti-TB and antitumour activities.** The I2C analogues **36 – 38** were assessed in Cihan-Üstündağ *et al* studies. The antiproliferative activity of CPF **39** was determined by Bourikas *et al*. The anti-TB activity of **39 – 41** and the antitumour activity of **40** and **41** against KNS42 cells were evaluated by our group in this PhD project.

#### 6.4. Design and Synthesis of Novel I2C-Based Small Molecules as Anti-TB and Antitumour Agents

The concept of drug repositioning (also termed as drug repurposing, drug re-tasking, drug reprofiling, or therapeutic switching) is firmly established in the literature (64-66). One of the famous examples of repurposed drugs is Pfizer's blockbuster drug sildenafil (Viagra®) which was originally developed for treating hypertension and angina pectoris. However, based on observations during clinical trials, sildenafil was serendipitously repositioned and marketed as a treatment for erectile dysfunction (64-66). Interestingly, many fluoroquinolone (FQ) drugs in the market (quinolone-based broad-spectrum antibiotics) were also found to have potent anticancer activity (67). In particular, CPF **39** (Figure 6.7), the well-known anti-TB drug, was previously shown to inhibit the proliferation and induce apoptosis in various cancer cell lines, including colon carcinoma, osteosarcoma, leukemia, and bladder carcinoma (68). The  $IC_{50}$  value of CPF was 9.46 µg/mL when tested against the proliferation of colon cancer cell line HT-29 (69).

Based on the well-documented antitumour activity of CPF, the adamantane-linked CPF analogue **40** (**Figure 6.7**) which exhibited an MIC value of 16 µg/mL against H37Rv strain (discussed in Chapter 5), was tested for its antiproliferative activity against paediatric GBM cell line KNS42. Our results revealed the potent growth inhibitory activity of this compound ( $IC_{50} \approx 8.2$  µg/mL) against KNS42 tumour cells (unpublished results), resembling the aforementioned antiproliferative activity of CPF against HT-29 tumour cells. These findings indicate the dual anti-TB and anti-tumour activity of CPF **39** and our *N*-adamantyl CPF analogue **40**. Therefore, the homologous *N*-adamantane quinolone-2-carboxamides and quinolone-3-carboxamides (discussed in Chapter 3) were further evaluated for their antitumour activities against KNS42 cells. The corresponding results are detailed and discussed in Chapter 7.

Motivated by the above-mentioned collated evidence on the antitumour potential of the I2Cs and the dual anti-TB and antitumour activities of compounds **36** and **37**, several new I2C analogues were designed and synthesised. All final compounds and one intermediate were evaluated for their growth inhibition against *M. tb* and grade IV GBM KNS42 tumour cells (results published in our 2021 research article). Several I2C derivatives showed dual potent anti-TB and cytotoxic activities against KNS42 cells. The most potent multi-target directed ligand was the *N*-rimantadine I2C derivative **41** (**Figure 6.7**; H37Rv MIC = 0.62 µM and KNS42 viability  $IC_{50}$  = 0.84 µM). Equally important, compound **41** showed limited cytotoxicity towards healthy Vero cells ( $IC_{50}$  = 39.9 µM), suggesting its selectivity towards *M. tb* and KNS42 tumour cells. The top potent I2C analogues in the proliferation and viability assays against KNS42 cells showed no inhibitory activity against *M. tb* H37Rv strain (MIC > 32 µg/mL). These most potent analogues were then evaluated against a panel of non-GBM grade IV paediatric tumours, namely teratoid/rhabdoid tumour cell lines BT12 and BT16 as well as medulloblastoma tumour cells DAOY. They were also tested for their cytotoxic activity against non-tumourigenic human fibroblasts HFF1 cells. Our recently published RSC Advances research article is enclosed herein.

## References

1. Baeyer A. Ueber die Reduction aromatischer Verbindungen mittelst Zinkstaub. *Justus Liebigs Annalen der Chemie*. 1866;140(3):295-6.
2. Robinson B. The Fischer Indole Synthesis. *Chemical Reviews*. 1963;63(4):373-401.
3. Van Order RB, Lindwall HG. Indole. *Chemical Reviews*. 1942;30(1):69-96.
4. Taber DF, Tirunahari PK. Indole synthesis: a review and proposed classification. *Tetrahedron*. 2011;67(38):7195-210.
5. Gribble GW. Recent developments in indole ring synthesis—methodology and applications. *Journal of the Chemical Society, Perkin Transactions 1*. 2000(7):1045-75.
6. de Sa Alves FR, Barreiro EJ, Fraga CA. From nature to drug discovery: the indole scaffold as a 'privileged structure'. *Mini Rev Med Chem*. 2009;9(7):782-93.
7. Evans BE, Rittle KE, Bock MG, DiPardo RM, Freidinger RM, Whitter WL, et al. Methods for drug discovery: development of potent, selective, orally effective cholecystokinin antagonists. *J Med Chem*. 1988;31(12):2235-46.
8. Welsch ME, Snyder SA, Stockwell BR. Privileged scaffolds for library design and drug discovery. *Curr Opin Chem Biol*. 2010;14(3):347-61.
9. Humphrey GR, Kuethe JT. Practical methodologies for the synthesis of indoles. *Chem Rev*. 2006;106(7):2875-911.
10. Kaushik NK, Kaushik N, Attri P, Kumar N, Kim CH, Verma AK, et al. Biomedical importance of indoles. *Molecules*. 2013;18(6):6620-62.
11. Gul W, Hamann MT. Indole alkaloid marine natural products: An established source of cancer drug leads with considerable promise for the control of parasitic, neurological and other diseases. *Life Sciences*. 2005;78(5):442-53.
12. Rosales PF, Bordin GS, Gower AE, Moura S. Indole alkaloids: 2012 until now, highlighting the new chemical structures and biological activities. *Fitoterapia*. 2020;143:104558.
13. Chung KR, Shilts T, Erturk U, Timmer LW, Ueng PP. Indole derivatives produced by the fungus *Colletotrichum acutatum* causing lime anthracnose and postbloom fruit drop of citrus. *FEMS Microbiol Lett*. 2003;226(1):23-30.
14. Kobayashi M, Aoki S, Gato K, Matsunami K, Kurosu M, Kitagawa I. Marine natural products. XXXIV. Trisindoline, a new antibiotic indole trimer, produced by a

bacterium of *Vibrio* sp. separated from the marine sponge *Hyrtilia altum*. *Chem Pharm Bull (Tokyo)*. 1994;42(12):2449-51.

15. Almeida MC, Resende D, da Costa PM, Pinto MMM, Sousa E. Tryptophan derived natural marine alkaloids and synthetic derivatives as promising antimicrobial agents. *Eur J Med Chem*. 2020;112945.
16. Slominski A, Semak I, Pisarchik A, Sweatman T, Szczesniowski A, Wortsman J. Conversion of L-tryptophan to serotonin and melatonin in human melanoma cells. *FEBS Lett*. 2002;511(1-3):102-6.
17. Slominski A, Pisarchik A, Semak I, Sweatman T, Wortsman J, Szczesniowski A, et al. Serotonergic and melatonergic systems are fully expressed in human skin. *FASEB J*. 2002;16(8):896-8.
18. Sravanthi TV, Manju SL. Indoles - A promising scaffold for drug development. *Eur J Pharm Sci*. 2016;91:1-10.
19. Chadha N, Silakari O. Indoles as therapeutics of interest in medicinal chemistry: Bird's eye view. *Eur J Med Chem*. 2017;134:159-84.
20. Garg V, Maurya RK, Thanikachalam PV, Bansal G, Monga V. An insight into the medicinal perspective of synthetic analogs of indole: A review. *Eur J Med Chem*. 2019;180:562-612.
21. Kumari A, Singh RK. Medicinal chemistry of indole derivatives: Current to future therapeutic prospectives. *Bioorg Chem*. 2019;89:103021.
22. Vicente R. Recent advances in indole syntheses: new routes for a classic target. *Org Biomol Chem*. 2011;9(19):6469-80.
23. Nosova EV, Lipunova GN, Charushin VN, Chupakhin ON. Fluorine-containing indoles: Synthesis and biological activity. *Journal of Fluorine Chemistry*. 2018;212:51-106.
24. Ciulla MG, Kumar K. The natural and synthetic indole weaponry against bacteria. *Tetrahedron Lett*. 2018;59(34):3223-33.
25. Dadashpour S, Emami S. Indole in the target-based design of anticancer agents: A versatile scaffold with diverse mechanisms. *Eur J Med Chem*. 2018;150:9-29.
26. Han Y, Dong W, Guo Q, Li X, Huang L. The importance of indole and azaindole scaffold in the development of antitumor agents. *Eur J Med Chem*. 2020;203:112506.
27. Jia Y, Wen X, Gong Y, Wang X. Current scenario of indole derivatives with potential anti-drug-resistant cancer activity. *Eur J Med Chem*. 2020;200:112359.



28. Wan Y, Li Y, Yan C, Yan M, Tang Z. Indole: A privileged scaffold for the design of anti-cancer agents. *Eur J Med Chem.* 2019;183:111691.
29. Zhang MZ, Chen Q, Yang GF. A review on recent developments of indole-containing antiviral agents. *Eur J Med Chem.* 2015;89:421-41.
30. Qin HL, Liu J, Fang WY, Ravindar L, Rakesh KP. Indole-based derivatives as potential antibacterial activity against methicillin-resistance *Staphylococcus aureus* (MRSA). *Eur J Med Chem.* 2020;194:112245.
31. Usach I, Melis V, Peris JE. Non-nucleoside reverse transcriptase inhibitors: a review on pharmacokinetics, pharmacodynamics, safety and tolerability. *J Int AIDS Soc.* 2013;16:1-14.
32. Perez EA. Microtubule inhibitors: Differentiating tubulin-inhibiting agents based on mechanisms of action, clinical activity, and resistance. *Mol Cancer Ther.* 2009;8(8):2086-95.
33. Bates D, Eastman A. Microtubule destabilising agents: far more than just antimetabolic anticancer drugs. *Br J Clin Pharmacol.* 2017;83(2):255-68.
34. Jordan MA, Himes RH, Wilson L. Comparison of the effects of vinblastine, vincristine, vindesine, and vinorelbine on microtubule dynamics and cell proliferation in vitro. *Cancer Res.* 1985;45(6):2741-7.
35. Lobert S, Vulevic B, Correia JJ. Interaction of vinca alkaloids with tubulin: a comparison of vinblastine, vincristine, and vinorelbine. *Biochemistry.* 1996;35(21):6806-14.
36. Bennouna J, Campone M, Delord JP, Pinel MC. Vinflunine: a novel antitubulin agent in solid malignancies. *Expert Opin Investig Drugs.* 2005;14(10):1259-67.
37. Jordan MA, Wilson L. Microtubules as a target for anticancer drugs. *Nat Rev Cancer.* 2004;4(4):253-65.
38. Keller L, Beaumont S, Liu JM, Thoret S, Bignon JS, Wdzieczak-Bakala J, et al. New C5-alkylated indolobenzazepinones acting as inhibitors of tubulin polymerization: cytotoxic and antitumor activities. *J Med Chem.* 2008;51(12):3414-21.
39. Putey A, Popowycz F, Do QT, Bernard P, Talapatra SK, Kozielski F, et al. Indolobenzazepin-7-ones and 6-, 8-, and 9-membered ring derivatives as tubulin polymerization inhibitors: synthesis and structure--activity relationship studies. *J Med Chem.* 2009;52(19):5916-25.
40. Das Mukherjee D, Kumar NM, Tantak MP, Das A, Ganguli A, Datta S, et al. Development of Novel Bis(indolyl)-hydrazide-Hydrazone Derivatives as Potent

Microtubule-Targeting Cytotoxic Agents against A549 Lung Cancer Cells. *Biochemistry*. 2016;55(21):3020-35.

41. Das Mukherjee D, Kumar NM, Tantak MP, Datta S, Ghosh Dastidar D, Kumar D, et al. NMK-BH2, a novel microtubule-depolymerising bis (indolyl)-hydrazide-hydrazone, induces apoptotic and autophagic cell death in cervical cancer cells by binding to tubulin at colchicine - site. *Biochim Biophys Acta Mol Cell Res*. 2020;1867(10):118762.

42. Lee T, Bian Z, Zhao B, Hogdal LJ, Sensintaffar JL, Goodwin CM, et al. Discovery and biological characterization of potent myeloid cell leukemia-1 inhibitors. *FEBS Lett*. 2017;591(1):240-51.

43. Pelz NF, Bian Z, Zhao B, Shaw S, Tarr JC, Belmar J, et al. Discovery of 2-Indole-acylsulfonamide Myeloid Cell Leukemia 1 (Mcl-1) Inhibitors Using Fragment-Based Methods. *J Med Chem*. 2016;59(5):2054-66.

44. Centonze M, Saponaro C, Mangia A. NHERF1 Between Promises and Hopes: Overview on Cancer and Prospective Openings. *Transl Oncol*. 2018;11(2):374-90.

45. Coluccia A, La Regina G, Naccarato V, Nalli M, Orlando V, Biagioni S, et al. Drug Design and Synthesis of First in Class PDZ1 Targeting NHERF1 Inhibitors as Anticancer Agents. *ACS Med Chem Lett*. 2019;10(4):499-503.

46. Ban F, Leblanc E, Li H, Munuganti RS, Frewin K, Rennie PS, et al. Discovery of 1H-indole-2-carboxamides as novel inhibitors of the androgen receptor binding function 3 (BF3). *J Med Chem*. 2014;57(15):6867-72.

47. Estebanez-Perpina E, Arnold LA, Nguyen P, Rodrigues ED, Mar E, Bateman R, et al. A surface on the androgen receptor that allosterically regulates coactivator binding. *Proc Natl Acad Sci U S A*. 2007;104(41):16074-9.

48. Dai Y, Guo Y, Guo J, Pease LJ, Li J, Marcotte PA, et al. Indole amide hydroxamic acids as potent inhibitors of histone deacetylases. *Bioorg Med Chem Lett*. 2003;13(11):1897-901.

49. Li Y, Seto E. HDACs and HDAC Inhibitors in Cancer Development and Therapy. *Cold Spring Harb Perspect Med*. 2016;6(10).

50. Lajiness JP, Robertson WM, Dunwiddie I, Broward MA, Vielhauer GA, Weir SJ, et al. Design, synthesis, and evaluation of duocarmycin O-amino phenol prodrugs subject to tunable reductive activation. *J Med Chem*. 2010;53(21):7731-8.

51. Wolfe AL, Duncan KK, Parelkar NK, Weir SJ, Vielhauer GA, Boger DL. A novel, unusually efficacious duocarmycin carbamate prodrug that releases no residual byproduct. *J Med Chem.* 2012;55(12):5878-86.
52. Wolfe AL, Duncan KK, Parelkar NK, Brown D, Vielhauer GA, Boger DL. Efficacious cyclic N-acyl O-amino phenol duocarmycin prodrugs. *J Med Chem.* 2013;56(10):4104-15.
53. Burlison JA, Avila C, Vielhauer G, Lubbers DJ, Holzbeierlein J, Blagg BS. Development of novobiocin analogues that manifest anti-proliferative activity against several cancer cell lines. *J Org Chem.* 2008;73(6):2130-7.
54. Shirude PS, Madhavapeddi P, Tucker JA, Murugan K, Patil V, Basavarajappa H, et al. Aminopyrazinamides: novel and specific GyrB inhibitors that kill replicating and nonreplicating Mycobacterium tuberculosis. *ACS Chem Biol.* 2013;8(3):519-23.
55. Montoir D, Barille-Nion S, Tonnerre A, Juin P, Duflos M, Bazin MA. Novel 1,6-naphthyridin-2(1H)-ones as potential anticancer agents targeting Hsp90. *Eur J Med Chem.* 2016;119:17-33.
56. Zhao H, Donnelly AC, Kusuma BR, Brandt GE, Brown D, Rajewski RA, et al. Engineering an antibiotic to fight cancer: optimization of the novobiocin scaffold to produce anti-proliferative agents. *J Med Chem.* 2011;54(11):3839-53.
57. Hu H, Wu J, Ao M, Wang H, Zhou T, Xue Y, et al. Synthesis, structure-activity relationship studies and biological evaluation of novel 2,5-disubstituted indole derivatives as anticancer agents. *Chem Biol Drug Des.* 2016;88(5):766-78.
58. Kempf C, Bathe F, Fischer R. Evidence that two Pcl-like cyclins control Cdk9 activity during cell differentiation in *Aspergillus nidulans* asexual development. *Eukaryot Cell.* 2013;12(1):23-36.
59. Rice AP. Cyclin-dependent kinases as therapeutic targets for HIV-1 infection. *Expert Opin Ther Targets.* 2016;20(12):1453-61.
60. Gokhale N, Panathur N, Dalimba U, Nayak PG, Pai KSR. Novel Indole-Quinazolinone Based Amides as Cytotoxic Agents. *J Heterocyclic Chem.* 2016;53(2):513-24.
61. Lu F, Chen B, Wang C, Zhuang C, Miao Z, Zhang X, et al. Design, synthesis, and biological evaluation of novel trimethoxyindole derivatives derived from natural products. *Monatshefte für Chemie - Chemical Monthly.* 2019;150(8):1545-52.
62. Cihan-Ustundag G, Capan G. Synthesis and evaluation of functionalized indoles as antimycobacterial and anticancer agents. *Mol Divers.* 2012;16(3):525-39.

63. Cihan-Ustundag G, Satana D, Ozhan G, Capan G. Indole-based hydrazide-hydrazones and 4-thiazolidinones: synthesis and evaluation as antitubercular and anticancer agents. *J Enzyme Inhib Med Chem*. 2016;31(3):369-80.
64. Pushpakom S, Iorio F, Eyers PA, Escott KJ, Hopper S, Wells A, et al. Drug repurposing: progress, challenges and recommendations. *Nat Rev Drug Discov*. 2019;18(1):41-58.
65. Talevi A, Bellera CL. Challenges and opportunities with drug repurposing: finding strategies to find alternative uses of therapeutics. *Expert Opin Drug Discov*. 2020;15(4):397-401.
66. Tartaglia LA. Complementary new approaches enable repositioning of failed drug candidates. *Expert Opin Investig Drugs*. 2006;15(11):1295-8.
67. Idowu T, Schweizer F. Ubiquitous Nature of Fluoroquinolones: The Oscillation between Antibacterial and Anticancer Activities. *Antibiotics (Basel)*. 2017;6(4).
68. Herold C, Ocker M, Ganslmayer M, Gerauer H, Hahn EG, Schuppan D. Ciprofloxacin induces apoptosis and inhibits proliferation of human colorectal carcinoma cells. *Br J Cancer*. 2002;86(3):443-8.
69. Bourikas LA, Kolios G, Valatas V, Notas G, Drygiannakis I, Pelagiadis I, et al. Ciprofloxacin decreases survival in HT-29 cells via the induction of TGF-beta1 secretion and enhances the anti-proliferative effect of 5-fluorouracil. *Br J Pharmacol*. 2009;157(3):362-70.

## STATEMENT OF CONTRIBUTION TO A CO-AUTHORED PUBLISHED PAPER

The second half of Chapter 6 includes a co-authored research article that has been published online in the RSC Advances journal (2021)

DOI: <https://doi.org/10.1039/D0RA10728J>

Publication link: <https://pubs.rsc.org/en/content/articlelanding/2021/ra/d0ra10728j>

Title: **Design, synthesis and evaluation of novel indole-2-carboxamides for growth inhibition of *Mycobacterium tuberculosis* and paediatric brain tumour cells**

Authors/Co-authors: **Shahinda S. R. Alsayed**, Shichun Lun, Anders W. Bailey, Amreena Suri, Chiang-Ching Huang, Mauro Mocerino, Alan Payne, Simone Treiger Sredni, William R. Bishai and Hendra Gunosewoyo

My contribution to the paper involved: 1) the conception, design, synthesis, purification, and chemical analysis of all the tested molecules, 2) interpreting all the results (chemistry and biology wise), 3) molecular docking of the compounds, 4) collecting and organising the information/data/references, 5) analysing the differential gene expression data and determining the potential mechanism of action of the novel analogues as antitumour agents, and 6) preparing and writing up the whole manuscript.

(Signed)  (Date) 20/09/2021

Shahinda Sayed Rabie Alsayed

(Countersigned)  (Date) 20/9/21

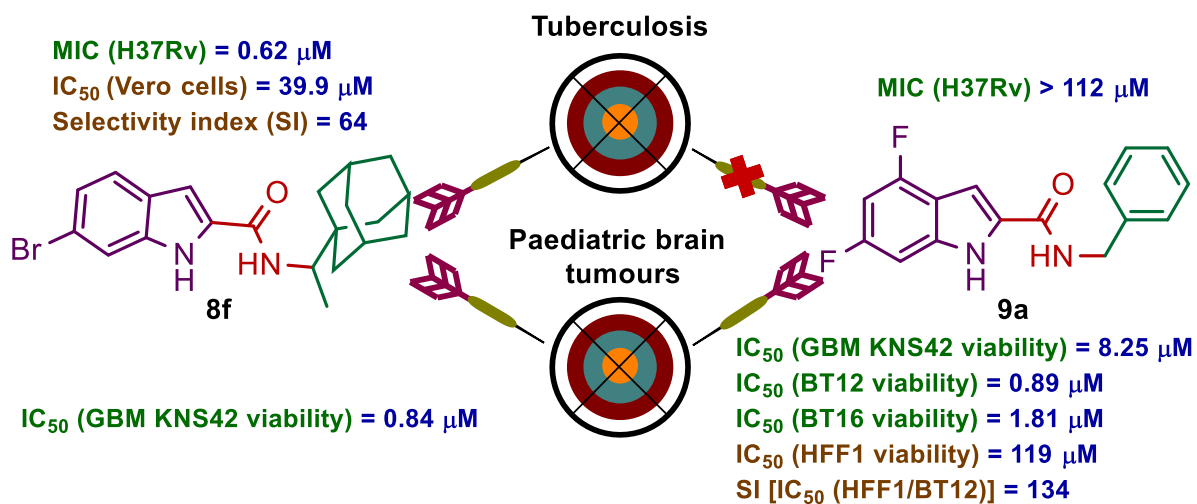
Corresponding author of the paper: Dr Hendra Gunosewoyo

(Countersigned)  (Date) 20/9/21

Main supervisor: Dr Hendra Gunosewoyo

# Graphical Abstract

## Polypharmacology of Indoleamide Chemotype




 Cite this: *RSC Adv.*, 2021, 11, 15497

# Design, synthesis and evaluation of novel indole-2-carboxamides for growth inhibition of *Mycobacterium tuberculosis* and paediatric brain tumour cells†

 Shahinda S. R. Alsayed,<sup>a</sup> Shichun Lun,<sup>b</sup> Anders W. Bailey,<sup>c</sup> Amreena Suri,<sup>c</sup> Chiang-Ching Huang,<sup>d</sup> Mauro Mocerino,<sup>e</sup> Alan Payne,<sup>e</sup> Simone Treiger Sredni,<sup>\*cf</sup> William R. Bishai<sup>\*bg</sup> and Hendra Gunosewoyo<sup>id</sup> <sup>\*a</sup>

The omnipresent threat of tuberculosis (TB) and the scant treatment options thereof necessitate the development of new antitubercular agents, preferably working *via* a novel mechanism of action distinct from the current drugs. Various studies identified the mycobacterial membrane protein large 3 transporter (MmpL3) as the target of several classes of compounds, including the indole-2-carboxamides. Herein, several indoleamide analogues were rationally designed, synthesised, and evaluated for their antitubercular and antitumour activities. Compound **8g** displayed the highest activity (MIC = 0.32  $\mu$ M) against the drug-sensitive (DS) *Mycobacterium tuberculosis* (*M. tb*) H37Rv strain. This compound also exhibited high selective activity towards *M. tb* over mammalian cells [IC<sub>50</sub> (Vero cells) = 40.9  $\mu$ M, SI = 128], suggesting its minimal cytotoxicity. In addition, when docked into the MmpL3 active site, **8g** adopted a binding profile similar to the indoleamide ligand ICA38. A related compound **8f** showed dual antitubercular (MIC = 0.62  $\mu$ M) and cytotoxic activities against paediatric glioblastoma multiforme (GBM) cell line KNS42 [IC<sub>50</sub> (viability) = 0.84  $\mu$ M]. Compound **8f** also showed poor cytotoxic activity against healthy Vero cells (IC<sub>50</sub> = 39.9  $\mu$ M). Compounds **9a** and **15**, which were inactive against *M. tb*, showed potent cytotoxic (IC<sub>50</sub> = 8.25 and 5.04  $\mu$ M, respectively) and antiproliferative activities (IC<sub>50</sub> = 9.85 and 6.62  $\mu$ M, respectively) against KNS42 cells. Transcriptional analysis of KNS42 cells treated with compound **15** revealed a significant downregulation in the expression of the carbonic anhydrase 9 (CA9) and the spleen tyrosine kinase (SYK) genes. The expression levels of these genes in GBM tumours were previously shown to contribute to tumour progression, suggesting their involvement in our observed antitumour activities. Compounds **9a** and **15** were selected for further evaluations against three different paediatric brain tumour cell lines (BT12, BT16 and DAOY) and non-neoplastic human fibroblast cells HFF1. Compound **9a** showed remarkable cytotoxic (IC<sub>50</sub> = 0.89 and 1.81  $\mu$ M, respectively) and antiproliferative activities (IC<sub>50</sub> = 7.44 and 6.06  $\mu$ M, respectively) against the two tested atypical teratoid/rhabdoid tumour (AT/RT) cells BT12 and BT16. Interestingly, compound **9a** was not cytotoxic when tested against non-neoplastic HFF1 cells [IC<sub>50</sub> (viability) = 119  $\mu$ M]. This suggests that an indoleamide scaffold can be fine-tuned to confer a set of derivatives with selective antitubercular and/or antitumour activities.

 Received 22nd December 2020  
 Accepted 10th April 2021

DOI: 10.1039/d0ra10728j

[rsc.li/rsc-advances](http://rsc.li/rsc-advances)

## 1. Introduction

*Mycobacterium tuberculosis* (*M. tb*), the causative agent of tuberculosis (TB), is a highly contagious airborne pathogen

infesting around 10 million people and claiming more than one million lives worldwide every year.<sup>1</sup> In 2019 before the COVID-19 pandemic, the inexorable TB burden together with the currently estimated one-quarter latent infections of global population

<sup>a</sup>Curtin Medical School, Faculty of Health Sciences, Curtin University, Bentley, Perth, WA 6102, Australia. E-mail: Hendra.Gunosewoyo@curtin.edu.au

<sup>b</sup>Center for Tuberculosis Research, Department of Medicine, Division of Infectious Disease, Johns Hopkins School of Medicine, 1550, Orleans Street, Baltimore, Maryland, 21231-1044, USA. E-mail: wbishai1@jhmi.edu

<sup>c</sup>Division of Pediatric Neurosurgery, Ann and Robert H. Lurie Children's Hospital of Chicago, Chicago, IL 60611, USA

<sup>d</sup>Department of Biostatistics, Zilber School of Public Health, University of Wisconsin, Milwaukee, WI 53205, USA

<sup>e</sup>School of Molecular and Life Sciences, Curtin University, Perth, WA 6102, Australia

<sup>f</sup>Department of Surgery, Northwestern University, Feinberg School of Medicine, Chicago, IL 60611, USA. E-mail: ssredni@northwestern.edu

<sup>g</sup>Howard Hughes Medical Institute, 4000 Jones Bridge Road, Chevy Chase, Maryland, 20815-6789, USA

† Electronic supplementary information (ESI) available. See DOI: 10.1039/d0ra10728j



ranked TB as the number one cause of mortality/morbidity from a single infectious agent (surpassing HIV/AIDS).<sup>1</sup> Due to the poor patient compliance to the onerous multi-drug first-line regimen, administered for at least 6 months, and the co-epidemic with HIV, vicious drug-resistant TB strains have emerged, perpetuating TB as a global health threat.<sup>2,3</sup> The insufficiency and limited efficacy of the drug options of multi- and extensively drug resistant TB (MDR- and XDR-TB, respectively) accompanied with their high cost, toxicity and drawn-out duration of therapy (up to 2 years) further exacerbate the TB resistance crisis.<sup>4</sup> Accordingly, it is imperative to revitalise the anti-TB drug discovery efforts and identify novel lead compounds inhibiting cellular targets different from the ones targeted by the current anti-TB drugs. This will presumably synergise their efficacy in combination with current agents in combating drug-sensitive (DS) and drug-resistant (DR) *M. tb*.

The mycobacterial membrane protein large 3 (MmpL3) is a vital transporter currently considered as one of the most druggable TB targets.<sup>5</sup> It is responsible for the translocation of mycolic acids (MAs) precursor, trehalose monomycolate (TMM), across the plasma membrane.<sup>6–11</sup> MAs are the major lipid component of the mycobacterial outer membrane and the main driving force behind its hydrophobicity and impermeability.<sup>12–14</sup> We previously illustrated the detailed biosynthetic machinery of MAs and their assembly into the mycobacterial cell envelope.<sup>15</sup> After the flipping and release of TMM from cytoplasm to periplasm *via* MmpL3, the cell wall core components serve as acceptors anchoring MAs and forming an intricate protective lipid bilayer. This coating insulates *M. tb* against exogenous substances, including antibiotics, and the host immune system.<sup>15</sup> The indispensable role of MmpL3 in *M. tb* growth and survival through shuttling TMM across the cytoplasmic membrane was verified when the downregulation of *mmpL3* expression led to an abrogation of cell division and rapid cell death. This was preceded by an intracellular accumulation of TMM and significant reduction of cell wall mycolation.<sup>16,17</sup>

A conspicuous trend of “high lipophilicity = high activity” was entrenched in many of the MmpL3 inhibitors reported to date. Recent literature revealed that five structurally distinct MmpL3 inhibitors indeed directly interact with MmpL3, while three of them additionally impact the proton motive force (PMF) in *M. tb*.<sup>18</sup> Of particular interest are the indoleamides in which NITD-304 (1, Fig. 1) and its analogous 4,6-difluoro derivative NITD-349 were identified as preclinical agents for treating MDR-TB.<sup>7</sup> We also identified the *N*-(1-adamantyl)-4,6-dimethylindole-2-carboxamide (2) as potent anti-TB agent (MIC = 0.012  $\mu$ M) with no cytotoxicity to healthy cells (IC<sub>50</sub> > 200  $\mu$ M).<sup>19</sup> Subsequent efforts, mainly directed towards non-tuberculous mycobacteria (NTM), identified the *N*-(1-adamantyl)-indole-2-carboxamide (3) and the *N*-rimantadine-4,6-dimethylindole-2-carboxamide (4) as highly potent anti-TB compounds with minimum inhibitory concentration (MIC) values of 0.68 and 0.88  $\mu$ M, respectively (Fig. 1).<sup>20</sup>

To date, several groups have reported the dual anti-TB and antineoplastic activities for a variety of scaffolds, including indole-2-carboxamides.<sup>21–25</sup> Our group has also demonstrated the selective cannabinoid receptor 2 (CB<sub>2</sub>) agonistic activity of

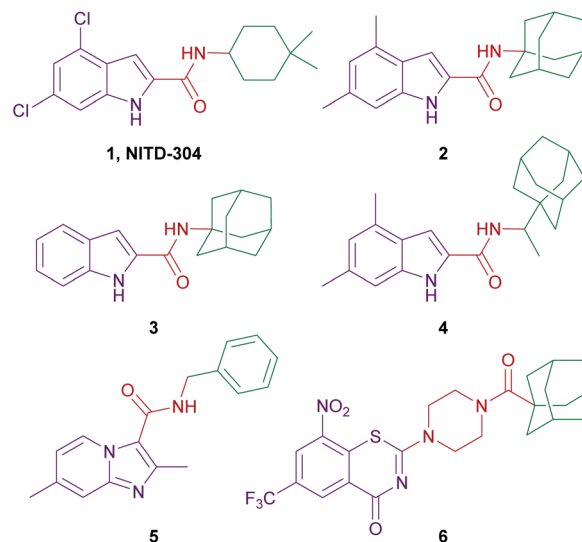


Fig. 1 Potent anti-TB compounds reported in the literature.

many indole-2-carboxamide derivatives, for instance compound 3 (EC<sub>50</sub> = 0.98  $\mu$ M).<sup>26</sup> Interestingly, in the same year, Franz *et al.* reported the potent anti-TB activity of compound 3 (MIC = 0.68  $\mu$ M).<sup>20</sup> Similarly, rimonabant, a cannabinoid receptor 1 (CB<sub>1</sub>) inverse agonist, was found to inhibit the growth of *M. tb* *via* targeting MmpL3.<sup>9</sup> The aforementioned two examples demonstrate the polypharmacological profile of various small molecules, a phenomenon that has been harnessed for drug repurposing, whereby new indications of existing agents/drugs can be identified.<sup>27,28</sup> This is well exemplified by the current repositioning of drugs in the COVID-19 era.<sup>29</sup> Towards this end, we were interested in exploring the antitumour activity that might be harboured in compound 3. We were particularly drawn into the paediatric brain tumours that are categorised as the highest-grade (grade IV) tumours according to the World Health Organisation (WHO). Paediatric gliomas represent the most common type of brain tumour and the leading cause of cancer-related death in children.<sup>30,31</sup> Glioblastoma multiforme (GBM) is a grade IV glioma that originate from the supportive cells of the brain and the spinal cord, known as the glial cells.<sup>32–34</sup> GBMs are among the most malignant, invasive and aggressive primary brain tumours which are usually refractory to current treatment, wherefore they remain largely incurable and are nearly universally fatal.<sup>35,36</sup> The mainstays of GBM treatment include gross total resection when feasible followed by focal radiotherapy combined with chemotherapy.<sup>37</sup> Many chemotherapeutic agents have been tested including temozolomide which is used in the treatment of adult GBM, but no clear benefit or remarkable improvement on survival has been achieved yet in paediatric GBM, likely due to its non-selective alkylating actions.<sup>38</sup> The dismal prognosis of GBM necessitates the discovery and development of new, more effective therapies for these tumours.

In the present study, we describe the design, synthesis, and *in vitro* biological evaluation of novel indole-2-carboxamide analogues as antitubercular agents. Upon assessing the drug-





like properties *in silico* using ACD Labs/Percepta, the designed compounds were predicted to cross the blood brain barrier (BBB). Accordingly, all synthesised compounds as well as compound **3** were also screened for their cytotoxic and anti-proliferative activities against the KNS42 tumor cell line (paediatric GBM). We subsequently performed a transcriptional analysis on the KNS42 cells treated with one of the most potent compounds in order to determine the potential mechanism of action of our indoleamide analogues. The top two potent compounds were then subjected to further evaluations against a panel of non-GBM high-grade paediatric brain tumor cell lines as well as non-tumor cells as control.

## 2. Results and discussion

### 2.1. Chemistry

The design of final compounds **8a-h**, **9a,b**, **11a,b**, **15** and **20** is depicted in Fig. 2. The indoleamides **8a-h** and **9a,b** were prepared in a one-pot amide coupling reaction as outlined in Scheme 1. First, since the *N*-rimantadine-indoleamide skeleton proved to have potent anti-TB activity,<sup>20</sup> we were interested in exploring the effect of different substitutions at various positions on the indole ring on the anti-TB activity. Towards this, commercially available indole-2-carboxylic acids **7a-h** were coupled with rimantadine hydrochloride. The amide coupling was carried out in the presence of 1-ethyl-3-(3-dimethylaminopropyl)carbodiimide hydrochloride (EDC·HCl), hydroxybenzotriazole hydrate (HOBT) and *N,N*-diisopropylethylamine (DIPEA) to deliver the requisite rimantadine-derived indoles **8a-h**. Compound **8a** was previously prepared using *N,N'*-dicyclohexylcarbodiimide (DCC) and 4-dimethylaminopyridine (DMAP) coupling reagents in a poor yield (31%).<sup>20</sup> The

other *N*-rimantadine analogue **4** prepared in the same report was also obtained in a similar low yield (29%).<sup>20</sup> However, upon employing EDC·HCl and HOBT coupling conditions in the current study, the *N*-rimantadine indoleamide derivatives were generated in significantly higher yields (66–99%).

Likewise, amide coupling of 4,6-difluoroindole-2-carboxylic acid **7h** with benzylamine or phenylhydrazine rendered amides **9a,b** in yields 98% and 93%, respectively. We used fragment-based drug design in compound **9a** in which we incorporated the benzyl group from the previously reported anti-TB compound **5** (ref. 39) into the indoleamide scaffold (Fig. 1 and 2). In Scheme 1, we also reacted the 4,6-difluoroindole **7h** with 1,1'-carbonyldiimidazole (CDI) and the resulting *N*-acylimidazole intermediate was treated *in situ* with ammonia (nucleophilic substitution reaction) to yield the amide **10**. The final imide derivatives **11a,b** were then formed *via* reacting **10** with either 3-fluorobenzoyl chloride or 3-chlorobenzoyl chloride, respectively, in pyridine.

Similar to **9a,b** and **11a,b**, we further probed the effect of extending the linker tethering the indole scaffold and the adamantane ring by introducing a carbonyl piperazine fragment as seen in the reported anti-TB derivative **6** (Fig. 1 and 2).<sup>40</sup> The diamides **15** and **20** were synthesised following the protocol delineated in Scheme 2. The synthesis of compound **15** was accomplished in three steps starting from coupling *N*-(*tert*-butoxycarbonyl) piperazine (*N*-Boc piperazine, **12**) with the carboxylic acid **7h** to give the amide analogue **13**. Subsequent *N*-Boc deprotection using trifluoroacetic acid (TFA) yielded the key indoleamide analogue **14** which was then converted to the final diamide **15** through a standard EDC-mediated coupling with 1-adamantanecarboxylic acid. On the other hand, compound **20**, entailing a phenyl group as a linker in place of piperazine, was

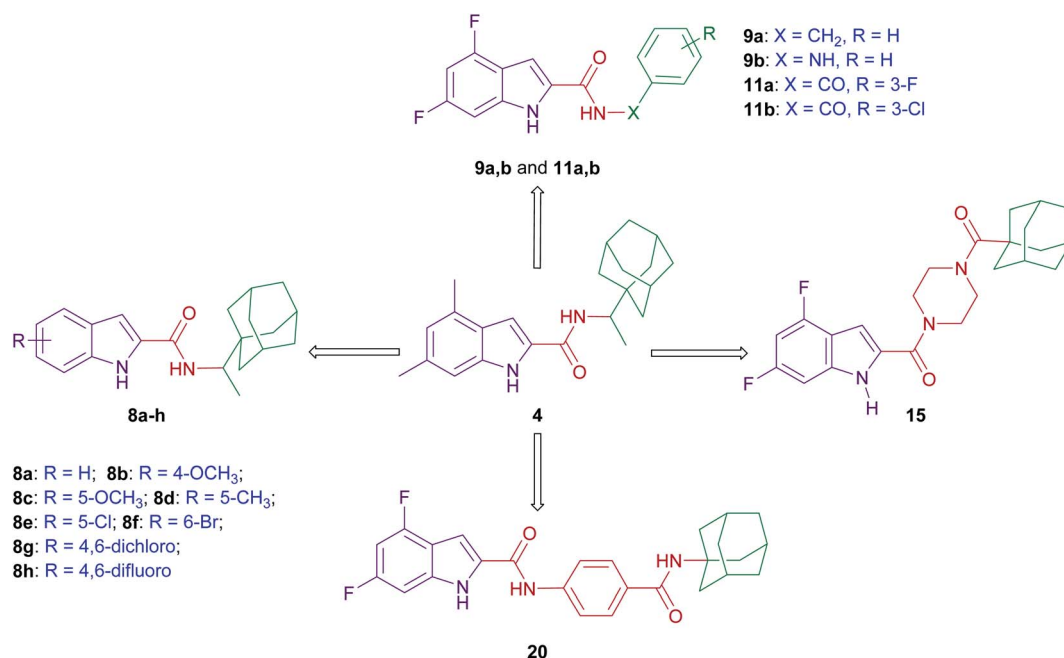
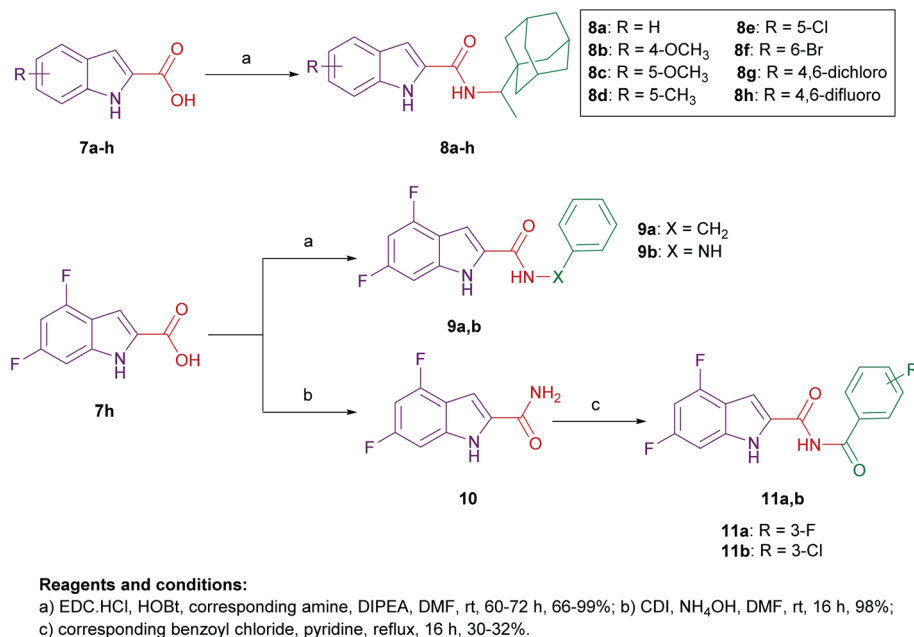


Fig. 2 A diagram summarising the design strategy of the target indoleamides.



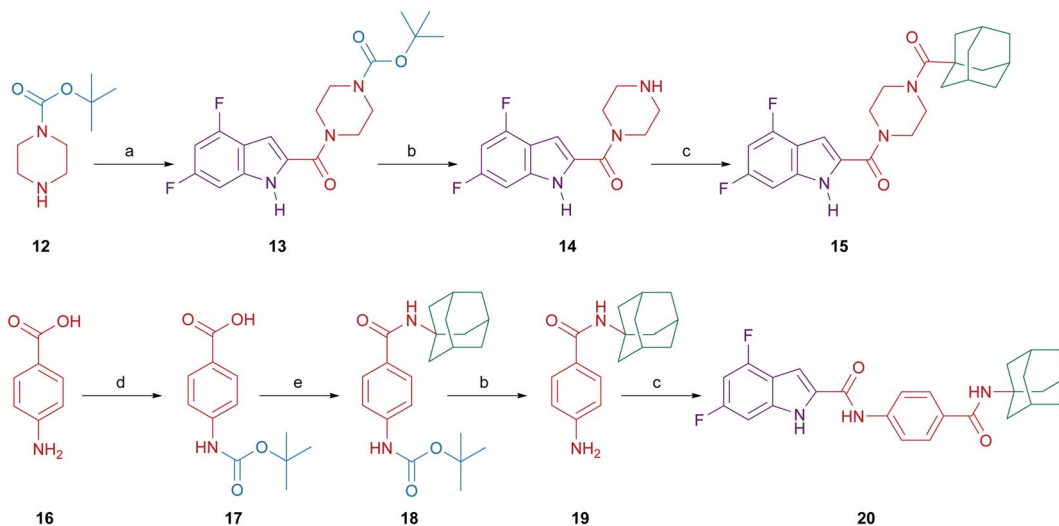


Scheme 1 General synthetic routes for compounds 8a–h, 9a,b, and 11a,b.

obtained in a four-step pathway. The amino group of the aniline **16** was initially protected using di-*tert*-butyl dicarbonate (Boc)<sub>2</sub>O to form the *N*-Boc derivative **17**. An amide linkage was formed thereafter connecting both **17** with the adamantane moiety, providing the crude *N*-Boc intermediate **18**. Next, cleaving the Boc group under acidic conditions (TFA) furnished the penultimate amidoadamantyl compound **19**. Finally, amide coupling of **19** with the carboxylic acid **7h** generated the desired dicarboxamide derivative **20**.

## 2.2. Antitubercular activity

Target compounds **8a–h**, **9a,b**, **11a,b**, **14**, **15** and **20** were screened *in vitro* against the wild-type *M. tb* strain (H37Rv) to obtain their respective MIC values (Table 1). Compounds **3** and **4** together with the two front-line anti-TB drugs, isoniazid (**INH**) and ethambutol (**EMB**) were used as positive controls. Franz *et al.* assessed the activity of both *N*-(1-adamantyl)-indole-2-carboxamide (**3**) and the *N*-rimantadine-4,6-dimethylindole-2-



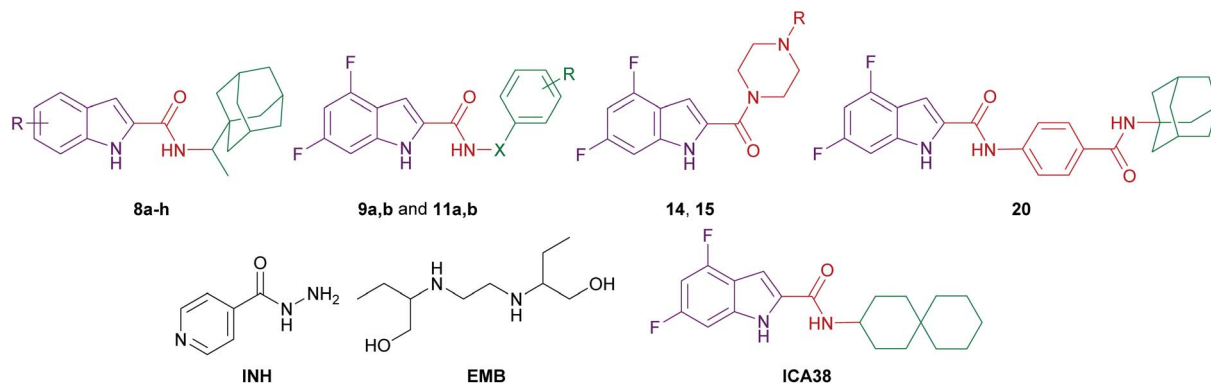
**Reagents and conditions:**

a) EDC.HCl, DMAP, 4,6-difluoroindole-2-carboxylic acid **7h**, DCM, THF, 72 h, 78%; b) TFA, DCM, rt, 12 h, 90-96%; c) EDC.HCl, HOBT, corresponding carboxylic acid, DIPEA, DMF, rt, 72 h, 25-75%; d) di-*tert*-butyl dicarbonate, triethylamine, dioxane, H<sub>2</sub>O, rt, 48 h, 86%; e) EDC.HCl, HOBT, 1-adamantylamine, DIPEA, DMF, rt, 72 h, 84%.

Scheme 2 General synthetic routes for compounds 15 and 20.



**Table 1** *In vitro* anti-TB activity in addition to cytotoxic and antiproliferative activity against KNS42 tumour cell line of compounds **8a–h**, **9a,b**, **11a,b**, **14**, **15**, and **20** as well as reference compounds **INH**, **EMB** and compounds **3**, **4**, **6**



| Cpd          | R                     | X               | H37Rv, MIC <sup>a</sup><br>( $\mu\text{g mL}^{-1}$ ) | H37Rv, MIC <sup>b</sup><br>( $\mu\text{M}$ ) | KNS42 viability,<br>IC <sub>50</sub> <sup>c</sup> ( $\mu\text{M}$ ) | KNS42 prolif.,<br>IC <sub>50</sub> <sup>d</sup> ( $\mu\text{M}$ ) | Clog P <sup>e</sup> |
|--------------|-----------------------|-----------------|--|--|---|---|---------------------|
| <b>8a</b>    | H                     | —               | 2  | 6.20   | >10   | >10   | 6.07                |
| <b>8b</b>    | 4-OCH <sub>3</sub>    | —               | 1  | 2.84   | 4.17  | >10   | 6.09                |
| <b>8c</b>    | 5-OCH <sub>3</sub>    | —               | 2  | 5.67   | 4.94  | >10   | 6.09                |
| <b>8d</b>    | 5-CH <sub>3</sub>     | —               | 1  | 2.97   | >10   | >10   | 6.57                |
| <b>8e</b>    | 5-Cl                  | —               | 1  | 2.80   | 3.13  | >10   | 6.89                |
| <b>8f</b>    | 6-Br                  | —               | <b>0.25</b>  | <b>0.62</b>                                  | <b>0.84</b>   | >10   | 7.04                |
| <b>8g</b>    | 4,6-Dichloro          | —               | <b>0.125</b>   | <b>0.32</b>                                  | >10   | >10   | 7.64                |
| <b>8h</b>    | 4,6-Difluoro          | —               | <b>0.25</b>  | <b>0.70</b>                                  | 5.66  | >10   | 6.50                |
| <b>9a</b>    | H                     | CH <sub>2</sub> | >32  | >112   | <b>8.25</b>   | <b>9.85</b>   | 3.84                |
| <b>9b</b>    | H                     | NH              | >32  | >111   | 4.45  | >10   | 2.42                |
| <b>11a</b>   | 3-F                   | CO              | >32  | >101   | 2.16  | >10   | 4.49                |
| <b>11b</b>   | 3-Cl                  | CO              | >32  | >96  | 6.65  | >10   | 5.06                |
| <b>14</b>    | H                     | —               | >32  | >121   | 1.34  | >10   | 1.54                |
| <b>15</b>    | Adamantane-1-carbonyl | —               | >32  | >75  | <b>5.04</b>   | <b>6.62</b>   | 3.80                |
| <b>20</b>    | —                     | —               | >32  | >71  | >10   | >10   | 5.29                |
| <b>INH</b>   | —                     | —               | 0.04 (ref. 6)  | 0.29   | ND <sup>f</sup>   | ND <sup>f</sup>   | −0.67               |
| <b>EMB</b>   | —                     | —               | 1 (ref. 6)   | 4.89   | ND <sup>f</sup>   | ND <sup>f</sup>   | 0.12                |
| <b>3</b>     | —                     | —               | 0.2 (ref. 20)  | 0.68 (ref. 20)                               | <b>0.33</b>   | >10   | 4.11                |
| <b>4</b>     | —                     | —               | 0.31 (ref. 20)                                       | 0.88 (ref. 20)                               | ND <sup>f</sup>   | ND <sup>f</sup>   | 7.07                |
| <b>6</b>     | —                     | —               | —  | 0.031 (ref. 40)                              | ND <sup>f</sup>   | ND <sup>f</sup>   | 4.25                |
| <b>ICA38</b> | —                     | —               | —  | 0.003 (ref. 42)                              | ND <sup>f</sup>   | ND <sup>f</sup>   | 5.90                |

<sup>a</sup> The lowest concentration of drug causing at least 90% reduction of bacterial growth by the microplate alamarBlue assay (MABA). The reported MIC values are an average of three individual measurements, in  $\mu\text{g mL}^{-1}$ . <sup>b</sup> The reported H37Rv MIC values converted to  $\mu\text{M}$ . <sup>c</sup> Compound dose required to achieve 50% inhibition of KNS42 cell viability, reflecting cytotoxicity. <sup>d</sup> Compound dose required to achieve 50% inhibition of KNS42 cell proliferation. <sup>e</sup> Calculated using ChemDraw 16.0. <sup>f</sup> Not determined.

carboxamide analogue (**4**) against several mycobacterial strains, including H37Rv *M. tb* strain (MIC = 0.68 and 0.88  $\mu\text{M}$ , respectively).<sup>20</sup> Within this context, we previously conducted a thorough antimycobacterial screening for several indole-2-carboxamide derivatives.<sup>6,19,41–43</sup> We found that the methyl groups located at the indole moiety in compound **2** present a potential metabolic liability (susceptible to metabolic oxidation). Accordingly, in order to explore the effects of various substituents on the indole ring, we synthesised several indoleamide derivatives **8a–h** bearing a rimantadine substituent in place of the adamantane ring. All of the tested *N*-rimantadine indoleamides had single digit micro- and submicro-molar MIC

values, with compounds **8f–h** exhibiting potencies (MIC = 0.32–0.70  $\mu\text{M}$ ) higher than compound **4**.

Upon re-evaluating the activity of the unsubstituted indole derivative **8a**, it displayed an MIC value of 6.20  $\mu\text{M}$ , which was lower than the published one (MIC > 15.5  $\mu\text{M}$  (ref. 20)). The 4-methoxyindole analogue **8b** showed a two-fold enhancement of activity compared to the 5-methoxy counterpart **8c** (MIC = 2.84 and 5.67  $\mu\text{M}$ , respectively). To further probe the effect of mono-substitution at position 5, more lipophilic methyl and chloro groups were installed. The observed activities of compounds **8d,e** (MIC = 2.97 and 2.80  $\mu\text{M}$ , respectively) were 2-fold higher than the respective 5-methoxy analogue **8c**. This could be attributed to the higher lipophilicity of **8d,e** (Clog P = 6.57 and



6.89, respectively) compared to **8c** (Clog  $P = 6.09$ ). These results suggest the lipophilicity-driven bioactivity of this series. Nevertheless, the fact that the 5-substituted indoles **8d,e** are equipotent to the 4-substituted analogue **8b**, despite the lower lipophilicity of the latter compared to the former derivatives, reflects the substitution preference for certain positions on the indole ring. Interestingly, the presence of a single bromo group at position 6 of the indole ring (**8f**: MIC = 0.62  $\mu\text{M}$ ) led to an approximately 10- and 4.5-fold increase in the activity in comparison to the unsubstituted and 5-halosubstituted indoles **8a,e**, respectively.

Next, we replaced the two methyl groups in compound **4** with metabolically stable halogens **8g,h**. It was pleasing to find that compound **8g** possessing 4,6-dichloro substituents on the indole core exhibited nearly a three-fold rise in activity (MIC = 0.32  $\mu\text{M}$ ) relative to compound **4** and a comparable potency to **INH** (MIC = 0.88 and 0.29  $\mu\text{M}$ , respectively). Of note is the fact that compound **8g** is the most lipophilic compound in our study (Clog  $P = 7.64$ ) that was translated into the highest activity as well which once again signifies the apparent influence of lipophilicity on the anti-TB activity. The 4,6-difluoro analogue **8h** (MIC = 0.70  $\mu\text{M}$ ) was more active than **4** and 2-fold less potent than the 4,6-dichloroindole counterpart **8g**. The consequential impact of the substitution pattern in the indole ring on activity, depicted earlier in compounds **8d,e** versus **8b**, was recapitulated in compound **8h** versus **8f** in which both compounds exhibited similar activities, although **8f** is more lipophilic than **8h** (Clog  $P = 7.04, 6.50$ , respectively). Importantly, the potency rendered by all the rimantadine analogues was comparable to or significantly higher than the first-line anti-TB drug **EMB** (MIC = 4.89  $\mu\text{M}$ ).

Similar to the other MmpL3 inhibitors, the inherent high lipophilicity of the foregoing series (Clog  $P = 6.07$ – $7.64$ ) likely endowed them with facilitated diffusion through the lipid-rich bilayer of *M. tb* where they presumably interacted with MmpL3 and elicited potent anti-TB activity. Nonetheless, it is worth noting that the anti-TB activities of the *N*-(rimantadine)-indole-2-carboxamides in our study are generally lower than the previously evaluated *N*-(1-adamantyl)-indole-2-carboxamide counterparts. Indeed, this was counterintuitive due to the high lipophilicity of the rimantadine derivatives compared to the corresponding 1-adamantane analogues.<sup>43</sup> The SAR hallmarks of these analogues, in which substitutions at the 4- and/or 6-positions of the indole ring was optimal for activity, together with the apparent impact of lipophilicity on the anti-TB activity, were consistent with our previous findings.<sup>19,42,43</sup> Therefore, in our subsequent evaluations in which we used the fragment-based drug design technique, 4,6-difluoroindole **7h** was the scaffold of choice, to which we attached different fragments from previously reported anti-TB agents with diverse mechanism of actions **5** and **6** (Fig. 1).

First, Moraski *et al.* called attention to the remarkable anti-TB potency of the *N*-benzyl imidazo[1,2-*a*]pyridine-3-carboxamide **5** (MIC = 0.37–1.9  $\mu\text{M}$  in three different media).<sup>39</sup> This compound also maintained its excellent potency when tested against a panel of single DR strains in addition to several MDR and XDR clinical isolates.<sup>39</sup> Imidazo[1,2-*a*]

pyridines were previously found to exert their anti-TB activity *via* inhibiting *M. tb* cytochrome b subunit of the cytochrome *bc1* complex (QcrB).<sup>44,45</sup> We, thereupon, appended a benzyl moiety to the 4,6-difluoroindoleamide architecture. Disappointingly, the tested benzylamide analogue **9a** was bereft of anti-TB activity (MIC > 112  $\mu\text{M}$ ). We also presumed that incorporating an NH or a carbonyl (C=O) group, instead of CH<sub>2</sub>, between the carboxamide moiety and the phenyl group would result in the formation of more hydrogen bonds with the hydrophilic residues in the S4 hydrophilic subsite of MmpL3,<sup>9</sup> leading to an improved binding and better activity. As reported previously,<sup>46</sup> when we introduced a C=O group between the 4,6-difluoroindoleamide and the adamantane moiety, the obtained imide derivative displayed moderate anti-TB activity (MIC = 22  $\mu\text{M}$ ). Unfortunately, this NH or C=O extension in compounds **9b** and **11a,b**, did not show any improved anti-TB activity (MIC > 96  $\mu\text{M}$ ).

It is noteworthy that the estimated lipophilicities of compounds **11a,b** (Clog  $P = 4.49$  and 5.06, respectively) are higher than that of **9a,b** (Clog  $P = 3.84$  and 2.42, respectively) which did not seemingly impact the anti-TB activity. Of interest is the fact that two *N*-phenyl indole-2-carboxamide analogues exhibited good anti-TB activities in our previous work (MIC = 1.7 and 3.8  $\mu\text{M}$ ).<sup>19</sup> This in turn suggests that introducing an extra spacer to the amide linker tethering the indole ring and the phenyl moiety is unfavourable. In the same report, on the contrary, we found that adding a methylene spacer between the amide nitrogen and a cyclohexyl ring elicited almost the same high potency as the desmethylene analogue (MIC = 0.88 and 0.93  $\mu\text{M}$ , respectively).<sup>19</sup> Evidently, the potent anti-TB activity manifested by the *N*-rimantadine indoleamide analogues **8a-h** in the present study corroborated the notion that incorporating an extra spacer next to the cycloaliphatic motifs is tolerated.

On the other hand, the nitrobenzothiazinone derivative **6**, bearing a carbonyl piperazine moiety (Fig. 1), was reported to have a potent anti-TB activity (MIC = 0.031  $\mu\text{M}$  (ref. 40)). The 1,3-benzothiazin-4-ones (BTZs) are a potent class of antimycobacterial agents that kill *M. tb in vitro, ex vivo* and in TB mouse models *via* targeting decaprenylphosphoryl- $\beta$ -D-ribose 2'-epimerase (DprE1) enzyme. Inhibition of the DprE1 enzymatic activity compromises the formation of a key precursor in the synthesis of cell wall arabinans, namely decaprenylphosphoryl arabinose, resulting in cell lysis and bacterial death.<sup>47</sup> Introducing a 4-carbonyl piperazine segment into the BTZ framework was well tolerated and led to compounds with enhanced aqueous solubility compared to other BTZ analogues in earlier reports.<sup>40</sup> This prompted us to integrate the carbonyl piperazine fragment into the *N*-(adamantyl)indoleamide structure core to verify its tolerability within this template. Initially, we examined the activity of the piperazinyndole intermediate **14** which displayed an MIC value > 121  $\mu\text{M}$ . This dramatic loss in activity could be ascribed to its diminished lipophilicity (Clog  $P = 1.54$ ) and the absence of the amide NH which is a crucial element for the hydrogen bonding with Asp645 in MmpL3.<sup>9</sup> The NH necessity was further emphasised when we increased the lipophilicity of **14** *via* attaching an adamantane ring, furnishing the 1,4-dicarbonyl piperazine **15** which was



Table 2 *In vitro* cytotoxicity (Vero cells) and molecular modelling results of compounds **8f** and **8g**

| Cpd          | MIC ( $\mu\text{M}$ ) | IC <sub>50</sub> <sup>a</sup> ( $\mu\text{M}$ ) | SI <sup>b</sup> | Docking score <sup>c</sup> (kcal mol <sup>-1</sup> ) | No. of H-bonds | Distance     | Amino acids      | Ligand atoms          |
|--------------|-----------------------|---|-----------------|--|----------------|--------------|------------------|-----------------------|
| <b>8f</b>    | 0.62                  | 39.9  | 64              | -13.9  | 2              | 2.51<br>2.66 | Asp645<br>Asp645 | Amide NH<br>Indole NH |
| <b>8g</b>    | 0.32                  | 40.9  | 128             | -14.4  | 2              | 2.55<br>2.62 | Asp645<br>Asp645 | Amide NH<br>Indole NH |
| <b>ICA38</b> | 0.003 (ref. 42)       | ND <sup>d</sup>                                 | ND <sup>d</sup> | -22.7  | 1              | 2.54         | Asp645           | Amide NH              |

<sup>a</sup> Cytotoxicity against Vero cells expressed as the half maximal inhibitory concentration of the drug by MABA. <sup>b</sup> Selectivity index (SI) = IC<sub>50</sub>(Vero)/MIC(H37Rv). <sup>c</sup> The lowest binding energy corresponding to the top-ranked pose. <sup>d</sup> Not determined.

devoid of activity (MIC > 75  $\mu\text{M}$ ) despite having a Clog *P* value of 3.80 that is higher than that of **14**.

A similar trend was observed in the analogous dicarboxamide **20**, in which a phenyl motif, *in lieu* of piperazine, was introduced in between the indole and adamantane rings. Despite its higher lipophilicity (Clog *P* = 5.29) and that the amide NH was preserved, compound **20** was inactive (MIC > 71  $\mu\text{M}$ ). Hence, it could be surmised that stretching the linker between the indole scaffold and the adamantane moiety *via* ring insertion is detrimental to the anti-TB activity, suggesting some steric requirements of the S4 subsite of MmpL3. The abolition of anti-TB activity pertaining to overextending the middle linker resonates with our previous findings.<sup>46</sup> Overall, whilst a positive correlation between lipophilicity and anti-TB activity was discernible in compounds **8a–h**, the rest of the tested analogues did not conform with this trend.

Motivated by the potent *in vitro* anti-TB activities of the rimantadine-derived indole derivatives **8a–h**, two compounds **8f** and **8g** (MIC = 0.62, 0.32  $\mu\text{M}$ , respectively) were selected for further cytotoxicity assessment and their selectivity index (SI) were subsequently calculated (Table 2). We were pleased to find that both compounds displayed high IC<sub>50</sub> values against Vero cells (IC<sub>50</sub> = 39.9 and 40.9  $\mu\text{M}$ , respectively). These values correspond to SI values of 64 and 128, respectively, indicating

minimal primary cytotoxicity of these derivatives against healthy mammalian cells.

Taking into consideration that MmpL3 is the most relevant potential enzymatic target of our analogues, molecular docking simulations were carried out to evaluate the possible binding mechanism of the rimantadine-based indoles within the MmpL3 active site (Table 2; Fig. 3 and 4). First, the co-crystallised ligand **ICA38** was re-docked into the MmpL3 binding site to validate the docking protocol as we reported before (Fig. 3).<sup>46</sup> In consonance with the previous findings,<sup>9</sup> the indole moiety and the spirocarbocyclic group of **ICA38** were both lodged in the bulky S3 and S5 hydrophobic subsites, respectively, forming hydrophobic contacts with the surrounding residues. The amide linker was positioned in the S4 hydrophilic subsite, wherein the amide NH of **ICA38** formed a hydrogen bond with Asp645. This Asp645 is a crucial part of the two Asp–Tyr pairs implicated in proton relay. Upon binding, **ICA38** inhibits the MmpL3 by occupying S3–S5 subsites in the proton transportation channel, disrupting the key components of the S4 subsite, namely the two Asp–Tyr pairs (Fig. 3), thereby blocking the PMF for substrate translocation.<sup>9</sup>

Both compounds **8f** and **8g**, typifying the rimantadine class, were oriented inside the MmpL3 binding pocket in a manner resembling **ICA38** (Fig. 4). The most favourable docking pose (*i.e.* lowest binding energy) retained the key interactions

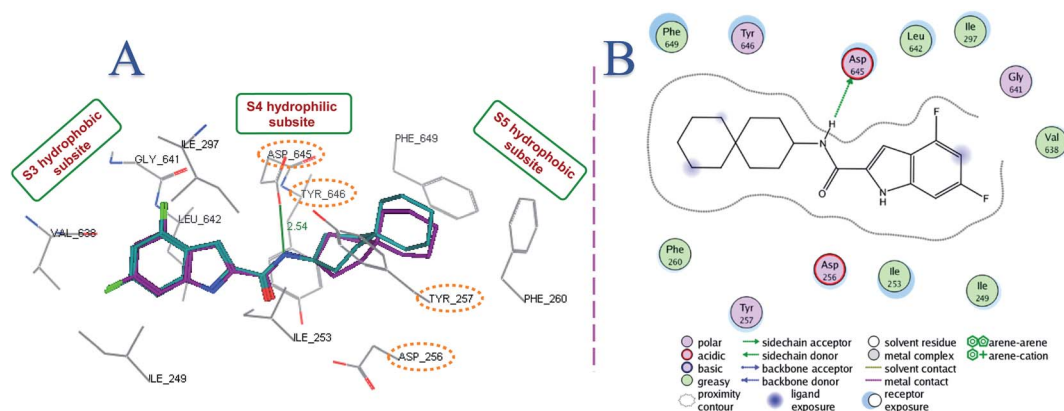


Fig. 3 Re-docking of **ICA38** (Cyan) in the MmpL3 active site (A), showing the S3–S5 subsites. The **ICA38** top pose was oriented almost at the same position as the original **ICA38** co-crystallised ligand (purple). The two key Asp–Tyr pairs, implicated in proton relay, located in the S4 subsite are marked in orange hashed ovals. The putative binding interactions of **ICA38** with the MmpL3 binding pocket is represented in 2D on the right panel (B).



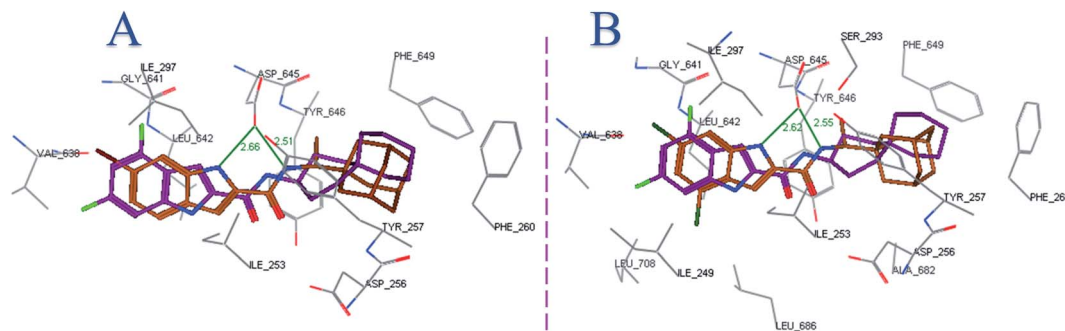


Fig. 4 Superposition of the top ranked docking pose of **8f** (A) and **8g** (B) (brown) and the co-crystallised ligand ICA38 (purple), showing the putative binding mode of both compounds in the MmpL3 active site.

observed in ICA38. The S3 hydrophobic subsite accommodated the indole nucleus, while the rimantadine moiety was embedded in the bulky S5 hydrophobic subsite, overlapping with the spirocyclic group of ICA38. Meanwhile, the amide NH in **8f** and **8g** was inserted in the S4 hydrophilic subsite, forming a hydrogen bond with Asp645 (distance = 2.51 and 2.55 Å, respectively). An additional hydrogen bond was formed between the indole NH of **8f** and **8g** with Asp645 (distance = 2.66 and 2.62 Å, respectively). They also showed high binding affinity to the MmpL3 active site (docking score =  $-13.9$  and  $-14.4$  kcal mol $^{-1}$ , respectively). The similarities between the binding modes of **8f** and **8g** and the MmpL3 inhibitor ICA38 suggest that this potent class of *N*-rimantadine indoleamides likely inhibit the same target *via* disrupting the two Asp–Tyr pairs that play a pivotal role in the proton translocation. It is worth mentioning that a recent study used a combination of *in vitro* and whole-cell-based approaches to determine whether a structurally distinct panel of MmpL3 inhibitors directly target the MmpL3 or dissipate the PMF from which this transporter derives its energy (indirect mechanism). They provided evidence that all compounds, including the indole-2-carboxamides, directly inhibit MmpL3, whether or not they exert an additional impact on the PMF that potentiate their activity.<sup>18</sup>

### 2.3. Cytotoxic and antiproliferative activity against paediatric GBM cells

All synthesised final compounds in addition to reference compound **3** were initially evaluated for their cytotoxicity and antiproliferative activities against paediatric KNS42 GBM cell line (Table 1). Compound **3**, which previously showed potent antitubercular activity against *M. tb* H37Rv strain (MIC = 0.68 μM (ref. 20)), displayed potent cytotoxicity against KNS42 cells with sub-micromolar inhibitory activity on cell viability (IC<sub>50</sub> = 0.33 μM). The cytotoxicity of compound **3** was previously evaluated against human THP-1 cells in which it was non-cytotoxic up to 50 μM.<sup>20</sup> Similarly, compound **8f** demonstrated excellent dual antitubercular and antitumour activity [MIC (H37Rv) = 0.62 μM, IC<sub>50</sub> (KNS42 viability) = 0.84 μM]. Importantly, compound **8f** also exhibited minimal cytotoxicity against healthy mammalian Vero cells with an IC<sub>50</sub> value of 39.9 μM

(Table 2). Nonetheless, both **8f** and reference compound **3** showed weak antiproliferative activities against KNS42 (IC<sub>50</sub> > 10 μM). Compounds **8b**, **8c**, **8e** and **8h** showed potent antitubercular activity and reduction of KNS42 cell viability [MIC (*M. tb*) and IC<sub>50</sub> (KNS42) < 6 μM].

On the other hand, compound **9a**, which was bereft of antitubercular activity, displayed good inhibitory activities against KNS42 cells in the viability and proliferation assays with IC<sub>50</sub> values of 8.25 and 9.85 μM, respectively. Similarly, compound **15** exhibited potent cytotoxic and antiproliferative activity against KNS42 cells (IC<sub>50</sub> = 5.04 and 6.62 μM, respectively). Additionally, compounds **9b**, **11a**, **11b** and **14** displayed high cytotoxic activities (IC<sub>50</sub> = 1.34–6.65 μM) and poor antiproliferative activity (IC<sub>50</sub> > 10 μM) against KNS42 cells.

### 2.4. Transcriptional analysis of KNS42 cells and compound 15-induced alterations to gene expression

To shed light on the potential mechanism of action of our indole-2-carboxamides as antitumour agents, we characterised the gene transcriptional response of the KNS42 cells upon exposure to compound **15**, using DNBSEQ Eukaryotic Stranded Transcriptome Resequencing. Of note, compound **15** was chosen in this respect due to its potent activity against KNS42 cells in both viability and proliferation assays (IC<sub>50</sub> = 5.04 and 6.62 μM, respectively). When we analysed the differential expression of the genes, in comparison to the control cells (untreated), we found that compound **15** downregulated the expression of 9 genes (fold change ≥ 8) with statistical significance ( $P < 0.05$ ). Two genes, namely the carbonic anhydrase 9 (CA9) and the spleen tyrosine kinase (SYK) stood out as potential targets of this compound, whereby it exerts its antitumour activity. Several reports previously showed that the expression levels of CA9 and SYK in GBM tumours are positively correlated to tumour growth/progression and negatively correlated to survival rates.<sup>48–50</sup> Therefore, downregulating the expression of these two genes could be conducive to the antitumour effects observed in compound **15**.

First, we found that the expression level of CA9 was downregulated by 15-fold ( $p < 0.01$ ) upon treating the KNS42 cells with compound **15**. CA9 is a hypoxia-responsive gene which is used as a hypoxia marker and a regulator of the pH of tumour



**Table 3** *In vitro* cytotoxicity and antiproliferation activity of compounds **9a** and **15** against different paediatric brain tumour cell lines (BT12, BT16 and DAOY) and non-neoplastic human fibroblasts (HFF1)

| Cpd       | BT12 viability, IC <sub>50</sub> (μM) | BT12 prolif., IC <sub>50</sub> (μM) | BT16 viability, IC <sub>50</sub> (μM) | BT16 prolif., IC <sub>50</sub> (μM) | DAOY viability, IC <sub>50</sub> (μM) | DAOY prolif., IC <sub>50</sub> (μM) | HFF1 viability, IC <sub>50</sub> (μM) | HFF1 prolif., IC <sub>50</sub> (μM) |
|-----------|---------------------------------------|-------------------------------------|---------------------------------------|-------------------------------------|---------------------------------------|-------------------------------------|---------------------------------------|-------------------------------------|
| <b>9a</b> | <b>0.89</b>                           | <b>7.44</b>                         | <b>1.81</b>                           | <b>6.06</b>                         | >10                                   | >10                                 | <b>119</b>                            | 65                                  |
| <b>15</b> | <b>3.16</b>                           | >10                                 | <b>5.89</b>                           | >10                                 | >10                                   | >10                                 | 19.35                                 | 17.41                               |

cells.<sup>51</sup> Hypoxia is a common feature of the majority of malignant tumours, in which extensively expanding and proliferating tumour tissues outgrow their blood supply resulting in hampered oxygen diffusion and hypoxic milieu.<sup>52</sup> CA9 expression is strongly induced by hypoxia, therefore it can serve as a marker that signifies aggressive rapidly proliferating tumours.<sup>50</sup> Hence, CA9 expression was found to be correlated to tumour progression in various human cancers.<sup>53</sup> Importantly, strong CA9 immunoreactivity was previously detected in HGGs, including GBM, whereas the normal brain cells showed no expression of CA9.<sup>53</sup> This tumour-exclusive expression pattern establishes CA9 as a feasible antitumour target. Indeed, Proescholdt *et al.* found that CA9 is expressed in the GBM tumours in all of the patients they investigated, whereby the expression levels were generally correlated with the overall prognosis.<sup>50</sup> Their survival analysis revealed that high expression levels of CA9 was associated with poor survival in GBM patients (15 months) compared to GBM patients with low CA9 expression (34 months). Therefore, high CA9 expression is considered a prognostic marker for poor survival in GBM patients.<sup>48,50</sup> Selective gene silencing of CA9 in GBM cells resulted in a profound reduction of cell attachment and invasion as well as a strong enhanced susceptibility to adjuvant chemotherapy and radiation treatment.<sup>50</sup> This was substantiated by Boyd *et al.*'s recent findings, in which concurrently using a CA9 inhibitor with temozolomide inhibited the growth of GBM cells and induced cell cycle arrest *in vitro*.<sup>51</sup> This combination was also efficacious in extending the survival of GBM-bearing mice. Taken together, the significant downregulation of CA9 gene in KNS42 cells induced by compound **15** suggest the involvement of CA9 in the cytotoxic and antiproliferative activities observed in this compound.

On the other hand, compound **15** also repressed the expression of the SYK by 9-fold with statistical significance ( $p < 0.05$ ). SYK is a non-receptor protein tyrosine kinase which is an essential component of the signalling machinery in the immune system.<sup>54</sup> It is mainly expressed in hematopoietic cells, including macrophages, B cells, neutrophils, monocytes, and natural killer cells.<sup>55</sup> SYK plays a key role in the oncogenesis and tumour promotion of various cancers, including gliomas.<sup>55</sup> Indeed, Moncayo and colleagues have recently found that SYK is overexpressed in the malignant gliomas, including GBM.<sup>49</sup> Their *in vitro* experiments showed that inhibiting or knocking down SYK activity resulted in blocking the proliferation and migration of GBM cell lines. Importantly, these findings were mirrored *in vivo* in nude mice injected with human GBM cells overexpressing SYK.<sup>49</sup> In this respect, SYK inhibition reduced

GBM cell proliferation and invasiveness *in vivo*. In addition, blocking the activity of SYK genetically or by inhibitors in tumour cells prolonged the life of treated mice and increased their survival.<sup>49</sup> Of note, our indoleamide derivative **15**, which significantly downregulated the expression of SYK protein, displayed the most potent antiproliferative activity in our set of analogues. This is in fact consistent with the Moncayo *et al.* findings. Overall, the evident downregulation of CA9 and SYK expression induced by compound **15** suggest that our observed antitumour effects could be correlated to modulating the activity of these two targets.

### 2.5. Cytotoxic and antiproliferative activities of the top potent compounds against different non-GBM paediatric brain tumour cells and non-neoplastic fibroblasts

Both compounds **9a** and **15** were selected for further *in vitro* viability and proliferation inhibition studies against different grade IV paediatric brain tumour cell lines and non-neoplastic mammalian cells (Table 3). Both compounds retained their potent cytotoxic activities against two atypical teratoid/rhabdoid tumour (AT/RT) cell lines BT12 and BT16. Remarkably, compound **9a** showed approximately 9- and 5-fold higher cytotoxic activity, respectively, when tested against the two fore-named cell lines compared to KNS42 [IC<sub>50</sub> = 0.89 (BT12), 1.81 (BT16) and 8.25 (KNS42) μM]. Compound **9a** also exhibited high antiproliferative activities against BT12 and BT16 cells [IC<sub>50</sub> = 7.44 and 6.06 μM, respectively]. Despite the potent antiproliferative activity of compound **15** against KNS42, this activity was not maintained against the two tested AT/RT cell lines (IC<sub>50</sub> > 10 μM). On the other hand, both compounds demonstrated a drop in both cytotoxic and antiproliferative activities when tested against the medulloblastoma cell line DAOY (IC<sub>50</sub> > 10 μM). To our delight, compound **9a** displayed negligible cytotoxicity when tested against the non-neoplastic human fibroblast cell line HFF1 (IC<sub>50</sub> = 119 μM), suggesting its selective cytotoxicity with an SI value up to 134 against tumour cells. Compound **15** displayed moderate cytotoxicity against HFF1 cells (IC<sub>50</sub> = 19.35 μM), giving low SI values.

The physicochemical properties of compound **9a** were predicted using ACD/Labs Percepta 2016 Build 2911 (13 Jul 2016). We evaluated the compliance of this compound with Lipinski's rule of five (RO5) in order to evaluate its drug-likeness.<sup>56</sup> Compound **9a** showed zero violations to the RO5, indicating the drug-like attributes of this compound, including its prospective *in vivo* bioavailability. Importantly, this compound is also expected to cross the BBB, whereupon it can elicit its antitumour activity. Overall, the aforementioned results establish



compound **9a** as a promising antitumour agent against various aggressive paediatric brain cancer cells, whilst being safe towards healthy cells.

### 3. Conclusions and future directions

In summary, we established a body of preliminary SAR for the *N*-rimantadine indoleamides **8a–h** as anti-TB agents, based on compound **4** which was obtained from a previous screening<sup>20</sup> against several mycobacterial strains. The SAR outcomes of this class were in harmony with our published findings,<sup>19,42,43</sup> highlighting the significance of both the substitution pattern of the indole moiety and the lipophilic nature of the substituents. In this study, a subsequent massive drop in the anti-TB activity ensued from the structural modifications implemented in compounds **9a,b**, **11a,b**, **14**, **15** and **20**. Although lipophilicity is a key driver for the anti-TB efficacy in **8a–h**, it is not the sole parameter influencing the potency in our study. The most active anti-TB compound identified in our study **8g** exhibited limited cytotoxic activity against Vero cells. A docking analysis was performed on compounds **8g** and **8f**, exemplifying the binding mode of the *N*-rimantadine indoleamide series. The similarity between the binding fashion of both compounds and **ICA38** in the same MmpL3 binding pocket support the high *in vitro* anti-TB potency of the amidorimantadine class. Since the indoleamide architecture was previously reported to have antitubercular and antitumour activities,<sup>22,23</sup> all compounds in the present study were tested for their antitumour activity against the paediatric GBM cell line KNS42. Some of the tested compounds demonstrated potent anti-TB activity and cytotoxicity towards KNS42 cells. Compound **8f** displayed the most potent dual activity while showing minimal cytotoxicity against non-neoplastic mammalian cells. Additionally, several compounds, which were devoid of anti-TB activity, showed potent cytotoxicity and/or antiproliferative activities against the KNS42 cell line.

Differential expression analysis of the genes in the KNS42 cells in response to compound **15** versus untreated cells revealed that this compound repressed the expression of CA9 ( $p < 0.01$ ) and SYK ( $p < 0.05$ ) genes by 15-fold and 9-fold, respectively. The expression levels of these genes in GBM tumours were previously shown to be directly correlated to the tumour growth and progression and inversely correlated to survival rates.<sup>48–50</sup> Indeed, knocking down the activity of each of these two genes was also found to inhibit the growth of GBM cells *in vitro*.<sup>49,51</sup> Accordingly, the cytotoxic and antiproliferative effects of compound **15** could be attributed to downregulating the activity of these two genes. Two compounds **9a** and **15**, which potently reduced cell viability and proliferation of KNS42 cells, were further evaluated against three paediatric brain tumour cell lines and non-neoplastic human fibroblasts. Compound **9a** stood out as the most promising antitumour agent, displaying excellent cytotoxic and antiproliferative activities against two AT/RT cell lines (BT12 and BT16) in addition to the GBM KNS42 cell line. The cytotoxicity of **9a** was nullified against non-neoplastic human cells, suggesting its selective activity towards tumour cells. Overall, the high activity against brain tumour cells, negligible cytotoxicity towards

non-neoplastic cells and *in silico* drug-like profile of the *N*-benzyl indoleamide **9a** establish this compound as a potential therapeutic agent that merits further investigation.

These findings foreground the indoleamides as a new class of compounds that could be fine-tuned to modulate their dual anti-TB and antitumour activities. In addition, our gene expression results lay the foundation for future studies to identify more indoleamide analogues as antitumour agents that can modulate the expression of CA9 and SYK genes. Unlike the conventional target identification approaches which employ determining the activity of a small molecule at a receptor or enzyme level, the transcriptional approach has the advantage of identifying the compound's impact on the absolute concentration of a target protein.<sup>57</sup> Future efforts will focus on confirming if the observed antitumour activity of the indoleamide scaffold in paediatric brain cancer cells is the direct consequence of inhibiting CA9 and/or SYK.

## 4. Experimental

### 4.1. Chemistry

**4.1.1. General.** All indole-2-carboxylic acids **7a–h** and rimantadine hydrochloride were purchased from Fluorochem, while the benzylamines were purchased from Sigma-Aldrich. *N*-Boc-piperazine and 4-aminobenzoic acid were purchased from AK Scientific. <sup>1</sup>H NMR and <sup>13</sup>C NMR spectra were recorded on a Bruker Avance III spectrometer at 400 and 100 MHz, respectively, with TMS as an internal standard. Standard abbreviations indicating multiplicity were as follows: s = singlet, d = doublet, dd = doublet of doublets, t = triplet, td = triplet of doublets, q = quadruplet, dq = doublet of quartets, m = multiplet and br = broad. HRMS experiments were done on a Thermo Scientific Q-Exactive Orbitrap mass spectrometer. TLC was carried out on Analtech silica gel TLC plates (200 microns, 20 × 20 cm). Flash chromatography was performed using a Teledyne Isco Combi-Flash Rf system with RediSep columns or manually using Sili-Cycle SiliaFlash® P60 Silica Gels [40–63 μm (230–400 mesh)]. The preparative HPLC (Shimadzu) employed a Phenomenex Luna® Omega 5 μm Polar C18 100A (150 × 21.2 mm) column, with detection at 254 and 280 nm on a Shimadzu SPD-20A detector, flow rate = 25.0 mL min<sup>-1</sup>. Method 1: 40–100% acetonitrile/H<sub>2</sub>O in 15 min; 100% acetonitrile in 10 min; 100–40% acetonitrile/H<sub>2</sub>O in 10 min. Method 2: 60–100% acetonitrile/H<sub>2</sub>O in 10 min; 100% acetonitrile in 15 min; 100–60% acetonitrile/H<sub>2</sub>O in 10 min. Method 3: 80–100% acetonitrile/H<sub>2</sub>O in 10 min; 100% acetonitrile in 15 min; 100–80% acetonitrile/H<sub>2</sub>O in 10 min. Both solvents contained 0.05 vol% of TFA. Purities of final compounds were established by analytical HPLC, which was conducted on Waters HPLC system (2487 dual wavelength absorbance detector, 1525 binary pump, and 717 plus autosampler) with a Phenomenex Luna® 5 μm C18(2) 100 Å (150 × 4.6 mm) column. Analytical HPLC method: flow rate = 1 mL min; gradient elution over 30 min. Gradient 1: 20–100% acetonitrile/H<sub>2</sub>O in 15 min; 100% acetonitrile in 10 min; 100–20% acetonitrile/H<sub>2</sub>O in 5 min. Gradient 2: 50–100% acetonitrile/H<sub>2</sub>O in 15 min; 100% acetonitrile in 10 min; 100–50% acetonitrile/H<sub>2</sub>O in 5 min. Again, 0.05 vol% of TFA was





incorporated in both solvents. Final compounds were already >95% pure after column chromatography or either purified by preparative HPLC or recrystallised from DMF to attain the needed purity as determined by the above-stated method.

#### 4.1.2. General procedure for amide coupling (method A).

To a solution of the appropriate carboxylic acid (1 mmol) in anhydrous dimethylformamide (DMF, 10 mL), EDC·HCl (2 mmol), HOBT (2 mmol), the corresponding amine (1.3 mmol) and DIPEA (3–6 equiv.) were added and the reaction mixture was stirred at room temperature (rt) until the disappearance of the starting material (usually 60–72 h). After this time water (50 mL) was added, and the mixture was extracted with EtOAc (3 × 50 mL). The combined organic layers were washed with water (5 × 50 mL), brine (1 × 25 mL), dried over anhydrous Na<sub>2</sub>SO<sub>4</sub>, filtered, and concentrated under reduced pressure. The residue was purified by flash chromatography or manual column using dichloromethane/methanol (DCM/MeOH) gradient. The purities of final compounds **8a**, **b**, **d**, **g**, **h** as well as **9a** were >95% after column chromatography as demonstrated by analytical HPLC. Compounds **8c**, **9b**, **15**, and **20** were further purified by preparative HPLC, whereas compounds **8e**, **f** were recrystallised from DMF to be procured in the requisite purity.

#### 4.1.3. General procedure for imide preparation (method B).

To a solution of 4,6-difluoro-1H-indole-2-carboxamide (**10**, 1 mmol) in pyridine (5 mL), the appropriate benzoyl chloride derivative (1.5 mmol) was added, and the reaction mixture was refluxed for 16 h. After cooling, 2 M HCl solution (25 mL) was added and the mixture was extracted with diethyl ether (1 × 25 mL) and EtOAc (3 × 25 mL). The organic layers were collected, washed with brine (1 × 25 mL), dried over anhydrous Na<sub>2</sub>SO<sub>4</sub>, filtered, concentrated under reduced pressure, and purified by flash chromatography using DCM/MeOH gradient. The obtained product was further purified by preparative HPLC to achieve >95% purity.

#### 4.1.4. General procedure for *N*-Boc deprotection (method C).

To a solution of the *N*-Boc protected amine (2 mmol) in 10 mL DCM, 4 mL TFA was added and the reaction mixture was stirred at rt for 12 h. The mixture was then concentrated *in vacuo* and NaHCO<sub>3</sub> solution was added for neutralisation, followed by extraction with DCM (3 × 50 mL). The combined organic phases were washed with brine (1 × 25 mL), dried over anhydrous Na<sub>2</sub>SO<sub>4</sub>, filtered, and concentrated under reduced pressure. The residue was purified by flash chromatography using DCM/MeOH gradient.

*N*-(1-(Adamantan-1-yl)ethyl)-1H-indole-2-carboxamide (**8a**). The title compound was obtained from indole-2-carboxylic acid (**7a**) and rimantadine hydrochloride employing method A and its <sup>1</sup>H NMR data matched the one reported in the literature.<sup>20</sup> White solid, yield: 91%. <sup>1</sup>H NMR (DMSO-*d*<sub>6</sub>) δ 11.50 (s, 1H), 7.86 (d, *J* = 9.5 Hz, 1H), 7.60 (d, *J* = 7.9 Hz, 1H), 7.42 (dd, *J* = 8.2, 0.6 Hz, 1H), 7.23 (d, *J* = 1.4 Hz, 1H), 7.19–7.13 (m, 1H), 7.05–6.99 (m, 1H), 3.83 (overlapping dq, *J* = 7.0 Hz, 1H), 1.94 (s, 3H), 1.72–1.44 (m, 12H), 1.08 (d, *J* = 7.1 Hz, 3H).

*N*-(1-(Adamantan-1-yl)ethyl)-4-methoxy-1H-indole-2-carboxamide (**8b**). The title compound was prepared from 4-methoxyindole-2-carboxylic acid (**7b**) and rimantadine hydrochloride employing method A. Yellow solid, yield: 95%. <sup>1</sup>H NMR

(DMSO-*d*<sub>6</sub>) δ 11.49 (s, 1H), 7.83 (d, *J* = 9.6 Hz, 1H), 7.33 (d, *J* = 1.6 Hz, 1H), 7.11–6.97 (m, 2H), 6.50 (d, *J* = 7.5 Hz, 1H), 3.88 (s, 3H), 3.81 (overlapping dq, *J* = 7.0 Hz, 1H), 1.94 (s, 3H), 1.69–1.47 (m, 12H), 1.06 (d, *J* = 6.9 Hz, 3H); <sup>13</sup>C NMR (DMSO-*d*<sub>6</sub>) δ 160.9, 154.0, 138.2, 131.0, 124.6, 118.6, 105.8, 100.8, 99.6, 55.4, 52.6, 38.6, 37.2, 36.7, 28.3, 14.5; HRMS (ESI) *m/z* calcd for C<sub>22</sub>H<sub>28</sub>N<sub>2</sub>O<sub>2</sub> ([M + H]<sup>+</sup>) *m/z* 353.2224; found 353.2217.

*N*-(1-(Adamantan-1-yl)ethyl)-5-methoxy-1H-indole-2-carboxamide (**8c**). 5-Methoxyindole-2-carboxylic acid (**7c**) and rimantadine hydrochloride were used to synthesise the title compound employing method A. White solid, yield: 99%. <sup>1</sup>H NMR (DMSO-*d*<sub>6</sub>) δ 11.34 (s, 1H), 7.81 (d, *J* = 9.5 Hz, 1H), 7.31 (d, *J* = 8.9 Hz, 1H), 7.13 (d, *J* = 1.5 Hz, 1H), 7.06 (d, *J* = 2.3 Hz, 1H), 6.83 (dd, *J* = 8.9, 2.4 Hz, 1H), 3.83 (overlapping dq, *J* = 7.0 Hz, 1H), 3.76 (s, 3H), 1.94 (s, 3H), 1.72–1.48 (m, 12H), 1.08 (d, *J* = 7.0 Hz, 3H); <sup>13</sup>C NMR (DMSO-*d*<sub>6</sub>) δ 161.0, 154.1, 132.8, 132.1, 127.9, 114.6, 113.5, 103.0, 102.4, 55.7, 52.6, 38.6, 37.1, 36.7, 28.3, 14.5; HRMS (ESI) *m/z* calcd for C<sub>22</sub>H<sub>28</sub>N<sub>2</sub>O<sub>2</sub> ([M + H]<sup>+</sup>) *m/z* 353.2224; found 353.2223.

*N*-(1-(Adamantan-1-yl)ethyl)-5-methyl-1H-indole-2-carboxamide (**8d**). This compound was obtained from 5-methylindole-2-carboxylic acid (**7d**) and rimantadine hydrochloride according to method A. White solid, yield: 66%. <sup>1</sup>H NMR (DMF-*d*<sub>7</sub>) δ 11.40 (s, 1H), 7.86 (d, *J* = 9.6 Hz, 1H), 7.43 (d, *J* = 8.4 Hz, 1H), 7.40 (d, *J* = 0.6 Hz, 1H), 7.27 (dd, *J* = 2.0, 0.6 Hz, 1H), 7.04 (dd, *J* = 8.4, 1.4 Hz, 1H), 3.94 (overlapping dq, *J* = 7.0 Hz, 1H), 2.38 (s, 3H), 1.93 (s, 3H), 1.75–1.53 (m, 12H), 1.12 (d, *J* = 7.0 Hz, 3H); <sup>13</sup>C NMR (DMF-*d*<sub>7</sub>) δ 161.6, 136.0, 133.2, 129.2, 128.7, 125.7, 121.5, 112.6, 102.7, 53.2, 39.1, 37.6, 37.2, 29.1, 21.4, 14.4; HRMS (ESI) *m/z* calcd for C<sub>22</sub>H<sub>28</sub>N<sub>2</sub>O ([M + H]<sup>+</sup>) *m/z* 337.2274; found 337.2269.

*N*-(1-(Adamantan-1-yl)ethyl)-5-chloro-1H-indole-2-carboxamide (**8e**). The title compound was synthesised from 5-chloroindole-2-carboxylic acid (**7e**) and rimantadine hydrochloride employing method A. White solid, yield: 98%. <sup>1</sup>H NMR (DMSO-*d*<sub>6</sub>) δ 11.68 (s, 1H), 7.97 (d, *J* = 9.5 Hz, 1H), 7.67 (d, *J* = 2.0 Hz, 1H), 7.43 (d, *J* = 8.7 Hz, 1H), 7.21 (d, *J* = 0.8 Hz, 1H), 7.16 (dd, *J* = 8.7, 2.1 Hz, 1H), 3.81 (overlapping dq, *J* = 7.0 Hz, 1H), 1.93 (s, 3H), 1.67–1.46 (m, 12H), 1.06 (d, *J* = 7.0 Hz, 3H); <sup>13</sup>C NMR (DMSO-*d*<sub>6</sub>) δ 160.7, 135.2, 133.9, 128.6, 124.6, 123.7, 120.9, 114.3, 102.8, 52.8, 38.6, 37.1, 36.7, 28.3, 14.4; HRMS (ESI) *m/z* calcd for C<sub>21</sub>H<sub>25</sub>ClN<sub>2</sub>O ([M + H]<sup>+</sup>) *m/z* 357.1728; found 357.1732.

*N*-(1-(Adamantan-1-yl)ethyl)-6-bromo-1H-indole-2-carboxamide (**8f**). This compound was obtained from 6-bromoindole-2-carboxylic acid (**7f**) and rimantadine hydrochloride according to method A. White solid, yield: 91%. <sup>1</sup>H NMR (DMSO-*d*<sub>6</sub>) δ 11.66 (s, 1H), 7.97 (d, *J* = 9.5 Hz, 1H), 7.63–7.52 (m, 2H), 7.28 (d, *J* = 1.4 Hz, 1H), 7.16 (dd, *J* = 8.6, 1.7 Hz, 1H), 3.83 (overlapping dq, *J* = 6.9 Hz, 1H), 1.94 (s, 3H), 1.75–1.38 (m, 12H), 1.08 (d, *J* = 7.0 Hz, 3H); <sup>13</sup>C NMR (DMSO-*d*<sub>6</sub>) δ 160.7, 137.5, 133.3, 126.6, 123.8, 123.1, 116.3, 115.1, 103.3, 52.8, 38.6, 37.1, 36.7, 28.3, 14.4; HRMS (ESI) *m/z* calcd for C<sub>21</sub>H<sub>25</sub>BrN<sub>2</sub>O ([M + H]<sup>+</sup>) *m/z* 401.1223; found 401.1224.

*N*-(1-(Adamantan-1-yl)ethyl)-4,6-dichloro-1H-indole-2-carboxamide (**8g**). This compound was prepared from 4,6-dichloroindole-2-carboxylic acid (**7g**) and rimantadine hydrochloride employing method A. White solid, yield: 87%. <sup>1</sup>H NMR



(DMSO- $d_6$ )  $\delta$  12.01 (d,  $J$  = 1.7 Hz, 1H), 8.13 (d,  $J$  = 9.5 Hz, 1H), 7.45–7.39 (m, 2H), 7.19 (d,  $J$  = 1.7 Hz, 1H), 3.82 (overlapping dq,  $J$  = 6.9 Hz, 1H), 1.91 (s, 3H), 1.66–1.45 (m, 12H), 1.06 (d,  $J$  = 7.0 Hz, 3H);  $^{13}\text{C}$  NMR (DMSO- $d_6$ )  $\delta$  160.2, 137.2, 134.1, 128.0, 126.7, 125.3, 119.8, 111.5, 101.2, 52.9, 38.6, 37.1, 36.7, 28.3, 14.4; HRMS (ESI)  $m/z$  calcd for  $\text{C}_{21}\text{H}_{24}\text{Cl}_2\text{N}_2\text{O}$  ( $[\text{M} + \text{H}]^+$ )  $m/z$  391.1338; found 391.1339.

*N*-(1-(Adamantan-1-yl)ethyl)-4,6-difluoro-1H-indole-2-carboxamide (**8h**). 4,6-Difluoroindole-2-carboxylic acid (**7h**) and rimantadine hydrochloride were used to afford the title compound following method A. White solid, yield: 85%.  $^1\text{H}$  NMR (DMSO- $d_6$ )  $\delta$  11.93 (s, 1H), 7.96 (d,  $J$  = 9.5 Hz, 1H), 7.38 (s, 1H), 7.02 (dd,  $J$  = 9.4, 1.7 Hz, 1H), 6.86 (td,  $J$  = 10.4, 2.0 Hz, 1H), 3.82 (overlapping dq,  $J$  = 6.9 Hz, 1H), 1.94 (s, 3H), 1.76–1.45 (m, 12H), 1.07 (d,  $J$  = 7.0 Hz, 3H);  $^{13}\text{C}$  NMR (DMSO- $d_6$ )  $\delta$  160.3, 159.6 (dd,  $J$  = 238.1, 12.1 Hz), 156.2 (dd,  $J$  = 248.5, 15.5 Hz), 138.0 (dd,  $J$  = 15.2, 13.3 Hz), 133.4 (d,  $J$  = 3.2 Hz), 113.6 (d,  $J$  = 21.6 Hz), 98.9, 95.4 (dd,  $J$  = 29.6, 23.3 Hz), 95.0 (dd,  $J$  = 25.9, 4.3 Hz), 52.8, 38.6, 37.1, 36.7, 28.3, 14.4; HRMS (ESI)  $m/z$  calcd for  $\text{C}_{21}\text{H}_{24}\text{F}_2\text{N}_2\text{O}$  ( $[\text{M} + \text{H}]^+$ )  $m/z$  359.1929; found 359.1924.

*N*-Benzyl-4,6-difluoro-1H-indole-2-carboxamide (**9a**). This compound was obtained from 4,6-difluoroindole-2-carboxylic acid (**7h**) and benzylamine employing method A. White solid, yield: 98%.  $^1\text{H}$  NMR (DMSO- $d_6$ )  $\delta$  12.05 (s, 1H), 9.13 (t,  $J$  = 5.9 Hz, 1H), 7.38–7.28 (m, 5H), 7.28–7.20 (m, 1H), 7.04 (dd,  $J$  = 9.4, 1.3 Hz, 1H), 6.87 (td,  $J$  = 10.4, 1.9 Hz, 1H), 4.52 (d,  $J$  = 6.0 Hz, 2H);  $^{13}\text{C}$  NMR (DMSO- $d_6$ )  $\delta$  160.8, 159.7 (dd,  $J$  = 237.0, 12.0 Hz), 156.2 (dd,  $J$  = 248.7, 15.6 Hz), 139.8, 138.1 (dd,  $J$  = 15.2, 13.2 Hz), 133.1 (d,  $J$  = 3.3 Hz), 128.8, 127.7, 127.3, 113.6 (d,  $J$  = 21.7 Hz), 98.9, 95.7 (dd,  $J$  = 29.6, 23.3 Hz), 95.1 (dd,  $J$  = 25.9, 4.4 Hz), 42.7; HRMS (ESI)  $m/z$  calcd for  $\text{C}_{16}\text{H}_{12}\text{F}_2\text{N}_2\text{O}$  ( $[\text{M} + \text{H}]^+$ )  $m/z$  287.0987; found 287.0990.

4,6-Difluoro-*N*-phenyl-1H-indole-2-carbohydrazide (**9b**). Compound **7h** and phenylhydrazine were reacted to deliver the title compound following method A. White solid, yield: 93%.  $^1\text{H}$  NMR (DMSO- $d_6$ )  $\delta$  12.11 (s, 1H), 10.45 (d,  $J$  = 2.0 Hz, 1H), 7.99 (d,  $J$  = 1.7 Hz, 1H), 7.38 (s, 1H), 7.16 (dd,  $J$  = 8.4, 7.4 Hz, 2H), 7.04 (dd,  $J$  = 9.4, 1.4 Hz, 1H), 6.92 (td,  $J$  = 10.4, 2.0 Hz, 1H), 6.78 (d,  $J$  = 7.7 Hz, 2H), 6.73 (t,  $J$  = 7.3 Hz, 1H);  $^{13}\text{C}$  NMR (DMSO- $d_6$ )  $\delta$  161.1, 159.8 (dd,  $J$  = 237.4, 12.1 Hz), 156.2 (dd,  $J$  = 248.9, 15.6 Hz), 149.8, 138.3 (dd,  $J$  = 15.3, 13.0 Hz), 131.4 (d,  $J$  = 3.3 Hz), 129.3, 119.2, 113.6 (d,  $J$  = 21.7 Hz), 112.7, 99.2, 95.9 (dd,  $J$  = 29.6, 23.3 Hz), 95.1 (dd,  $J$  = 25.9, 4.3 Hz); HRMS (ESI)  $m/z$  calcd for  $\text{C}_{15}\text{H}_{11}\text{F}_2\text{N}_3\text{O}$  ( $[\text{M} + \text{H}]^+$ )  $m/z$  288.0943; found 288.0939.

4,6-Difluoro-1H-indole-2-carboxamide (**10**). The title compound was prepared following the procedure published in our previous report and the  $^1\text{H}$  NMR data matched the one therein.<sup>46</sup> Buff solid, yield: 98%.  $^1\text{H}$  NMR (DMSO- $d_6$ )  $\delta$  11.97 (s, 1H), 8.03 (s, 1H), 7.44 (s, 1H), 7.22 (s, 1H), 7.01 (dd,  $J$  = 9.4, 1.9 Hz, 1H), 6.86 (td,  $J$  = 10.5, 2.0 Hz, 1H).

4,6-Difluoro-*N*-(3-fluorobenzoyl)-1H-indole-2-carboxamide (**11a**). The title compound was prepared from **7h** and 3-fluorobenzoyl chloride employing method B. White solid, yield: 32%.  $^1\text{H}$  NMR (DMSO- $d_6$ )  $\delta$  12.31 (s, 1H), 11.31 (s, 1H), 7.79–7.69 (m, 3H), 7.64–7.55 (m, 1H), 7.54–7.46 (m, 1H), 7.07 (dd,  $J$  = 9.3, 1.3 Hz, 1H), 6.95 (td,  $J$  = 10.4, 2.0 Hz, 1H);  $^{13}\text{C}$  NMR (DMSO- $d_6$ )  $\delta$  166.6 (d,  $J$  = 2.6 Hz), 162.2 (d,  $J$  = 244.7 Hz), 160.6 (dd,  $J$  =

240.6, 12.1 Hz), 160.0, 156.7 (dd,  $J$  = 250.4, 15.7 Hz), 139.1 (dd,  $J$  = 15.4, 12.6 Hz), 136.8 (d,  $J$  = 7.1 Hz), 131.5 (d,  $J$  = 3.2 Hz), 131.0 (d,  $J$  = 8.0 Hz), 125.3 (d,  $J$  = 2.8 Hz), 119.8 (d,  $J$  = 21.2 Hz), 115.9 (d,  $J$  = 23.1 Hz), 113.5 (dd,  $J$  = 22.0, 0.5 Hz), 103.8, 96.3 (dd,  $J$  = 30.0, 23.1 Hz), 95.2 (dd,  $J$  = 26.0, 4.6 Hz); HRMS (ESI)  $m/z$  calcd for  $\text{C}_{16}\text{H}_9\text{F}_3\text{N}_2\text{O}_2$  ( $[\text{M} + \text{H}]^+$ )  $m/z$  319.0689; found 319.0686.

*N*-(3-Chlorobenzoyl)-4,6-difluoro-1H-indole-2-carboxamide (**11b**). This compound was synthesised from **7h** and 3-chlorobenzoyl chloride following method B. White solid, yield: 30%.  $^1\text{H}$  NMR (DMSO- $d_6$ )  $\delta$  12.30 (s, 1H), 11.35 (s, 1H), 7.95 (s, 1H), 7.85 (d,  $J$  = 7.8 Hz, 1H), 7.72 (s, 1H), 7.70 (d,  $J$  = 1.0 Hz, 1H), 7.57 (t,  $J$  = 7.9 Hz, 1H), 7.07 (dd,  $J$  = 9.3, 1.2 Hz, 1H), 6.95 (td,  $J$  = 10.4, 1.8 Hz, 1H);  $^{13}\text{C}$  NMR (DMSO- $d_6$ )  $\delta$  166.7, 160.6 (dd,  $J$  = 240.5, 12.2 Hz), 160.1, 156.7 (dd,  $J$  = 250.4, 15.6 Hz), 139.1 (dd,  $J$  = 15.4, 12.6 Hz), 136.6, 133.5, 132.7, 131.5 (d,  $J$  = 2.5 Hz), 130.8, 128.8, 127.8, 113.5 (d,  $J$  = 21.9 Hz), 103.8, 96.3 (dd,  $J$  = 29.9, 23.1 Hz), 95.2 (dd,  $J$  = 25.9, 4.6 Hz); HRMS (ESI)  $m/z$  calcd for  $\text{C}_{16}\text{H}_9\text{ClF}_2\text{N}_2\text{O}_2$  ( $[\text{M} + \text{H}]^+$ )  $m/z$  335.0393; found 335.0393.

*tert*-Butyl 4-(4,6-difluoro-1H-indole-2-carbonyl)piperazine-1-carboxylate (**13**). A mixture of 4,6-difluoroindole **7h** (1.5 mmol), *N*-Boc-piperazine **12** (1.8 mmol), EDC·HCl (1.8 mmol), and DMAP (1.8 mmol) in a 1 : 1 mixture of tetrahydrofuran (THF) and DCM (10 mL each) was stirred at rt for 72 h. The reaction mixture was then quenched with saturated aqueous solution of ammonium chloride (50 mL) and extracted with DCM (3  $\times$  25 mL) and ethyl acetate (3  $\times$  25 mL). The combined organic layers were washed with brine (1  $\times$  25 mL), dried over anhydrous  $\text{Na}_2\text{SO}_4$ , filtered, and concentrated under reduced pressure. The obtained residue was used for the next reaction without further purification; buff solid, yield: 78%.

(4,6-Difluoro-1H-indol-2-yl)(piperazin-1-yl)methanone (**14**). The crude product **13** was *N*-Boc deprotected employing method C to afford the title compound which was >95% pure after flash chromatography. Buff solid, yield: 90%.  $^1\text{H}$  NMR (DMSO- $d_6$ )  $\delta$  7.03 (dd,  $J$  = 9.4, 1.4 Hz, 1H), 6.77 (d,  $J$  = 0.6 Hz, 1H), 6.71 (td,  $J$  = 10.3, 2.0 Hz, 1H), 3.64 (s, 4H), 2.73 (s, 4H);  $^{13}\text{C}$  NMR (DMSO- $d_6$ )  $\delta$  161.5, 159.5 (dd,  $J$  = 238.3, 12.1 Hz), 156.0 (dd,  $J$  = 248.8, 15.5 Hz), 137.6 (dd,  $J$  = 15.2, 13.2 Hz), 131.5 (d,  $J$  = 3.3 Hz), 113.2 (d,  $J$  = 21.7 Hz), 99.9, 95.6 (dd,  $J$  = 29.6, 23.3 Hz), 94.8 (dd,  $J$  = 25.9, 4.4 Hz), 46.1 (br, 4C).

(Adamantan-1-yl)(4-(4,6-difluoro-1H-indole-2-carbonyl)piperazin-1-yl)methanone (**15**). This compound was prepared following method A entailing compound **14** and 1-adamantanecarboxylic acid. White solid, yield: 75%.  $^1\text{H}$  NMR (DMSO- $d_6$ )  $\delta$  12.02 (s, 1H), 7.04 (dd,  $J$  = 9.3, 1.3 Hz, 1H), 6.92 (d,  $J$  = 1.3 Hz, 1H), 6.88 (dd,  $J$  = 10.4, 1.6 Hz, 1H), 3.70 (s, 8H), 1.98 (s, 3H), 1.92 (s, 6H), 1.69 (q,  $J$  = 12.1 Hz, 6H);  $^{13}\text{C}$  NMR (DMSO- $d_6$ )  $\delta$  175.1, 161.6, 159.7 (dd,  $J$  = 238.5, 12.0 Hz), 156.1 (dd,  $J$  = 248.8, 15.4 Hz), 137.7 (dd,  $J$  = 15.2, 13.2 Hz), 131.2 (d,  $J$  = 3.3 Hz), 113.3 (d,  $J$  = 21.6 Hz), 100.5, 95.7 (dd,  $J$  = 29.6, 23.3 Hz), 94.9 (dd,  $J$  = 25.9, 4.3 Hz), 45.1 (br, 4C), 41.4, 38.8, 36.5, 28.4; HRMS (ESI)  $m/z$  calcd for  $\text{C}_{24}\text{H}_{27}\text{F}_2\text{N}_3\text{O}_2$  ( $[\text{M} + \text{H}]^+$ )  $m/z$  428.2131; found 428.2130.

4-((*tert*-Butoxycarbonyl)amino)benzoic acid (**17**). To a solution of 4-aminobenzoic acid (**16**, 3 mmol) in a 1 : 2 mixture of water (10 mL) and dioxane (20 mL), di-*tert*-butyl dicarbonate ( $\text{Boc}_2\text{O}$ , 6 mmol) and triethylamine ( $\text{Et}_3\text{N}$ , 6 mmol) were added and the



reaction mixture was stirred at rt for 48 h. Three quarters of the solvent were then evaporated *in vacuo* and the residue was acidified with 3 M aqueous HCL solution. The formed precipitate was filtered off, washed with water, and dried. The  $^1\text{H}$  NMR data was in agreement with the reported one.<sup>58</sup> White solid, yield: 86%.  $^1\text{H}$  NMR (DMSO- $d_6$ )  $\delta$  9.71 (s, 1H), 7.83 (d,  $J$  = 8.5 Hz, 2H), 7.55 (d,  $J$  = 8.4 Hz, 2H), 1.48 (s, 9H).

*tert*-Butyl (4-((adamantan-1-yl)carbamoyl)phenyl)carbamate (**18**). Compound **17** and 1-adamantylamine were reacted according to method A and the residue, obtained after evaporating the EtOAc extract, was used in the next step without further purification; white solid, yield: 84%.

*N*-(1-Adamantyl)-4-aminobenzamide (**19**). The crude product **18** was *N*-Boc deprotected following method C to deliver the title compound. Brown solid, yield: 96%.  $^1\text{H}$  NMR (DMSO- $d_6$ )  $\delta$  7.51 (dd,  $J$  = 8.5, 1.8 Hz, 2H), 7.02 (s, 1H), 6.50 (dd,  $J$  = 8.5, 1.9 Hz, 2H), 5.50 (s, 2H), 2.03 (s, 9H), 1.64 (s, 6H);  $^{13}\text{C}$  NMR (DMSO- $d_6$ )  $\delta$  166.4, 151.7, 129.2, 123.0, 112.8, 51.5, 41.6, 36.6, 29.4.

*N*-(4-((Adamantan-1-yl)carbamoyl)phenyl)-4,6-difluoro-1*H*-indole-2-carboxamide (**20**). The indole **7h** was coupled with **19** following method A to afford the title compound. White solid, yield: 25%.  $^1\text{H}$  NMR (DMSO- $d_6$ )  $\delta$  12.21 (s, 1H), 10.42 (s, 1H), 7.89–7.80 (m, 4H), 7.58 (d,  $J$  = 1.5 Hz, 1H), 7.49 (s, 1H), 7.08 (dd,  $J$  = 9.3, 1.4 Hz, 1H), 6.94 (td,  $J$  = 10.4, 2.0 Hz, 1H), 2.08 (s, 6H), 2.06 (s, 3H), 1.67 (s, 6H);  $^{13}\text{C}$  NMR (DMSO- $d_6$ )  $\delta$  165.9, 160.1 (dd,  $J$  = 239.4, 12.1 Hz), 159.5, 156.4 (dd,  $J$  = 249.2, 15.6 Hz), 141.4, 138.5 (dd,  $J$  = 15.3, 12.9 Hz), 132.7 (d,  $J$  = 3.3 Hz), 131.4, 128.6, 119.5, 113.6 (d,  $J$  = 21.8 Hz), 100.5, 96.0 (dd,  $J$  = 29.7, 23.2 Hz), 95.2 (dd,  $J$  = 25.9, 4.4 Hz), 51.9, 41.4, 36.6, 29.4; HRMS (ESI)  $m/z$  calcd for  $\text{C}_{26}\text{H}_{25}\text{F}_2\text{N}_3\text{O}_2$  ( $[\text{M} + \text{H}]^+$ )  $m/z$  450.1988; found 450.1987.

## 4.2. Biology

**4.2.1. Anti-TB activity.** MIC was determined using Microplate alamarBlue assay (MABA) as previously reported.<sup>59,60</sup> MABA format was also used in the cytotoxicity evaluation on Vero Cells.<sup>6</sup>

### 4.2.2. Antitumour activity

**4.2.2.1. Cell culture.** The four well-established paediatric brain tumour cell lines were all derived from humans and were used to assess the effects on proliferation and viability when treated with the indole-2-carboxamides. KNS42 (glioblastoma multiforme – GBM), BT-12 and BT-16 (atypical teratoid rhabdoid tumour – AT/RT) cell lines were gifts from Dr Hashizume, Northwestern University, whereas DAOY cells (medulloblastoma – MB) were obtained from ATCC. The human fibroblasts HFF1 (obtained from ATCC) were used as non-neoplastic controls. The KNS42, BT-12 and BT-16 cell lines were maintained in Roswell Park Memorial Institute (RPMI) medium supplemented with 10% fetal bovine serum (FBS). The DAOY cell line was maintained in Eagle's minimal essential medium (EMEM) supplemented with 10% FBS. The HFF1 were maintained in Dulbecco's modified Eagle's medium (DMEM) supplemented with 15% FBS. All media contained 1% penicillin/streptomycin. The cells were incubated at 37 °C in 5%  $\text{CO}_2$ .

**4.2.2.2. Screening.** After extensive optimization at various concentrations and time-points, the compounds were screened in the GBM cell line (KNS42) to assess the impact on proliferation and viability (described below). The cells were treated with 0.5, 1, 2.5, 5, 7.5 and 10  $\mu\text{M}$  of each compound and assessed after 72 hours of treatment, whereupon their  $\text{IC}_{50}$  values were calculated. The top potent compounds with  $\text{IC}_{50}$  values <10  $\mu\text{M}$  were further screened in multiple paediatric brain cancer cell lines, BT-12, BT-16 and DAOY in addition to the non-neoplastic cell line HFF1 to assess their impact on proliferation and viability (described below). The cells were treated with 0.5, 1, 2.5, 5, 7.5 and 10  $\mu\text{M}$  of each compound and assessed after 72 h of treatment.

**4.2.2.3. Cell proliferation assay.** All cell lines were seeded in 96-well plates, at 2000 cells per well, except KNS42 which was seeded at 4000 cell per well. After incubating overnight in normal growth media, the media was aspirated off and 100  $\mu\text{l}$  of treatment media was added. Media containing 0.1% DMSO was used as a control. After 72 h of incubation, the MTT proliferation assay reagents were added as previously described.<sup>61</sup> The absorbance of the assay (570 nm/600 nm) was measured using the CLARIOstar (BMG Lab Tech, USA) and exported into excel, where the data was normalized by removing the background absorbance. The data was analysed and  $\text{IC}_{50}$  values were calculated using PRISM 8 (GraphPad, USA).

**4.2.2.4. Cell viability assay.** All cell lines were seeded at 2000 cells per well, except KNS42 which was seeded at 4000 cell per well, in 96-well plates. After an overnight incubation in normal growth media, the media was aspirated off and 100  $\mu\text{l}$  of treatment media was added. 0.1% DMSO was used in the control media. After 72 h of incubation, the PrestoBlue Viability (ThermoFisher Scientific, USA) was added, per the manufacturer's instructions. The fluorescence of the assay (560 nm/590 nm) was measured using the CLARIOstar (BMG Lab Tech, USA) and exported into Excel, where the data was normalized by removing the background fluorescence. The data was analysed and  $\text{IC}_{50}$  values were calculated using PRISM 8 (GraphPad, USA).

**4.2.2.5. Transcriptional analysis of KNS42 cells.** The KNS42 cell line was maintained in Roswell Park Memorial Institute (RPMI) medium supplemented with 10% fetal bovine serum (FBS) and 1% penicillin/streptomycin and incubated at 37 °C in 5%  $\text{CO}_2$ . The cells were treated with 10  $\mu\text{M}$  of compound **15**. The cells were washed with  $1\times$  PBS, scraped with a cell scraper and centrifuged to collect cell pellets after 72 hours of treatment. RNA was extracted from the cell pellets using TRIzol reagent (Thermo Fisher, USA) and following the protocol from Cold Spring Harbor Laboratory Press.<sup>62</sup> The RNA pellet was resuspended in 50  $\mu\text{l}$  of sterile diethylpyrocarbonate (DEPC) treated water. Concentration of the RNA was measured using the standard Qubit RNA Broad-Range Assay kit (Thermo Fisher, USA) according to the manufacturer's instructions. The RNA samples were submitted to BGI Americas for DNBSEQ Eukaryotic Stranded Transcriptome Resequencing.



### 4.3. Molecular modelling

*In silico* molecular docking analysis was undertaken using the Molecular Operating Environment MOE software version 2008.10 (Chemical Computing Group, Montreal, Canada). The crystal structure of MmpL3 in complex with ICA38 (6AJJ) was retrieved from the protein data bank (PDB) and the docking protocol was similar to our previous report.<sup>46</sup>

## Conflicts of interest

The authors declare no conflict of interest.

## Acknowledgements

SSRA acknowledges Curtin University for the support through Curtin International Postgraduate Research Scholarship (CIPRS). WRB is grateful for the support of NIH grants AI 37856 and HL 133190. HG is thankful for the ARC Discovery Early Career Researcher Award DE160100482.

## References

- World Health Organization, *Global Tuberculosis Report*, Geneva, 2020, retrieved from <https://apps.who.int/iris/bitstream/handle/10665/336069/9789240013131-eng.pdf>.
- K. Dheda, C. E. Barry III and G. Maartens, *Lancet*, 2016, **387**, 1211–1226.
- S. Keshavjee and P. E. Farmer, *N. Engl. J. Med.*, 2012, **367**, 931–936.
- J. A. Caminero, G. Sotgiu, A. Zumla and G. B. Migliori, *Lancet Infect. Dis.*, 2010, **10**, 621–629.
- N. Chim, R. Torres, Y. Liu, J. Capri, G. Batot, J. P. Whitelegge and C. W. Goulding, *Chem. Biol.*, 2015, **22**, 1098–1107.
- S. Lun, H. Guo, O. K. Onajole, M. Pieroni, H. Gunosewoyo, G. Chen, S. K. Tipparaju, N. C. Ammerman, A. P. Kozikowski and W. R. Bishai, *Nat. Commun.*, 2013, **4**, 2907.
- S. P. Rao, S. B. Lakshminarayana, R. R. Kondreddi, M. Herve, L. R. Camacho, P. Bifani, S. K. Kalapala, J. Jiricek, N. L. Ma, B. H. Tan, S. H. Ng, M. Nanjundappa, S. Ravindran, P. G. Seah, P. Thayalan, S. H. Lim, B. H. Lee, A. Goh, W. S. Barnes, Z. Chen, K. Gagaring, A. K. Chatterjee, K. Pethe, K. Kuhen, J. Walker, G. Feng, S. Babu, L. Zhang, F. Blasco, D. Beer, M. Weaver, V. Dartois, R. Glynne, T. Dick, P. W. Smith, T. T. Diagana and U. H. Manjunatha, *Sci. Transl. Med.*, 2013, **5**, 214ra168.
- K. Tahlan, R. Wilson, D. B. Kastrinsky, K. Arora, V. Nair, E. Fischer, S. W. Barnes, J. R. Walker, D. Alland, C. E. Barry III and H. I. Boshoff, *Antimicrob. Agents Chemother.*, 2012, **56**, 1797–1809.
- B. Zhang, J. Li, X. Yang, L. Wu, J. Zhang, Y. Yang, Y. Zhao, L. Zhang, X. Yang, X. Yang, X. Cheng, Z. Liu, B. Jiang, H. Jiang, L. W. Guddat, H. Yang and Z. Rao, *Cell*, 2019, **176**, 636–648.
- Z. Xu, V. A. Meshcheryakov, G. Poce and S. S. Chng, *Proc. Natl. Acad. Sci. U. S. A.*, 2017, **114**, 7993–7998.
- A. E. Grzegorzewicz, H. Pham, V. A. Gundi, M. S. Scherman, E. J. North, T. Hess, V. Jones, V. Gruppo, S. E. Born, J. Kordulakova, S. S. Chavadi, C. Morisseau, A. J. Lenaerts, R. E. Lee, M. R. McNeil and M. Jackson, *Nat. Chem. Biol.*, 2012, **8**, 334–341.
- P. J. Brennan, *Tuberculosis*, 2003, **83**, 91–97.
- C. Hoffmann, A. Leis, M. Niederweis, J. M. Plitzko and H. Engelhardt, *Proc. Natl. Acad. Sci. U. S. A.*, 2008, **105**, 3963–3967.
- J. Liu, C. E. Barry III, G. S. Besra and H. Nikaido, *J. Biol. Chem.*, 1996, **271**, 29545–29551.
- S. S. R. Alsayed, C. C. Beh, N. R. Foster, A. D. Payne, Y. Yu and H. Gunosewoyo, *Curr. Mol. Pharmacol.*, 2019, **12**, 27–49.
- G. Degiacomi, A. Benjak, J. Madacki, F. Boldrin, R. Proveddi, G. Palu, J. Kordulakova, S. T. Cole and R. Manganeli, *Sci. Rep.*, 2017, **7**, 43495.
- W. Li, A. Obregon-Henao, J. B. Wallach, E. J. North, R. E. Lee, M. Gonzalez-Juarrero, D. Schnappinger and M. Jackson, *Antimicrob. Agents Chemother.*, 2016, **60**, 5198–5207.
- W. Li, C. M. Stevens, A. N. Pandya, Z. Darzynkiewicz, P. Bhattarai, W. Tong, M. Gonzalez-Juarrero, E. J. North, H. I. Zgurskaya and M. Jackson, *ACS Infect. Dis.*, 2019, **5**, 1001–1012.
- O. K. Onajole, M. Pieroni, S. K. Tipparaju, S. Lun, J. Stec, G. Chen, H. Gunosewoyo, H. Guo, N. C. Ammerman, W. R. Bishai and A. P. Kozikowski, *J. Med. Chem.*, 2013, **56**, 4093–4103.
- N. D. Franz, J. M. Belardinelli, M. A. Kaminski, L. C. Dunn, V. Calado Nogueira de Moura, M. A. Blaha, D. D. Truong, W. Li, M. Jackson and E. J. North, *Bioorg. Med. Chem.*, 2017, **25**, 3746–3755.
- L. F. Castano, V. Cuartas, A. Bernal, A. Insuasty, J. Guzman, O. Vidal, V. Rubio, G. Puerto, P. Lukac, V. Vimberg, G. Balikova-Novtona, L. Vannucci, J. Janata, J. Quiroga, R. Abonia, M. Noguerras, J. Cobo and B. Insuasty, *Eur. J. Med. Chem.*, 2019, **176**, 50–60.
- G. Cihan-Ustundag and G. Capan, *Mol. Diversity*, 2012, **16**, 525–539.
- G. Cihan-Ustundag, D. Satana, G. Ozhan and G. Capan, *J. Enzyme Inhib. Med. Chem.*, 2016, **31**, 369–380.
- I. Correia, P. Adao, S. Roy, M. Wahba, C. Matos, M. R. Maurya, F. Marques, F. R. Pavan, C. Q. F. Leite, F. AVECILLA and J. Costa Pessoa, *J. Inorg. Biochem.*, 2014, **141**, 83–93.
- T. Taj, R. R. Kamble, T. M. Gireesh, R. K. Hunnur and S. B. Margankop, *Eur. J. Med. Chem.*, 2011, **46**, 4366–4373.
- Y. Shi, Y. H. Duan, Y. Y. Ji, Z. L. Wang, Y. R. Wu, H. Gunosewoyo, X. Y. Xie, J. Z. Chen, F. Yang, J. Li, J. Tang, X. Xie and L. F. Yu, *J. Med. Chem.*, 2017, **60**, 7067–7083.
- A. Moya-Garcia, T. Adeyelu, F. A. Kruger, N. L. Dawson, J. G. Lees, J. P. Overington, C. Orengo and J. A. G. Ranea, *Sci. Rep.*, 2017, **7**, 10102.
- A. S. Reddy and S. Zhang, *Expert Rev. Clin. Pharmacol.*, 2013, **6**, 41–47.
- A. A. Elfiky, *Life Sci.*, 2020, **248**, 117477.



- 30 Q. T. Ostrom, H. Gittleman, P. Liao, C. Rouse, Y. Chen, J. Dowling, Y. Wolinsky, C. Kruchko and J. Barnholtz-Sloan, *Neuro-Oncology*, 2014, **16**(Suppl 4), iv1–iv63.
- 31 A. T. Reddy, *Curr. Neurol. Neurosci. Rep.*, 2001, **1**, 137–143.
- 32 F. He and Y. E. Sun, *Int. J. Biochem. Cell Biol.*, 2007, **39**, 661–665.
- 33 K. R. Jessen and R. Mirsky, *Nature*, 1980, **286**, 736–737.
- 34 D. N. Louis, A. Perry, G. Reifenberger, A. von Deimling, D. Figarella-Branger, W. K. Cavenee, H. Ohgaki, O. D. Wiestler, P. Kleihues and D. W. Ellison, *Acta Neuropathol.*, 2016, **131**, 803–820.
- 35 K. Aldape, K. M. Brindle, L. Chesler, R. Chopra, A. Gajjar, M. R. Gilbert, N. Gottardo, D. H. Gutmann, D. Hargrave, E. C. Holland, D. T. W. Jones, J. A. Joyce, P. Kearns, M. W. Kieran, I. K. Mellingshoff, M. Merchant, S. M. Pfister, S. M. Pollard, V. Ramaswamy, J. N. Rich, G. W. Robinson, D. H. Rowitch, J. H. Sampson, M. D. Taylor, P. Workman and R. J. Gilbertson, *Nat. Rev. Clin. Oncol.*, 2019, **16**, 509–520.
- 36 F. Hanif, K. Muzaffar, K. Perveen, S. M. Malhi and S. U. Simjee, *Asian Pac. J. Cancer Prev.*, 2017, **18**, 3–9.
- 37 J. Fangusaro, *Front. Oncol.*, 2012, **2**, 105.
- 38 Z. Miklja, A. Pasternak, S. Stallard, T. Nicolaidis, C. Kline-Nunnally, B. Cole, R. Beroukhim, P. Bandopadhyay, S. Chi, S. H. Ramkissoon, B. Mullan, A. K. Bruzek, A. Gauthier, T. Garcia, C. Atchison, B. Marini, M. Fouladi, D. W. Parsons, S. Leary, S. Mueller, K. L. Ligon and C. Koschmann, *Neuro-Oncology*, 2019, **21**(8), 968–980.
- 39 G. C. Moraski, L. D. Markley, P. A. Hipkind, H. Boshoff, S. Cho, S. G. Franzblau and M. J. Miller, *ACS Med. Chem. Lett.*, 2011, **2**, 466–470.
- 40 C. T. Peng, C. Gao, N. Y. Wang, X. Y. You, L. D. Zhang, Y. X. Zhu, Y. Xv, W. Q. Zuo, K. Ran, H. X. Deng, Q. Lei, K. J. Xiao and L. T. Yu, *Bioorg. Med. Chem. Lett.*, 2015, **25**, 1373–1376.
- 41 A. P. Kozikowski, O. K. Onajole, J. Stec, C. Dupont, A. Viljoen, M. Richard, T. Chaira, S. Lun, W. Bishai, V. S. Raj, D. Ordway and L. Kremer, *J. Med. Chem.*, 2017, **60**, 5876–5888.
- 42 J. Stec, O. K. Onajole, S. Lun, H. Guo, B. Merenbloom, G. Vistoli, W. R. Bishai and A. P. Kozikowski, *J. Med. Chem.*, 2016, **59**, 6232–6247.
- 43 S. S. R. Alsayed, S. Lun, A. Payne, W. R. Bishai and H. Gunosewoyo, *Bioorg. Chem.*, 2021, **106**, 104486.
- 44 K. A. Abrahams, J. A. Cox, V. L. Spivey, N. J. Loman, M. J. Pallen, C. Constantinidou, R. Fernandez, C. Alemparte, M. J. Remuinan, D. Barros, L. Ballell and G. S. Besra, *PLoS One*, 2012, **7**, e52951.
- 45 G. C. Moraski, P. A. Miller, M. A. Bailey, J. Ollinger, T. Parish, H. I. Boshoff, S. Cho, J. R. Anderson, S. Mulugeta, S. G. Franzblau and M. J. Miller, *ACS Infect. Dis.*, 2015, **1**, 85–90.
- 46 S. S. R. Alsayed, S. Lun, G. Luna, C. C. Beh, A. D. Payne, N. Foster, W. R. Bishai and H. Gunosewoyo, *RSC Adv.*, 2020, **10**, 7523–7540.
- 47 V. Makarov, G. Manina, K. Mikusova, U. Mollmann, O. Ryabova, B. Saint-Joanis, N. Dhar, M. R. Pasca, S. Buroni, A. P. Lucarelli, A. Milano, E. De Rossi, M. Belanova, A. Bobovska, P. Dianiskova, J. Kordulakova, C. Sala, E. Fullam, P. Schneider, J. D. McKinney, P. Brodin, T. Christophe, S. Waddell, P. Butcher, J. Albrethsen, I. Rosenkrands, R. Brosch, V. Nandi, S. Bharath, S. Gaonkar, R. K. Shandil, V. Balasubramanian, T. Balganes, S. Tyagi, J. Grosset, G. Riccardi and S. T. Cole, *Science*, 2009, **324**, 801–804.
- 48 B. Cetin, I. I. Gonul, O. Gumusay, I. Bilgetekin, E. Algin, A. Ozet and A. Uner, *Neuropathology*, 2018, **38**, 457–462.
- 49 G. Moncayo, M. Grzmil, T. Smirnova, P. Zmarz, R. M. Huber, D. Hynx, H. Kohler, Y. Wang, H. R. Hotz, N. E. Hynes, G. Keller, S. Frank, A. Merlo and B. A. Hemmings, *Neuro-Oncology*, 2018, **20**, 621–631.
- 50 M. A. Proescholdt, M. J. Merrill, E. M. Stoerr, A. Lohmeier, F. Pohl and A. Brawanski, *Neuro-Oncology*, 2012, **14**, 1357–1366.
- 51 N. H. Boyd, K. Walker, J. Fried, J. R. Hackney, P. C. McDonald, G. A. Benavides, R. Spina, A. Audia, S. E. Scott, C. J. Libby, A. N. Tran, M. O. Bevensee, C. Griguer, S. Nozell, G. Y. Gillespie, B. Nabors, K. P. Bhat, E. E. Bar, V. Darley-Usmar, B. Xu, E. Gordon, S. J. Cooper, S. Dedhar and A. B. Hjelmeland, *JCI Insight*, 2017, **2**(24), e92928.
- 52 B. Muz, P. de la Puente, F. Azab and A. K. Azab, *Hypoxia*, 2015, **3**, 83–92.
- 53 S. Ivanov, S. Y. Liao, A. Ivanova, A. Danilkovitch-Miagkova, N. Tarasova, G. Weirich, M. J. Merrill, M. A. Proescholdt, E. H. Oldfield, J. Lee, J. Zavada, A. Waheed, W. Sly, M. I. Lerman and E. J. Stanbridge, *Am. J. Pathol.*, 2001, **158**, 905–919.
- 54 M. O. Krisenko and R. L. Geahlen, *Biochim. Biophys. Acta*, 2015, **1853**, 254–263.
- 55 J. Fueyo, M. M. Alonso, B. C. Parker Kerrigan and C. Gomez-Manzano, *Neuro-Oncology*, 2018, **20**, 582–583.
- 56 C. A. Lipinski, F. Lombardo, B. W. Dominy and P. J. Feeney, *Adv. Drug Delivery Rev.*, 2001, **46**, 3–26.
- 57 A. Heguy, A. A. Stewart, J. D. Haley, D. E. Smith and J. G. Foulkes, *Gene Expression*, 1995, **4**, 337–344.
- 58 M. W. Jones, G. Mantovani, C. A. Blindauer, S. M. Ryan, X. Wang, D. J. Brayden and D. M. Haddleton, *J. Am. Chem. Soc.*, 2012, **134**, 7406–7413.
- 59 L. Collins and S. G. Franzblau, *Antimicrob. Agents Chemother.*, 1997, **41**, 1004–1009.
- 60 M. Pieroni, S. K. Tipparaju, S. Lun, Y. Song, A. W. Sturm, W. R. Bishai and A. P. Kozikowski, *ChemMedChem*, 2011, **6**, 334–342.
- 61 S. T. Sredni, M. Suzuki, J. P. Yang, J. Topczewski, A. W. Bailey, T. Gokirmak, J. N. Gross, A. de Andrade, A. Kondo, D. R. Piper and T. Tomita, *Pediatr. Blood Cancer*, 2017, **64**(11), e26551.
- 62 D. C. Rio, M. Ares Jr, G. J. Hannon and T. W. Nilsen, *Cold Spring Harb. Protoc.*, 2010, **2010**, pdb prot5439.



## Conclusions

A literature review on the antitumour potential of the I2Cs was performed in this Chapter with the goal of: 1) analysing and comparing the impact of these compounds on different tumour cells, 2) highlighting the mechanisms of action, whereby the I2Cs elicit their antitumour activity, and 3) exploring the prospect of developing an I2C derivative with dual anti-TB and antitumour activities. Inspired by the well-established potent antitumour activities of various I2Cs against a wide array of tumour cell lines, we reported the anti-TB and antitumour activities of several novel I2C analogues. The preliminary antitumour screening was carried out using paediatric GBM tumour cell line KNS42. Pleasingly, some of our tested derivatives were endowed with dual potent anti-TB and antitumour activities. In addition, other I2C derivatives in our study demonstrated selective potencies towards either TB or grade IV brain tumour cells. Indeed, the *N*-rimantadine-4,6-dichloroindole analogue exhibited the most potent anti-TB activity in our report, whilst showing no antitumour activity against KNS42 cells at 10  $\mu$ M concentration. Of note, the observed TB-related SAR trends augmented our earlier SAR outcomes, documented in our 2021 Bioorganic Chemistry paper (Chapter 4). On the other hand, two compounds, which were bereft of anti-TB efficacy, showed potent inhibitory activities against different tested brain tumour cells. Since, to the best of my knowledge, no I2C analogue was previously tested against KNS42 cells, the mechanism by which our compounds inhibited the proliferation and viability of these tumour cells represented an uncharted territory. In other words, choosing any tumour-related protein target to test our compounds against its activity would have been a mere conjecture. Therefore, we opted alternatively for conducting gene expression profiling of KNS42 cells before and after being treated with one of our two most active compounds. The differential gene expression analysis revealed the significant downregulation of two oncogenes, CA9 and SYK, indicating their likely involvement in the observed antitumour activity of this compound. Overall, the notion of testing the I2Cs against TB and cancer has proven to be a fruitful approach, as evidenced by the promising compounds identified in our most recently published RSC Advances article.

## **Chapter 7**

### **Correlation Between Modulation of Cannabinoid Receptors and the Antitumour Activity of Indole-2-Carboxamides**

## Background

In ongoing efforts towards identifying novel indole-2-carboxamide (I2C) derivatives with polypharmacology profiles, novel I2C analogues and bioisosteres were designed, synthesised, and biologically evaluated for their antitumour and anti-TB activities. It was intriguing to find that cannabinoid receptor 1 (CB<sub>1</sub>R) is overexpressed in the paediatric glioblastoma (GBM) KNS42 cells, used in our preliminary proliferation and viability inhibition screening assays. Within this context, several synthetic cannabinoid receptor modulators (SCRMs) were reported in the literature as potent antitumour agents. In addition, upon looking into previously reported I2Cs with potent cannabinoid (CB) receptors 1 and 2 (CB<sub>1</sub>R and CB<sub>2</sub>R) modulatory activities, uncanny similarities in the chemical structures of these CB receptor modulators and our compounds were detected. Therefore, we were prompted to investigate the functional activities of our most potent antitumour compounds at CB<sub>1</sub>R and CB<sub>2</sub>R. In this regard, the decision to assess the CB functional profiles of our active analogues was predicated on the presumption that CB<sub>1</sub>R and CB<sub>2</sub>R could be involved in our observed antitumour activities. Accordingly, well-known CB receptor modulators were also simultaneously evaluated for their antiproliferative and cytotoxic activities against the tested paediatric brain tumour cell lines for comparison. The cytotoxicities of the most active derivatives and CB receptor reference ligand WIN55,212-2 against non-tumourigenic cells were probed in the healthy human fibroblast cell line HFF1. Additionally, the gene expression profile of KNS42 cells treated with one of our potent antitumour I2C hit compounds was analysed relative to that of the untreated control cells. A set of seven oncogenes were found to be significantly downregulated in comparison to the untreated KNS42 cells, suggesting their involvement in the observed antitumour activity of this I2C analogue.



## 7.1. Introduction

The discovery and validation of many famous multi-target ligands has driven researchers to find new therapeutic applications for existing drugs, clinical candidates, and promising molecules. The concept of drug repurposing was generally correlated with serendipity, in which the unintended effects of chemical compounds led to the beneficial discovery of new indications, exemplified by sildenafil. However, it must be taken into consideration that a strong drug promiscuity can backfire and result in many undesired side effects. In the previous Chapter, several I2Cs with anti-TB and/or antitumour activities were identified (published in our RSC Advances 2021 article). Interestingly, some of these analogues showed negligible cytotoxicity towards healthy cells, suggesting their selective activity against TB and tumour cells. Fascinated by the promising results documented therein, a follow-up work on the I2Cs and some I2C bioisosteres was conducted (discussed later in this Chapter).

Upon studying the characteristics of paediatric KNS42 cell line, used in our preliminary antitumour screening, we found that these GBM cells overexpress CB<sub>1</sub>R, which is encoded by the *CNR1* gene (data not shown). A plethora of literature reports documented that CB receptors constitute viable targets for the treatment of cancer, owing to their ability to regulate key signalling pathways implicated in cell growth and survival (1). Indeed, the antitumour activities of several well-known cannabinoids were previously correlated to their activities at CB receptors (2). For instance, rimonabant (**1**, SR141716, **Figure 7.1**), a CB<sub>1</sub>R inverse agonist/antagonist was previously found to inhibit the growth of human breast cancer cells (overexpressing CB<sub>1</sub>R), both *in vitro* and *in vivo*, via CB<sub>1</sub>R-mediated mechanism (3). These findings were further substantiated by the lack of activity of this compound against Chinese hamster ovary cell (CHO), wherein CB<sub>1</sub>R expression was not detected (3).

Similarly, Flygare *et al* demonstrated that several CB receptor ligands, including rimonabant, suppress the growth and viability in addition to inducing apoptosis in mantle cell lymphoma (MCL) cell lines expressing high levels of CB<sub>1</sub>R and moderate levels of CB<sub>2</sub>R (4). In contrast, their control cells, lacking CB<sub>1</sub>R, were not affected by the tested CB receptor ligands, indicating the involvement of CB receptors in their observed antitumour activities (4). Other studies also showed the potent antiproliferative and/or apoptotic effects of rimonabant against other tumour cells and

xenografts, such as colorectal cancer (CRC) cells and leukemia (5-9). Importantly, rimonabant demonstrated low/no toxicity against healthy normal cell, suggesting its selectivity against tumour cells (5, 8). Of note, the authors of these studies also proposed other different underlying mechanisms of the antitumour activity of rimonabant, apart from its CB<sub>1</sub>R modulation (5-8).

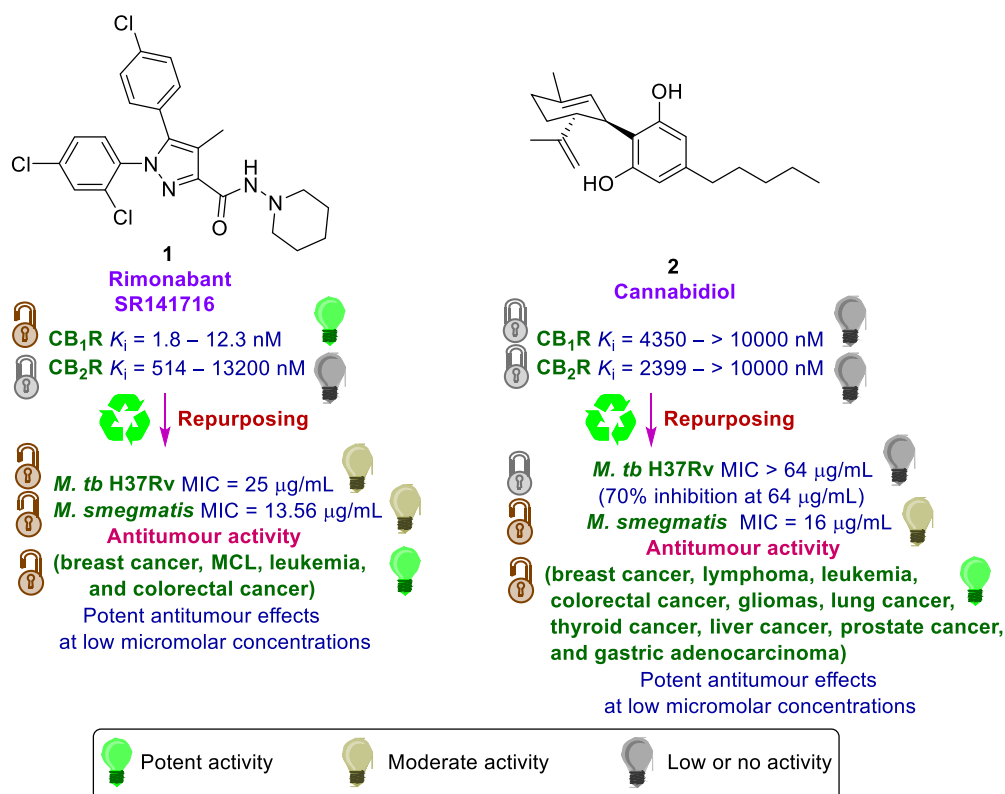


**Figure 7.1. Repurposing of CB receptors ligands rimonabant and cannabidiol against *M. tb*, *M. smegmatis*, and various tumour cells.**

Rimonabant **1** was found to have pleiotropic effects in various diseases (10). The most prominent function of rimonabant is its anorectic effect. In fact, it was approved as an antiobesity drug in 2006 by the European Medicines Agency (EMA), but it was withdrawn from the market globally in 2008 as its post marketing surveillance revealed that it caused serious psychiatric side effects, such as suicidal ideation (11, 12). The antiobesity attribute of rimonabant is derived from its ability to block the CB<sub>1</sub>R, which regulates food intake at both the peripheral and central levels (6). Indeed, rimonabant showed significantly higher affinity for CB<sub>1</sub>R ( $K_i = 1.8 - 12.3$  nM) over CB<sub>2</sub>R ( $K_i = 514 - 13200$  nM) (13, 14). Interestingly, in line with the polypharmacology scope of this

Chapter, when rimonabant was subsequently repurposed as an antimycobacterial agent, it manifested an appreciable inhibitory activity against *Mycobacterium tuberculosis* (*M. tb*) H37Rv strain [minimum inhibitory concentration (MIC) = 25 µg/mL] via targeting MmpL3 (15-17). It also inhibited the growth of *Mycobacterium smegmatis* (*M. smegmatis*) with an MIC value of 13.56 µg/mL (15).

Similar to rimonabant, cannabidiol (CBD, **2**, **Figure 7.1**) is a non-psychoactive phytocannabinoid that acts as an inverse agonist/antagonist at CB<sub>1</sub>R and CB<sub>2</sub>R and was extensively reported in the literature as an antitumour agent (13, 18-20). It has a low affinity for both CB<sub>1</sub>R ( $K_i = 4350 - > 10000$  nM) and CB<sub>2</sub>R ( $K_i = 2399 - > 10000$  nM) (13). Therefore, the antitumour effects of CBD were found to be likely attributed to CB receptors-independent mechanisms (2). However, McKallip *et al* previously demonstrated that CBD reduced cell viability and induced apoptosis in leukemia cells, both *in vitro* and *in vivo*, through CB<sub>2</sub>R-mediated mechanism (21). In fact, human lymphomas and leukemias were shown to express significantly higher levels of CB<sub>2</sub>R compared to other tumours, explaining the sensitivity of leukemia cells to CBD (18).

Importantly, CBD inhibited the viability of human GBM cells U87 and U373 with IC<sub>50</sub> values around 25 µM (22). The observed antiproliferative effect of CBD in these glioma cells was partially counteracted by CB<sub>2</sub>R antagonist SR144528 but was not affected by CB<sub>1</sub>R antagonist SR141716 (rimonabant). Neither of the preceding antagonists was able to reverse the CBD-induced glioma cell death (22). Nonetheless, the antitumour attributes of CBD against gliomas are predominately reported to be independent of CB<sub>1</sub>R and CB<sub>2</sub>R (23-26). Of note, CBD showed potent antiproliferative activity against other GBM cell lines with IC<sub>50</sub> values less than 10 µM, such as U251, U87, and SF126 cell lines (IC<sub>50</sub> = 0.6 – 1.2 µM) (27-29). In addition to its activity against the foregoing tumours, CBD showed potent antineoplastic activities at low micromolar concentrations against other tumour cell lines, such as CRC, prostate cancer, breast cancer, lung cancer, thyroid cancer, liver cancer, and gastric adenocarcinoma (27, 28, 30). The antitumour effects of CBD run the gamut from inhibition of proliferation/growth, viability, migration, invasion, and metastasis to the induction of tumour cell death (apoptosis) (28).

In terms of paediatric oncology, there is a paucity of research on the activity of medicinal cannabinoids therein (31). In 2021, Andradas *et al* collated the data reported

in the literature on the activity of cannabinoids, including CBD, against paediatric tumours (31). Interestingly, in a clinical study conducted on the effects of CBD in 119 cancer patients, a male child (5 years old) with posterior fossa ependymoma, a very rare brain tumour, manifested the best response to the CBD treatment (32). After undergoing standard treatments, including surgeries, chemotherapy, and radiotherapy, this child was left with no other therapeutic option (32). He was then prescribed CBD as a sole treatment in February 2016. Remarkably, when a magnetic resonance imaging was carried out on his brain in December 2016, after nearly 10 months of CBD treatment, an approximately 60% reduction in tumour volume was discerned (32). Significant decreases in tumour volumes were also detected in other elderly patients with different types of cancer, such as oesophageal cancer, breast cancer, and prostate cancer. More importantly, the maximum tolerated dose of CBD in this study could not be determined owing to the complete absence of side effects (32).

Apart from its antitumour effects, the antimicrobial potential of CBD was investigated in a wide range of Gram-positive and Gram-negative bacteria in a recent study, wherein it showed potent activities (MIC = 0.25 – 4 µg/mL) against multiple strains, such as *Staphylococcus aureus* (*S. aureus*) and *Streptococcus pneumoniae* (33). When the authors evaluated the antimycobacterial activity of CBD, it showed marginal activity against *M. tb* (70% inhibition against H37Rv strain at 64 µg/mL) and moderate potency against *M. smegmatis* (MIC = 16 µg/mL) (33). However, the mechanisms of action of CBD as antimycobacterial agent are yet to be determined. Overall, both rimonabant and CBD were shown to be multi-target directed agents, impacting different disease pathways, including TB and cancer (**Figure 7.1**). In addition, cannabinoids generally possess promising antitumour effects against a vast array of human neoplasms, dependently or independently of their CB receptors modulatory functions (2, 34, 35).

## **7.2. Indole-Based SCRM: Transition From the Indole-3-Carboxamide (I3C) Scaffold to The I2C**

SCRMs constitute an ever-growing class of recreational/psychoactive "designer drugs" with a wide degree of structural heterogeneity (36). Indeed, to bypass legal prohibitions, new unregulated psychoactive SCRMs have been produced in the illicit

markets of recreational drugs. These SCRM typically act as agonists at both the CB<sub>1</sub>R and CB<sub>2</sub>R. The psychoactivity is attributed to the ability of these compounds to activate CB<sub>1</sub>R, which is predominantly located in the central nervous system (CNS) (36). Compared to  $\Delta^9$ -tetrahydrocannabinol ( $\Delta^9$ -THC, the psychoactive constituent of marijuana), which is a partial agonist at CB<sub>1</sub>R, most of the SCRM are full agonists at CB<sub>1</sub>R with significantly higher potency and efficacy than  $\Delta^9$ -THC, accounting for more dangerous side-effects (37).

A myriad of I3C analogues have been developed and identified as potent CB<sub>1</sub>R and CB<sub>2</sub>R agonists (38-42). Interestingly, there were no prior reports on some of these I3C-based SCRM in the literature at the time they were detected and identified in seized "Spice-like" products. For instance, the *N*-(1-adamantyl)-1-pentyl-1*H*-indole-3-carboxamide (APICA, SDB-001, **3**, **Figure 7.2**) and 5-fluoro-APICA (STS-135, **4**) were unprecedented before their discovery in psychotropic substances in the Japanese illegal market (43-45). In 2013, Banister *et al* performed structure-activity relationship (SAR) studies on APICA and reported the *N*-benzyl I3C cannabimimetic derivative SDB-006 (**5**), which was detected alongside its 5-fluoropentyl analogue (5-F-SDB-006, **6**) in Finland in the same year (36). The foregoing I3C analogues **3** – **6** were found to function as mixed CB<sub>1</sub>R and CB<sub>2</sub>R agonists with EC<sub>50</sub> values of 13 – 134 nM (41) (**Figure 7.2**).

In 2017, Shi *et al* investigated the effect of shifting the amide handle from position 3 to position 2 of the indole ring (46). Intriguingly, all the tested I2C analogues in their study behaved as selective CB<sub>2</sub>R agonists, while they failed to activate or antagonise the CB<sub>1</sub>R at 10  $\mu$ M concentration, suggesting the lack of psychoactive effects of these compounds (46). The I2C-derived APICA analogue **7** (**Figure 7.2**) displayed an EC<sub>50</sub> value of 0.72  $\mu$ M at the CB<sub>2</sub>R. The highlight of their study was the homologous *N*-adamantyl-1-(4-hydroxybutyl)-I2C derivative **8** (**Figure 7.2**) which showed an EC<sub>50</sub> value of approximately 0.12  $\mu$ M (118 nM) at the CB<sub>2</sub>R (46). Surprisingly, the functional activity of the *N*-1 unsubstituted I2C compound **9** at the CB receptors (no agonism or antagonism at CB<sub>1</sub>R at 10  $\mu$ M concentration, CB<sub>2</sub>R EC<sub>50</sub> = 0.98  $\mu$ M) resembled that of the 1-pentane-I2C analogue **7** (**Figure 7.2**). Similarly, the despentyl APICA analogue (*N*-adamantyl-1*H*-I3C) behaved as a selective CB<sub>2</sub>R agonist (EC<sub>50</sub> = 0.63  $\mu$ M), with no stimulation or antagonism showed at CB<sub>1</sub>R at 10  $\mu$ M concentration (46). Thus far, the preceding findings indicate that switching the 3-amido pendant to position

2 of the indole ring brings about selectivity at CB<sub>2</sub>R over CB<sub>1</sub>R. In addition, removing indole *N*-1 substituents in the I3C and I2C SCRMs seems to help overturn the activity at CB<sub>1</sub>R.

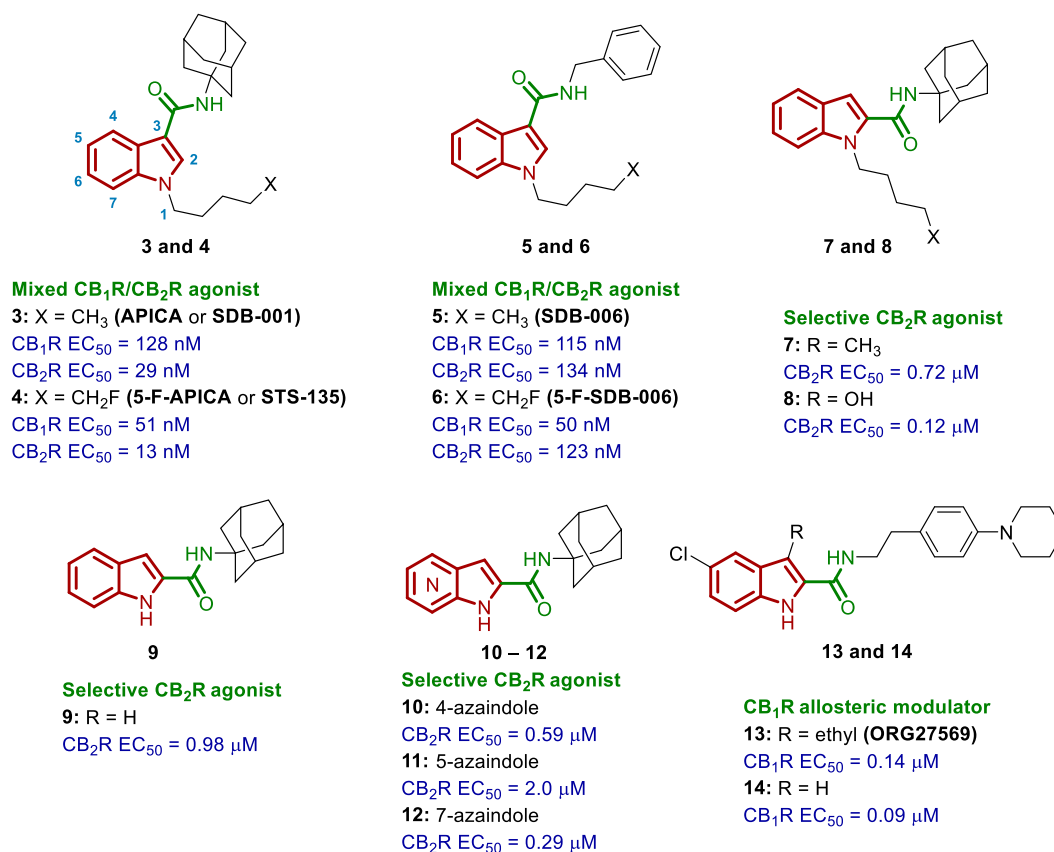


**Figure 7.2. Selected I3C and I2C analogues with potent modulatory activities at CB<sub>1</sub>R and/or CB<sub>2</sub>R receptors.**

In 2019, with the intent of improving the water solubility, the same group bioisosterically replaced the indole ring of I2Cs with an azaindole nucleus (47). Similar to compound **9**, the 4-, 5-, and 7-azaindole derivatives **10 – 12** (**Figure 7.2**) were found to be selective CB<sub>2</sub>R agonists [EC<sub>50</sub> CB<sub>2</sub>R = 0.59, 2.0, and 0.29, respectively; EC<sub>50</sub> CB<sub>1</sub>R = not active (NA) at 10 μM]. When these three 1*H*-azaindoles **10 – 12** were substituted at position 1 of the indole ring with an *n*-pentyl group, the resulting *N*-1 substituted derivatives remained inactive at CB<sub>1</sub>R. At CB<sub>2</sub>R, the despentyl azaindoles **10 – 12** showed agonistic activities comparable to or higher than the corresponding 1-pentane-azaindoles-2-carboxamides (47). In the same year, Moir *et al*/investigated the functional activities of numerous *N*-1 substituted azaindole analogues at CB<sub>1</sub>R and

CB<sub>2</sub>R (48). They showed that moving the amide appendage from position 3 of the azaindole ring to position 2 imparts selectivity at CB<sub>2</sub>R, corroborating Shi *et al*/findings (48).

Prior to the aforementioned investigations on the I2C framework as a replacement to the I3C one, several *N*-phenylethyl-1*H*-I2C analogues were extensively researched and were found to act as allosteric modulators of CB<sub>1</sub>R. Allosteric ligands bind to a site topographically distinct from the binding site of the orthosteric/endogenous ligands (49). The therapeutic potential of the CB receptor allosteric ligands is attributed to their lack of intrinsic efficacy when administered alone, although there are some exceptions (50). Indeed, they can enhance [positive allosteric modulators (PAMs)], diminish [negative allosteric modulators (NAMs)], or do not affect [neutral allosteric ligands (NALs)] the response of orthosteric/endogenous ligands at the CB receptors. In other words, allosteric ligands allow for the modulation of CB receptors signalling without the desensitisation, dependence, or tolerance (50). CB<sub>1</sub>R allosteric modulators possess multiple potential advantages, such as circumventing the CB<sub>1</sub>R-mediated side effects (associated with some orthosteric ligands) and providing a mechanism for more precise regulation of the downstream events (51, 52). Accordingly, allosterically modulating CB<sub>1</sub>R signalling may enable the separation between the side effects and the therapeutic benefits (49).

The first CB<sub>1</sub>R allosteric modulators were documented by Price *et al*/in 2005. The three I2C derivatives, exemplified by Org27569 (**13**, **Figure 7.2**), investigated in their study were shown to allosterically modulate CB<sub>1</sub>R (53). These I2C analogues markedly increased the binding of the CB<sub>1</sub>R and CB<sub>2</sub>R non-selective agonist CP55940 at CB<sub>1</sub>R, behaving as PAMs. In contrast, the same compounds significantly decreased the binding of CB<sub>1</sub>R inverse agonist/antagonist SR141716 (rimonabant), acting as NAMs (53). Following this report, numerous research efforts were focused on incorporating various structural modifications into the I2C framework and investigating the impact thereof on the CB<sub>1</sub>R allosteric modulation (54-59). In general, the 3,5-disubstituted-*N*-phenethyl-1*H*-indole-2-carboxamide architecture of Org27569 was retained in most of the subsequently designed analogues, which, expectedly, spawned a subset of new I2C analogues with potent allosteric modulatory activities at CB<sub>1</sub>R (54-59). Of note, most of these reports maintained the 5-chloro functionality on the indole ring, suggesting that it is critical for the allosteric activity at CB<sub>1</sub>R (54-58). Nonetheless, in

2016, when Kulkarni *et al* replaced the 5-chloro group in Org27569 with 5-isothiocyanate (5-NCS) functionality, the resulting isothiocyanate-containing analogue showed an improved allosteric activity profile compared to Org27569 (59, 60).

Interestingly, in 2012, Piscitelli *et al* demonstrated that compound **14** (**Figure 7.2**), in which they excised the ethyl group at position 3 of the indole ring in Org27569, maintained the positive allosteric modulation behaviour (61). In fact, compound **14** potently stimulated the binding of CP55940 at CB<sub>1</sub>R in a nanomolar EC<sub>50</sub> value, showing higher activity compared to that of Org27569 (EC<sub>50</sub> = 90 nM and 0.14 μM, respectively) (61). On the other hand, several 5-chloro and 5-cyano I2C derivatives were found to behave as CB<sub>1</sub>R antagonists when different substituents were introduced to position 1 of the indole ring in studies carried out by Cowley *et al* in 2011 (62, 63). Overall, a multitude of 1*H*-I2Cs were documented in the literature as potent CB receptor ligands with various functional activities, acting as selective CB<sub>2</sub>R agonists, CB<sub>1</sub>R allosteric modulators, or CB<sub>1</sub>R antagonists.

### 7.3. I2Cs with Polypharmacology Profile Resembling Cannabinoids

As mentioned in the previous section, in 2017, Shi *et al* documented the selective CB<sub>2</sub>R agonistic activity of the *N*-adamantyl I2C analogue **9** (EC<sub>50</sub> = 0.98 μM) (46). In the same year, Franz *et al* discovered the potent antimycobacterial activity of this compound (64) (**Figure 7.3**). Indeed, this I2C derivative not only displayed excellent activity against *M. tb* (MIC = 0.68 μM), but it also showed potent efficacy against six tested non-tuberculous mycobacterial (NTM) strains (MIC = 0.85 – 5.3 μM) and moderate activity against *Mycobacterium avium* (*M. avium*, MIC = 27 μM). In the same report, when compound **9** was evaluated against other bacterial strains, namely *Pseudomonas aeruginosa* (*P. aeruginosa*) and *S. aureus*, it was devoid of activity (MIC > 543 μM) (64). The discrepancies in the activity of this I2C analogue against the foregoing microbes suggest its selective antibacterial activity against the mycobacterium species, which further verify the mycobacterial membrane protein large 3 (MmpL3) as the target of this molecule. In addition, this compound showed no cytotoxicity against human THP-1 cell line up to 50 μM concentration (64). In our 2021 published article in the RSC Advances journal (Chapter 6), the I2C analogue **9** was synthesised and evaluated for its antitumour activity against paediatric GBM KNS42 cell line. Pleasingly, it showed potent inhibitory activity against the viability of KNS42



cells ( $IC_{50} = 0.33 \mu\text{M}$ ), while the proliferation of the cells remained unaffected at  $10 \mu\text{M}$  concentration. Taken together, the polypharmacology profile of the *N*-adamantyl I2C derivative **9** (Figure 7.3) is indeed reminiscent of rimonabant and CBD activity profiles (Figure 7.1).

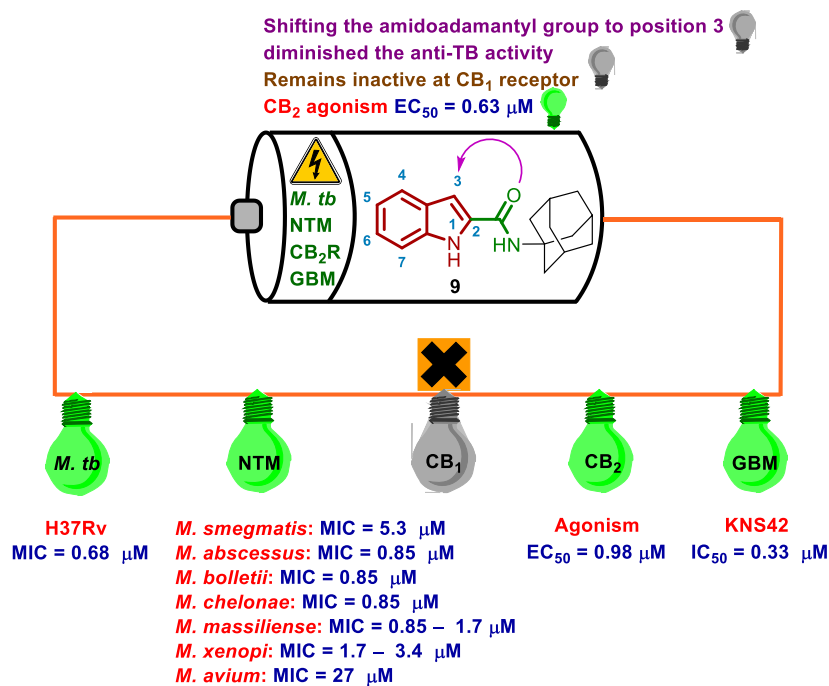


Figure 7.3. The *N*-adamantyl I2C analogue **9** as a multi-target directed ligand.

#### 7.4. Multimodality of Quinolone-3-Carboxylic Acids/Carboxamides

Quinolones represent the first set of fully synthetic anti-infective agents to be discovered that were not knowingly modelled after any antibacterial natural products (65). FQs were subsequently foregrounded, constituting a class of broad-spectrum antibiotics and an integral component of Gram-negative and Gram-positive bacterial infections therapy. FQs are privileged antibiotics that are endowed with wide therapeutic indices, favourable physicochemical properties, and synthetic tractability (65), all of which accounted for the success of the FQs. These favourable characteristics made the FQs ideal compounds for repurposing and development of new biologically active agents. Indeed, several FQs were shown to behave as multimodal drugs (65). For instance, an oscillation between antimicrobial and antitumour activities was demonstrated in CPF (Chapter 6). In addition to its

remarkable antibacterial activities, CPF inhibited the growth of colon cancer HT-29 cell line and leukemia Jurkat cell line with  $IC_{50}$  values of 9.46 and 25  $\mu\text{g}/\text{mL}$ , respectively (66, 67).

Similar to the I3C analogues, a multitude of quinolone-3-carboxamides were reported in the literature as CB receptor modulators (68, 69). In this regard, a group in Italy carried out a series of investigations on the biological potential of the 4-quinolone-3-carboxylic acid/carboxamide framework (70-76). They highlighted numerous 4-quinolone-3-carboxamides as selective  $CB_2R$  ligands; they acted as agonists (with potent antinociceptive effects *in vivo*) or inverse agonists at  $CB_2R$ , with  $K_i$  values in the sub-nanomolar or low nanomolar range (71-76). In 2008 (71), they discovered the high  $CB_2R$  affinity and selectivity of the *N*-adamantyl-4-quinolone-3-carboxamide derivative **15** ( $CB_1R$   $K_i$  = 1220 nM and  $CB_2R$   $K_i$  = 6.3 nM, **Figure 7.4**). This compound produced analgesia in formalin-treated mice via acting as a potent  $CB_2R$  agonist. Indeed, compound **15**-induced inhibition of the formalin-caused nocifensive response in mice was attenuated when AM630, a  $CB_2R$  antagonist, was administered to mice beforehand (71). The same group published a report in 2009, documenting the diverse biological activities of the quinolone analogues (77). In 2019, the prototype compound **15**, which was assigned the name COR167, was evaluated for its antitumour activity against human GBM and astrocytoma cells obtained from specimens collected during neurosurgical operations (78). Remarkably, this compound inhibited the proliferation of the preceding tumour cells at 10 nM concentration by 50.3 – 53% and 49.5 – 51.7%, respectively. Importantly, the antiproliferative effects of COR167 was completely reversed in the presence of the  $CB_2R$  antagonist AM630, indicating that the antitumour potential of COR167 in these glioma cells is attributed to its binding to the  $CB_2R$  expressed therein (78).

In 2015, the 2-quinolone-3-carboxamide and 2-oxo-1,8-naphthyridine-3-carboxamide derivatives **16** and **17** (**Figure 7.4**) were identified as highly selective  $CB_2R$  ligands ( $CB_1R$   $K_i$  = 227 and 138.5 nM, respectively, and  $CB_2R$   $K_i$  = 1.5 and 0.75 nM, respectively) (79). While compound **16** acted as a full agonist at  $CB_2R$ , the naphthyridine analogue **17** behaved as a partial agonist at  $CB_2R$ . In the same report, when these analogues were evaluated against prostate cancer LNCaP cell line expressing  $CB_2R$ , potent cytotoxic activities were observed [ $IC_{50}$  (viability) = 3.90 and 2.08  $\mu\text{M}$ , respectively]. When the LNCaP cells were pretreated with a  $CB_2R$  antagonist

previously synthesised by the same group, the cytotoxic activities induced by compounds **16** and **17** were reversed, resulting in restorations of cell viability at levels comparable to the control (79). Accordingly, similar to COR167, the antitumour effects of **16** and **17** in LNCaP cells are ascribed to their CB<sub>2</sub>R agonistic activities. The therapeutic utility of CB<sub>2</sub>R ligands in cancer and various other diseases is detailed in several review articles (80-82). Overall, while the quinolone-3-carboxylic acid architecture was proven to have potent antibacterial and antitumour activities, the quinolone-3-carboxamide framework was shown to possess affinities at CB<sub>2</sub>R higher than that of CB<sub>1</sub>R. The CB<sub>2</sub>R agonistic effects of some quinolone-3-carboxamides were correlated with potent analgesic and/or antitumour activities.

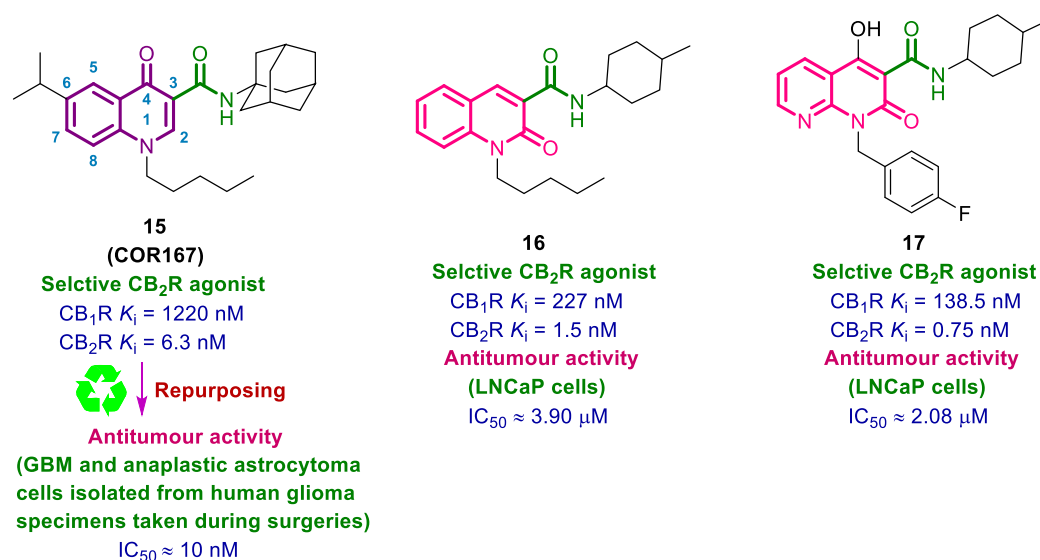
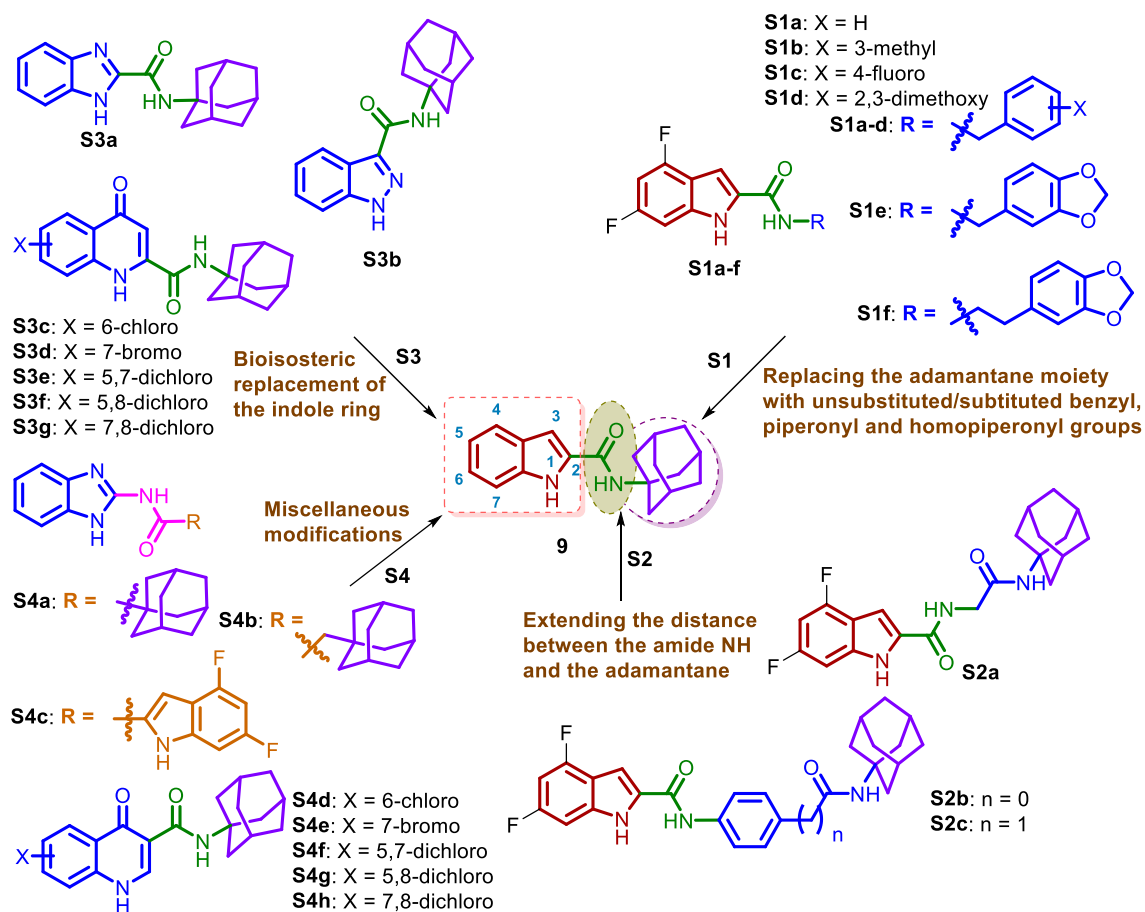


Figure 7.4. Functional activities at CB receptors and antitumour activities of quinolone-3-carboxamides **15** – **17**.

## 7.5. Design/Repurposing, Synthesis, and Biological Evaluation of Novel I2C Derivatives and Bioisosteres against *M. tb* and Paediatric Brain Tumour Cells

Following the identification of several I2C analogues possessing potent anti-TB and antitumour activities (RSC Advances 2021 article, Chapter 6), further SAR studies were undertaken to identify more potent derivatives with polypharmacology profiles. Our results were recently published in the RSC Medicinal Chemistry journal. Using the *N*-adamantyl I2C derivative **9** as a lead compound, the design strategies (S1 – S4) of the new analogues are summarised in **Figure 7.5**. All final compounds were initially

tested for their growth inhibitory activities against *M. tb* and paediatric GBM KNS42 cell line. Since KNS42 cells were found to be overexpressing CB<sub>1</sub>R (data not shown), well-known non-selective and selective CB receptor ligands were evaluated for their antitumour activities and used for comparison.



**Figure 7.5.** Design strategies of new and repurposed analogues as antitumour agents

The first strategy (S1) entailed maintaining the indole moiety and the carboxamide linker, while replacing the adamantane ring with an unsubstituted/substituted benzyl (**S1a-d**), a piperonyl (**S1e**), or a homopiperonyl group (**S1f**). The second strategy (S2) comprised stretching the linker between the indole ring and the adamantane (**S2a-c**). Next (S3), the indole ring was biososterically replaced with a benzimidazole (**S3a**), an indazole (**S3b**), or a substituted quinolone motif (**S3c-g**). Of note, while the benzimidazole-2-carboxamide and indazole-3-carboxamide motifs were previously shown to behave as potent CB receptor ligands (36, 47), the functional profile of the

quinolone-2-carboxamide scaffold at CB receptors has not been addressed yet. Finally (S4), miscellaneous changes were simultaneously incorporated in the I2C framework of **9** including: 1) while a benzimidazole ring was introduced instead of the indole moiety, the amide linker at position 2 was reversed and the adamantane moiety was either maintained (**S4a,b**) or replaced with a 4,6-difluoroindole ring (**S4c**), and 2) several substituted quinolones (**S4d-h**) were further probed, wherein the carboxamide moiety was shifted from position 2 to position 3 (**Figure 7.5**). As previously mentioned in this Chapter, like the I3C architecture, the quinolone-3-carboxamide framework modulates the activity of the CB receptors.

All the synthesised analogues were evaluated for their growth inhibition against *M. tb*. The anti-TB activities of the quinolone-containing compounds **S3c-g** and **S4d-h** were documented in our 2020 RSC Advances article (Chapter 3). All the quinoloneamides were inactive against *M. tb* H37Rv strain (MIC  $\geq$  32  $\mu\text{g/mL}$ ), except for the 7-bromo and 5,7-dichloro-4-quinolone-2-carboxamide derivatives **S3d,e**, which showed moderate activities (MIC = 8 and 16  $\mu\text{g/mL}$ , respectively). Both compounds demonstrated no antiproliferative or cytotoxic activities against paediatric GBM KNS42 cells at 10  $\mu\text{M}$  concentration. Importantly, the most potent derivative against KNS42 cells in the quinolone set of compounds was the 5,8-dichloro-4-quinolone-3-carboxamide analogue **S4g** [IC<sub>50</sub> (viability and proliferation) = 9.06 and 2.92  $\mu\text{M}$ , respectively].

The anti-TB activities of the two adamantane-based benzimidazoles, with reversed amide linker **S4a,b**, were assessed in our Bioorganic Chemistry article, published in 2021 (Chapter 4). While **S4a** showed good inhibitory activity against *M. tb* H37Rv strain (MIC = 4  $\mu\text{g/mL}$ ), compound **S4b** demonstrated no activity with an MIC value > 32  $\mu\text{g/mL}$ . Conversely, compound **S4a** displayed no inhibitory activity against KNS42 cells in the viability and proliferation assays, whilst compound **S4b** showed moderate antiproliferative activity with IC<sub>50</sub> value of 6.46  $\mu\text{M}$ . The rest of the final compounds **S1a-f**, **S2a-c**, **S3a,b**, and **S4c** were inactive when tested against *M. tb* H37Rv strain (MIC > 32  $\mu\text{g/mL}$ , unpublished results). However, when tested against KNS42 cells, several analogues showed potent inhibitory activities against the viability and proliferation of KNS42 cells. Importantly, selective CB<sub>2</sub>R agonist **8** (**Figure 7.2**) was one of the reference compounds that was synthesised and evaluated for its anti-TB and antitumour activity. It demonstrated no inhibitory activity against *M. tb* H37Rv

strain (MIC > 64 µg/mL), in line with the previous inactivity (83) encountered when the indole NH was substituted. Compound **8** inhibited the viability of KNS42 cells with an IC<sub>50</sub> value of 4.75 µM, while the proliferation of the cells remained unaffected at 10 µM concentration. In contrast, compounds **S3a,b** which were previously reported to act as selective CB<sub>2</sub>R agonists (CB<sub>2</sub>R EC<sub>50</sub> = 0.52 and 0.086 µM, respectively, CB<sub>1</sub>R EC<sub>50</sub> > 10 µM (47)), failed to inhibit the viability and proliferation of KNS42 cells.

The novel *N*-homopiperonyl-I2C analogue **S1f** showed potent cytotoxic and antiproliferative activities against all tested brain tumour cell lines in our study. Interestingly, when we evaluated **S1f** for its functional activity at CB receptors, it behaved as a selective CB<sub>1</sub>R antagonist (IC<sub>50</sub> = 0.373 µM); it showed no activation or inhibition at CB<sub>2</sub>R (EC<sub>50</sub>/IC<sub>50</sub> > 10 µM). In general, the most active compounds in our study were evaluated for their agonistic and antagonistic activities at both CB<sub>1</sub>R and CB<sub>2</sub>R. Dissonance was discerned between their antitumour activities and functional profiles at CB receptors. Of note, further studies will be undertaken in the future to examine the allosteric modulation potential of the top potent compounds at CB receptors. Similar to the strategy adopted in the recently published RSC advances article (Chapter 6), a gene transcriptional analysis of KNS42 cells before and after being treated with one of the most active compounds was performed. The recently published RSC Medicinal Chemistry article is included herein.

## References

1. Bifulco M, Malfitano AM, Pisanti S, Laezza C. Endocannabinoids in endocrine and related tumours. *Endocr Relat Cancer*. 2008;15(2):391-408.
2. Laezza C, Pagano C, Navarra G, Pastorino O, Proto MC, Fiore D, et al. The Endocannabinoid System: A Target for Cancer Treatment. *Int J Mol Sci*. 2020;21(3).
3. Sarnataro D, Pisanti S, Santoro A, Gazzo P, Malfitano AM, Laezza C, et al. The cannabinoid CB1 receptor antagonist rimonabant (SR141716) inhibits human breast cancer cell proliferation through a lipid raft-mediated mechanism. *Mol Pharmacol*. 2006;70(4):1298-306.
4. Flygare J, Gustafsson K, Kimby E, Christensson B, Sander B. Cannabinoid receptor ligands mediate growth inhibition and cell death in mantle cell lymphoma. *FEBS Lett*. 2005;579(30):6885-9.
5. Fiore D, Ramesh P, Proto MC, Piscopo C, Franceschelli S, Anzelmo S, et al. Rimonabant Kills Colon Cancer Stem Cells without Inducing Toxicity in Normal Colon Organoids. *Front Pharmacol*. 2017;8:949.
6. Santoro A, Pisanti S, Grimaldi C, Izzo AA, Borrelli F, Proto MC, et al. Rimonabant inhibits human colon cancer cell growth and reduces the formation of precancerous lesions in the mouse colon. *Int J Cancer*. 2009;125(5):996-1003.
7. Proto MC, Fiore D, Piscopo C, Franceschelli S, Bizzarro V, Laezza C, et al. Inhibition of Wnt/beta-Catenin pathway and Histone acetyltransferase activity by Rimonabant: a therapeutic target for colon cancer. *Sci Rep*. 2017;7(1):11678.
8. Gallotta D, Nigro P, Cotugno R, Gazzo P, Bifulco M, Belisario MA. Rimonabant-induced apoptosis in leukemia cell lines: activation of caspase-dependent and -independent pathways. *Biochem Pharmacol*. 2010;80(3):370-80.
9. Gazzo P, Malfitano AM, Proto MC, Santoro A, Pisanti S, Caruso MG, et al. Synergistic inhibition of human colon cancer cell growth by the cannabinoid CB1 receptor antagonist rimonabant and oxaliplatin. *Oncol Rep*. 2010;23(1):171-5.
10. Bifulco M, Grimaldi C, Gazzo P, Pisanti S, Santoro A. Rimonabant: just an antiobesity drug? Current evidence on its pleiotropic effects. *Mol Pharmacol*. 2007;71(6):1445-56.
11. Moreira FA, Crippa JA. The psychiatric side-effects of rimonabant. *Braz J Psychiatry*. 2009;31(2):145-53.

12. Sam AH, Salem V, Ghatei MA. Rimonabant: From RIO to Ban. *J Obes.* 2011;2011:432607.
13. Pertwee RG, Howlett AC, Abood ME, Alexander SP, Di Marzo V, Elphick MR, et al. International Union of Basic and Clinical Pharmacology. LXXIX. Cannabinoid receptors and their ligands: beyond CB(1) and CB(2). *Pharmacol Rev.* 2010;62(4):588-631.
14. Song KS, Lee SH, Chun HJ, Kim JY, Jung ME, Ahn K, et al. Design, synthesis and biological evaluation of piperazine analogues as CB1 cannabinoid receptor ligands. *Bioorg Med Chem.* 2008;16(7):4035-51.
15. Gajbhiye JM, More NA, Patil MD, Ummanni R, Kotapalli SS, Yogeeswari P, et al. Discovery of Rimonabant and its potential analogues as anti-TB drug candidates. *Med Chem Res.* 2015;24(7):2960-71.
16. Ramesh R, Shingare RD, Kumar V, Anand A, B S, Veeraraghavan S, et al. Repurposing of a drug scaffold: Identification of novel sila analogues of rimonabant as potent antitubercular agents. *Eur J Med Chem.* 2016;122:723-30.
17. Zhang B, Li J, Yang X, Wu L, Zhang J, Yang Y, et al. Crystal Structures of Membrane Transporter MmpL3, an Anti-TB Drug Target. *Cell.* 2019;176(3):636-48 e13.
18. Massi P, Solinas M, Cinquina V, Parolaro D. Cannabidiol as potential anticancer drug. *Br J Clin Pharmacol.* 2013;75(2):303-12.
19. Kis B, Ifrim FC, Buda V, Avram S, Pavel IZ, Antal D, et al. Cannabidiol-from Plant to Human Body: A Promising Bioactive Molecule with Multi-Target Effects in Cancer. *Int J Mol Sci.* 2019;20(23).
20. Wang F, Multhoff G. Repurposing Cannabidiol as a Potential Drug Candidate for Anti-Tumor Therapies. *Biomolecules.* 2021;11(4).
21. McKallip RJ, Jia W, Schlomer J, Warren JW, Nagarkatti PS, Nagarkatti M. Cannabidiol-induced apoptosis in human leukemia cells: A novel role of cannabidiol in the regulation of p22phox and Nox4 expression. *Mol Pharmacol.* 2006;70(3):897-908.
22. Massi P, Vaccani A, Ceruti S, Colombo A, Abbracchio MP, Parolaro D. Antitumor effects of cannabidiol, a nonpsychoactive cannabinoid, on human glioma cell lines. *J Pharmacol Exp Ther.* 2004;308(3):838-45.
23. Solinas M, Massi P, Cinquina V, Valenti M, Bolognini D, Gariboldi M, et al. Cannabidiol, a non-psychoactive cannabinoid compound, inhibits proliferation and



invasion in U87-MG and T98G glioma cells through a multitarget effect. *PLoS One*. 2013;8(10):e76918.

24. Massi P, Valenti M, Vaccani A, Gasperi V, Perletti G, Marras E, et al. 5-Lipoxygenase and anandamide hydrolase (FAAH) mediate the antitumor activity of cannabidiol, a non-psychoactive cannabinoid. *J Neurochem*. 2008;104(4):1091-100.
25. Vaccani A, Massi P, Colombo A, Rubino T, Parolaro D. Cannabidiol inhibits human glioma cell migration through a cannabinoid receptor-independent mechanism. *Br J Pharmacol*. 2005;144(8):1032-6.
26. Massi P, Vaccani A, Bianchessi S, Costa B, Macchi P, Parolaro D. The non-psychoactive cannabidiol triggers caspase activation and oxidative stress in human glioma cells. *Cell Mol Life Sci*. 2006;63(17):2057-66.
27. Ligresti A, Moriello AS, Starowicz K, Matias I, Pisanti S, De Petrocellis L, et al. Antitumor activity of plant cannabinoids with emphasis on the effect of cannabidiol on human breast carcinoma. *J Pharmacol Exp Ther*. 2006;318(3):1375-87.
28. Seltzer ES, Watters AK, MacKenzie D, Jr., Granat LM, Zhang D. Cannabidiol (CBD) as a Promising Anti-Cancer Drug. *Cancers (Basel)*. 2020;12(11).
29. Marcu JP, Christian RT, Lau D, Zielinski AJ, Horowitz MP, Lee J, et al. Cannabidiol enhances the inhibitory effects of delta9-tetrahydrocannabinol on human glioblastoma cell proliferation and survival. *Mol Cancer Ther*. 2010;9(1):180-9.
30. Ramer R, Merkord J, Rohde H, Hinz B. Cannabidiol inhibits cancer cell invasion via upregulation of tissue inhibitor of matrix metalloproteinases-1. *Biochem Pharmacol*. 2010;79(7):955-66.
31. Andradas C, Truong A, Byrne J, Endersby R. The Role of Cannabinoids as Anticancer Agents in Pediatric Oncology. *Cancers (Basel)*. 2021;13(1).
32. Kenyon J, Liu W, Dalglish A. Report of Objective Clinical Responses of Cancer Patients to Pharmaceutical-grade Synthetic Cannabidiol. *Anticancer Res*. 2018;38(10):5831-5.
33. Blaskovich MAT, Kavanagh AM, Elliott AG, Zhang B, Ramu S, Amado M, et al. The antimicrobial potential of cannabidiol. *Commun Biol*. 2021;4(1):7.
34. Bogdanovic V, Mrdjanovic J, Borisev I. A Review of the Therapeutic Antitumor Potential of Cannabinoids. *J Altern Complement Med*. 2017;23(11):831-6.
35. Nikan M, Nabavi SM, Manayi A. Ligands for cannabinoid receptors, promising anticancer agents. *Life Sci*. 2016;146:124-30.

36. Banister SD, Connor M. The Chemistry and Pharmacology of Synthetic Cannabinoid Receptor Agonist New Psychoactive Substances: Evolution. *Handb Exp Pharmacol.* 2018;252:191-226.
37. Pacher P, Steffens S, Hasko G, Schindler TH, Kunos G. Cardiovascular effects of marijuana and synthetic cannabinoids: the good, the bad, and the ugly. *Nat Rev Cardiol.* 2018;15(3):151-66.
38. Banister SD, Adams A, Kevin RC, Macdonald C, Glass M, Boyd R, et al. Synthesis and pharmacology of new psychoactive substance 5F-CUMYL-P7AICA, a scaffold-hopping analog of synthetic cannabinoid receptor agonists 5F-CUMYL-PICA and 5F-CUMYL-PINACA. *Drug Test Anal.* 2019;11(2):279-91.
39. Banister SD, Longworth M, Kevin R, Sachdev S, Santiago M, Stuart J, et al. Pharmacology of Valinate and tert-Leucinate Synthetic Cannabinoids 5F-AMBICA, 5F-AMB, 5F-ADB, AMB-FUBINACA, MDMB-FUBINACA, MDMB-CHMICA, and Their Analogues. *ACS Chem Neurosci.* 2016;7(9):1241-54.
40. Banister SD, Moir M, Stuart J, Kevin RC, Wood KE, Longworth M, et al. Pharmacology of Indole and Indazole Synthetic Cannabinoid Designer Drugs AB-FUBINACA, ADB-FUBINACA, AB-PINACA, ADB-PINACA, 5F-AB-PINACA, 5F-ADB-PINACA, ADBICA, and 5F-ADBICA. *ACS Chem Neurosci.* 2015;6(9):1546-59.
41. Banister SD, Stuart J, Kevin RC, Edington A, Longworth M, Wilkinson SM, et al. Effects of bioisosteric fluorine in synthetic cannabinoid designer drugs JWH-018, AM-2201, UR-144, XLR-11, PB-22, 5F-PB-22, APICA, and STS-135. *ACS Chem Neurosci.* 2015;6(8):1445-58.
42. Banister SD, Wilkinson SM, Longworth M, Stuart J, Apetz N, English K, et al. The synthesis and pharmacological evaluation of adamantane-derived indoles: cannabimimetic drugs of abuse. *ACS Chem Neurosci.* 2013;4(7):1081-92.
43. Uchiyama N, Kawamura M, Kikura-Hanajiri R, Goda Y. Identification of two new-type synthetic cannabinoids, N-(1-adamantyl)-1-pentyl-1H-indole-3-carboxamide (APICA) and N-(1-adamantyl)-1-pentyl-1H-indazole-3-carboxamide (APINACA), and detection of five synthetic cannabinoids, AM-1220, AM-2233, AM-1241, CB-13 (CRA-13), and AM-1248, as designer drugs in illegal products. *Forensic Toxicol.* 2012;30(2):114-25.
44. Uchiyama N, Kawamura M, Kikura-Hanajiri R, Goda Y. URB-754: A new class of designer drug and 12 synthetic cannabinoids detected in illegal products. *Forensic Sci Int.* 2013;227(1):21-32.

45. Uchiyama N, Matsuda S, Kawamura M, Kikura-Hanajiri R, Goda Y. Two new-type cannabimimetic quinolinyl carboxylates, QUPIC and QUCHIC, two new cannabimimetic carboxamide derivatives, ADB-FUBINACA and ADBICA, and five synthetic cannabinoids detected with a thiophene derivative  $\alpha$ -PVT and an opioid receptor agonist AH-7921 identified in illegal products. *Forensic Toxicol.* 2013;31(2):223-40.
46. Shi Y, Duan YH, Ji YY, Wang ZL, Wu YR, Gunosewoyo H, et al. Amidoalkylindoles as Potent and Selective Cannabinoid Type 2 Receptor Agonists with in Vivo Efficacy in a Mouse Model of Multiple Sclerosis. *J Med Chem.* 2017;60(16):7067-83.
47. Ji YY, Wang ZL, Pei FN, Shi JJ, Li JJ, Gunosewoyo H, et al. Introducing nitrogen atoms to amidoalkylindoles: potent and selective cannabinoid type 2 receptor agonists with improved aqueous solubility. *Medchemcomm.* 2019;10(12):2131-9.
48. Moir M, Lane S, Lai F, Connor M, Hibbs DE, Kassiou M. Strategies to develop selective CB2 receptor agonists from indole carboxamide synthetic cannabinoids. *Eur J Med Chem.* 2019;180:291-309.
49. An D, Peigneur S, Hendrickx LA, Tytgat J. Targeting Cannabinoid Receptors: Current Status and Prospects of Natural Products. *Int J Mol Sci.* 2020;21(14).
50. Gado F, Meini S, Bertini S, Digiacoio M, Macchia M, Manera C. Allosteric modulators targeting cannabinoid cb1 and cb2 receptors: implications for drug discovery. *Future Med Chem.* 2019;11(15):2019-37.
51. Dopart R, Lu D, Lichtman AH, Kendall DA. Allosteric modulators of cannabinoid receptor 1: developing compounds for improved specificity. *Drug Metab Rev.* 2018;50(1):3-13.
52. Khajehali E, Malone DT, Glass M, Sexton PM, Christopoulos A, Leach K. Biased Agonism and Biased Allosteric Modulation at the CB1 Cannabinoid Receptor. *Mol Pharmacol.* 2015;88(2):368-79.
53. Price MR, Baillie GL, Thomas A, Stevenson LA, Easson M, Goodwin R, et al. Allosteric modulation of the cannabinoid CB1 receptor. *Mol Pharmacol.* 2005;68(5):1484-95.
54. Mahmoud MM, Ali HI, Ahn KH, Damaraju A, Samala S, Pulipati VK, et al. Structure-activity relationship study of indole-2-carboxamides identifies a potent allosteric modulator for the cannabinoid receptor 1 (CB1). *J Med Chem.* 2013;56(20):7965-75.

55. Khurana L, Ali HI, Olszewska T, Ahn KH, Damaraju A, Kendall DA, et al. Optimization of chemical functionalities of indole-2-carboxamides to improve allosteric parameters for the cannabinoid receptor 1 (CB1). *J Med Chem*. 2014;57(7):3040-52.
56. Cawston EE, Connor M, Di Marzo V, Silvestri R, Glass M. Distinct Temporal Fingerprint for Cyclic Adenosine Monophosphate (cAMP) Signaling of Indole-2-carboxamides as Allosteric Modulators of the Cannabinoid Receptors. *J Med Chem*. 2015;58(15):5979-88.
57. Nguyen T, German N, Decker AM, Li JX, Wiley JL, Thomas BF, et al. Structure-activity relationships of substituted 1H-indole-2-carboxamides as CB1 receptor allosteric modulators. *Bioorg Med Chem*. 2015;23(9):2195-203.
58. Qiao CJ, Ali HI, Ahn KH, Kolluru S, Kendall DA, Lu D. Synthesis and biological evaluation of indole-2-carboxamides bearing photoactivatable functionalities as novel allosteric modulators for the cannabinoid CB1 receptor. *Eur J Med Chem*. 2016;121:517-29.
59. Kulkarni PM, Kulkarni AR, Korde A, Tichkule RB, Laprairie RB, Denovan-Wright EM, et al. Novel Electrophilic and Photoaffinity Covalent Probes for Mapping the Cannabinoid 1 Receptor Allosteric Site(s). *J Med Chem*. 2016;59(1):44-60.
60. Abood ME. Allosteric Modulators: A Side Door. *J Med Chem*. 2016;59(1):42-3.
61. Piscitelli F, Ligresti A, La Regina G, Coluccia A, Morera L, Allara M, et al. Indole-2-carboxamides as allosteric modulators of the cannabinoid CB(1) receptor. *J Med Chem*. 2012;55(11):5627-31.
62. Cowley PM, Baker J, Barn DR, Buchanan KI, Carlyle I, Clark JK, et al. The discovery of novel indole-2-carboxamides as cannabinoid CB(1) receptor antagonists. *Bioorg Med Chem Lett*. 2011;21(1):497-501.
63. Cowley PM, Baker J, Buchanan KI, Carlyle I, Clark JK, Clarkson TR, et al. Pharmacokinetic optimisation of novel indole-2-carboxamide cannabinoid CB1 antagonists. *Bioorg Med Chem Lett*. 2011;21(7):2034-9.
64. Franz ND, Belardinelli JM, Kaminski MA, Dunn LC, Calado Nogueira de Moura V, Blaha MA, et al. Design, synthesis and evaluation of indole-2-carboxamides with pan anti-mycobacterial activity. *Bioorg Med Chem*. 2017;25(14):3746-55.
65. Idowu T, Schweizer F. Ubiquitous Nature of Fluoroquinolones: The Oscillation between Antibacterial and Anticancer Activities. *Antibiotics (Basel)*. 2017;6(4).
66. Bourikas LA, Kolios G, Valatas V, Notas G, Drygiannakis I, Pelagiadis I, et al. Ciprofloxacin decreases survival in HT-29 cells via the induction of TGF-beta1

secretion and enhances the anti-proliferative effect of 5-fluorouracil. *Br J Pharmacol.* 2009;157(3):362-70.

67. Koziel R, Szczepanowska J, Magalska A, Piwocka K, Duszynski J, Zablocki K. Ciprofloxacin inhibits proliferation and promotes generation of aneuploidy in Jurkat cells. *J Physiol Pharmacol.* 2010;61(2):233-9.

68. Stern E, Muccioli GG, Bosier B, Hamtiaux L, Millet R, Poupaert JH, et al. Pharmacomodulations around the 4-oxo-1,4-dihydroquinoline-3-carboxamides, a class of potent CB2-selective cannabinoid receptor ligands: consequences in receptor affinity and functionality. *J Med Chem.* 2007;50(22):5471-84.

69. Spinelli F, Capparelli E, Abate C, Colabufo NA, Contino M. Perspectives of Cannabinoid Type 2 Receptor (CB2R) Ligands in Neurodegenerative Disorders: Structure-Affinity Relationship (SAfiR) and Structure-Activity Relationship (SAR) Studies. *J Med Chem.* 2017;60(24):9913-31.

70. Pasquini S, Mugnaini C, Tintori C, Botta M, Trejos A, Arvela RK, et al. Investigations on the 4-quinolone-3-carboxylic acid motif. 1. Synthesis and structure-activity relationship of a class of human immunodeficiency virus type 1 integrase inhibitors. *J Med Chem.* 2008;51(16):5125-9.

71. Pasquini S, Botta L, Semeraro T, Mugnaini C, Ligresti A, Palazzo E, et al. Investigations on the 4-quinolone-3-carboxylic acid motif. 2. Synthesis and structure-activity relationship of potent and selective cannabinoid-2 receptor agonists endowed with analgesic activity in vivo. *J Med Chem.* 2008;51(16):5075-84.

72. Pasquini S, Ligresti A, Mugnaini C, Semeraro T, Cicione L, De Rosa M, et al. Investigations on the 4-quinolone-3-carboxylic acid motif. 3. Synthesis, structure-affinity relationships, and pharmacological characterization of 6-substituted 4-quinolone-3-carboxamides as highly selective cannabinoid-2 receptor ligands. *J Med Chem.* 2010;53(16):5915-28.

73. Pasquini S, De Rosa M, Pedani V, Mugnaini C, Guida F, Luongo L, et al. Investigations on the 4-quinolone-3-carboxylic acid motif. 4. Identification of new potent and selective ligands for the cannabinoid type 2 receptor with diverse substitution patterns and antihyperalgesic effects in mice. *J Med Chem.* 2011;54(15):5444-53.

74. Mugnaini C, Nocerino S, Pedani V, Pasquini S, Tafi A, De Chiaro M, et al. Investigations on the 4-quinolone-3-carboxylic acid motif part 5: modulation of the

physicochemical profile of a set of potent and selective cannabinoid-2 receptor ligands through a bioisosteric approach. *ChemMedChem*. 2012;7(5):920-34.

75. Pasquini S, De Rosa M, Ligresti A, Mugnaini C, Brizzi A, Caradonna NP, et al. Investigations on the 4-quinolone-3-carboxylic acid motif. 6. Synthesis and pharmacological evaluation of 7-substituted quinolone-3-carboxamide derivatives as high affinity ligands for cannabinoid receptors. *Eur J Med Chem*. 2012;58:30-43.

76. Mugnaini C, Brizzi A, Ligresti A, Allara M, Lamponi S, Vacondio F, et al. Investigations on the 4-Quinolone-3-carboxylic Acid Motif. 7. Synthesis and Pharmacological Evaluation of 4-Quinolone-3-carboxamides and 4-Hydroxy-2-quinolone-3-carboxamides as High Affinity Cannabinoid Receptor 2 (CB2R) Ligands with Improved Aqueous Solubility. *J Med Chem*. 2016;59(3):1052-67.

77. Mugnaini C, Pasquini S, Corelli F. The 4-quinolone-3-carboxylic acid motif as a multivalent scaffold in medicinal chemistry. *Curr Med Chem*. 2009;16(14):1746-67.

78. Cioni C, Tassi M, Marotta G, Mugnaini C, Corelli F, Annunziata P. A Novel Highly Selective Cannabinoid CB2 Agonist Reduces in vitro Growth and TGF-beta Release of Human Glial Cell Tumors. *Cent Nerv Syst Agents Med Chem*. 2019;19(3):206-14.

79. Manera C, Malfitano AM, Parkkari T, Lucchesi V, Carpi S, Fogli S, et al. New quinolone- and 1,8-naphthyridine-3-carboxamides as selective CB2 receptor agonists with anticancer and immuno-modulatory activity. *Eur J Med Chem*. 2015;97:10-8.

80. Han S, Thatte J, Buzard DJ, Jones RM. Therapeutic utility of cannabinoid receptor type 2 (CB(2)) selective agonists. *J Med Chem*. 2013;56(21):8224-56.

81. Aghazadeh Tabrizi M, Baraldi PG, Borea PA, Varani K. Medicinal Chemistry, Pharmacology, and Potential Therapeutic Benefits of Cannabinoid CB2 Receptor Agonists. *Chem Rev*. 2016;116(2):519-60.

82. Mangiatordi GF, Intranuovo F, Delre P, Abatematteo FS, Abate C, Niso M, et al. Cannabinoid Receptor Subtype 2 (CB2R) in a Multitarget Approach: Perspective of an Innovative Strategy in Cancer and Neurodegeneration. *J Med Chem*. 2020;63(23):14448-69.

83. Onajole OK, Pieroni M, Tipparaju SK, Lun S, Stec J, Chen G, et al. Preliminary structure-activity relationships and biological evaluation of novel antitubercular indolecarboxamide derivatives against drug-susceptible and drug-resistant *Mycobacterium tuberculosis* strains. *J Med Chem*. 2013;56(10):4093-103.

## STATEMENT OF CONTRIBUTION TO A CO-AUTHORED PUBLISHED PAPER

The second half of Chapter 7 includes a co-authored research article that has been published online in the RSC Medicinal Chemistry journal (2021)

DOI: <https://doi.org/10.1039/D1MD00065A>

Publication link: <https://pubs.rsc.org/en/content/articlelanding/2021/md/d1md00065a>

**Title: Synthesis and antitumour evaluation of indole-2-carboxamides against paediatric brain cancer cells**

**Authors/Co-authors: Shahinda S. R. Alsayed, Amreena Suri, Anders W. Bailey, Samuel Lane, Eryn L. Werry, Chiang-Ching Huang, Li-Fang Yu, Michael Kassiou, Simone Treiger Sredni and Hendra Gunosewoyo**

My contribution to the paper involved: 1) the conception, design, synthesis, purification, and chemical analysis of all the tested molecules, 2) interpreting all the results (chemistry and biology wise), 3) collecting and organising the information/data/references, 4) analysing the differential gene expression data and determining the potential mechanism of action of the novel analogues as antitumour agents, and 5) preparing and writing up the whole manuscript.

(Signed)  (Date) 20/09/2021

Shahinda Sayed Rabie Alsayed

(Countersigned)  (Date) 20/9/21

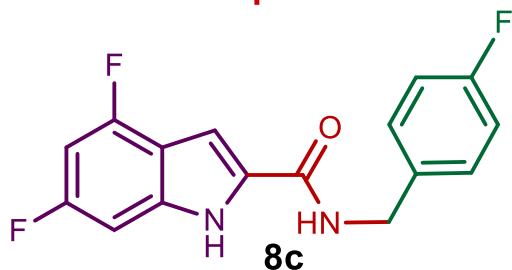
Corresponding author of the paper: Dr Hendra Gunosewoyo

(Countersigned)  (Date) 20/9/21

Main supervisor: Dr Hendra Gunosewoyo

## Graphical abstract

### Indole-2-carboxamides: Antitumour potential and selectivity against paediatric glioma



**GBM KNS42 cells:**

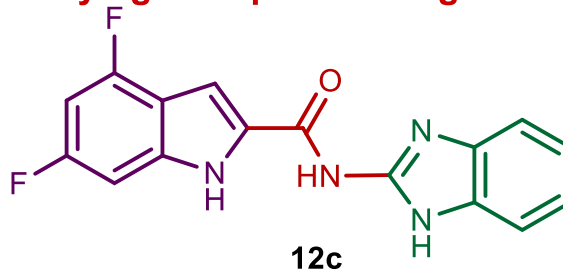
Viability  $IC_{50}$  = 3.41  $\mu$ M

**AT/RT and DAOY tumour cells:**

Viability  $IC_{50}$  = 4.10 – 9.23  $\mu$ M

**non-neoplastic HFF1 cells:**

Viability  $IC_{50}$  = 281  $\mu$ M



**GBM KNS42 cells:**

Viability  $IC_{50}$  = 4.49  $\mu$ M

**AT/RT and DAOY tumour cells:**

Viability  $IC_{50}$  = 1.02 – 7.65  $\mu$ M

**non-neoplastic HFF1 cells:**

Viability  $IC_{50}$  = 115  $\mu$ M



Cite this: *RSC Med. Chem.*, 2021, 12, 1910

# Synthesis and antitumour evaluation of indole-2-carboxamides against paediatric brain cancer cells†

Shahinda S. R. Alsayed,<sup>a</sup> Amreena Suri,<sup>b</sup> Anders W. Bailey,<sup>b</sup> Samuel Lane,<sup>c</sup> Eryn L. Werry,<sup>cd</sup> Chiang-Ching Huang,<sup>e</sup> Li-Fang Yu,<sup>f</sup> Michael Kassiou,<sup>g\*</sup> Simone Treiger Sredni<sup>h\*bg</sup> and Hendra Gunosewoyo<sup>id\*<sup>a</sup></sup>

Paediatric glioblastomas are rapidly growing, devastating brain neoplasms with an invasive phenotype. Radiotherapy and chemotherapy, which are the current therapeutic adjuvant to surgical resection, are still associated with various toxicity profiles and only marginally improve the course of the disease and life expectancy. A considerable body of evidence supports the antitumour and apoptotic effects of certain cannabinoids, such as WIN55,212-2, against a wide spectrum of cancer cells, including gliomas. In fact, we previously highlighted the potent cytotoxic activity of the cannabinoid ligand **5** against glioblastoma KNS42 cells. Taken together, in this study, we designed, synthesised, and evaluated several indoles and indole bioisosteres for their antitumour activities. Compounds **8a**, **8c**, **8f**, **12c**, and **24d** demonstrated significant inhibitory activities against the viability ( $IC_{50} = 2.34\text{--}9.06\ \mu\text{M}$ ) and proliferation ( $IC_{50} = 2.88\text{--}9.85\ \mu\text{M}$ ) of paediatric glioblastoma KNS42 cells. All five compounds further retained their antitumour activities against two atypical teratoid/rhabdoid tumour (AT/RT) cell lines. When tested against a medulloblastoma DAOY cell line, only **8c**, **8f**, **12c**, and **24d** maintained their viability inhibitory activities. The viability assay against non-neoplastic human fibroblast HFF1 cells suggested that compounds **8a**, **8c**, **8f**, and **12c** act selectively towards the panel of paediatric brain tumour cells. In contrast, compound **24d** and WIN55,212-2 were highly toxic toward HFF1 cells. Due to their structural resemblance to known cannabimimetics, the most potent compounds were tested in cannabinoid 1 and 2 receptor (CB<sub>1</sub>R and CB<sub>2</sub>R) functional assays. Compounds **8a**, **8c**, and **12c** failed to activate or antagonise both CB<sub>1</sub>R and CB<sub>2</sub>R, whereas compounds **8f** and **24d** antagonised CB<sub>1</sub>R and CB<sub>2</sub>R, respectively. We also performed a transcriptional analysis on KNS42 cells treated with our prototype compound **8a** and highlighted a set of seven genes that were significantly downregulated. The expression levels of these genes were previously shown to be positively correlated with tumour growth and progression, indicating their implication in the antitumour activity of **8a**. Overall, the drug-like and selective antitumour profiles of indole-2-carboxamides **8a**, **8c**, **8f**, and **12c** substantiate the versatility of the indole scaffold in cancer drug discovery.

Received 26th February 2021,  
Accepted 5th August 2021

DOI: 10.1039/d1md00065a

rsc.li/medchem

<sup>a</sup> Curtin Medical School, Faculty of Health Sciences, Curtin University, Bentley, Perth, WA 6102, Australia. E-mail: Hendra.Gunosewoyo@curtin.edu.au<sup>b</sup> Division of Pediatric Neurosurgery, Ann and Robert H. Lurie Children's Hospital of Chicago, Chicago, IL 60611, USA. E-mail: simone.sredni@gmail.com<sup>c</sup> School of Chemistry, The University of Sydney, NSW, 2006, Australia. E-mail: michael.kassiou@sydney.edu.au<sup>d</sup> Faculty of Medicine and Health, The University of Sydney, NSW 2006, Australia<sup>e</sup> Department of Biostatistics, Zilber School of Public Health, University of Wisconsin, Milwaukee, WI 53205, USA<sup>f</sup> Shanghai Engineering Research Center of Molecular Therapeutics and New Drug Development, School of Chemistry and Molecular Engineering, East China Normal University, 3663 North Zhongshan Road, Shanghai 200062, China<sup>g</sup> Department of Surgery, Northwestern University, Feinberg School of Medicine, Chicago, IL 60611, USA

† Electronic supplementary information (ESI) available. See DOI: 10.1039/d1md00065a

## 1. Introduction

Gliomas are brain tumours that originate from non-neuronal supportive cells, called glial cells, which are the most abundant cell types in the central nervous system (CNS).<sup>1,2</sup> Paediatric gliomas represent the most common CNS tumours and the leading cause of cancer-related death in children. The average annual incidence rate of CNS tumours in children (0–14 years old) is 5.26 per 100 000 with gliomas accounting for approximately 53% of tumours in this age cohort.<sup>3</sup> Gliomas are classified based on the histological criteria of neoplasms into a grading system of malignancy by the World Health Organisation (WHO). The three main categories of gliomas are low grade gliomas (LGGs, WHO grade I and II), high grade gliomas (HGGs, WHO grade III

and IV) and diffuse midline gliomas (DMGs).<sup>4</sup> These three tumour entities require different treatment and/or management strategies. Paediatric HGGs are nearly universally fatal brain tumours associated with dismal prognosis, with a median survival of 1–2 years.<sup>5</sup> A key element hampering the development of new targeted therapies is the relative shortage of paediatric glioma cell lines.<sup>6</sup> Despite the clear histopathological similarities between HGGs of all ages, the well-established commonly used adult cell lines are not truly representative of the distinct molecular signatures of childhood HGGs.<sup>6–8</sup> Hence, there is a pressing need to develop novel therapeutic agents that effectively target paediatric brain tumours.

We are particularly interested in paediatric glioblastoma multiforme (GBM or grade IV astrocytoma) which is among the most malignant, aggressive and invasive CNS tumours in children.<sup>3</sup> The mainstays of treatment of GBM are only palliative, including surgical resection when applicable followed by focal radiotherapy combined with chemotherapy. Many chemotherapeutic agents have been tested including temozolomide, but no remarkable improvement on survival has been achieved in paediatric GBM.<sup>5,9</sup> The druggable molecular targets in paediatric HGGs and their corresponding drug candidates that are currently in clinical trials have been recently reviewed.<sup>10</sup> In the adult GBM counterpart, Guzman *et al.* first reported their pilot phase I clinical trial findings on the efficacy of the phytocannabinoid derivative  $\Delta^9$ -tetrahydrocannabinol ( $\Delta^9$ -THC, **1**, Fig. 1) delivered intracranially to nine patients.<sup>11</sup> This cannabinoid was found to be fairly safe (no overt psychoactive effects) and inhibited tumour cell proliferation in a subset of patients.<sup>11</sup>

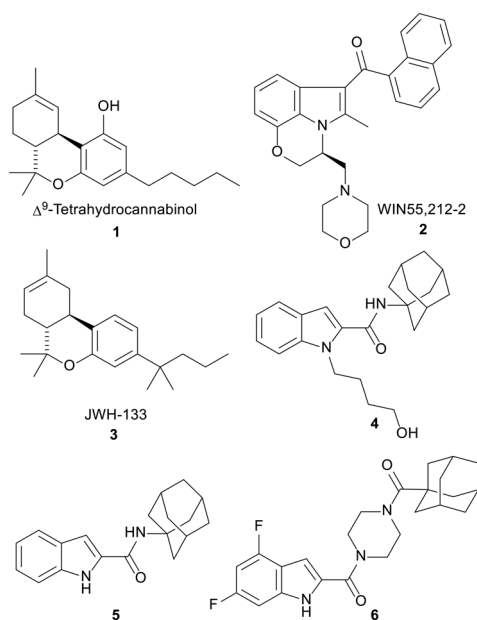


**Fig. 1** CB ligands **1–5** as well as the antitumour indoleamide analogue **6** which was identified in our previous report.  $\Delta^9$ -Tetrahydrocannabinol (**1**) and WIN55,212-2 (**2**) are mixed CB<sub>1</sub>R/CB<sub>2</sub>R agonists, while compounds **3–5** are selective CB<sub>2</sub>R agonists.

In fact, since the *in vitro* antitumour potential of  $\Delta^9$ -THC was first reported in 1975,<sup>12</sup> an accumulating body of research has demonstrated the antineoplastic effects of many endogenous, naturally occurring, and synthetic cannabinoids against various tumour cells, including gliomas.<sup>13–20</sup> These compounds produce most of their biological effects by targeting cannabinoid 1 and 2 receptors (CB<sub>1</sub>R and CB<sub>2</sub>R) which are present in the brain and the periphery.<sup>21</sup> In particular, two mixed CB<sub>1</sub>R and CB<sub>2</sub>R agonists,  $\Delta^9$ -THC (**1**) and WIN55,212-2 (**2**), in addition to the selective CB<sub>2</sub>R agonist JWH-133 (**3**), Fig. 1, were shown to inhibit the growth of malignant gliomas and impair tumour angiogenesis *in vitro* and in animal models. They also induced apoptosis in glioma cells *in vitro* and tumour regression *in vivo*.<sup>22–28</sup> A number of reports ascribed the antitumour activities of cannabinoids to the CB receptors, whilst others demonstrated that their antitumour activities are independent of CB receptors.<sup>24–26,29–36</sup> Hence, the mechanism of action of cannabinoids as antitumour agents is still debatable.

In light of the widely reported antitumour activities of cannabinoids, we were interested in exploring the structure–antitumour activity relationship of the indole-containing cannabimimetic agents, exemplified by WIN55,212-2. Indeed, we previously reported several indolecarboxamide derivatives as potent CB<sub>1</sub>R and/or CB<sub>2</sub>R ligands.<sup>37</sup> The potent CB<sub>2</sub>R agonist *N*-(1-adamantyl)-1-(4-hydroxybutyl)-indole-2-carboxamide (**4**) was the highlight of our previous work (CB<sub>2</sub>R EC<sub>50</sub> = 0.12  $\mu$ M) which showed no agonist or antagonist activity at CB<sub>1</sub>R. We also found in the same report that the *N*-unsubstituted indole **5** exhibited a similar selective CB<sub>2</sub>R functional activity (EC<sub>50</sub> = 0.98  $\mu$ M) to the *N*-alkylated indole **4**.<sup>37</sup> Importantly, we demonstrated the potent inhibitory activity of compound **5** against the viability of paediatric GBM KNS42 cells (IC<sub>50</sub> = 0.33  $\mu$ M).<sup>38</sup> In this report, we brought to light the cytotoxic and antiproliferative activities of the indole-2-carboxamide **6** against different malignant brain tumour cells.

Accordingly, in the current study, we describe the design, synthesis, and biological evaluation of several *N*-unsubstituted indoles and indole bioisosteres as antitumour agents. All final analogues as well as reference ligands WIN55,212-2, JWH-133, and compound **4** were screened *in vitro* for their viability and proliferation inhibitory activities against paediatric GBM KNS42 cells. KNS42 was the cell line of choice in our primary antitumour screening as it is reported to overexpress CB<sub>1</sub>R (encoded by the *CNR1* gene).<sup>39</sup> The antitumour and safety profiles of the most potent compounds were then scrutinised in non-GBM high-grade paediatric brain tumour cells [teratoid/rhabdoid AT/RT (BT12 and BT16) and medulloblastoma (DAOY)] as well as non-neoplastic HFF1 cells. In addition, the functional activities of the top active compounds at CB<sub>1</sub>R and CB<sub>2</sub>R were assessed and a transcriptional analysis of KNS42 cells treated with the *N*-benzylindoleamide analogue **8a** was conducted. The drug-likeness of the most active compounds was also predicted using ACD/Labs Percepta.

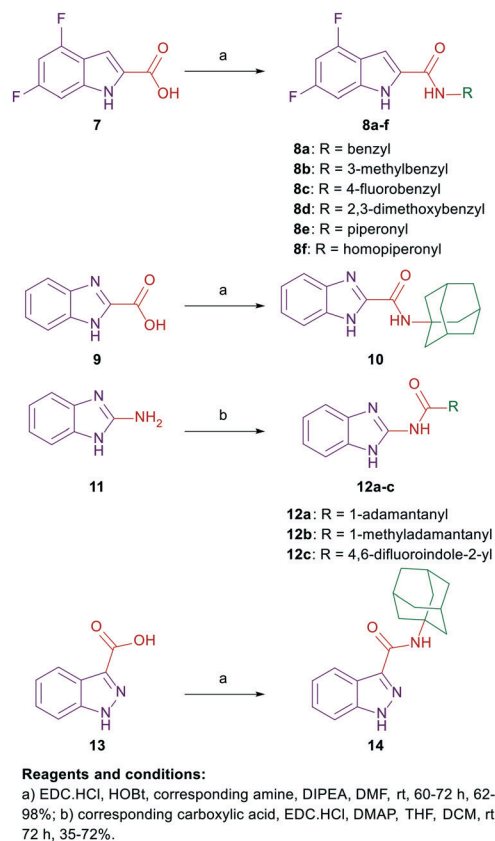
## 2. Design

In compounds **8a–f**, a 4,6-difluoro-1*H*-indole nucleus was used instead of the unsubstituted-1*H*-indole in compound **5**, while the adamantane ring was replaced with benzyl, piperonyl, and homopiperonyl motifs. The 4,6-difluoroindole was the scaffold of choice in our study as it has higher lipophilicity ( $\text{Clog}P = 2.6$ ) compared to the unsubstituted indole ring ( $\text{Clog}P = 2.1$ ). In this respect, the slight increase in lipophilicity of the 4,6-difluoroindole-containing compounds may enhance their uptake by tumour cells<sup>40</sup> which can lead to an improved antitumour activity profile without significantly impacting the drug-like properties. We also probed the activity of the benzimidazole and indazole cores as bioisosteric replacements to the indole moiety while retaining the adamantane appendage in compounds **10**, **12a–c**, and **14**. In a different approach, we also investigated the activity of some adamantane-derived indoles, wherein extra spacers were introduced to the amide linker between the 4,6-difluoroindole core and the adamantane ring, forming the diamides **18** and **23a** and **b**. It is noteworthy that compound **23a** was previously evaluated in our recent report<sup>38</sup> and is reincorporated herein to be compared to compound **23b**.

On the other hand, *N*-(1-adamantyl)-1-alkylquinolone-3-carboxamides were widely reported in the literature as cannabinoid receptor modulators.<sup>41–44</sup> In addition, some quinolone-3-carboxamides with selective CB<sub>2</sub>R affinity previously showed potent reduction of the viability of the LNCaP prostatic cancer cell line, displaying IC<sub>50</sub> values significantly lower than that of JWH-133 (**3**).<sup>45</sup> Accordingly, in line with the aforementioned strategies, we tested several *N*-unsubstitutedquinolone-3-carboxamides **24a–e** and their analogous quinolone-2-carboxamide counterparts **25a–e** for their antitumour activities. Of note, all of the tested quinolonecarboxamides **24a–e** and **25a–e** were previously evaluated for their antitubercular activity, whereupon most of them were found to be inactive.<sup>46</sup>

## 3. Chemistry

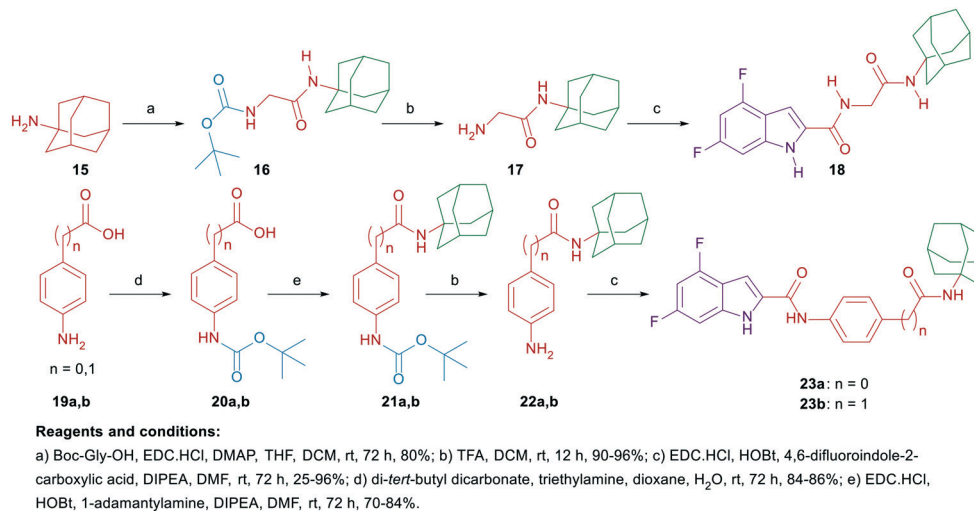
The synthetic strategies of all the final compounds are depicted in Schemes 1 and 2. Reference cannabimimetic indoles **4** and **5** were synthesised according to the reported procedure.<sup>37</sup> Indoles **8a–f**, benzimidazoles **10** and **12a–c**, and indazole derivative **14** were synthesised in a one-step amide coupling reaction (method A or B). The indole-2-carboxamides **8a–f** and benzimidazole-2-carboxamide **10** were obtained *via* reacting the carboxylic acid derivatives **7** and **9**, respectively, with the corresponding amines in the presence of 1-ethyl-3-(3-dimethylaminopropyl)carbodiimide hydrochloride (EDC·HCl), hydroxybenzotriazole hydrate (HOBt) and *N,N*-diisopropylethylamine (DIPEA) (method A). Method B [EDC·HCl and 4-dimethylaminopyridine (DMAP)] was conducted between compound **11** and the corresponding carboxylic acids to generate the benzimidazole derivatives **12a–c**. The indazole-3-carboxamide derivative **14** was formed



**Scheme 1** General synthetic approach for compounds **8a–f**, **10**, **12a–c**, and **14**.

following the amide coupling protocol A between compound **13** and 1-adamantylamine (Scheme 1).

On the other hand, the synthesis of the adamantane-derived indole dicarboxamide derivatives **18** and **23a** and **b** is illustrated in Scheme 2. Compound **18** was prepared in three steps starting from coupling 1-adamantylamine (**15**) with *N*-(*tert*-butoxycarbonyl)glycine (Boc-Gly-OH) following a reported procedure<sup>47</sup> to give the *N*-(Boc) adamantane derivative **16**. Cleavage of the Boc group thereof using trifluoroacetic acid (TFA) yielded the aminoacetamide intermediate **17**. Employing method A of amide coupling, compound **17** was reacted with 4,6-difluoroindole-2-carboxylic acid (**7**) to afford the final compound **18**. Similar to our previously reported compound **23a**,<sup>38</sup> the dicarboxamide analogue **23b** was obtained in a four-step pathway starting from the initial protection of the amino group in the aniline **19b** using di-*tert*-butyl dicarbonate (Boc)<sub>2</sub>O. Thereafter, the *N*-Boc derivative **20b** was subjected to amide coupling (method A) with 1-adamantylamine to provide compound **21b**. Subsequent *N*-Boc deprotection of the crude product **21b** under acidic conditions furnished the key intermediate **22b**. Finally, amide coupling of **22b** with **7** (method A) delivered the desired dicarboxamide analogue **23b** (Scheme 2). Compounds **24a–e** and **25a–e** were synthesised as reported in our previous work.<sup>46</sup>



Scheme 2 General synthetic approach for compounds 18 and 23a and b.

## 4. Results and discussion

### 4.1. Biological evaluation and SAR analysis

**4.1.1. Cytotoxicity and antiproliferative activity against paediatric KNS42 GBM cells.** All the synthesised final compounds **8a–f**, **10**, **12a–c**, **14**, **18**, **23a and b**, **24a–e**, and **25a–e** were evaluated for their viability inhibition and antiproliferative activities against paediatric GBM KNS42 cells (Table 1). CB receptor ligands WIN55,212-2 (**2**), JWH-133 (**3**), **4**, and **5** were used as positive controls. Of note, WIN55,212-2 is a non-selective CB<sub>1</sub>R/CB<sub>2</sub>R agonist (CB<sub>1</sub>R EC<sub>50</sub> = 0.284 μM, CB<sub>2</sub>R EC<sub>50</sub> = 0.062 μM), whereas JWH-133 (CB<sub>2</sub>R K<sub>i</sub> = 0.0034 μM) and compounds **4** and **5** are selective CB<sub>2</sub>R agonists (CB<sub>2</sub>R EC<sub>50</sub> = 0.12 and 0.98 μM, respectively).<sup>37,48,49</sup> Reference compounds **2**, **4**, and **5** showed moderate to high cytotoxic activities with low micro- and sub-micromolar inhibitory activities on cell viability (IC<sub>50</sub> = 8.02, 4.75, and 0.33 μM, respectively). The selective CB<sub>2</sub>R agonist JWH-133 (**3**) showed no inhibitory activity at 10 μM concentration against KNS42 cells in both viability and proliferation studies. WIN55,212-2 was the only active control that inhibited the proliferation of KNS42 cells (IC<sub>50</sub> = 8.07 μM). The cytotoxic effects of selective CB<sub>2</sub>R agonists **4** and **5** versus the inactivity of JWH-133 towards KNS42 cells suggest that these compounds may be impacting the cell viability of KNS42 cells *via* a CB receptor-independent mechanism. This notion is reinforced with many previous reports excluding the involvement of CB receptors in the antiproliferative and apoptotic effects of numerous cannabinoids.<sup>22,26,31–36,50</sup>

The first round of our investigations was focused on exploring the antitumour activity of the 4,6-difluoroindoleamides **8a–f**, benzimidazoleamides **10** and **12a–c**, and indazoleamide **14**. The *N*-benzyl-indoleamide analogue **8a** was previously evaluated in our recently published report.<sup>38</sup> It displayed an activity profile similar to WIN55,212-2 against KNS42 cells [IC<sub>50</sub> (viability and proliferation) = 8.25 and 9.85 μM, respectively]. We then

probed the effect of incorporating different substituents on the benzyl group in **8a** on the antitumour activity. Introducing a methyl group at position 3 to the *N*-linked benzyl group in compound **8b** diminished the antitumour activity (IC<sub>50</sub> > 10 μM). The *N*-(4-fluorobenzyl)indoleamide **8c** exhibited approximately 2-fold higher cytotoxicity and antiproliferative activities (IC<sub>50</sub> = 3.41 and 4.34 μM, respectively) compared to the unsubstituted amidobenzyl counterpart **8a**. Similar to **8b**, disubstituting the benzyl moiety at positions 2 and 3 with methoxy groups **8d** led to a drop in both cytotoxic and antiproliferative activities (IC<sub>50</sub> > 10 μM). The *N*-piperonyl-indoleamide analogue **8e**, containing a 1,3-benzodioxole group in lieu of the phenyl ring in **8a**, was devoid of activity in the viability and proliferation assays (IC<sub>50</sub> > 10 μM). Surprisingly, the *N*-homopiperonyl analogue **8f**, entailing an extra methylene group between the amide linkage and piperonyl motif, showed nearly 3.5-fold higher inhibitory activities (IC<sub>50</sub> = 2.34 and 2.88 μM, respectively) compared to **8a** against KNS42 cells' viability and proliferation, respectively.

Bioisosteric replacement of the indole ring in reference compound **5** [IC<sub>50</sub> (viability) = 0.33 μM] with a benzimidazole scaffold **10** resulted in a dramatic attenuation in the cytotoxic activity against KNS42 cells (IC<sub>50</sub> > 10 μM). Of note, compound **10** previously showed high selective agonistic activity towards CB<sub>2</sub>R (EC<sub>50</sub> = 0.52 μM), without observable activity at CB<sub>1</sub>R.<sup>51</sup> Nevertheless, unlike compounds **4** and **5**, compound **10** was inactive against KNS42 cells. Next, we evaluated the antitumour activity of benzimidazole derivatives **12a–c**, featuring a reversed amide linker. Akin to compound **10**, the benzimidazoleamide analogue **12a** failed to inhibit the viability and proliferation of KNS42 cells at 10 μM concentration. Introducing a methylene group spacer between the amide linker and the adamantane moiety in **12b** led to an improvement in the antiproliferative activity, while the cell viability remained unaffected (IC<sub>50</sub> = 6.46 and > 10 μM, respectively). On the other hand, the benzimidazole-

**Table 1** *In vitro* viability and proliferation inhibitory activities of compounds **8a–f**, **10**, **12a–c**, **14**, **18**, **23a** and **b**, **24a–e**, and **25a–e** as well as reference compounds **2–6** against KNS42 cells

| Cpd                      | R                       | R <sup>1</sup> | Viability IC <sub>50</sub> <sup>a</sup> (μM) | Proliferation IC <sub>50</sub> <sup>b</sup> (μM) |
|--------------------------|-------------------------|----------------|--|--|
| <b>8a</b>                | Benzyl                  | —              | 8.25 ± 1.25                                  | 9.85 ± 2.76                                      |
| <b>8b</b>                | 3-Methylbenzyl          | —              | >10  | >10  |
| <b>8c</b>                | 4-Fluorobenzyl          | —              | 3.41 ± 0.49                                  | 4.34 ± 0.46                                      |
| <b>8d</b>                | 2,3-Dimethoxybenzyl     | —              | >10  | >10  |
| <b>8e</b>                | Piperonyl               | —              | >10  | >10  |
| <b>8f</b>                | Homopiperonyl           | —              | 2.34 ± 0.19                                  | 2.88 ± 0.25                                      |
| <b>10</b>                | —                       | —              | >10  | >10  |
| <b>12a</b>               | Adamantane-1-yl         | —              | >10  | >10  |
| <b>12b</b>               | 1-Methyladamantane      | —              | >10  | 6.46   |
| <b>12c</b>               | 4,6-Difluoroindole-2-yl | —              | 4.49 ± 0.63                                  | 4.03 ± 0.01                                      |
| <b>14</b>                | —                       | —              | >10  | >10  |
| <b>18</b>                | —                       | —              | >10  | >10  |
| <b>23a</b>               | —                       | —              | >10  | >10  |
| <b>23b</b>               | —                       | —              | >10  | 4.90   |
| <b>24a</b>               | —                       | 6-Chloro       | >10  | >10  |
| <b>24b</b>               | —                       | 7-Bromo        | >10  | >10  |
| <b>24c</b>               | —                       | 5,7-Dichloro   | >10  | 9.17   |
| <b>24d</b>               | —                       | 5,8-Dichloro   | 9.06 ± 0.79                                  | 2.92 ± 0.43                                      |
| <b>24e</b>               | —                       | 7,8-Dichloro   | >10  | 8.05 ± 4.15                                      |
| <b>25a</b>               | —                       | 6-Chloro       | >10  | 6.11 ± 0.91                                      |
| <b>25b</b>               | —                       | 7-Bromo        | >10  | >10  |
| <b>25c</b>               | —                       | 5,7-Dichloro   | >10  | >10  |
| <b>25d</b>               | —                       | 5,8-Dichloro   | >10  | >10  |
| <b>25e</b>               | —                       | 7,8-Dichloro   | >10  | >10  |
| WIN55,212-2 ( <b>2</b> ) | —                       | —              | 8.02 ± 0.25                                  | 8.07 ± 0.29                                      |
| JWH-133 ( <b>3</b> )     | —                       | —              | >10  | >10  |
| <b>4</b>                 | —                       | —              | 4.75 ± 0.93                                  | >10  |
| <b>5</b>                 | —                       | —              | 0.33 ± 0.14                                  | >10  |
| <b>6</b>                 | —                       | —              | 5.04 ± 0.65                                  | 6.62 ± 2.01                                      |

<sup>a</sup> Compound dose required to achieve 50% inhibition of KNS42 cell viability, reflecting cytotoxicity. <sup>b</sup> Compound dose required to achieve 50% inhibition of KNS42 cell proliferation.

indole (BZ-IND) **12c** hybrid, linked through an amide group, equally inhibited the viability and proliferation of KNS42 cells (IC<sub>50</sub> = 4.49 and 4.03 μM, respectively). In this hybrid, the indole-2-carboxamide framework integrated into compounds **8a–f** was preserved, while the benzimidazole nucleus served as the *N*-linked moiety which may explain the higher activity of this derivative compared to the other benzimidazole analogues **10**, **12a**, and **12b**.

Similar to the *N*-(adamantyl)benzimidazole derivative **10**, integrating an indazole scaffold, in place of the indole nucleus, into compound **14** led to a drastic drop in the cytotoxic activity against KNS42 cells (IC<sub>50</sub> > 10 μM). It is worth noting that the same report which documented the CB<sub>2</sub>R selective activity of compound **10** showed that compound **14** has higher agonistic

activity towards CB<sub>2</sub>R over CB<sub>1</sub>R (CB<sub>2</sub>R EC<sub>50</sub> = 0.086 μM, CB<sub>1</sub>R EC<sub>50</sub> = 17.1 μM).<sup>51</sup> Thus far, the difference in the antitumour activity of **5** versus **10**, **12a**, and **14** suggests that the cytotoxic activity of the *N*-(adamantyl)indoleamide framework against KNS42 cells is superior to the benzimidazole and indazole counterparts. In addition, using the 4,6-difluoroindole scaffold in lieu of the unsubstituted indole ring featured in compound **5**, while concomitantly replacing the adamantane group therein with a 4-fluorobenzyl or homopiperonyl motif, was beneficial for the cytotoxic and antiproliferative activities against KNS42 cells.

Based on these findings and the potentiation of the antitumour activity seen in **8f** (upon extending the linker connecting the indole ring and the piperonyl motif), in our

subsequent round of evaluations, the 4,6-difluoroindole was maintained, while extra spacers were added in between the indole and adamantane moieties (Table 1). First, the adamantane-based indolecarboxamide **18** showed no inhibitory activity against KNS42 cells in the viability and proliferation studies ( $IC_{50} > 10 \mu\text{M}$ ). Similarly, in our previous report, compound **23a**, containing a phenyl group as a middle linker between the indole and adamantane rings, showed no activity at  $10 \mu\text{M}$  concentration in both assays.<sup>38</sup> However, when we introduced an extra methylene spacer between the phenyl group and the amidoadamantyl motif in compound **23b**, a reduction in KNS42 cell proliferation was manifested ( $IC_{50} = 4.90 \mu\text{M}$ ), while the cell viability remained unaffected. It is noteworthy that the antiproliferative activity of **23b** is comparable to that of our recently reported indoleamide **6** ( $IC_{50} = 6.62 \mu\text{M}$ ), entailing a piperazine ring connecting the indole and the adamantane rings. These results suggest that stretching the middle linker connecting the indole and the adamantane moieties could be tolerated in certain structural settings.

The final modification in our study entailed replacing the indole ring in the *N*-(1-adamantyl)indoleamide framework with a quinolone moiety. Although the majority of the *N*-(1-adamantyl)quinolone-3-carboxamides that were reported to modulate the activity of CB receptors are *N*-alkylated at position 1 of the quinolone ring, few *N*-unsubstituted quinolone analogues were endowed with high affinity and selectivity for CB<sub>2</sub>R.<sup>41–44</sup> Therefore, in accordance with our foregoing strategies, we assessed the cytotoxicity and antiproliferative activities of the adamantane-derived 1*H*-quinolone-3-carboxamides **24a–e**. Monosubstituted quinolones **24a** and **b** failed to inhibit the viability and proliferation of KNS42 cells at  $10 \mu\text{M}$  concentration. Disubstituted quinolones **24c–e**, on the other hand, demonstrated good inhibitory activities against proliferation and/or viability of KNS42 cells. The 5,8-dichloroquinolone **24d** was the most active compound in this series with cytotoxicity ( $IC_{50} = 9.06 \mu\text{M}$ ) and antiproliferative effects ( $IC_{50} = 2.92 \mu\text{M}$ ) against KNS42 cells. The 5,7- and 7,8-disubstituted quinolones **24c** and **24e** exhibited  $IC_{50}$  values of 9.17 and 8.05  $\mu\text{M}$ , respectively, in the proliferation assay, while they manifested lower inhibitory activities in the viability study ( $IC_{50} > 10 \mu\text{M}$ ).

Shifting the amidoadamantyl motif from the 3-position of the quinolone scaffold to the 2-position in **25a–e** diminished the cytotoxic and antiproliferative activities ( $IC_{50} > 10 \mu\text{M}$ ), except for compound **25a**. Unlike compound **24a**, the 6-chloroquinolone-2-carboxamide analogue **25a** showed only moderate antiproliferative activity against KNS42 cells ( $IC_{50} = 6.11 \mu\text{M}$ ). Overall, the indole-2-carboxamide architecture appears to be preferable to the benzimidazole, indazole, and quinolone counterparts as antitumour agents.

**4.1.2. Cytotoxicity and antiproliferative activities of the most potent compounds against different paediatric brain tumour cells and non-neoplastic fibroblasts.** The top potent compounds in the viability and proliferation assays against

KNS42 cells, **8a**, **8c**, **8f**, **12c**, and **24d** ( $IC_{50} \leq 10 \mu\text{M}$ ) as well as WIN55,212-2 (**2**), were selected for further cytotoxicity and antiproliferative evaluations against a panel of grade IV paediatric brain tumour cells and non-neoplastic human fibroblasts (Table 2). All five compounds and WIN55,212-2 retained their viability and proliferation inhibitory activities ( $IC_{50} \leq 10 \mu\text{M}$ ) against the two AT/RT tumour cell lines (BT12 and BT16). When tested against the medulloblastoma cells DAOY, the *N*-benzylindoleamide **8a** was devoid of antitumour activity ( $IC_{50} > 10 \mu\text{M}$ ), as per our previous report.<sup>38</sup> However, the *N*-(4-fluorobenzyl)indole analogue **8c** demonstrated moderate cytotoxic activity ( $IC_{50} = 4.10 \mu\text{M}$ ) and weak antiproliferative activity ( $IC_{50} > 10 \mu\text{M}$ ) against DAOY cells. Similarly, the *N*-(homopiperonyl)-indoleamide analogue **8f** showed appreciable reduction of cell viability and moderate antiproliferative activity against DAOY cells ( $IC_{50} = 3.65$  and  $9.91 \mu\text{M}$ , respectively). Interestingly, the BZ-IND hybrid **12c** exhibited remarkable cytotoxic and antiproliferative activities against all tested paediatric tumour cells (KNS24, BT12, BT16, and DAOY). Compound **12c** also showed the most potent viability and proliferation inhibitory activities against DAOY cells ( $IC_{50} = 1.02$  and  $2.31 \mu\text{M}$ , respectively).

A similar pan-tumour cell viability and/or proliferation inhibition was manifested in the 5,8-dichloroquinolone-3-carboxamide derivative **24d** and WIN55,212-2. As we previously reported,<sup>38</sup> compound **8a**, which was cytotoxic against KNS42, BT12, and BT16 cells, exhibited limited cytotoxicity against healthy human fibroblasts, HFF1 cells ( $IC_{50} = 119 \mu\text{M}$ ). Remarkably, compounds **8c**, **8f**, and **12c**, which demonstrated potent cytotoxicity against all paediatric brain tumour cell lines in our study, showed negligible cytotoxicity against HFF1 cells ( $IC_{50} = 281$ ,  $81$ , and  $115 \mu\text{M}$ , respectively). However, compounds **8f** and **12c** inhibited the proliferation of HFF1 cells at concentrations  $< 10 \mu\text{M}$ . On the other hand, compound **24d** and WIN55,212-2 demonstrated potent viability and proliferation inhibitory activities against non-neoplastic HFF1 cells, indicating the non-selectivity and significant toxicity of these two compounds. Consistent with this observation, Ellert-Miklaszewska *et al.* also demonstrated that the increase of proapoptotic Bad protein activity is linked to WIN55,212-2's cytotoxic activity.<sup>25</sup>

#### 4.2. Functional activity at the cannabinoid receptors

Given the structural resemblance of the synthesised molecules to the known cannabinoids, the most active compounds **8a**, **8c**, **8f**, **12c**, and **24d** in our study in addition to our recently reported indoleamide **6** were further evaluated *in vitro* for their ability to activate or antagonise human CB<sub>1</sub>R and CB<sub>2</sub>R expressed in mouse AtT-20 neuroblastoma cells (Table 3). All six compounds showed no agonistic activity at both CB receptors. These findings were in fact counterintuitive owing to the previously reported potent agonistic profile of the analogous two indoleamide reference compounds **4** and **5** as well as WIN55,212-2 (**2**). Nonetheless,

**Table 2** *In vitro* cytotoxicity and antiproliferative effects of compounds **8a**, **8c**, **8f**, **12c**, and **24d** as well as WIN55,212-2 (**2**) against different paediatric brain cancer cell lines (BT12, BT16 and DAOY) and healthy human fibroblasts (HFF1)

| Cpd        | BT12 viability                     | BT12 Prolif.                       | BT16 viability                     | BT16 Prolif.                       | DAOY viability                     | DAOY Prolif.                       | HFF1 viability                     | HFF1 Prolif.                       |
|------------|------------------------------------|------------------------------------|------------------------------------|------------------------------------|------------------------------------|------------------------------------|------------------------------------|------------------------------------|
|            | IC <sub>50</sub> <sup>a</sup> (μM) | IC <sub>50</sub> <sup>b</sup> (μM) | IC <sub>50</sub> <sup>a</sup> (μM) | IC <sub>50</sub> <sup>b</sup> (μM) | IC <sub>50</sub> <sup>a</sup> (μM) | IC <sub>50</sub> <sup>b</sup> (μM) | IC <sub>50</sub> <sup>a</sup> (μM) | IC <sub>50</sub> <sup>b</sup> (μM) |
| <b>8a</b>  | 0.89 ± 0.12                        | 7.44 ± 0.59                        | 1.81 ± 0.21                        | 6.06 ± 0.69                        | >10                                | >10                                | 119 ± 19.78                        | 65 ± 8.73                          |
| <b>8c</b>  | 9.23 ± 0.35                        | 8.87 ± 0.63                        | 5.50 ± 0.76                        | 9.79 ± 0.89                        | 4.10 ± 0.50                        | >10                                | 281 ± 28.42                        | 40 ± 9.81                          |
| <b>8f</b>  | 6.08 ± 0.32                        | 4.10 ± 0.40                        | 2.72 ± 0.33                        | 7.53 ± 0.46                        | 3.65 ± 0.22                        | 9.91 ± 0.97                        | 81 ± 20.26                         | 6.98 ± 1.23                        |
| <b>12c</b> | 7.65 ± 0.38                        | 1.79 ± 0.21                        | 1.37 ± 0.13                        | 5.41 ± 0.55                        | 1.02 ± 0.07                        | 2.31 ± 0.38                        | 115 ± 11.85                        | 3.03 ± 0.55                        |
| <b>24d</b> | 5.15 ± 0.17                        | 3.59 ± 0.27                        | 1.96 ± 0.39                        | 4.88 ± 5.89                        | 1.54 ± 0.17                        | 4.71 ± 0.24                        | 7.04 ± 0.87                        | 3.85 ± 0.47                        |
| <b>2</b>   | 8.60 ± 0.78                        | 9.32 ± 0.47                        | 4.74 ± 3.77                        | 4.57 ± 2.71                        | >10 ± 3.4                          | 6.09 ± 0.22                        | 0.023 ± 0.04                       | 1.82 ± 0.42                        |

<sup>a</sup> Compound dose required to achieve 50% inhibition of tumour/healthy cell viability, reflecting cytotoxicity. <sup>b</sup> Compound dose required to achieve 50% inhibition of tumour/healthy cell proliferation.

upon evaluating the antagonistic activity of **8a**, **8c**, **8f**, **12c**, and **24d** at CB<sub>1</sub>R and CB<sub>2</sub>R, we observed some mixed results. The indole-based dicarboxamide analogue **6** and the two *N*-(benzyl)indoleamide derivatives **8a** and **8c** failed to antagonise the response of CP55940, a non-selective CB<sub>1</sub>R/CB<sub>2</sub>R agonist. On the other hand, the *N*-(homopiperonyl) indoleamide **8f** potently inhibited the CP55940-mediated CB<sub>1</sub>R activation with an IC<sub>50</sub> value of 0.373 μM, whilst the CP55940-mediated CB<sub>2</sub>R response remained unaffected at 10 μM concentration. The BZ-IND hybrid **12c** was inactive as an antagonist at both receptors. Contrary to compound **8f**, the quinolone-3-carboxamide **24d** failed to inhibit the CP55940-mediated response at CB<sub>1</sub>R at 10 μM concentration while displaying potent antagonism at CB<sub>2</sub>R (IC<sub>50</sub> = 1.28 μM). These results suggest that the antitumour activities of our most potent compounds are unlikely to be a direct result of activity at CB<sub>1</sub>R or CB<sub>2</sub>R.

This was further corroborated by our previous highlights regarding the different cytotoxicity profiles of selective CB<sub>2</sub>R agonists JWH-133 (**3**), **10** and **14** versus compounds **4** and **5** against KNS42 cells. In fact, the two *N*-benzylindoleamides **8a** and **8c** as well as the BZ-IND hybrid **12c** which exhibited potent antitumour profiles in our study showed no agonistic or antagonistic activity at both receptors. However, compounds **8f** and **24d** were shown in the functional assay to

be CB ligands. Taken together, it is plausible that the antitumour activities observed in our compounds as well as WIN55,212-2 are not mediated by their action on CB receptors. Indeed, several studies have substantiated the CB-receptor independent induction of tumour cell death and antiproliferative effects exerted by many cannabinoids.

In this respect, in 1998, Sanchez *et al.* revealed that Δ<sup>9</sup>-THC-induced apoptosis and sphingomyelin breakdown in C6 glioma cells (expressing CB<sub>1</sub>R) were not prevented by the CB<sub>1</sub>R antagonist SR141716. Their results suggested that the observed antitumour effects of Δ<sup>9</sup>-THC are mediated through a CB<sub>1</sub>R-independent mechanism.<sup>22</sup> This was further supported by Ruiz *et al.*'s findings in 1999 who also inferred that Δ<sup>9</sup>-THC-induced apoptosis in human prostate tumour cells is independent of cannabinoid receptors.<sup>50</sup> However, Sanchez *et al.* showed in their subsequent reports that the three cannabinoids [Δ<sup>9</sup>-THC (**1**), WIN55,212-2 (**2**), and JWH-133 (**3**)] induced apoptosis in C6 glioma cells *via* a CB<sub>1</sub>R or CB<sub>2</sub>R-dependent pathway, as well as sustained accumulation of pro-apoptotic ceramide.<sup>24,29,30</sup> Ensuing reports demonstrated that the antitumour activities of cannabinoids are independent of cannabinoid receptors.<sup>26,31–36</sup> These conflicting results highlight the elusive mechanism of action of cannabinoids as antitumour agents. Overall, the preceding findings suggest that the antitumour activity observed in our most potent analogues is likely independent of CB receptors.

**Table 3** Functional profile of compounds **6**, **8a**, **8c**, **8f**, **12c**, and **24d** as well as cannabimimetic controls **2**, **4**, and **5**

| Cpd        | Agonism EC <sub>50</sub> (μM) |                   | Antagonism IC <sub>50</sub> (μM) |                   |
|------------|-------------------------------|-------------------|----------------------------------|-------------------|
|            | CB <sub>1</sub> R             | CB <sub>2</sub> R | CB <sub>1</sub> R                | CB <sub>2</sub> R |
| <b>6</b>   | NA <sup>a</sup>               | NA <sup>a</sup>   | NA <sup>a</sup>                  | NA <sup>a</sup>   |
| <b>8a</b>  | NA <sup>a</sup>               | NA <sup>a</sup>   | NA <sup>a</sup>                  | NA <sup>a</sup>   |
| <b>8c</b>  | NA <sup>a</sup>               | NA <sup>a</sup>   | NA <sup>a</sup>                  | NA <sup>a</sup>   |
| <b>8f</b>  | NA <sup>a</sup>               | NA <sup>a</sup>   | 0.373                            | NA <sup>a</sup>   |
| <b>12c</b> | NA <sup>a</sup>               | NA <sup>a</sup>   | NA <sup>a</sup>                  | NA <sup>a</sup>   |
| <b>24d</b> | NA <sup>a</sup>               | NA <sup>a</sup>   | NA <sup>a</sup>                  | 1.28              |
| <b>2</b>   | 0.284 (ref. 48)               | 0.062 (ref. 48)   | ND <sup>b</sup>                  | ND <sup>b</sup>   |
| <b>4</b>   | NA <sup>a</sup>               | 0.12 (ref. 37)    | NA <sup>a</sup>                  | NA <sup>a</sup>   |
| <b>5</b>   | NA <sup>a</sup>               | 0.98 (ref. 37)    | NA <sup>a</sup>                  | NA <sup>a</sup>   |

<sup>a</sup> NA: not active, defined as <50% activation or inhibition at 10 μM.

<sup>b</sup> ND: not determined.

### 4.3. Differential gene expression analysis of KNS42 cells treated with compound **8a**

In order to unravel the mechanism of action of the indole-2-carboxamides, we previously performed a transcriptional analysis on KNS42 cells treated with compound **6** versus the untreated control cell counterparts.<sup>38</sup> Upon examining the differential expression of the genes therein, we found that compound **6** downregulated the expression of two key genes, denominated carbonic anhydrase 9 (CA9) and spleen tyrosine kinase (SYK), with statistical significance ( $p < 0.05$ ).<sup>38</sup> Indeed, since knocking down the activity of each of these two genes has been previously shown to inhibit the cell proliferation, invasion, and/or migration of GBM tumours, we concluded in our previous report that the antitumour activities of this

indoleamide molecule could be ascribed to repressing the expression of these two genes.<sup>38</sup> In the current study, we investigated the gene transcriptional response of KNS42 cells before and after they were treated with the *N*-benzylindoleamide **8a**, employing the DNBSEQ Eukaryotic Stranded Transcriptome Resequencing technique.

Inspecting the differential expression of the genes in the treated cells in comparison to the control cells revealed that compound **8a** downregulated the expression of 33 genes (fold change  $\geq 5$ ) with statistical significance ( $p < 0.05$ ) (Table S1, ESI†). Seven genes were previously shown to promote the progression, proliferation, migration, and/or invasion of various tumours.<sup>52–69</sup> Accordingly, compound **8a**-induced downregulation of these genes could be the reason behind the antitumour attributes of this indoleamide against GBM KNS42 cells. Interestingly, neither the *CA9* nor *SYK* expression was significantly affected in **8a**-treated KNS42 cells.

These seven downregulated genes are: 1) placenta specific protein 1 (*PLAC1*), 2) Rho GTPase-activating protein 9 (*ARHGAP9*), 3) apelin early ligand A (*APELA*) gene, 4) NADH dehydrogenase [ubiquinone] 1 alpha subcomplex subunit 4-like 2 (*NDUFA4L2*), 5) mitogen-activated protein kinase 4 (*MAPK4*), 6) L-amino acid transporter 1 (*LAT1* or *SLC7A5*), and 7) angiopoietin-related protein 4 (*ANGPTL4*). It is noteworthy that the expression levels of *CNR1* and *CNR2* genes were not significantly altered in KNS42 cells treated with compound **6** or **8a**, further corroborating the premise that the CB receptors are presumably uninvolved in our observed antitumour activities. Importantly, upon retrospectively inspecting the differential gene expression data of KNS42 cells treated with our previously reported indoleamide analogue **6**, we did not observe any significant alteration in the expression levels of the preceding seven genes. Taken together, these findings suggest that despite both compounds **6** and **8a** bearing the same 4,6-difluoroindole-2-carboxamide structure core, the mechanisms through which they exert their antitumour effects are seemingly different.

First, *PLAC1*, the expression of which is restricted to placental tissues, wherein it plays a key role in the development and function of placenta, was previously found to be highly expressed and aberrantly activated in a wide variety of human cancers.<sup>52–54,70</sup> In addition, *PLAC1* serves as a biomarker signifying the presence and prognosis of certain tumours.<sup>71–73</sup> Indeed, apart from the placenta, no detectable expression of the *PLAC1* gene was found in any normal human tissues; therefore it is considered a cancer/placenta-specific gene and was designated as cancer-placenta antigen 1 (CP1).<sup>54</sup> A growing body of evidence has demonstrated the oncogenic potential of *PLAC1* in various human malignancies, where its expression was shown to be attributed to tumour progression.<sup>52–54</sup> Equally important, these studies revealed that silencing *PLAC1* in different cancer cells resulted in an inhibition in the proliferation and viability thereof, in addition to induction of apoptosis and cell cycle arrest. Knocking down *PLAC1* also impaired the

migration and invasion of tumour cells which are metastasis-related phenomena that represent the hallmark of malignancy.<sup>52–54</sup> When the KNS42 cells were treated with **8a**, *PLAC1* was the most downregulated gene with high statistical significance (fold change = 30,  $p < 0.005$ ). This profound suppression of *PLAC1* expression could have contributed to the observed cytotoxic and antiproliferative activities of compound **8a** against GBM KNS42 cells.

Two other genes that are potentially involved in the antitumour effects of **8a** are *ARHGAP9* and *MAPK4*. The protein encoded by *ARHGAP9* belongs to the Rho family of GTPases which principally modulate cytoskeletal dynamics.<sup>55</sup> Interestingly, *ARHGAP9* was previously shown to serve as a docking protein for mitogen-activated protein kinases (MAPKs).<sup>74</sup> Indeed, the interaction observed between *ARHGAP9* and MAPKs represents a key crosstalk mechanism between the Rho GTPase and MAPK signalling pathways that is potentially implicated in regulating actin remodelling.<sup>74</sup> It was, therefore, intriguing to find that *ARHGAP9* and *MAPK4* were downregulated in **8a**-treated KNS42 cells with high statistical significance (fold change = 12 and 6, respectively,  $p < 0.0005$ ). However, whether the observed suppression of *ARHGAP9* and *MAPK4* expression is intertwined, or a mere coincidence requires further investigation. Of note, similar to *PLAC1*, the abnormal expression of *ARHGAP9* and *MAPK4* was found to be correlated with poor patient survival as well as the genesis and development/progression of various tumours.<sup>55–58</sup> Therefore, it has been proposed that both genes can be used as prognostic biomarkers for these tumours.<sup>55,57</sup> Within this context, Wang *et al.* demonstrated that silencing *ARHGAP9* in different human breast cancer cells resulted in a marked decrease in cell proliferation, migration, and invasion, as well as inducing cell cycle arrest and apoptosis thereof.<sup>56</sup> Similarly, knocking down the expression of *MAPK4* inhibited the proliferation and growth of different human tumour cells and xenografts.<sup>57,58</sup> Thus far, although the exact effects of *PLAC1*, *ARHGAP9*, and *MAPK4* expression in HGGs are yet to be determined, their highly significant downregulation in **8a**-treated KNS42 cells suggests, for the first time, their involvement in the tumorigenicity of the GBM tumours.

On the other hand, the oncogenic roles of *APELA*, *NDUFA4L2*, *SLC7A5*, and *ANGPTL4* in gliomas, including GBM, were previously demonstrated in the literature.<sup>59,60,62,66,75</sup> Accordingly, these four genes were highlighted by researchers as prospective therapeutic targets in malignant gliomas. The protein encoded by the *APELA* gene binds to the Apelin receptor and promotes the formation of human embryonic vasculature and the growth of embryonic stem cells.<sup>59</sup> Since many signalling networks function in both embryogenesis and cancers, Yi *et al.* investigated the expression of the *APELA* gene in normal tissues *vs.* cancer tissues.<sup>61</sup> They found that this gene is highly expressed in GBM tissues compared to LGGs. In the same study, the *APELA* overexpression in ovarian cancers was found to promote cell growth and migration as well as cell



cycle progression. Indeed, in the *APELA* knockout ovarian cancer cells, the loss of *APELA* led to an inhibition in cell proliferation and migration *in vitro*. Similar results were discerned in a model of ovarian cancer xenograft bearing mice, in which the size of *APELA* knockout tumours was significantly decreased compared to the wild-type tumours, supporting the role of *APELA* in ovarian cancer growth and progression and suggesting its pro-tumorigenic effects *in vivo*.<sup>61</sup>

In a subsequent report by Ganguly *et al.*, *APELA* was found to be expressed at high levels in glioma patients and its upregulation was negatively correlated with patient survival.<sup>59</sup> In this respect, there was a significant difference between high and low *APELA* expressing glioma patients, with high *APELA* expression being associated with poor patient survival. In fact, the authors showed a direct correlation between *APELA* expression and glioma grade, wherein the highest *APELA* expression was found in GBM tumours (grade IV), in resonance with Yi *et al.*'s findings.<sup>59,61</sup> Interestingly, unlike the *APELA* gene, the expression of the Apelin receptor gene in these patients was not associated with glioma grade or survival rates.<sup>59</sup> The significant downregulation of *APELA* in **8a**-treated KNS42 cells (fold change = 11,  $p < 0.05$ ) accorded with the preceding findings, supporting the role of *APELA* in the growth of GBM tumours and suggesting that its suppression in KNS42 cells likely contributed to the observed antitumour effects of **8a**.

Similar to *APELA*, *NDUFA4L2* was shown to act as an oncogene in different tumours, including GBM.<sup>60</sup> *NDUFA4L2* is a subunit of the mitochondrial respiratory chain complex I, which is implicated in oxidative stress and metabolic reprogramming in various cancers. Indeed, many interesting findings were documented in a very recent study, published in 2021, supporting the role of *NDUFA4L2* in promoting GBM progression.<sup>60</sup> Chen *et al.* reported therein that the *NDUFA4L2* mRNA and protein were markedly upregulated in human GBM tissues and these elevated levels were associated with shorter survival times in GBM patients. Therefore, they suggested that the high expression of *NDUFA4L2* can be regarded as an independent prognostic biological marker for the overall survival of GBM patients.<sup>60</sup> Like *APELA*, the expression levels of *NDUFA4L2* in GBM tissues were found to be highly increased, compared to LGGs and normal brain tissues. More importantly, they found that knocking down the *NDUFA4L2* gene, both *in vitro* and *in vivo*, suppressed tumour cell proliferation and increased apoptosis, whilst protective mitophagy was initiated. They also discovered that apatinib, a multikinase inhibitor that displayed promising antitumour effects in various clinical trials, can effectively target *NDUFA4L2*, recapitulating the effects brought forth by *NDUFA4L2* gene knockdown.<sup>60</sup> Indeed, apatinib efficiently reduced the expression of *NDUFA4L2*, causing cell cycle arrest, enhanced apoptosis, and initiation of protective mitophagy, both *in vitro* and *in vivo*. This study was the first to demonstrate the tumorigenic role of *NDUFA4L2* in GBM tumours.<sup>60</sup> Interestingly, compound **8a** inhibited the

expression of *NDUFA4L2* by 7-fold with high statistical significance ( $p < 0.0005$ ). Resonating with the preceding antitumour characteristics of apatinib, **8a**-induced downregulation of *NDUFA4L2* likely contributed to the observed antiproliferative and cytotoxic effects of **8a** against GBM cells.

The next gene that we determined to be potentially implicated in **8a**-induced antitumour effects is *SLC7A5*, also referred to as *LAT1*. This gene belongs to system L transporters, which is accountable for the cellular uptake of most essential amino acids.<sup>76</sup> *LAT1* was found to be upregulated in various types of cancer, with predominant expression in metastatic lesions and primary tumours; therefore it is considered a cancer-type amino acid transporter.<sup>76</sup> Indeed, its high expression was previously shown to be closely related to growth, progression, and aggressiveness of different tumours.<sup>62–65</sup> Therefore, it was also suggested that *LAT1* can be used as an independent marker for poor prognosis in different types of cancer.<sup>63</sup> Its tumour-promoting activity was proven *in vivo* when *LAT1* knockdown metastatic prostatic cancer xenografts showed suppressed cell cycle progression, tumour growth, and spontaneous metastasis.<sup>64</sup> Importantly, accumulating literature reports have highlighted several *LAT1* inhibitors that displayed reduction of cellular uptake of leucine, tumour cell proliferation, and cell cycle progression in various cancer cell lines *in vitro*, as well as inhibiting tumour growth *in vivo*.<sup>63,76,77</sup> Within this context, Kobayashi *et al.* demonstrated that 2-aminobicyclo-(2, 2, 1)-heptane-2-carboxylic acid (BCH), a classical *LAT1* inhibitor, displayed remarkable cytostatic (reduced proliferation) and cytotoxic (increased apoptosis) effects in glioma cells overexpressing the *LAT1* gene.<sup>62</sup> They also found that increasing the expression of *LAT1* significantly enhanced the rate of tumour growth in glioma cells with low endogenous expression of *LAT1* in mice. Additionally, *LAT1* was found to be expressed at higher levels in human HGGs, including GBM, compared to LGGs, while being undetected in non-neoplastic brain tissues, correlating the expression levels of *LAT1* with the malignant status of glioma.<sup>62</sup> This was further substantiated by Haining *et al.*'s study which associated *LAT1* upregulation with the histopathological grade, proliferation, and angiogenesis of gliomas, in addition to the poor prognosis of glioma patients.<sup>66</sup> The 5-fold downregulation of *LAT1* with a very high statistical significance ( $p < 0.0001$ ) manifested in **8a**-treated KNS42 cells, together with the aforementioned compelling findings, supports the possible involvement of *LAT1* in the proliferation and viability inhibition of GBM cells induced by **8a**.

Finally, we found that *ANGPTL4* was 5-fold downregulated in **8a**-treated KNS42 cells with statistical significance ( $p < 0.05$ ). This gene is involved in numerous physiological and pathological functions, such as lipid metabolism, angiogenesis, cell differentiation, and tumorigenesis.<sup>78</sup> Several studies demonstrated that high levels of *ANGPTL4* are correlated with poorer prognosis in patients with solid

tumours, including GBM, suggesting its role in cancer onset, angiogenesis, progression, and metastasis.<sup>67–69</sup> Importantly, Katanasaka *et al.* showed that upregulating the expression of *ANGPTLA* promotes tumour angiogenesis in GBM.<sup>75</sup> In addition, constitutive knockdown of the *ANGPTLA* gene in GBM cells resulted in a significant reduction in the angiogenesis and growth of the corresponding tumour xenografts. This in turn suggests the likely involvement of this gene in the antitumour effects detected in compound **8a**.

Overall, we identified seven genes whose expression levels were previously correlated with growth, progression, and poor prognosis of various tumours. Targeting the activity of each of these seven genes genetically and/or chemically was also shown to abrogate tumour growth in several reports. Accordingly, the antitumour activity of **8a** could be accredited to modulating the expression levels of these oncogenes.

#### 4.4. ADME profiling

The top potent derivatives **8a**, **8c**, **8f**, **12c**, and **24d** in addition to WIN55,212-2 (**2**) were evaluated for their drug-likeness (Table 4) through assessing their conformity to Lipinski's rule of five (RO5) using ACD/Labs Percepta 2016 Build 2911 (13 Jul 2016). The log BB values of these compounds were also predicted *in silico* to examine their BBB permeability potential. The indole-2-carboxamide derivatives **8a**, **8c**, **8f**, and **12c** as well as WIN55,212-2 showed no violation to the RO5, indicating the drug-like attributes of these compounds. The small size and optimum lipophilicity (Log *P* = 2.69–3.23) of the preceding four indole-2-carboxamides suggest the prospective bioavailability of these analogues. On the contrary, the high lipophilicity of the quinolone derivative **24d** (log *P* = 5.07) accounted for the one minor violation observed therein. All five compounds and WIN55,212-2 (**2**) are also expected to traverse the BBB, whereupon they may exert their antitumor activities.

## 5. Conclusions

Motivated by the previously reported antitumour activity of the indole-based CB ligands WIN55,212-2 and compound **5**,

several analogous arylcarboxamide derivatives were designed, synthesised and evaluated for their cytotoxicity and antiproliferative activities against paediatric GBM KNS42 cells. The structure–antitumour activity relationship of our analogues led to the following highlights: (a) the indole-2-carboxamide framework is superior to the benzimidazole, indazole and quinolone counterparts; (b) replacing the adamantane moiety in **5** with benzyl or homopiperonyl groups was favourable; (c) mixed results were manifested when the linker connecting the indole moiety and adamantane group was overextended. Derivatives **8a**, **8c**, **8f**, **12c**, and **24d** displayed the most potent inhibitory activities against the viability and proliferation of KNS42 cells. WIN55,212-2 and selective CB<sub>2</sub>R agonists **4** and **5** showed potent cytotoxic activities against KNS42 cells, whilst JWH-133 was devoid of activity. Compounds **8a**, **8c**, **8f**, **12c**, and **24d** maintained their potent antitumour activities against the other tested grade IV non-GBM paediatric brain tumour cells BT12 and BT16 (AT/RT). When tested against the DAOY (medulloblastoma) cells, these compounds were mostly active, with the exception of **8a**. All indole-2-carboxamides **8a**, **8c**, **8f**, and **12c** showed no cytotoxicity against non-neoplastic human fibroblasts HFF1, suggesting their selective activity towards tumour cells. On the contrary, the quinolone-3-carboxamide **24d** and reference compound WIN55,212-2 were toxic towards HFF-1 cells.

Based on the structural similarities between the newly synthesised compounds and known indole-based cannabinoids, CB functional assays were performed. None of our five most active compounds showed agonistic activity at CB<sub>1</sub>R or CB<sub>2</sub>R. In the antagonist mode, compounds **8a**, **8c**, and **12c** failed to inhibit the CP55940-mediated response at both receptors. On the contrary, compounds **8f** and **24d** behaved as antagonists at CB<sub>1</sub>R and CB<sub>2</sub>R, respectively. The discrepancies observed between the antitumour activities of our compounds and their CB functional profiles suggest a complex interplay between CB receptor modulation and CB-independent antitumour mechanisms which remain to be determined. This was further supported by previous reports indicating the non-involvement of CB receptors in the antitumour activity of several cannabinoids.<sup>22,26,31–36,50,79</sup> We further substantiated this premise when we performed a transcriptional analysis on KNS42 cells, wherein neither compound **6** nor **8a** altered the expression of *CNR1* and *CNR2* genes. Contrary to our recent findings on compound **6**,<sup>38</sup> the *N*-benzylindoleamide **8a** did not show a significant modification in the expression of *CA9* and *SYK* genes. Alternatively, we found a set of seven oncogenes that were significantly downregulated in **8a**-treated KNS42 cells.

The expression levels of each of these seven genes was previously shown to be positively correlated with the growth, progression, migration, invasion, and/or prognosis of various tumours.<sup>52–64,66–69</sup> Since genetically and/or chemically inhibiting the expression of these genes has been previously shown to suppress tumour growth, the antitumour activity of **8a** could be attributed to downregulating the expression of

**Table 4** Calculated drug-like properties of the top potent compounds **8a**, **8c**, **8f**, **12c**, and **24d** in addition to reference compound **2** using ACD/Labs Percepta 2016 build 2911 (13 Jul 2016)

| Cpd        | MW     | HBD | HBA | log <i>P</i> | NRB | TPSA  | Log BB |
|------------|--------|-----|-----|--------------|-----|-------|--------|
| <b>8a</b>  | 286.28 | 2   | 3   | 3.17         | 3   | 44.89 | 0.08   |
| <b>8c</b>  | 304.27 | 2   | 3   | 3.23         | 3   | 44.89 | −0.20  |
| <b>8f</b>  | 344.31 | 2   | 5   | 3.02         | 4   | 63.35 | −0.15  |
| <b>12c</b> | 312.27 | 3   | 5   | 2.69         | 2   | 73.57 | −0.64  |
| <b>24d</b> | 391.29 | 2   | 4   | 5.07         | 2   | 58.20 | 0.21   |
| <b>2</b>   | 426.51 | 0   | 5   | 4.13         | 4   | 43.70 | −0.23  |

MW: molecular weight, HBD: H-bond donors, HBA: H-bond acceptors, log *P*: octanol–water partition coefficient, NRB: number of rotatable bonds, TPSA: topological polar surface area, Log BB: [log (C brain/C blood)].

these genes. Upon performing a retrospective examination on the differential expression of the genes in compound **6**-treated KNS42 cells, we found that the expression levels of the seven genes, potentially implicated in **8a** antitumour activity, are not significantly changed. This in turn suggests that despite the structural homology between compounds **6** and **8a**, both compounds seemingly inhibit the proliferation and viability of GBM cells *via* different mechanisms of action. Overall, the drug-like profile, *in vitro* antitumour activities, and preliminary safety towards non-tumour cells of **8a**, **8c**, **8f**, and **12c** establish the indole-2-carboxamides as potential therapeutic agents that can efficiently target malignant brain tumours.

## 6. Experimental section

### 6.1. Chemistry

**General information.** The following starting materials: 4,6-difluoroindole-2-carboxylic acid (**7**) and 1-adamantylamine (**15**) were purchased from Fluorochem, while 2-aminobenzimidazole (**11**) was purchased from AlfaAesar. Benzimidazole-2-carboxylic acid (**9**), indazole-3-carboxylic acid (**13**), and 4-aminophenylacetic acid (**19b**) were purchased from AK Scientific. WIN55,212-2 and JWH-133 were purchased from Cayman Chemical. <sup>1</sup>H NMR and <sup>13</sup>C NMR spectra were recorded on a Bruker Avance III spectrometer at 400 and 100 MHz, respectively, with TMS as an internal standard. Standard abbreviations indicating multiplicity were as follows: s = singlet, d = doublet, dd = doublet of doublets, t = triplet, q = quadruplet, m = multiplet and br = broad. HRMS experiments were carried out on a Thermo Scientific Q-Exactive Orbitrap mass spectrometer. TLC was performed on Analtech silica gel TLC plates (200 microns, 20 × 20 cm). Flash chromatography was conducted using a Teledyne Isco CombiFlash Rf system with RediSep columns or manually using SiliCycle SiliaFlash® P60 silica gels [40–63 μm (230–400 mesh)]. The final compounds were purified by preparative HPLC unless otherwise stated. The preparative HPLC employed an Omega 5 μm Polar C18 (21.2 × 150 mm) column, with detection at 254 and 280 nm on a Shimadzu SPD-20A detector, flow rate = 25.0 mL min<sup>-1</sup>. Method 1: 40–100% acetonitrile/H<sub>2</sub>O in 10 min; 100% acetonitrile in 15 min; 100–40% acetonitrile/H<sub>2</sub>O in 10 min. Method 2: 50–100% acetonitrile/H<sub>2</sub>O in 10 min; 100% acetonitrile in 15 min; 100–50% acetonitrile/H<sub>2</sub>O in 10 min. Method 3: 60–100% acetonitrile/H<sub>2</sub>O in 10 min; 100% acetonitrile in 15 min; 100–60% acetonitrile/H<sub>2</sub>O in 10 min. Both solvents contained 0.05 vol% of trifluoroacetic acid (TFA). The purities of the final compounds were established by analytical HPLC, which was carried out using a Waters 1525 HPLC system with a Phenomenex 5 μm C18 (2) (150 × 4.6 mm), on a Waters 2487 dual wavelength detector. Analytical HPLC method: flow rate = 1 mL min<sup>-1</sup>; gradient elution over 35 min. Gradient: 20–100% acetonitrile/H<sub>2</sub>O in 15 min; 100% acetonitrile in 10 min; 100–20% acetonitrile/H<sub>2</sub>O in 5 min. Both solvents incorporated 0.05 vol% of TFA. The purity of all tested

compounds was at least 95% as determined by the method described above.

#### 6.1.1. General procedure for amide coupling (method A).

To a solution of the appropriate carboxylic acid (1 equiv.) in anhydrous dimethylformamide (DMF, 10 mL mmol<sup>-1</sup>), HOBt (2 equiv.) and EDC·HCl (2 equiv.) were added at room temperature (rt). After stirring for 10 min, the corresponding amine (1.2 equiv.) and DIPEA (6 equiv.) were added, and the reaction mixture was stirred at room temperature (rt) until the disappearance of the starting material (usually 60–72 h). After this time, water (50 mL) was added, and the mixture was extracted with EtOAc (3 × 50 mL). The combined organic layers were washed with water (5 × 25 mL) and brine (1 × 25 mL), dried over anhydrous Na<sub>2</sub>SO<sub>4</sub>, filtered, and concentrated under reduced pressure. The residue was purified by flash chromatography using a dichloromethane/methanol (DCM/MeOH) gradient prior to further preparative HPLC purification unless otherwise stated.

#### 6.1.2. General procedure for amide coupling (method B).

A mixture of 2-aminobenzimidazole (1 mmol), EDC·HCl (1.2 mmol), DMAP (1.2 mmol) and the appropriate carboxylic acid (1.2 mmol) in a (1 : 1) 20 mL mixture of anhydrous DCM and anhydrous tetrahydrofuran (THF) was stirred at room temperature (rt) for 72 h. In compounds **12a** and **12c**, the reaction mixture was quenched with saturated NH<sub>4</sub>Cl solution (50 mL) and extracted with DCM (3 × 25 mL) and ethyl acetate (3 × 25 mL). The combined organic layers were washed with brine (1 × 50 mL), dried over anhydrous Na<sub>2</sub>SO<sub>4</sub>, filtered, and concentrated under reduced pressure. The residue was purified by flash chromatography using a DCM/MeOH gradient. The two compounds were then further purified *via* preparative HPLC to attain >95% purity. In compound **12b**, after 72 h of stirring at rt, the solvent was evaporated under vacuum and the residue was purified by manual column chromatography. The obtained product was already >95% pure.

#### 6.1.3. General procedure for *N*-Boc protection (method C).

To a solution of the appropriate amine (3 mmol) in 30 mL of water:dioxane (1:2), di-*tert*-butyl dicarbonate (Boc<sub>2</sub>O, 6 mmol) and triethylamine (Et<sub>3</sub>N, 6 mmol) were added and the reaction mixture was stirred at rt for 72 h. Three quarters of the solvent was then evaporated *in vacuo* and the residue was acidified with 3 M aqueous HCl. The formed precipitate was filtered off, washed with water, and dried.

#### 6.1.4. General procedure for *N*-Boc deprotection (method D).

To a solution of the *N*-Boc protected amine (1 mmol) in 5 mL DCM, 2 mL TFA was added. The reaction mixture was stirred for 12 h and concentrated *in vacuo* then Na<sub>2</sub>HCO<sub>3</sub> solution was added for neutralisation, followed by extraction with DCM (3 × 50 mL). The combined organic phases were washed with brine (1 × 25 mL), dried over anhydrous Na<sub>2</sub>SO<sub>4</sub>, filtered, and concentrated under reduced pressure. The residue was purified by flash chromatography using a DCM/MeOH gradient.

**6.1.5. Preparation of synthetic intermediates 20a, 21a, 22a, and final compound 23a.** The synthesis of the title

compounds and their chemical characterisation are delineated in our recent article.<sup>38</sup>

**6.1.6. Preparation of the tested quinoloneamides.** The tested quinolones **24a–e** and **25a–e** were synthesised and characterised as we previously reported.<sup>46</sup>

*N*-Benzyl-4,6-difluoro-1*H*-indole-2-carboxamide (**8a**). This compound was obtained from 4,6-difluoroindole-2-carboxylic acid (**7**) and benzylamine employing method A. White solid, yield: 98%. Its chemical characterisation is detailed in our recently published report.<sup>38</sup> <sup>1</sup>H NMR (DMSO-*d*<sub>6</sub>) δ 12.05 (s, 1H), 9.13 (t, *J* = 5.9 Hz, 1H), 7.38–7.28 (m, 5H), 7.28–7.20 (m, 1H), 7.04 (dd, *J* = 9.4, 1.3 Hz, 1H), 6.87 (td, *J* = 10.4, 1.9 Hz, 1H), 4.52 (d, *J* = 6.0 Hz, 2H).

4,6-Difluoro-*N*-(3-methylbenzyl)-1*H*-indole-2-carboxamide (**8b**). 4,6-Difluoroindole-2-carboxylic acid (**7**) and 3-methylbenzyl amine were used to deliver the title compound following method A. It was >95% pure after flash chromatography. White solid, yield: 90%. <sup>1</sup>H NMR (DMSO-*d*<sub>6</sub>) δ 12.04 (s, 1H), 9.09 (t, *J* = 6.0 Hz, 1H), 7.30 (s, 1H), 7.22 (t, *J* = 7.5 Hz, 1H), 7.17–7.00 (m, 4H), 6.87 (td, *J* = 10.4, 1.8 Hz, 1H), 4.49 (d, *J* = 6.0 Hz, 2H); <sup>13</sup>C NMR (DMSO-*d*<sub>6</sub>) δ 160.8, 159.7 (dd, *J* = 237.0, 12.0 Hz), 156.2 (dd, *J* = 248.7, 15.5 Hz), 139.7138.1 (dd, *J* = 15.2, 13.2 Hz), 137.9, 133.1 (d, *J* = 3.2 Hz), 128.7, 128.3, 128.0, 124.8, 113.6 (d, *J* = 21.9 Hz), 98.8, 95.7 (dd, *J* = 29.7, 23.2 Hz), 95.1 (dd, *J* = 25.9, 4.4 Hz), 42.7, 21.5; HRMS (ESI) *m/z* calcd for C<sub>17</sub>H<sub>14</sub>F<sub>2</sub>N<sub>2</sub>O ([M + H]<sup>+</sup>) *m/z* 301.1147; found 301.1141.

4,6-Difluoro-*N*-(4-fluorobenzyl)-1*H*-indole-2-carboxamide (**8c**). The title compound was obtained from 4,6-difluoroindole-2-carboxylic acid (**7**) and 4-fluorobenzyl amine employing method A. This compound was purified by crystallisation from DMF and was obtained in >95% purity. Off white solid, yield: 76%. <sup>1</sup>H NMR (DMSO-*d*<sub>6</sub>) δ 12.04 (s, 1H), 9.13 (t, *J* = 6.0 Hz, 1H), 7.46–7.33 (m, 2H), 7.27 (s, 1H), 7.21–7.11 (m, 2H), 7.03 (dd, *J* = 9.4, 1.5 Hz, 1H), 6.88 (td, *J* = 10.4, 2.0 Hz, 1H), 4.49 (d, *J* = 5.9 Hz, 2H); <sup>13</sup>C NMR (DMSO-*d*<sub>6</sub>) δ 161.7 (d, *J* = 242.3 Hz), 160.8, 159.7 (dd, *J* = 237.0, 12.0 Hz), 156.2 (dd, *J* = 248.8, 15.6 Hz), 138.1 (dd, *J* = 15.0, 13.3 Hz), 136.0 (d, *J* = 3.0 Hz), 133.0 (d, *J* = 3.1 Hz), 129.7 (d, *J* = 8.1 Hz), 115.5 (d, *J* = 21.3 Hz), 113.6 (d, *J* = 21.8 Hz), 98.9, 95.7 (dd, *J* = 29.7, 23.3 Hz), 95.1 (dd, *J* = 25.9, 4.3 Hz), 42.0; HRMS (ESI) *m/z* calcd for C<sub>16</sub>H<sub>11</sub>F<sub>3</sub>N<sub>2</sub>O ([M + H]<sup>+</sup>) *m/z* 305.0896; found 305.0894.

*N*-(2,3-Dimethoxybenzyl)-4,6-difluoro-1*H*-indole-2-carboxamide (**8d**). This compound was synthesised from 4,6-difluoroindole-2-carboxylic acid (**7**) and 2,3-dimethoxybenzyl amine following method A. White solid, yield: 78%. <sup>1</sup>H NMR (DMSO-*d*<sub>6</sub>) δ 12.05 (s, 1H), 9.07 (t, *J* = 5.9 Hz, 1H), 7.29 (s, 1H), 7.03 (dd, *J* = 9.4, 1.3 Hz, 1H), 6.97 (d, *J* = 1.5 Hz, 1H), 6.85–6.92 (m, 3H), 4.44 (d, *J* = 5.9 Hz, 2H), 3.74 (s, 3H), 3.72 (s, 3H); <sup>13</sup>C NMR (DMSO-*d*<sub>6</sub>) δ 160.7, 159.6 (dd, *J* = 238.3, 12.1 Hz), 156.2 (dd, *J* = 248.6, 15.6 Hz), 149.1, 148.3, 138.1 (dd, *J* = 15.2, 13.3 Hz), 133.2 (d, *J* = 3.2 Hz), 132.2, 120.0, 113.6 (d, *J* = 22.0 Hz), 112.3, 112.0, 98.9, 95.6 (dd, *J* = 29.7, 23.2 Hz), 95.1 (dd, *J* = 25.9, 4.4 Hz), 56.0, 55.9, 42.5; HRMS (ESI) *m/z* calcd for C<sub>18</sub>H<sub>16</sub>F<sub>2</sub>N<sub>2</sub>O<sub>3</sub> ([M + H]<sup>+</sup>) *m/z* 347.1202; found 347.1202.

*N*-(Piperonyl)-4,6-difluoro-1*H*-indole-2-carboxamide (**8e**). This compound was obtained from 4,6-difluoroindole-2-carboxylic acid (**7**) and piperonylamine following method A. It was 95% pure after flash chromatography. Buff solid, yield: 93%. <sup>1</sup>H NMR (DMSO-*d*<sub>6</sub>) δ 12.03 (s, 1H), 9.05 (t, *J* = 6.0 Hz, 1H), 7.26 (s, 1H), 7.02 (dd, *J* = 9.4, 1.5 Hz, 1H), 6.93–6.84 (m, 3H), 6.81 (dd, *J* = 8.0, 1.5 Hz, 1H), 5.98 (s, 2H), 4.41 (d, *J* = 6.0 Hz, 2H); <sup>13</sup>C NMR (DMSO-*d*<sub>6</sub>) δ 160.7, 159.7 (dd, *J* = 238.4, 12.2 Hz), 156.2 (dd, *J* = 248.7, 15.5 Hz), 147.7, 146.6, 138.1 (dd, *J* = 15.3, 13.2 Hz), 133.7, 133.1 (d, *J* = 3.3 Hz), 121.0, 113.6 (d, *J* = 22.5 Hz), 108.5, 108.4, 101.3, 98.8, 95.7 (dd, *J* = 29.7, 23.3 Hz), 95.1 (dd, *J* = 25.8, 4.4 Hz), 42.5; HRMS (ESI) *m/z* calcd for C<sub>17</sub>H<sub>12</sub>F<sub>2</sub>N<sub>2</sub>O<sub>3</sub> ([M + H]<sup>+</sup>) *m/z* 331.0889; found 331.0881.

*N*-(Homopiperonyl)-4,6-difluoro-1*H*-indole-2-carboxamide (**8f**). The title compound was synthesised from 4,6-difluoroindole-2-carboxylic acid (**7**) and homopiperonylamine following method A. It was >95% pure after flash chromatography. White solid, yield: 73%. <sup>1</sup>H NMR (DMSO-*d*<sub>6</sub>) δ 11.97 (s, 1H), 8.60 (t, *J* = 5.6 Hz, 1H), 7.19 (d, *J* = 1.1 Hz, 1H), 7.02 (dd, *J* = 9.4, 1.4 Hz, 1H), 6.88 (overlapping td, *J* = 10.4, 2.0 Hz, 1H), 6.84 (d, *J* = 1.6 Hz, 1H), 6.81 (d, *J* = 7.9 Hz, 1H), 6.69 (dd, *J* = 7.9, 1.6 Hz, 1H), 5.95 (s, 2H), 3.47 (q, *J* = 6.7 Hz, 2H), 2.77 (t, *J* = 7.2 Hz, 2H); <sup>13</sup>C NMR (DMSO-*d*<sub>6</sub>) δ 160.7, 159.6 (dd, *J* = 238.3, 12.1 Hz), 156.1 (dd, *J* = 248.5, 15.6 Hz), 147.7, 146.0, 138.0 (dd, *J* = 15.2, 13.2 Hz), 133.6, 133.3 (d, *J* = 3.3 Hz), 122.0, 113.6 (d, *J* = 21.1 Hz), 109.5, 108.6, 101.1, 98.5, 95.6 (dd, *J* = 29.6, 23.3 Hz), 95.1 (dd, *J* = 25.9, 4.4 Hz), 41.1, 35.2; HRMS (ESI) *m/z* calcd for C<sub>19</sub>H<sub>20</sub>F<sub>2</sub>N<sub>2</sub>O<sub>2</sub> ([M + H]<sup>+</sup>) *m/z* 345.1045; found 345.1038.

*N*-(1-Adamantyl)-1*H*-benzimidazol-2-carboxamide (**10**). The title compound was synthesised from benzimidazole-2-carboxylic acid (**9**) and 1-adamantylamine following method A. The <sup>1</sup>H NMR data matched the one reported in the literature.<sup>51</sup> It was >95% pure after flash chromatography. White solid, yield: 66%. <sup>1</sup>H NMR (DMSO-*d*<sub>6</sub>) δ 13.11 (s, 1H), 7.74 (s, 1H), 7.61 (s, 2H), 7.31–7.24 (m, 2H), 2.10 (s, 6H), 2.08 (s, 3H), 1.67 (s, 6H).

*N*-(1*H*-Benzimidazol-2-yl)adamantane-1-carboxamide (**12a**). The title compound was synthesised from 2-aminobenzimidazole (**11**) and 1-adamantanecarboxylic acid according to method B and its <sup>1</sup>H NMR data matched the one we reported before.<sup>80</sup> White solid, yield: 41%. The <sup>1</sup>H NMR (DMSO-*d*<sub>6</sub>) δ 7.61 (s, 2H), 7.32 (s, 2H), 2.05 (s, 3H), 1.97 (s, 6H), 1.72 (s, 6H).

2-(1-Adamantyl)-*N*-(1*H*-benzimidazol-2-yl)acetamide (**12b**). This compound was obtained from 2-aminobenzimidazole (**11**) and 1-adamantanecarboxylic acid employing method B and it was >95% pure after flash chromatography. Its <sup>1</sup>H NMR data matched the one we reported before.<sup>80</sup> White solid, yield: 72%. <sup>1</sup>H NMR (DMSO-*d*<sub>6</sub>) δ 12.05 (s, 1H), 11.41 (s, 1H), 7.43 (s, 2H), 7.15–6.95 (m, 2H), 2.19 (s, 2H), 1.91 (s, 3H), 1.74–1.49 (m, 12H).

*N*-(1*H*-Benzimidazol-2-yl)-4,6-difluoro-1*H*-indole-2-carboxamide (**12c**). This compound was obtained via amide coupling 2-aminobenzimidazole (**11**) and 4,6-difluoroindole-2-carboxylic acid (**6**) following method B. White solid, yield:

35%.  $^1\text{H}$  NMR (DMSO- $d_6$ )  $\delta$  12.34 (s, 1H), 7.67 (s, 1H), 7.62 (s, 2H), 7.32 (dd,  $J = 5.3, 2.2$  Hz, 2H), 7.14 (dd,  $J = 9.3, 1.8$  Hz, 1H), 6.96 (td,  $J = 10.3, 2.0$  Hz, 1H);  $^{13}\text{C}$  NMR (DMSO- $d_6$ )  $\delta$  160.8, 160.6 (dd,  $J = 240.5, 12.0$  Hz), 156.6 (dd,  $J = 250.3, 15.6$  Hz), 146.3, 139.1 (overlapping dd,  $J = 14.0$  Hz, 1H), 131.4, 124.0, 113.9, 113.8, 113.7, 102.8, 96.4 (dd,  $J = 30.0, 23.0$  Hz), 95.4 (dd,  $J = 26.0, 4.1$  Hz); HRMS (ESI)  $m/z$  calcd for  $\text{C}_{17}\text{H}_{14}\text{F}_2\text{N}_2\text{O}$  ( $[\text{M} + \text{H}]^+$ )  $m/z$  301.1147; found 301.1141.

*N*-(1-Adamantyl)-1H-indazole-3-carboxamide (**14**). The title compound was synthesised from indazole-3-carboxylic acid (**13**) and 1-adamantylamine following method A. It was >95% pure after flash chromatography. The  $^1\text{H}$  NMR data matched the one reported in the literature.<sup>51</sup> White solid, yield: 62%.  $^1\text{H}$  NMR (DMSO- $d_6$ )  $\delta$  13.47 (s, 1H), 8.14 (d,  $J = 8.2$  Hz, 1H), 7.59 (d,  $J = 8.4$  Hz, 1H), 7.40 (t,  $J = 7.6$  Hz, 1H), 7.27–7.17 (m, 2H), 2.11 (s, 6H), 2.07 (s, 3H), 1.68 (s, 6H).

*tert*-Butyl (2-(adamantan-1-ylamino)-2-oxoethyl)carbamate (**16**). The title compound was prepared from 1-adamantylamine (**15**) according to the reported procedure.<sup>47</sup> The obtained crude residue was used without further purification in the next step; white solid, yield: 80%.

*N*-(1-Adamantyl)-2-aminoacetamide (**17**). This compound was synthesised using the crude product **16** employing method D. The  $^1\text{H}$ NMR data matched the one reported in the literature.<sup>47</sup> White solid, yield: 92%.  $^1\text{H}$  NMR (DMSO- $d_6$ )  $\delta$  7.48 (s, 1H), 3.12 (s, 2H), 2.01 (s, 3H), 1.92 (d,  $J = 2.6$  Hz, 6H), 1.62 (s, 6H).

*N*-(2-((Adamantan-1-yl)amino)-2-oxoethyl)-4,6-difluoro-1H-indole-2-carboxamide (**18**). This compound was prepared from compound **17** and 4,6-difluoroindole-2-carboxylic acid (**7**) following method A. White solid, yield: 82%.  $^1\text{H}$  NMR (DMSO- $d_6$ )  $\delta$  12.02 (s, 1H), 8.71 (t,  $J = 5.9$  Hz, 1H), 7.38 (s, 1H), 7.25 (d,  $J = 1.7$  Hz, 1H), 7.04 (dd,  $J = 9.3, 1.5$  Hz, 1H), 6.88 (td,  $J = 10.4, 1.8$  Hz, 1H), 3.85 (d,  $J = 5.9$  Hz, 2H), 2.01 (s, 3H), 1.94 (s, 6H), 1.62 (s, 6H);  $^{13}\text{C}$  NMR (DMSO- $d_6$ )  $\delta$  168.0, 161.0, 159.7 (dd,  $J = 238.5, 12.1$  Hz), 156.2 (dd,  $J = 248.7, 15.5$  Hz), 138.1 (dd,  $J = 15.2, 13.2$  Hz), 133.0 (d,  $J = 3.3$  Hz), 113.6 (d,  $J = 21.7$  Hz), 99.0, 95.7 (dd,  $J = 29.6, 23.3$  Hz), 95.0 (dd,  $J = 25.9, 4.4$  Hz), 51.3, 42.8, 41.5, 36.5, 29.3; HRMS (ESI)  $m/z$  calcd for  $\text{C}_{21}\text{H}_{23}\text{F}_2\text{N}_3\text{O}_2$  ( $[\text{M} + \text{H}]^+$ )  $m/z$  388.1831; found 388.1830.

2-(4-((*tert*-Butoxycarbonyl)amino)phenyl)acetic acid (**20b**). This compound was obtained *via* *N*-Boc protection of 4-aminophenylacetic acid **19b** following method C. The  $^1\text{H}$ -NMR data matched the one reported in the literature.<sup>81</sup> White solid, yield: 84%.  $^1\text{H}$  NMR (DMSO- $d_6$ )  $\delta$  7.89 (d,  $J = 8.2$  Hz, 2H), 7.45 (t,  $J = 6.0$  Hz, 1H), 7.34 (d,  $J = 8.2$  Hz, 2H), 4.18 (d,  $J = 6.1$  Hz, 2H), 1.39 (s, 9H).

*tert*-Butyl (4-(2-((adamantan-1-yl)amino)-2-oxoethyl)phenyl)carbamate (**21b**). The title compound was prepared *via* amide coupling **20b** and 1-adamantylamine employing method A. The collected crude product after evaporating the EtOAc extract was used without further purification in the next step; buff solid, yield: 70%.

*N*-(1-Adamantyl)-2-(4-aminophenyl)acetamide (**22b**). This compound was obtained *via* *N*-Boc deprotection (method D) of the crude product **21b**. Buff solid, yield: 90%.  $^1\text{H}$  NMR (DMSO- $d_6$ )  $\delta$  10.06 (t,  $J = 5.7$  Hz, 1H), 7.74 (d,  $J = 8.2$  Hz, 2H),

7.54 (s, 1H), 7.31 (d,  $J = 8.2$  Hz, 2H), 4.42 (d,  $J = 5.8$  Hz, 2H), 2.06 (s, 9H), 1.65 (s, 6H);  $^{13}\text{C}$  NMR (DMSO- $d_6$ )  $\delta$  170.8, 147.3, 129.7, 124.4, 114.3, 51.1, 42.9, 41.5, 36.5, 29.3.

*N*-(4-(2-((Adamantan-1-yl)amino)-2-oxoethyl)phenyl)-4,6-difluoro-1H-indole-2-carboxamide (**23b**). This compound was obtained *via* amide coupling 4,6-difluoroindole-2-carboxylic acid (**7**) and **22b** employing method A. The product was further crystallised from a 70% DCM/30% MeOH mixture and was obtained in >95% purity. White solid, yield: 96%.  $^1\text{H}$  NMR (DMSO- $d_6$ )  $\delta$  12.15 (s, 1H), 10.24 (s, 1H), 7.68 (d,  $J = 8.6$  Hz, 2H), 7.52 (s, 2H), 7.23 (d,  $J = 8.6$  Hz, 2H), 7.07 (dd,  $J = 9.4, 1.4$  Hz, 1H), 6.91 (td,  $J = 10.4, 2.1$  Hz, 1H), 3.32 (s, 2H), 1.98 (s, 3H), 1.92 (s, 6H), 1.59 (s, 6H);  $^{13}\text{C}$  NMR (DMSO- $d_6$ )  $\delta$  170.0, 159.9 (dd,  $J = 239.0, 12.1$  Hz), 159.3, 156.3 (dd,  $J = 249.0, 15.5$  Hz), 138.4 (dd,  $J = 15.3, 13.0$  Hz), 137.3, 133.0 (d,  $J = 3.2$  Hz), 132.9, 129.6, 120.6, 113.6 (d,  $J = 21.9$  Hz), 99.9, 95.9 (dd,  $J = 29.8, 23.2$  Hz), 95.1 (dd,  $J = 25.9, 4.4$  Hz), 51.2, 43.0, 41.4, 36.5, 29.3; HRMS (ESI)  $m/z$  calcd for  $\text{C}_{27}\text{H}_{27}\text{F}_2\text{N}_3\text{O}_2$  ( $[\text{M} + \text{H}]^+$ )  $m/z$  464.2144; found 464.2138.

## 6.2. Biological evaluation

**6.2.1. Antitumour activity.** The four well-established paediatric brain tumour cell lines were all derived from humans and were used to assess the effects on proliferation and viability when treated with the indole and indole bioisostere carboxamide derivatives. KNS42 (glioblastoma multiforme – GBM), BT-12 and BT-16 (atypical teratoid rhabdoid tumour – AT/RT) cell lines were gifts from Dr. Hashizume, Northwestern University, whereas DAOY cells (medulloblastoma – MB) were obtained from ATCC. The human fibroblasts HFF1 (obtained from ATCC) were used as non-neoplastic controls. The cells were cultured and the compounds were screened for their proliferation and viability inhibitory activities following the protocol described in our previous report.<sup>38</sup> Each experiment was executed in triplicate.

**6.2.2. Transcriptional analysis of KNS42 cells.** The KNS42 cells were maintained in Roswell Park Memorial Institute (RPMI) medium supplemented with 10% fetal bovine serum (FBS) and 1% penicillin/streptomycin and incubated at 37 °C in 5%  $\text{CO}_2$ . The cells were treated with 10  $\mu\text{M}$  compound **8a**. The cells were washed with 1 $\times$  PBS, scraped with a cell scraper and centrifuged to collect cell pellets after 72 hours of treatment. The RNA samples were then prepared according to our previous report<sup>38</sup> and were submitted to BGI Americas for DNBSEQ Eukaryotic Stranded Transcriptome Resequencing.

**6.2.3. *In vitro* functional activity assay at CB<sub>1</sub>R and CB<sub>2</sub>R.** Mouse AtT-20 neuroblastoma cells stably transfected with human CB<sub>1</sub>R or human CB<sub>2</sub>R were used for evaluation of membrane potential responses as previously reported.<sup>82,83</sup> In antagonist mode, cells were pre-incubated with the vehicle or compounds for 60 minutes, before addition of 500 nM CP 55940. Data were analysed with PRISM (GraphPad Software Inc., San Diego, CA), using four-parameter non-linear regression to fit agonist ( $\text{EC}_{50}$ ) and antagonist ( $\text{IC}_{50}$ ) concentration response curves.

## Conflicts of interest

There are no conflicts to declare.

## Acknowledgements

SSRA acknowledges Curtin University for the support through a Curtin International Postgraduate Research Scholarship (CIPRS). HG is thankful for the ARC Discovery Early Career Researcher Award DE160100482.

## References

- 1 F. He and Y. E. Sun, *Int. J. Biochem. Cell Biol.*, 2007, **39**, 661–665.
- 2 K. R. Jessen and R. Mirsky, *Nature*, 1980, **286**, 736–737.
- 3 Q. T. Ostrom, H. Gittleman, P. Liao, C. Rouse, Y. Chen, J. Dowling, Y. Wolinsky, C. Kruchko and J. Barnholtz-Sloan, *Neuro-Oncology*, 2014, **16**(Suppl 4), iv1–iv63.
- 4 D. N. Louis, A. Perry, G. Reifenberger, A. von Deimling, D. Figarella-Branger, W. K. Cavenee, H. Ohgaki, O. D. Wiestler, P. Kleihues and D. W. Ellison, *Acta Neuropathol.*, 2016, **131**, 803–820.
- 5 Z. Miklja, A. Pasternak, S. Stallard, T. Nicolaides, C. Kline-Nunnally, B. Cole, R. Beroukhim, P. Bandopadhyay, S. Chi, S. H. Ramkissoon, B. Mullan, A. K. Bruzek, A. Gauthier, T. Garcia, C. Atchison, B. Marini, M. Fouladi, D. W. Parsons, S. Leary, S. Mueller, K. L. Ligon and C. Koschmann, *Neuro-Oncology*, 2019, **21**(8), 968–980.
- 6 D. A. Bax, S. E. Little, N. Gaspar, L. Perryman, L. Marshall, M. Viana-Pereira, T. A. Jones, R. D. Williams, A. Grigoriadis, G. Vassal, P. Workman, D. Sheer, R. M. Reis, A. D. Pearson, D. Hargrave and C. Jones, *PLoS One*, 2009, **4**, e5209.
- 7 K. Ichimura, R. Nishikawa and M. Matsutani, *Neuro-Oncology*, 2012, **14**(Suppl 4), iv90–iv99.
- 8 C. Jones, L. Perryman and D. Hargrave, *Nat. Rev. Clin. Oncol.*, 2012, **9**, 400–413.
- 9 N. Gaspar, L. Marshall, L. Perryman, D. A. Bax, S. E. Little, M. Viana-Pereira, S. Y. Sharp, G. Vassal, A. D. Pearson, R. M. Reis, D. Hargrave, P. Workman and C. Jones, *Cancer Res.*, 2010, **70**, 9243–9252.
- 10 T. Mueller, A. S. G. Stucklin, A. Postlmayr, S. Metzger, N. Gerber, C. Kline, M. Grotzer, J. Nazarian and S. Mueller, *Curr. Treat. Options Neurol.*, 2020, **22**, 43.
- 11 M. Guzman, M. J. Duarte, C. Blazquez, J. Ravina, M. C. Rosa, I. Galve-Roperh, C. Sanchez, G. Velasco and L. Gonzalez-Feria, *Br. J. Cancer*, 2006, **95**, 197–203.
- 12 A. E. Munson, L. S. Harris, M. A. Friedman, W. L. Dewey and R. A. Carchman, *J. Natl. Cancer Inst.*, 1975, **55**, 597–602.
- 13 B. Chakravarti, J. Ravi and R. K. Ganju, *Oncotarget*, 2014, **5**, 5852–5872.
- 14 S. Sarfaraz, V. M. Adhami, D. N. Syed, F. Afaq and H. Mukhtar, *Cancer Res.*, 2008, **68**, 339–342.
- 15 P. Massi, M. Valenti, M. Solinas and D. Parolaro, *Cancers*, 2010, **2**, 1013–1026.
- 16 D. Parolaro and P. Massi, *Expert Rev. Neurother.*, 2008, **8**, 37–49.
- 17 F. C. Rocha, J. G. Dos Santos Junior, S. C. Stefano and D. X. da Silveira, *J. Neuro-Oncol.*, 2014, **116**, 11–24.
- 18 G. Velasco, A. Carracedo, C. Blazquez, M. Lorente, T. Aguado, A. Haro, C. Sanchez, I. Galve-Roperh and M. Guzman, *Mol. Neurobiol.*, 2007, **36**, 60–67.
- 19 G. Velasco, C. Sanchez and M. Guzman, *Nat. Rev. Cancer*, 2012, **12**, 436–444.
- 20 G. Velasco, C. Sanchez and M. Guzman, *Curr. Oncol.*, 2016, **23**, S23–S32.
- 21 M. Guzman, *Nat. Rev. Cancer*, 2003, **3**, 745–755.
- 22 C. Sanchez, I. Galve-Roperh, C. Canova, P. Brachet and M. Guzman, *FEBS Lett.*, 1998, **436**, 6–10.
- 23 C. Blazquez, L. Gonzalez-Feria, L. Alvarez, A. Haro, M. L. Casanova and M. Guzman, *Cancer Res.*, 2004, **64**, 5617–5623.
- 24 I. Galve-Roperh, C. Sanchez, M. L. Cortes, T. Gomez del Pulgar, M. Izquierdo and M. Guzman, *Nat. Med.*, 2000, **6**, 313–319.
- 25 A. Ellert-Miklaszewska, B. Kaminska and L. Konarska, *Cell. Signalling*, 2005, **17**, 25–37.
- 26 C. Blazquez, M. Salazar, A. Carracedo, M. Lorente, A. Egia, L. Gonzalez-Feria, A. Haro, G. Velasco and M. Guzman, *Cancer Res.*, 2008, **68**, 1945–1952.
- 27 R. Ramer and B. Hinz, *Int. Rev. Cell Mol. Biol.*, 2015, **314**, 43–116.
- 28 C. Blazquez, M. L. Casanova, A. Planas, T. Gomez Del Pulgar, C. Villanueva, M. J. Fernandez-Acenero, J. Aragonés, J. W. Huffman, J. L. Jorcano and M. Guzman, *FASEB J.*, 2003, **17**, 529–531.
- 29 T. Gomez del Pulgar, G. Velasco, C. Sanchez, A. Haro and M. Guzman, *Biochem. J.*, 2002, **363**, 183–188.
- 30 C. Sanchez, M. L. de Ceballos, T. Gomez del Pulgar, D. Rueda, C. Corbacho, G. Velasco, I. Galve-Roperh, J. W. Huffman, S. Ramon y Cajal and M. Guzman, *Cancer Res.*, 2001, **61**, 5784–5789.
- 31 S. Fogli, P. Nieri, A. Chicca, B. Adinolfi, V. Mariotti, P. Iacopetti, M. C. Breschi and S. Pellegrini, *FEBS Lett.*, 2006, **580**, 1733–1739.
- 32 S. B. Gustafsson, T. Lindgren, M. Jonsson and S. O. Jacobsson, *Cancer Chemother. Pharmacol.*, 2009, **63**, 691–701.
- 33 P. Massi, A. Vaccani, S. Ceruti, A. Colombo, M. P. Abbracchio and D. Parolaro, *J. Pharmacol. Exp. Ther.*, 2004, **308**, 838–845.
- 34 P. Massi, A. Vaccani, S. Bianchessi, B. Costa, P. Macchi and D. Parolaro, *Cell. Mol. Life Sci.*, 2006, **63**, 2057–2066.
- 35 K. P. Sarker and I. Maruyama, *Cell. Mol. Life Sci.*, 2003, **60**, 1200–1208.
- 36 A. Vaccani, P. Massi, A. Colombo, T. Rubino and D. Parolaro, *Br. J. Pharmacol.*, 2005, **144**, 1032–1036.
- 37 Y. Shi, Y. H. Duan, Y. Y. Ji, Z. L. Wang, Y. R. Wu, H. Gunosewoyo, X. Y. Xie, J. Z. Chen, F. Yang, J. Li, J. Tang, X. Xie and L. F. Yu, *J. Med. Chem.*, 2017, **60**, 7067–7083.
- 38 S. S. R. Alsayed, S. Lun, A. W. Bailey, A. Suri, C.-C. Huang, M. Mocerino, A. Payne, S. T. Sredni, W. R. Bishai and H. Gunosewoyo, *RSC Adv.*, 2021, **11**, 15497–15511.
- 39 A. D. Rouillard, G. W. Gundersen, N. F. Fernandez, Z. Wang, C. D. Monteiro, M. G. McDermott and A. Ma'ayan, *Database*, 2016, **2016**, baw100.

- 40 S. P. Oldfield, M. D. Hall and J. A. Platts, *J. Med. Chem.*, 2007, **50**, 5227–5237.
- 41 C. Mugnaini, A. Brizzi, A. Ligresti, M. Allara, S. Lamponi, F. Vacondio, C. Silva, M. Mor, V. Di Marzo and F. Corelli, *J. Med. Chem.*, 2016, **59**, 1052–1067.
- 42 S. Pasquini, M. De Rosa, V. Pedani, C. Mugnaini, F. Guida, L. Luongo, M. De Chiaro, S. Maione, S. Dragoni, M. Frosini, A. Ligresti, V. Di Marzo and F. Corelli, *J. Med. Chem.*, 2011, **54**, 5444–5453.
- 43 S. Pasquini, A. Ligresti, C. Mugnaini, T. Semeraro, L. Cicione, M. De Rosa, F. Guida, L. Luongo, M. De Chiaro, M. G. Cascio, D. Bolognini, P. Marini, R. Pertwee, S. Maione, V. Di Marzo and F. Corelli, *J. Med. Chem.*, 2010, **53**, 5915–5928.
- 44 E. Stern, G. G. Muccioli, R. Millet, J. F. Goossens, A. Farce, P. Chavatte, J. H. Poupaert, D. M. Lambert, P. Depreux and J. P. Henichart, *J. Med. Chem.*, 2006, **49**, 70–79.
- 45 C. Manera, A. M. Malfitano, T. Parkkari, V. Lucchesi, S. Carpi, S. Fogli, S. Bertini, C. Laezza, A. Ligresti, G. Saccomanni, J. R. Savinainen, E. Ciaglia, S. Pisanti, P. Gazzero, V. Di Marzo, P. Nieri, M. Macchia and M. Bifulco, *Eur. J. Med. Chem.*, 2015, **97**, 10–18.
- 46 S. S. R. Alsayed, S. Lun, G. Luna, C. C. Beh, A. D. Payne, N. Foster, W. R. Bishai and H. Gunosewoyo, *RSC Adv.*, 2020, **10**, 7523–7540.
- 47 P. Kancharla, J. X. Kelly and K. A. Reynolds, *J. Med. Chem.*, 2015, **58**, 7286–7309.
- 48 S. D. Banister, J. Stuart, R. C. Kevin, A. Edington, M. Longworth, S. M. Wilkinson, C. Beinat, A. S. Buchanan, D. E. Hibbs, M. Glass, M. Connor, I. S. McGregor and M. Kassiou, *ACS Chem. Neurosci.*, 2015, **6**, 1445–1458.
- 49 R. G. Pertwee, *Expert Opin. Invest. Drugs*, 2000, **9**, 1553–1571.
- 50 L. Ruiz, A. Miguel and I. Diaz-Laviada, *FEBS Lett.*, 1999, **458**, 400–404.
- 51 Y. Y. Ji, Z. L. Wang, F. N. Pei, J. J. Shi, J. J. Li, H. Gunosewoyo, F. Yang, J. Tang, X. Xie and L. F. Yu, *MedChemComm*, 2019, **10**, 2131–2139.
- 52 M. Koslowski, U. Sahin, R. Mitnacht-Kraus, G. Seitz, C. Huber and O. Tureci, *Cancer Res.*, 2007, **67**, 9528–9534.
- 53 C. Lin, P. Qian, Y. Zhang, Z. Liu, K. Dai and D. Sun, *Tissue Cell*, 2021, **69**, 101480.
- 54 Y. Wu, X. Lin, X. Di, Y. Chen, H. Zhao and X. Wang, *Oncol. Rep.*, 2017, **37**, 465–473.
- 55 C. Han, S. He, R. Wang, X. Gao, H. Wang, J. Qiao, X. Meng, Y. Li and L. Yu, *J. Transl. Med.*, 2021, **19**, 65.
- 56 T. Wang and M. Ha, *J. Cell. Biochem.*, 2018, **119**, 7747–7756.
- 57 W. Wang, T. Shen, B. Dong, C. J. Creighton, Y. Meng, W. Zhou, Q. Shi, H. Zhou, Y. Zhang, D. D. Moore and F. Yang, *J. Clin. Invest.*, 2019, **129**, 1015–1029.
- 58 T. Shen, W. Wang, W. Zhou, I. Coleman, Q. Cai, B. Dong, M. M. Ittmann, C. J. Creighton, Y. Bian, Y. Meng, D. R. Rowley, P. S. Nelson, D. D. Moore and F. Yang, *J. Clin. Invest.*, 2021, **131**(4), e135465.
- 59 D. Ganguly, C. Cai, M. M. Sims, C. H. Yang, M. Thomas, J. Cheng, A. G. Saad and L. M. Pfeffer, *Pharmaceuticals*, 2019, **12**(1), 45.
- 60 Z. Chen, X. Wei, X. Wang, X. Zheng, B. Chang, L. Shen, H. Zhu, M. Yang, S. Li and X. Zheng, *Cell Death Dis.*, 2021, **12**, 377.
- 61 Y. Yi, S. H. Tsai, J. C. Cheng, E. Y. Wang, M. S. Anglesio, D. R. Cochrane, M. Fuller, E. A. Gibb, W. Wei, D. G. Huntsman, A. Karsan and P. A. Hoodless, *Gynecol. Oncol.*, 2017, **147**, 663–671.
- 62 K. Kobayashi, A. Ohnishi, J. Promsuk, S. Shimizu, Y. Kanai, Y. Shiokawa and M. Nagane, *Neurosurgery*, 2008, **62**(2), 493–504.
- 63 Y. Ohshima, K. Kaira, A. Yamaguchi, N. Oriuchi, H. Tominaga, S. Nagamori, Y. Kanai, T. Yokobori, T. Miyazaki, T. Asao, Y. Tsushima, H. Kuwano and N. S. Ishioka, *Cancer Sci.*, 2016, **107**, 1499–1505.
- 64 Q. Wang, J. Tiffen, C. G. Bailey, M. L. Lehman, W. Ritchie, L. Fazli, C. Metierre, Y. J. Feng, E. Li, M. Gleave, G. Buchanan, C. C. Nelson, J. E. Rasko and J. Holst, *J. Natl. Cancer Inst.*, 2013, **105**, 1463–1473.
- 65 J. Wang, X. Chen, L. Su, P. Li, B. Liu and Z. Zhu, *Biomed. Pharmacother.*, 2013, **67**, 693–699.
- 66 Z. Haining, N. Kawai, K. Miyake, M. Okada, S. Okubo, X. Zhang, Z. Fei and T. Tamiya, *BMC Clin. Pathol.*, 2012, **12**, 4.
- 67 T. Nakayama, H. Hirakawa, K. Shibata, A. Nazneen, K. Abe, T. Nagayasu and T. Taguchi, *Oncol. Rep.*, 2011, **25**, 929–935.
- 68 Y. T. Tsai, A. C. Wu, W. B. Yang, T. J. Kao, J. Y. Chuang, W. C. Chang and T. I. Hsu, *Int. J. Mol. Sci.*, 2019, **20**(22), 5625.
- 69 Z. Wang, B. Han, Z. Zhang, J. Pan and H. Xia, *Biomarkers*, 2010, **15**, 39–46.
- 70 M. Cocchia, R. Huber, S. Pantano, E. Y. Chen, P. Ma, A. Forabosco, M. S. Ko and D. Schlessinger, *Genomics*, 2000, **68**, 305–312.
- 71 Y. Yin, X. Zhu, S. Huang, J. Zheng, M. Zhang, W. Kong, Q. Chen, Y. Zhang, X. Chen, K. Lin and X. Ouyang, *Tumor Biol.*, 2017, **39**, 1010428317699131.
- 72 H. Yuan, V. Chen, M. Boisvert, C. Isaacs and R. I. Glazer, *PLoS One*, 2018, **13**, e0192106.
- 73 J. Mahmoudian, R. Ghods, M. Nazari, M. Jeddi-Tehrani, M. H. Ghahremani, S. N. Ostad and A. H. Zarnani, *Exp. Oncol.*, 2019, **41**, 7–13.
- 74 B. K. Ang, C. Y. Lim, S. S. Koh, N. Sivakumar, S. Taib, K. B. Lim, S. Ahmed, G. Rajagopal and S. H. Ong, *J. Mol. Signaling*, 2007, **2**, 1.
- 75 Y. Katanasaka, Y. Kodera, Y. Kitamura, T. Morimoto, T. Tamura and F. Koizumi, *Mol. Cancer*, 2013, **12**, 31.
- 76 P. Kongpracha, S. Nagamori, P. Wiriyasermkul, Y. Tanaka, K. Kaneda, S. Okuda, R. Ohgaki and Y. Kanai, *J. Pharmacol. Sci.*, 2017, **133**, 96–102.
- 77 K. Oda, N. Hosoda, H. Endo, K. Saito, K. Tsujihara, M. Yamamura, T. Sakata, N. Anzai, M. F. Wempe, Y. Kanai and H. Endou, *Cancer Sci.*, 2010, **101**, 173–179.
- 78 L. La Paglia, A. Listi, S. Caruso, V. Amodeo, F. Passiglia, V. Bazan and D. Fanale, *PPAR Res.*, 2017, **2017**, 8187235.
- 79 A. Carracedo, M. Lorente, A. Egia, C. Blazquez, S. Garcia, V. Giroux, C. Malicet, R. Villuendas, M. Gironella, L. Gonzalez-Feria, M. A. Piris, J. L. Iovanna, M. Guzman and G. Velasco, *Cancer Cell*, 2006, **9**, 301–312.

- 80 S. S. R. Alsayed, S. Lun, A. Payne, W. R. Bishai and H. Gunosewoyo, *Bioorg. Chem.*, 2021, **106**, 104486.
- 81 K. Urgan, M. Jida, K. Ehrhardt, T. Muller, M. Lanzer, L. Maes, M. Elhabiri and E. Davioud-Charvet, *Molecules*, 2017, **22**, 161.
- 82 A. Knapman, M. Santiago, Y. P. Du, P. R. Bennallack, M. J. Christie and M. Connor, *J. Biomol. Screening*, 2013, **18**, 269–276.
- 83 M. Moir, S. Lane, F. Lai, M. Connor, D. E. Hibbs and M. Kassiou, *Eur. J. Med. Chem.*, 2019, **180**, 291–309.



## Conclusions

When paediatric GBM KNS42 cells were found to be overexpressing CB<sub>1</sub>R, a closer look at the antitumour potential of cannabinoids was taken. Numerous natural and synthetic-based cannabinoids, including  $\Delta^9$ -THC, CBD, WIN55,212-2, JWH-133, and rimonabant, were demonstrated to have potent antitumour activities. Some reports showed that the antitumour potential of cannabinoids is attributed to modulating the activity of CB receptors. Nonetheless, numerous studies attested that the antitumour activities of several cannabinoids are independent of CB receptors. Similar to the foregoing cannabinoids, the I2C architecture was proven to act as a potent modulator of CB receptors. In addition, some I2C analogues were shown to have dual pharmacology profiles as potent anti-TB and anti-tumour agents in our 2021 RSC Advances article (Chapter 6). Accordingly, several I2C analogues and bioisosteres were designed, synthesised, and evaluated for their anti-TB and antitumour activities. When assessed for their anti-TB activities, all the newly designed I2C analogues, benzimidazoles, and indazole-3-carboxamide were devoid of anti-TB activity. Therefore, the focus of our RSC Medicinal Chemistry was directed towards the antitumour potential of these I2C analogues and bioisosteres. The top potent compounds were evaluated for their agonistic and antagonistic activities at CB<sub>1</sub>R and CB<sub>2</sub>R. No correlation was clearly discerned between the antitumour activities and CB receptor modulation profiles of our tested compounds. Differential gene expression analysis was performed on KNS42 cells treated with one of the top potent compounds versus the untreated cells. A set of seven oncogenes were found to be downregulated in the I2C-treated KNS42 cells compared to the control cells. Overall, the I2C architecture seems to be a multi-target directed ligand, in which it can be structurally modified to obtain molecules with specific biological activities or polypharmacology profiles.

In Chapters 1 – 7 of this thesis, "every reasonable effort has been made to acknowledge the owners of copyright material. I would be pleased to hear from any copyright owner who has been omitted or incorrectly acknowledged."

## **Chapter 8**

### **Conclusions and Future Directions**

## 8.1. Conclusions

Despite the discovery of the tubercle bacilli more than a century ago by Robert Koch as the causative agent of TB, this infectious disease remains one of the leading causes of deaths worldwide, especially in underprivileged societies. The two monumental hurdles thwarting the global TB control efforts are the HIV epidemic and the growing ubiquity of the drug-resistant (DR) *Mycobacterium tuberculosis* (*M. tb*) strains. Therefore, new anti-TB agents with novel mechanisms of action are desperately needed to outmanoeuvre the mycobacterial resistance mechanisms against current antibiotics.

This project was mainly focused on the development of novel anti-TB agents effective against both drug-sensitive (DS) and DR *M. tb* strains. In addition, several molecules were repurposed/developed as antitumour agents. The major aims achieved in this project are the following:

- 1- Investigating the role of phosphorylation and dephosphorylation in the biosynthesis of mycolic acids (MAs) in *M. tb* as part of the mycobacterial mechanism in eluding the host's immune response.
- 2- Designing, synthesising, and biologically evaluating various indole-2-carboxamide (I2C) analogues and bioisosteres as potent anti-TB agents.
- 3- Structurally modifying isoniazid (INH), pyrazinamide (PZA), and ciprofloxacin (CPF) to optimise their physicochemical properties and discover new anti-TB analogues.
- 4- Highlighting the polypharmacology profile of the I2C framework through the identification of several I2C analogues and bioisosteres showing potent anti-TB and antitumour activities.

Chapter 1 entails a general introduction on TB statistics, pathogenesis, current treatment regimens, and hot targets in *M. tb* with their related drug candidates. This introduction is intended to be later prepared as a manuscript to be submitted for publication as a review article. The first major aim was rigorously addressed in a review article published in 2019 in Current Molecular Pharmacology journal (Chapter 2). The ability of *M. tb* to modulate the functional activity of several enzymes involved in the MAs synthesis was summarised therein. In this respect, *M. tb* uses phosphorylation and dephosphorylation machineries to modify its cell wall composition in response to

different environmental conditions, allowing for the bacterial virulence and survival within the host. Prior to incorporating the review article in this Chapter, the role of *M. tb*-secreted kinases and phosphatases in establishing infection inside the granuloma and evading the phagosome-lysosome fusion was thoroughly discussed. This unpublished part is also intended to be later submitted as a review article. Taken together, targeting mycobacterial protein kinases and phosphatases that are implicated in the *M. tb* survival mechanisms represents a novel and unorthodox approach that could be further exploited in the future to develop new anti-TB agents.

The second major aim entailed the rational design and synthesis of novel anti-TB compounds employing the I2C framework as a template (Chapter 3; RSC Advances 2020 article). To this end, the indole ring was replaced by various bioisosteres or scaffold hops, while the carboxamide and the *N*-linked cycloaliphatic moiety were maintained. The most successful replacement in this strategy was the naphthalene moiety [minimum inhibitory concentration (MIC) = 3.27 – 13.10  $\mu$ M (1 – 4  $\mu$ g/mL)] against DS and DR *M. tb* strains. These naphthalene analogues showed no cytotoxicities against normal mammalian cells (Vero cells), suggesting their selective activities against *M. tb*. Since the indole scaffold proved to be superior to the other structural subunits used in its place, the next strategy was to retain the indole moiety and the *N*-linked moiety, while modifying the central amide linker. Introducing a carbonyl group between the amide group and the cycloaliphatic tail (imide linker) was the most tolerated change to the amide connector [MIC = 22.32  $\mu$ M (8  $\mu$ g/mL)]. Docking studies using the MmpL3 crystal structure were conducted to shed light on the potential mode of action of the top potent compounds. The virtual binding modes of the new active analogues within the MmpL3 active site were similar to the co-crystallised I2C ligand.

On the other hand, the main structural modification entailed in Chapter 4 (Bioorganic Chemistry 2021 article) was the introduction of a hydroxyl group to the *N*-linked adamantane moiety, while the indole ring and the amide group were preserved. The reason behind this approach was to improve the water solubility of the *N*-cycloaliphatic I2C framework while maintaining optimum lipophilicity for eliciting good anti-TB activity. Three *N*-adamantanol I2C analogues showed potent activities against DS, multidrug-resistant (MDR), and extensively drug-resistant (XDR) *M. tb* isolates (MIC = 0.66 – 5.77  $\mu$ M). These derivatives also displayed negligible cytotoxicities against

Vero cells, indicating their preliminary safety profiles as well as their selectivity towards *M. tb*. Expectedly, the binding profiles of the most active *N*-adamantanol I2C analogues were similar to the co-crystallised I2C ligand. Upon experimentally determining the water solubility of some representative analogues, the adamantanol containing compounds demonstrated 2- to 3-fold improvement in their kinetic aqueous solubility compared to the homologous bare adamantane derivatives. In addition, an overall improvement in the *in silico* physicochemical parameters of the adamantanol analogues was observed in comparison to the unsubstituted adamantane counterparts. Accordingly, the adamantanol ring constitutes a valid replacement to the less polar adamantane moiety, wherein a potent anti-TB activity was retained while the drug-like properties were improved.

Contrary to the aforementioned strategies applied to the I2C framework, the third major aim involved increasing the lipophilicity of some TB antibiotics, namely INH, PZA, and CPF, via attaching an adamantane moiety (Chapter 5; Chemical Biology and Drug Design 2021 article). In addition, several hybrids were synthesised, in which two pharmacophores from various anti-TB agents with different mechanisms of action were conjugated. The hybrid incorporating both INH and PZA was shown to be the most active compound in this study (MIC = 2 – 4 µg/mL against DS *M. tb*), while displaying no cytotoxicity against Vero cells (MIC ≥ 64 µg/mL). Unfortunately, this hybrid was stripped of its activity when tested against DR *M. tb* isolates (MIC > 32 µg/mL), suggesting that it targets a mechanistic pathway similar to INH and PZA. Tethering the I2C framework with INH and PZA resulted in a drastic drop in the anti-TB activity (MIC > 64 µg/mL).

Since the I2C architecture was integrated in several reported antitumour agents, a comprehensive literature review was conducted to highlight their mechanisms of action in addition to the structural features required to elicit potent antitumour activities (Chapter 6). These findings prompted the design and synthesis of numerous I2C analogues to be evaluated for their anti-TB and antitumour activities (RSC Advances 2021 article; Chapter 6). This repurposing strategy revealed the dual pharmacology profile of several *N*-rimantadine I2C derivatives. In fact, all the rimantadine-containing compounds showed potent anti-TB activities against DS *M. tb* H37Rv strain (MIC = 0.32 – 6.20 µM). All derivatives were preliminary evaluated for their antitumour activities against paediatric glioblastoma (GBM) KNS42 cell line. The *N*-rimantadine-

6-bromo-I2C analogue showed the most promising multi-target activity profile [MIC (H37Rv) = 0.62  $\mu$ M and IC<sub>50</sub> (KNS42 viability) = 0.84  $\mu$ M]. Apart from the rimantadine derivatives, the other tested I2C analogues in our study were devoid of anti-TB activity, while most of them displayed potent inhibitory activities against the viability of KNS42 cells (IC<sub>50</sub> = 1.34 – 8.25  $\mu$ M). The most potent antitumour I2C derivative entailed a piperazine ring as the middle linker between the indole ring and the adamantane moiety. Upon analysing the differential gene expression of KNS42 cells treated with this piperazine derivative versus the untreated control cells, two oncogenes were found to be significantly downregulated (fold change = 9 and 15;  $p < 0.05$ ). While this piperazine-linked I2C compound retained its potent antitumour activity against the viability of teratoid/rhabdoid (AT/RT) BT12 and BT16 tumour cell lines, it showed moderate cytotoxicity against non-tumourigenic human fibroblasts HFF1 cells.

Intriguingly, KNS42 cells were reported to overexpress cannabinoid receptor 1 gene (*CNR1*). Therefore, a thorough literature search was conducted, wherein compounds with polypharmacology activities against *M. tb*, tumour cells, and cannabinoid (CB) receptors were highlighted (Chapter 7). Equally important, the correlation between the antitumour activities of several cannabinoids and their CB receptor modulatory effects was discussed. The polypharmacology potential of the I2C framework, discussed in the first half of both Chapters 6 and 7, is intended to be later prepared and submitted as a review article. In the second half of Chapter 7, several I2C analogues were designed, synthesised, and biologically evaluated for their antitumour activities (RSC Medicinal Chemistry 2021). The anti-TB activities of the new derivatives in this article were also determined, in which they were devoid of potency against *M. tb* H37Rv strain. Several I2C analogues demonstrated potent antiproliferative and cytotoxic activities against KNS42 cells and a panel of paediatric grade IV brain tumour cells, namely AT/RT BT12 and BT16 tumour cell lines and the medulloblastoma DAOY cell line (IC<sub>50</sub> < 10  $\mu$ M). Importantly, the top potent I2C analogues in our study exhibited limited cytotoxic activities against non-tumourigenic HFF1 human fibroblasts, suggesting their selective cytotoxicities against tumour cells. The next logical step was to test the activities of the most active compounds at cannabinoid receptors 1 and 2 (CB<sub>1</sub>R and CB<sub>2</sub>R). No direct correlation between the antitumour activities of these analogues and CB receptor agonism/antagonism or lack thereof was observed. Accordingly, gene sequencing analysis of KNS42 cells treated with one of the most

potent I2Cs versus the untreated control cells was performed. A set of seven oncogenes was found to be downregulated in response to this I2C analogue.

Overall, the research outcome in this thesis points to the following highlights: 1) the quinolone and the naphthalene rings may serve as potential replacements for the indole moiety in the I2C-derived MmpL3 inhibitors, 2) substituting the 4 and/or 6 positions at the indole ring is favourable for the anti-TB activity, 3) extending the amide linker between the indole ring and the cycloaliphatic group in the I2C framework led to unfruitful anti-TB activities, 4) the I2C-appended adamantanol moiety is superior to the bare adamantane ring in terms of water solubility, while maintaining appreciable anti-TB activity, 5) while attaching an adamantane ring to INH, PZA, and CPF increases the lipophilicity of these drugs, the *in vitro* anti-TB activities of the resulting derivatives were disappointing, 6) the I2C skeleton possesses the potential to hit multiple targets and can be fine-tuned to elicit a particular biological activity, and 7) differential gene expression analysis represents a viable approach that can be employed to identify potential mechanisms of action of novel antitumour agents. These findings pave the way for possible future investigations aimed at determining the *in vivo* anti-TB and antitumour activities of the most potent compounds that were pinpointed throughout this thesis.

## 8.2. Future Directions

Although several promising research avenues were unfolded in the present work, some important facets could not be investigated due to time constraints. First, like most of the antibiotics in the market, all the tested compounds in this work were evaluated against actively replicating *M. tb*. Therefore, it would be interesting to develop novel anti-TB agents effective against the non- or slowly replicating persistent mycobacteria. These recalcitrant mycobacterial subpopulations prevail during latent TB infections and are phenotypically tolerant towards antibiotics, accounting for the long-drawn-out treatment course of TB. One way to target these mycobacterial persisters is to modulate the phosphorylation/dephosphorylation-based immune evasion mechanisms of *M. tb* which could extricate the macrophages from the *M. tb* counterforces (Chapter 2). Indeed, targeting *M. tb*-secreted kinases and phosphatases using chemical probes, would result in unbridled macrophages with restored inherent killing qualities. This underexploited approach represents a new

horizon for the development of novel anti-TB agents effective against the quiescent mycobacteria.

Interestingly, the skeleton of AX20017 (**Figure 8.1**) bears some outward resemblance to the multi-target directed ligand *N*-adamantyl I2C molecule (NAI2C, **Figure 8.1**). AX20017 is a potent protein kinase G (PknG) inhibitor that killed the *M. tb* cells residing inside the macrophage while displaying no activity against mycobacterial growth *in vitro* (Chapter 2). In contrast, NAI2C exhibited potent anti-TB activity against *M. tb* H37Rv strain *in vitro* (MIC = 0.68  $\mu$ M) through blocking the flippase activity of MmpL3 that translocates the MAs precursor from cytoplasm to the periplasm. It would therefore be intriguing to investigate the anti-TB activity of some hybrid molecules possessing structural features of both AX20017 and NAI2C. In this respect, some examples of future explorations are summarised in **Figure 8.1** which involve the following: 1) replacing the 4,5,6,7-tetrahydrobenzo[*b*]thiophene moiety of AX20017 with an indole ring while maintaining the rest of AX20017 functional groups (**S1**), 2) integrating the whole I2C architecture (with unreversed amide-linked cyclopropyl at position 2) with the amide group at position 3 (**S2**), 3) shifting the amide moiety from position 3 of the indole ring to position 4 (**S3,4**), and 4) replacing the amide group at position 3 or 4 of the indole ring with a carbohydrazide moiety (**S1-4**). These newly designed derivatives are proposed to be evaluated for their anti-TB activities both *in vitro* and intramacrophage. Indeed, depending on the activity profiles of these new analogues, further studies may be initiated to determine whether they target PknG, MmpL3, both PknG and MmpL3, or a totally different protein.

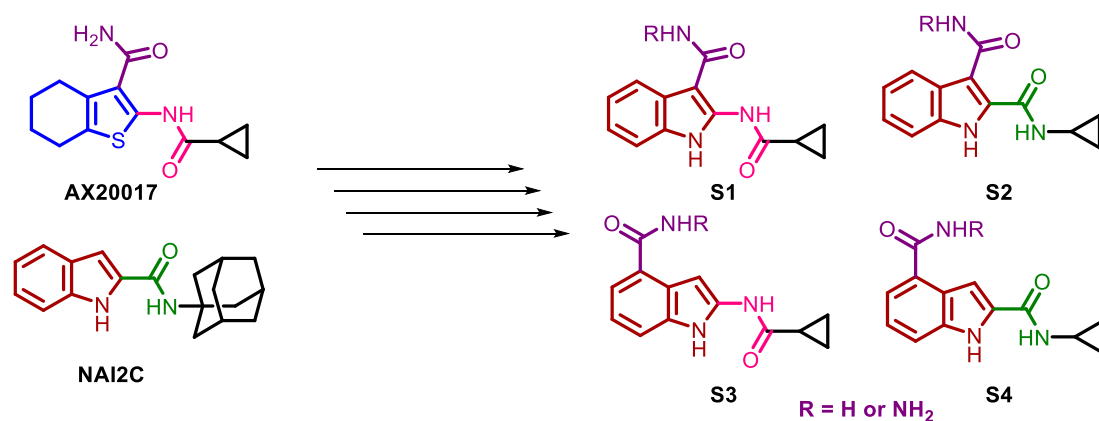


**Figure 8.1.** Design of new potential anti-TB analogues via conjugating fragments from AX20017 and NAI2C.



Regarding the promising antitumour derivatives (Chapters 6 and 7), the likelihood of blood brain barrier (BBB) penetration should be experimentally examined. Additionally, in the future design strategies of antitumour agents, the central nervous system multiparameter optimisation (CNS MPO) tool will be taken into consideration to increase the chances of compound's nomination for clinical development. One of the main criteria required to attain desirable CNS MPO scores is that the ClogP of the designed molecule should be ideally  $\leq 3$ . Since lowering the ClogP value generally compromises the anti-TB efficacy of the I2C framework (Chapter 4), implementing the CNS MPO paradigm will help tailor unique I2C drug candidates with selective antitumour activities. Further functional studies at CB receptors will be also conducted on several I2C analogues (synthesised herein in addition to others that will be prepared in the future). In this respect, since several I2C derivatives identified in this thesis structurally resemble the I2C-based positive allosteric modulator (PAM) of CB<sub>1</sub>R Org27569 (Chapter 7), the allosteric modulation potential of our homologous I2Cs at both CB<sub>1</sub>R and CB<sub>2</sub>R will be scrutinised.

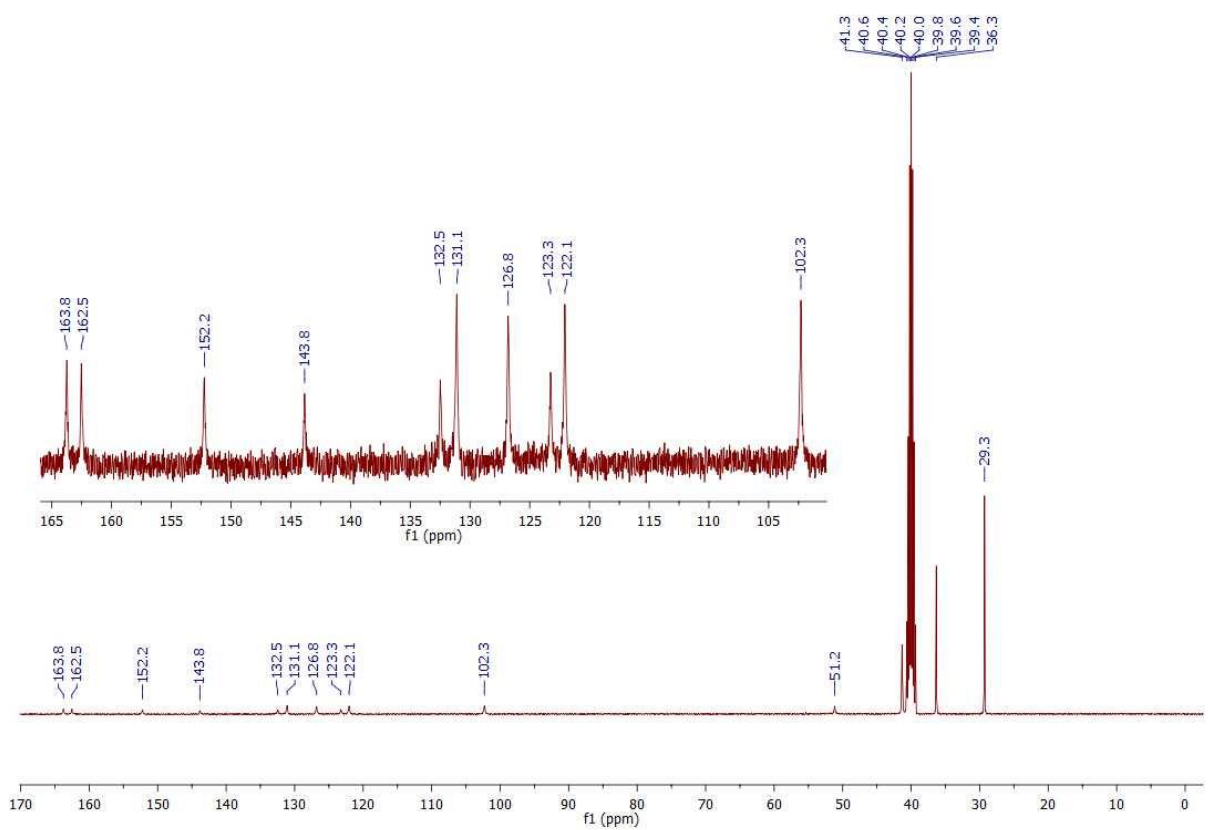
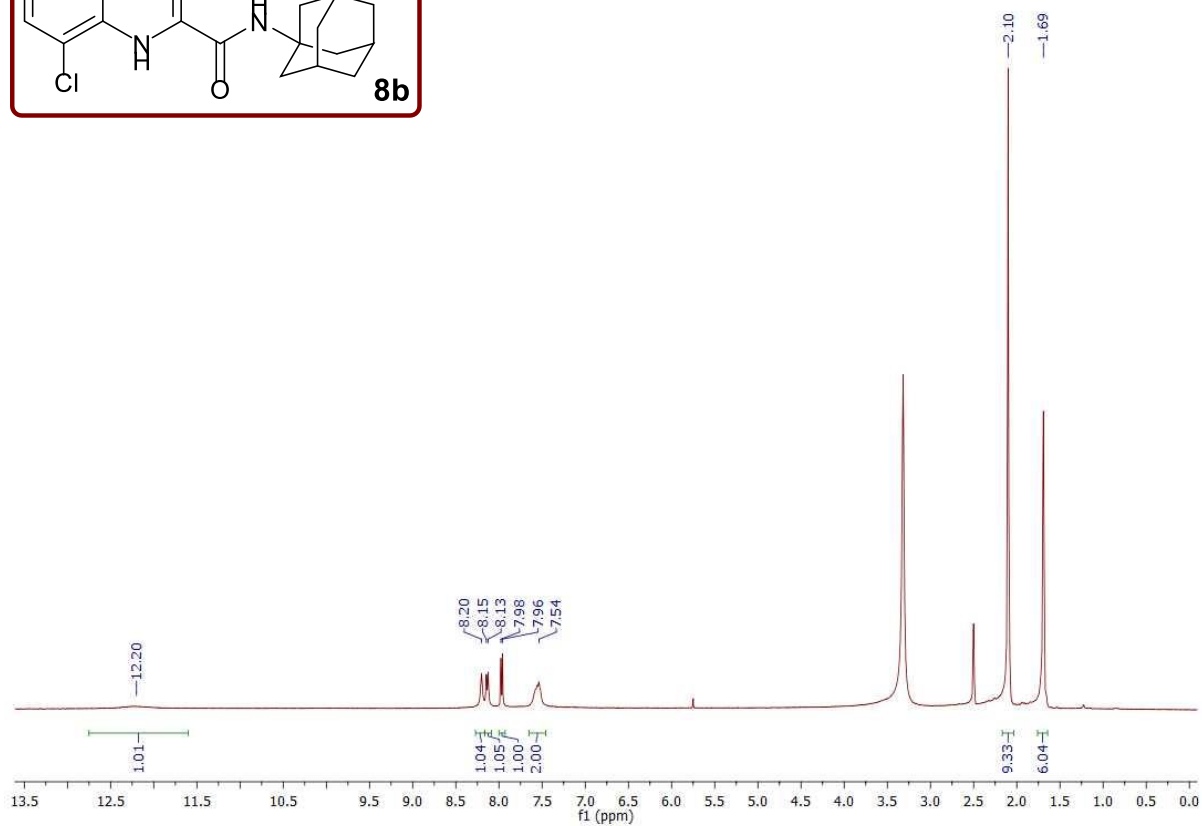
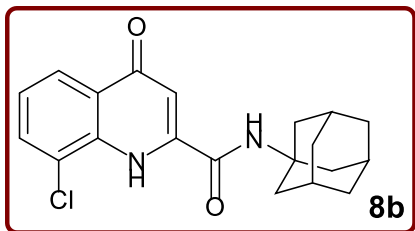
On the other hand, while *in silico* predictions of the drug-like properties were performed on the top potent compounds identified herein, experimental determination of such parameters would paint a more accurate picture of their drug-likeness. In this regard, the most active analogues highlighted in the five research articles incorporated in this thesis merit further investigations into their pharmacokinetic (PK) properties, including absorption, distribution, metabolism, and excretion (ADME). In addition, more toxicological assessments should be undertaken to ensure the safety of these compounds towards normal human cells, including cytochrome P450 (CYP) inhibition studies, cardiotoxicity (hERG channel inhibition), hepatotoxicity, and genotoxicity. The most promising analogues that show acceptable ADME/PK and toxicology profiles can then be subjected to *in vivo* anti-TB and/or antitumour screenings. If successfully developed, these preclinical candidates may amount to new arsenals that could be utilised in combating DR-TB and grade IV brain cancers. Indeed, the provision of such potent, safe and orally bioavailable molecules could be invaluable in rejuvenating the TB and cancer drug discovery field.

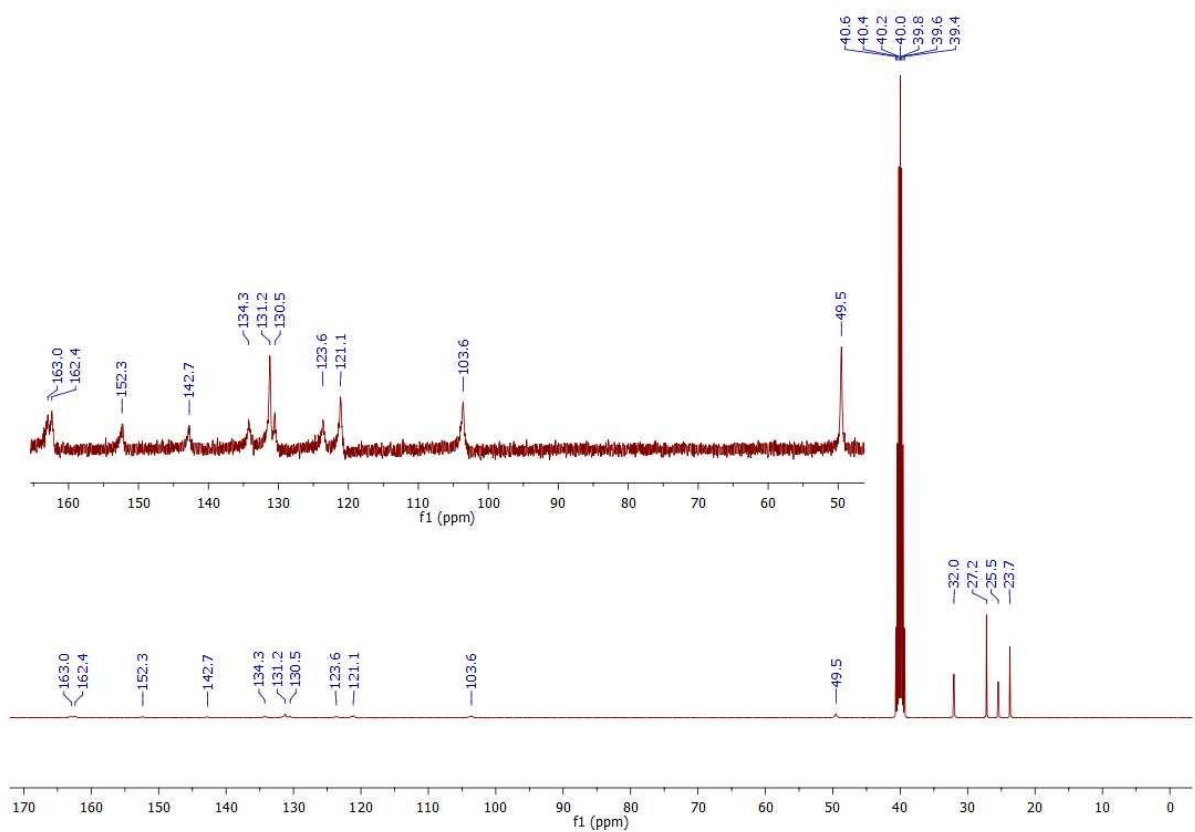
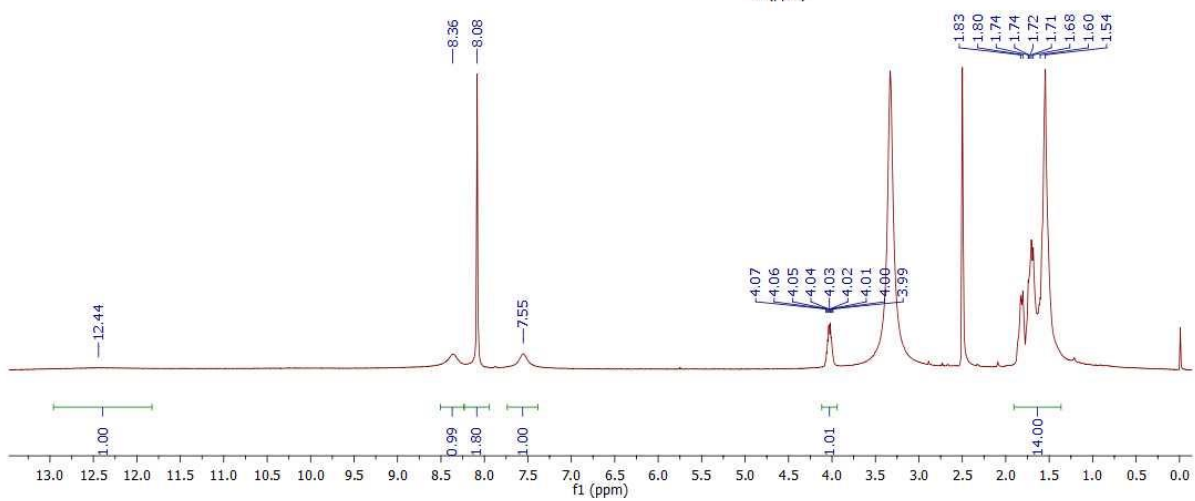
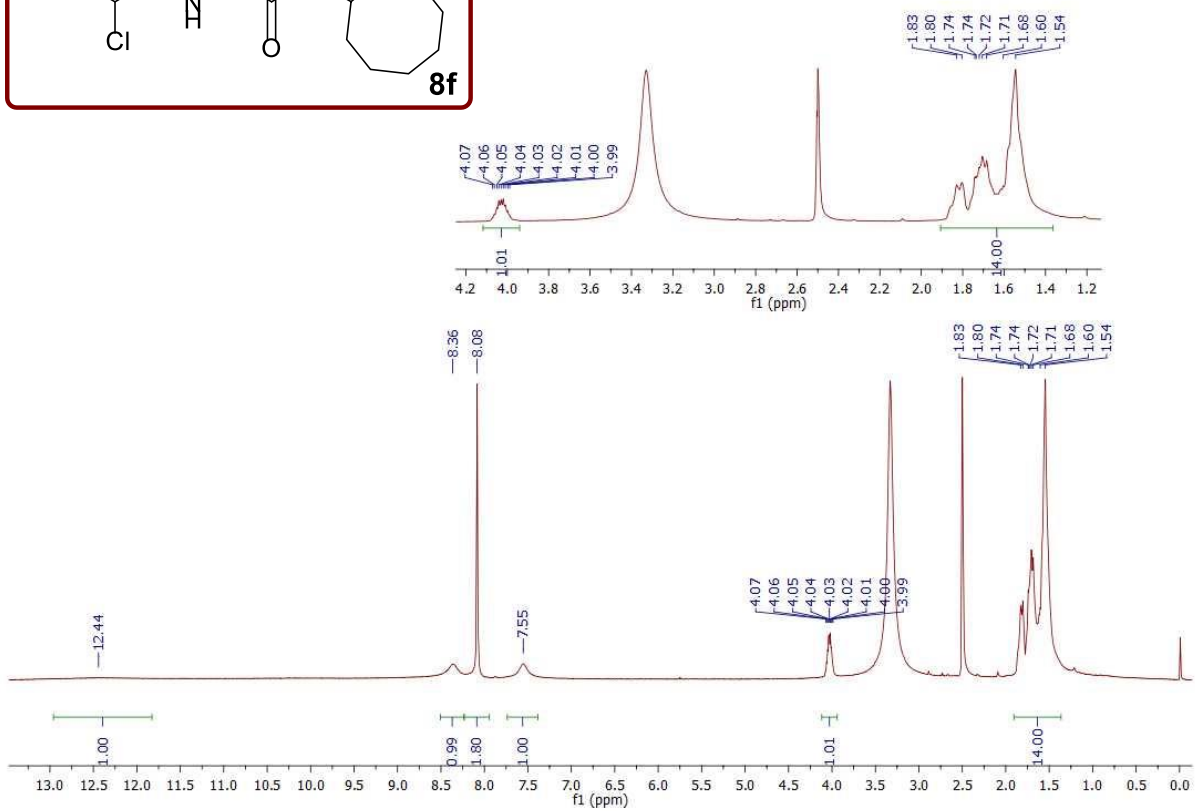
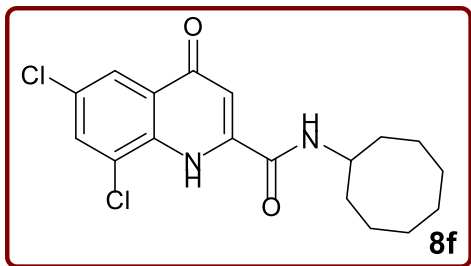
# Appendices

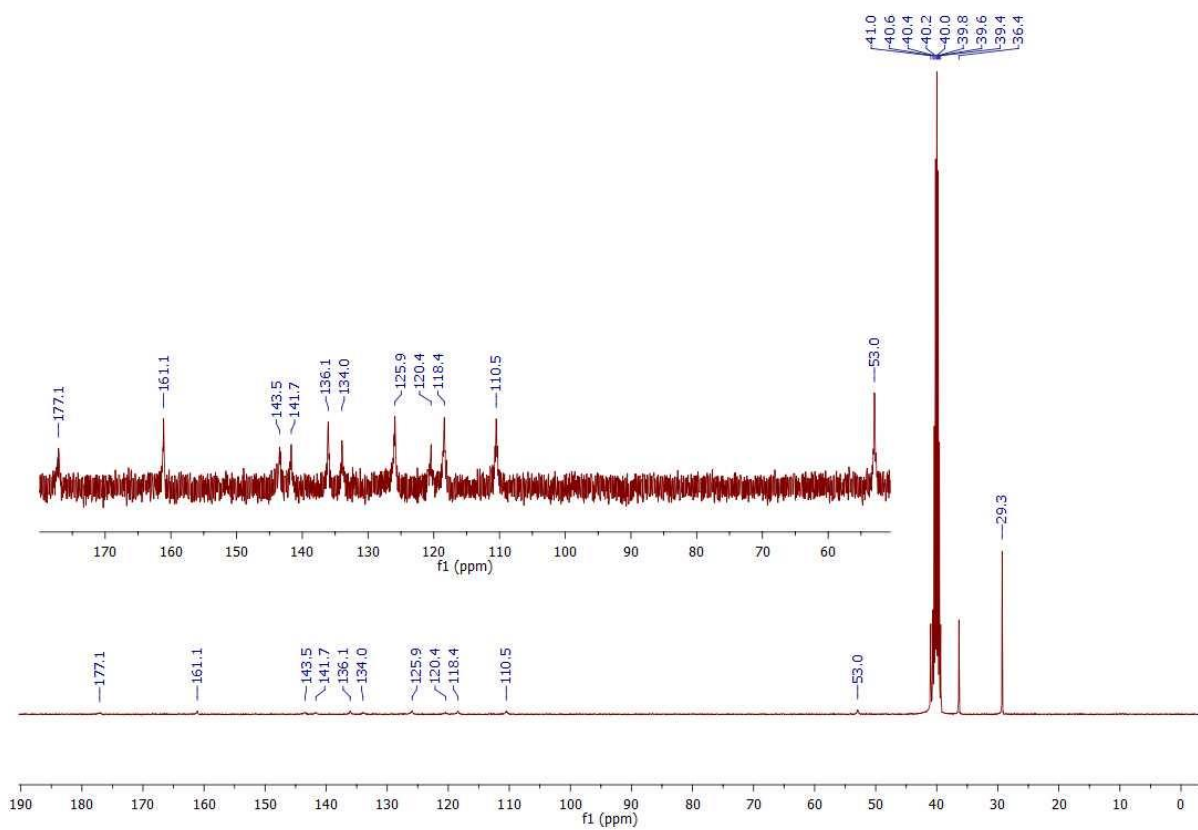
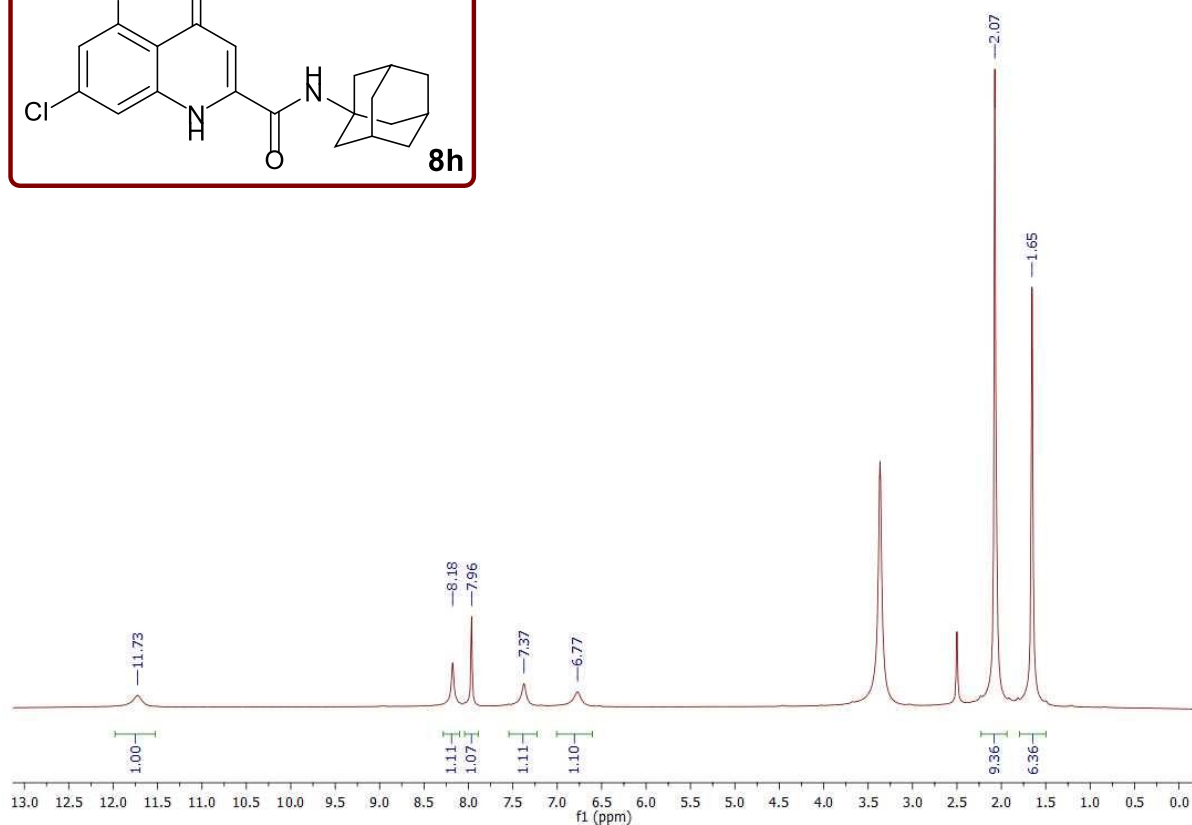
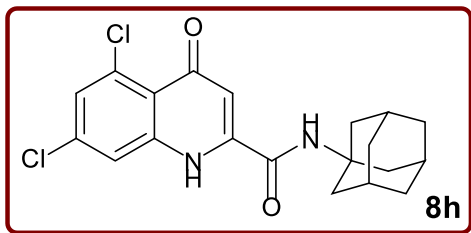
# **Appendix I**

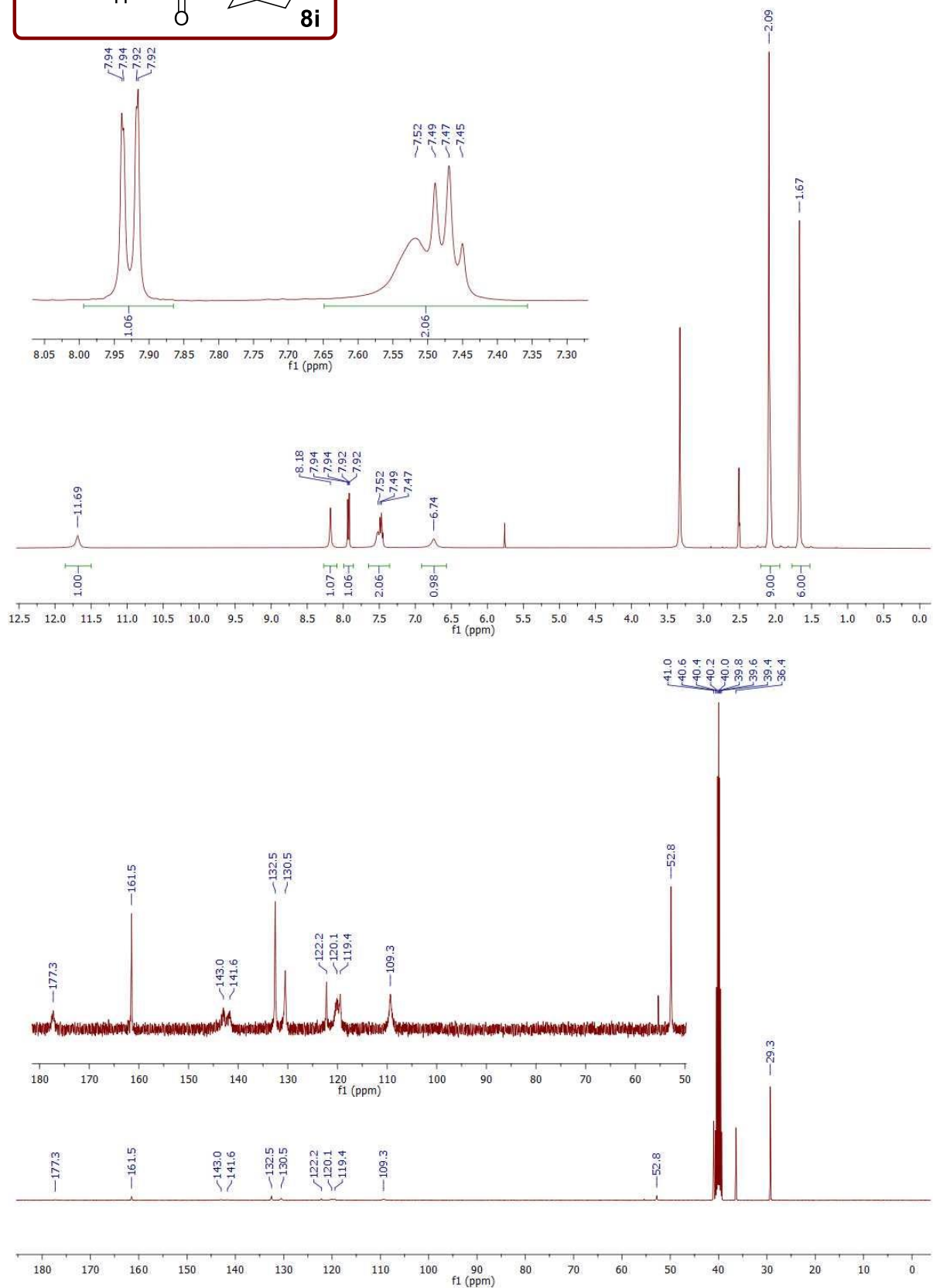
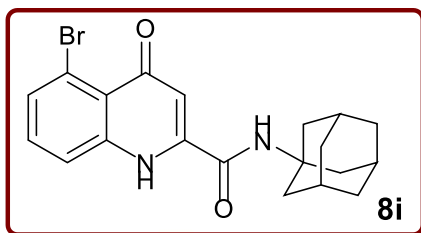
## **Supplementary Information**

**Supplementary Information – Chapter 3**  
**(RSC Advances 2020 Article)**

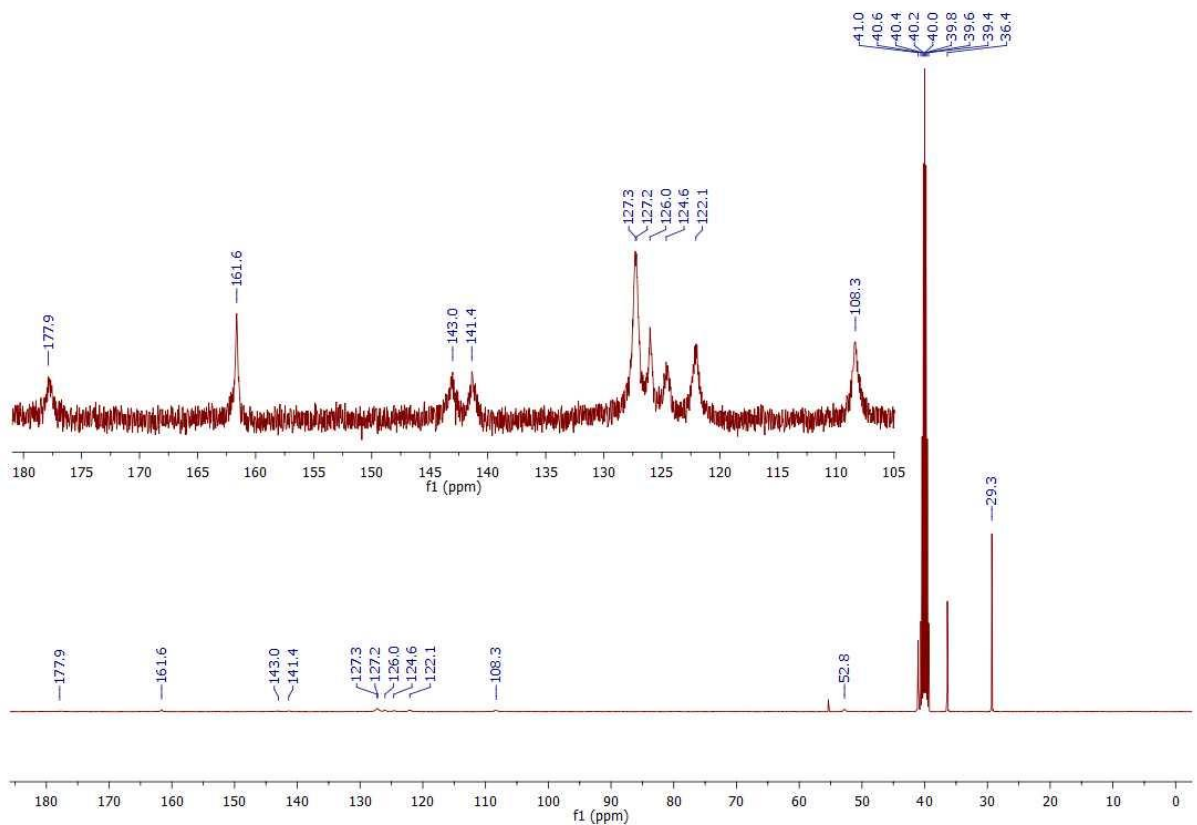
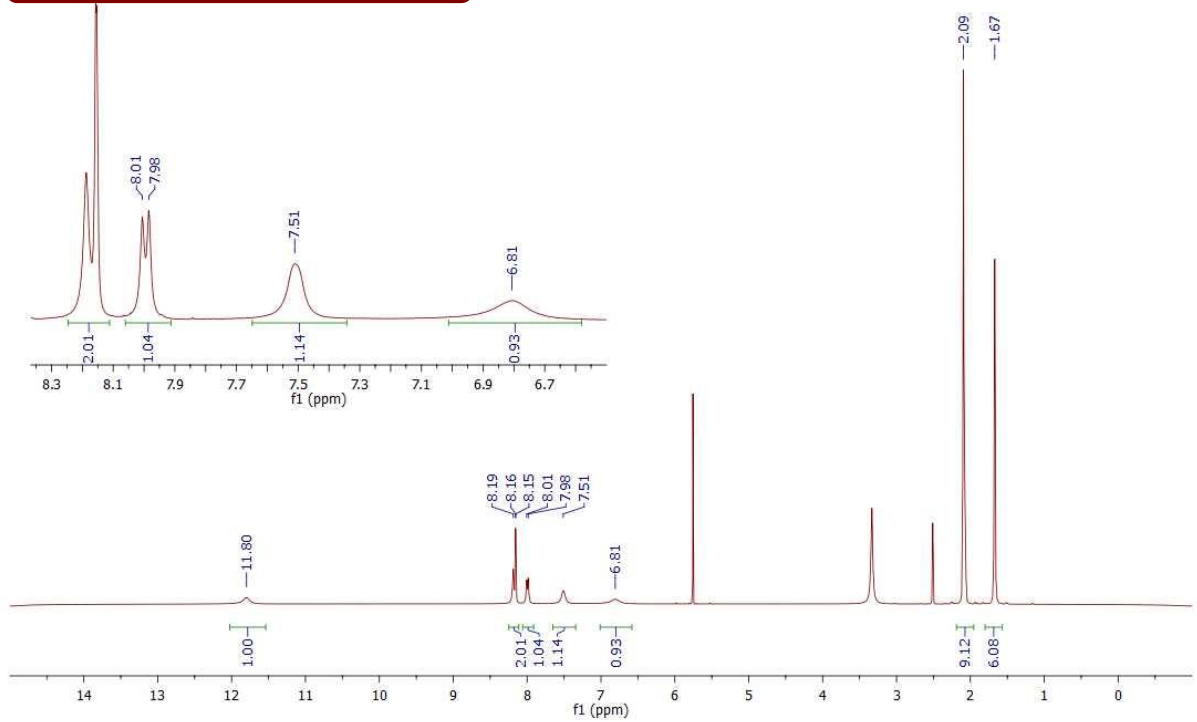
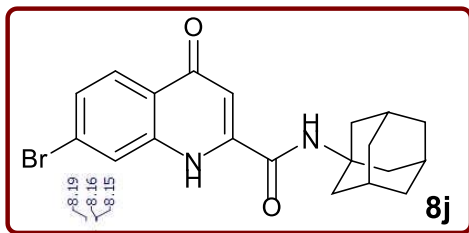


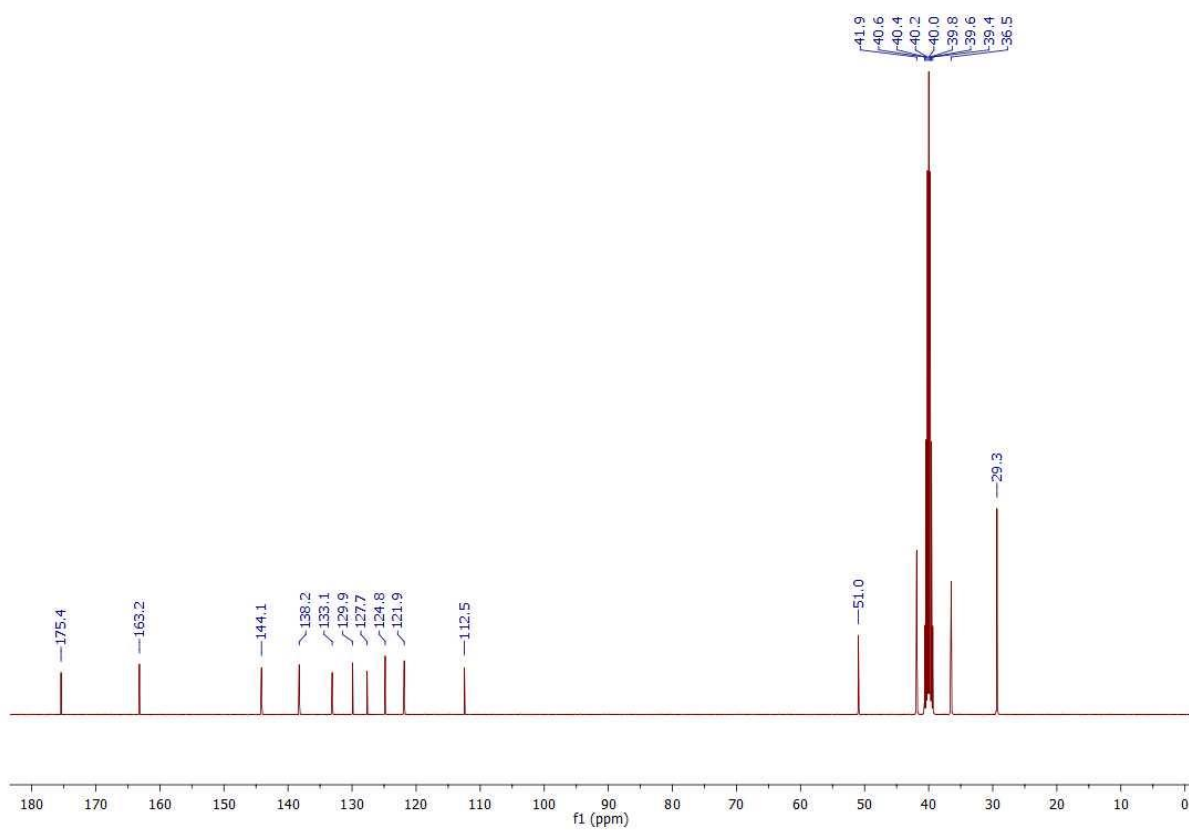
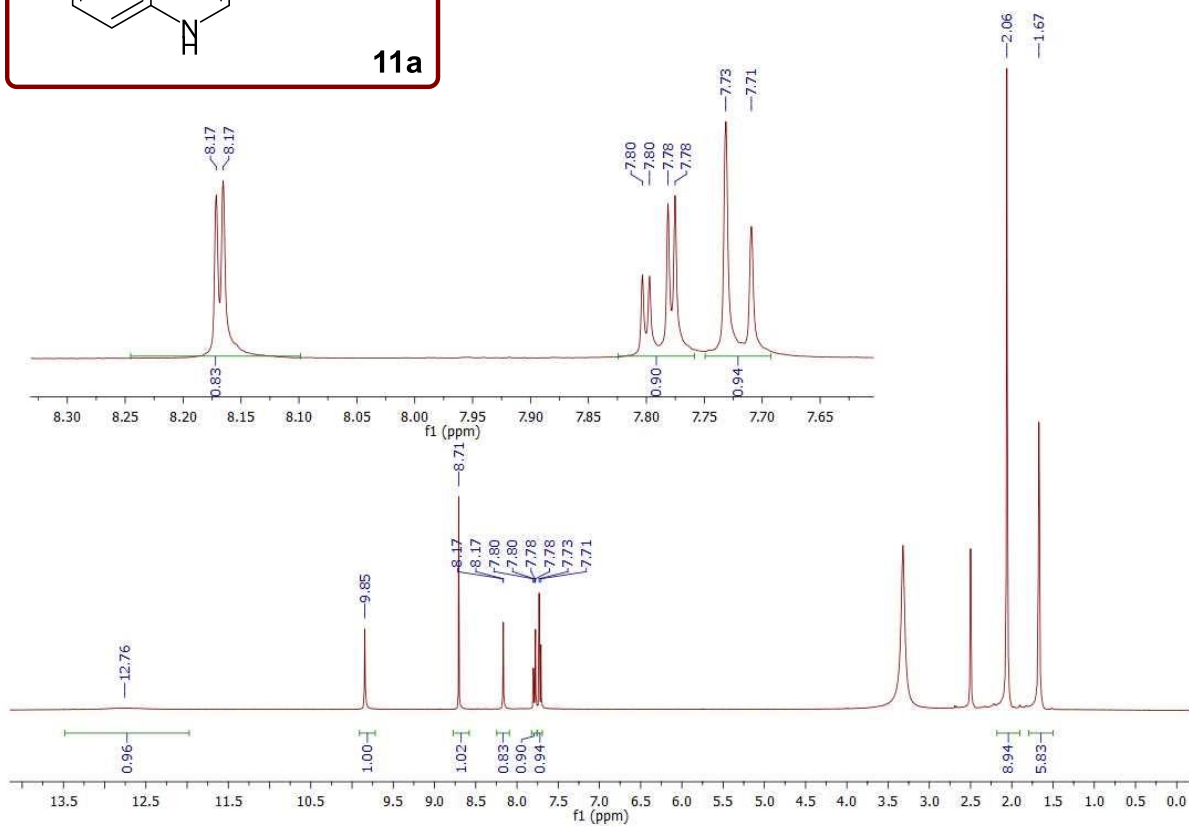
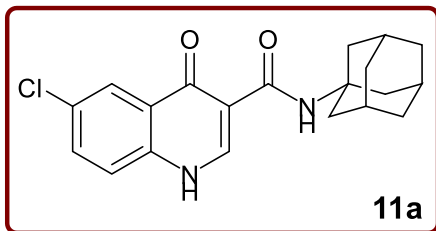


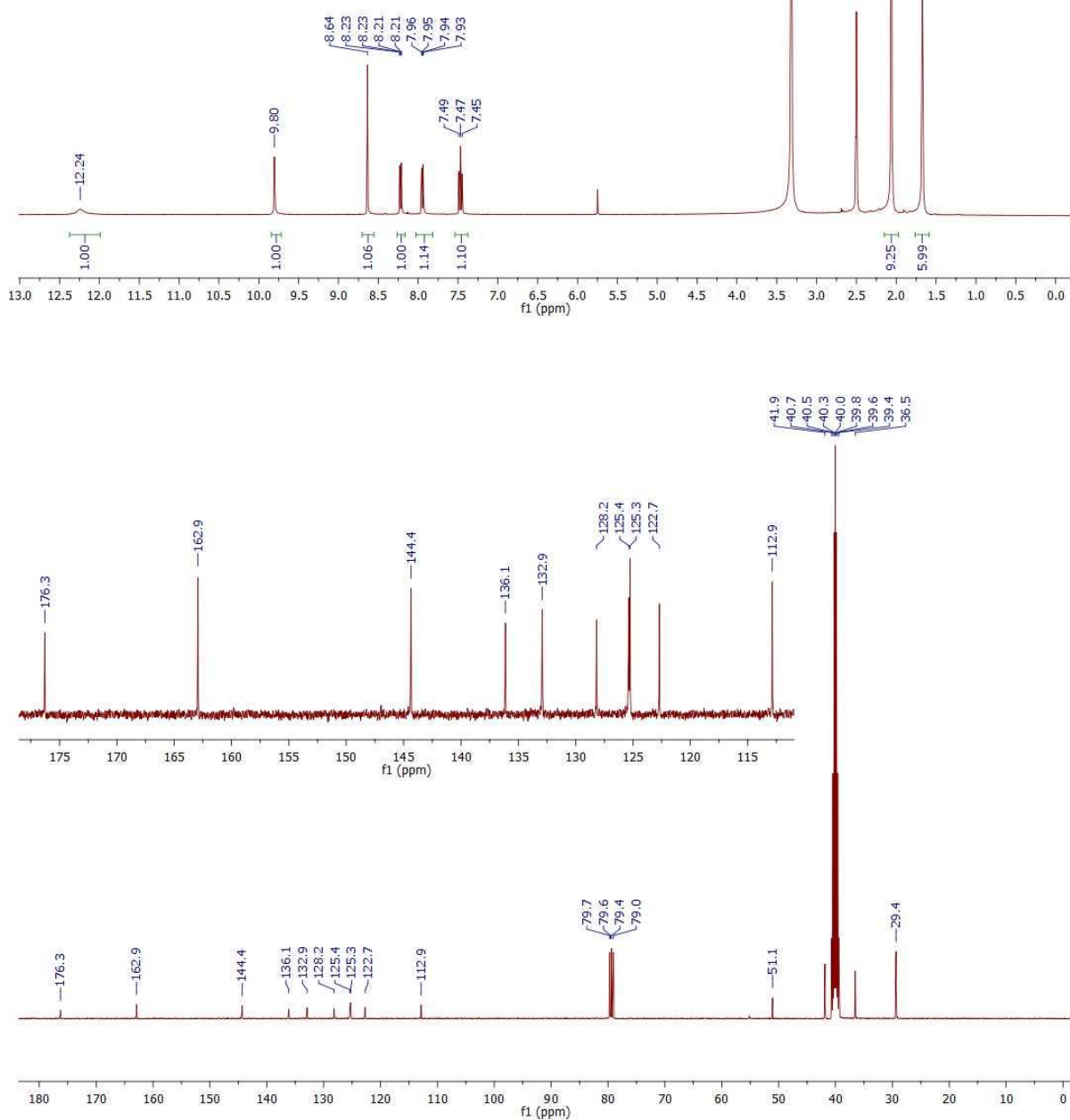
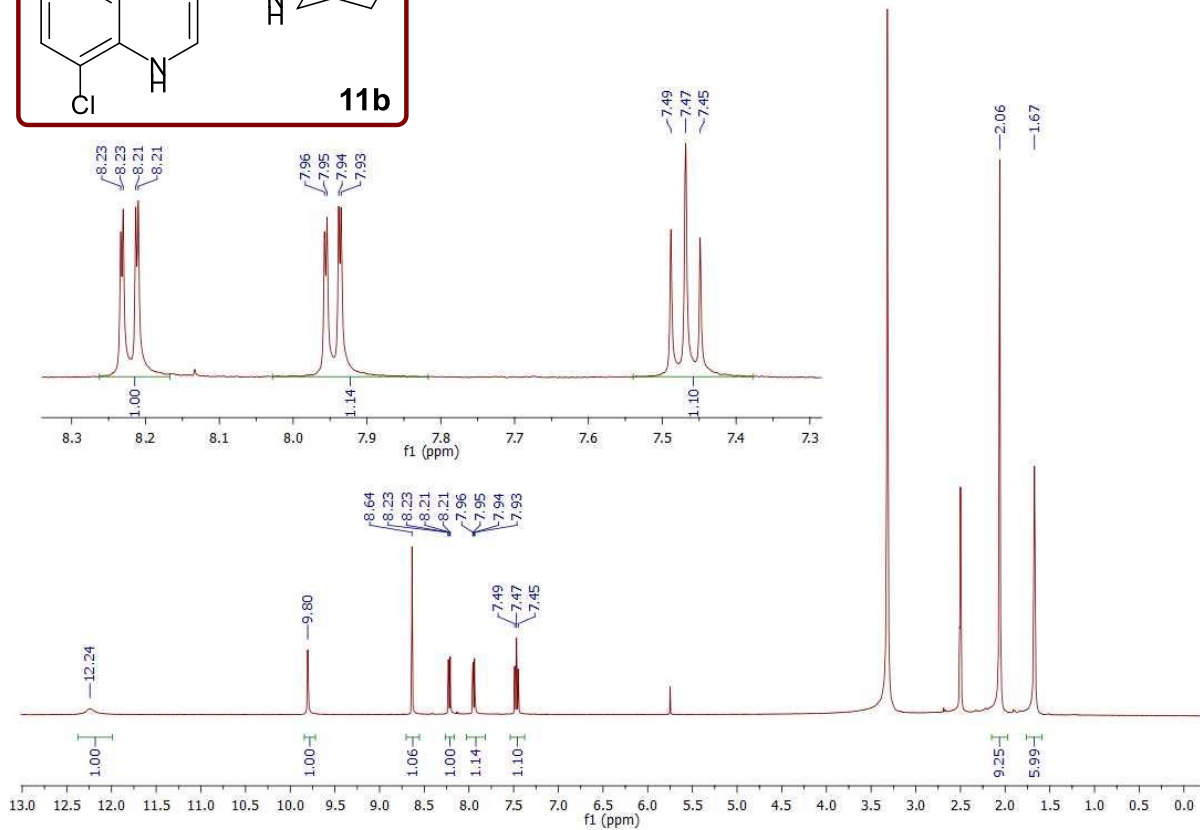
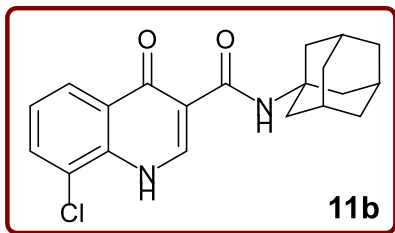


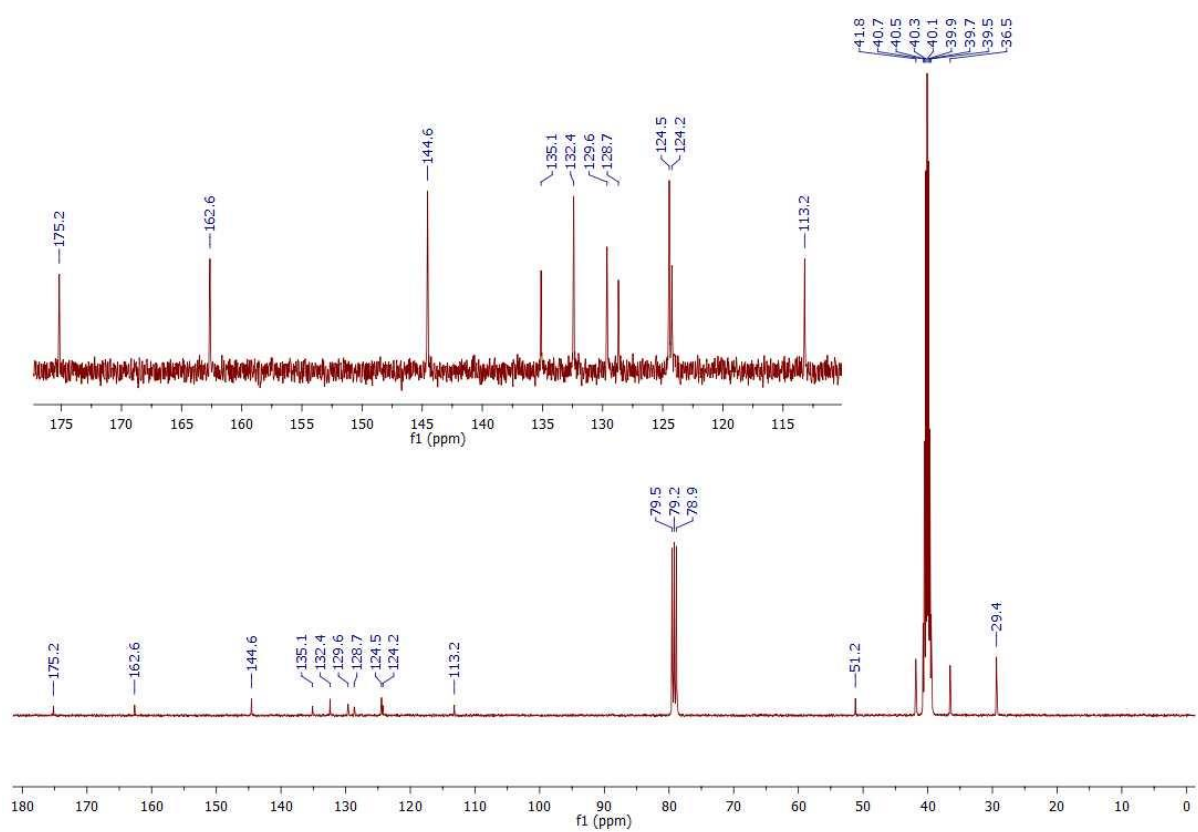
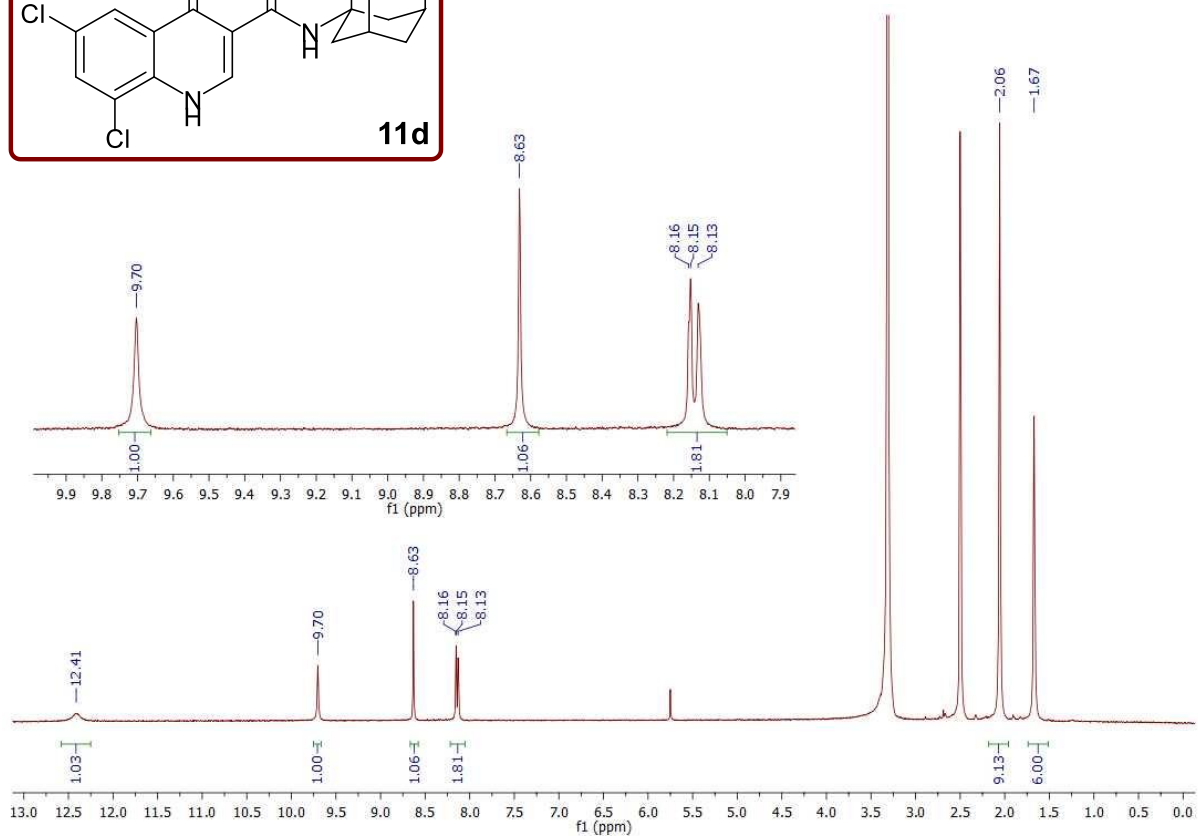
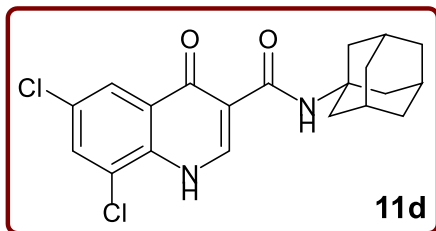


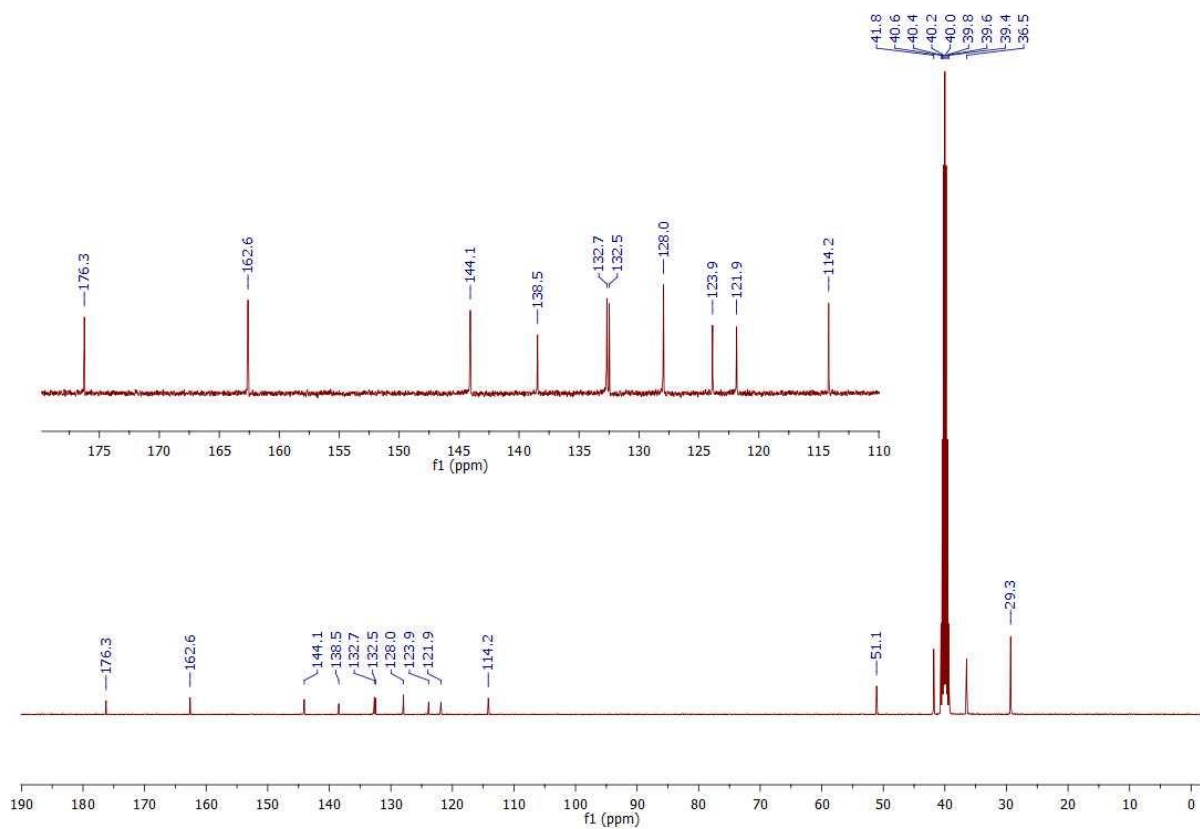
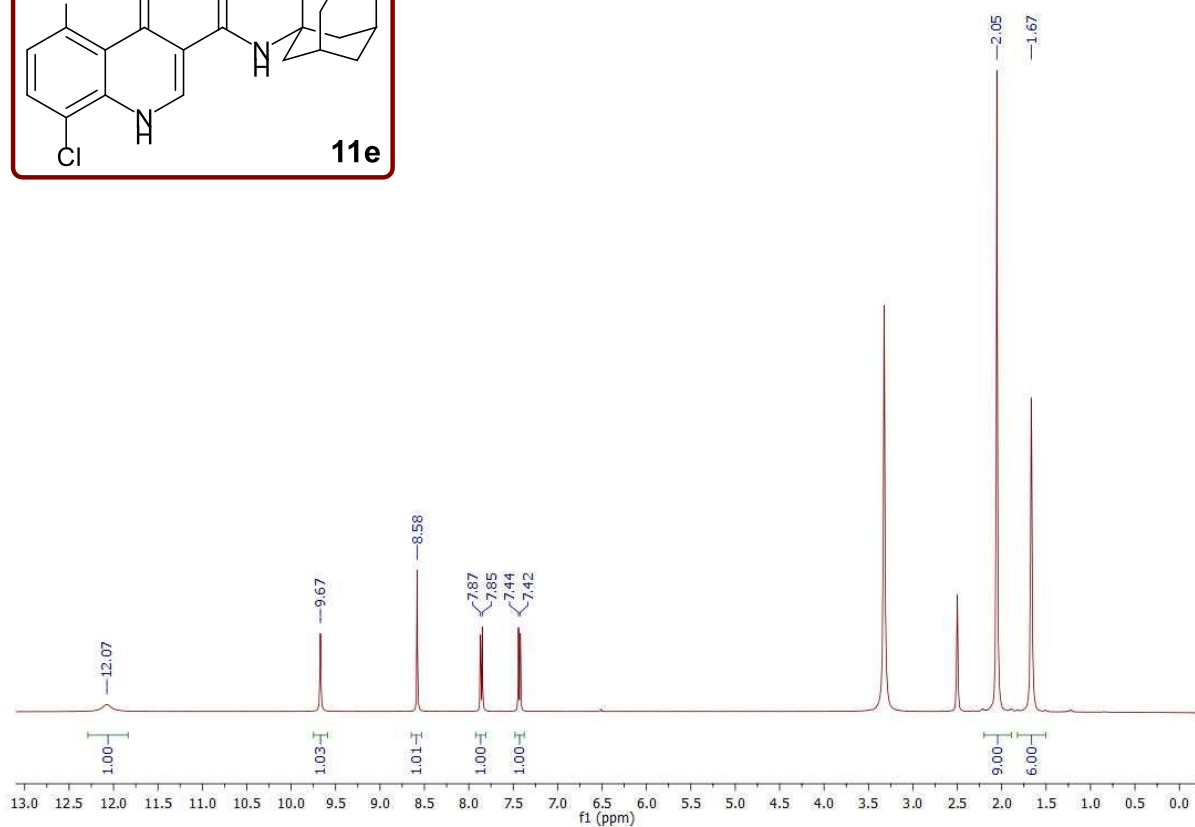
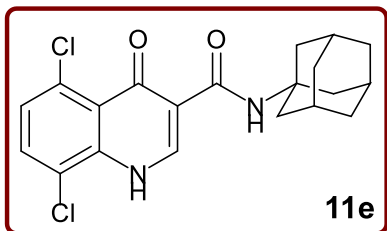


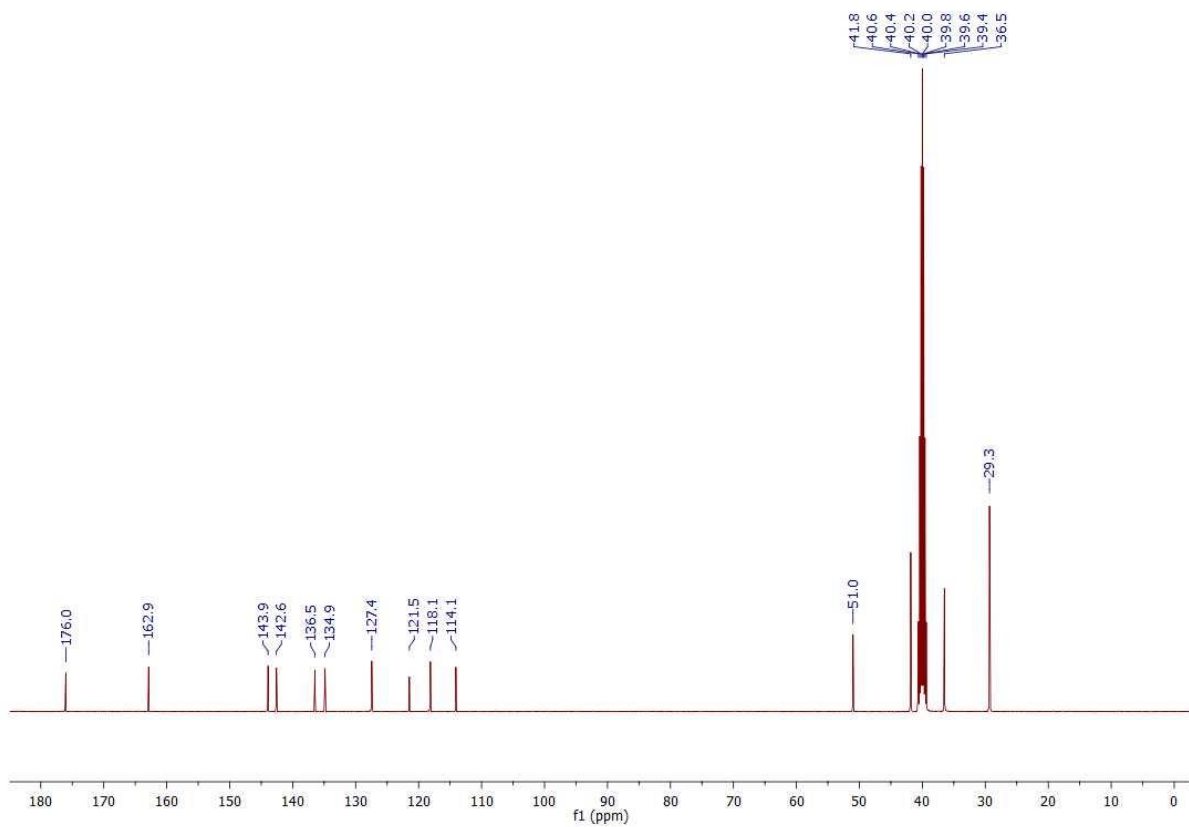
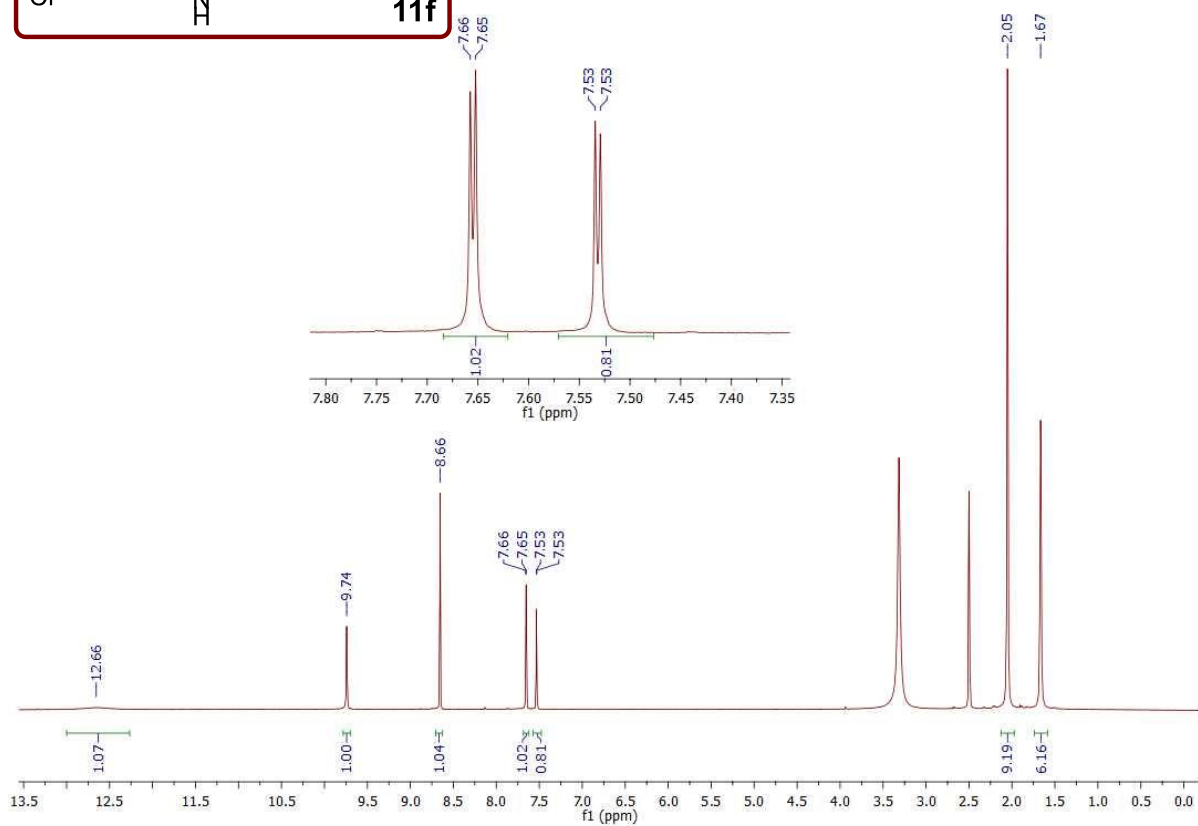
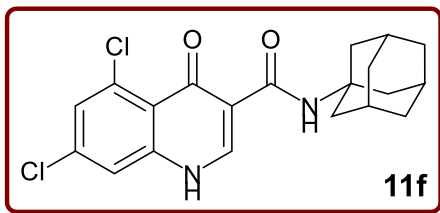


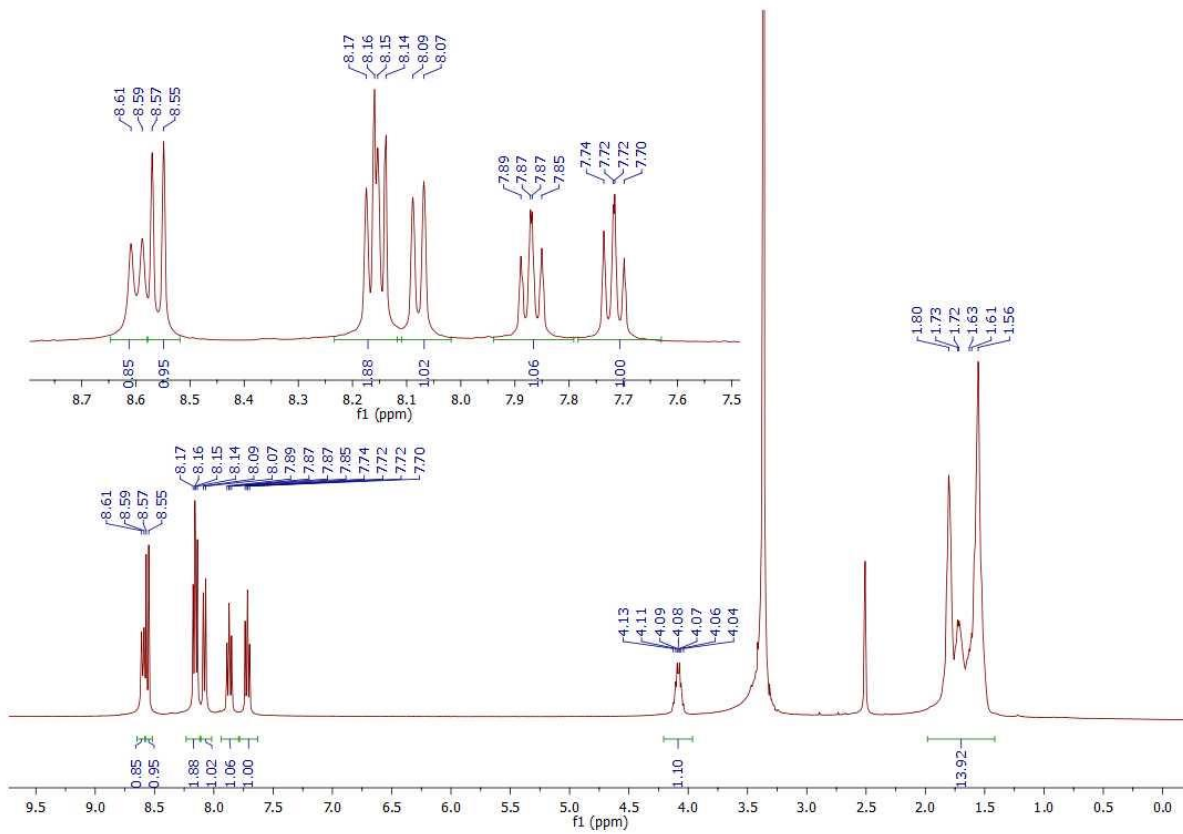
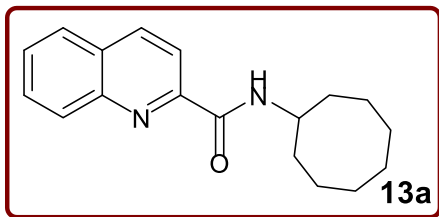


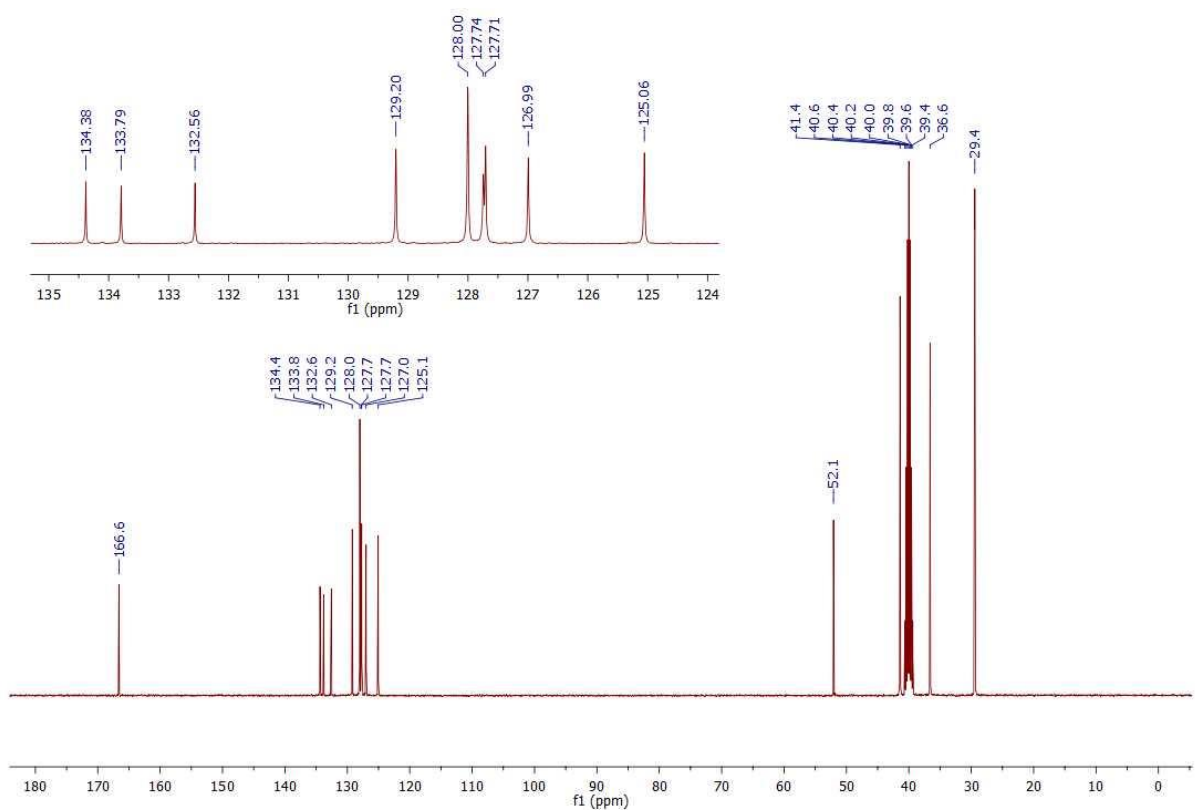
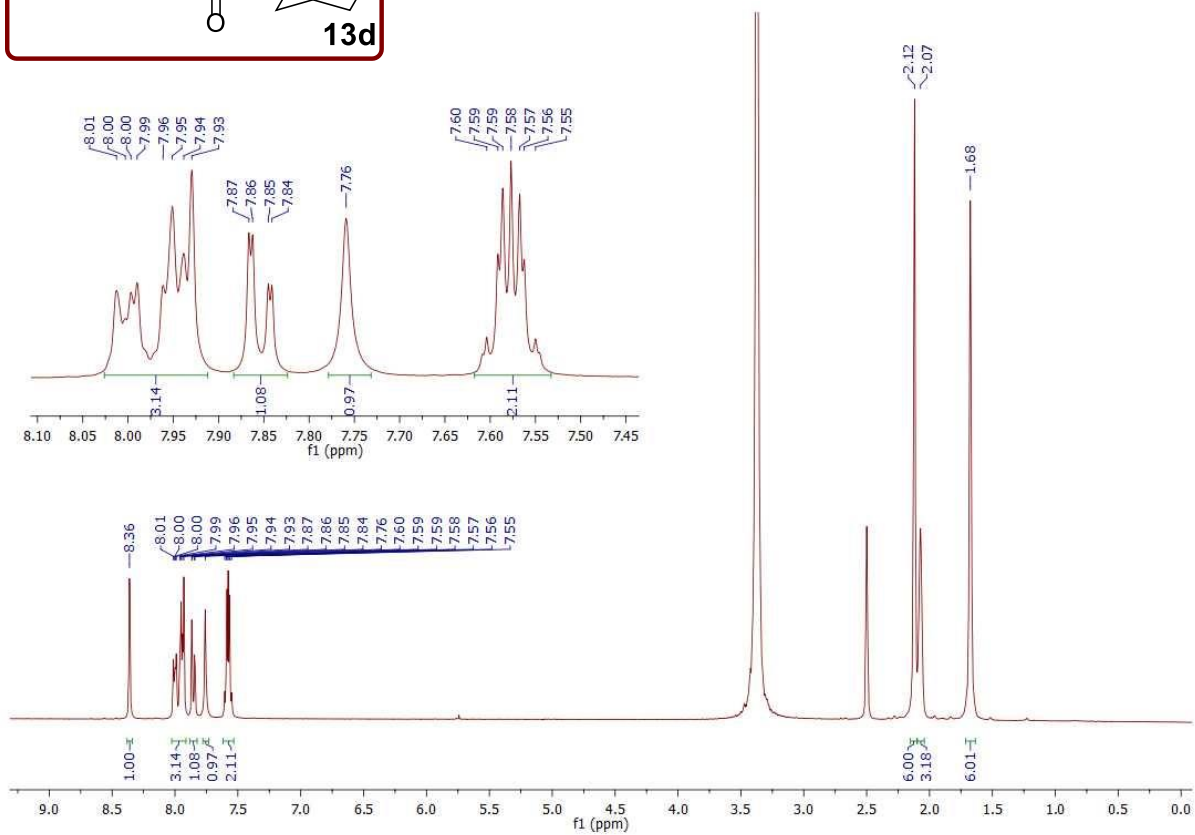
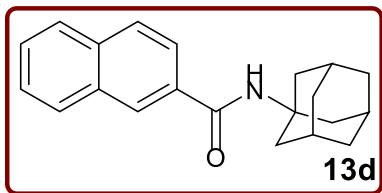




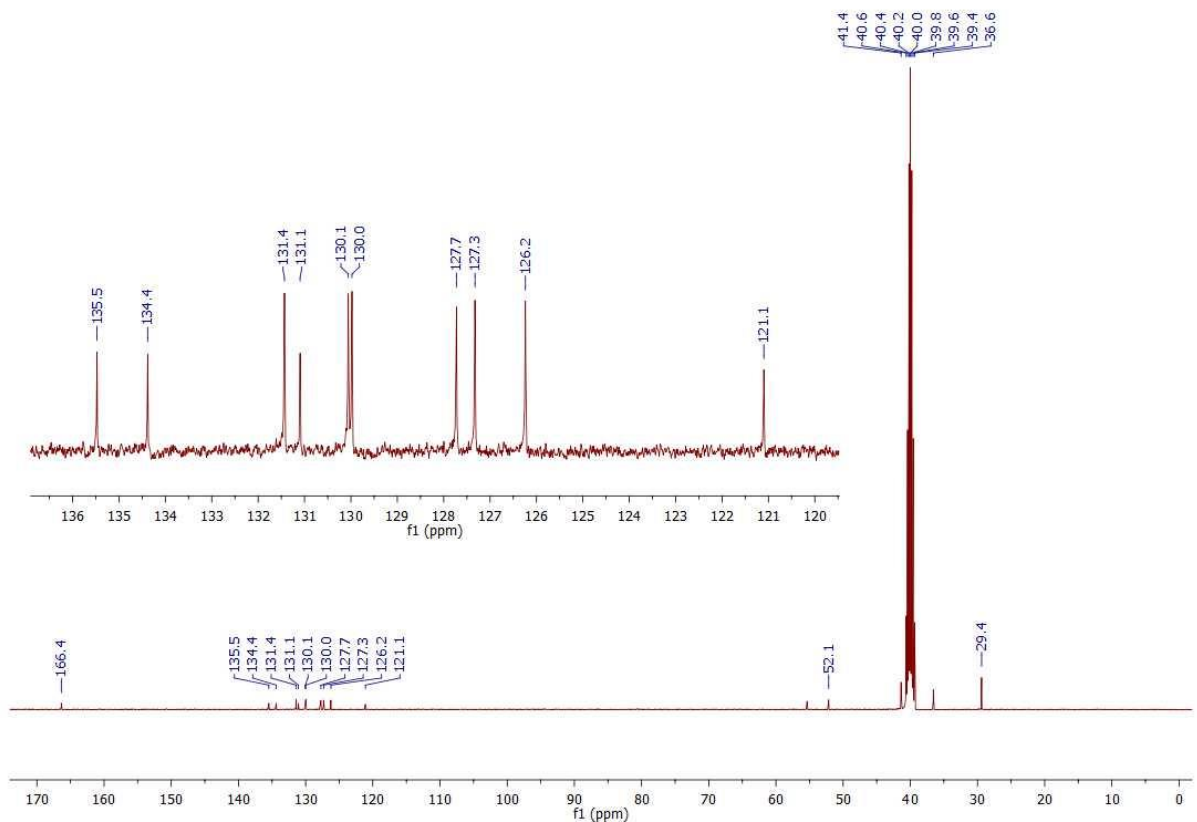
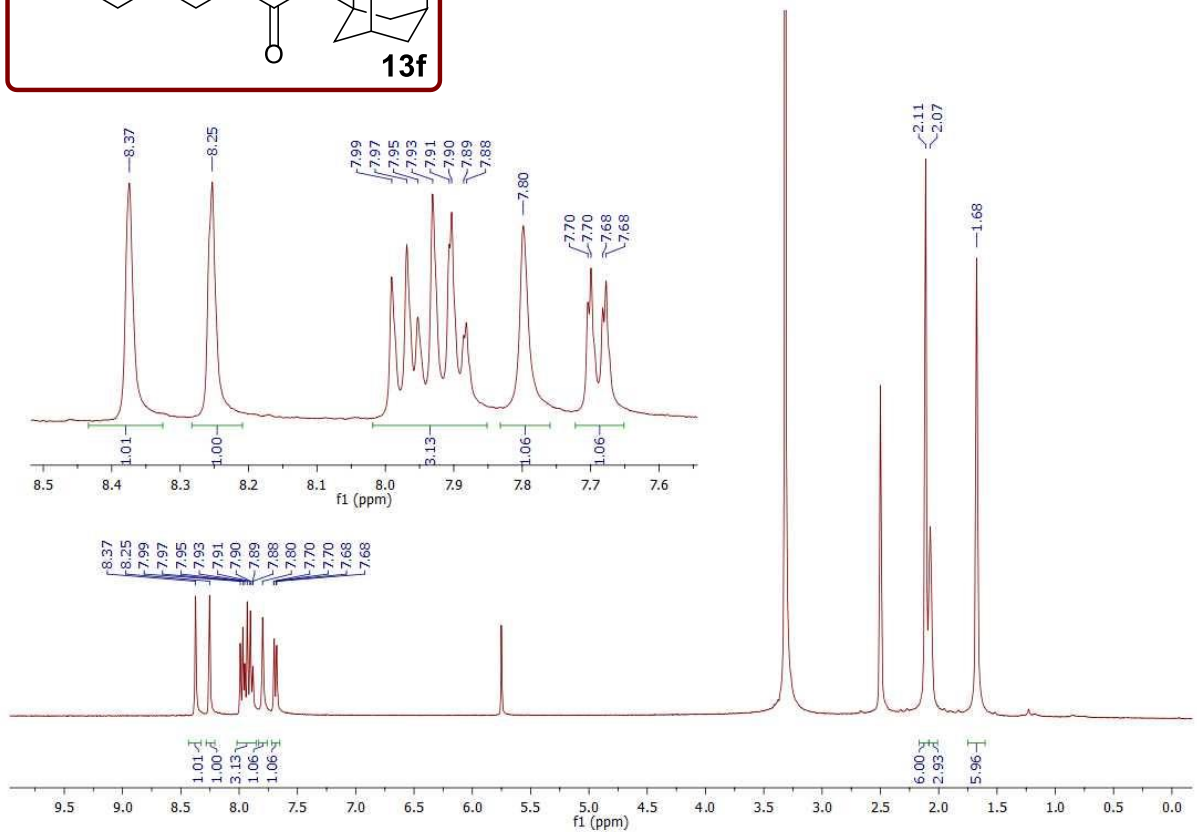
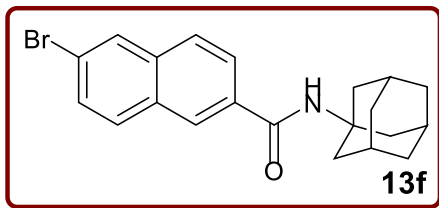


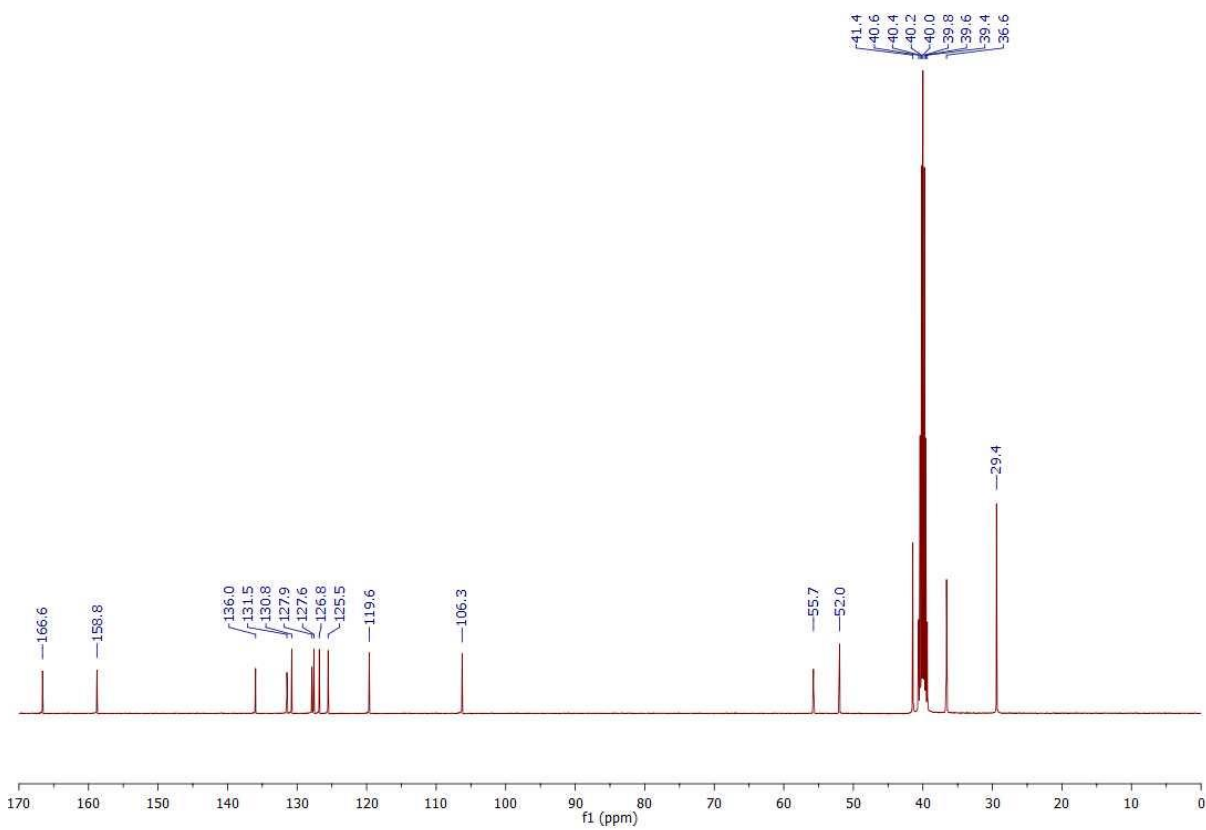
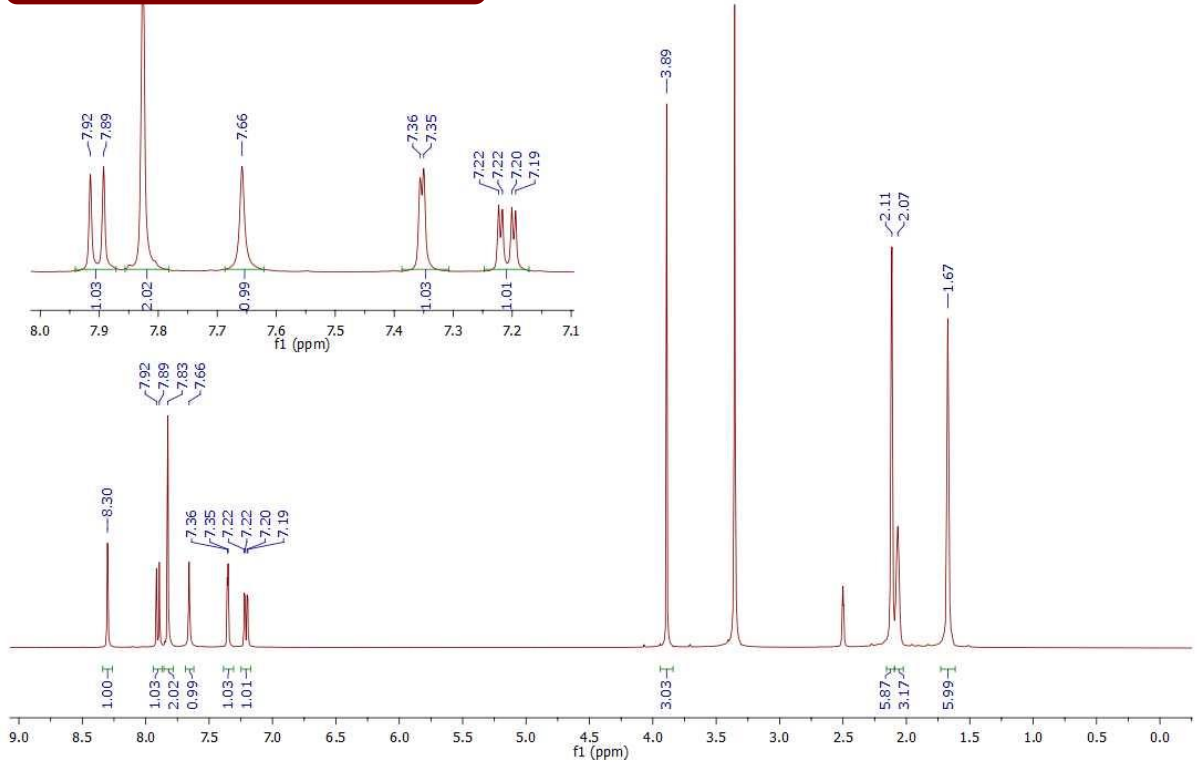
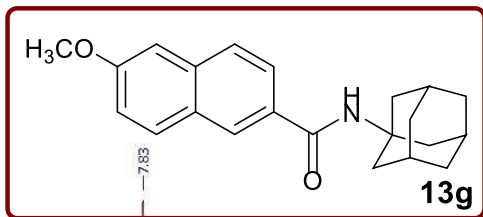


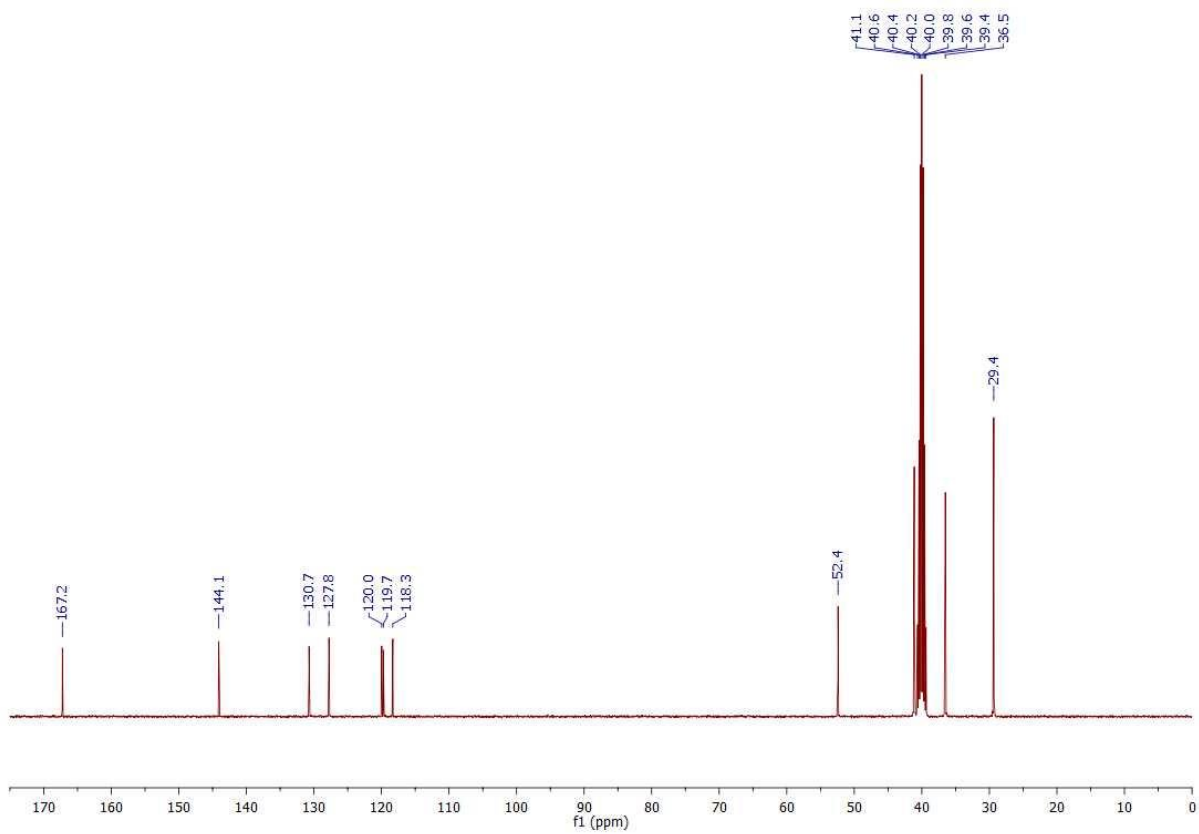
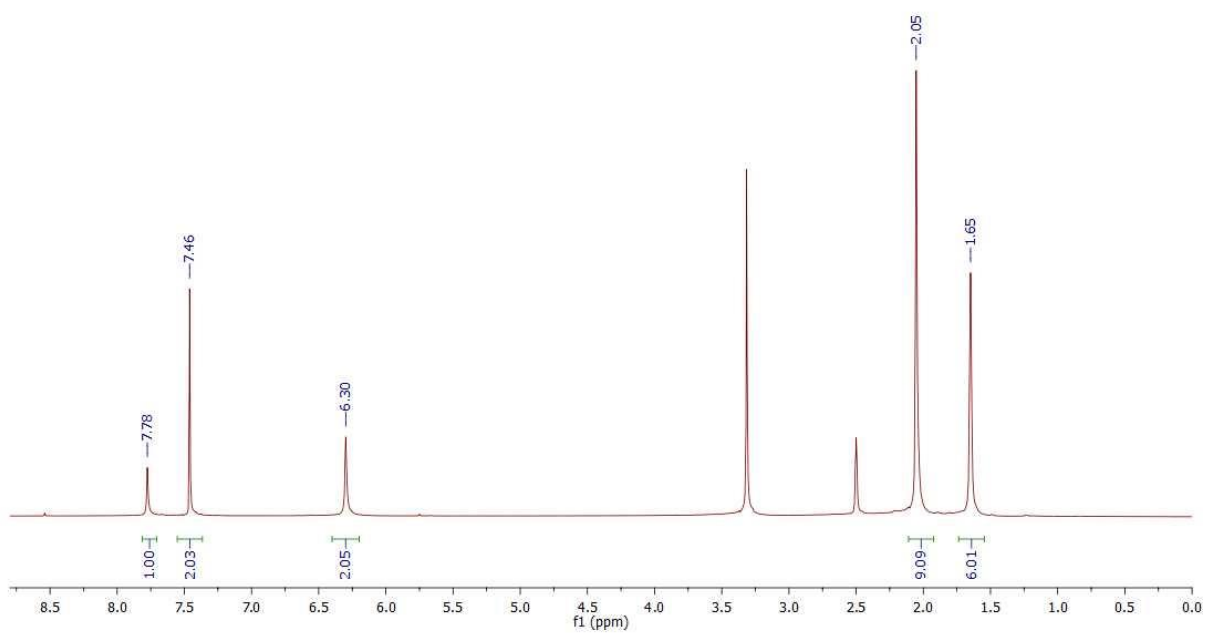
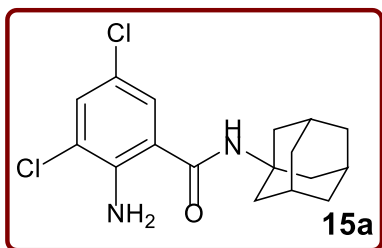


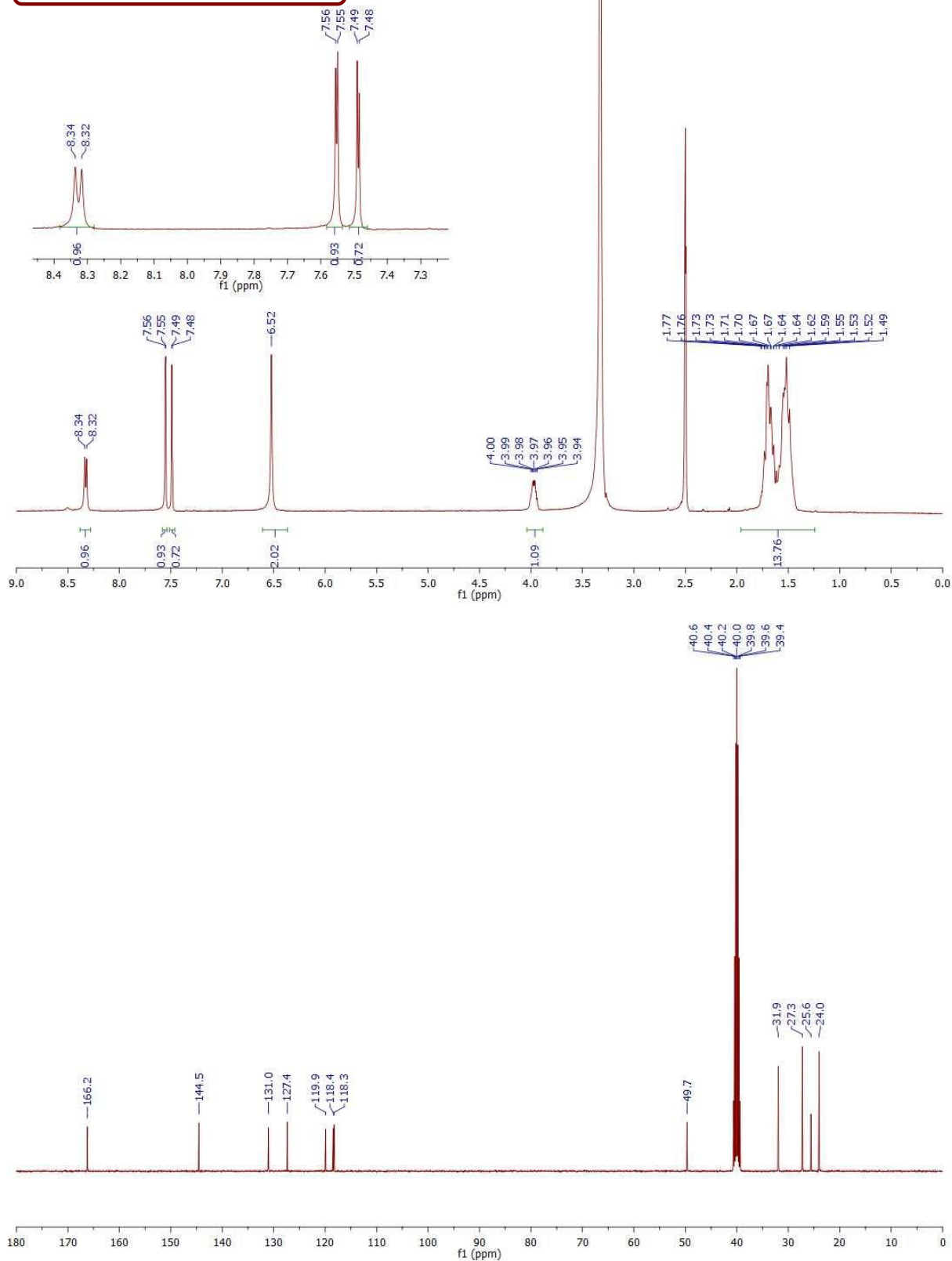
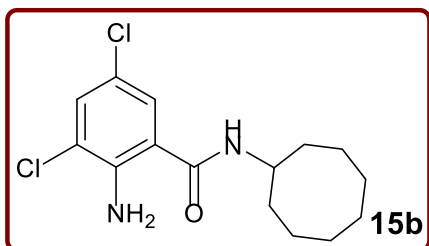


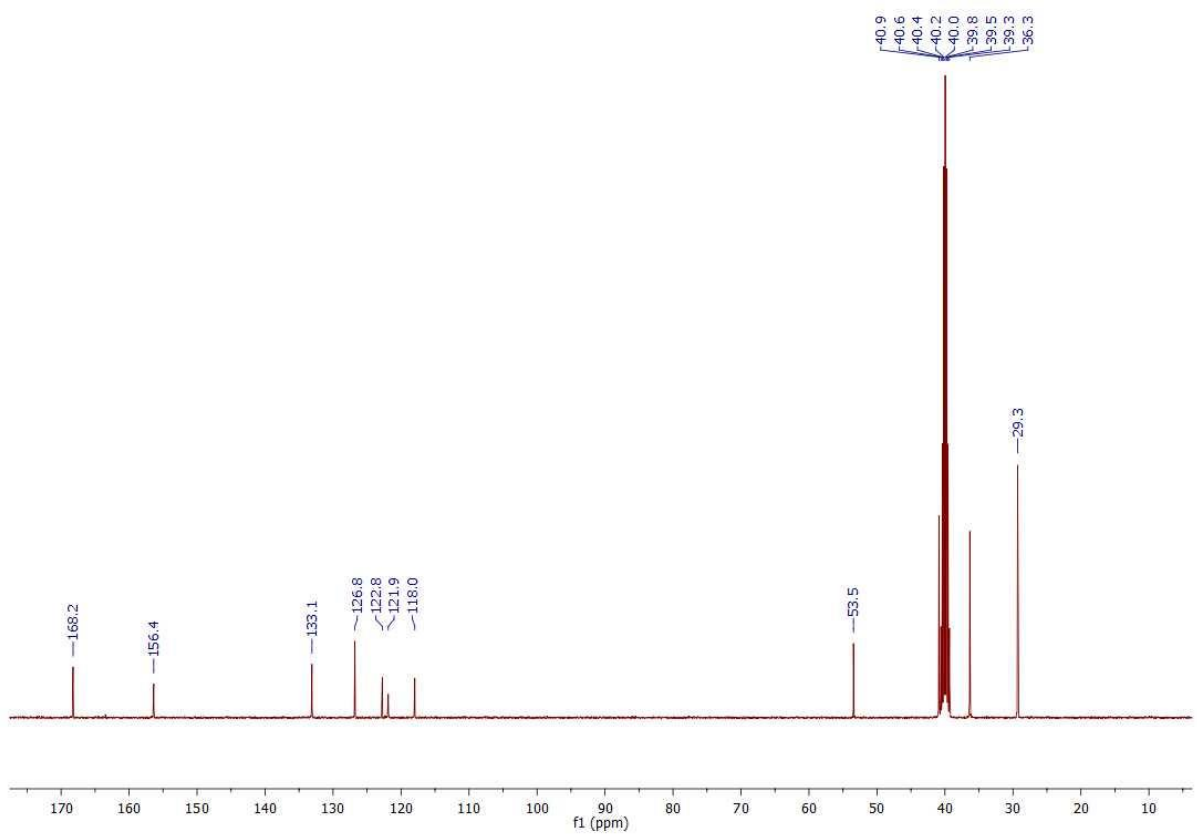
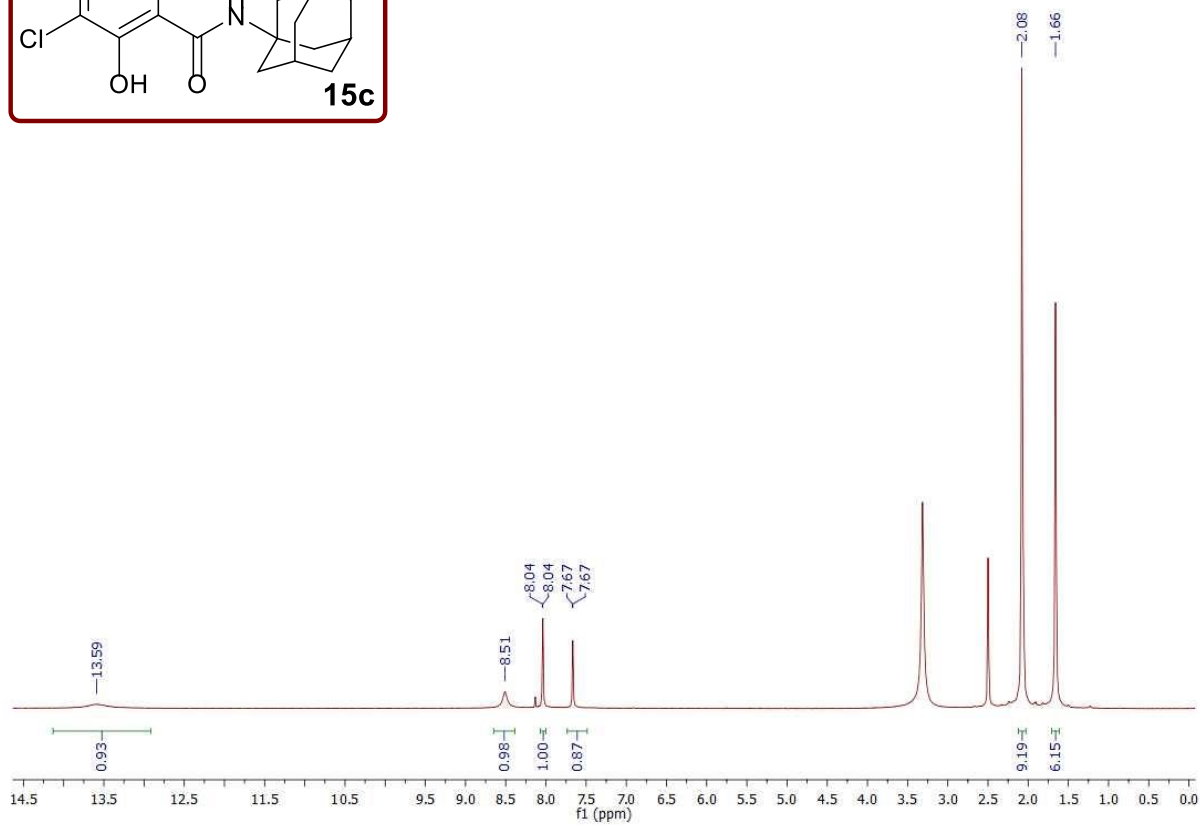
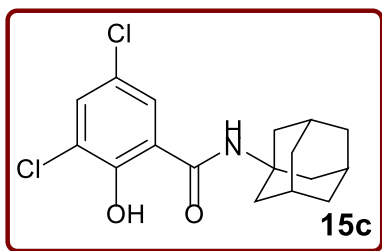


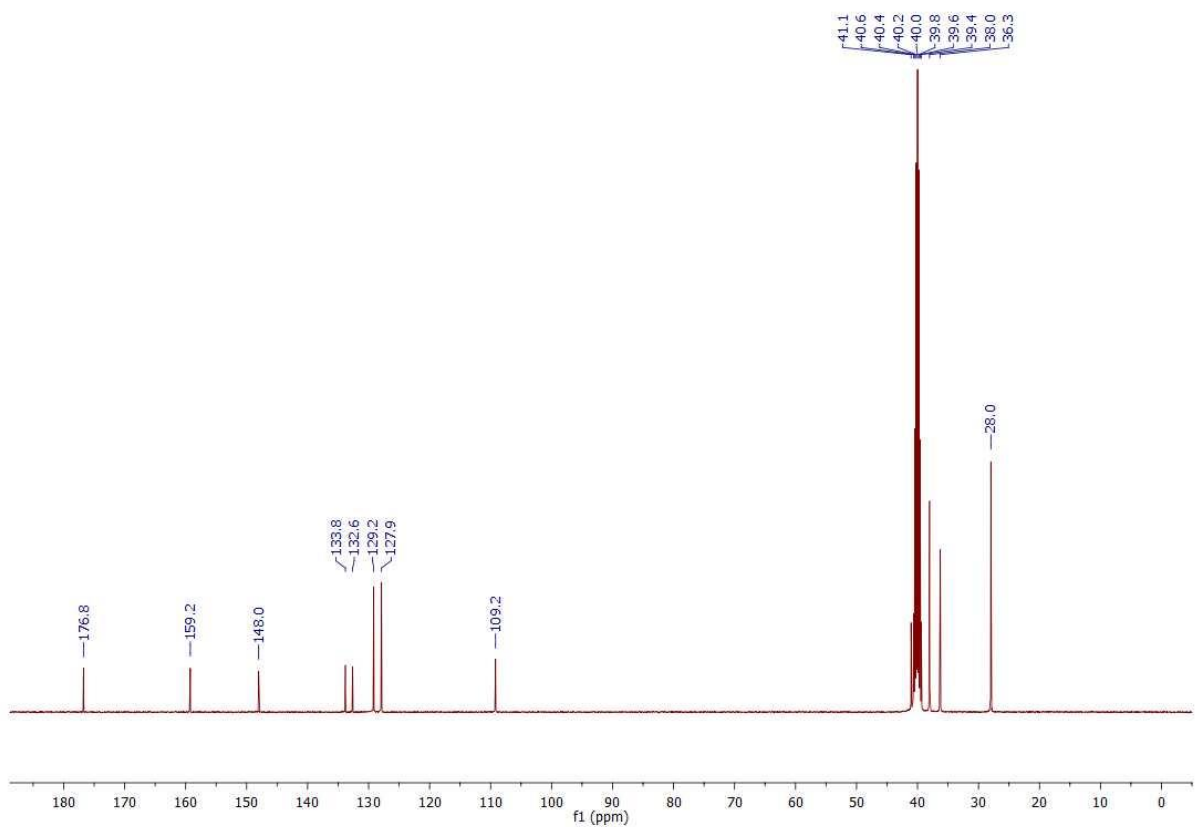
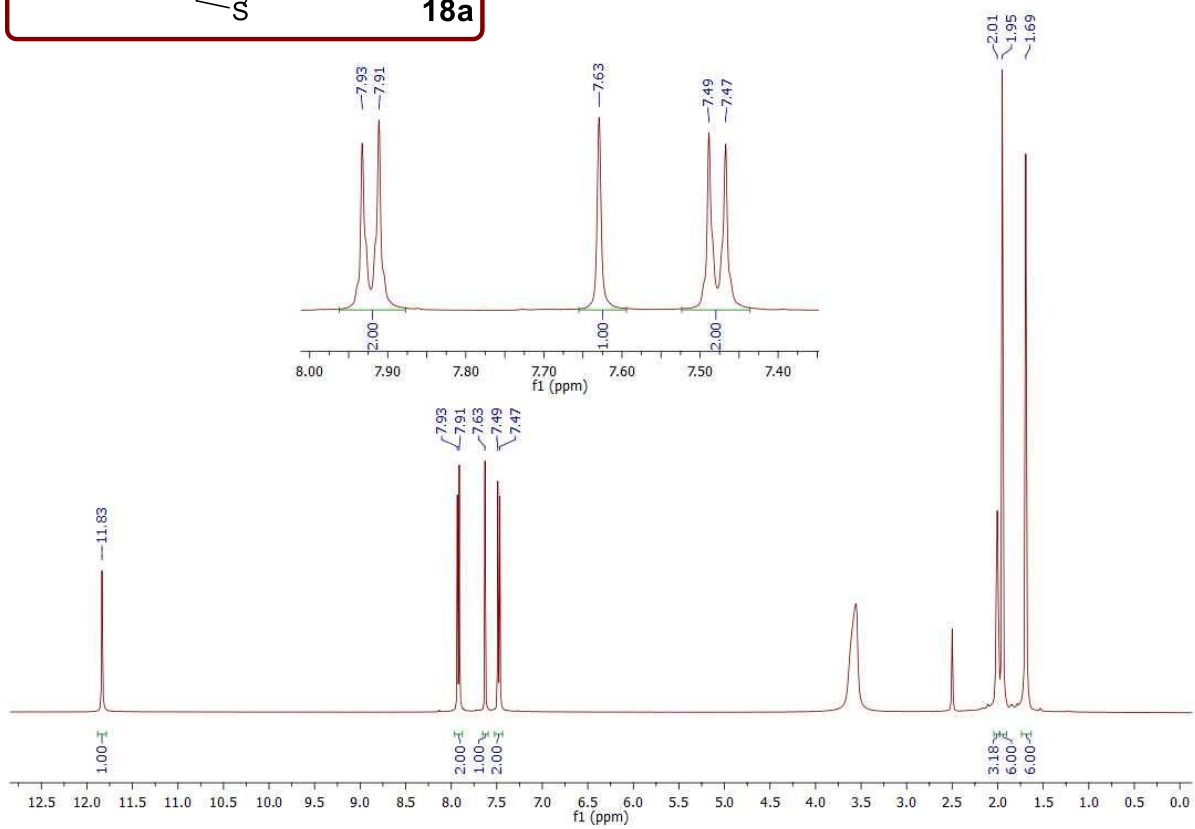
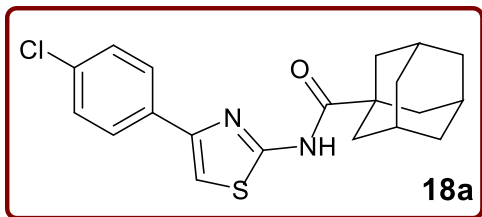


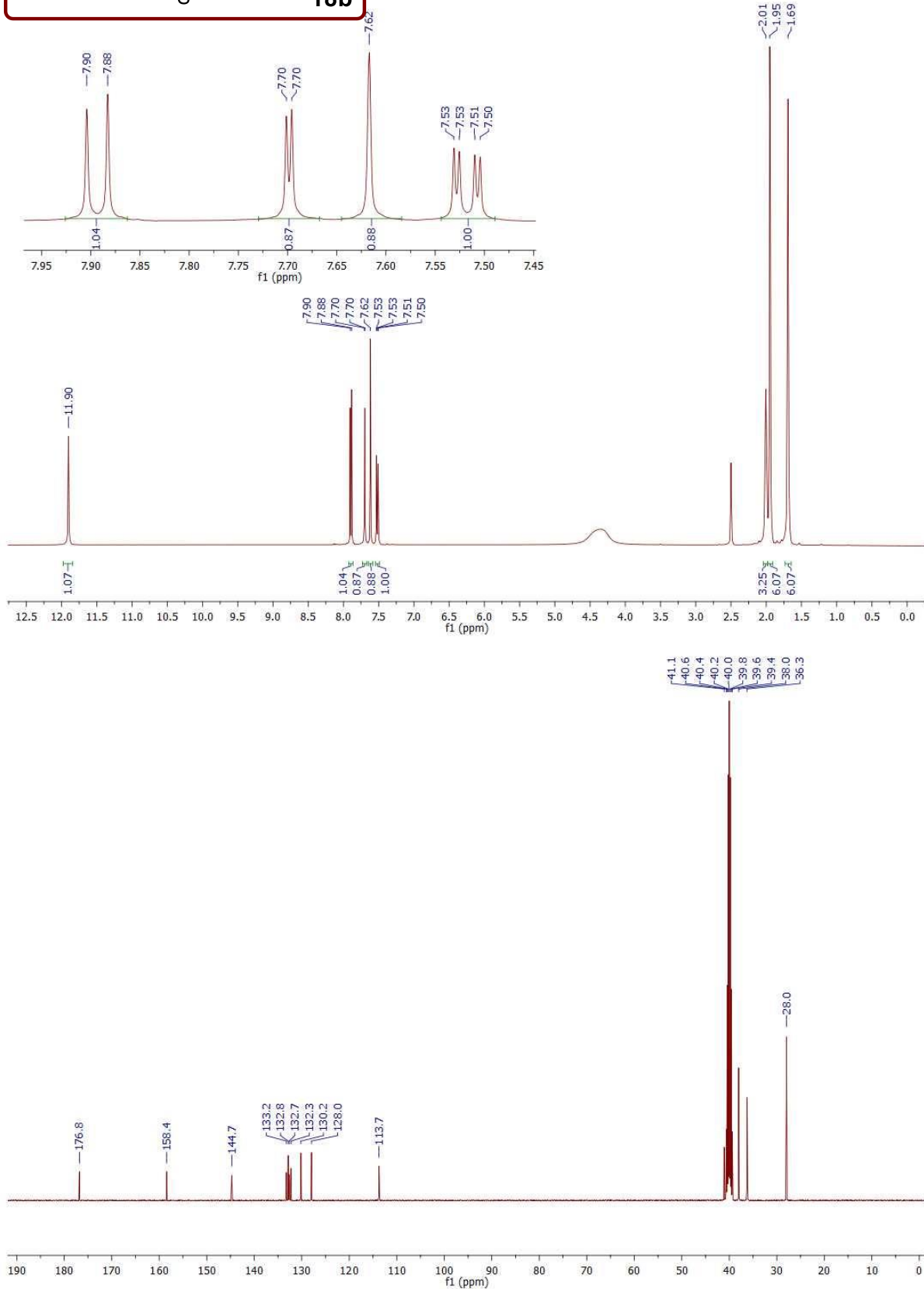
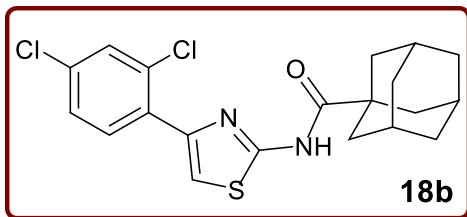


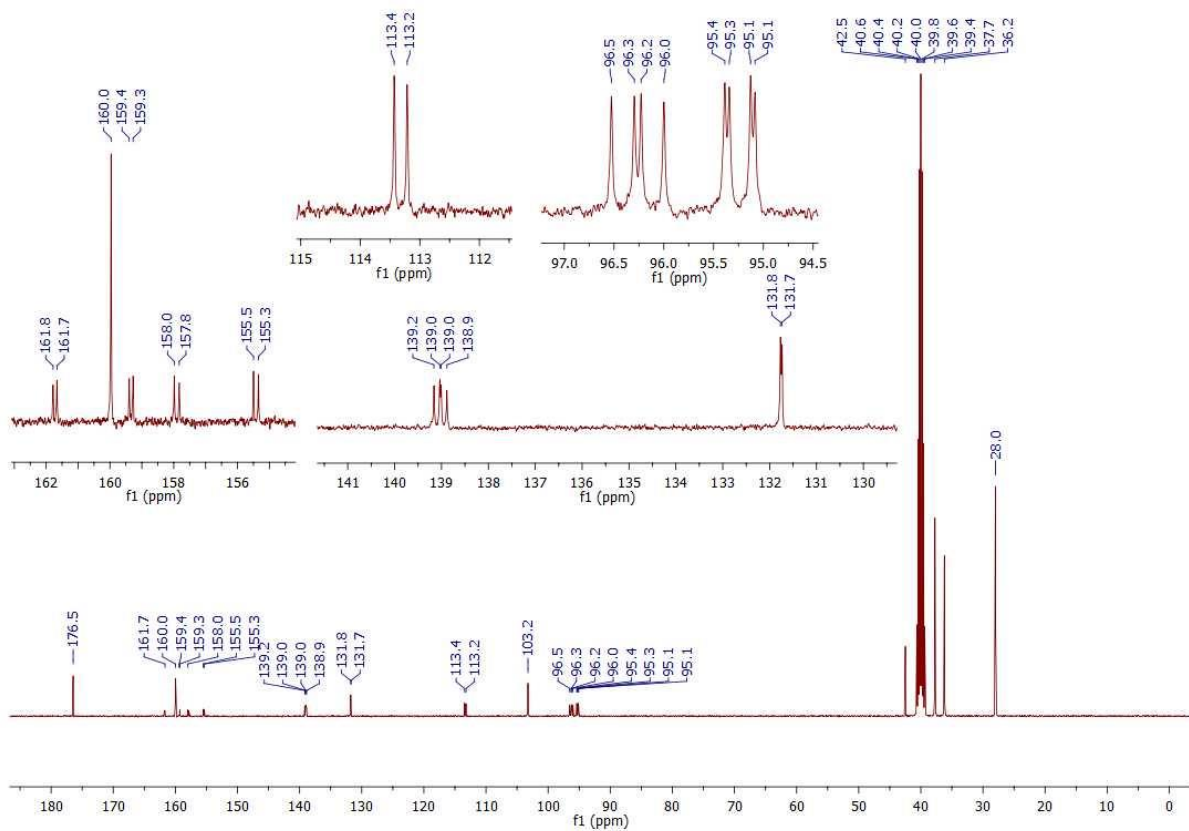
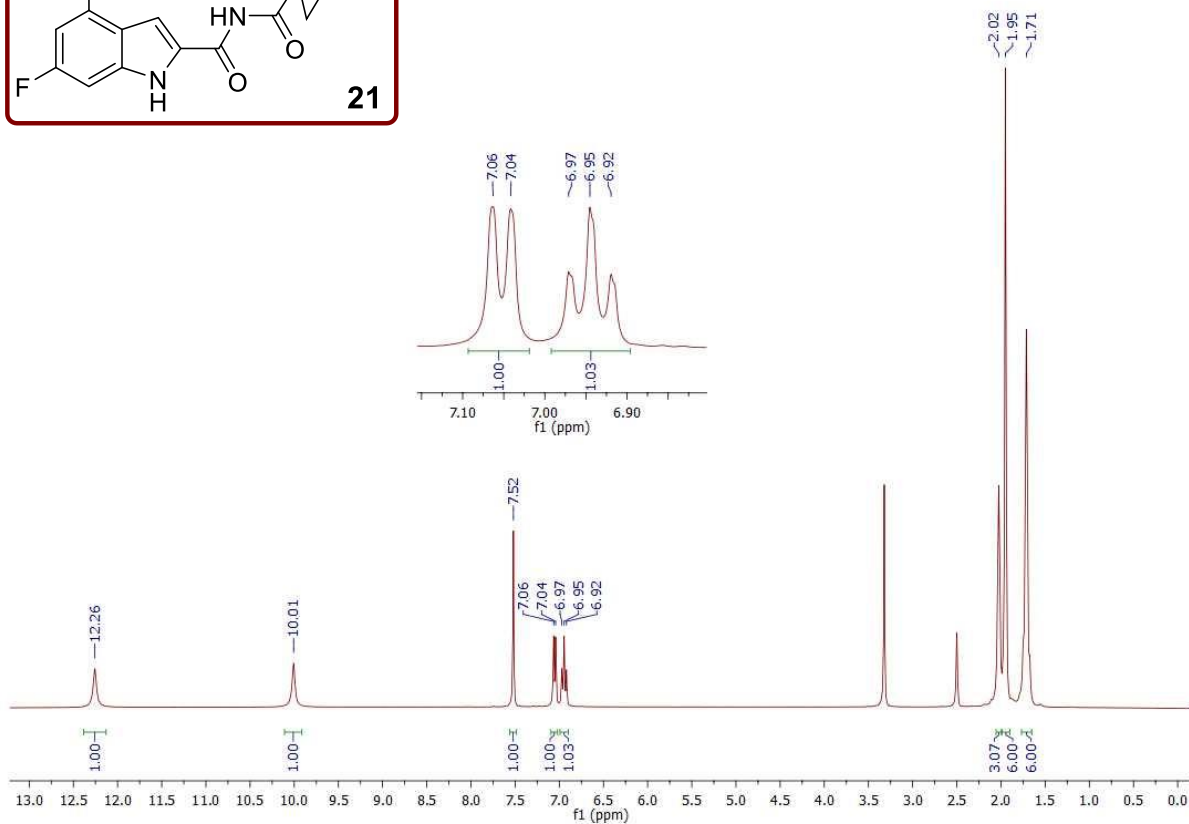
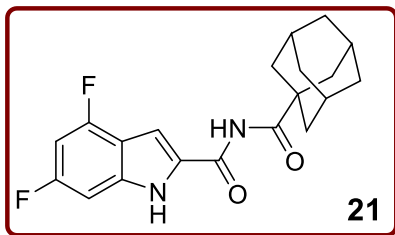




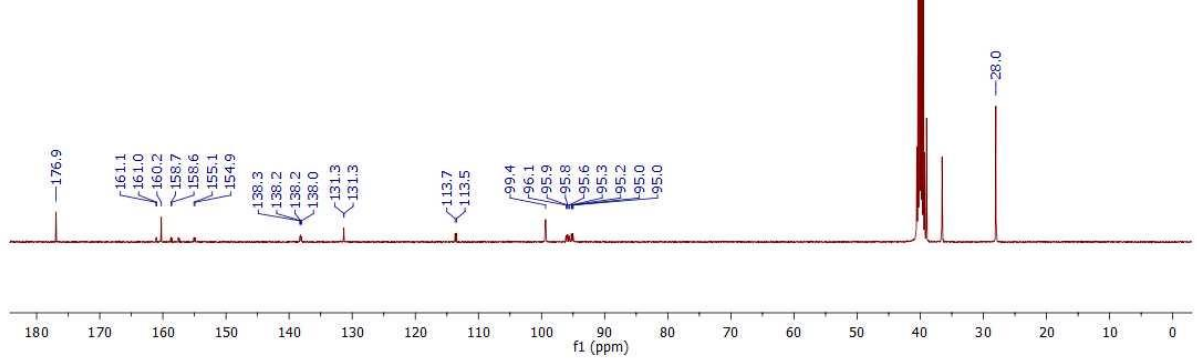
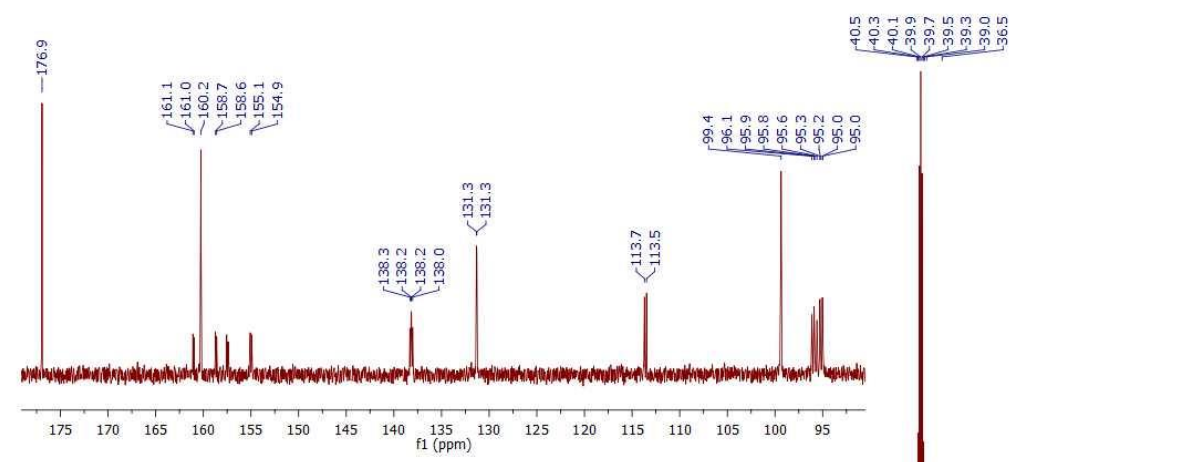
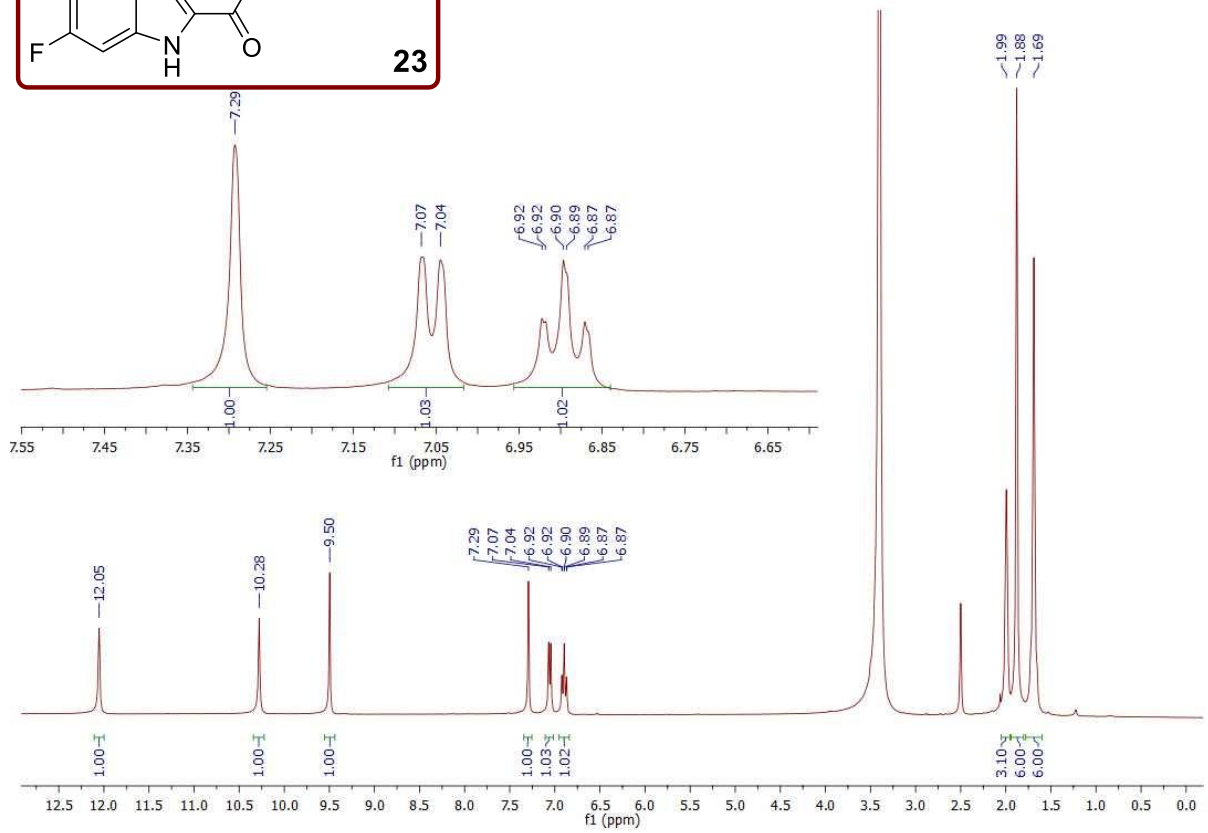
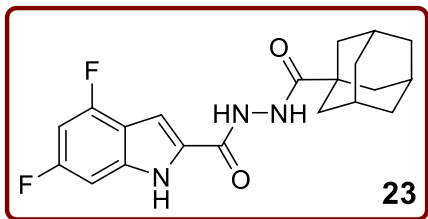


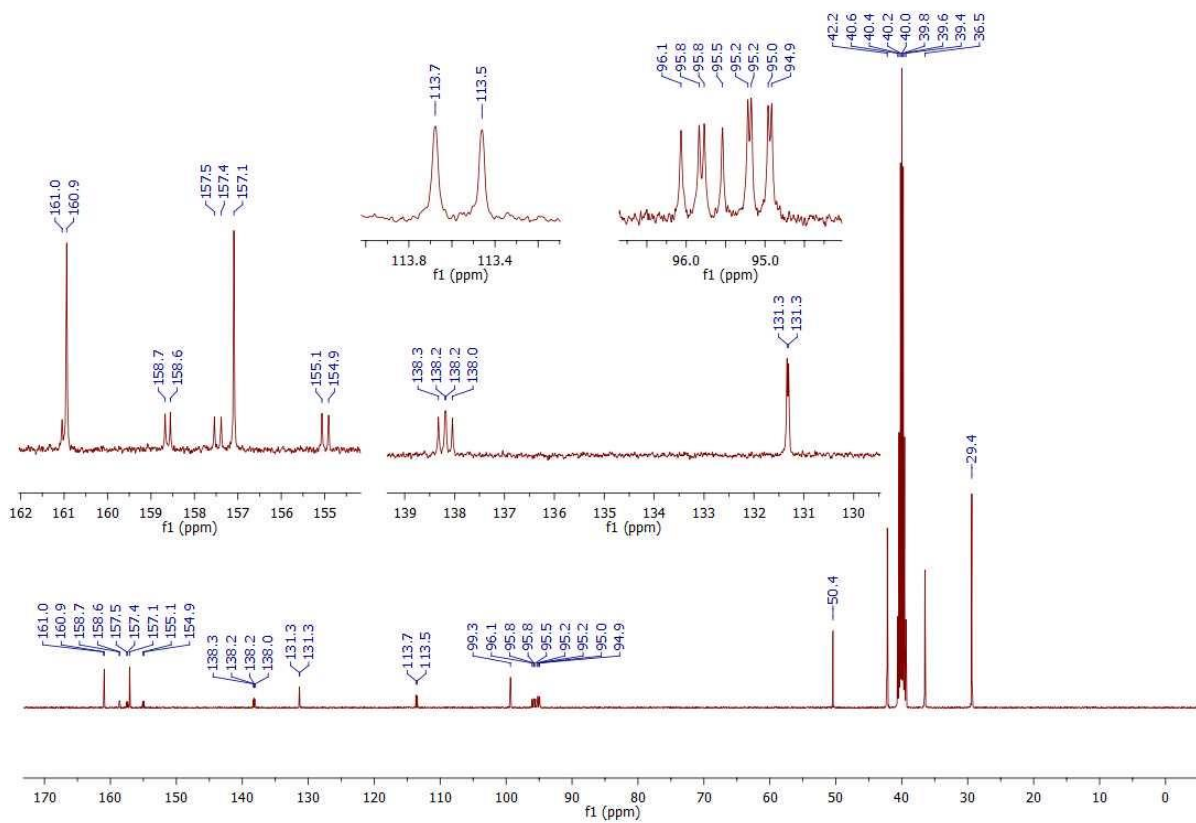
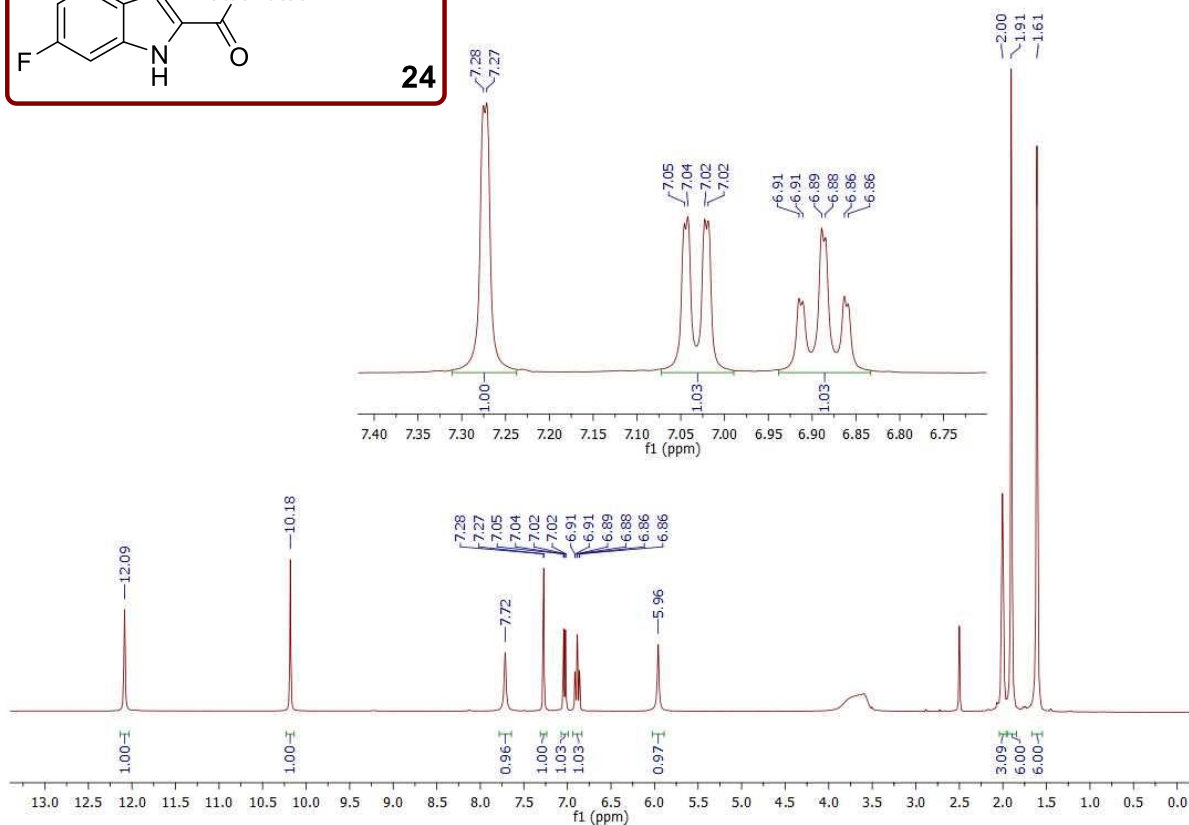
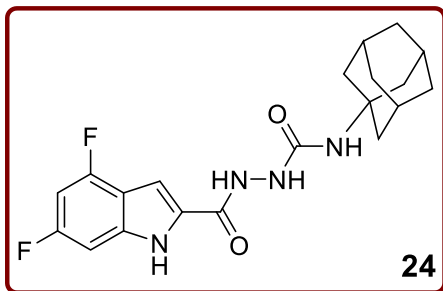


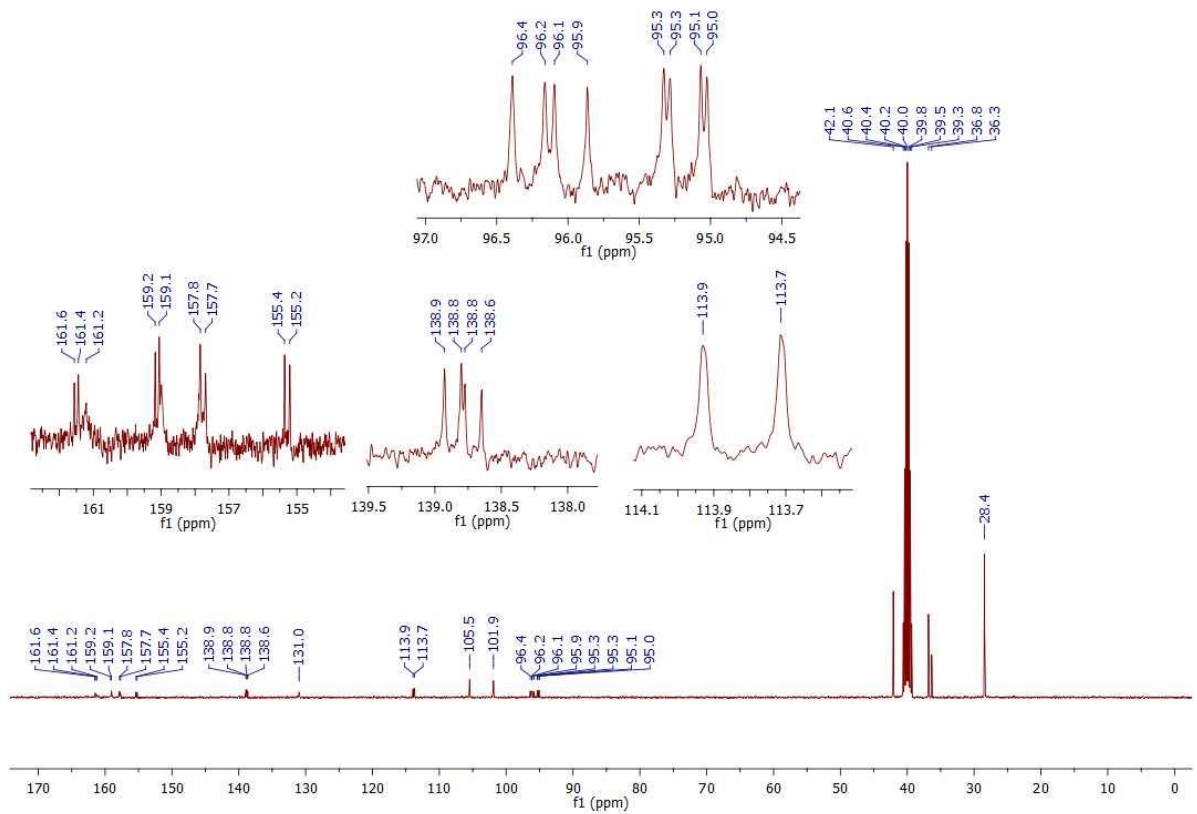
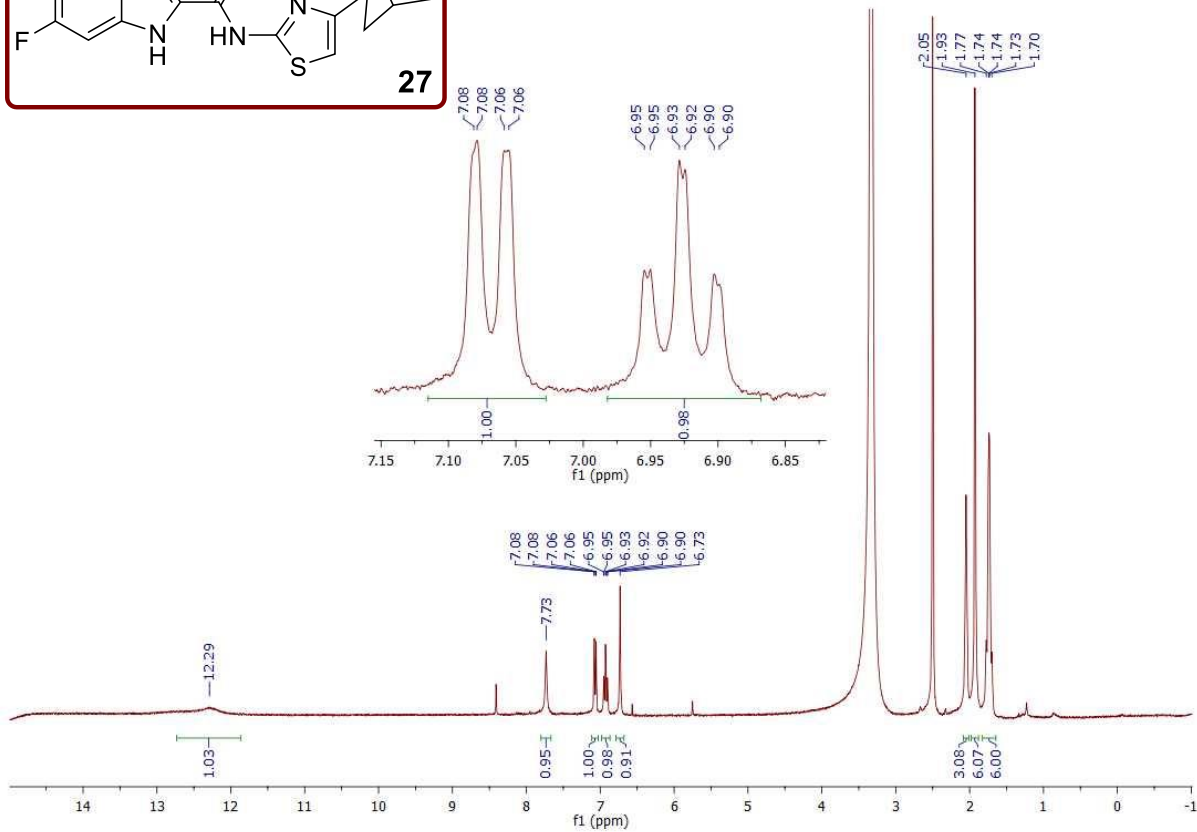
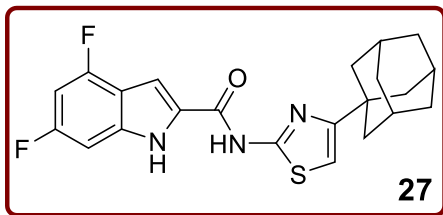




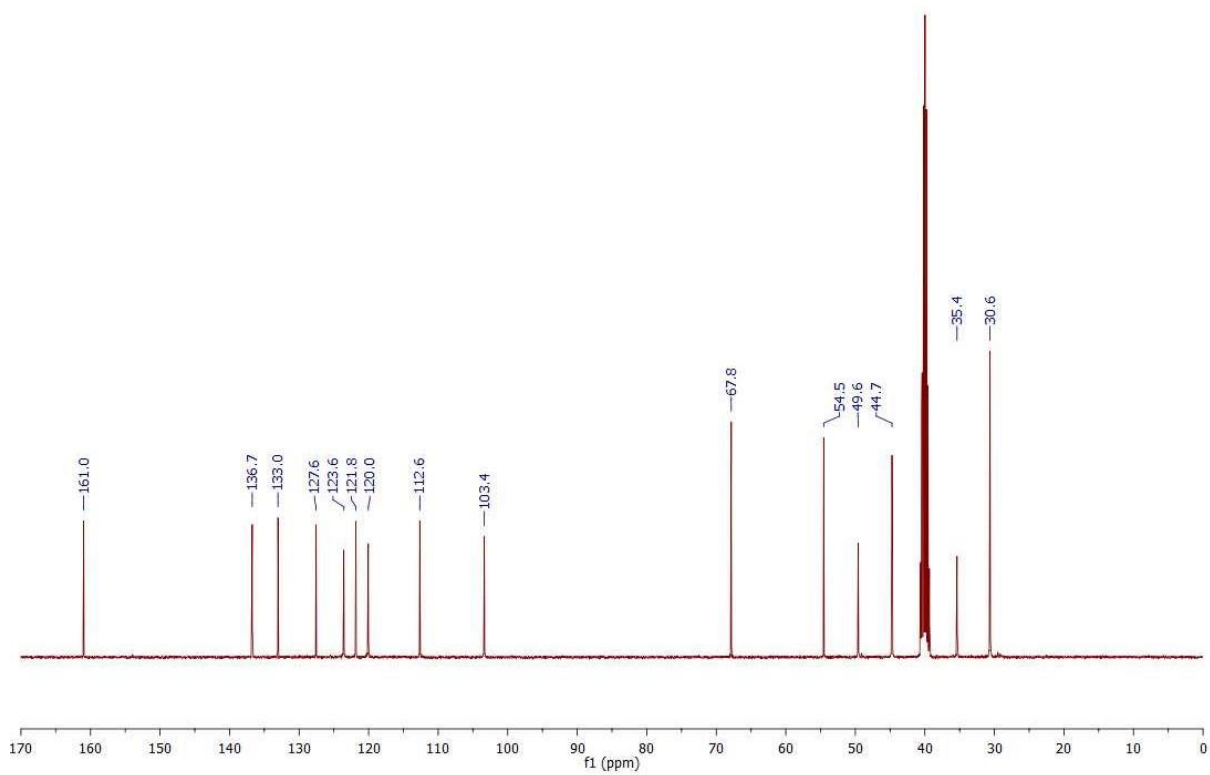
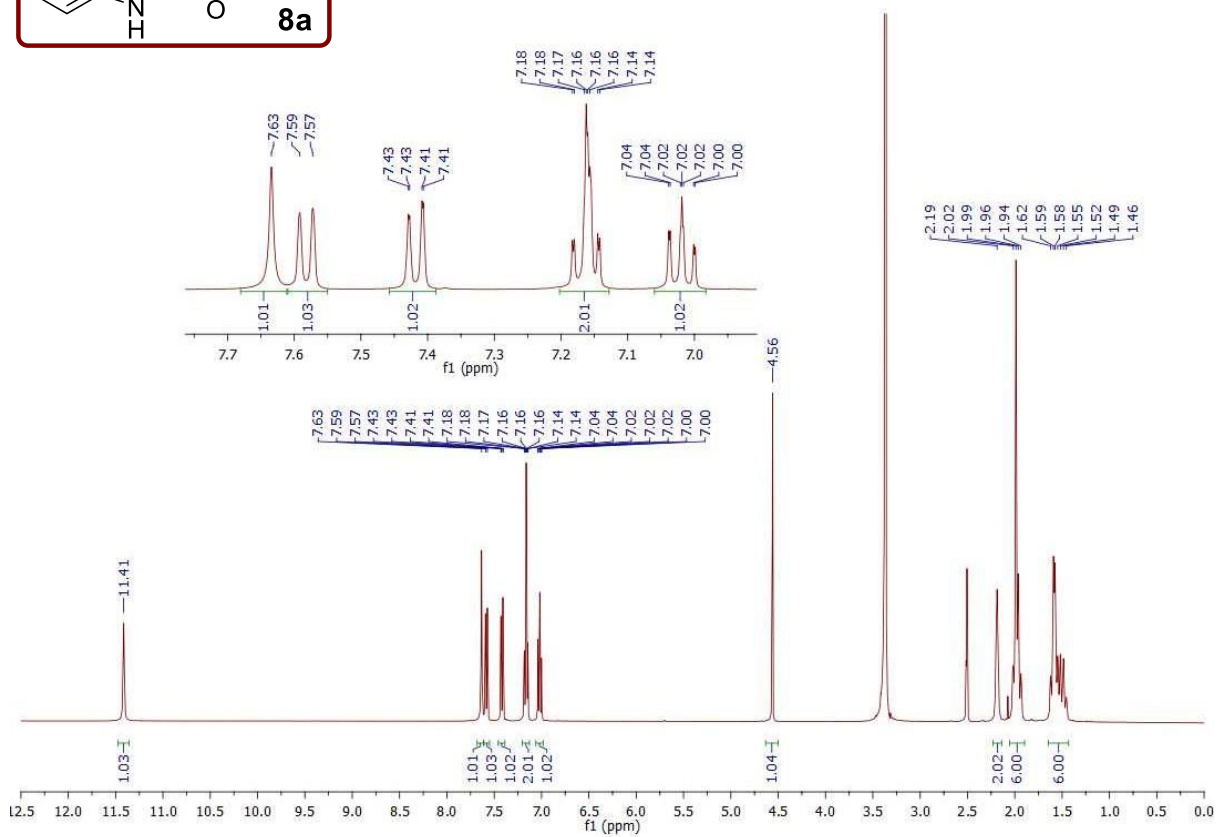
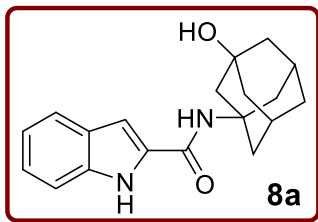


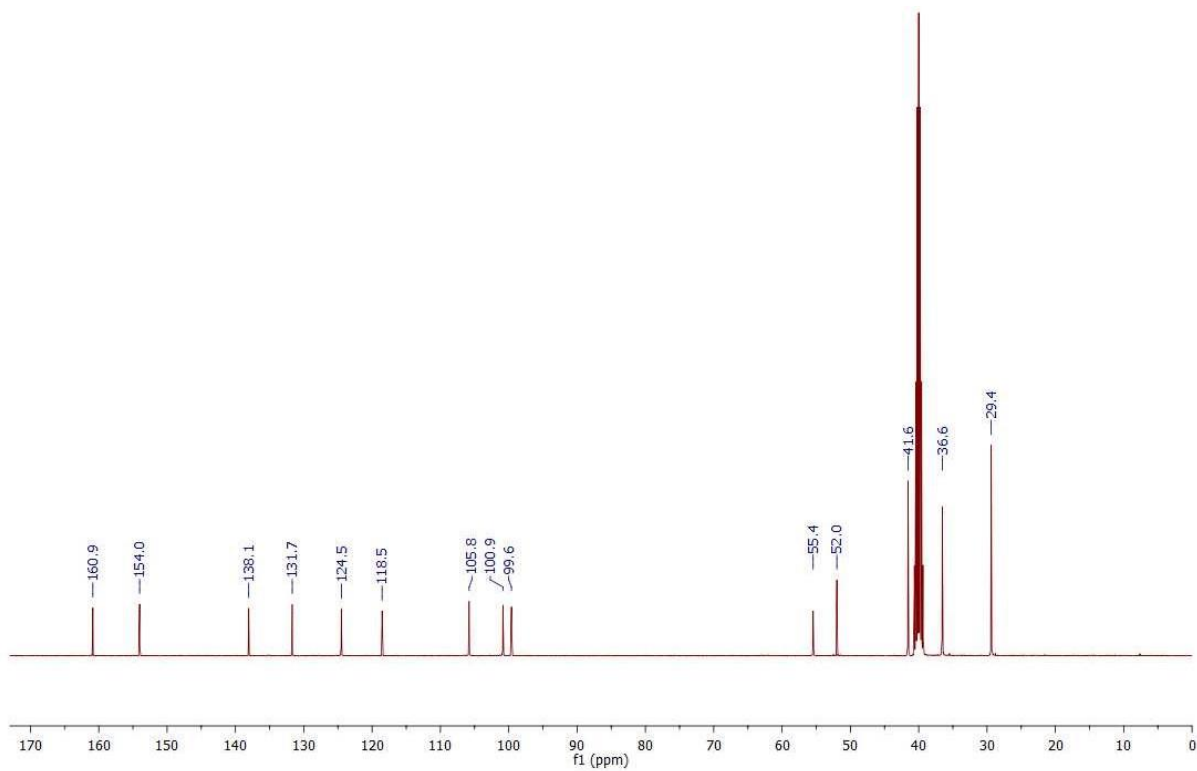
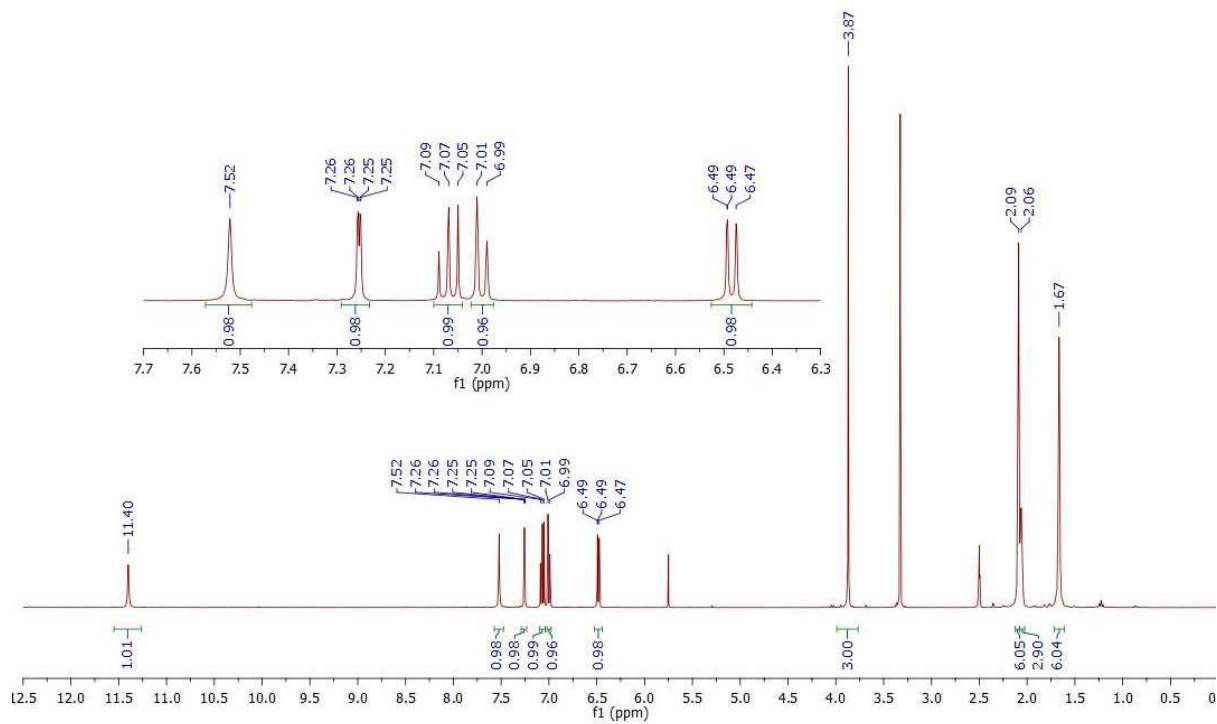
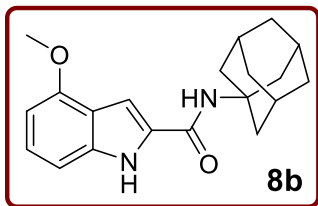


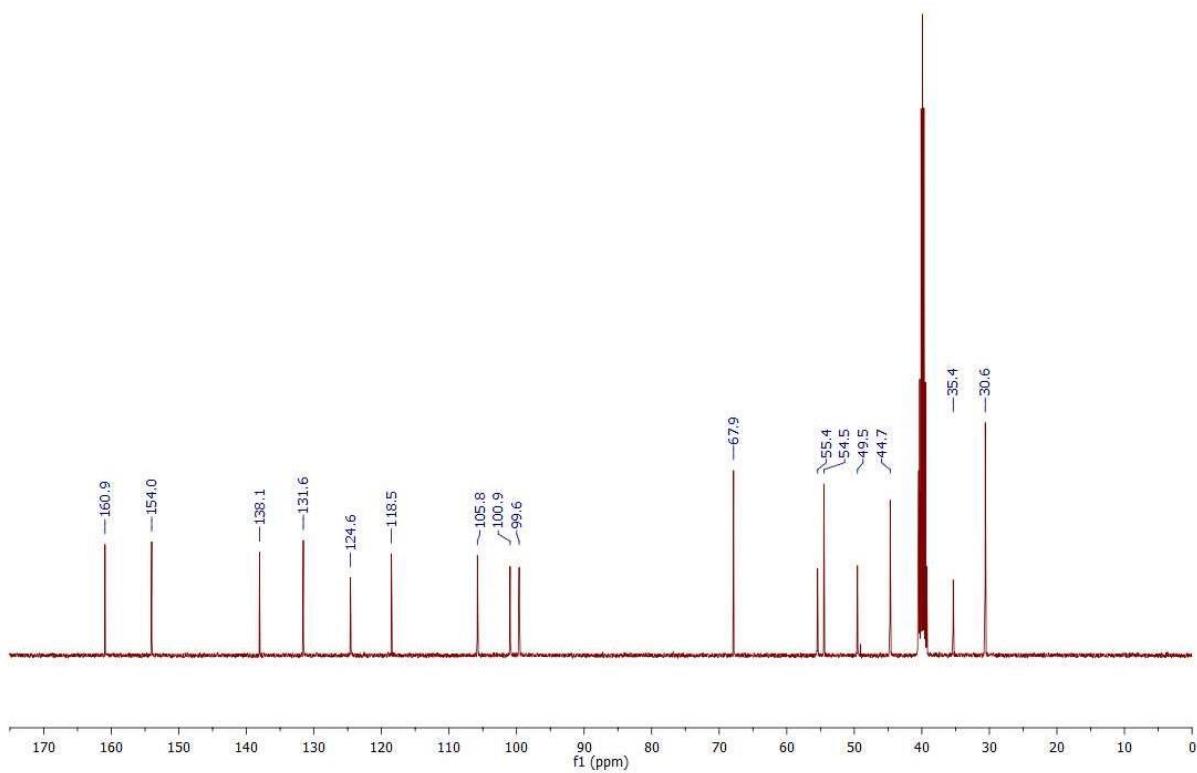
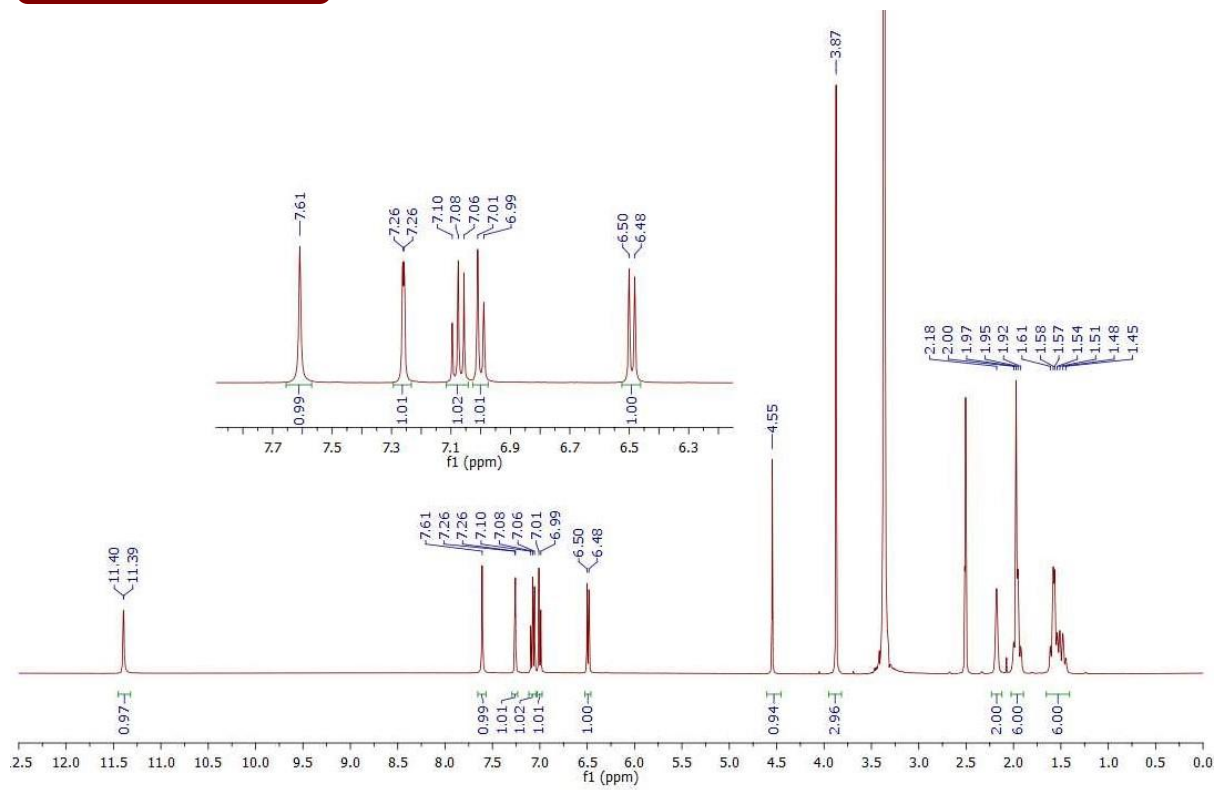
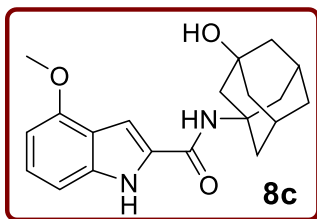


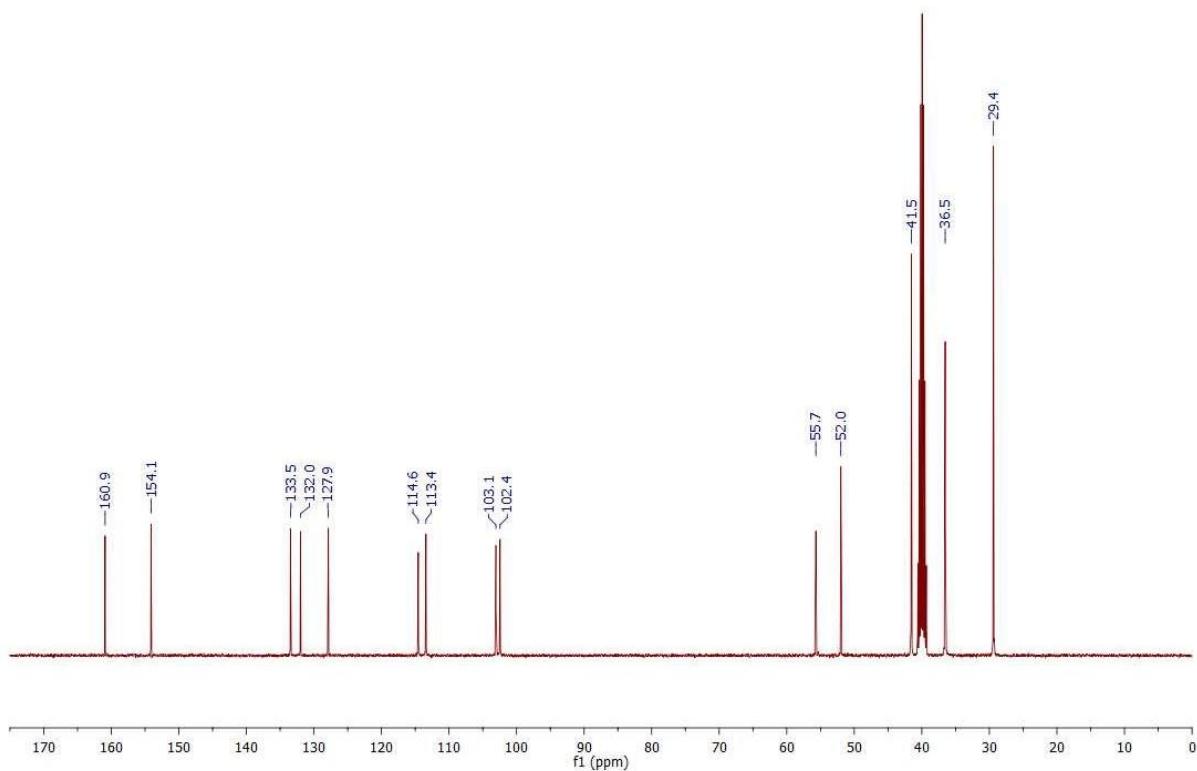
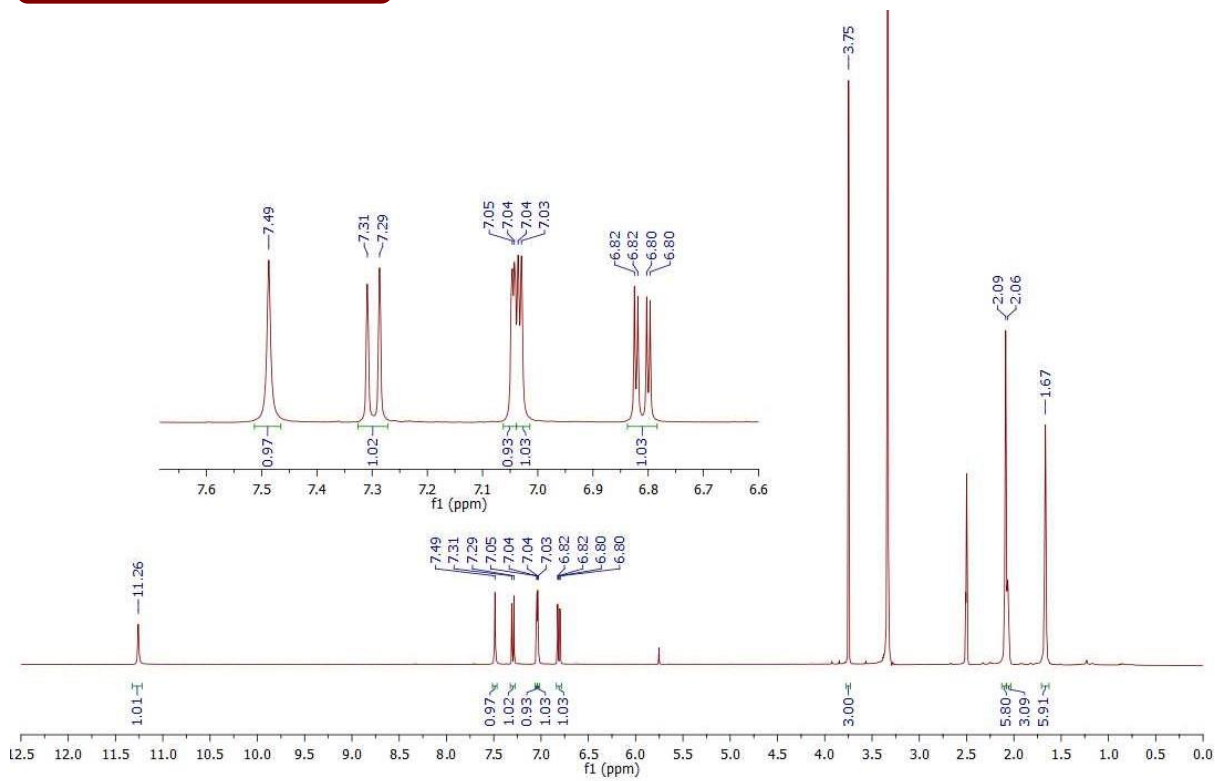
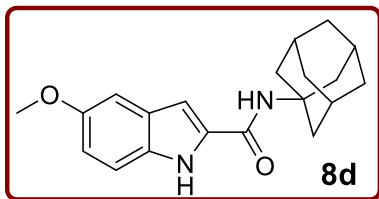


**Supplementary Information – Chapter 4**  
**(Bioorganic Chemistry 2021 Article)**

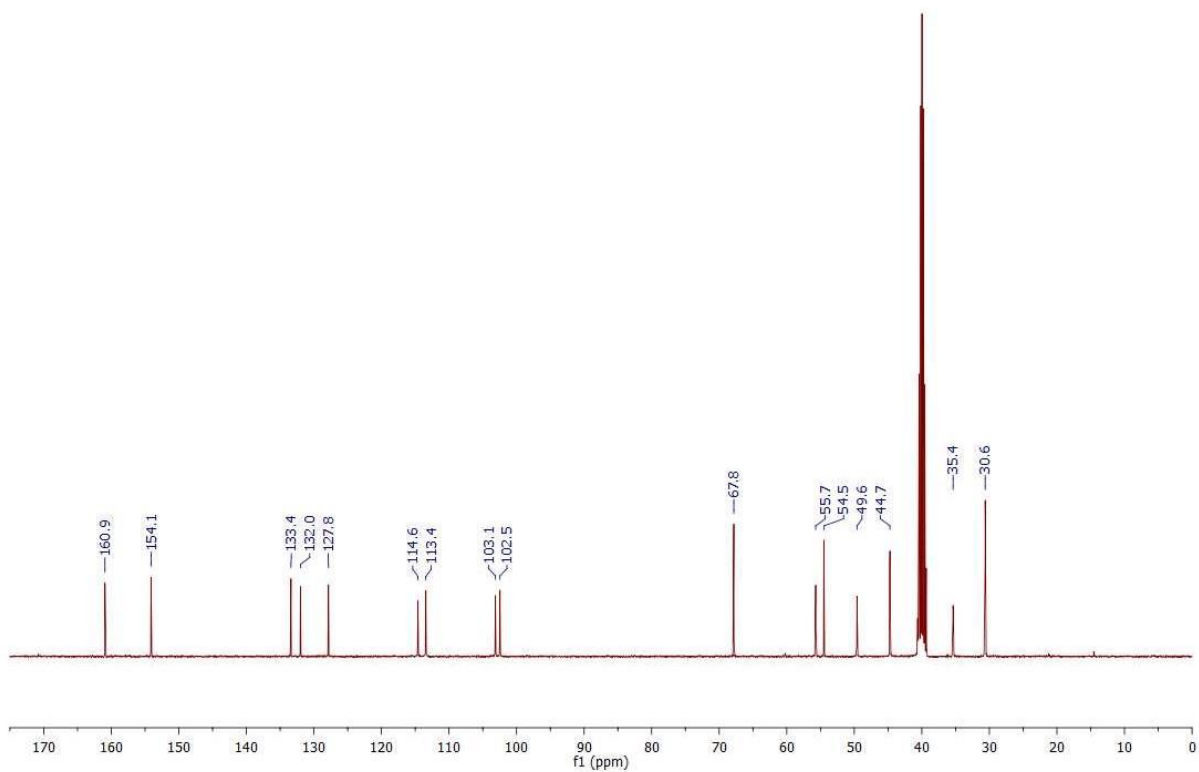
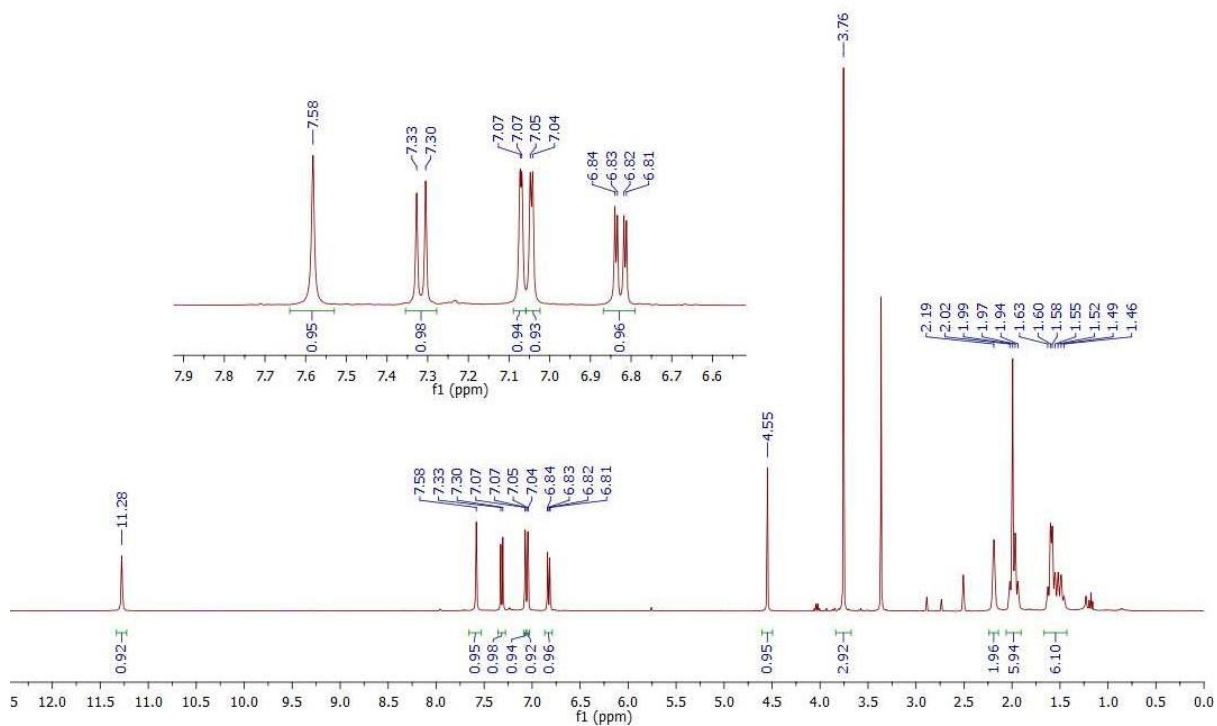
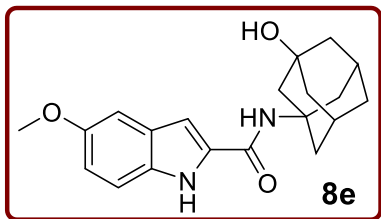


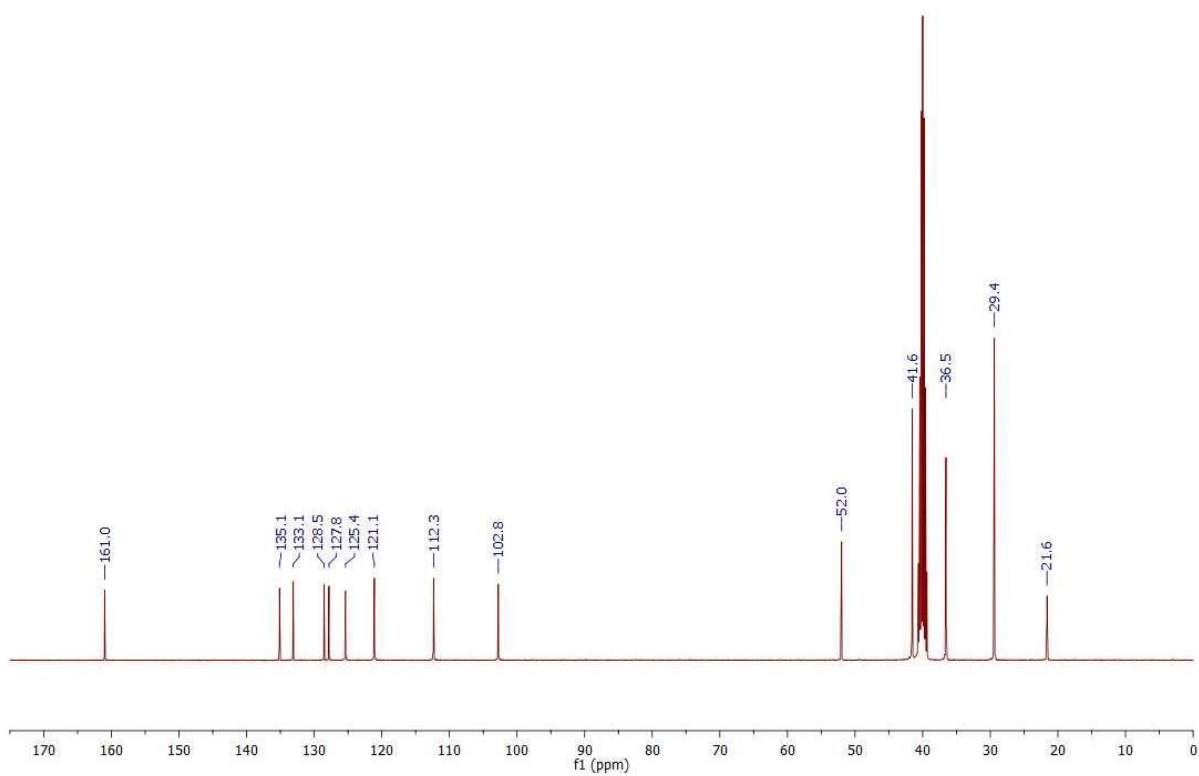
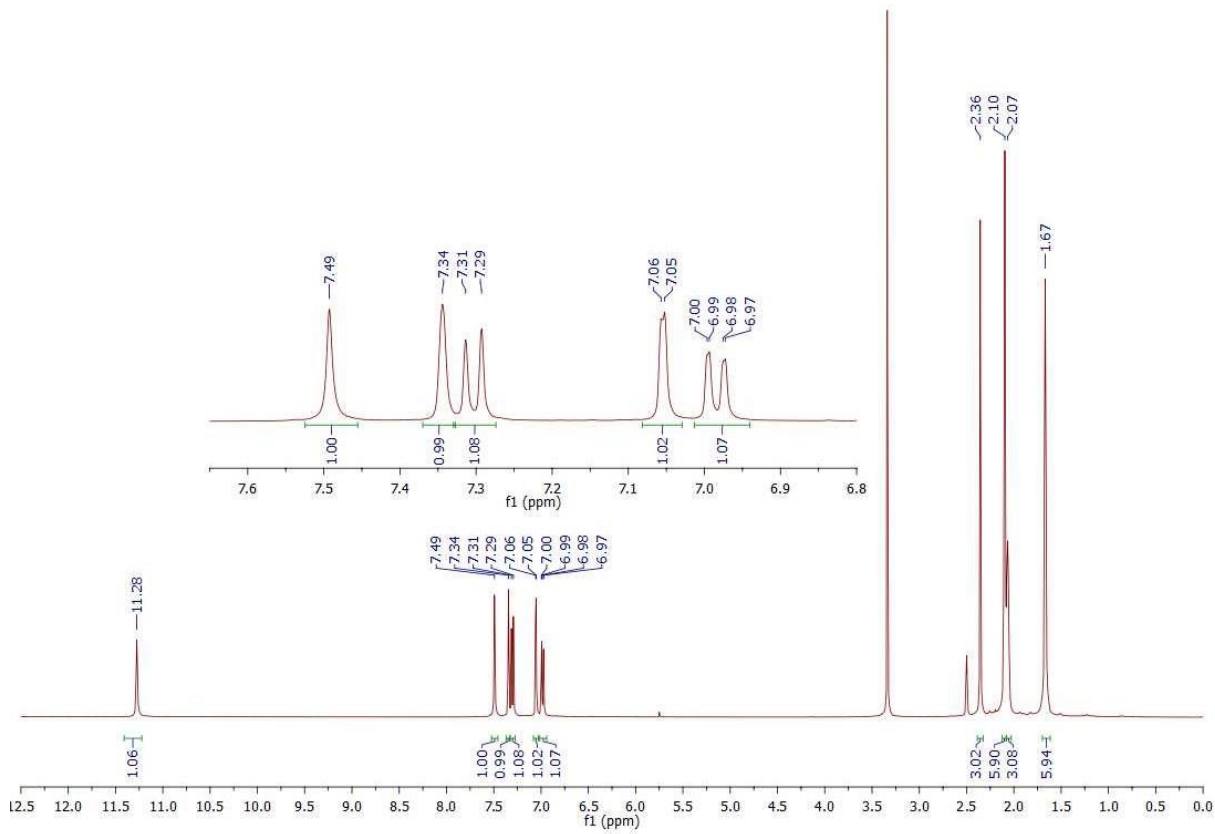
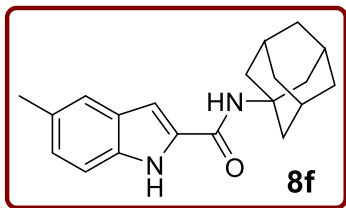


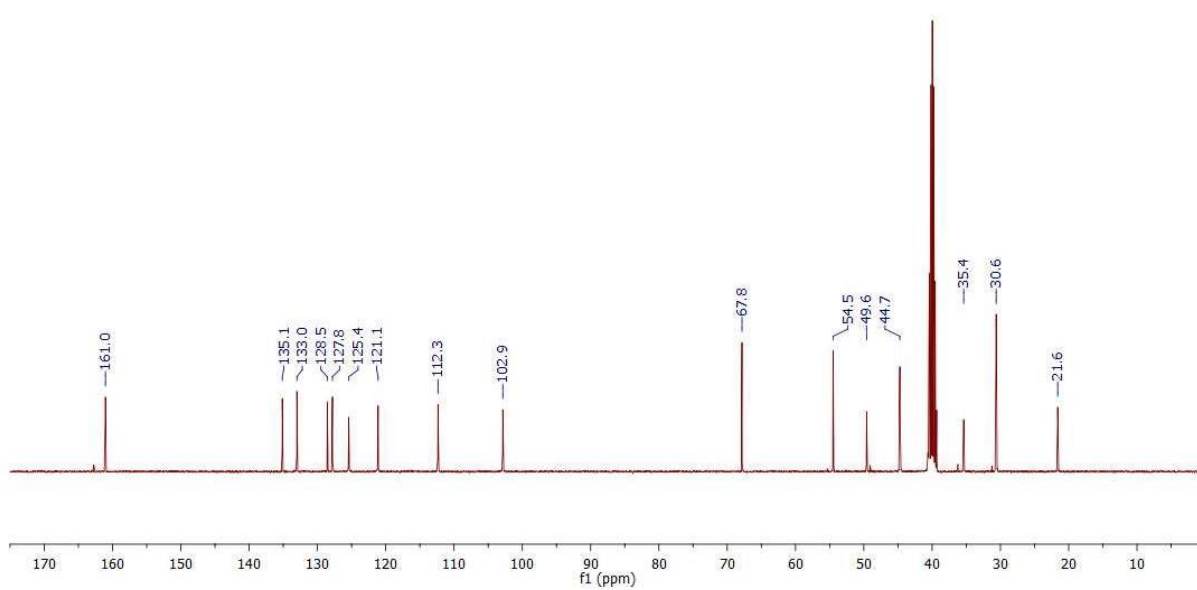
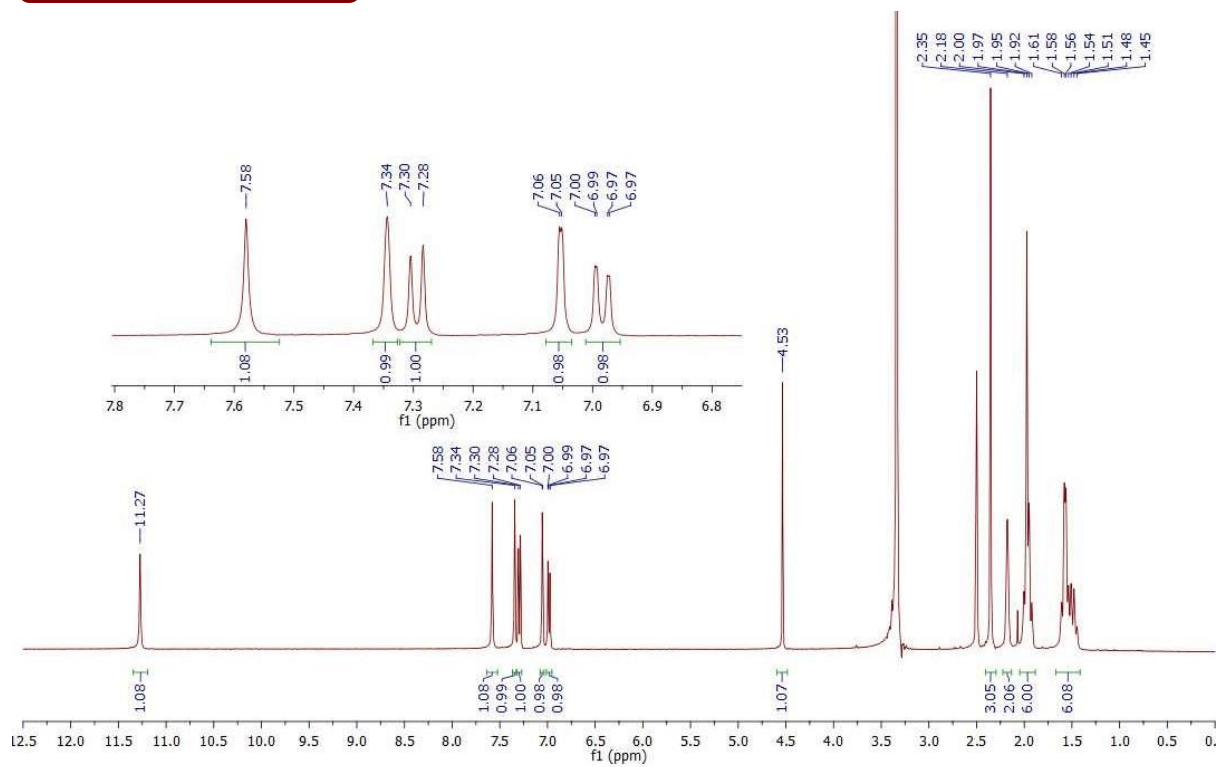
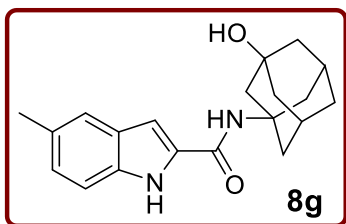


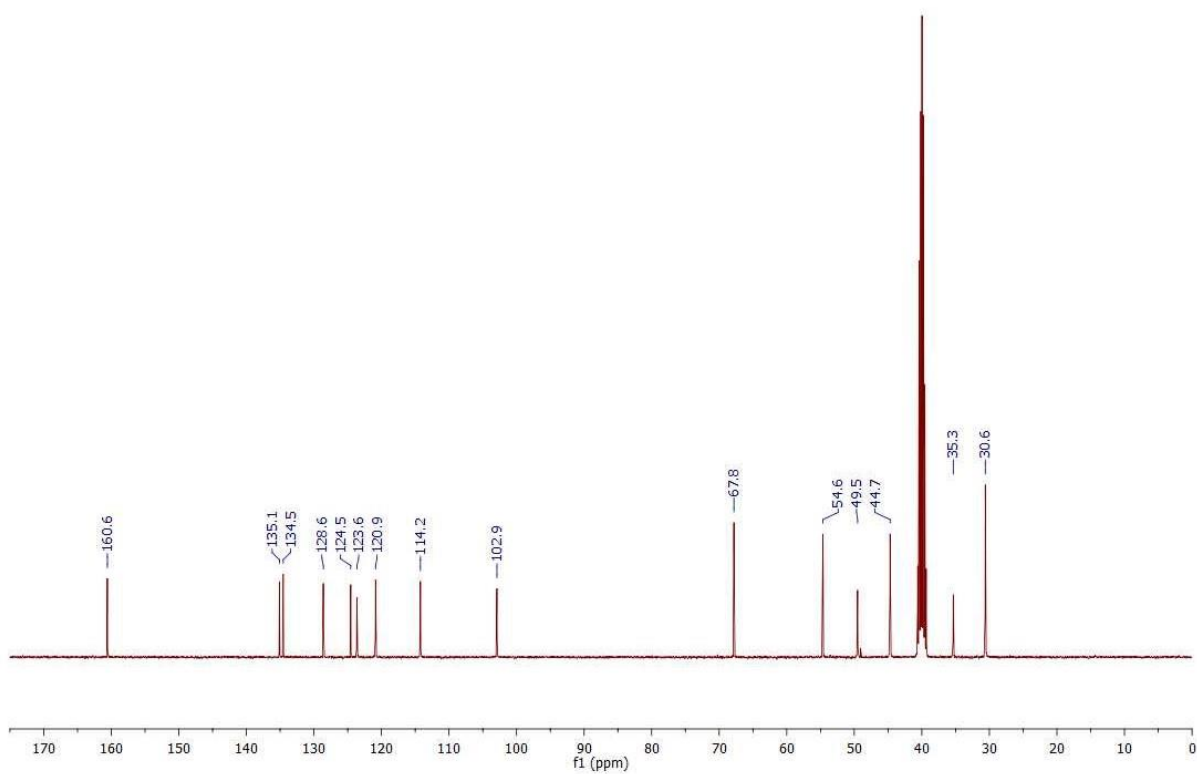
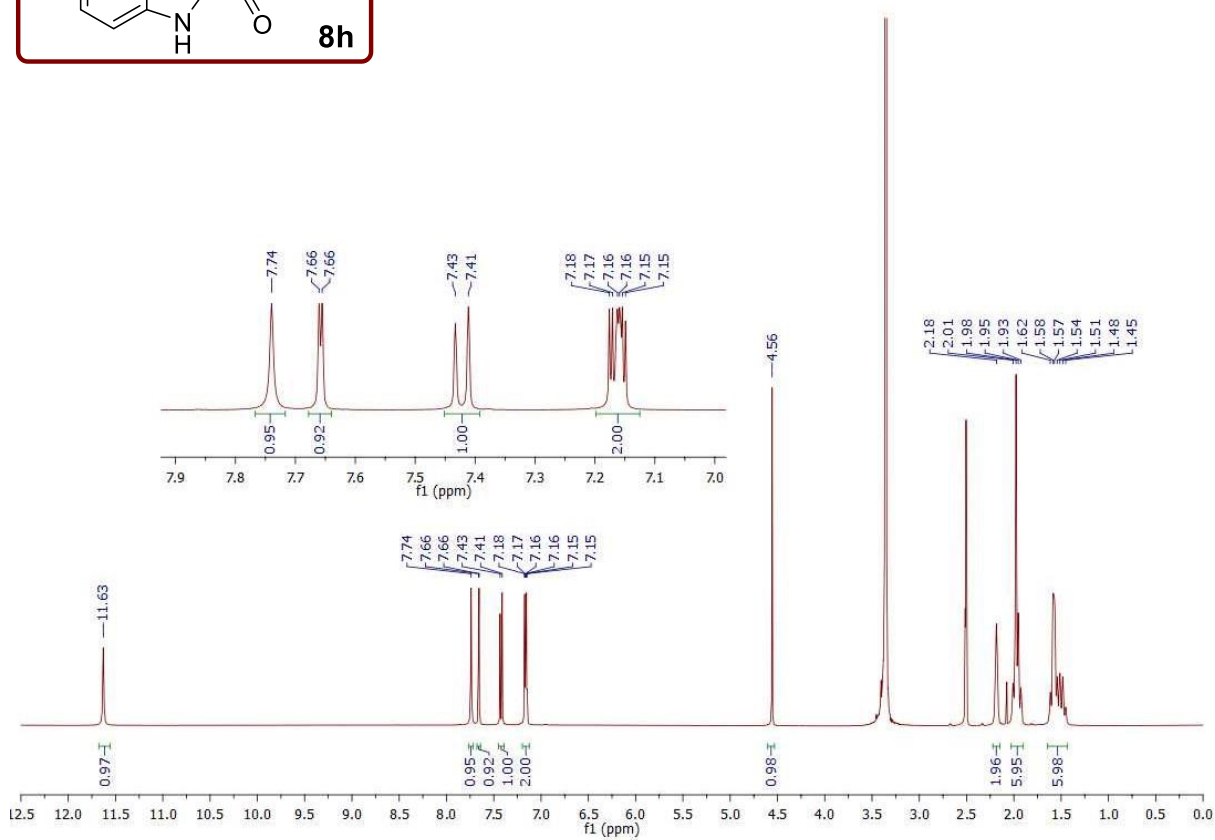
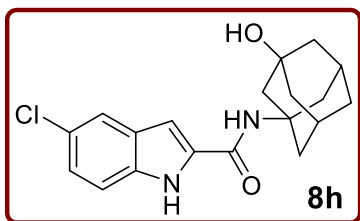


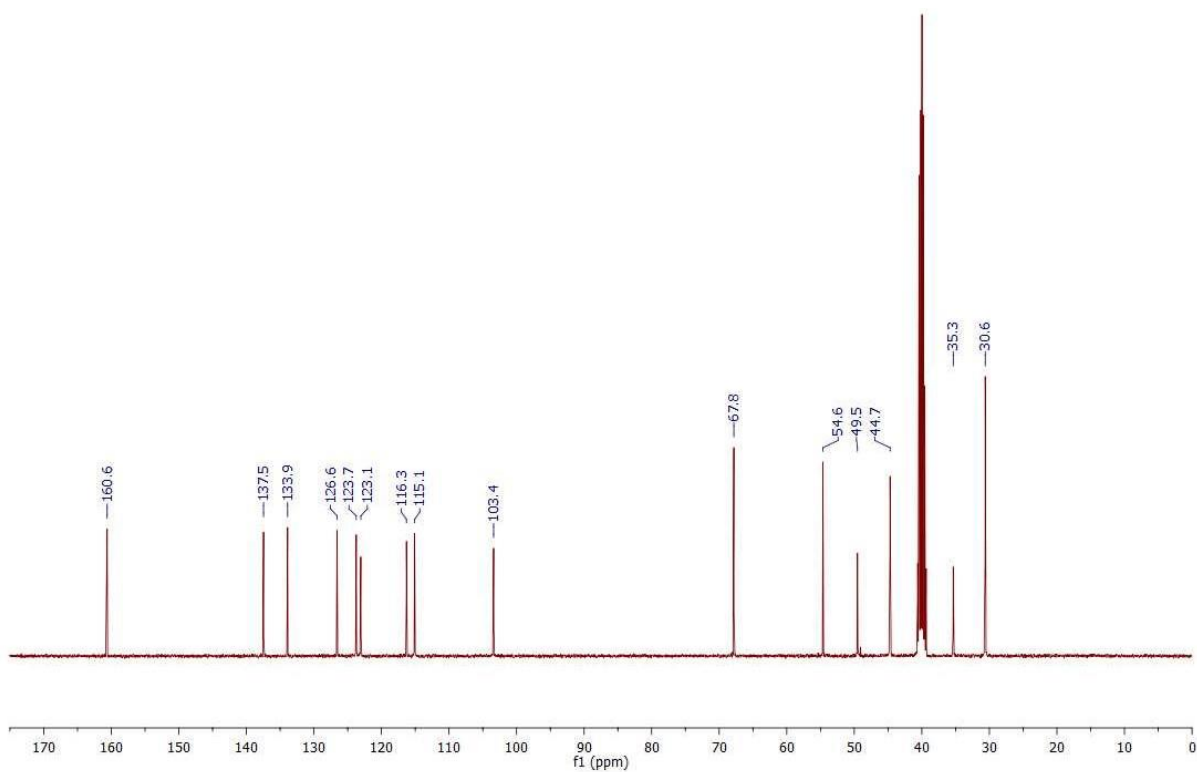
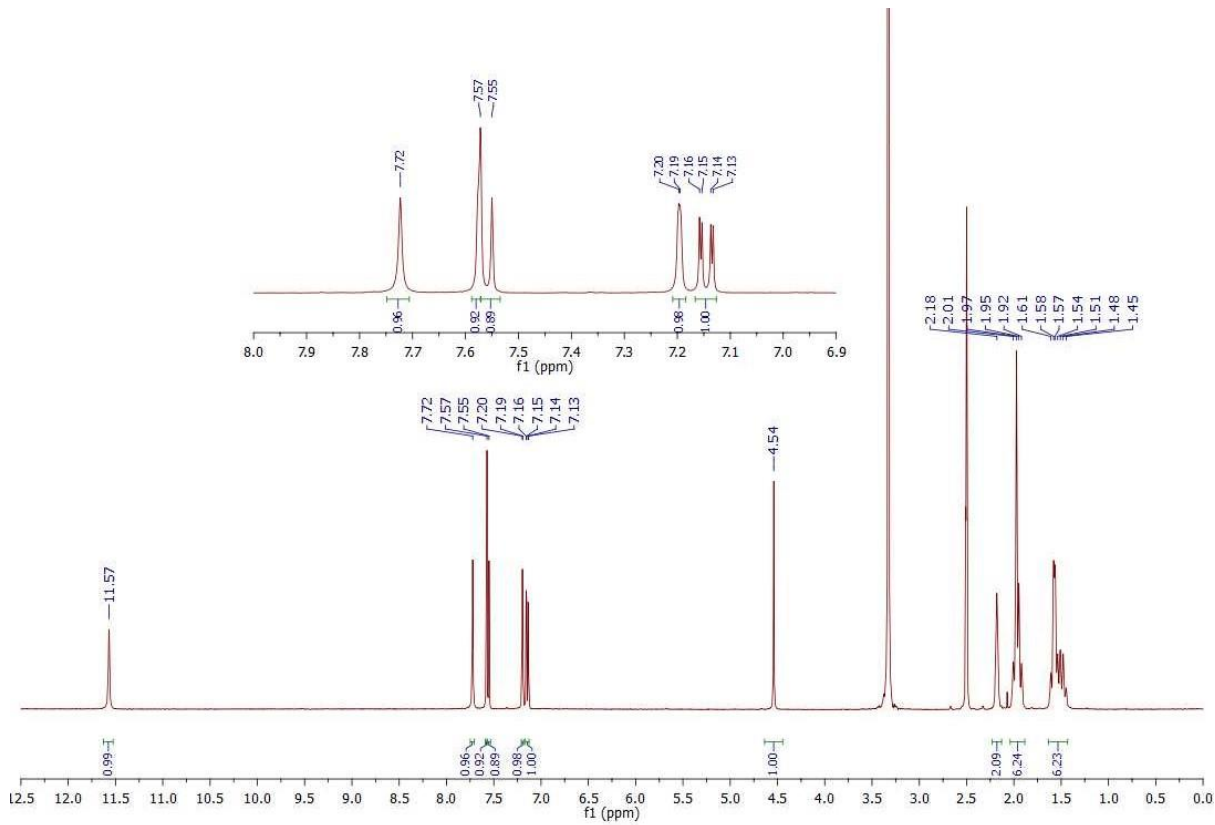
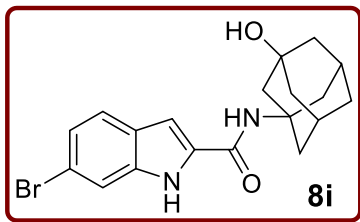


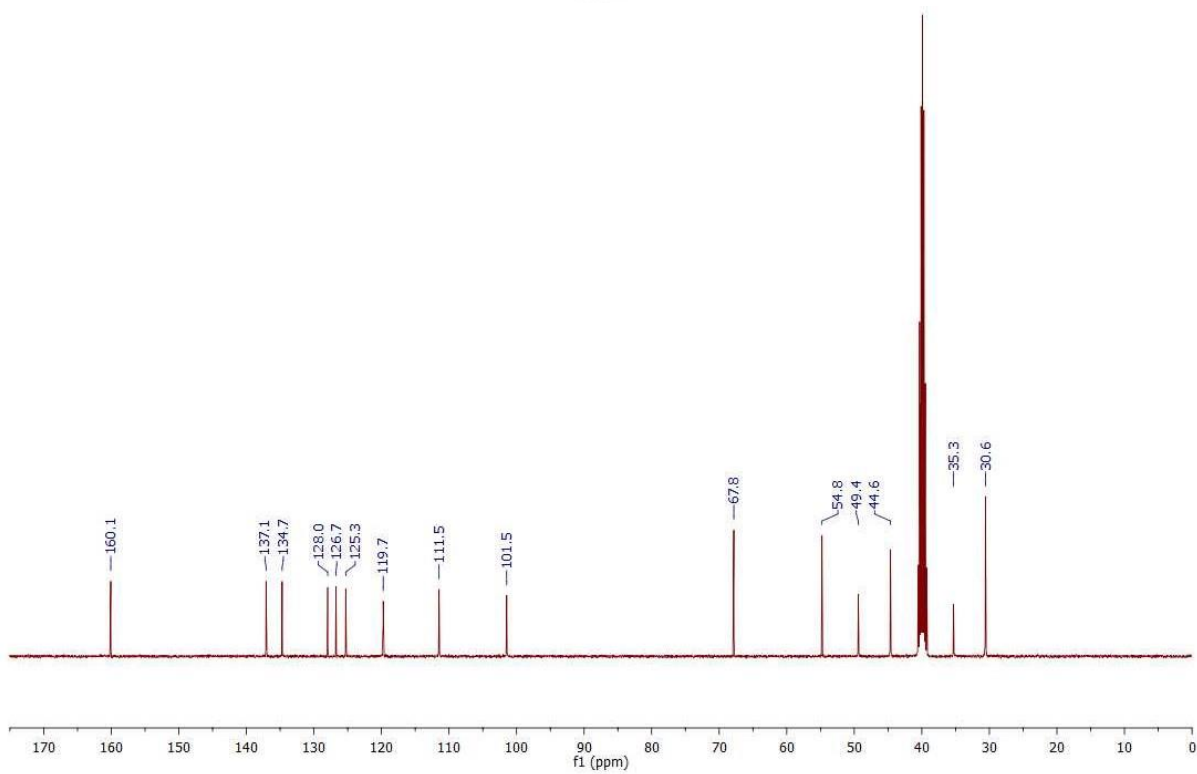
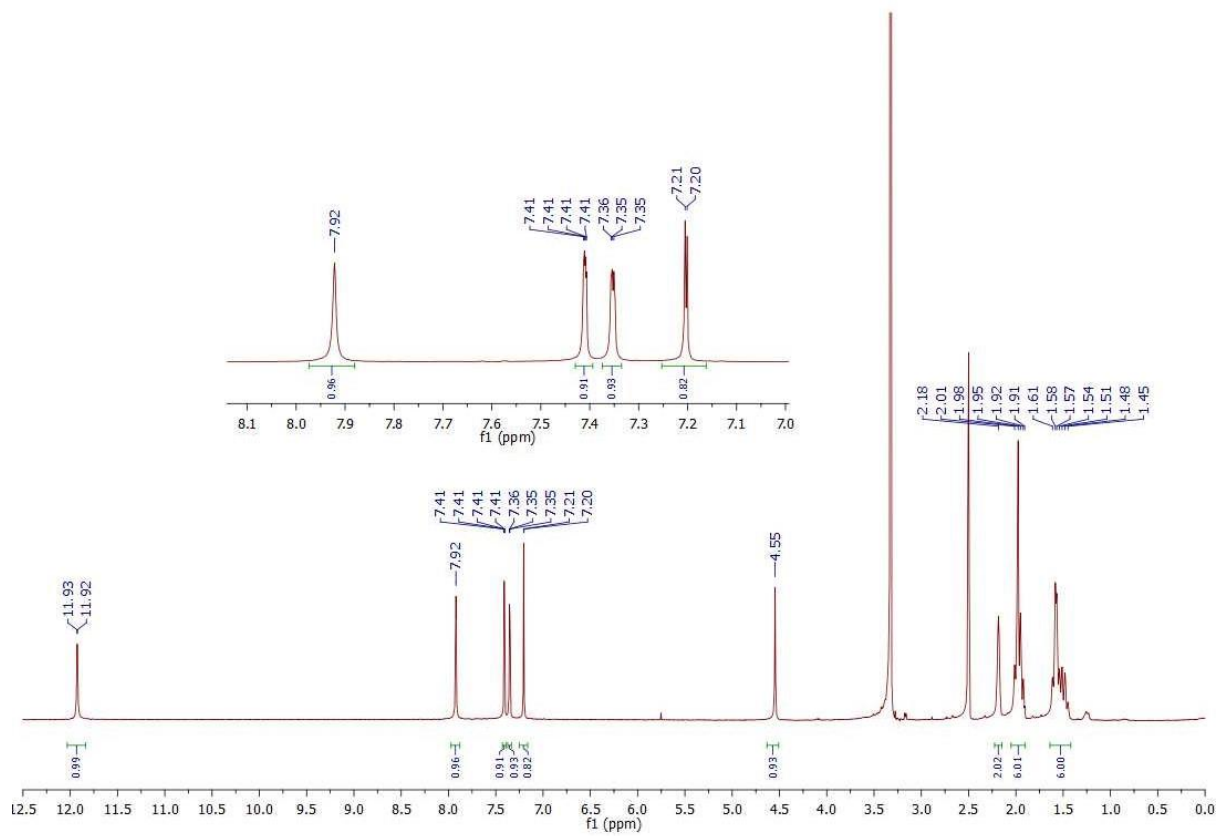
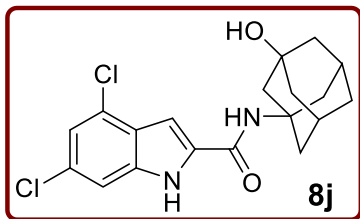


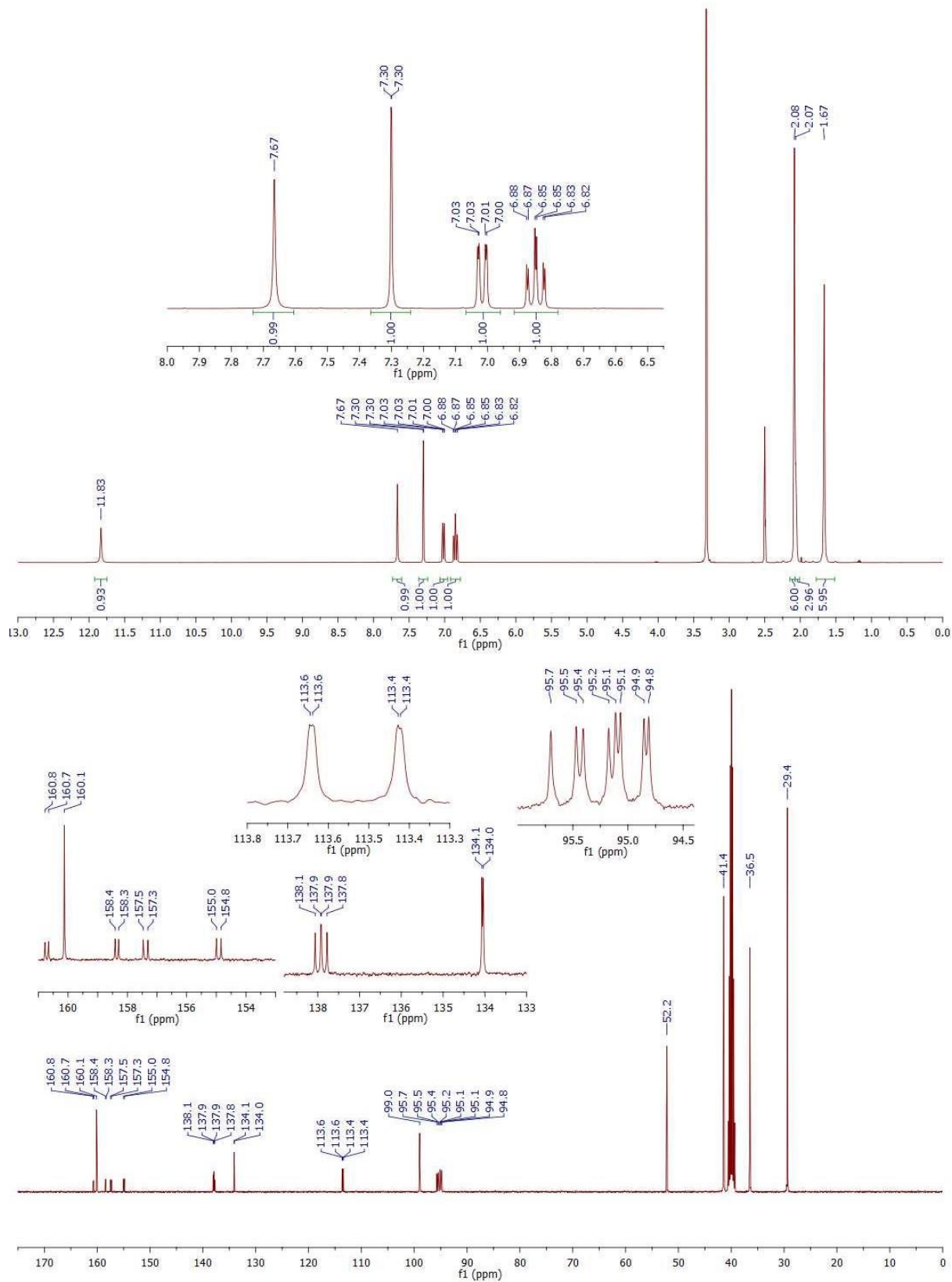
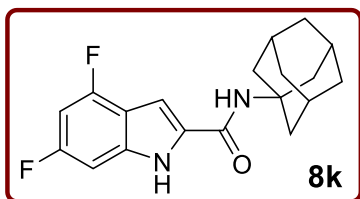


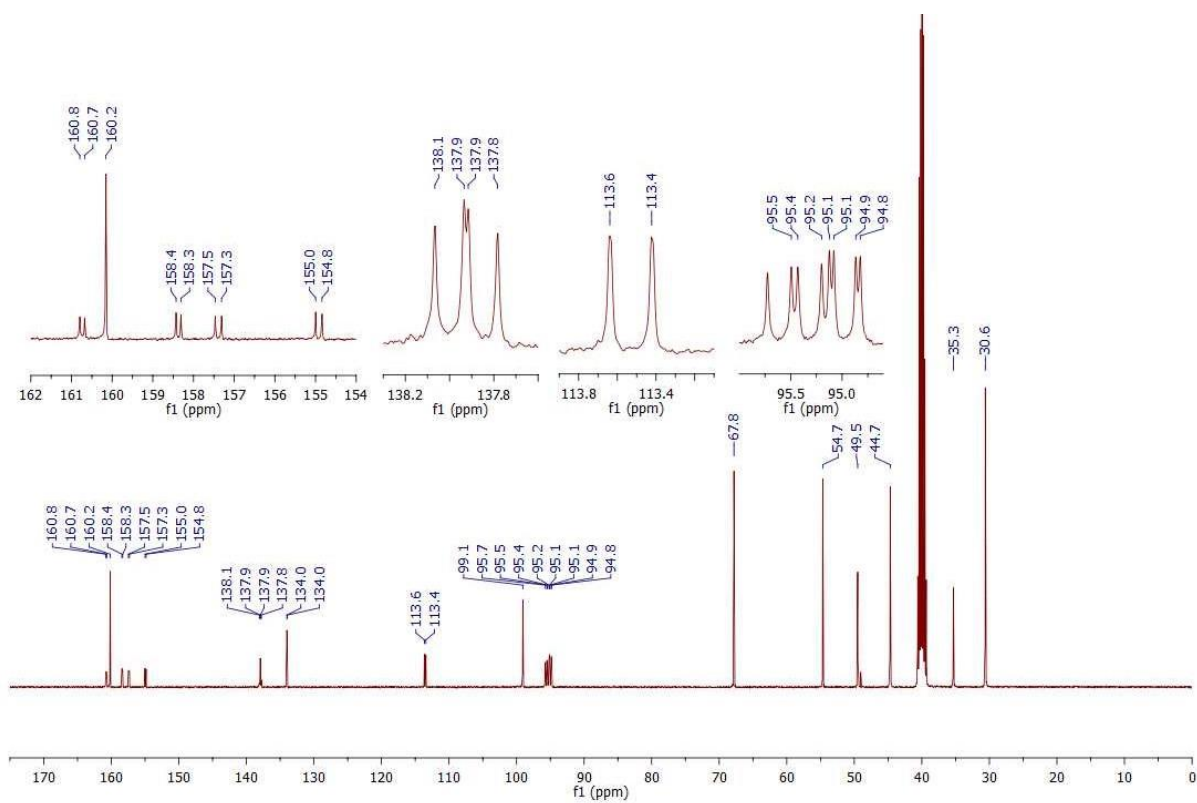
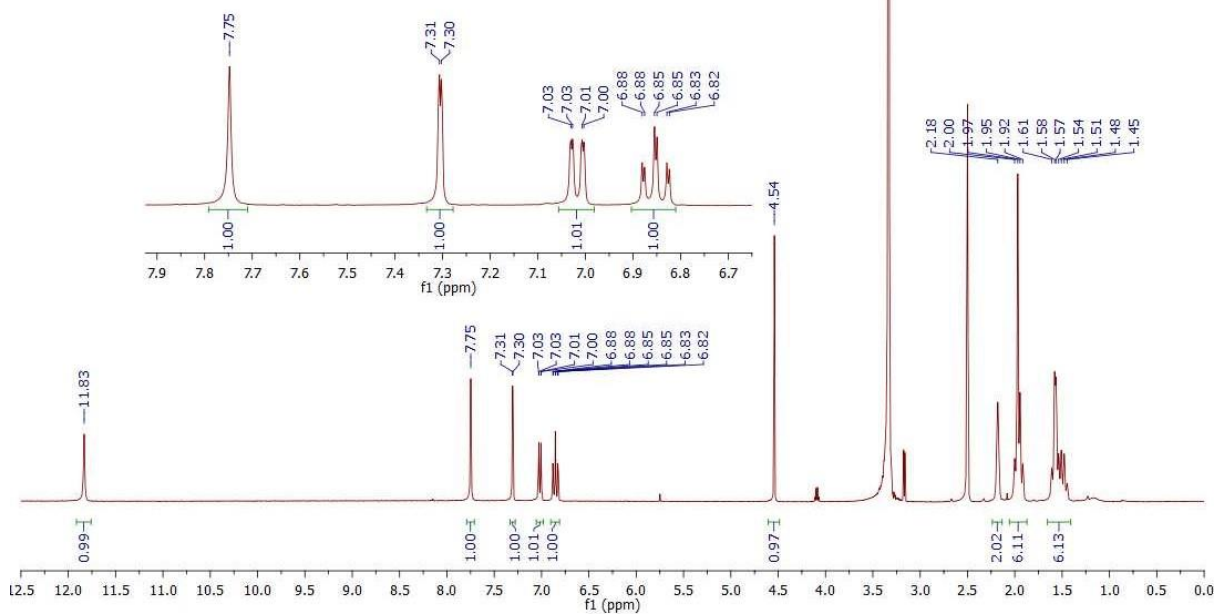
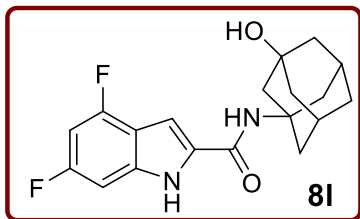




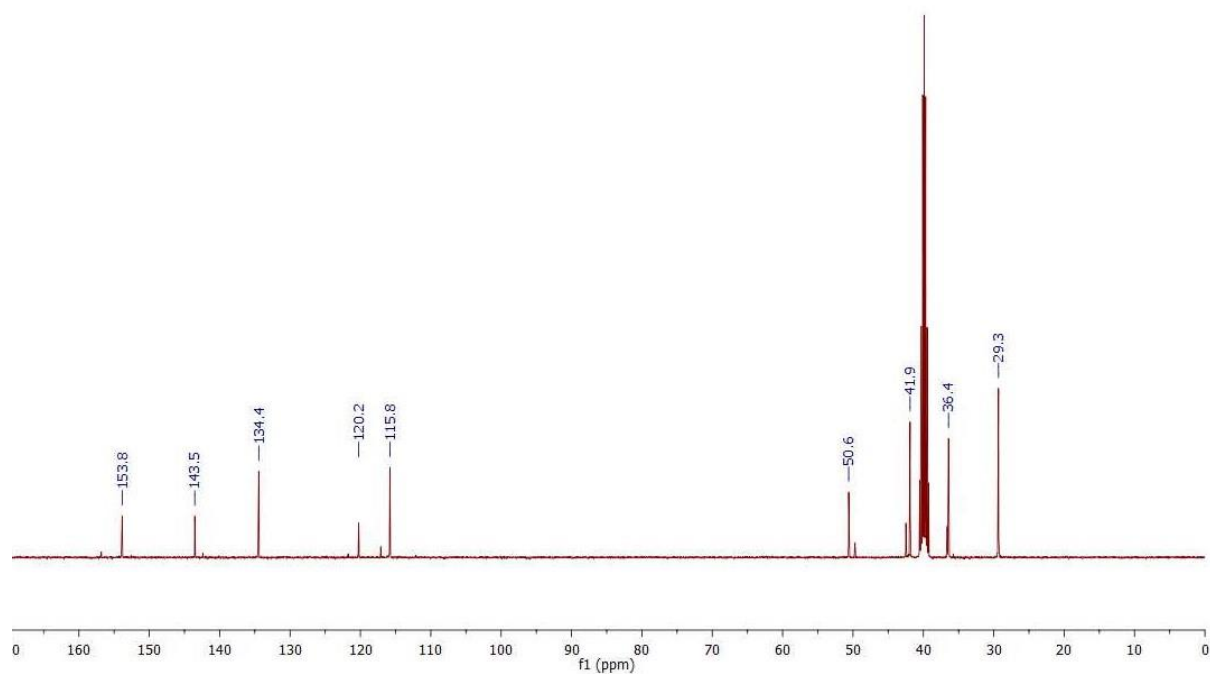
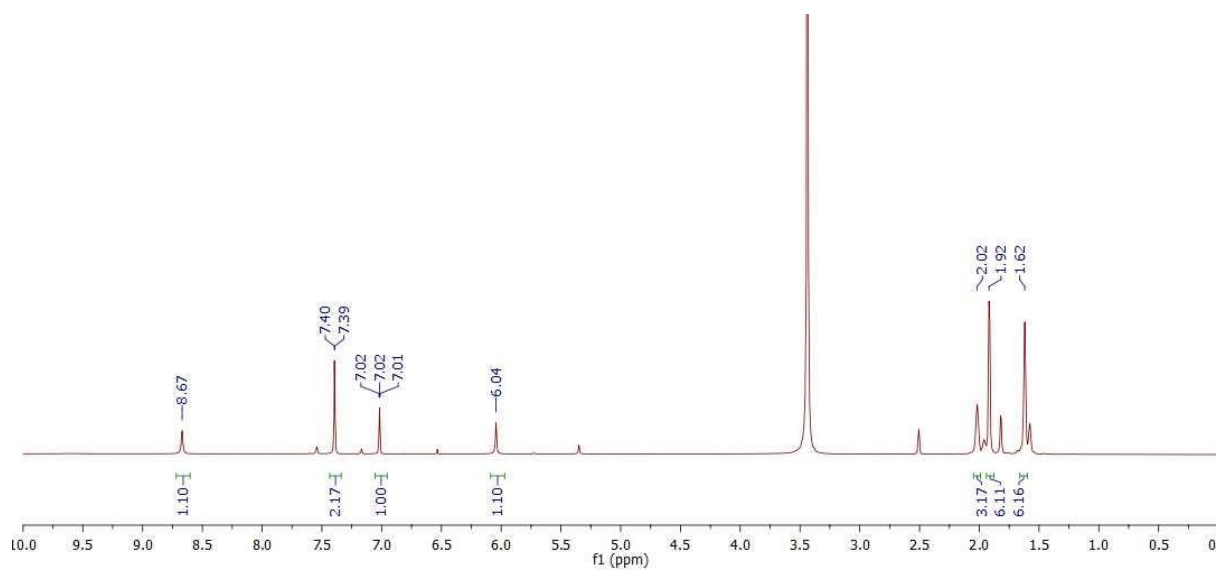
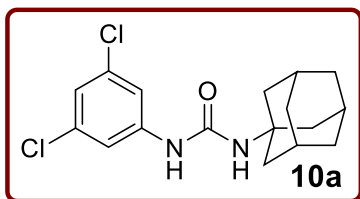


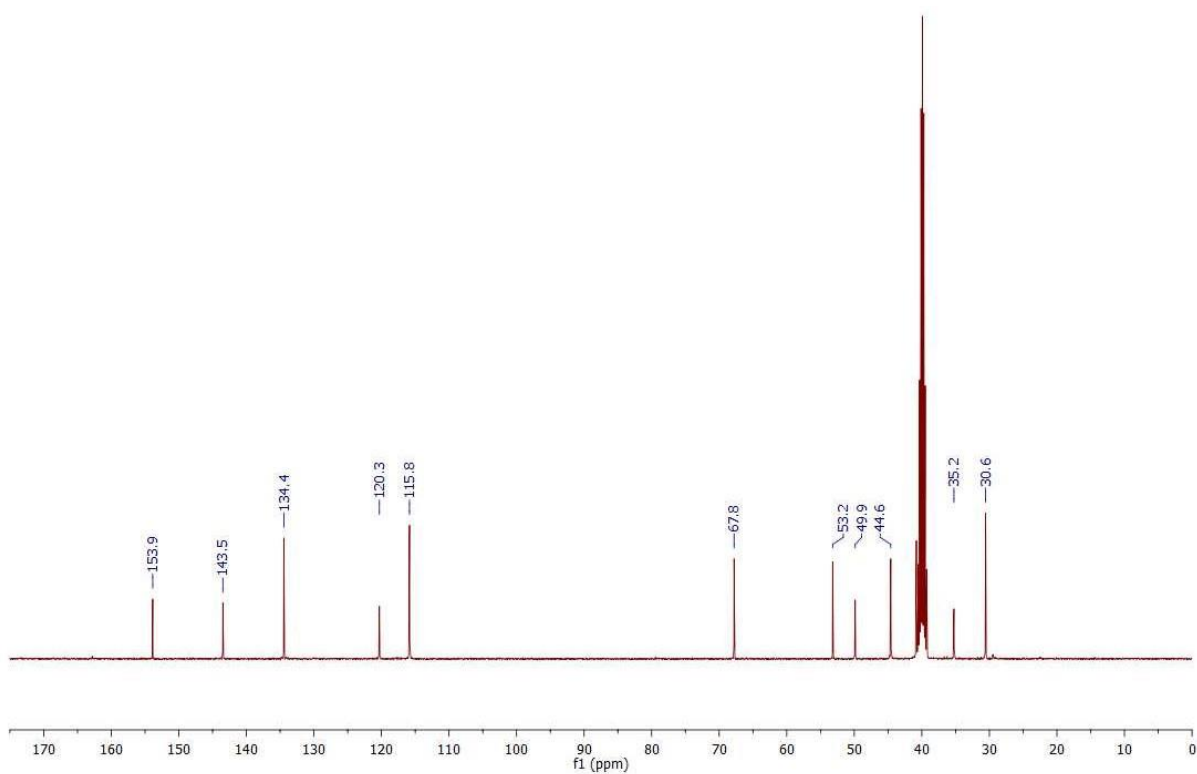
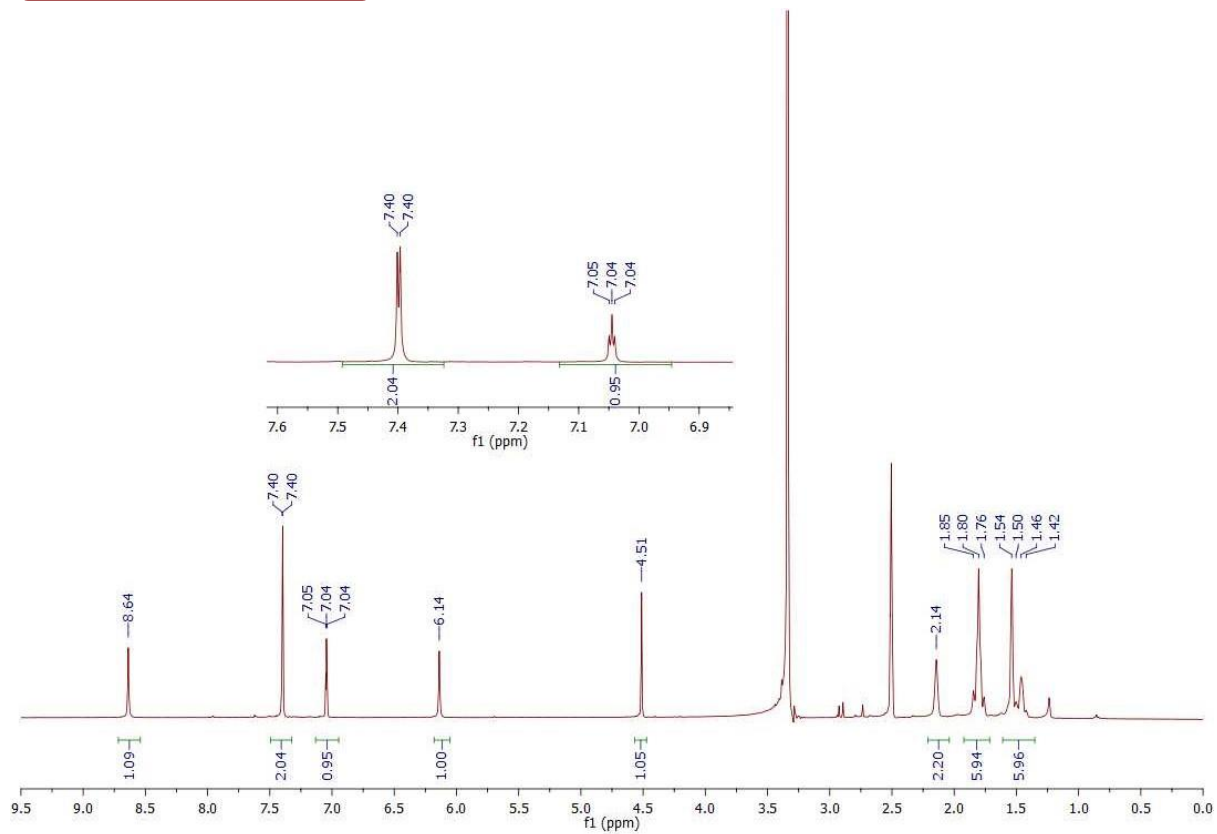
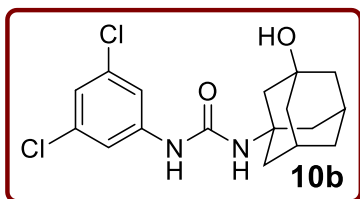


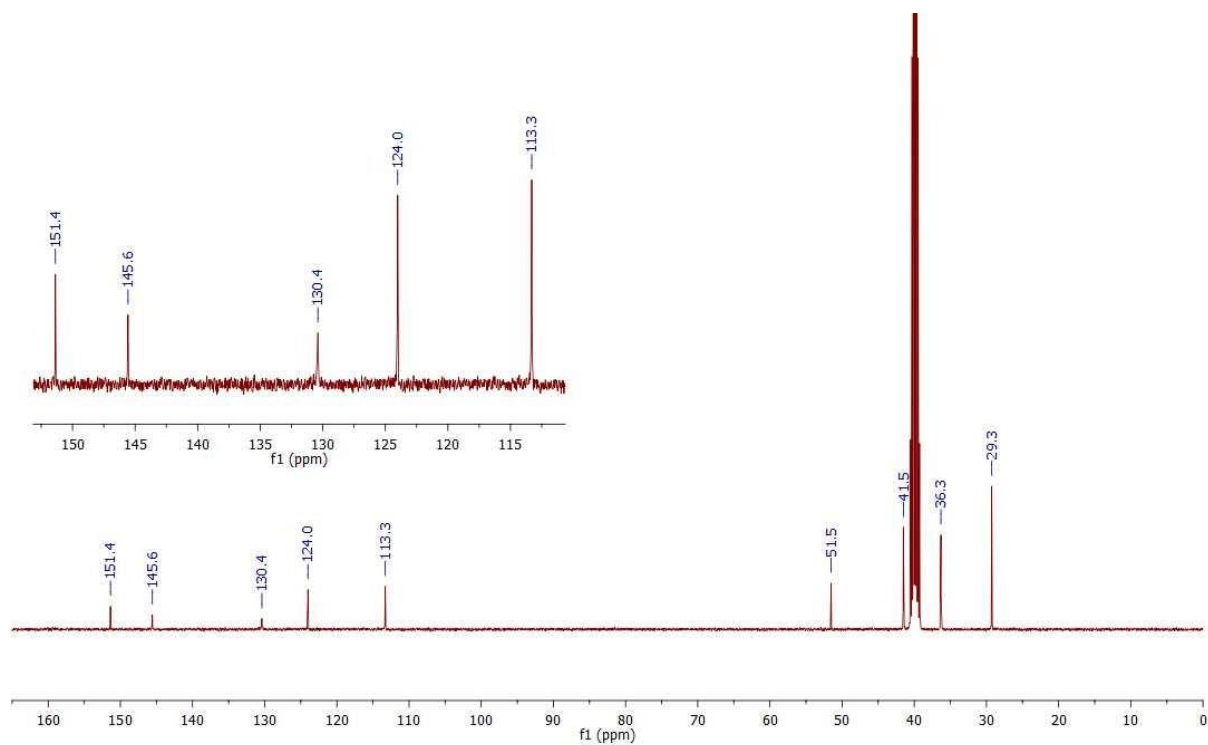
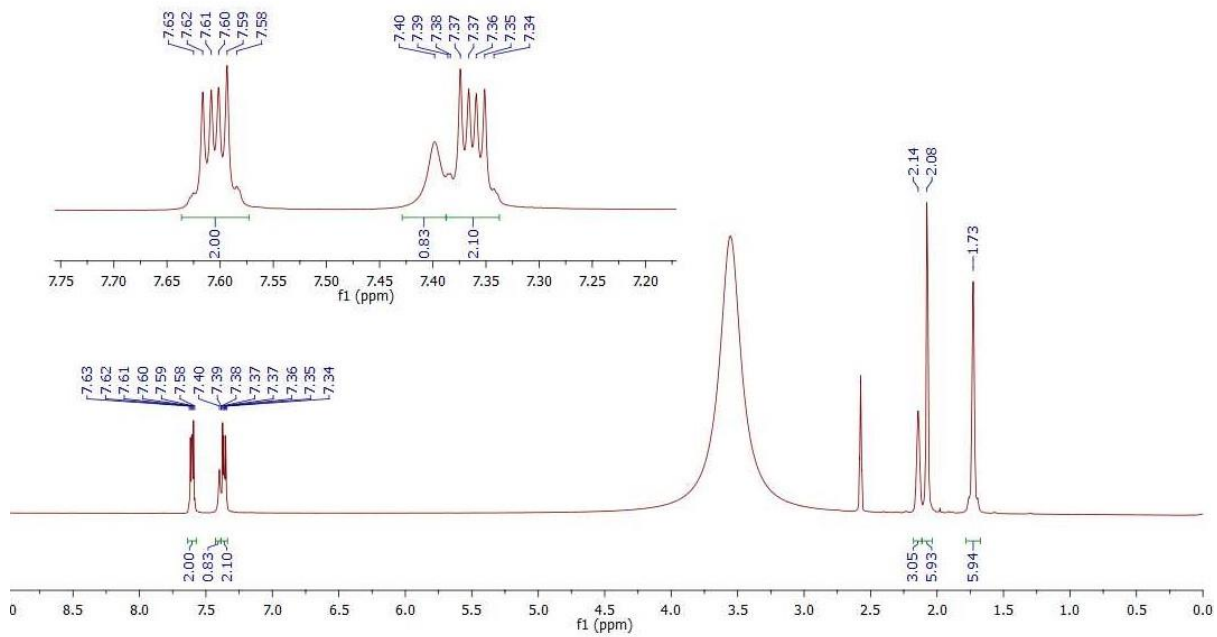
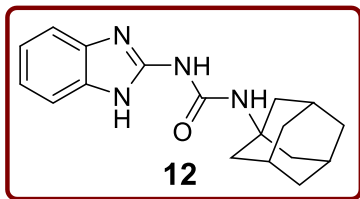


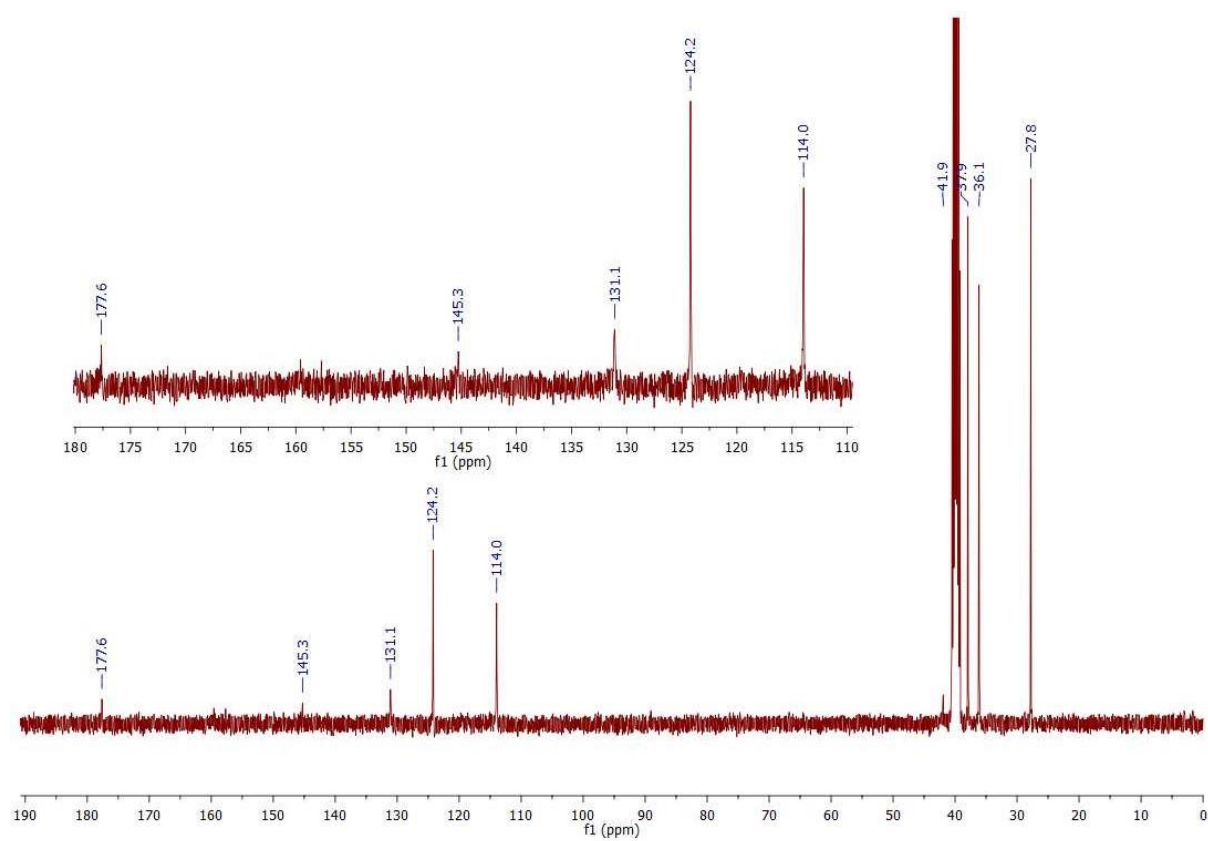
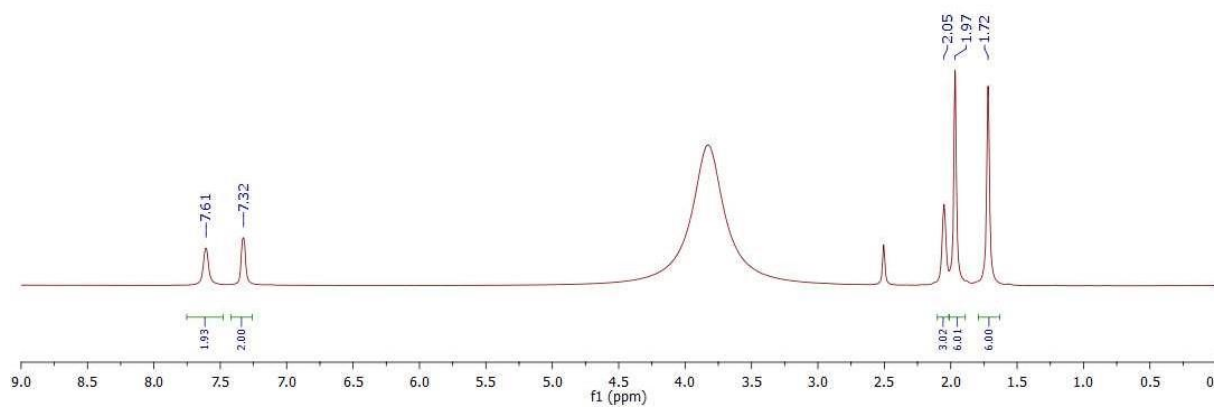
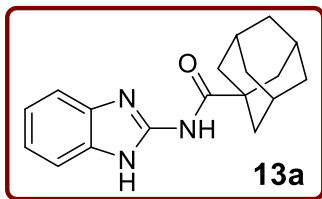


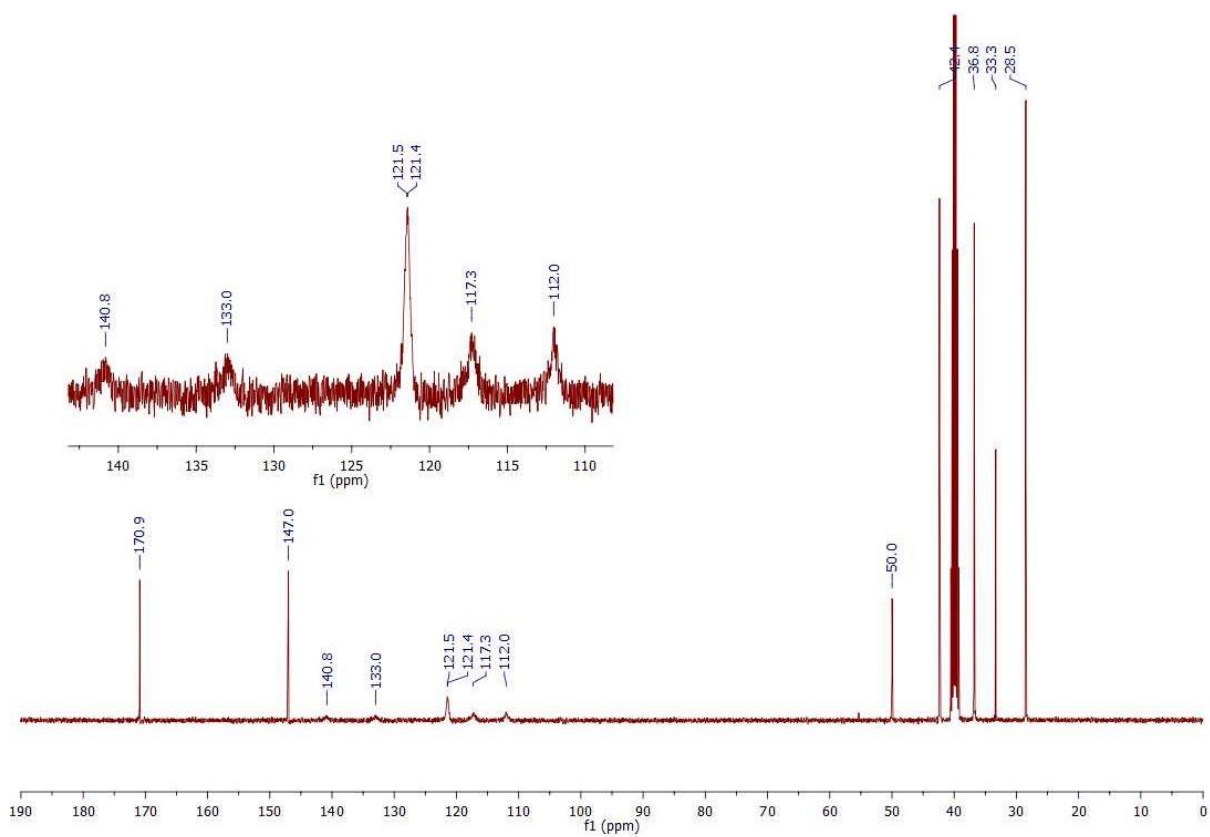
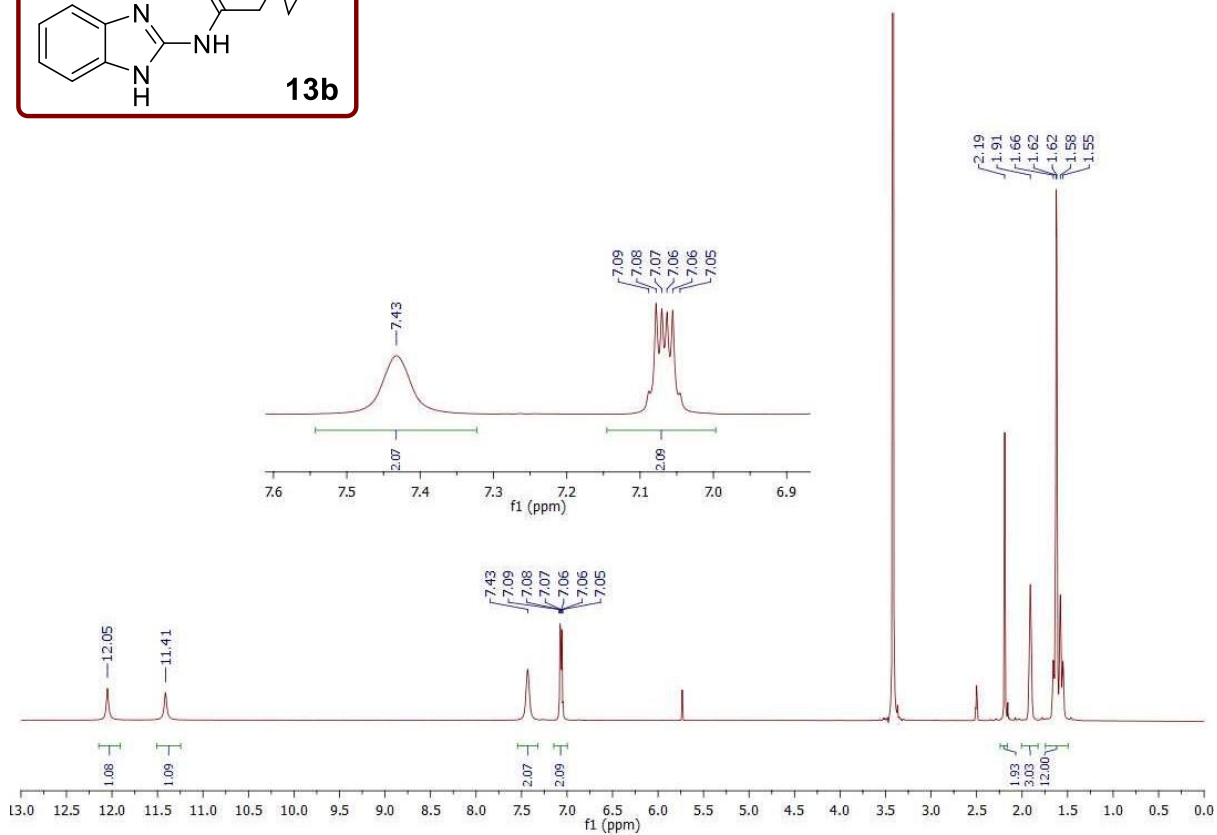
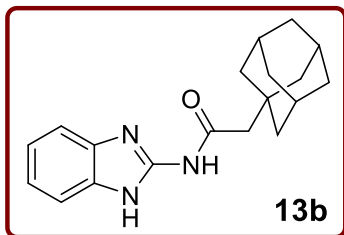




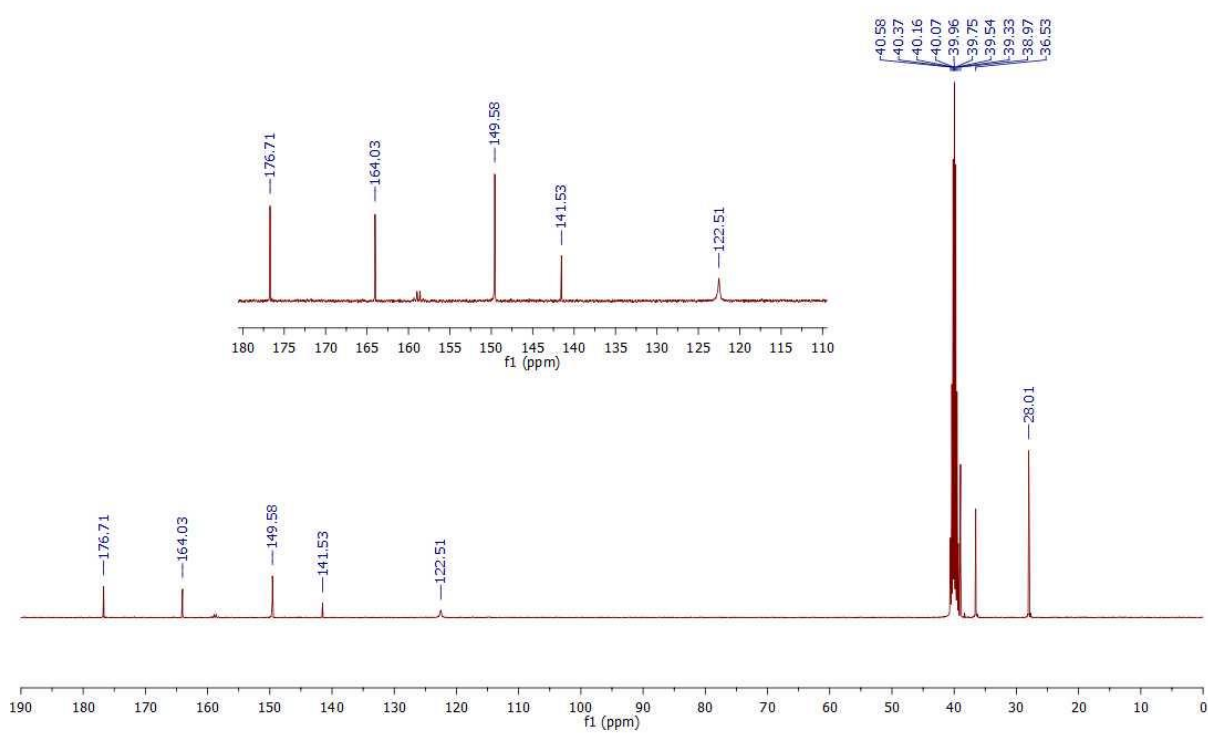
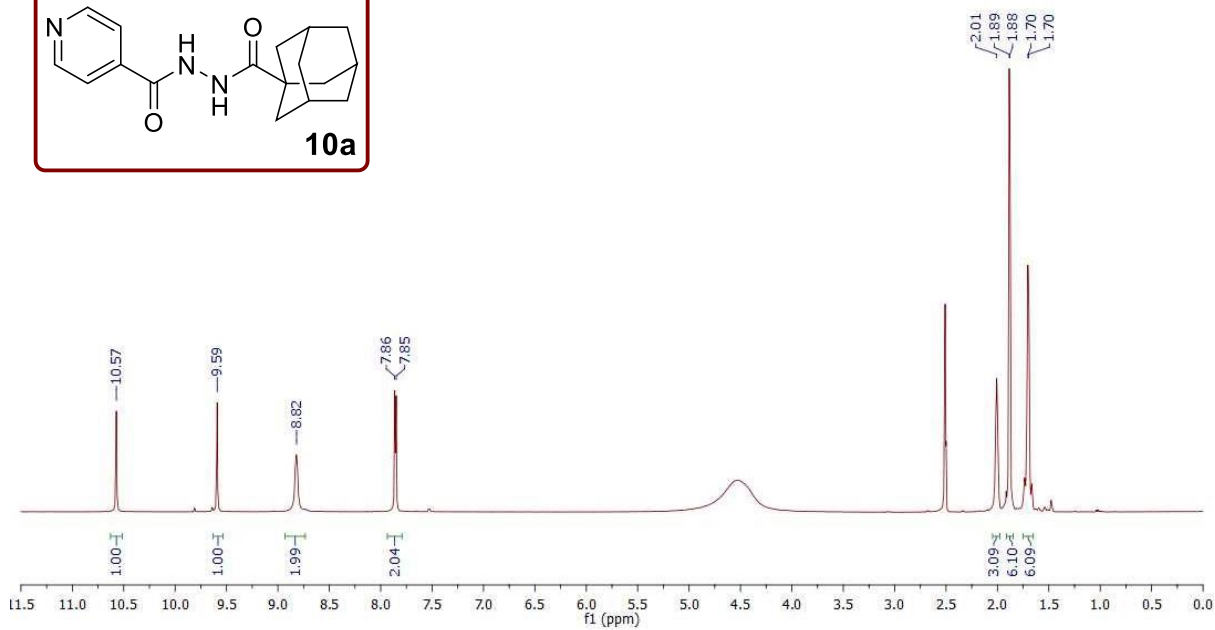
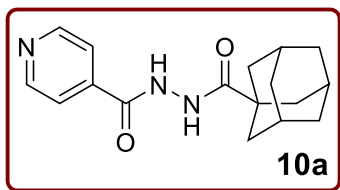


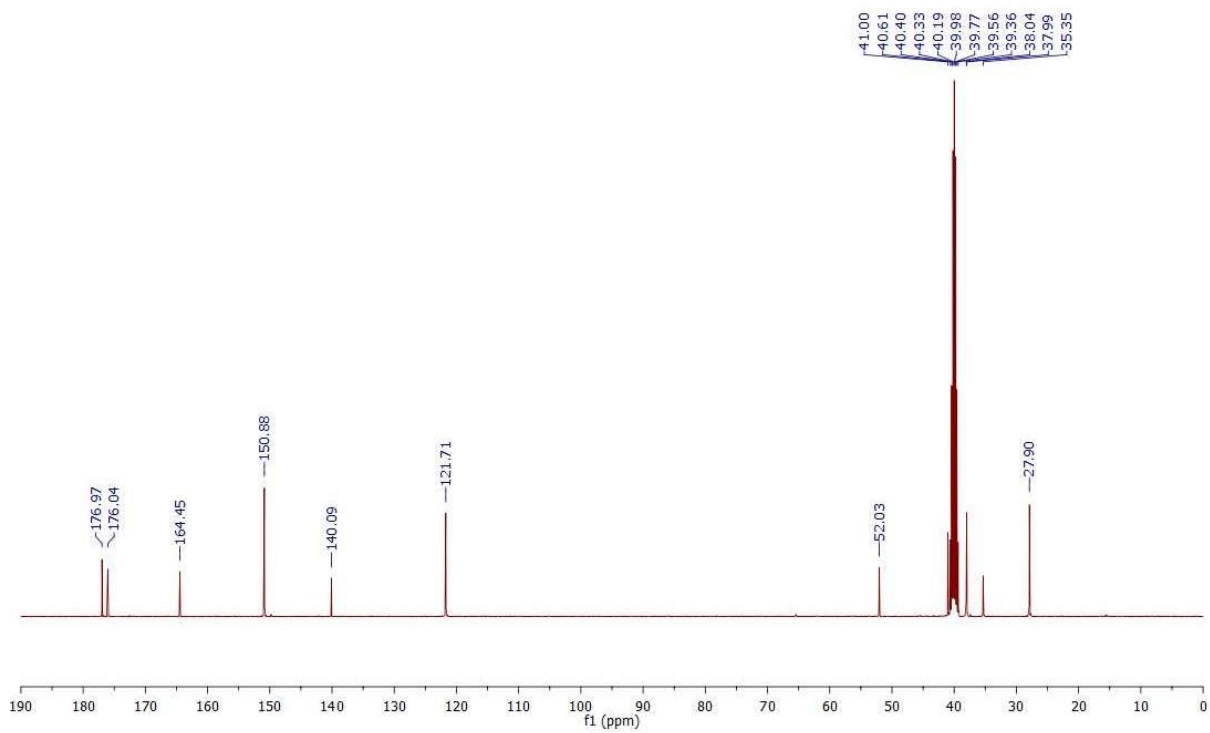
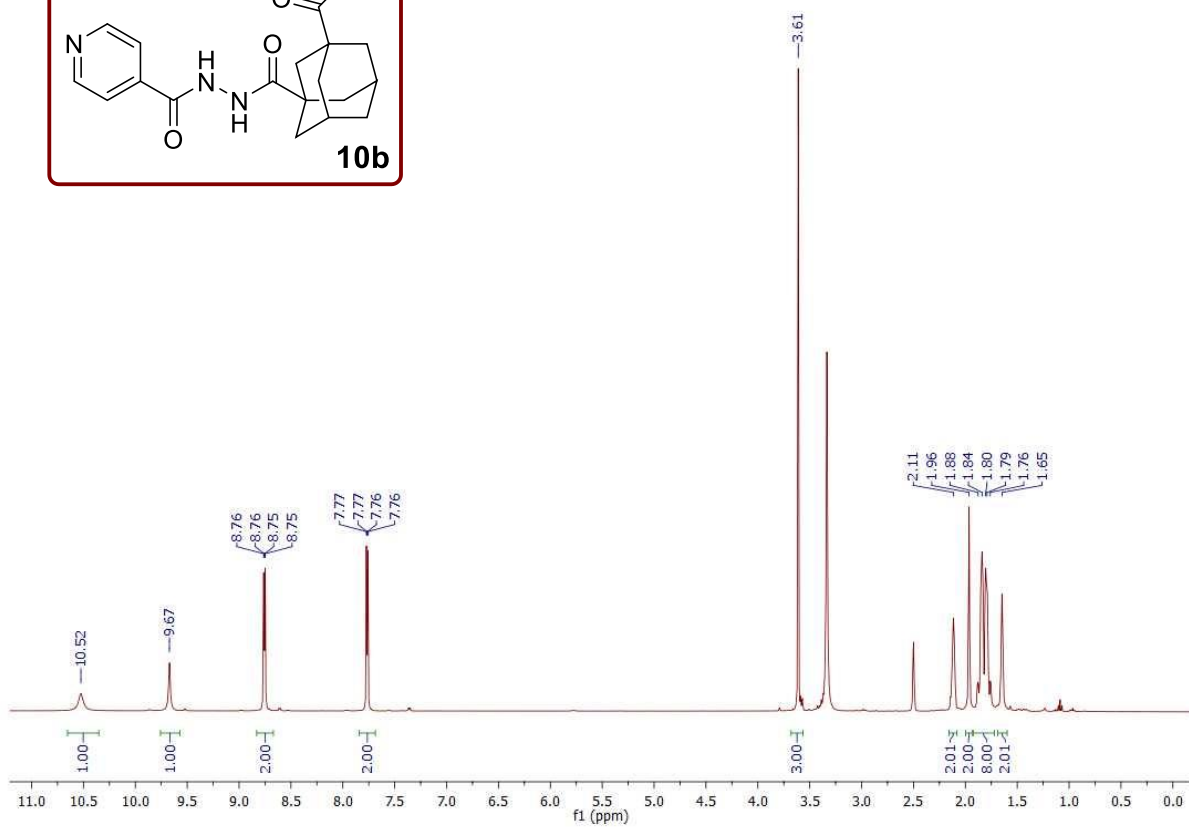
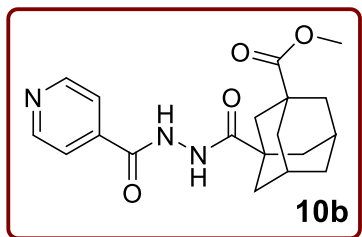




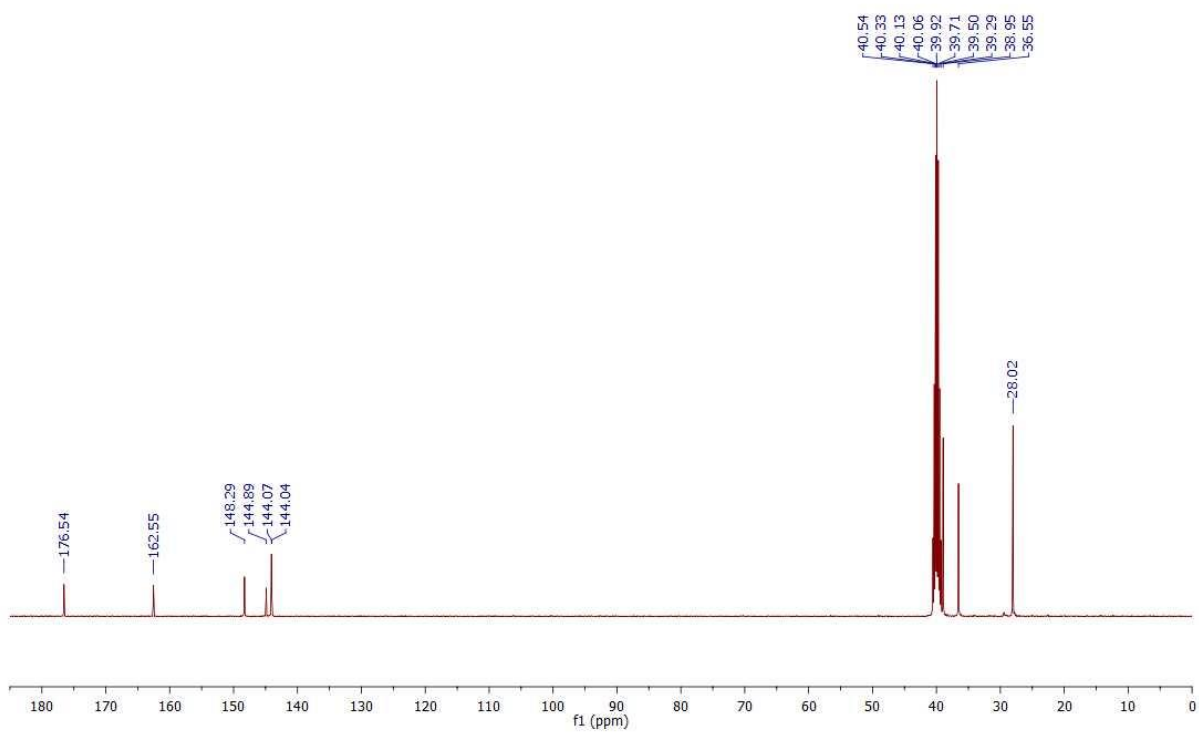
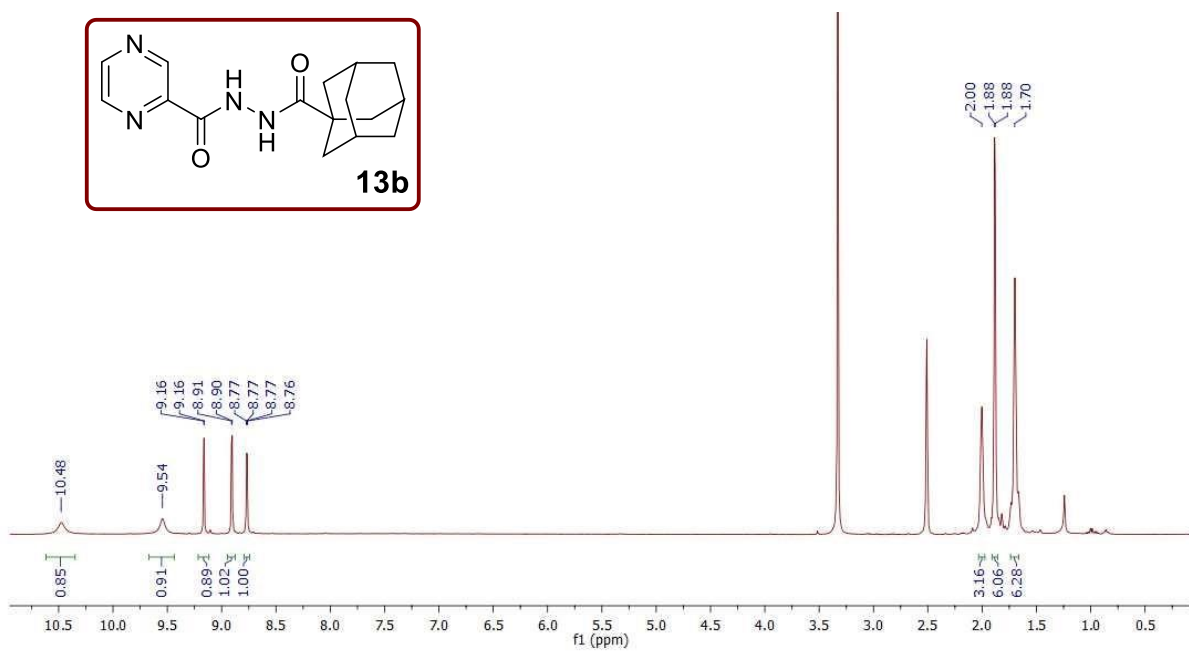
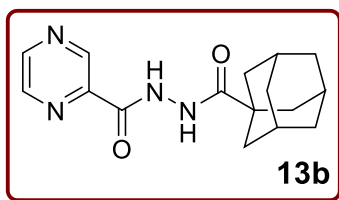


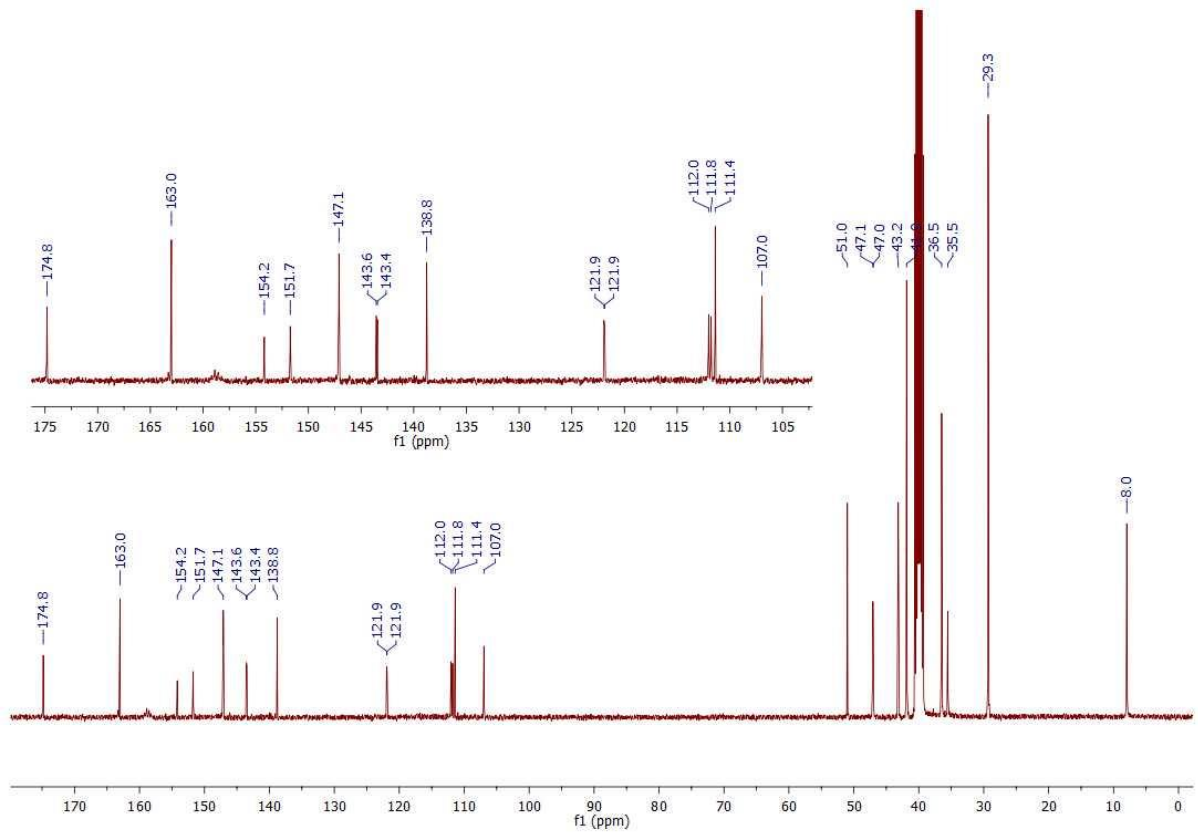
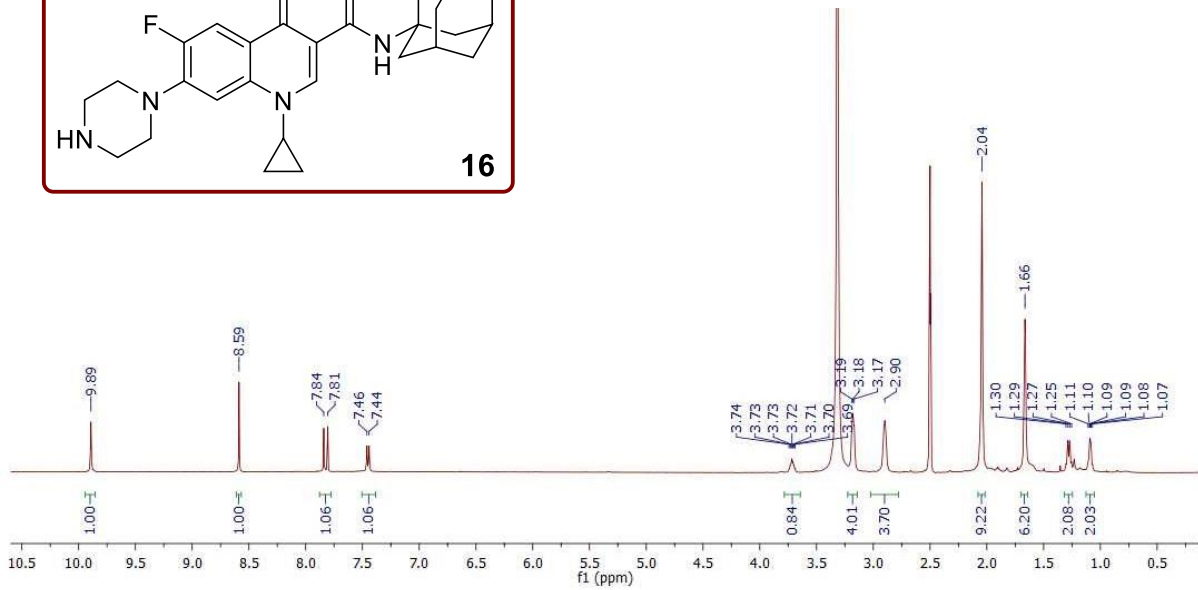
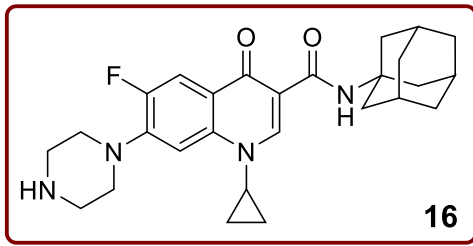
**Supplementary Information – Chapter 5**  
**(Chemical Biology and Drug Design 2021 Article)**

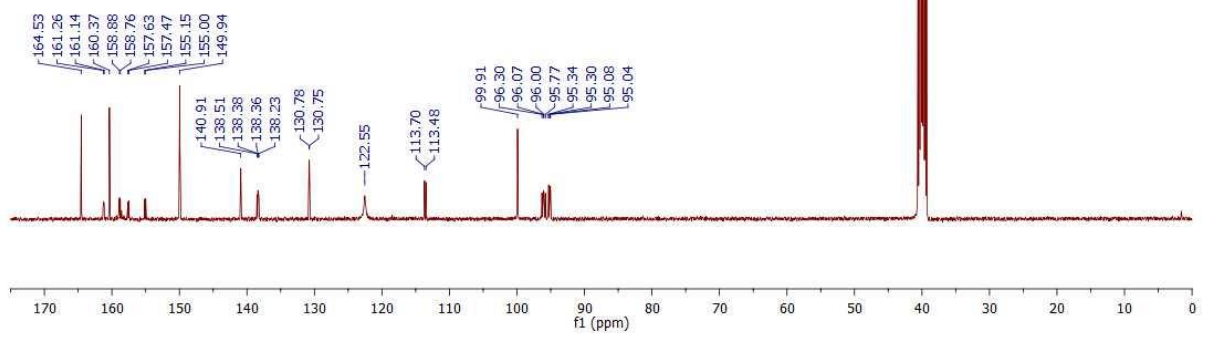
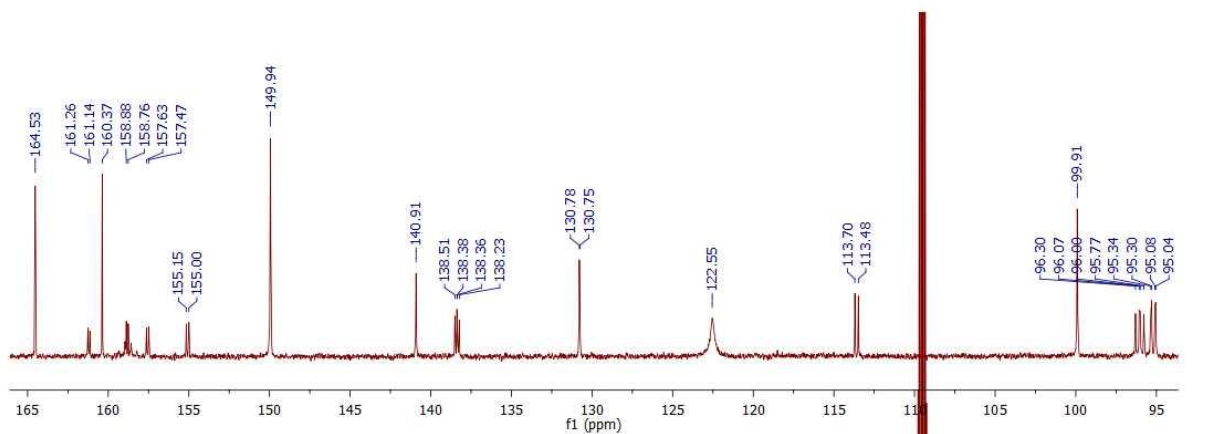
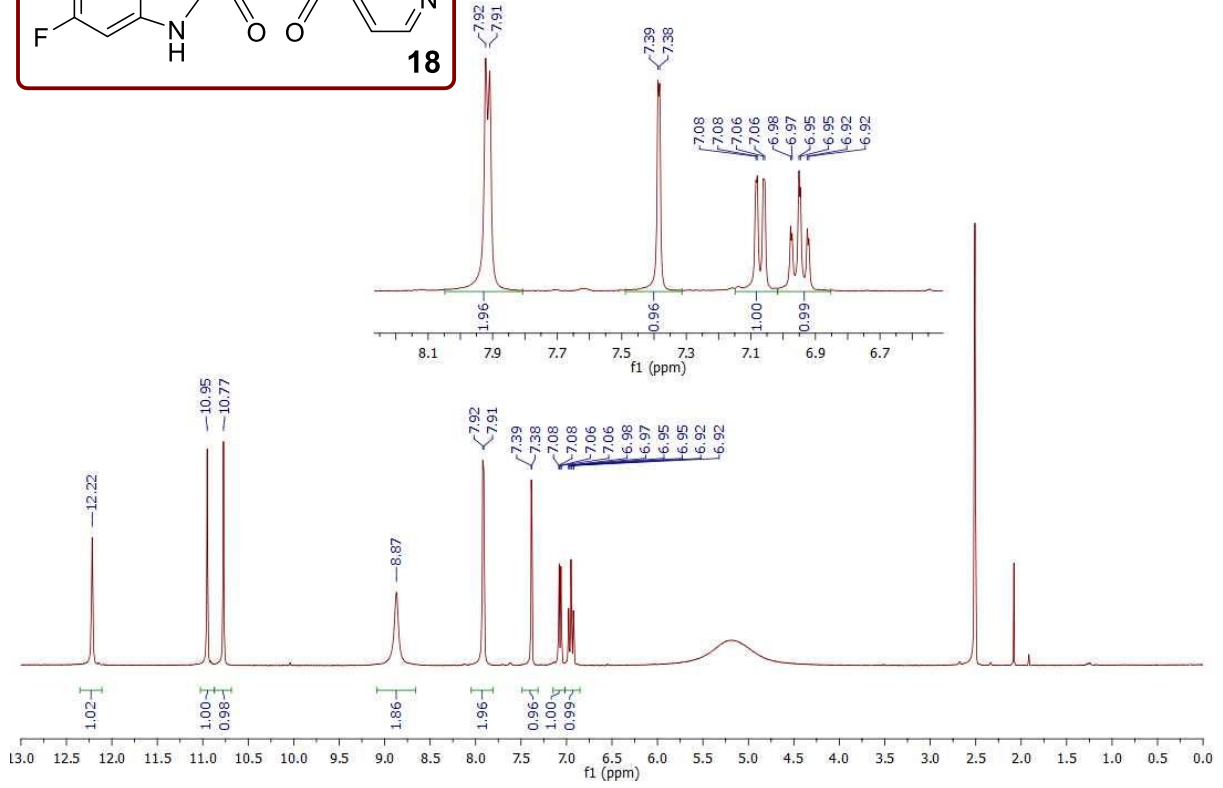
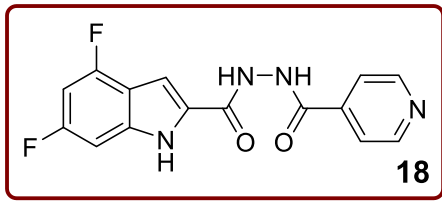


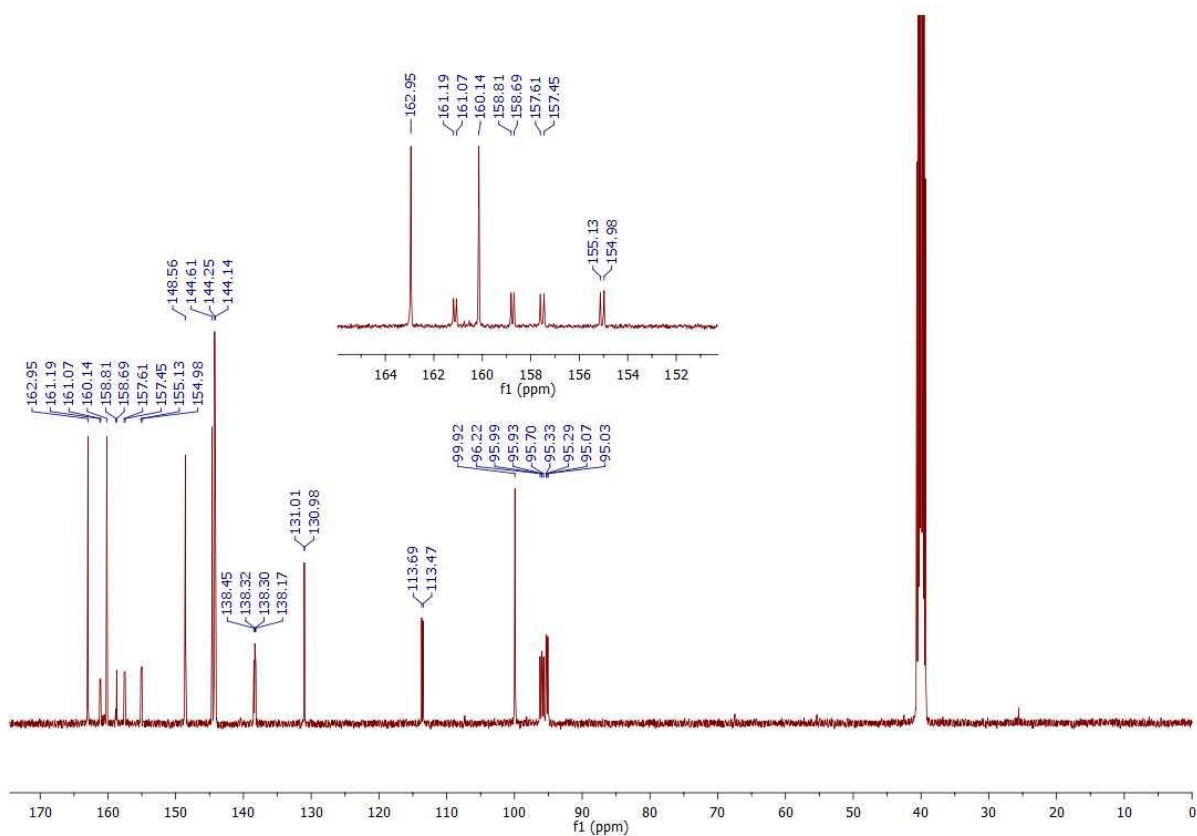
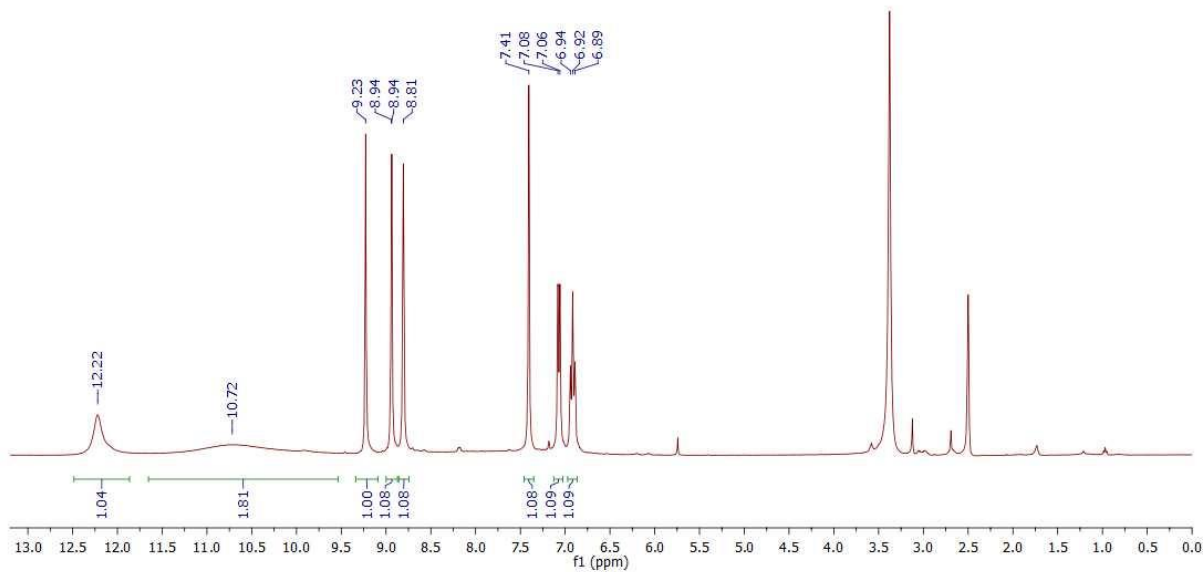
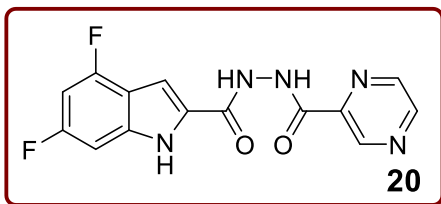


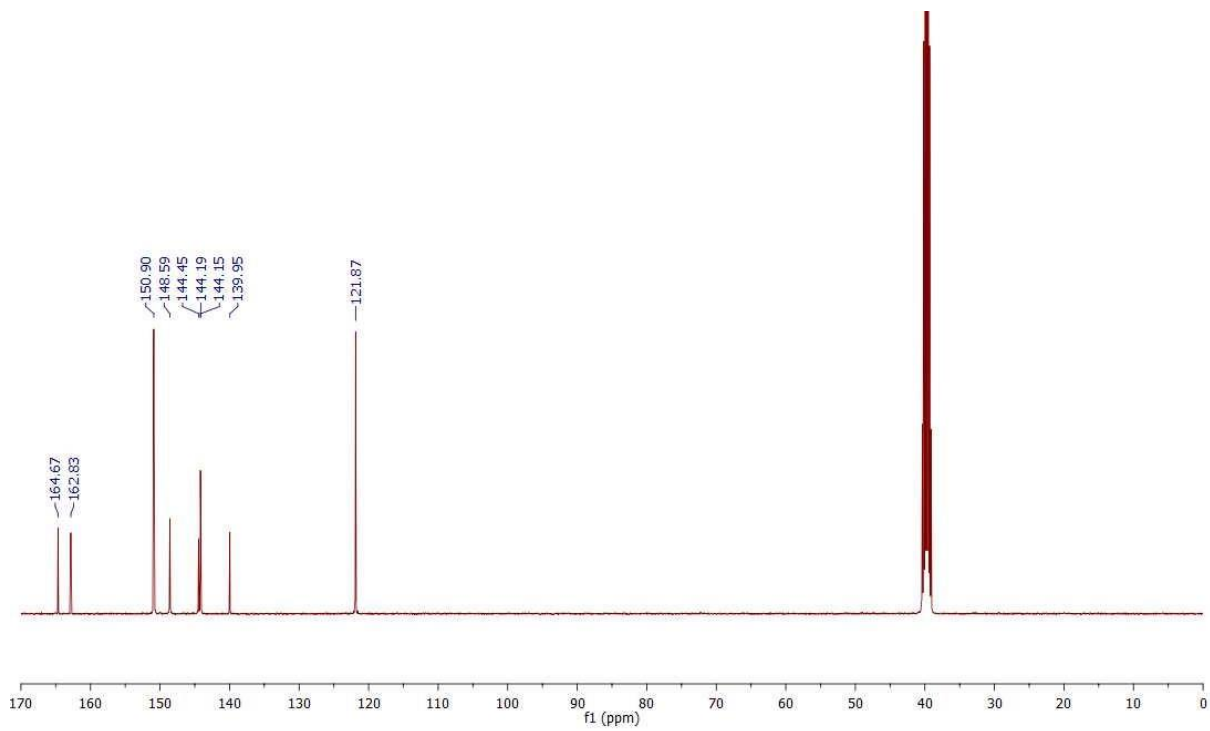
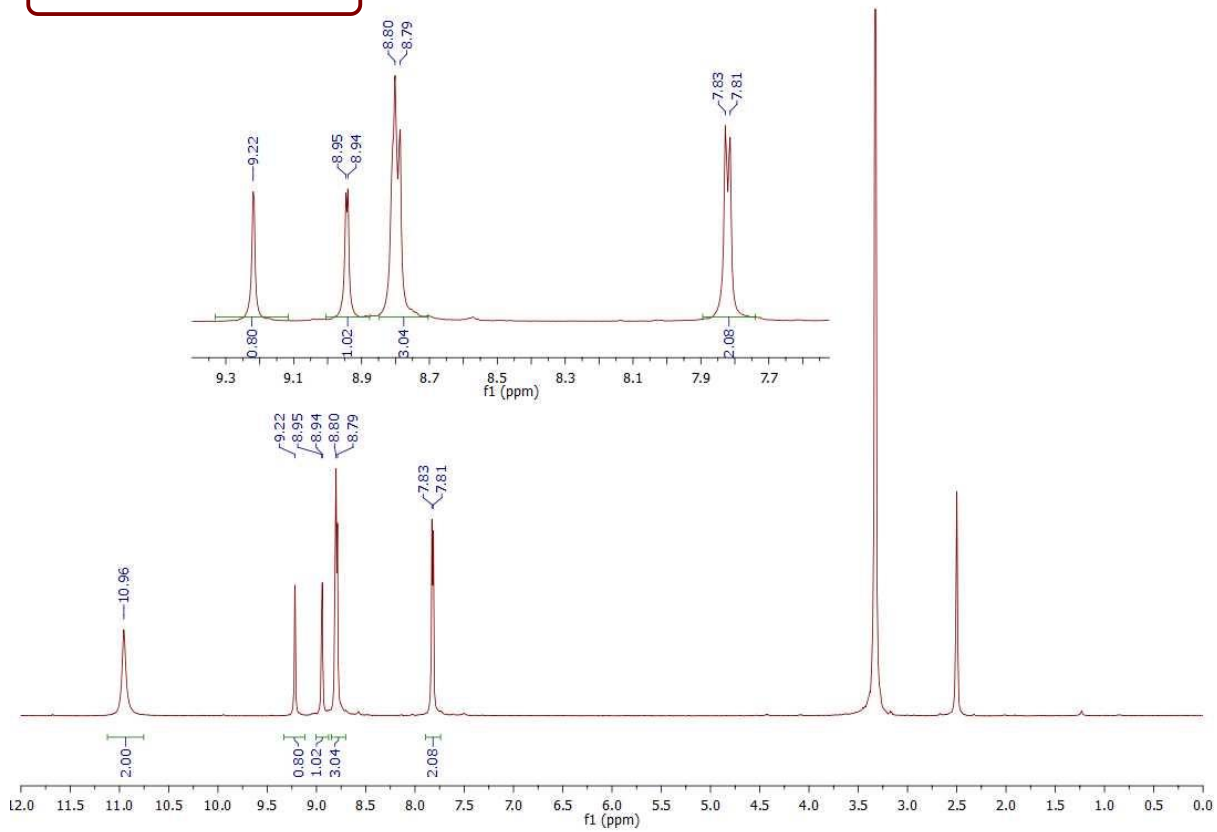
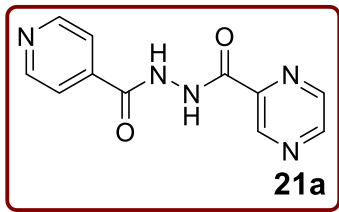


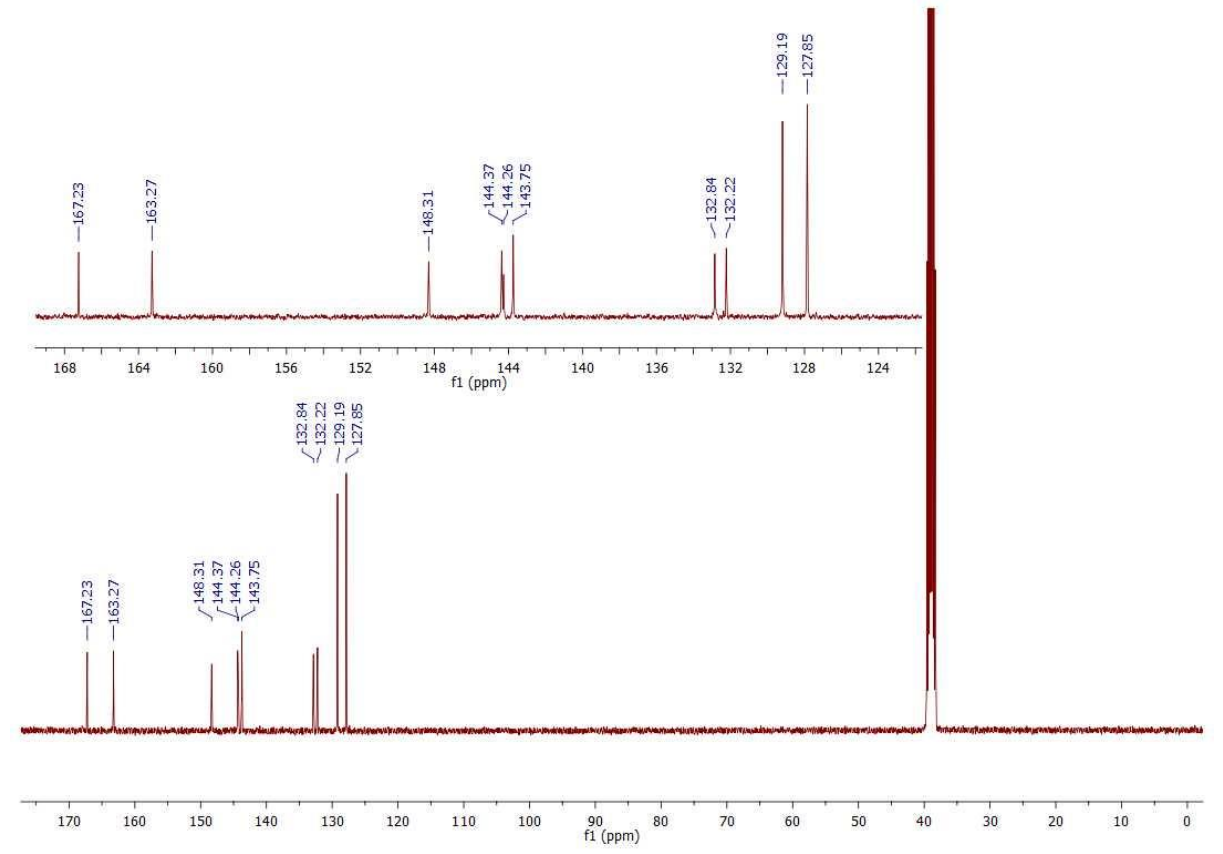
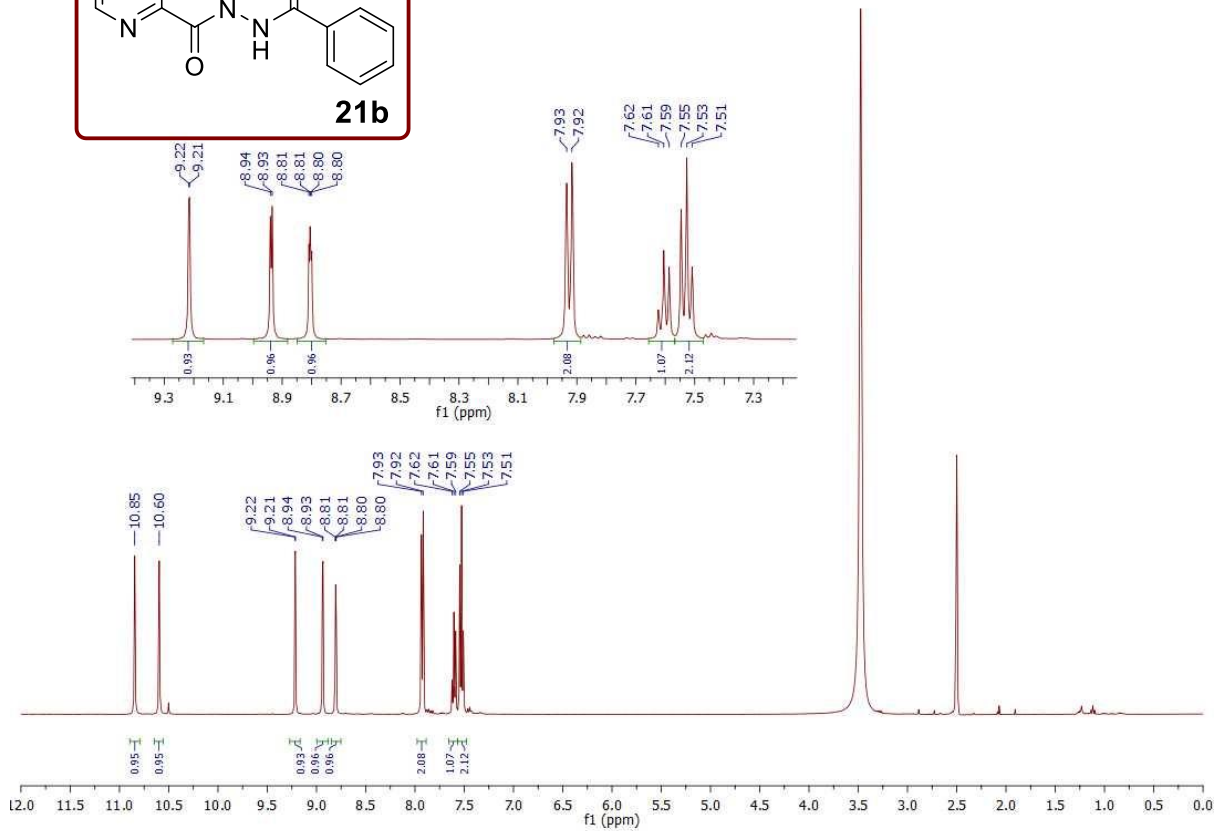
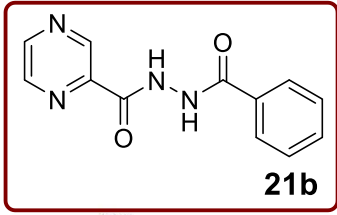












**Supplementary Information – Chapter 6**  
**(RSC Advances 2021 Article)**

Retrieved from: <https://doi.org/10.1039/D0RA10728J>

## **Design, Synthesis and Evaluation of Novel Indole-2-Carboxamides for Growth Inhibition of *Mycobacterium tuberculosis* and Paediatric Brain Tumour Cells**

Shahinda S. R. Alsayed,<sup>a</sup> Shichun Lun,<sup>b</sup> Anders W. Bailey,<sup>c</sup> Amreena Suri,<sup>c</sup> Chiang-Ching Huang,<sup>d</sup> Mauro Mocerino,<sup>e</sup> Alan Payne,<sup>e</sup> Simone Treiger Sredni,<sup>c,f,\*</sup> William R. Bishai,<sup>b,g,\*</sup> and Hendra Gunosewoyo<sup>a,\*</sup>

<sup>a</sup> Curtin Medical School, Faculty of Health Sciences, Curtin University, Bentley, Perth, WA 6102, Australia

<sup>b</sup> Center for Tuberculosis Research, Department of Medicine, Division of Infectious Disease, Johns Hopkins School of Medicine, 1550, Orleans Street, Baltimore, Maryland, 21231-1044, United States

<sup>c</sup> Division of Pediatric Neurosurgery, Ann and Robert H. Lurie Children's Hospital of Chicago, Chicago, IL 60611, USA

<sup>d</sup> Department of Biostatistics, Zilber School of Public Health, University of Wisconsin, Milwaukee, WI 53205, USA

<sup>e</sup> School of Molecular and Life Sciences, Curtin University, Perth, WA 6102, Australia

<sup>f</sup> Department of Surgery, Northwestern University, Feinberg School of Medicine, Chicago, IL 60611, USA

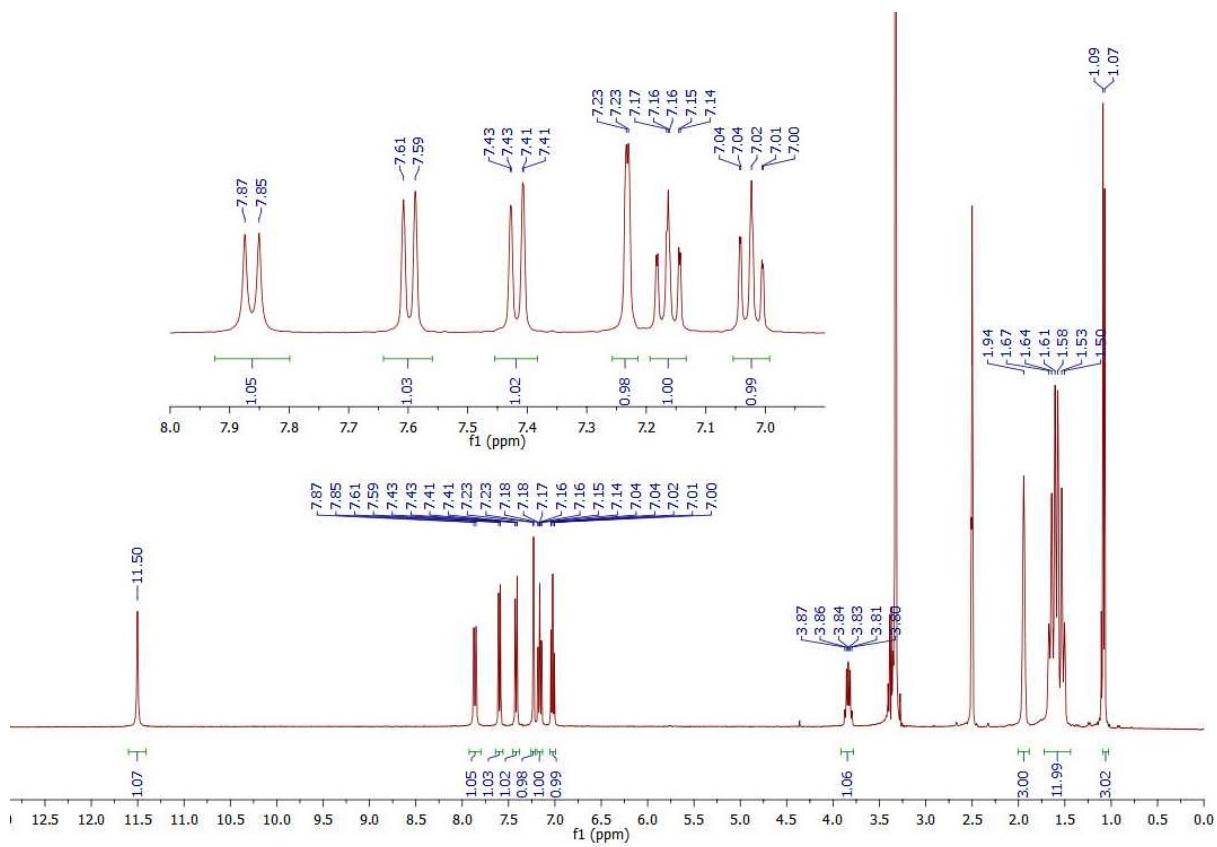
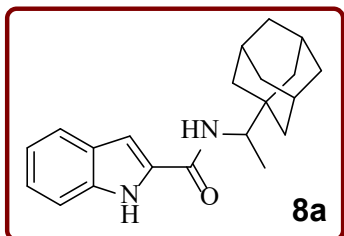
<sup>g</sup> Howard Hughes Medical Institute, 4000 Jones Bridge Road, Chevy Chase, Maryland, 20815-6789, United States

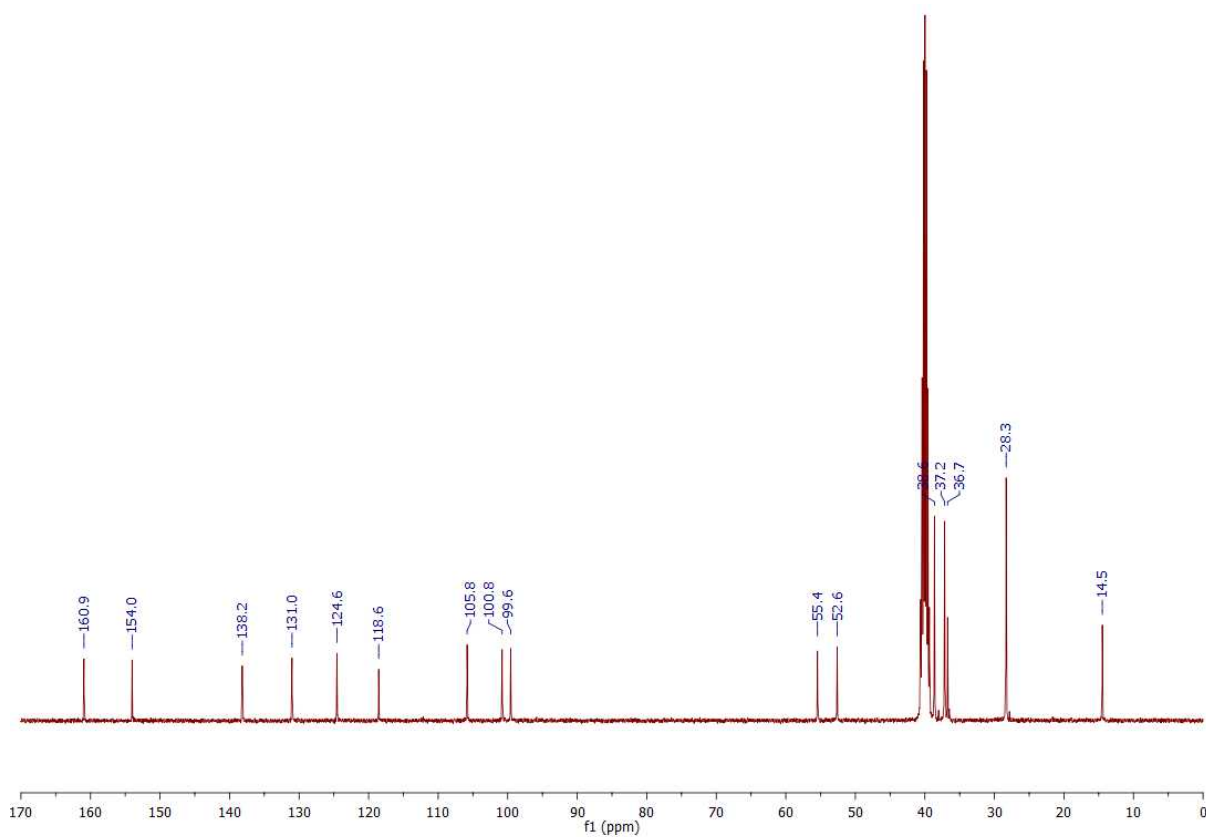
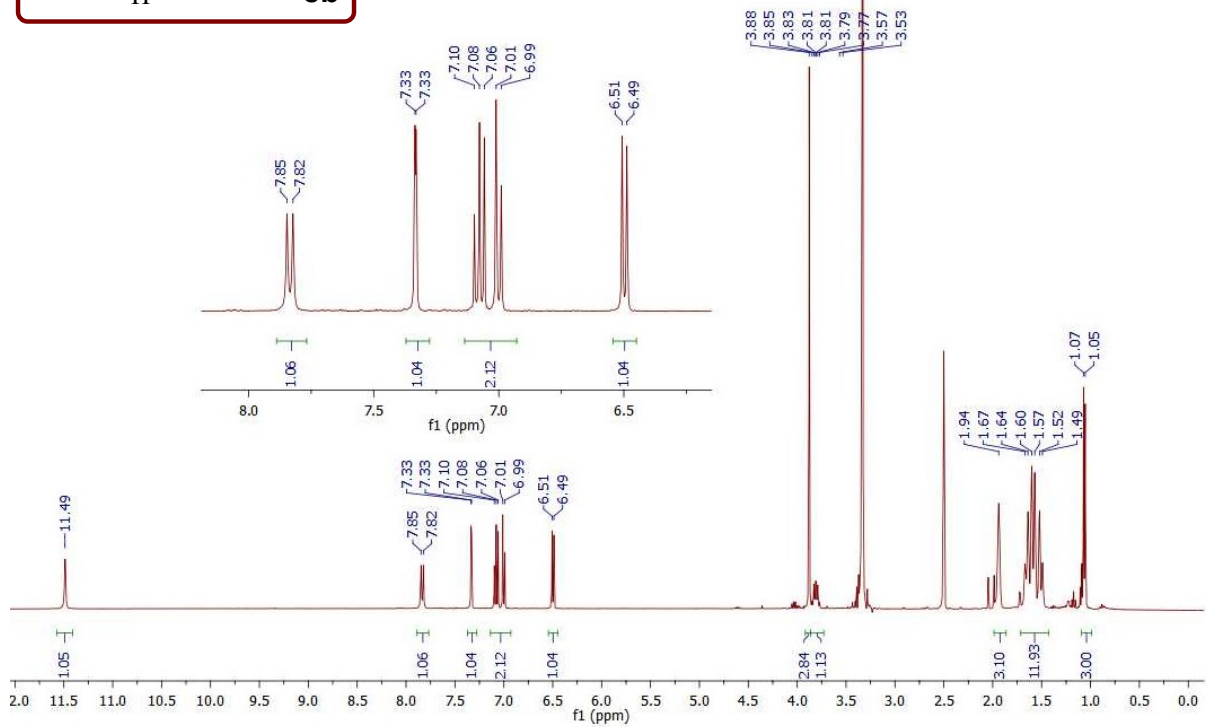
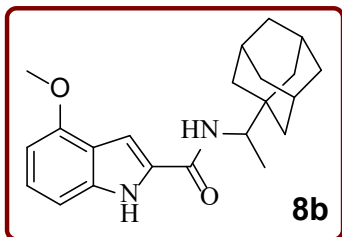
\* Corresponding author. Hendra Gunosewoyo: [Hendra.Gunosewoyo@curtin.edu.au](mailto:Hendra.Gunosewoyo@curtin.edu.au)

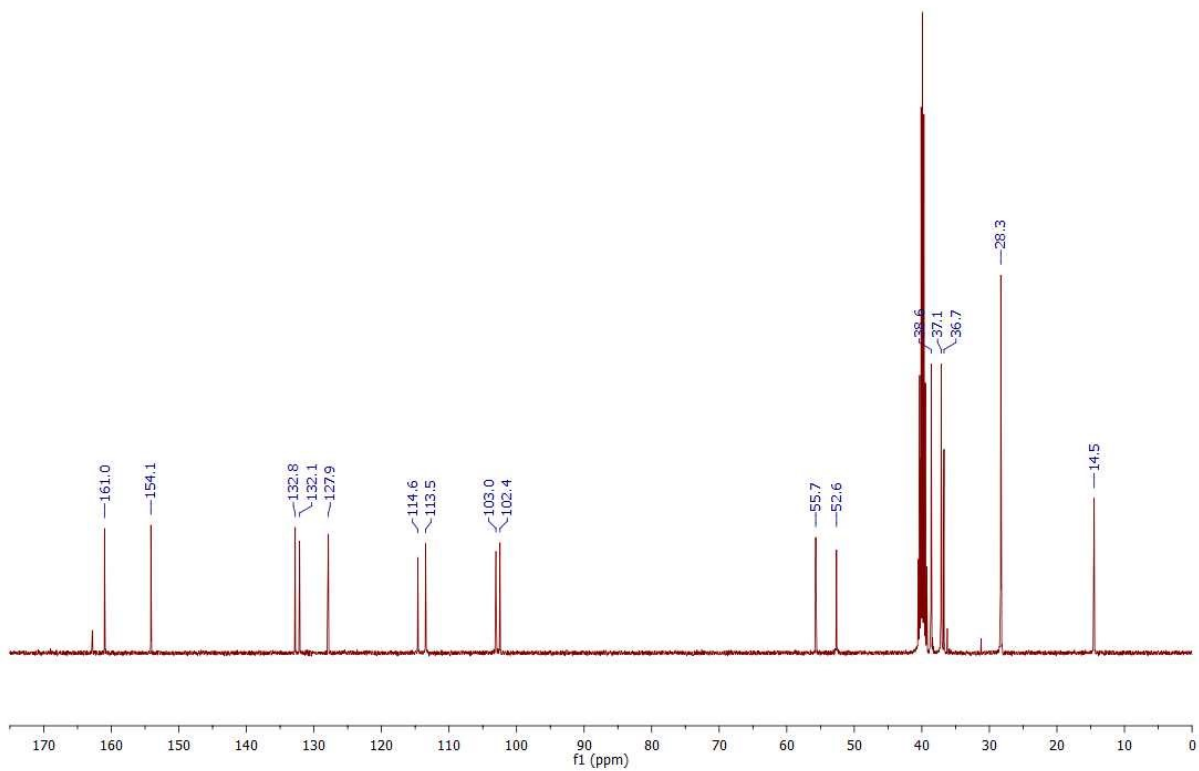
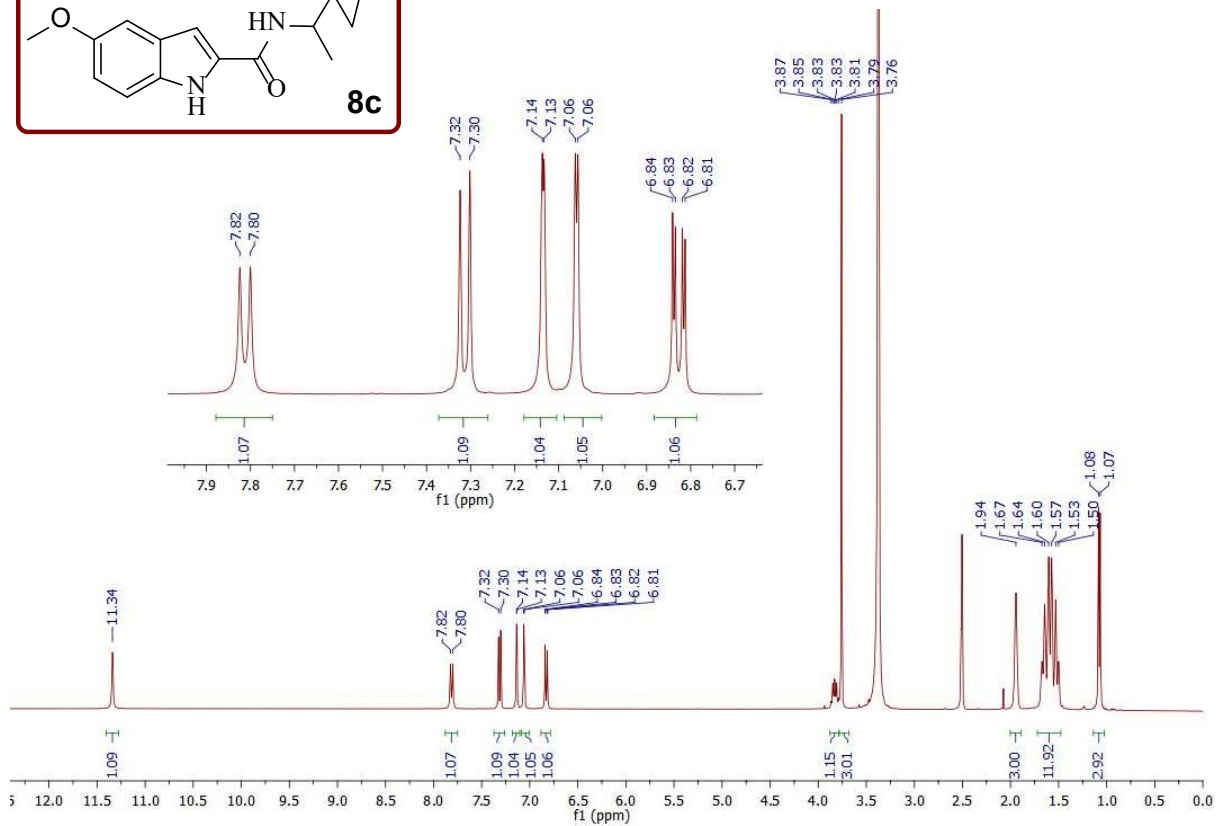
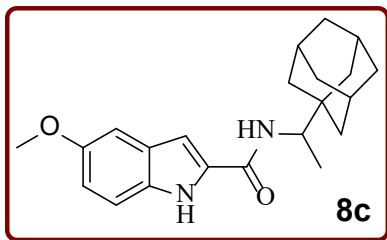
\* Corresponding author. William R. Bishai: [wbishai1@jhmi.edu](mailto:wbishai1@jhmi.edu)

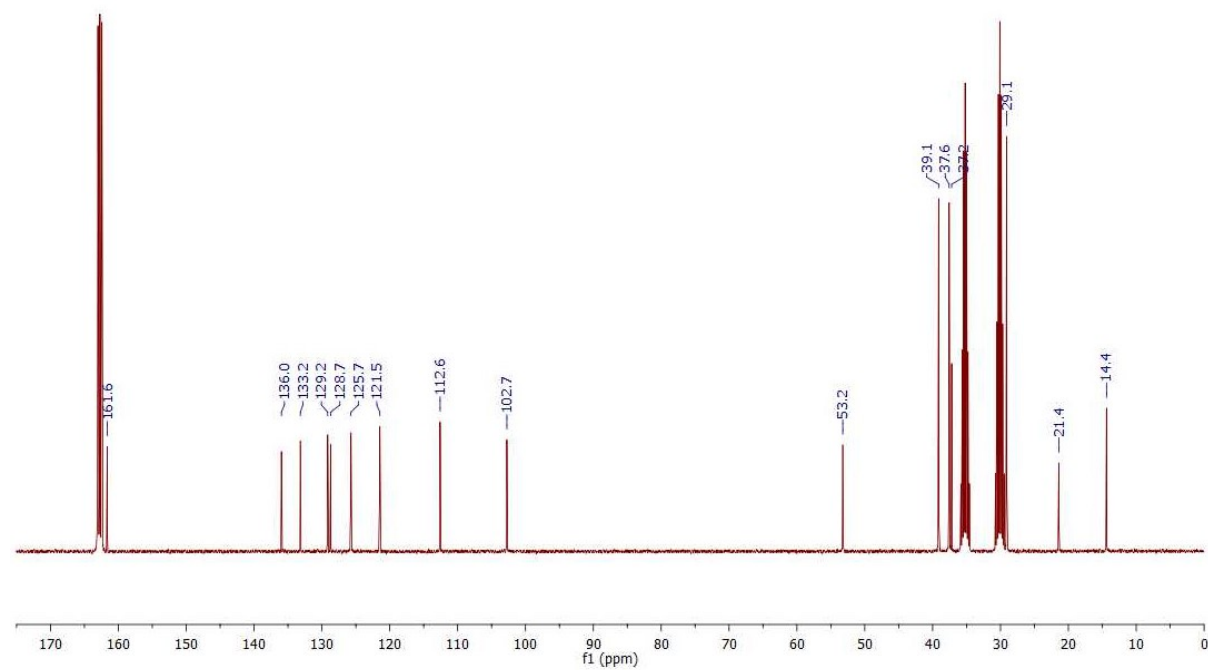
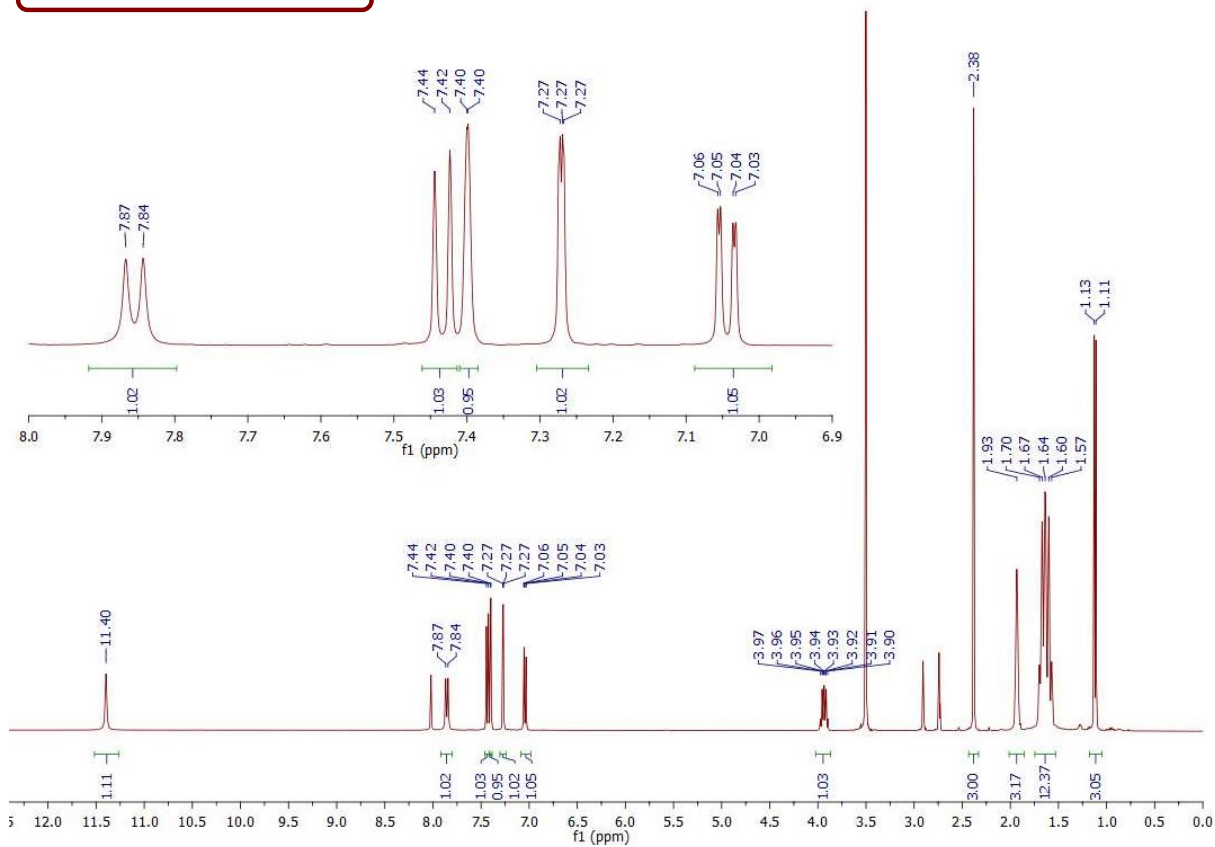
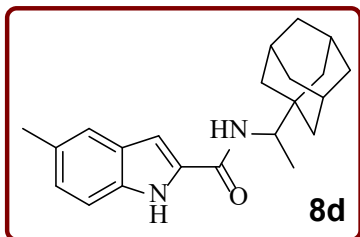
\* Corresponding author. Simone Treiger Sredni: [ssredni@northwestern.edu](mailto:ssredni@northwestern.edu)

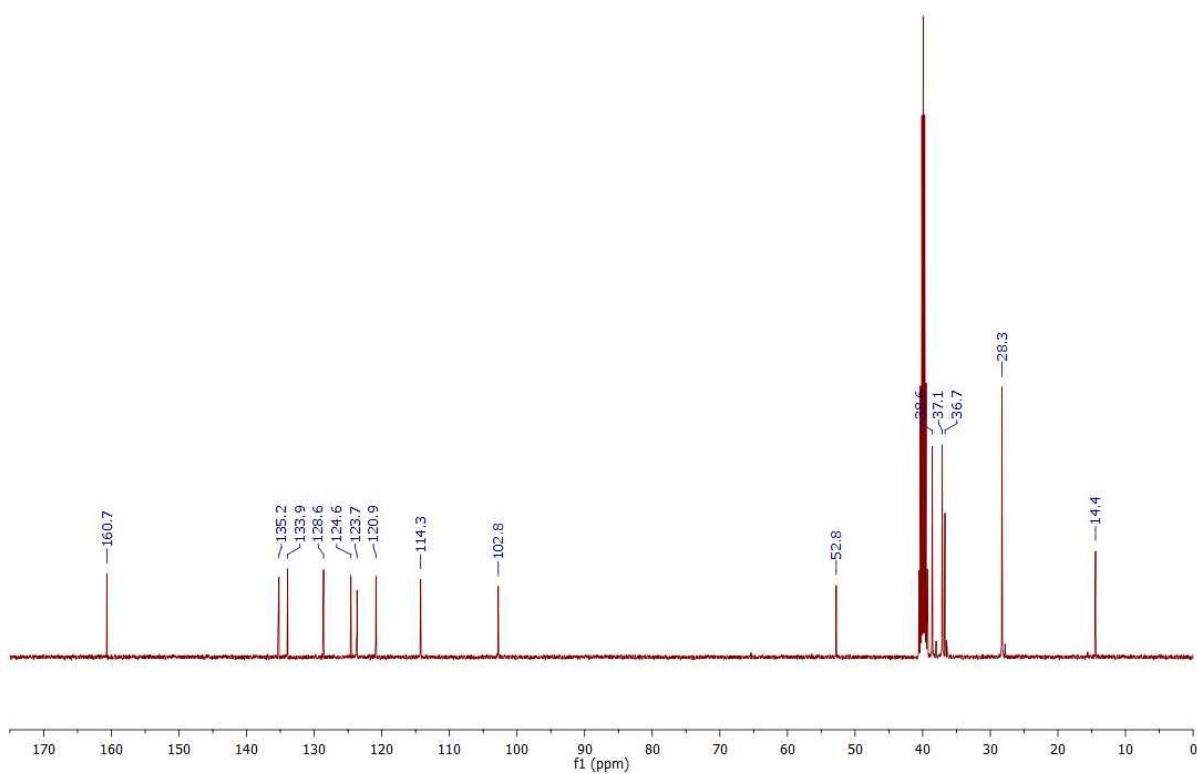
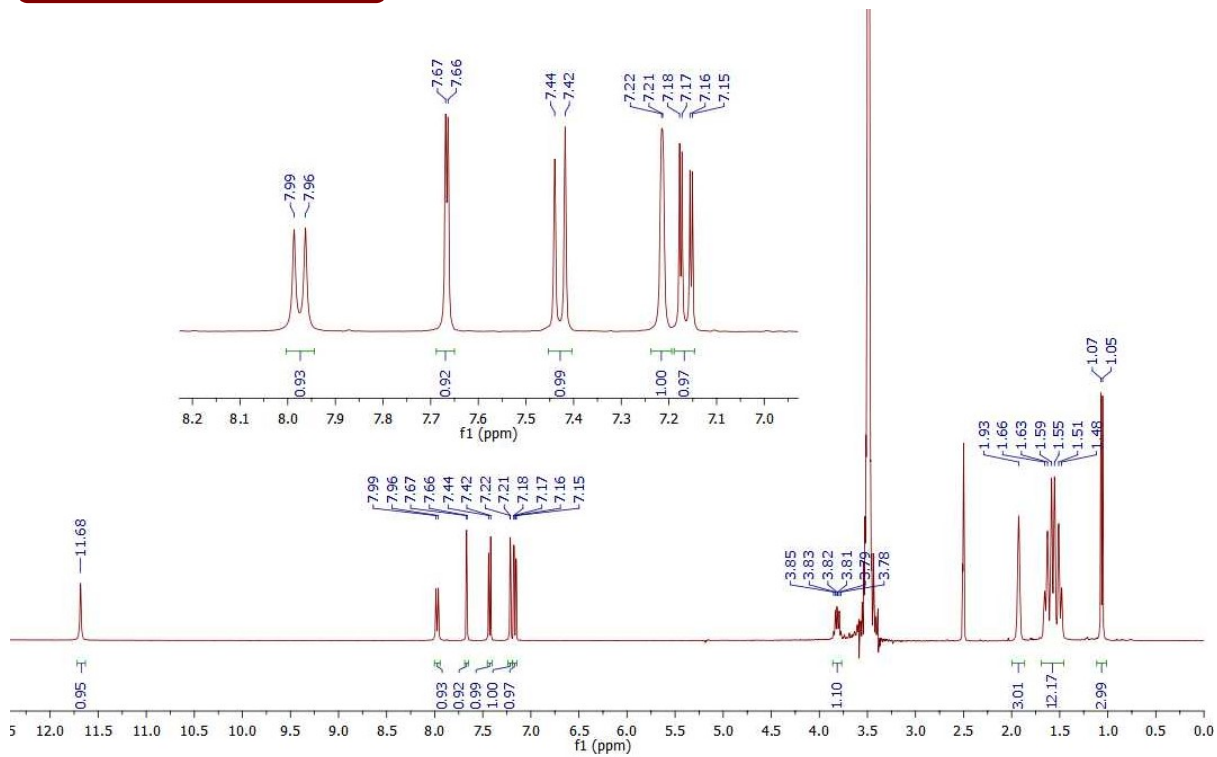
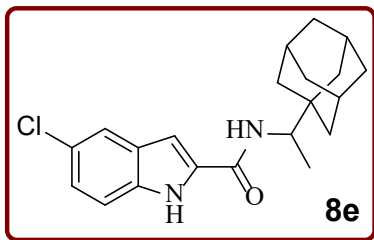


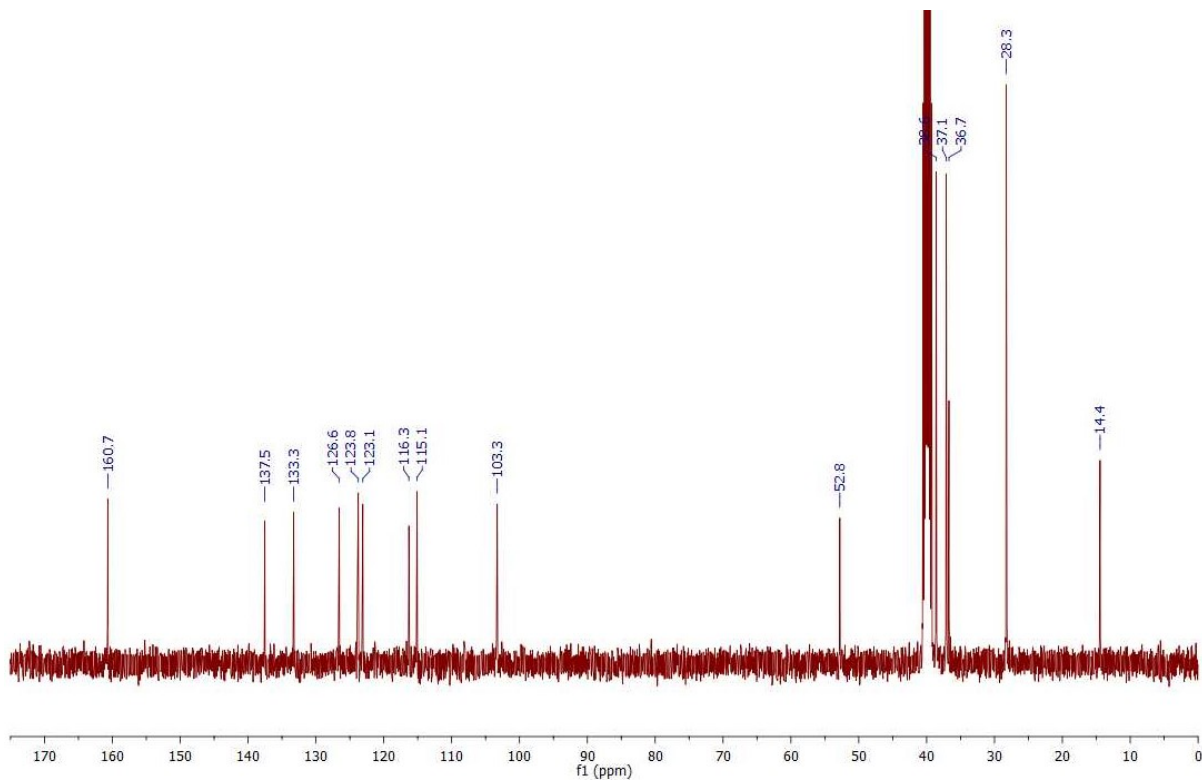
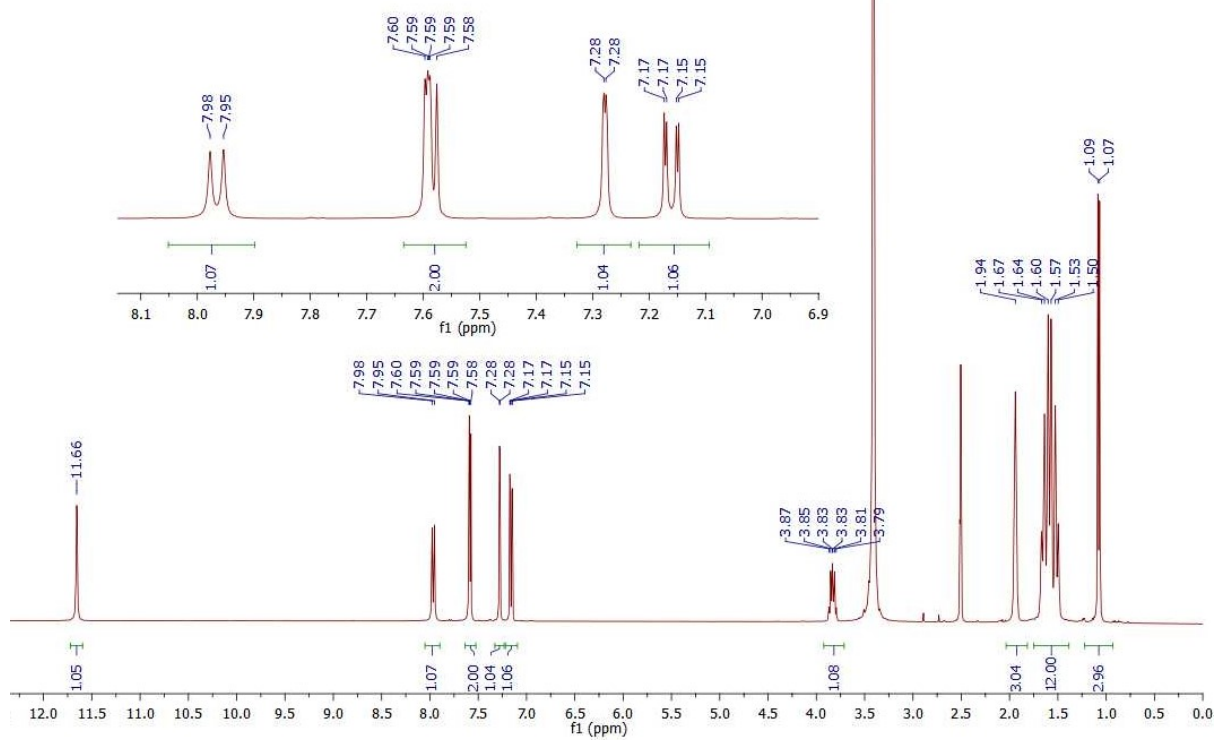
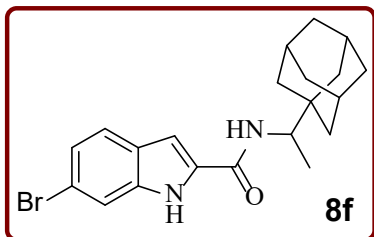


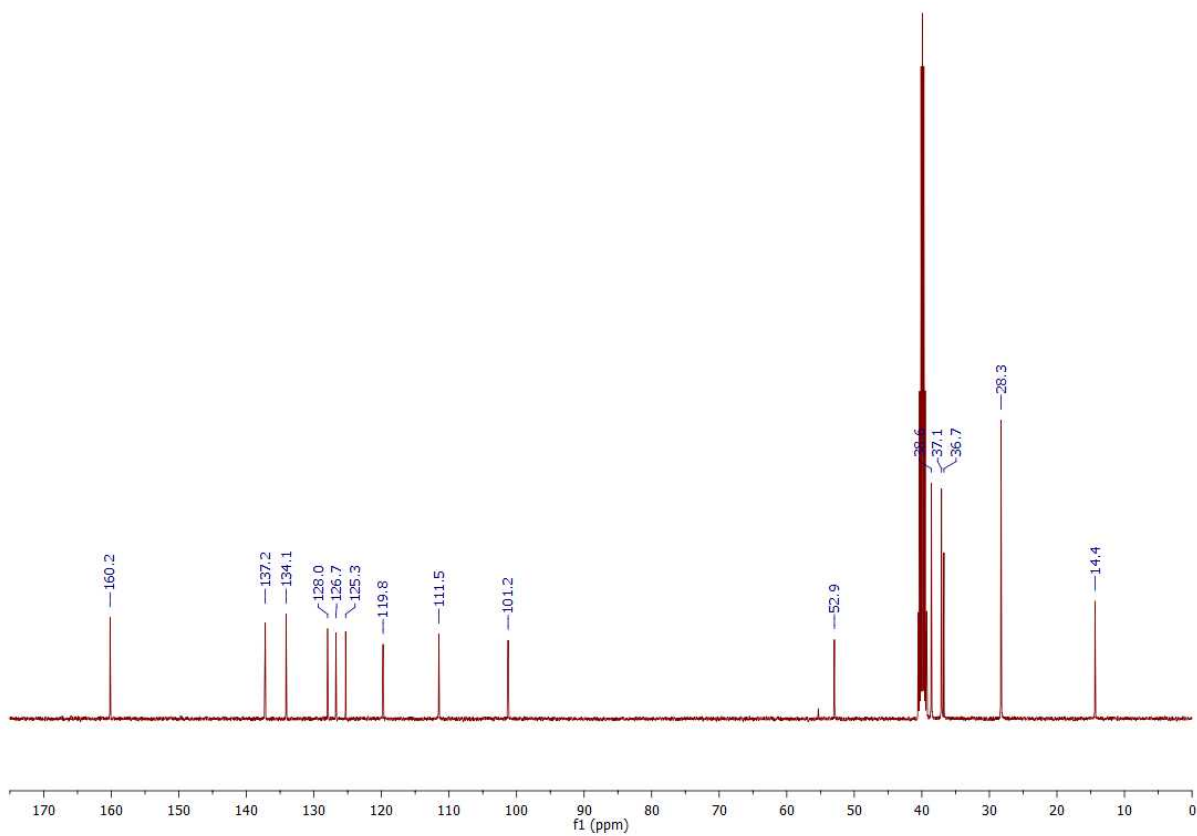
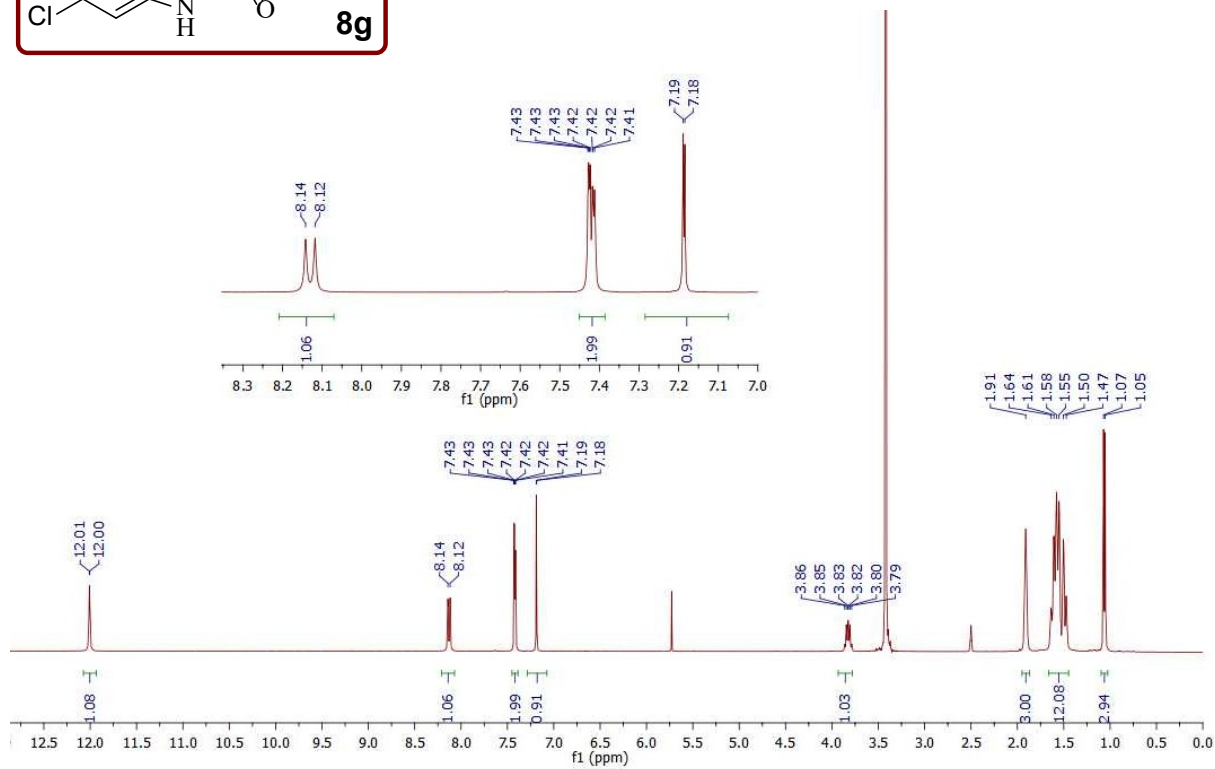
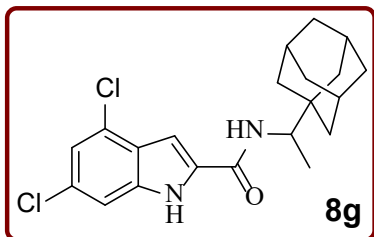


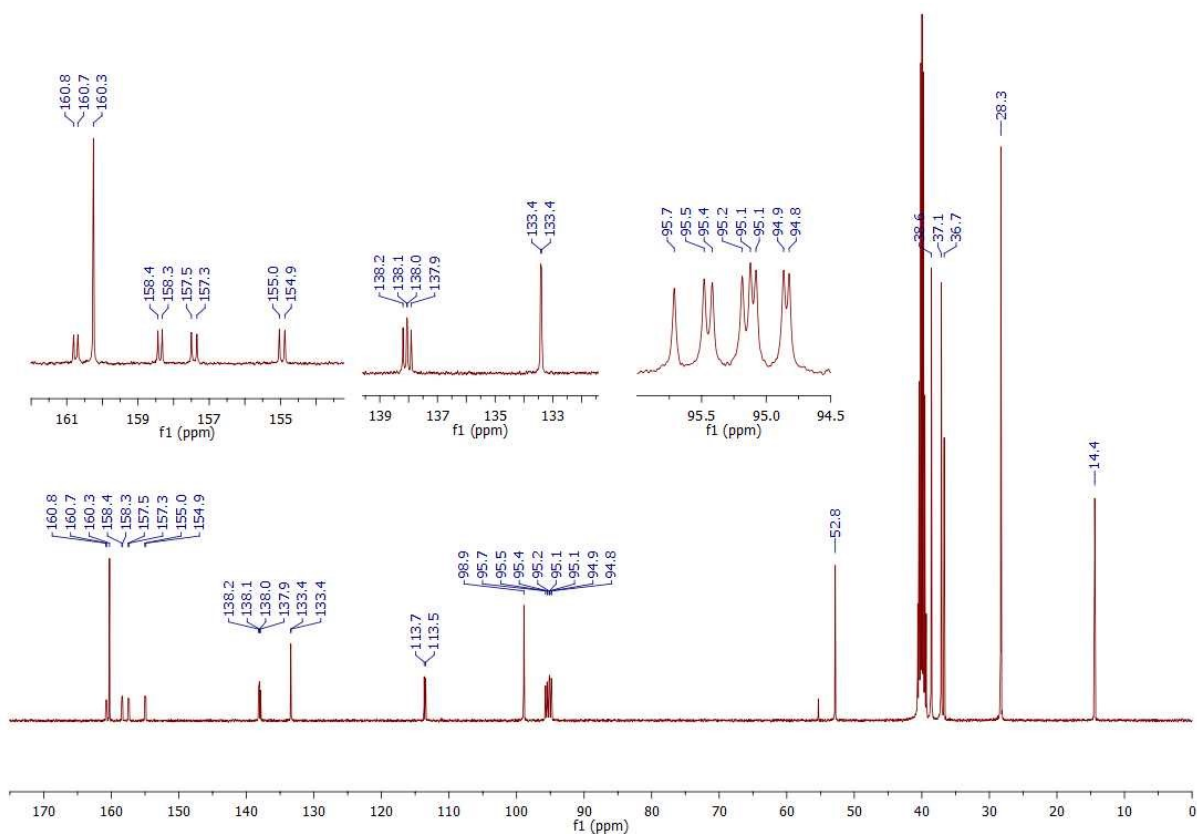
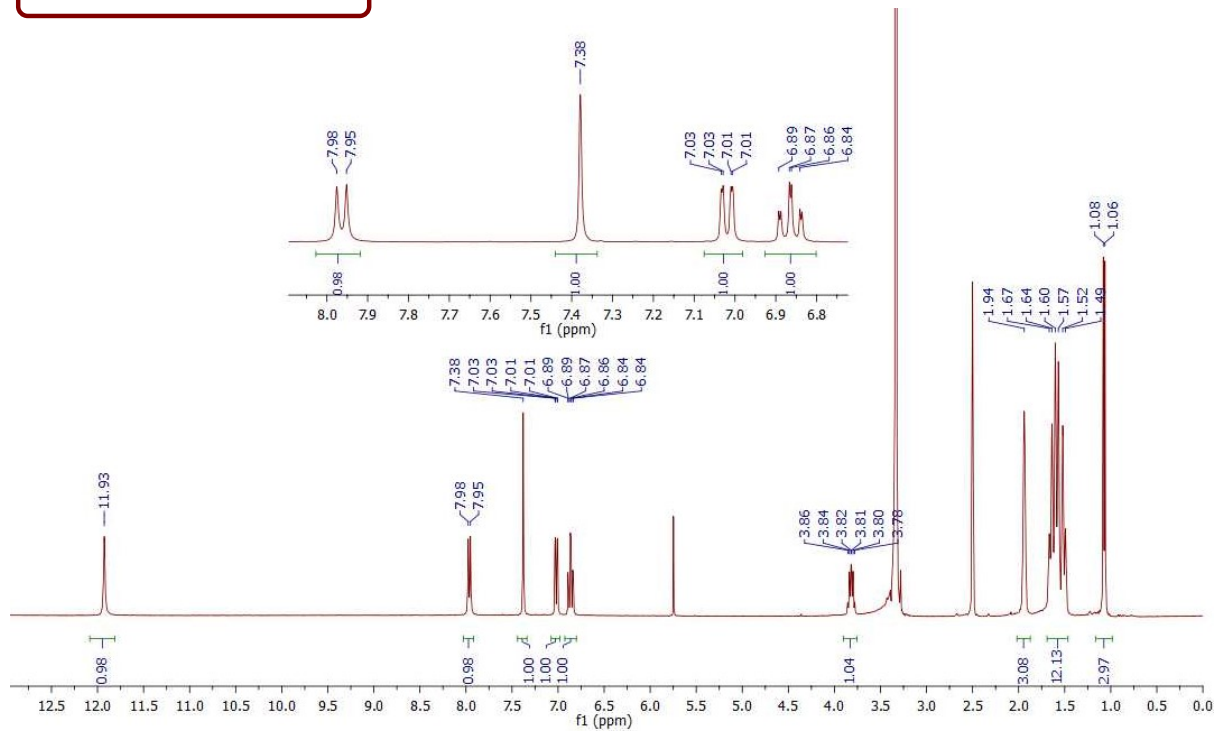
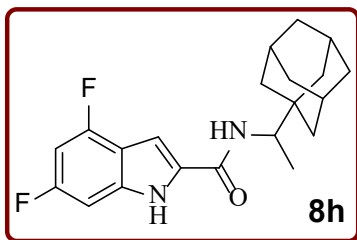




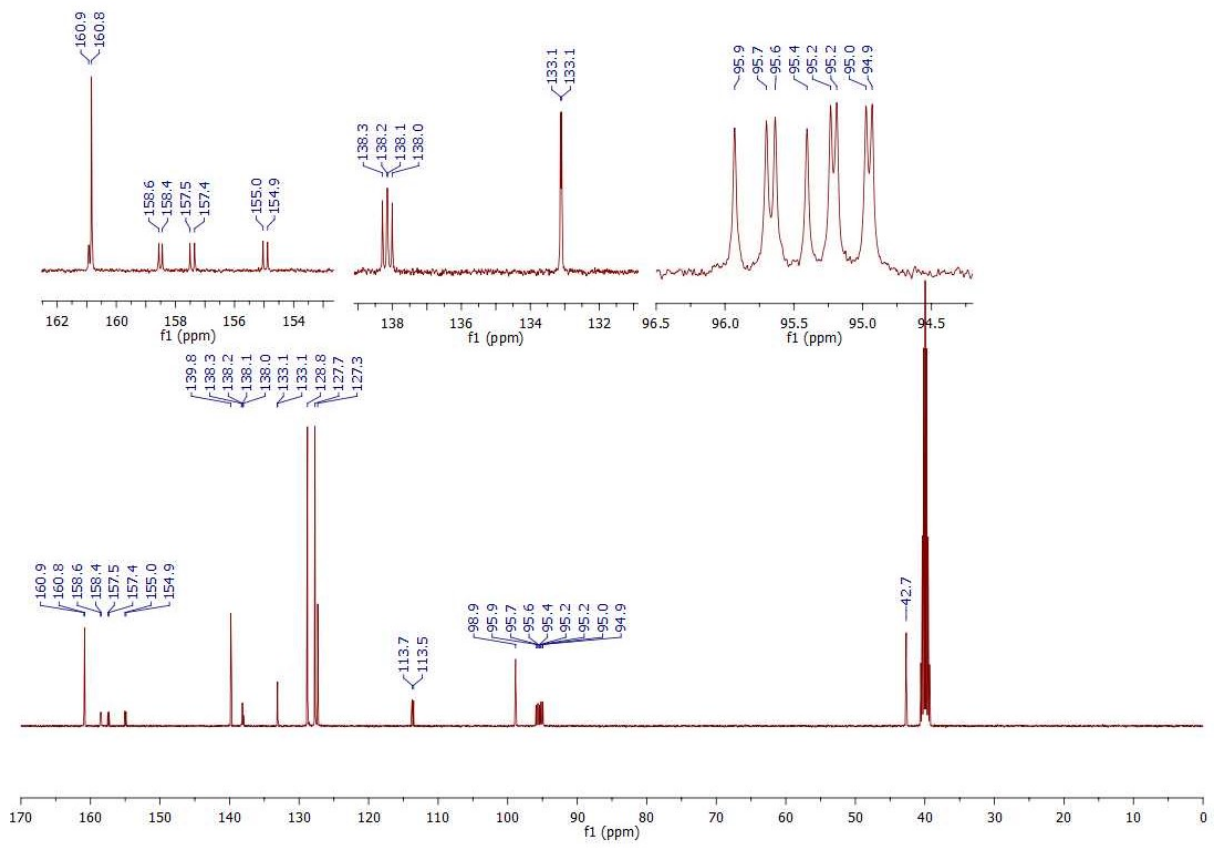
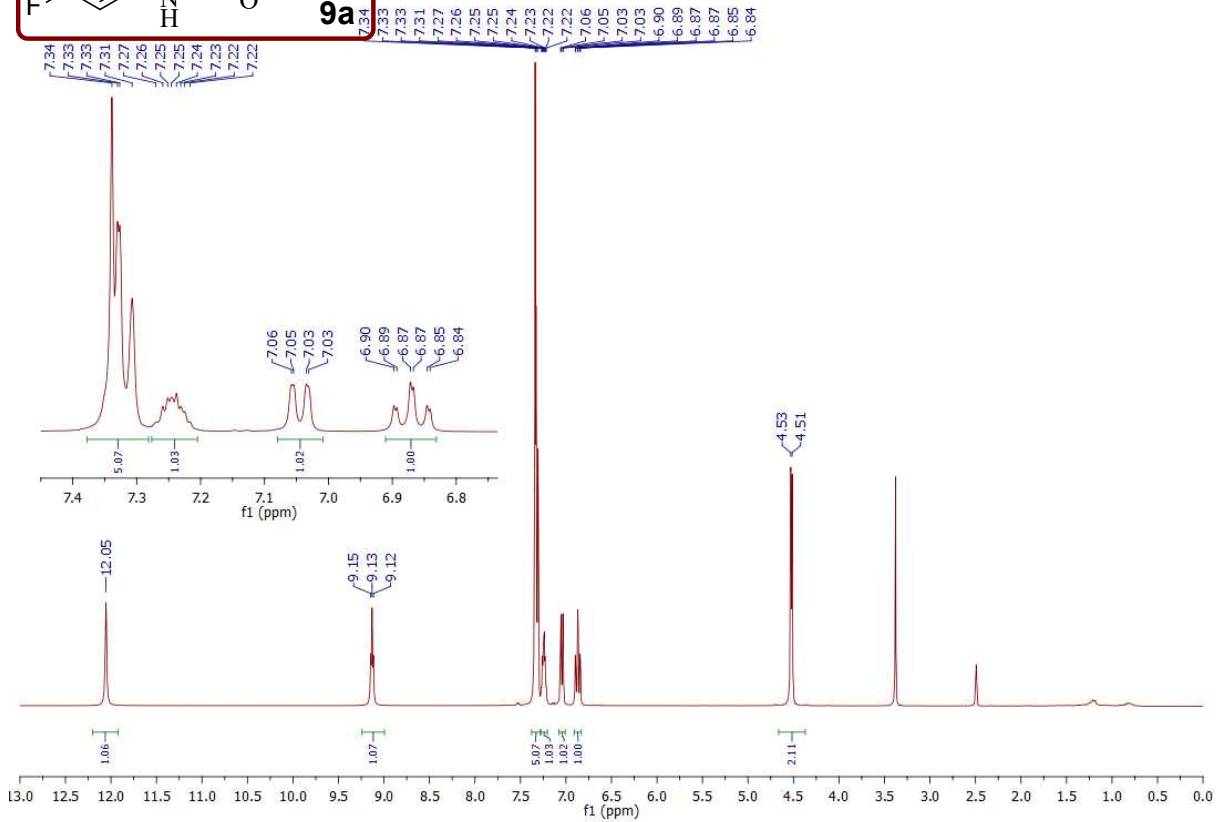
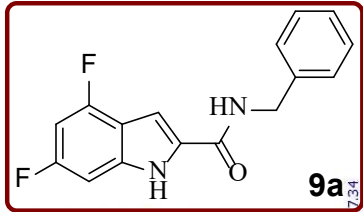


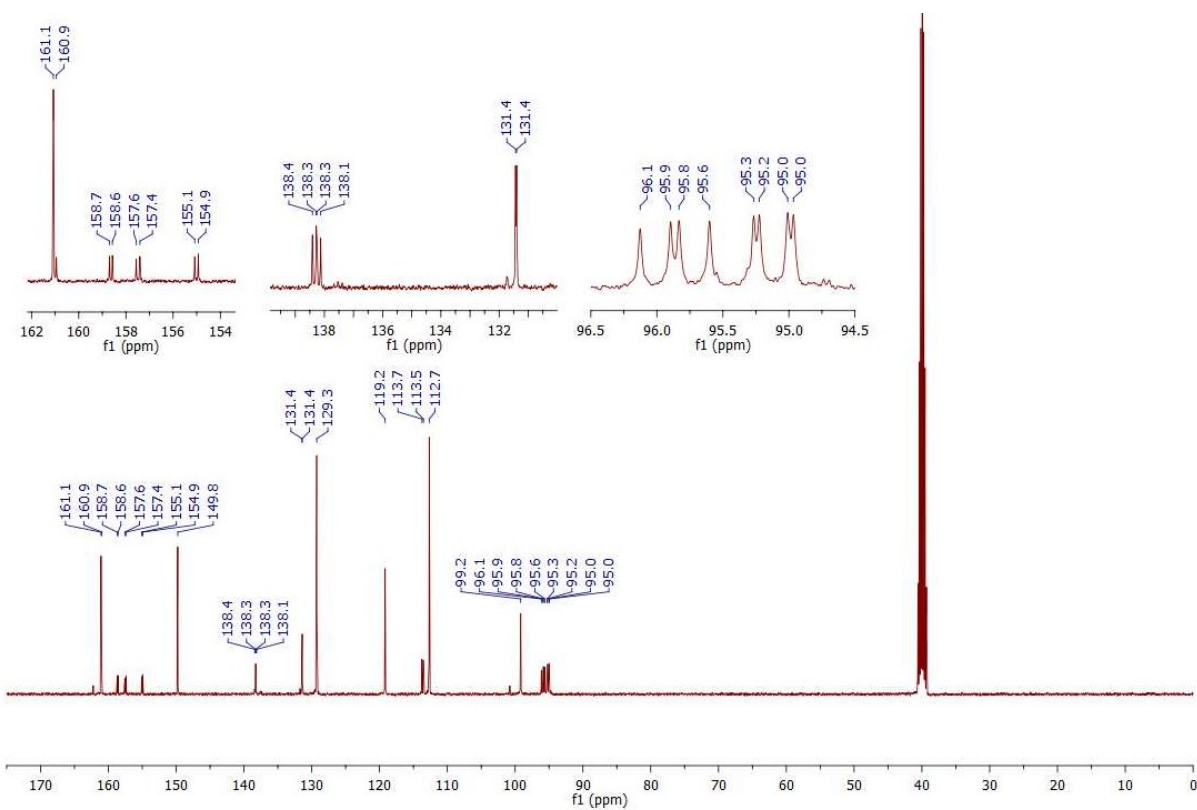
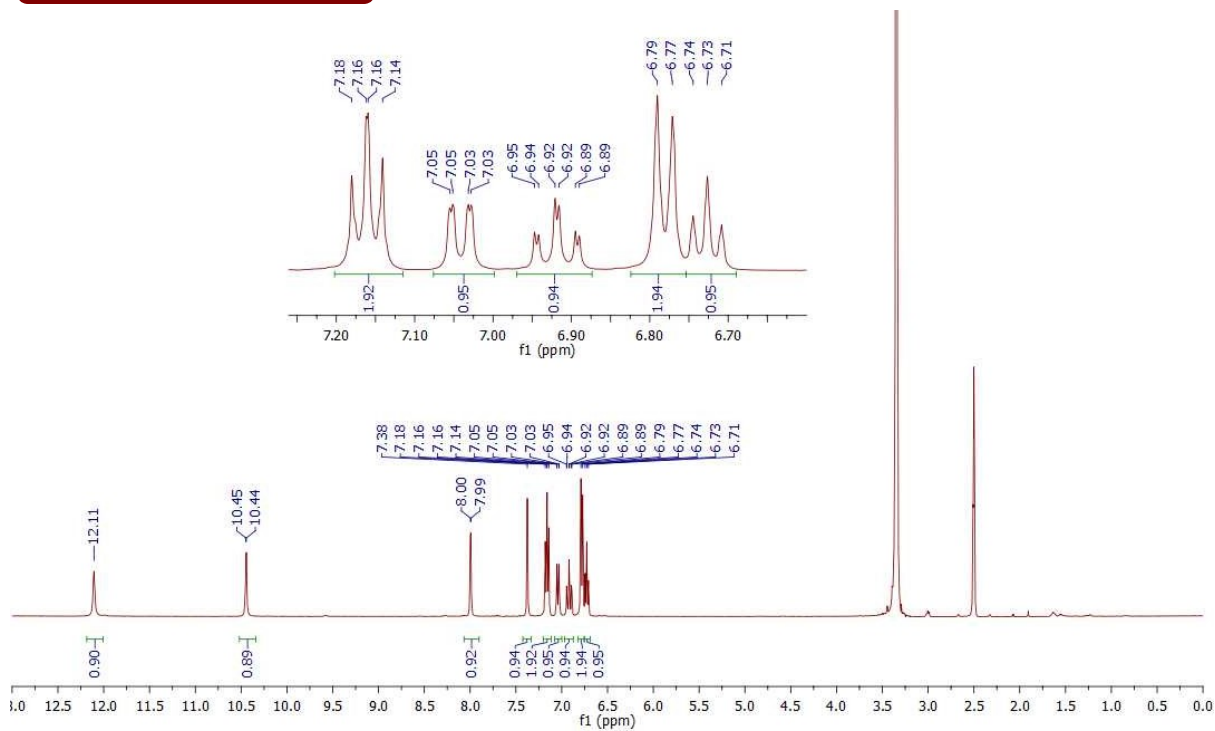
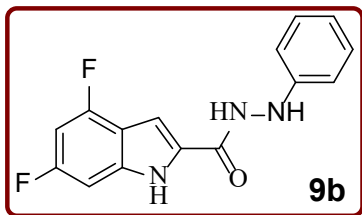


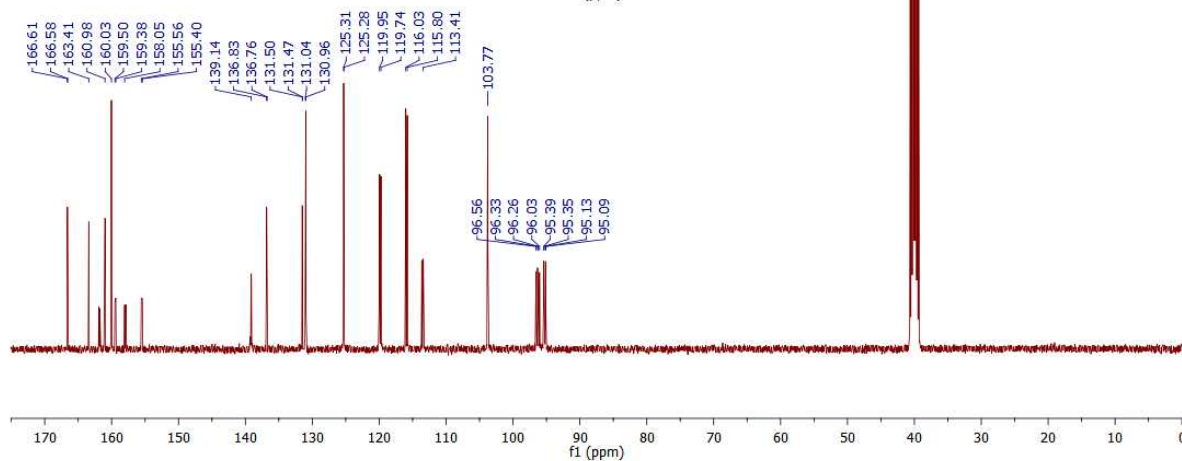
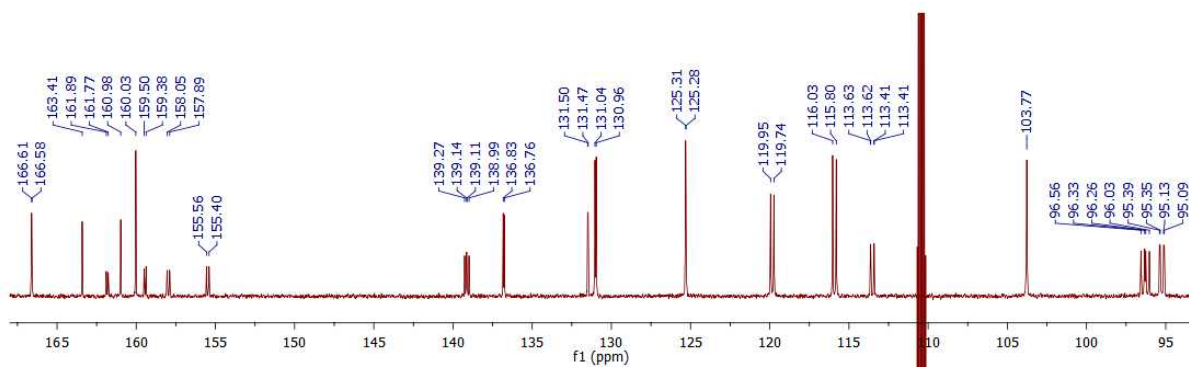
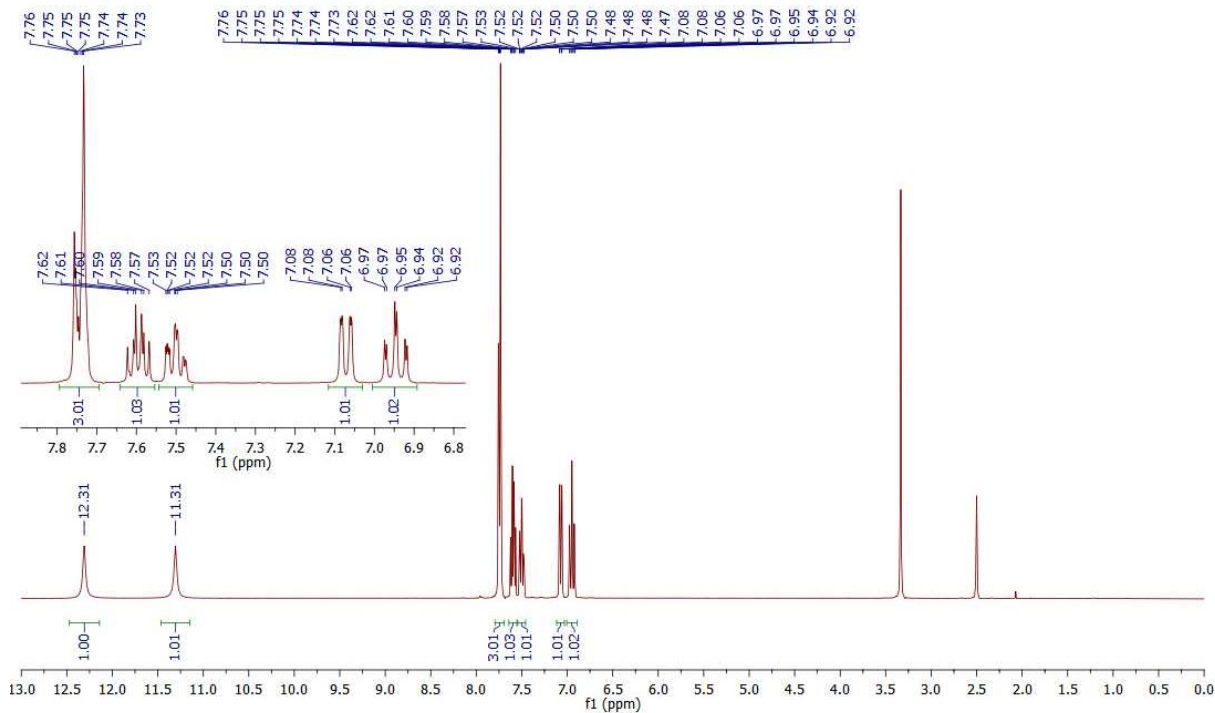
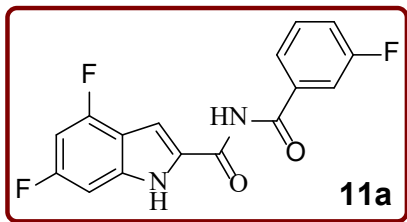


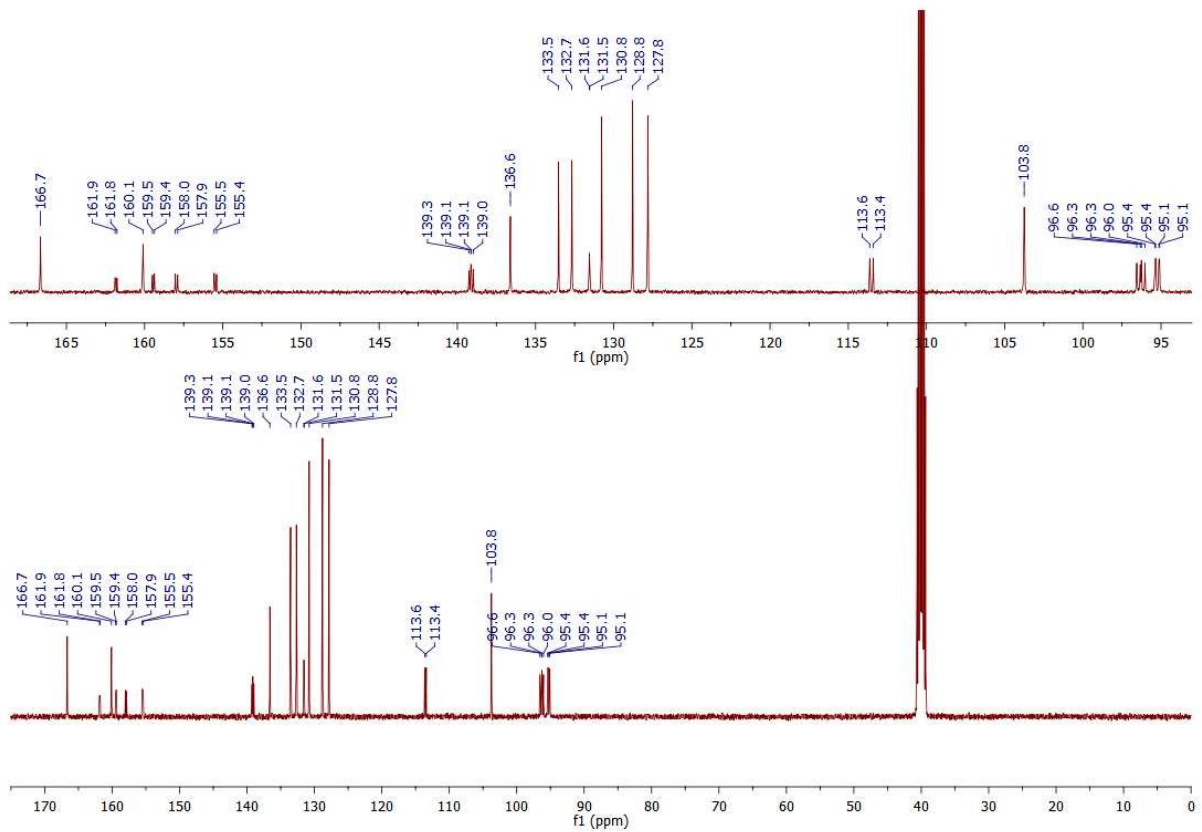
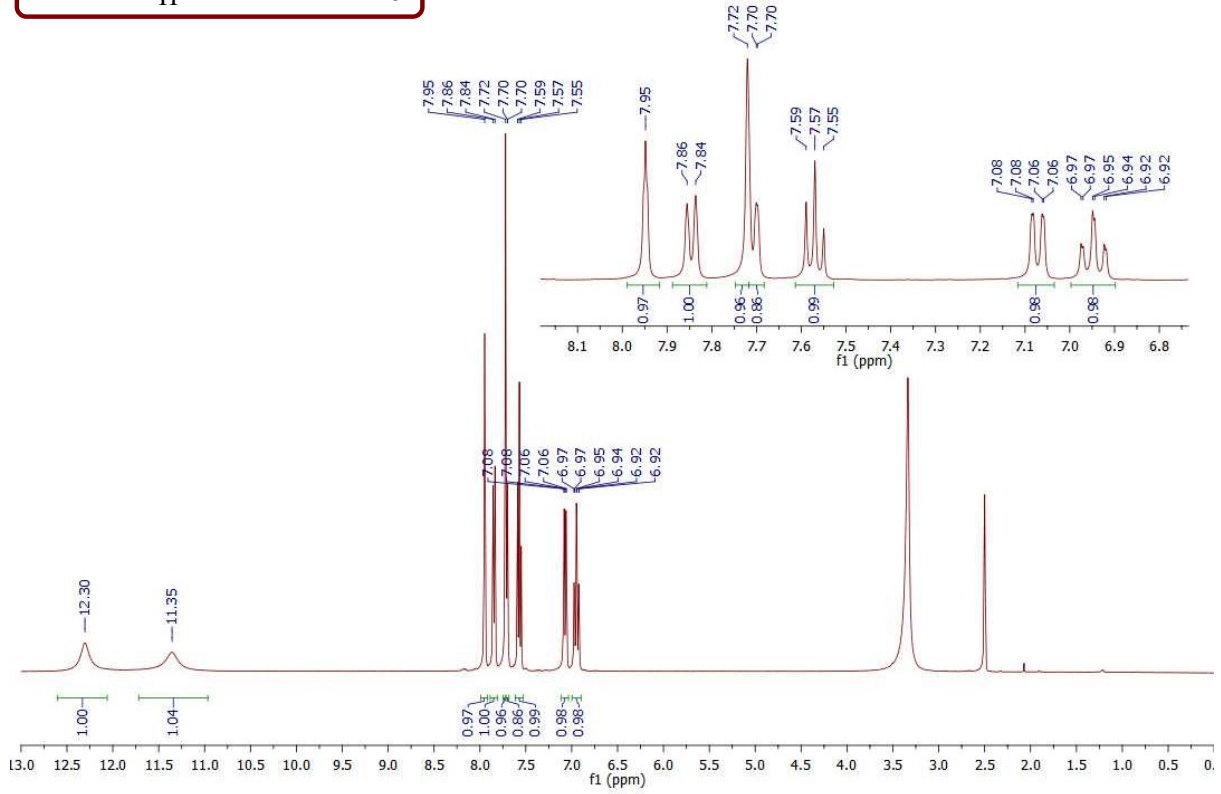
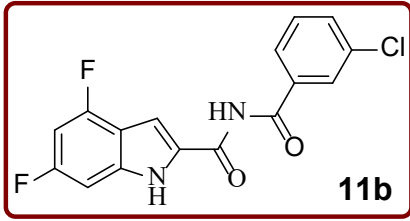


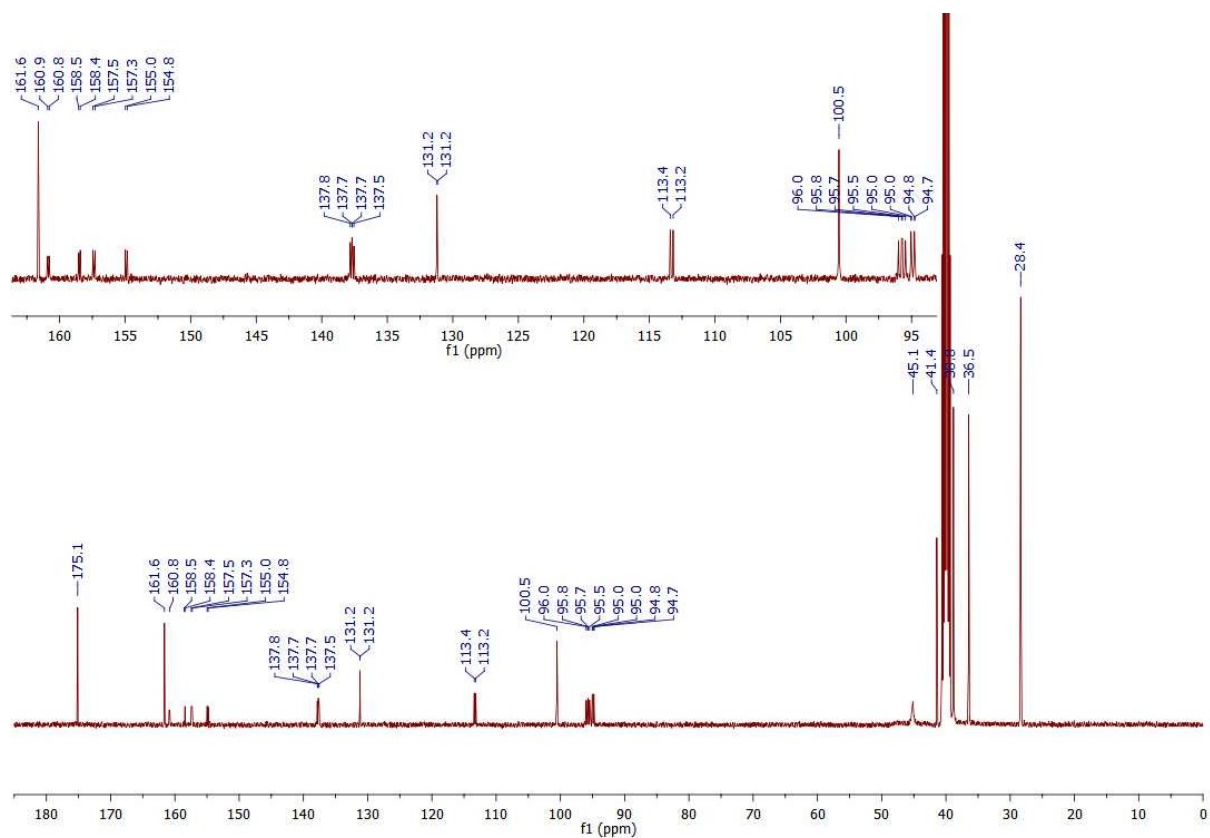
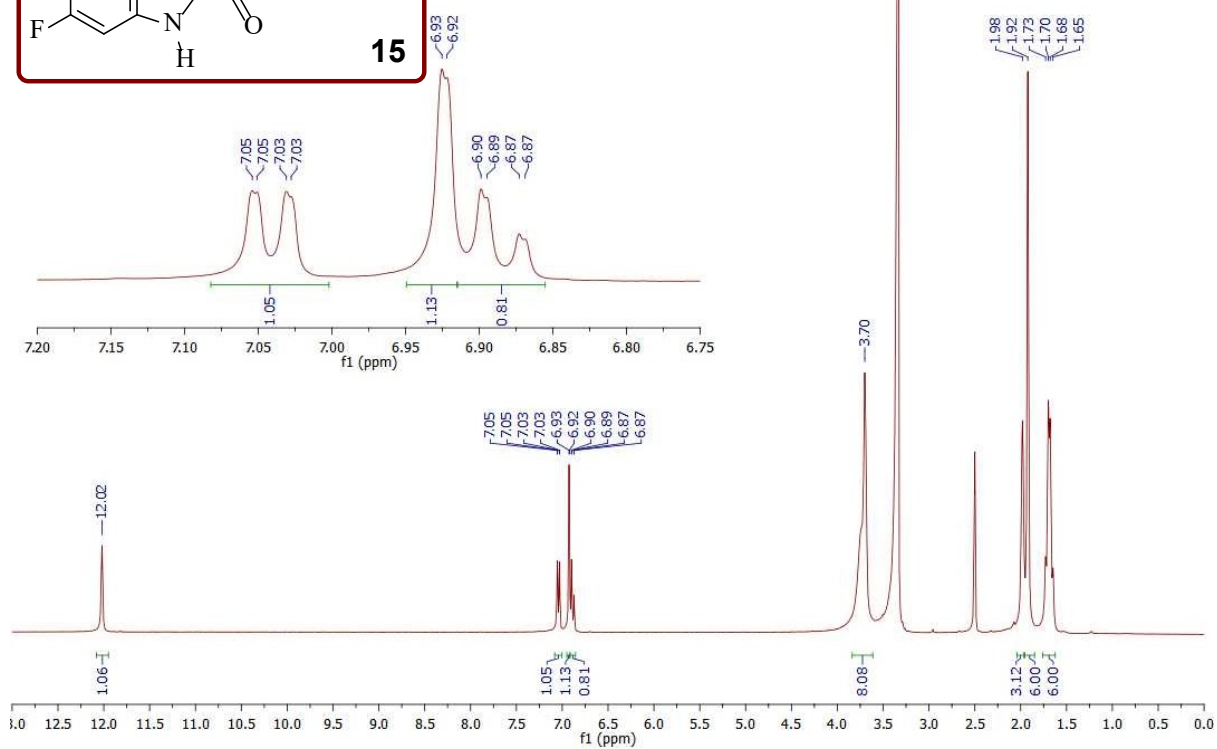
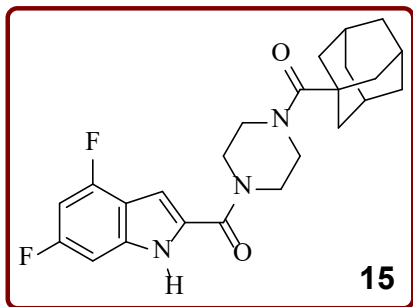


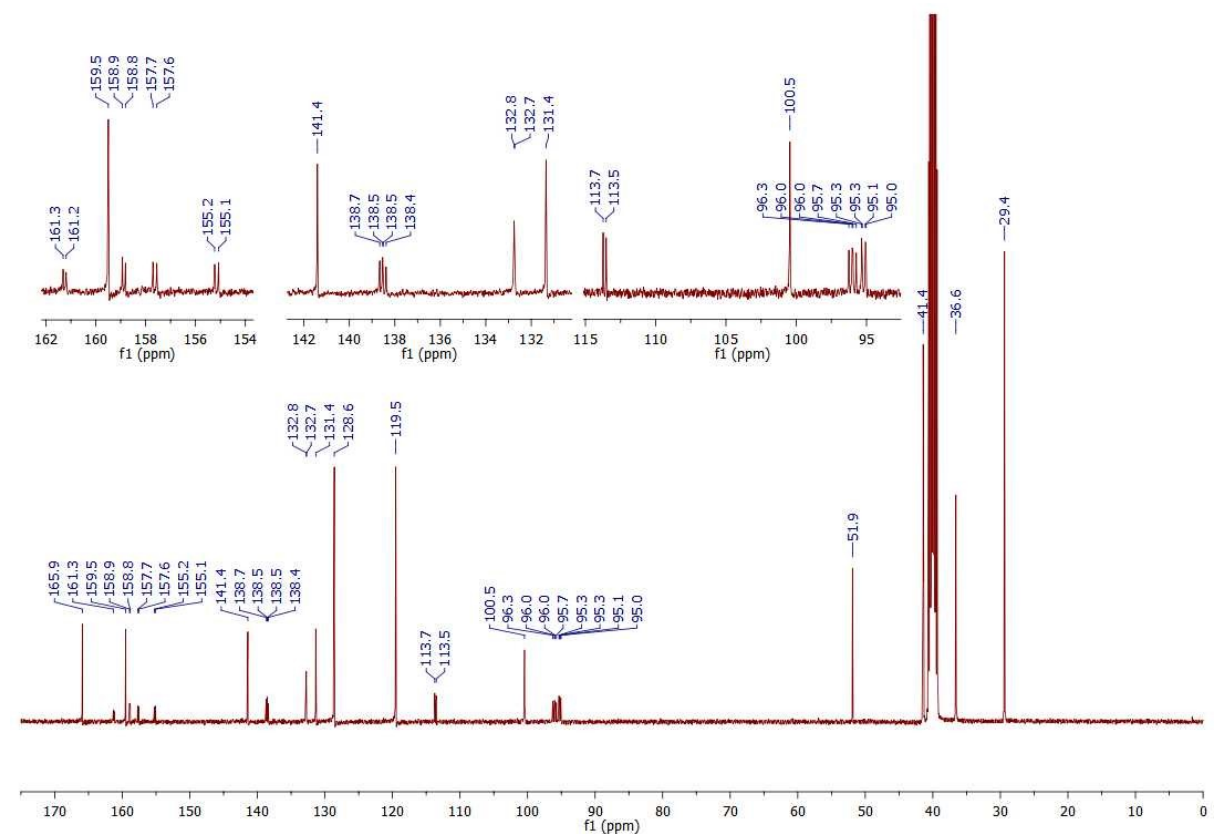
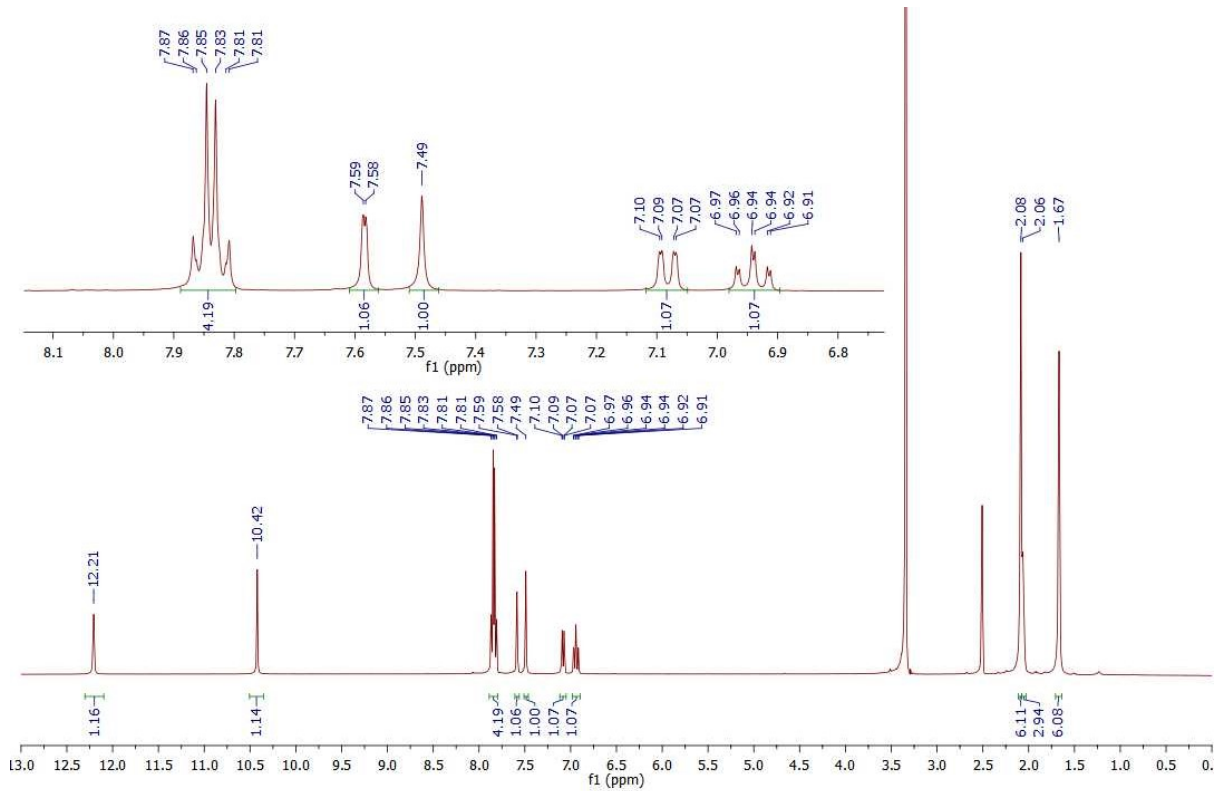
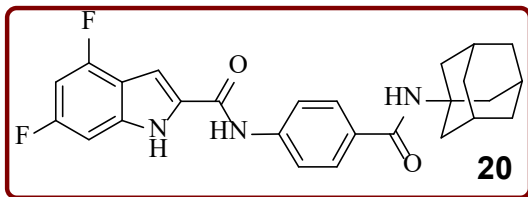












**Supplementary Information – Chapter 7**  
**(RSC Medicinal Chemistry 2021 Article)**

## Synthesis and Antitumour Evaluation of Indole-2-Carboxamides against Paediatric Brain Cancer Cells

Shahinda S. R. Alsayed<sup>a</sup>, Amreena Suri<sup>b</sup>, Anders W. Bailey<sup>b</sup>, Samuel Lane<sup>c</sup>, Eryn L Werry<sup>c,d</sup>, Chiang-Ching Huang<sup>e</sup>, Li-Fang Yu<sup>f</sup>, Michael Kassiou<sup>c,\*</sup>, Simone Treiger Sredni<sup>b,g,\*</sup>, and Hendra Gunosewoyo<sup>a,\*</sup>

<sup>a</sup> Curtin Medical School, Faculty of Health Sciences, Curtin University, Bentley, Perth, WA 6102, Australia

<sup>b</sup> Division of Pediatric Neurosurgery, Ann and Robert H. Lurie Children's Hospital of Chicago, Chicago, IL 60611, USA

<sup>c</sup> School of Chemistry, The University of Sydney, NSW, 2006, Australia

<sup>d</sup> Faculty of Medicine and Health, The University of Sydney, NSW 2006, Australia

<sup>e</sup> Department of Biostatistics, Zilber School of Public Health, University of Wisconsin, Milwaukee, WI 53205, USA

<sup>f</sup> Shanghai Engineering Research Center of Molecular Therapeutics and New Drug Development, School of Chemistry and Molecular Engineering, East China Normal University, 3663 North Zhongshan Road, Shanghai 200062, China

<sup>g</sup> Department of Surgery, Northwestern University, Feinberg School of Medicine, Chicago, IL 60611, USA

\* Corresponding author. Michael Kassiou: [michael.kassiou@sydney.edu.au](mailto:michael.kassiou@sydney.edu.au)

\* Corresponding author. Simone Treiger Sredni: [simone.sredni@gmail.com](mailto:simone.sredni@gmail.com)

\* Corresponding author. Hendra Gunosewoyo: [Hendra.Gunosewoyo@curtin.edu.au](mailto:Hendra.Gunosewoyo@curtin.edu.au)



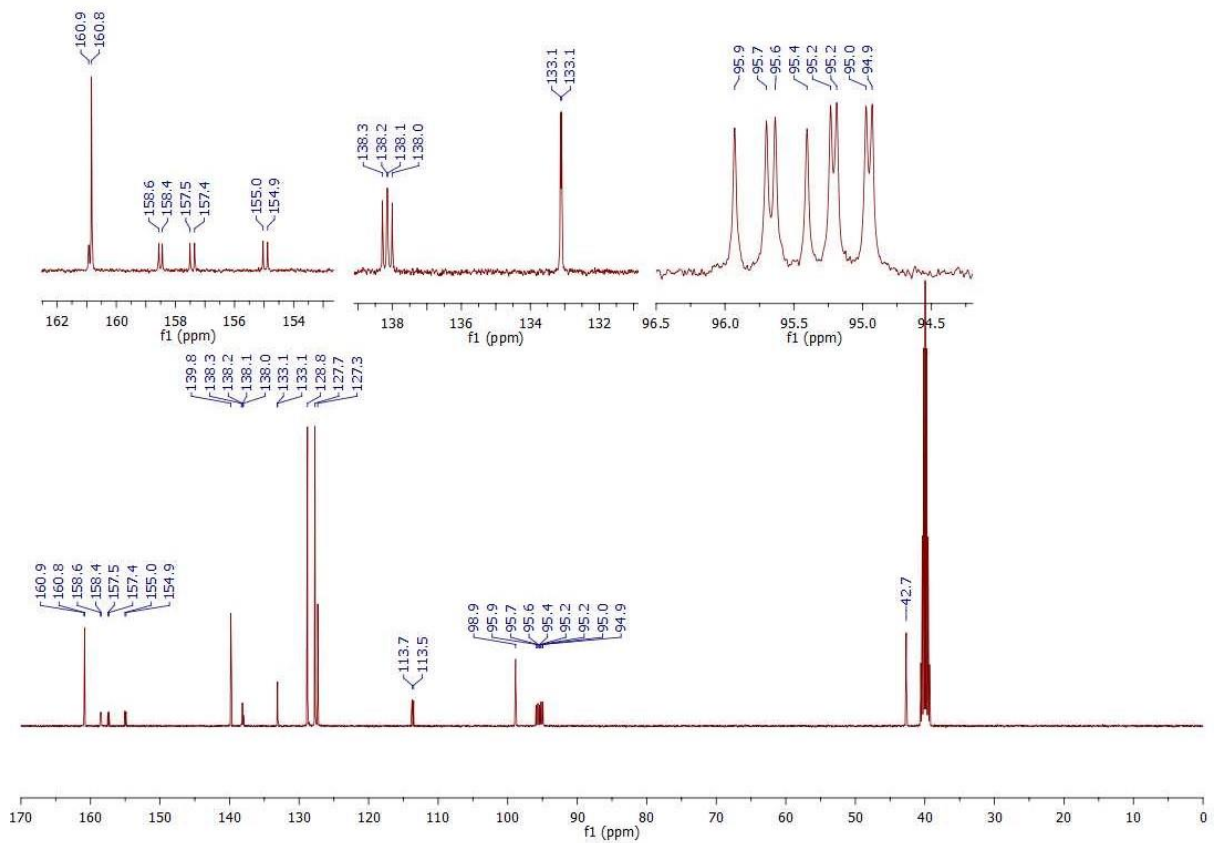
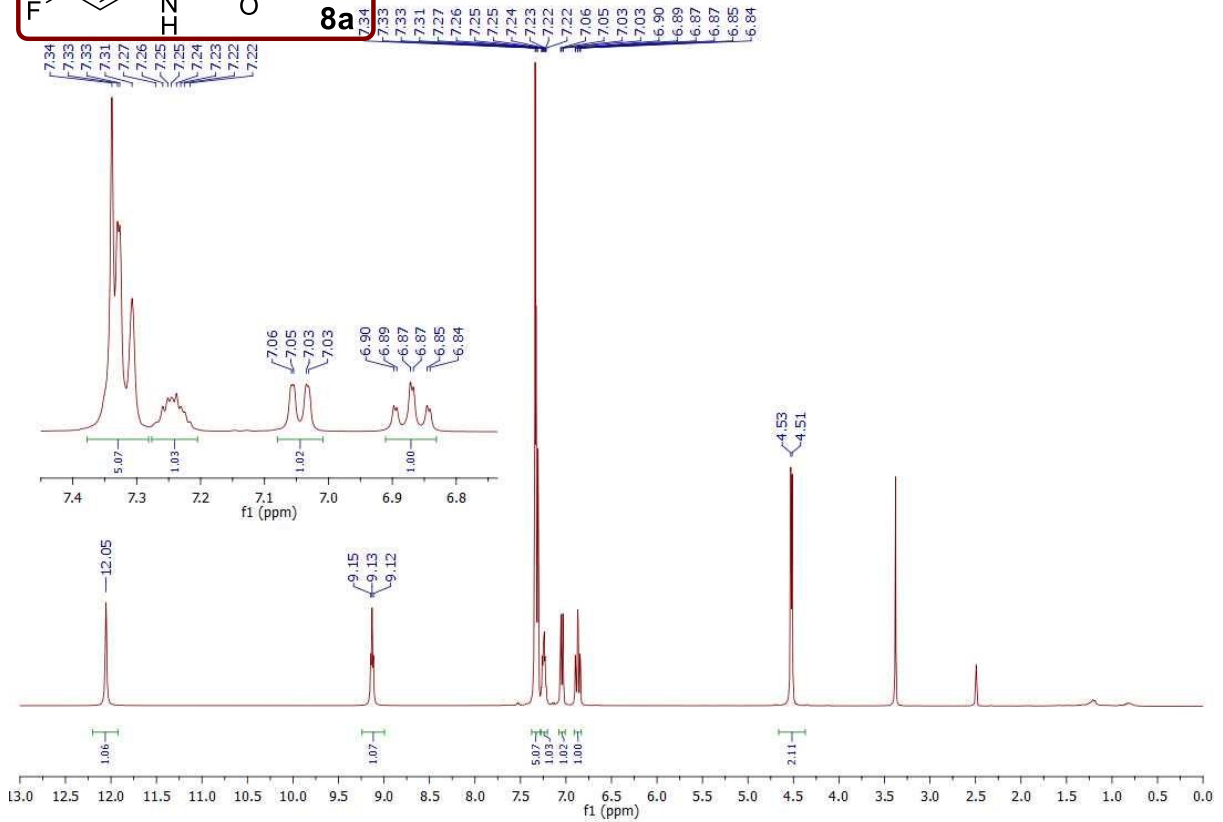
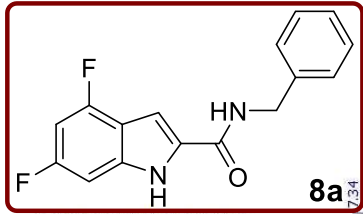
**Table S1. Downregulated genes in 8a-treated KNS42 cells**

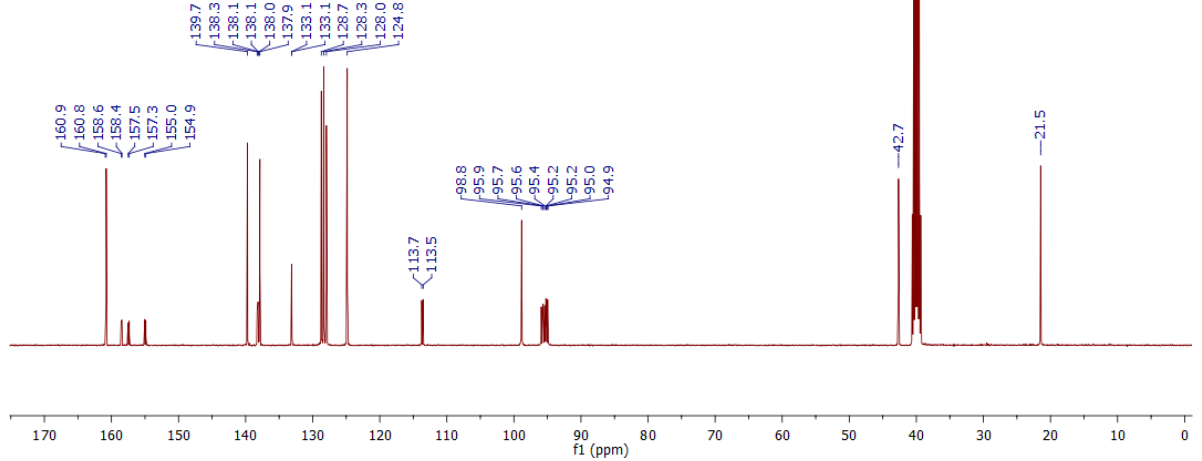
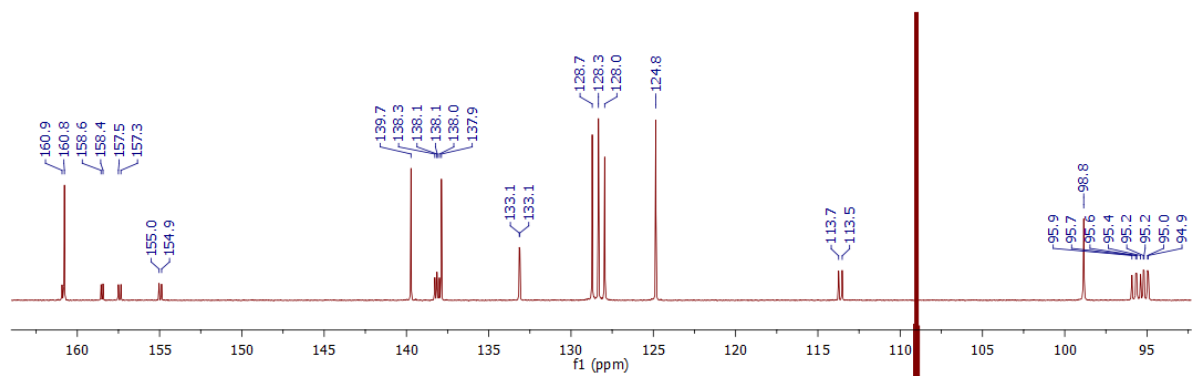
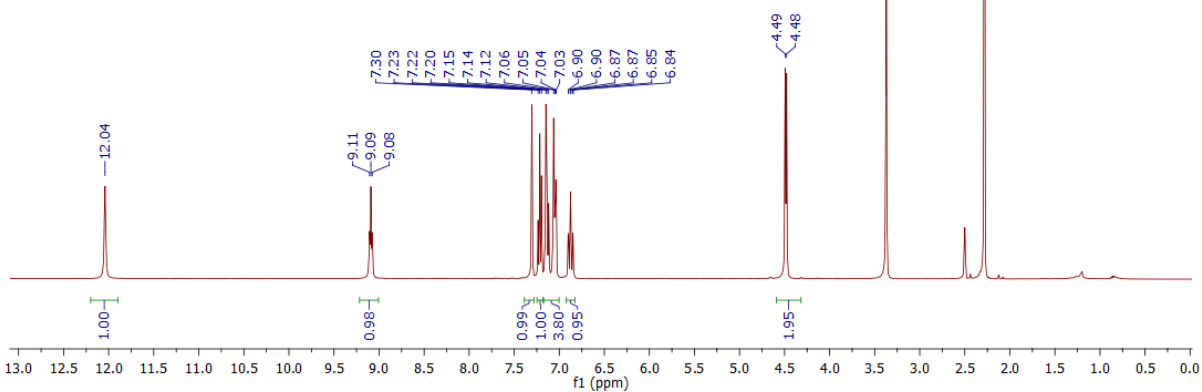
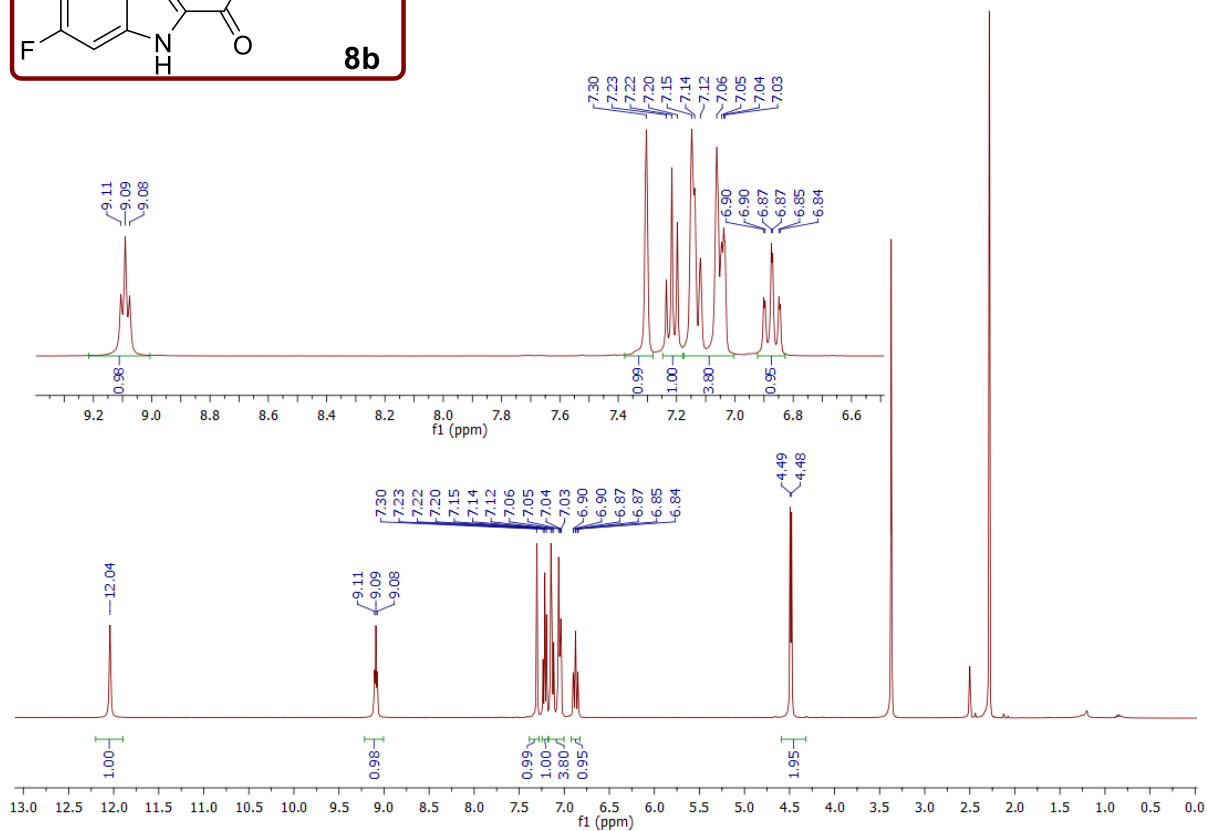
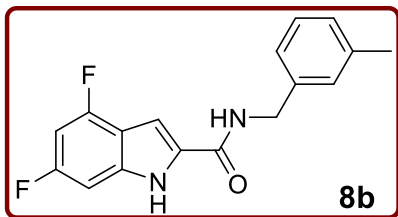
| Gene Symbol          | Description <sup>a</sup>  | Fold Change | P value   | Function <sup>a</sup>  |
|----------------------|---|-------------|-----------|--|
| <b>PLAC1</b>         | Placenta specific protein1  | 30          | 0.0028    | Placental development  |
| <b>CLECL1</b>        | C-type lectin-like domain family 1                                  | 19          | 0.0123    | Immune response regulation   |
| <b>ETV7</b>          | ETS Variant Transcription Factor 7                                  | 19          | 0.0057    | Transcriptional repressor  |
| <b>TNS1</b>          | Tensin-1  | 18          | 0.0100    | Fibrillar adhesion and crosslinking actin filaments  |
| <b>KCNJ12</b>        | ATP-sensitive inward rectifier potassium channel 12                 | 17          | 0.0060    | Potassium ion transfer   |
| <b>NT5C1B</b>        | Cytosolic 5'-nucleotidase 1B  | 14          | 0.0124    | Adenosine level regulation   |
| <b>TREH</b>          | Trehalase   | 13          | 0.0154    | Trehalose hydrolysis   |
| <b>FAM186A</b>       | Family with sequence similarity 186, member A                       | 13          | 0.0286    | ND <sup>b</sup>  |
| <b>LOC105377622</b>  | A non-coding RNA (ncRNA) gene                                       | 13          | 0.0221    | ND <sup>b</sup>  |
| <b>OPCML</b>         | Opioid-binding protein/cell adhesion molecule-like                  | 13          | 0.0204    | Cell contact regulation  |
| <b>DNASE2B</b>       | Deoxyribonuclease-2-beta  | 13          | 0.0254    | DNA degradation  |
| <b>ARHGAP9</b>       | Rho GTPase-activating protein 9                                     | 12          | 1.23E-12  | Cytoskeletal dynamics regulation <sup>1</sup>  |
| <b>APELA</b>         | Apelin receptor early endogenous ligand                             | 11          | 0.0159    | Cardiovascular homeostasis   |
| <b>MISP</b>          | Mitotic interactor and substrate of PLK1                            | 10          | 0.0181    | Cell division and migration  |
| <b>JSRP1</b>         | Junctional sarcoplasmic reticulum protein 1                         | 10          | 0.0215    | Modulation of Skeletal muscle excitation-contraction coupling  |
| <b>CCDC42</b>        | Coiled-coil domain-containing protein 42                            | 10          | 0.0104    | Sperm development  |
| <b>KNCN</b>          | Kinocilin   | 10          | 0.0374    | Vacuolar trafficking   |
| <b>FLG</b>           | Filaggrin   | 9           | 3.05E-88  | Keratinisation   |
| <b>ADM2</b>          | Adrenomedullin 2  | 8           | 1.08E-47  | Gastrointestinal and cardiovascular homeostasis  |
| <b>CHAC1</b>         | Glutathione-specific gamma-glutamylcyclotransferase 1               | 8           | 2.69E-76  | neuronal differentiation and Glutathione level Modulation  |
| <b>IRX3</b>          | Iroquois Homeobox 3   | 7           | 0.0329    | Neural development   |
| <b>GPR45</b>         | G Protein-Coupled Receptor 45                                       | 7           | 0.0306    | Mediation of Signalling processes  |
| <b>NDUFA4L2</b>      | NADH dehydrogenase [ubiquinone] 1 alpha subcomplex subunit 4-like 2 | 7           | 0.0002    | Cell survival regulation <sup>2</sup>  |
| <b>TESC</b>          | Tescalcin or Calcineurin B homologous protein 3                     | 6           | 0.0009    | Cell pH regulation   |
| <b>MAPK4</b>         | Mitogen-Activated Protein Kinase 4                                  | 6           | 0.0001    | Phosphorylation of microtubule-associated protein 2 (MAP2) <sup>3</sup>  |
| <b>SH2D3C</b>        | SH2 domain-containing protein 3C                                    | 6           | 0.0237    | Mediation of cell signalling pathways implicated in cell adhesion, migration, and invasion   |
| <b>CABP1</b>         | Calcium-binding protein 1   | 5           | 0.0254    | Signal transduction  |
| <b>SLC7A5 (LAT1)</b> | Large neutral amino acids transporter small subunit 1               | 5           | 5.30E-217 | Amino acid exchanger   |
| <b>ANGPTL4</b>       | Angiopietin-related protein 4                                       | 5           | 0.0106    | Regulation of insulin sensitivity, glucose homeostasis, and lipid metabolism   |
| <b>MIOX</b>          | Myo-Inositol Oxygenase  | 5           | 4.55E-08  | ND <sup>b</sup>  |
| <b>PLIN5</b>         | Perilipin-5   | 5           | 0.0017    | Maintaining the balance between lipolysis and lipogenesis.   |
| <b>ACTN3</b>         | Actinin Alpha 3   | 5           | 0.0221    | Crosslinking actin with various intracellular structures (a bundling protein)  |
| <b>CCKAR</b>         | Cholecystokinin receptor type A                                     | 5           | 0.0346    | Mediator of smooth muscle contraction of stomach and gallbladder, as well as pancreatic enzyme secretion and growth. Regulation of satiety and release of dopamine and β-endorphin |

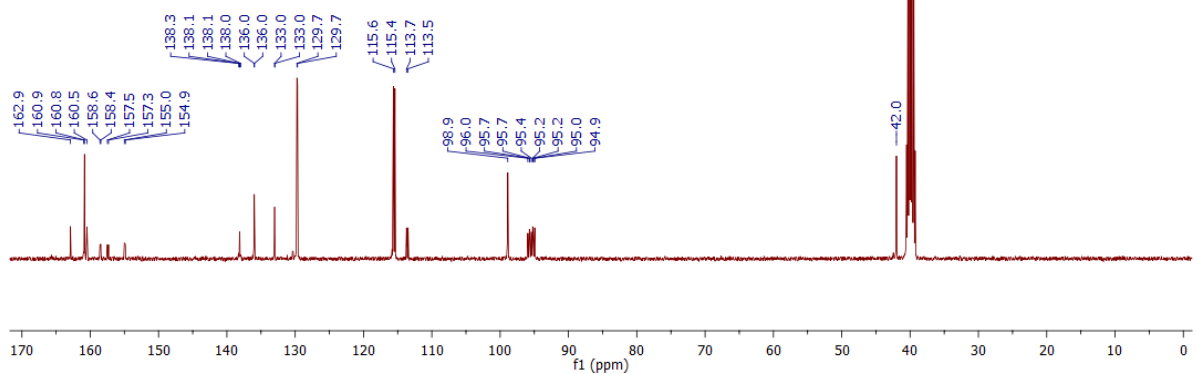
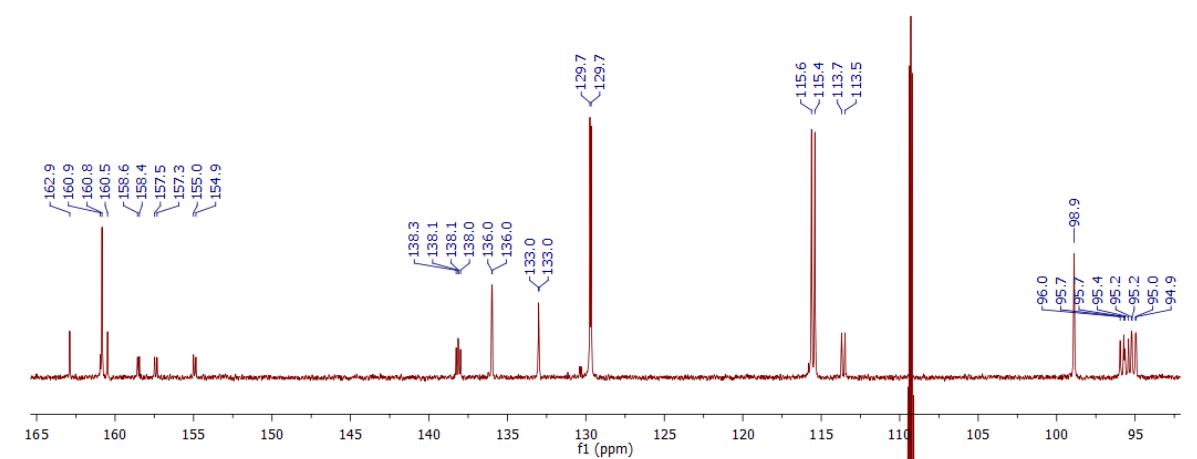
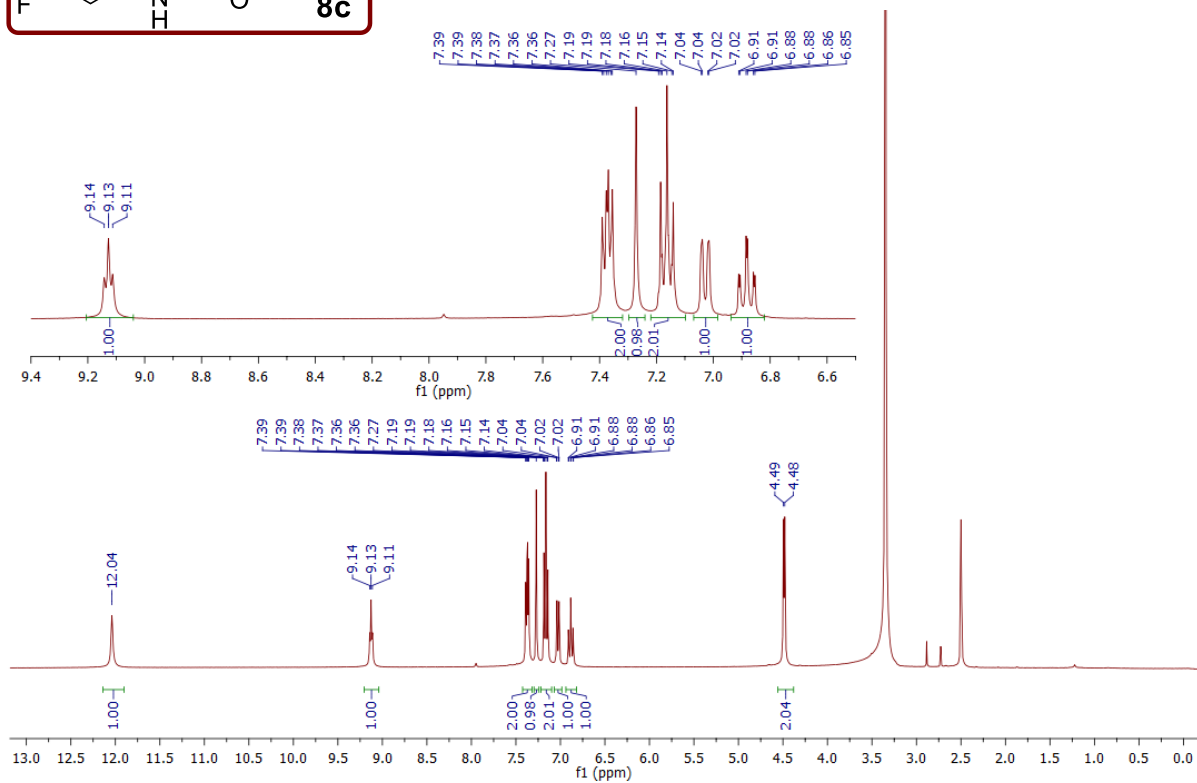
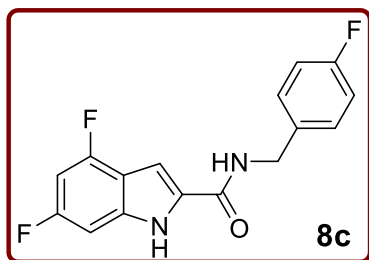
<sup>a</sup> All descriptions and functions were retrieved from uniprot (<https://www.uniprot.org/>) and/or genecards (<https://www.genecards.org/>) websites. In addition, other relevant references are interspersed therein. <sup>b</sup> ND: not determined.

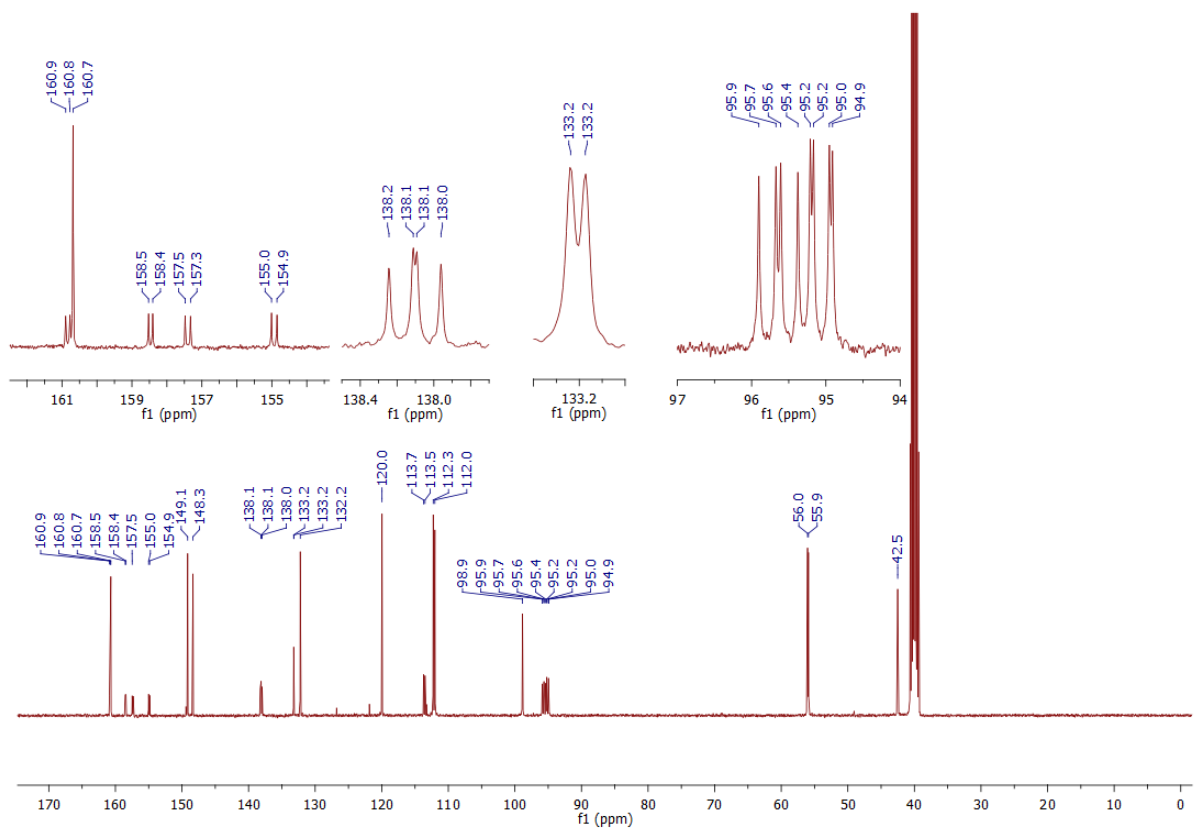
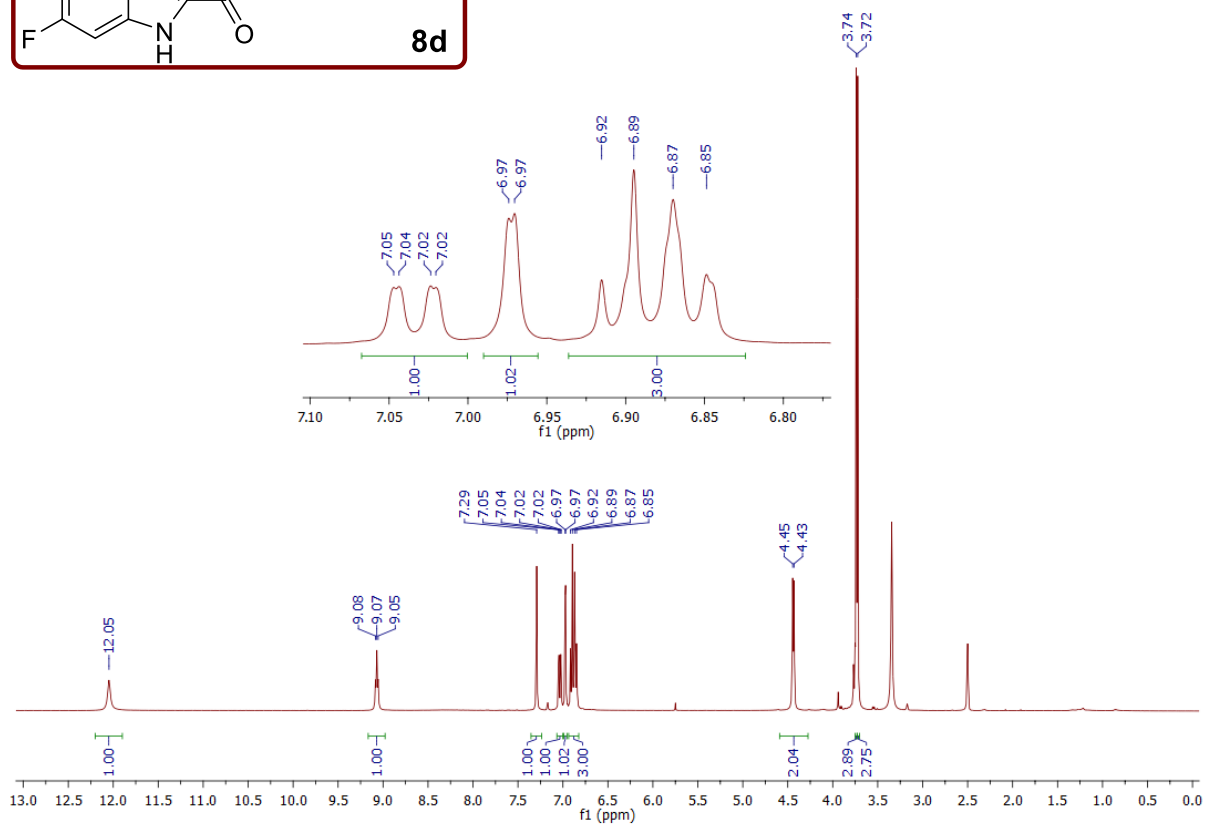
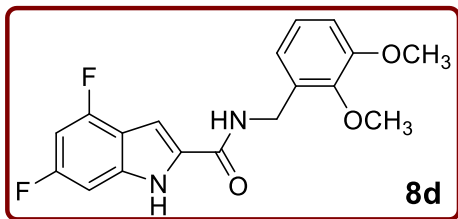
## References:

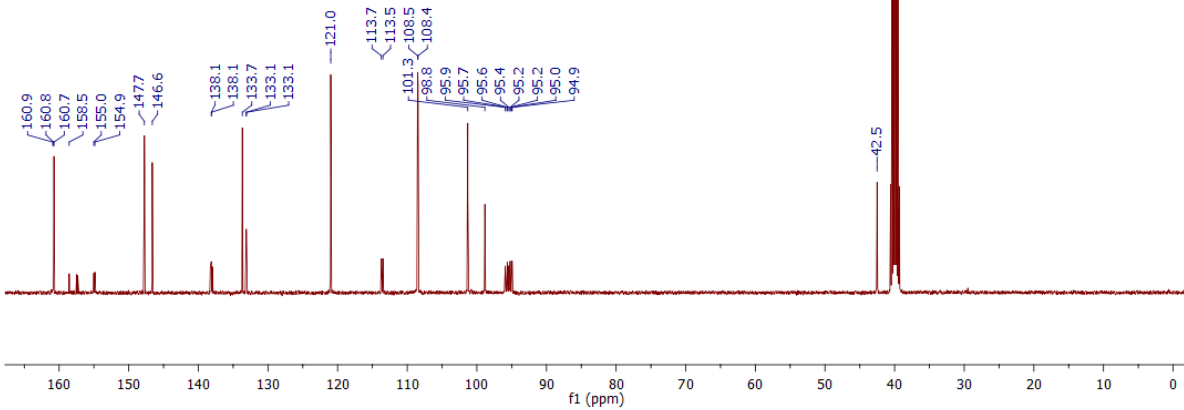
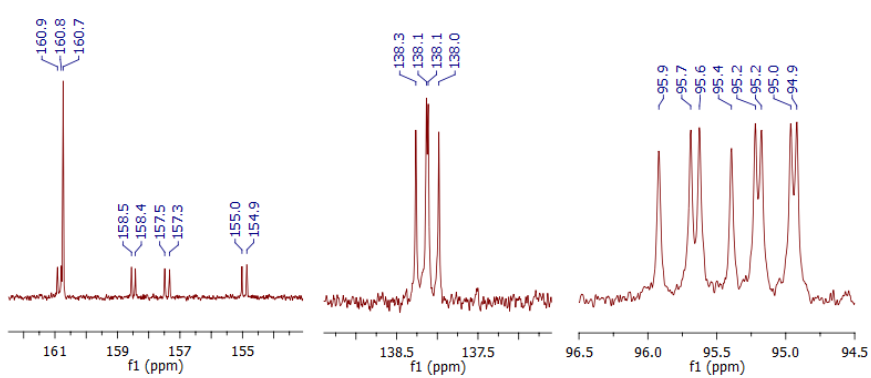
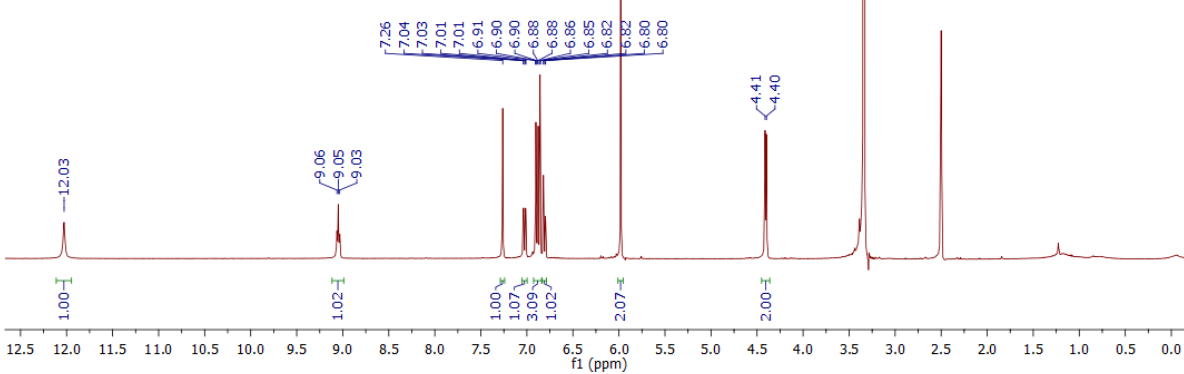
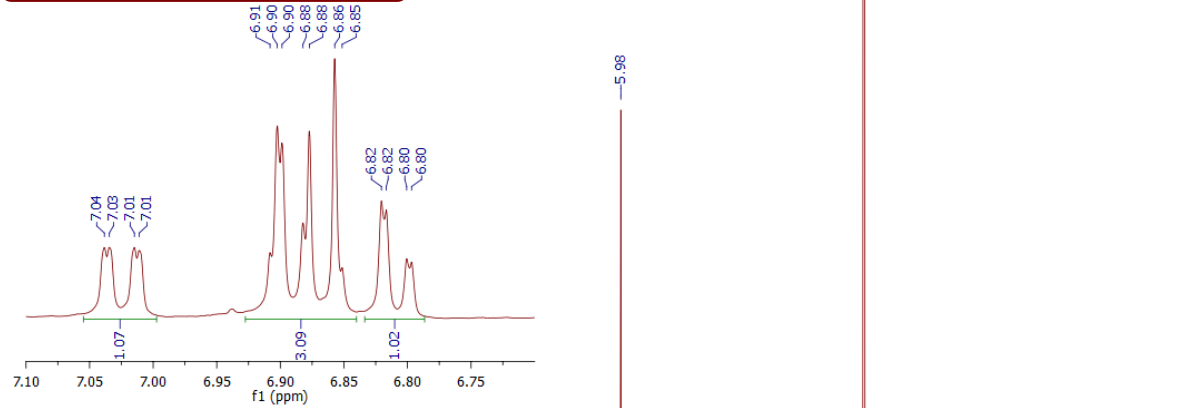
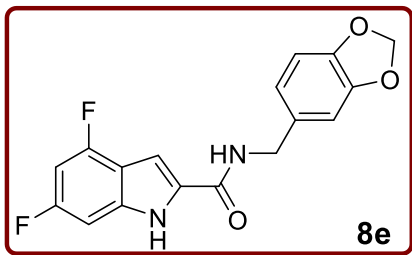
1. C. Han, S. He, R. Wang, X. Gao, H. Wang, J. Qiao, X. Meng, Y. Li and L. Yu, *J. Transl. Med.*, 2021, **19**, 65.
2. L. Meng, X. Yang, X. Xie and M. Wang, *Thorac. Cancer*, 2019, **10**, 676-685.
3. C. Sanchez, J. Diaz-Nido and J. Avila, *Prog. Neurobiol.*, 2000, **61**, 133-168.

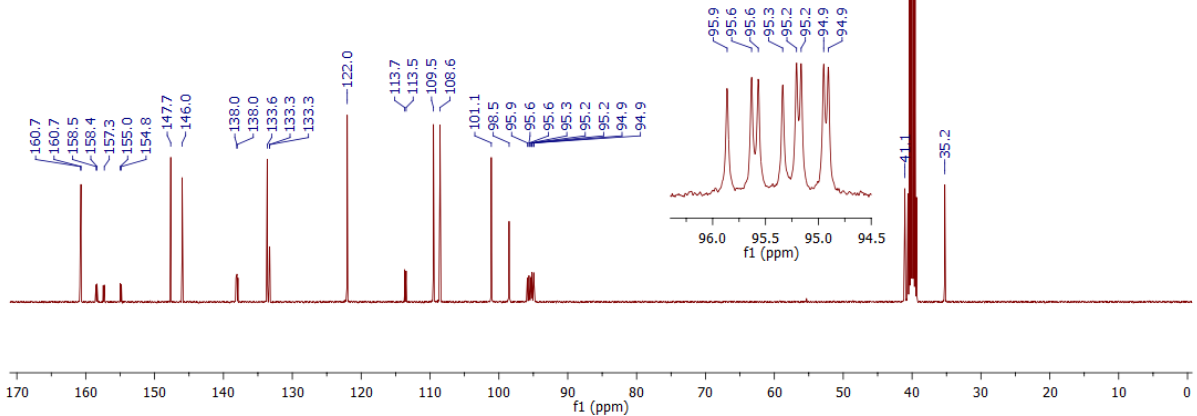
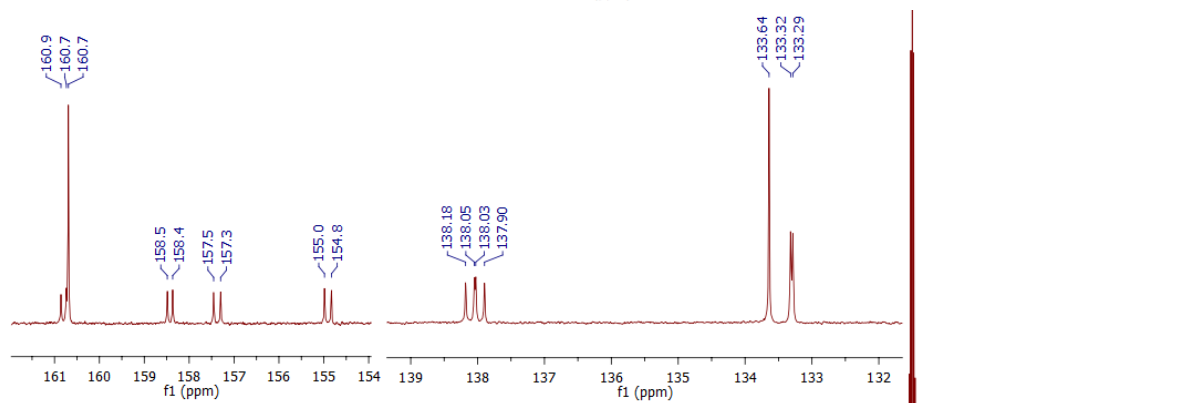
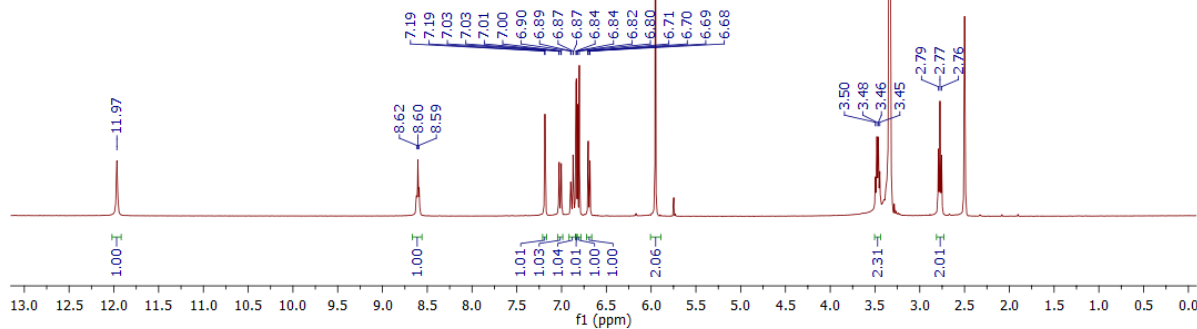
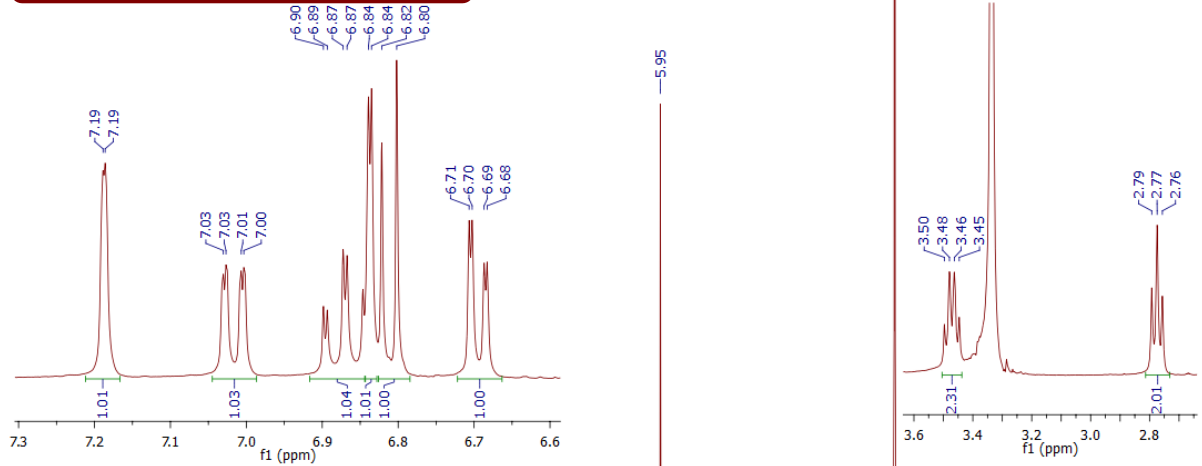
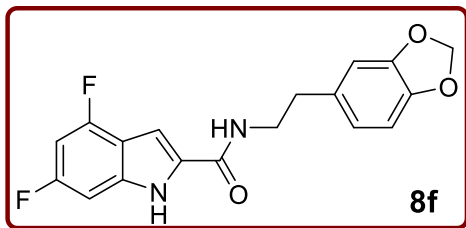




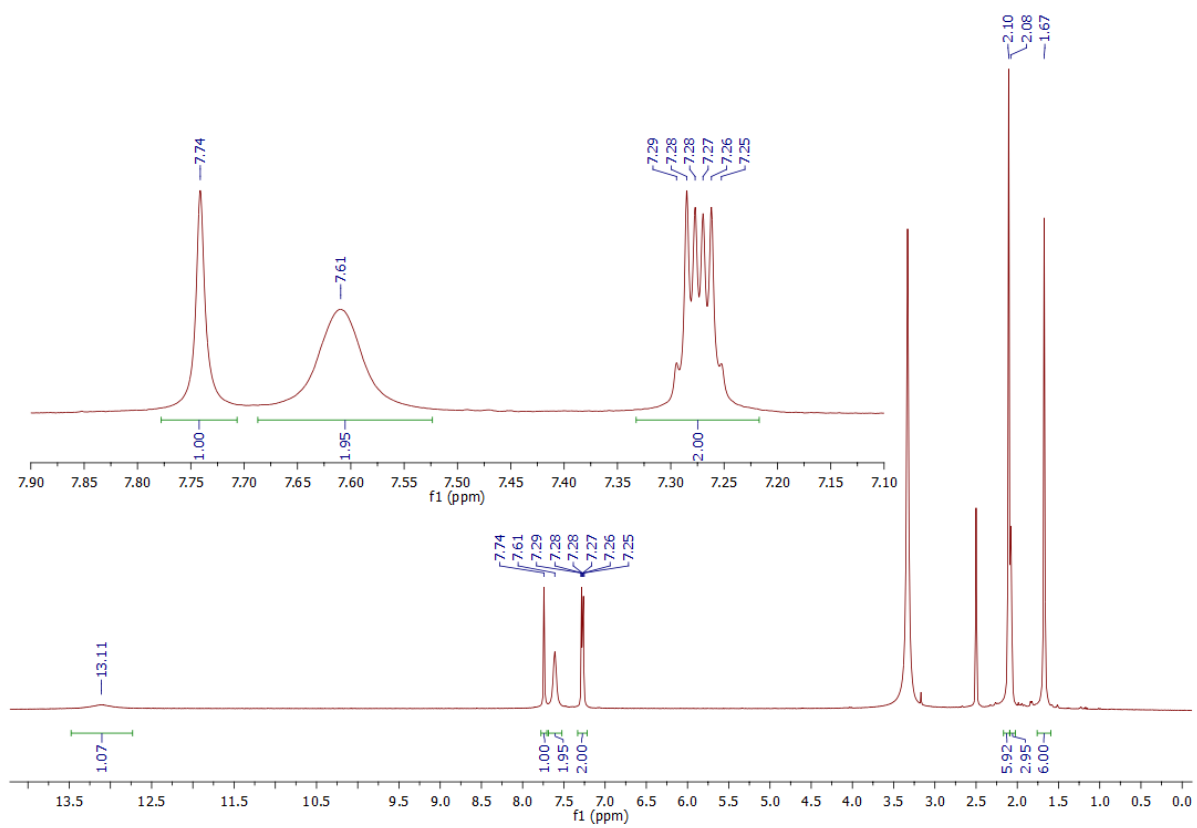
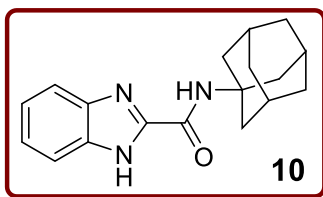


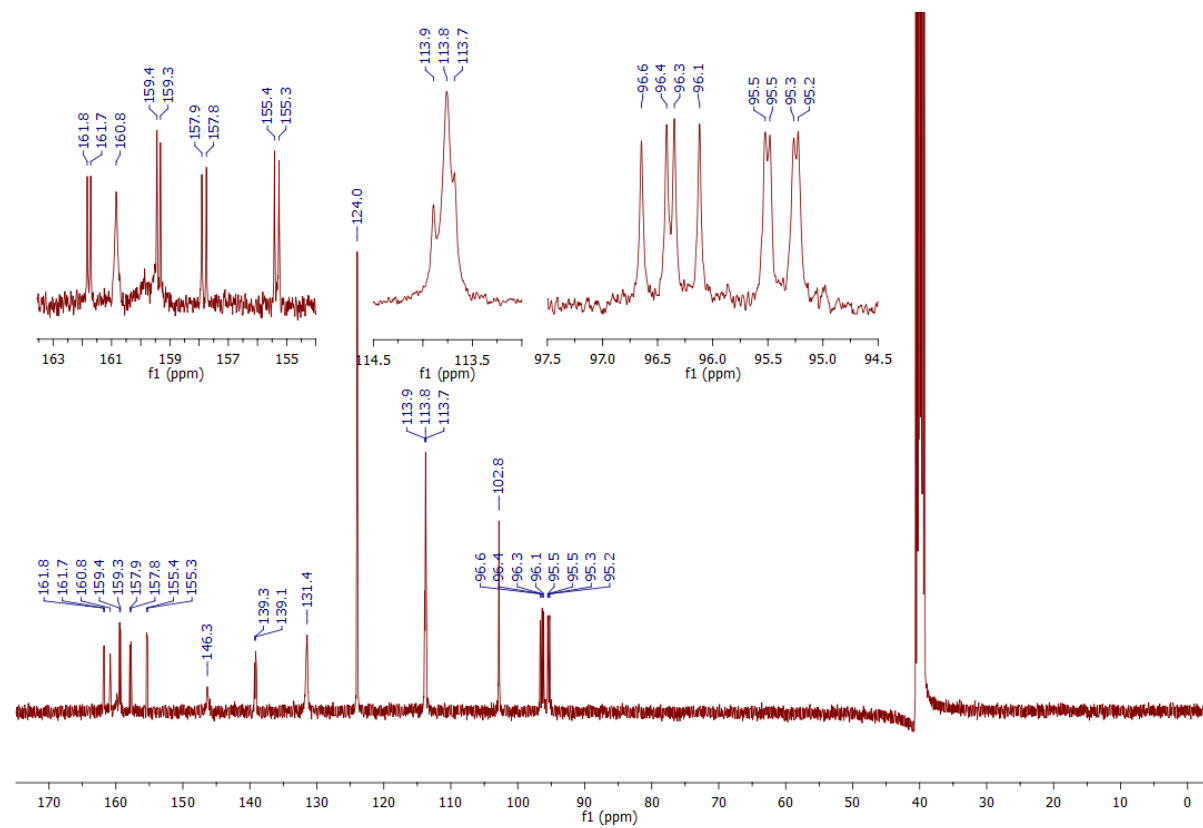
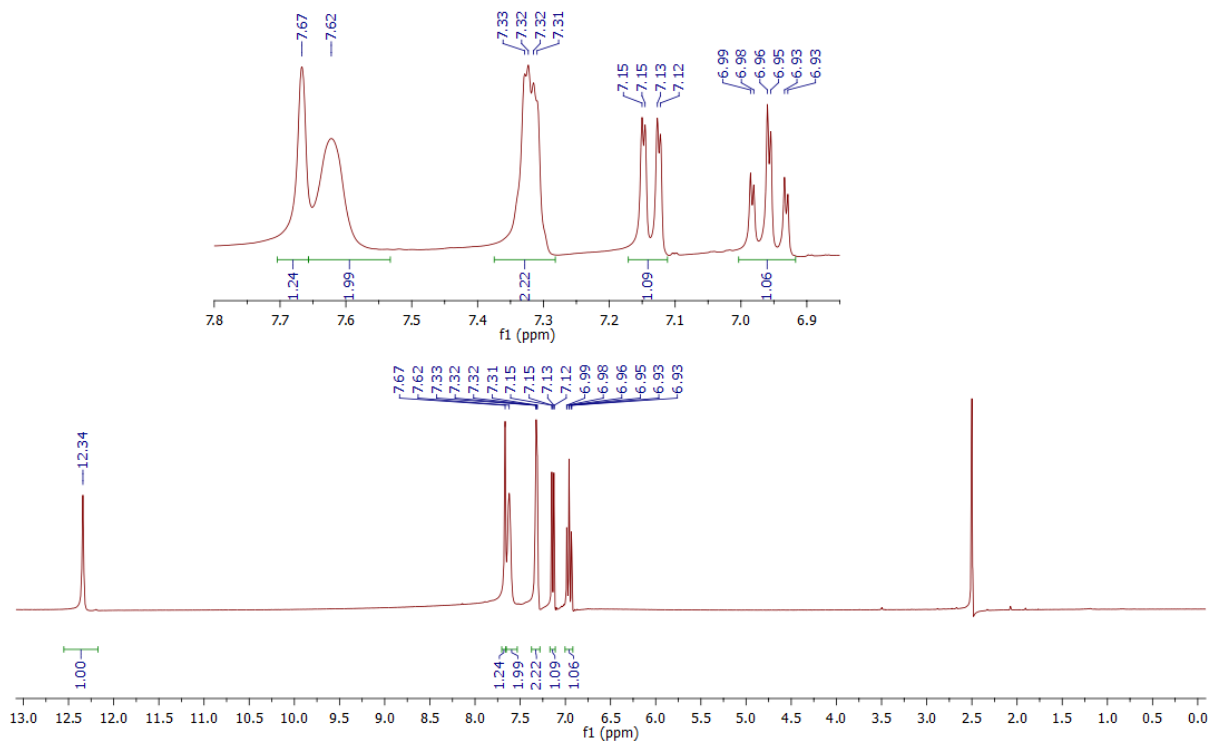
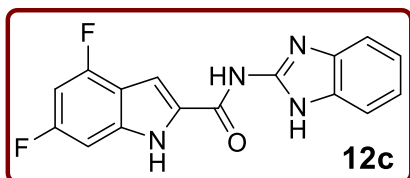


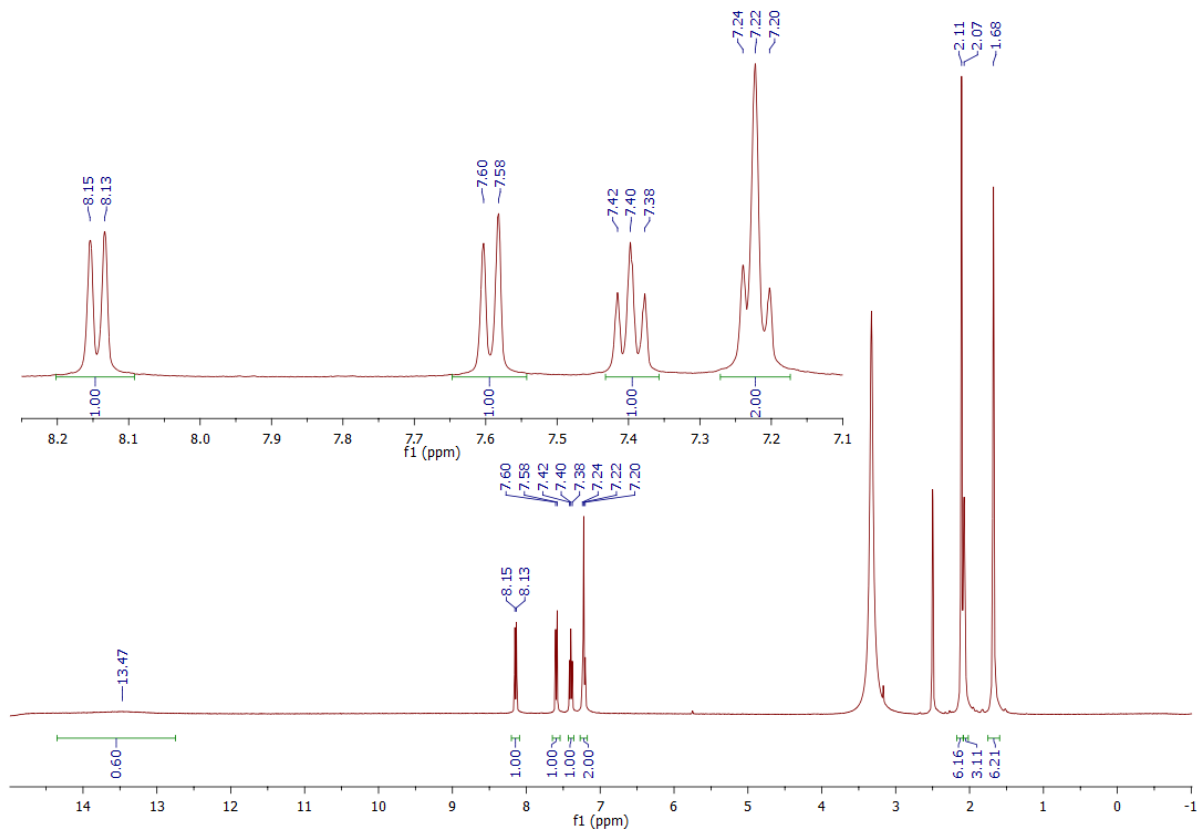
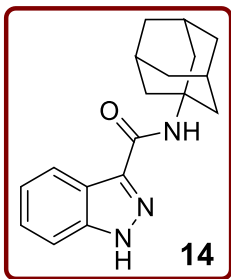


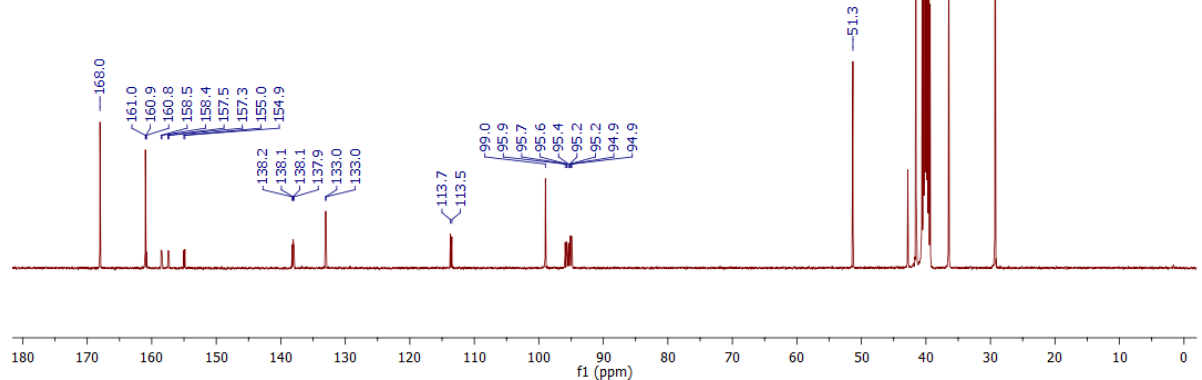
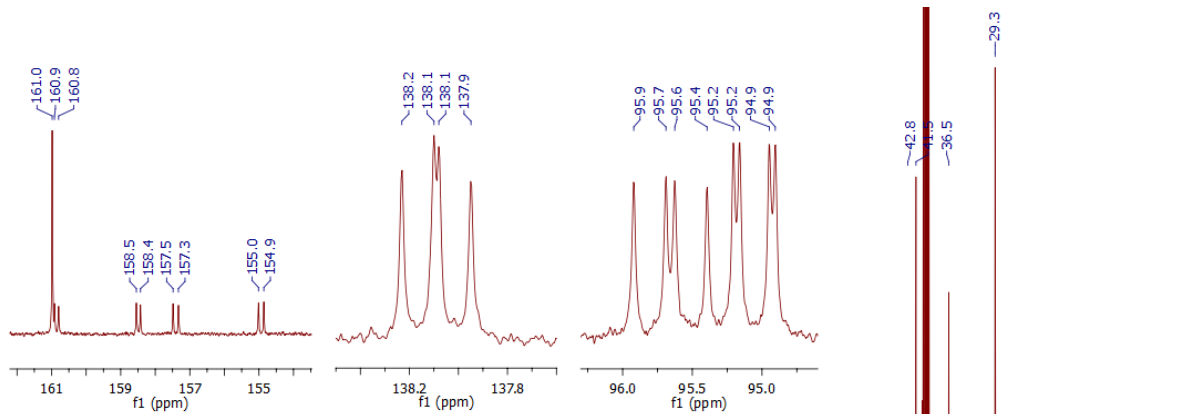
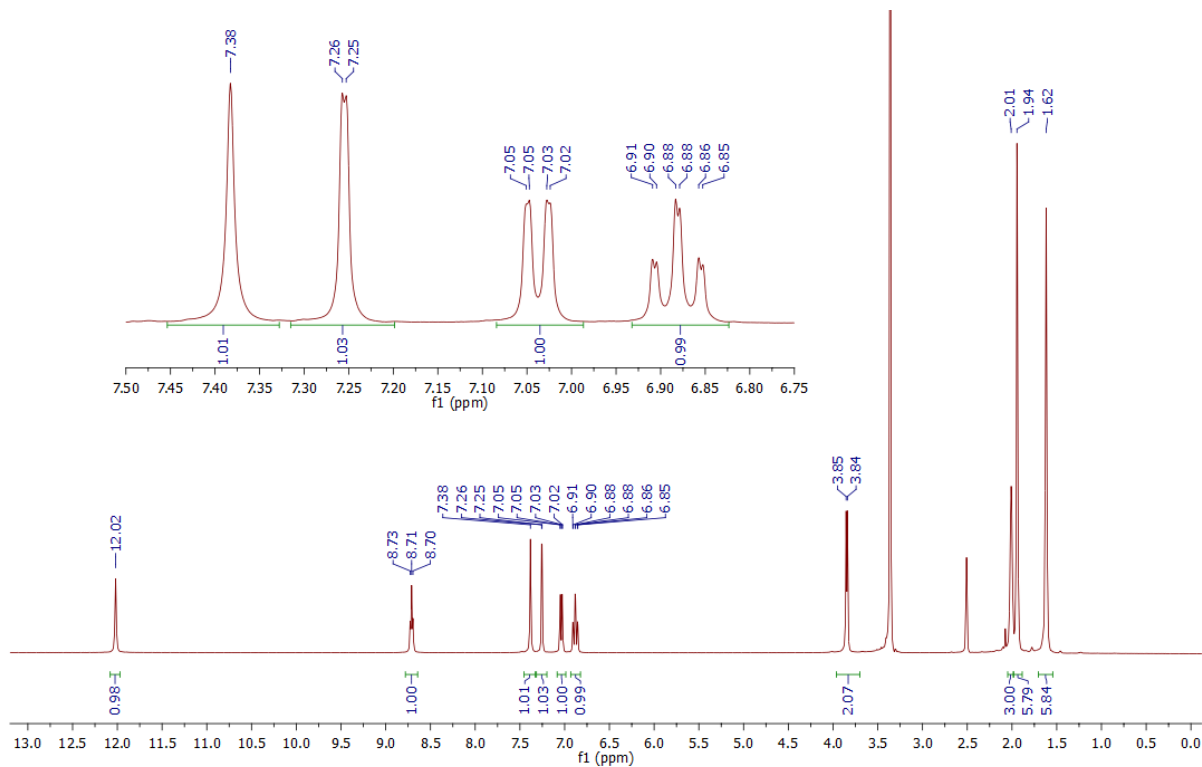
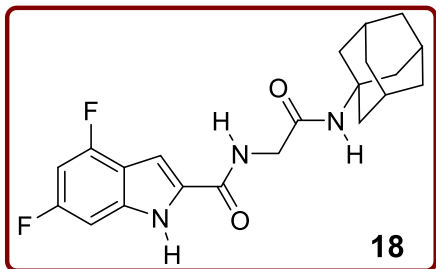


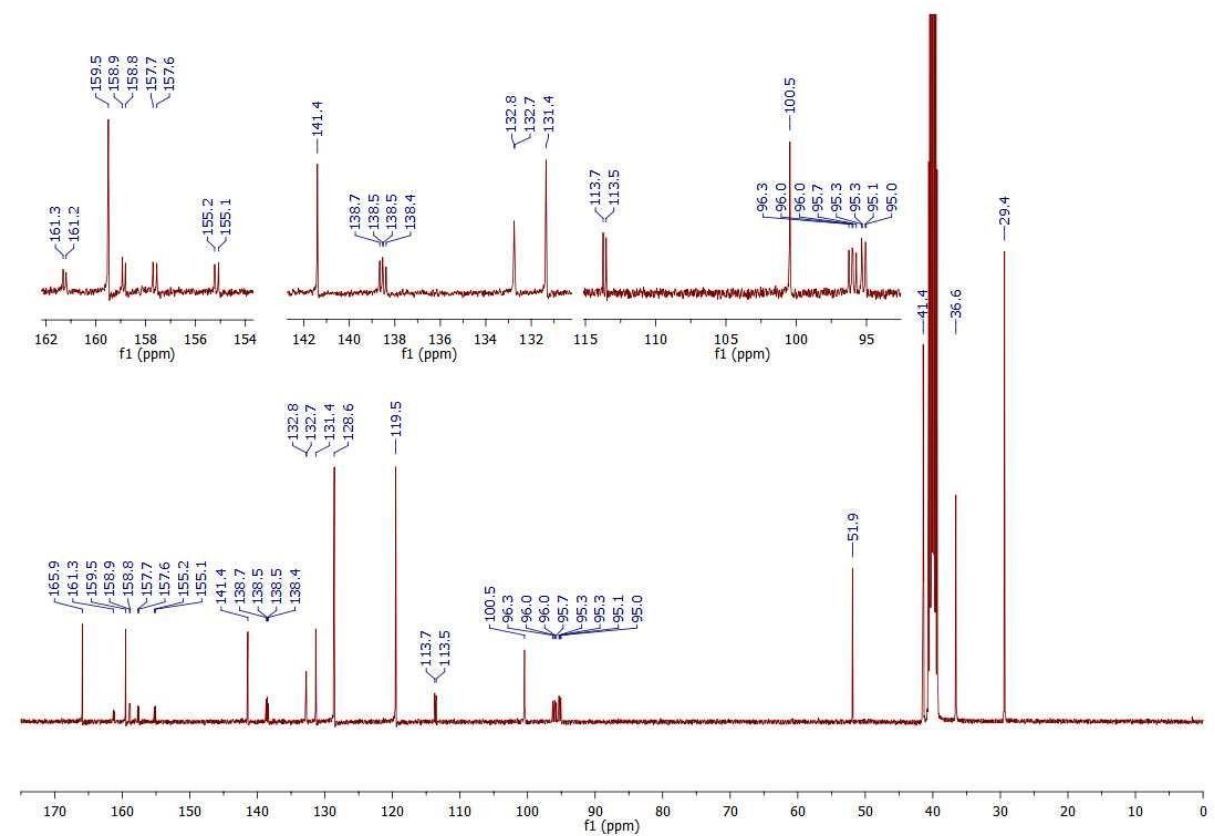
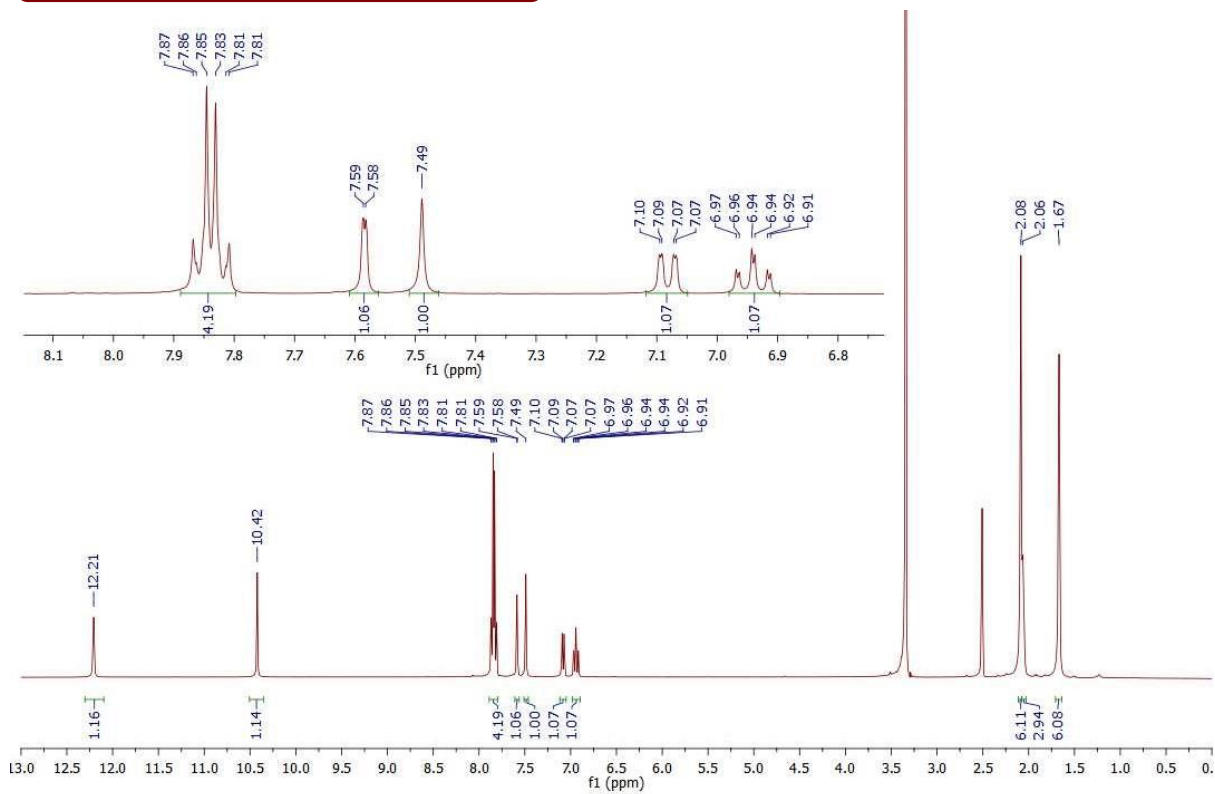
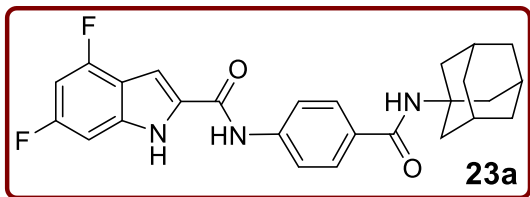


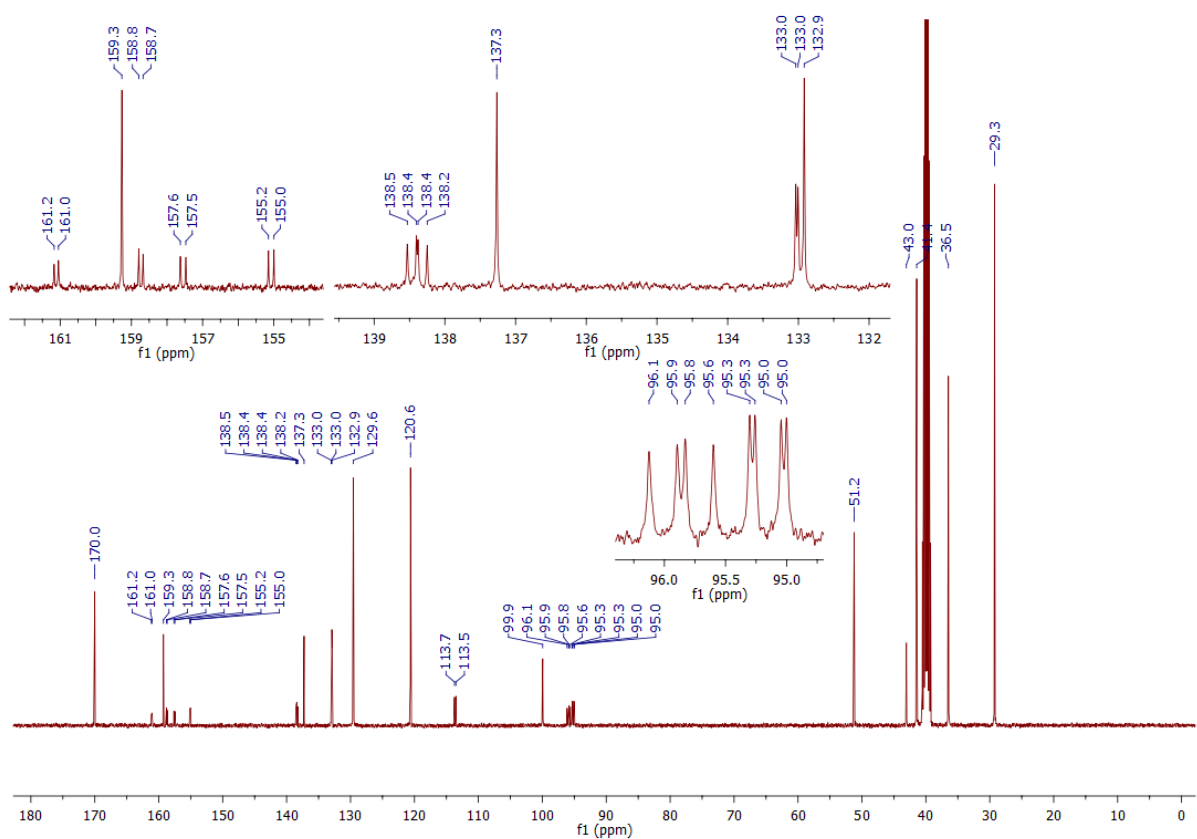
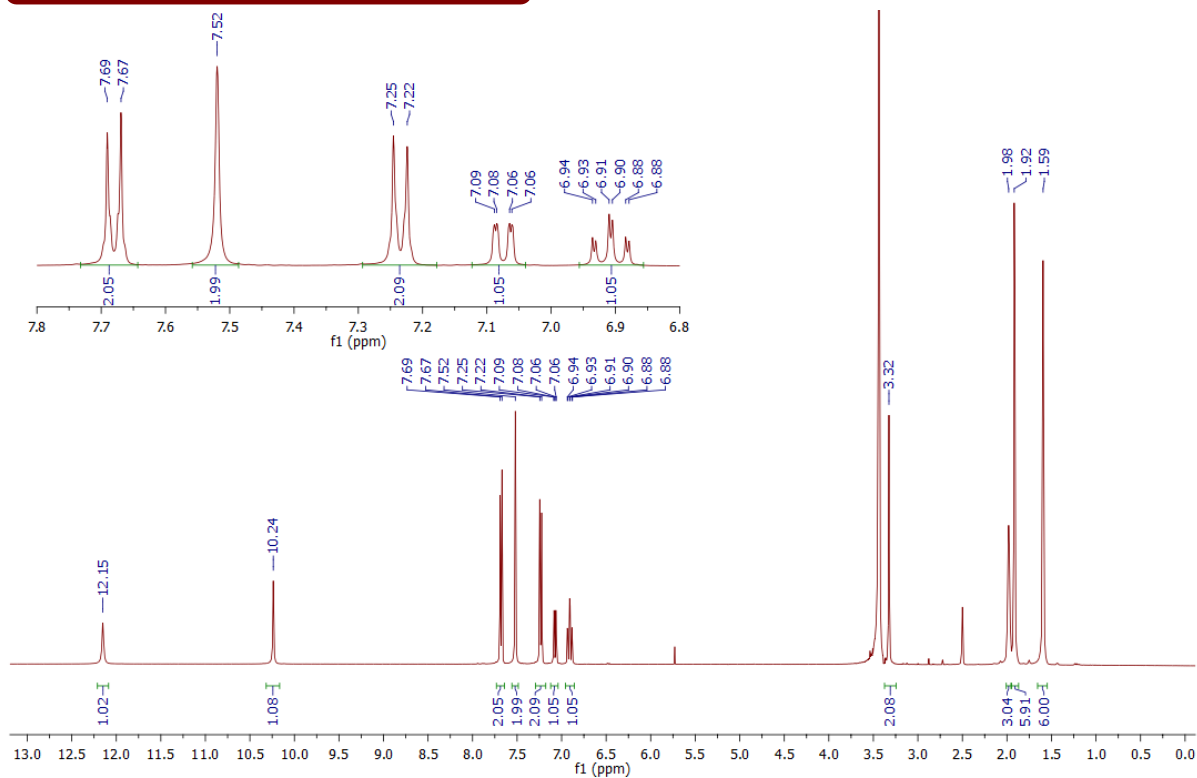
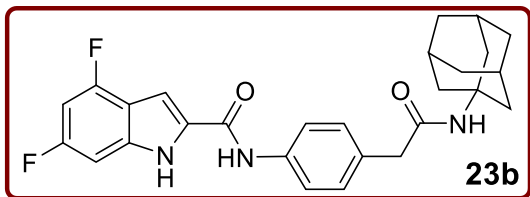












# **Appendix II**

## **Copyright Permissions**

**Current Molecular Pharmacology**  
**(Chapter 2, 2019 Article)**





## EUREKA SCIENCE (FZC) - License Terms and Conditions

This is a License Agreement between Shahinda S. R. Alsayed ("You") and EUREKA SCIENCE (FZC) ("Publisher") provided by Copyright Clearance Center ("CCC"). The license consists of your order details, the terms and conditions provided by EUREKA SCIENCE (FZC), and the CCC terms and conditions.

All payments must be made in full to CCC.

|                  |             |                   |                                    |
|------------------|-------------|-------------------|------------------------------------|
| Order Date       | 25-Jan-2021 | Type of Use       | Republish in a thesis/dissertation |
| Order license ID | 1092675-1   | Publisher Portion | BENTHAM SCIENCE Chapter/article    |
| ISSN             | 1874-4702   |                   |                                    |

### LICENSED CONTENT

|                   |   |                  |         |
|-------------------|---|------------------|---------|
| Publication Title | CURRENT MOLECULAR PHARMACOLOGY  | Publication Type | Journal |
| Article Title     | Kinase Targets for Mycolic Acid Biosynthesis in Mycobacterium tuberculosis. | Start Page       | 27      |
|                   |   | End Page         | 49      |
|                   |   | Issue            | 1       |
|                   |   | Volume           | 12      |
| Date              | 01/01/2007  |                  |         |
| Language          | English   |                  |         |
| Country           | Netherlands   |                  |         |
| Rightsholder      | EUREKA SCIENCE (FZC)  |                  |         |

### REQUEST DETAILS

|                                 |   |                             |   |
|---------------------------------|---|-----------------------------|---|
| Portion Type                    | Chapter/article                         | Rights Requested            | Main product, any product related to main product, and other compilations/derivative products |
| Page range(s)                   | 27-49                                   | Distribution                | Worldwide   |
| Total number of pages           | 23                                      | Translation                 | Original language of publication  |
| Format (select all that apply)  | Print, Electronic                       | Copies for the disabled?    | No  |
| Who will republish the content? | Academic institution                    | Minor editing privileges?   | No  |
| Duration of Use                 | Life of current and all future editions | Incidental promotional use? | No  |
| Lifetime Unit Quantity          | Up to 4,999                             | Currency                    | AUD   |

### NEW WORK DETAILS

|                 |                        |                            |                   |
|-----------------|------------------------|----------------------------|-------------------|
| Title           | Dissertation for a PhD | Institution name           | Curtin University |
| Instructor name | Shahinda S.R. Alsayed  | Expected presentation date | 2021-03-15        |

## ADDITIONAL DETAILS

---

|                        |     |   |                        |
|------------------------|-----|---|------------------------|
| Order reference number | N/A | The requesting person / organization to appear on the license | Shahinda S. R. Alsayed |
|------------------------|-----|---|------------------------|

## REUSE CONTENT DETAILS

---

|   |  |   |  |
|---|--|---|--|
| Title, description or numeric reference of the portion(s) | DOI :<br>10.2174/187446721166618102511114  | Title of the portion is from                    | Kinase Targets for Mycolic Acid Biosynthesis in Mycobacterium tuberculosis.                      |
| Editor of portion(s)                                      | Yu, Yu; Payne, Alan D; Gunosewoyo, Hendra; Foster, Neil R; Beh, Chau Chun; Alsayed, Shahinda S R | Author of portion(s)                            | Yu, Yu; Payne, Alan D; Gunosewoyo, Hendra; Foster, Neil R; Beh, Chau Chun; Alsayed, Shahinda S R |
| Volume of serial or monograph                             | 12   | Issue, if republishing an article from a serial | 1  |
| Page or page range of portion                             | 27-49  | Publication date of portion                     | 2019-01-11   |

## CCC Republication Terms and Conditions

1. Description of Service; Defined Terms. This Republication License enables the User to obtain licenses for republication of one or more copyrighted works as described in detail on the relevant Order Confirmation (the "Work(s)"). Copyright Clearance Center, Inc. ("CCC") grants licenses through the Service on behalf of the rightsholder identified on the Order Confirmation (the "Rightsholder"). "Republication", as used herein, generally means the inclusion of a Work, in whole or in part, in a new work or works, also as described on the Order Confirmation. "User", as used herein, means the person or entity making such republication.
2. The terms set forth in the relevant Order Confirmation, and any terms set by the Rightsholder with respect to a particular Work, govern the terms of use of Works in connection with the Service. By using the Service, the person transacting for a republication license on behalf of the User represents and warrants that he/she/it (a) has been duly authorized by the User to accept, and hereby does accept, all such terms and conditions on behalf of User, and (b) shall inform User of all such terms and conditions. In the event such person is a "freelancer" or other third party independent of User and CCC, such party shall be deemed jointly a "User" for purposes of these terms and conditions. In any event, User shall be deemed to have accepted and agreed to all such terms and conditions if User republishes the Work in any fashion.
3. Scope of License; Limitations and Obligations.
  - 3.1. All Works and all rights therein, including copyright rights, remain the sole and exclusive property of the Rightsholder. The license created by the exchange of an Order Confirmation (and/or any invoice) and payment by User of the full amount set forth on that document includes only those rights expressly set forth in the Order Confirmation and in these terms and conditions, and conveys no other rights in the Work(s) to User. All rights not expressly granted are hereby reserved.
  - 3.2. General Payment Terms: You may pay by credit card or through an account with us payable at the end of the month. If you and we agree that you may establish a standing account with CCC, then the following terms apply: Remit Payment to: Copyright Clearance Center, 29118 Network Place, Chicago, IL 60673-1291. Payments Due: Invoices are payable upon their delivery to you (or upon our notice to you that they are available to you for downloading). After 30 days, outstanding amounts will be subject to a service charge of 1-1/2% per month or, if less, the maximum rate allowed by applicable law. Unless otherwise specifically set forth in the Order Confirmation or in a separate written agreement signed by CCC, invoices are due

and payable on "net 30" terms. While User may exercise the rights licensed immediately upon issuance of the Order Confirmation, the license is automatically revoked and is null and void, as if it had never been issued, if complete payment for the license is not received on a timely basis either from User directly or through a payment agent, such as a credit card company.

- 3.3. Unless otherwise provided in the Order Confirmation, any grant of rights to User (i) is "one-time" (including the editions and product family specified in the license), (ii) is non-exclusive and non-transferable and (iii) is subject to any and all limitations and restrictions (such as, but not limited to, limitations on duration of use or circulation) included in the Order Confirmation or invoice and/or in these terms and conditions. Upon completion of the licensed use, User shall either secure a new permission for further use of the Work(s) or immediately cease any new use of the Work(s) and shall render inaccessible (such as by deleting or by removing or severing links or other locators) any further copies of the Work (except for copies printed on paper in accordance with this license and still in User's stock at the end of such period).
  - 3.4. In the event that the material for which a republication license is sought includes third party materials (such as photographs, illustrations, graphs, inserts and similar materials) which are identified in such material as having been used by permission, User is responsible for identifying, and seeking separate licenses (under this Service or otherwise) for, any of such third party materials; without a separate license, such third party materials may not be used.
  - 3.5. Use of proper copyright notice for a Work is required as a condition of any license granted under the Service. Unless otherwise provided in the Order Confirmation, a proper copyright notice will read substantially as follows: "Republished with permission of [Rightsholder's name], from [Work's title, author, volume, edition number and year of copyright]; permission conveyed through Copyright Clearance Center, Inc. " Such notice must be provided in a reasonably legible font size and must be placed either immediately adjacent to the Work as used (for example, as part of a by-line or footnote but not as a separate electronic link) or in the place where substantially all other credits or notices for the new work containing the republished Work are located. Failure to include the required notice results in loss to the Rightsholder and CCC, and the User shall be liable to pay liquidated damages for each such failure equal to twice the use fee specified in the Order Confirmation, in addition to the use fee itself and any other fees and charges specified.
  - 3.6. User may only make alterations to the Work if and as expressly set forth in the Order Confirmation. No Work may be used in any way that is defamatory, violates the rights of third parties (including such third parties' rights of copyright, privacy, publicity, or other tangible or intangible property), or is otherwise illegal, sexually explicit or obscene. In addition, User may not conjoin a Work with any other material that may result in damage to the reputation of the Rightsholder. User agrees to inform CCC if it becomes aware of any infringement of any rights in a Work and to cooperate with any reasonable request of CCC or the Rightsholder in connection therewith.
4. Indemnity. User hereby indemnifies and agrees to defend the Rightsholder and CCC, and their respective employees and directors, against all claims, liability, damages, costs and expenses, including legal fees and expenses, arising out of any use of a Work beyond the scope of the rights granted herein, or any use of a Work which has been altered in any unauthorized way by User, including claims of defamation or infringement of rights of copyright, publicity, privacy or other tangible or intangible property.
  5. Limitation of Liability. UNDER NO CIRCUMSTANCES WILL CCC OR THE RIGHTSHOLDER BE LIABLE FOR ANY DIRECT, INDIRECT, CONSEQUENTIAL OR INCIDENTAL DAMAGES (INCLUDING WITHOUT LIMITATION DAMAGES FOR LOSS OF BUSINESS PROFITS OR INFORMATION, OR FOR BUSINESS INTERRUPTION) ARISING OUT OF THE USE OR INABILITY TO USE A WORK, EVEN IF ONE OF THEM HAS BEEN ADVISED OF THE POSSIBILITY OF SUCH DAMAGES. In any event, the total liability of the Rightsholder and CCC (including their respective employees and directors) shall not exceed the total amount actually paid by User for this license. User assumes full liability for the actions and omissions of its principals, employees, agents, affiliates, successors and assigns.
  6. Limited Warranties. THE WORK(S) AND RIGHT(S) ARE PROVIDED "AS IS". CCC HAS THE RIGHT TO GRANT TO USER

THE RIGHTS GRANTED IN THE ORDER CONFIRMATION DOCUMENT. CCC AND THE RIGHTSHOLDER DISCLAIM ALL OTHER WARRANTIES RELATING TO THE WORK(S) AND RIGHT(S), EITHER EXPRESS OR IMPLIED, INCLUDING WITHOUT LIMITATION IMPLIED WARRANTIES OF MERCHANTABILITY OR FITNESS FOR A PARTICULAR PURPOSE. ADDITIONAL RIGHTS MAY BE REQUIRED TO USE ILLUSTRATIONS, GRAPHS, PHOTOGRAPHS, ABSTRACTS, INSERTS OR OTHER PORTIONS OF THE WORK (AS OPPOSED TO THE ENTIRE WORK) IN A MANNER CONTEMPLATED BY USER; USER UNDERSTANDS AND AGREES THAT NEITHER CCC NOR THE RIGHTSHOLDER MAY HAVE SUCH ADDITIONAL RIGHTS TO GRANT.

7. Effect of Breach. Any failure by User to pay any amount when due, or any use by User of a Work beyond the scope of the license set forth in the Order Confirmation and/or these terms and conditions, shall be a material breach of the license created by the Order Confirmation and these terms and conditions. Any breach not cured within 30 days of written notice thereof shall result in immediate termination of such license without further notice. Any unauthorized (but licensable) use of a Work that is terminated immediately upon notice thereof may be liquidated by payment of the Rightsholder's ordinary license price therefor; any unauthorized (and unlicensable) use that is not terminated immediately for any reason (including, for example, because materials containing the Work cannot reasonably be recalled) will be subject to all remedies available at law or in equity, but in no event to a payment of less than three times the Rightsholder's ordinary license price for the most closely analogous licensable use plus Rightsholder's and/or CCC's costs and expenses incurred in collecting such payment.
8. Miscellaneous.
  - 8.1. User acknowledges that CCC may, from time to time, make changes or additions to the Service or to these terms and conditions, and CCC reserves the right to send notice to the User by electronic mail or otherwise for the purposes of notifying User of such changes or additions; provided that any such changes or additions shall not apply to permissions already secured and paid for.
  - 8.2. Use of User-related information collected through the Service is governed by CCC's privacy policy, available online here:<https://marketplace.copyright.com/rs-ui-web/mp/privacy-policy>
  - 8.3. The licensing transaction described in the Order Confirmation is personal to User. Therefore, User may not assign or transfer to any other person (whether a natural person or an organization of any kind) the license created by the Order Confirmation and these terms and conditions or any rights granted hereunder; provided, however, that User may assign such license in its entirety on written notice to CCC in the event of a transfer of all or substantially all of User's rights in the new material which includes the Work(s) licensed under this Service.
  - 8.4. No amendment or waiver of any terms is binding unless set forth in writing and signed by the parties. The Rightsholder and CCC hereby object to any terms contained in any writing prepared by the User or its principals, employees, agents or affiliates and purporting to govern or otherwise relate to the licensing transaction described in the Order Confirmation, which terms are in any way inconsistent with any terms set forth in the Order Confirmation and/or in these terms and conditions or CCC's standard operating procedures, whether such writing is prepared prior to, simultaneously with or subsequent to the Order Confirmation, and whether such writing appears on a copy of the Order Confirmation or in a separate instrument.
  - 8.5. The licensing transaction described in the Order Confirmation document shall be governed by and construed under the law of the State of New York, USA, without regard to the principles thereof of conflicts of law. Any case, controversy, suit, action, or proceeding arising out of, in connection with, or related to such licensing transaction shall be brought, at CCC's sole discretion, in any federal or state court located in the County of New York, State of New York, USA, or in any federal or state court whose geographical jurisdiction covers the location of the Rightsholder set forth in the Order Confirmation. The parties expressly submit to the personal jurisdiction and venue of each such federal or state court. If you have any comments or questions about the Service or Copyright Clearance Center, please contact us at 978-750-8400 or send an e-mail to [support@copyright.com](mailto:support@copyright.com).

**RSC Advances**  
**(Chapter 3, 2020 Article)**

Issue 13, 2020, Issue in Progress

Previous Article

Next Article

From the journal:  
RSC Advances

## Design, synthesis, and biological evaluation of novel arylcarboxamide derivatives as anti-tubercular agents



Shahinda S. R. Alsayed,<sup>a</sup> Shichun Lun,<sup>b</sup> Giuseppe Luna,<sup>a</sup> Chau Chun Beh,<sup>c</sup> Alan D. Payne,<sup>d</sup> Neil Foster,<sup>c</sup> William R. Bishai<sup>\*bc</sup> and Hendra Gunosewoyo<sup>id \*a</sup>

⊕ Author affiliations

### Abstract

Our group has previously reported several indolecarboxamides exhibiting potent antitubercular activity. Herein, we rationally designed several arylcarboxamides based on our previously reported homology model and the recently published crystal structure of the mycobacterial membrane protein large 3 (MmpL3). Many analogues showed considerable anti-TB activity against drug-sensitive (DS) *Mycobacterium tuberculosis* (*M. tb*) strain. Naphthamide derivatives **13c** and **13d** were the most active compounds in our study (MIC: 6.55, 7.11  $\mu\text{M}$ , respectively), showing comparable potency to the first line anti-tuberculosis (anti-TB) drug ethambutol (MIC: 4.89  $\mu\text{M}$ ). In addition to the naphthamide derivatives, we also identified the quinolone-2-carboxamides and 4-arylthiazole-2-carboxamides as potential MmpL3 inhibitors in which compounds **8i** and **18b** had MIC values of 9.97 and 9.82  $\mu\text{M}$ , respectively. All four compounds retained their high activity against multidrug-resistant (MDR) and extensively drug-resistant (XDR) *M. tb* strains. It is worth noting that the two most active compounds **13c** and **13d** also exhibited the highest selective activity towards DS, MDR and XDR *M. tb* strains over mammalian cells [ $\text{IC}_{50}$  (Vero cells)  $\geq 227 \mu\text{M}$ ], indicating their potential lack of cytotoxicity. The four compounds were docked into the MmpL3 active site and were studied for their

About

Cited by

Related

### Design, synthesis, and biological evaluation of novel arylcarboxamide derivatives as anti-tubercular agents

S. S. R. Alsayed, S. Lun, G. Luna, C. C. Beh, A. D. Payne, N. Foster, W. R. Bishai and H. Gunosewoyo, *RSC Adv.*, 2020, **10**, 7523 DOI: 10.1039/C9RA10663D

This article is licensed under a [Creative Commons Attribution-NonCommercial 3.0 Unported Licence](#). You can use material from this article in other publications, without requesting further permission from the RSC, provided that the correct acknowledgement is given and it is not used for commercial purposes.

To request permission to reproduce material from this article in a commercial publication, please go to the [Copyright Clearance Center request page](#).

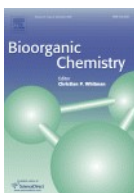
If you are an author contributing to an RSC publication, you do not need to request permission provided correct acknowledgement is given.

If you are the author of this article, you do not need to request permission to reproduce figures and diagrams provided correct acknowledgement is given. If you want to reproduce the whole article in a third-party commercial publication (excluding your thesis/dissertation for which permission is not required) please go to the [Copyright Clearance Center request page](#).

Read more about [how to correctly acknowledge RSC content](#).

# **Bioorganic Chemistry**

**(Chapter 4, 2021 Article)**



### Design, synthesis and antimycobacterial evaluation of novel adamantane and adamantanol analogues effective against drug-resistant tuberculosis

**Author:** Shahinda S.R. Alsayed, Shichun Lun, Alan Payne, William R. Bishai, Hendra Gunosewoyo

**Publication:** Bioorganic Chemistry

**Publisher:** Elsevier

**Date:** January 2021

© 2020 Elsevier Inc. All rights reserved.

Please note that, as the author of this Elsevier article, you retain the right to include it in a thesis or dissertation, provided it is not published commercially. Permission is not required, but please ensure that you reference the journal as the original source. For more information on this and on your other retained rights, please visit: <https://www.elsevier.com/about/our-business/policies/copyright#Author-rights>

BACK

CLOSE WINDOW



# **Chemical Biology and Drug Design**

**(Chapter 5, 2021 Article)**

**WILEY**

RESEARCHERS



THE WILEY NETWORK / HOME / HOW TO CLEAR PERMISSIONS FOR A THESIS OR DISSERTATION

R RESEARCHERS

## How to Clear Permissions for a Thesis or Dissert

**Leah Alaani**, Marketing Manager, Wiley

November 16, 2020

So, you're ready to finish your thesis...

The time has come. You've done the research; you've written the dissertation. You're gearing up to defend your work and your right to scholarly achievement.

But wait: in addition to some last-minute citation formatting, there's one more box you need to tick as you finalize your manuscript. You need to clear permissions.

### What are permissions?

Every good scholar knows how to cite her sources. But in cases where someone else's work is directly copied or quoted at length— even with an accurate citation — you may need a license that grants you the legal right to reproduce another person's intellectual property.

The reuse of intellectual property is protected by law. Content creators need to formally request permission to republish or otherwise reuse existing content in new works. This applies to all types of new content, including theses and dissertations. Make sure that you review your manuscript for any quoted content, third-party charts or graphs, and other elements that you have incorporated from existing intellectual property.

# WILEY

RESEARCHERS



## Wanted: rights holder

Once you've identified the content that will need a reuse license, you'll need to submit requests to the rights holder of each piece of intellectual property and ask them to grant permission for you to use this content in your work.

The rights holder could be the author or the publisher of the content. The rights holder will be specified in the copyright line of a publication. You can also find rights holder information by searching through the [Copyright Clearance Center](#).

## Reusing Wiley content

If you're reusing Wiley content in your thesis or dissertation, rights will be granted at no cost to you if the content meets these requirements:

- **Your thesis or dissertation is not being used for commercial purposes.** This means that you're submitting it only for graduation requirements. You don't currently have a deal with a commercial publisher, and you won't otherwise be benefitting financially from the publication of your thesis.
- **Wiley is the rights holder of the content you are seeking to reuse.** Usually, Wiley holds the rights to our content, but occasionally the rights holder will be an author or sponsoring organization. In those cases, Wiley cannot guarantee free reuse.

While Wiley does grant free reuse of content in thesis and dissertation projects, we do still require a record of use so that we can issue you a license agreement.

If you publish your thesis or dissertation through a commercial publisher in the future, you will need to reapply for commercial reuse licenses. The legal rights granted for content reuse in non-commercial publications, such as a thesis or dissertation, are different from the rights required by commercial publishers to legally republish third-party content.

## Do I need to request permission to use my own work as my dissertation?

If you are the author of a published Wiley article, you have the right to reuse the full text of your published article as part of your thesis or dissertation. In this situation, you do not need to request permission from Wiley for this use.

**RSC Advances**  
**(Chapter 6, 2021 Article)**

Issue 26, 2021, Issue in Progress

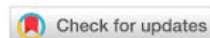
Previous Article

Next Article



From the journal:  
**RSC Advances**

## Design, synthesis and evaluation of novel indole-2-carboxamides for growth inhibition of *Mycobacterium tuberculosis* and paediatric brain tumour cells†



Shahinda S. R. Alsayed,<sup>a</sup> Shichun Lun,<sup>b</sup> Anders W. Bailey,<sup>c</sup> Amreena Suri,<sup>c</sup> Chiang-Ching Huang,<sup>d</sup> Mauro Mocerino,<sup>e</sup> Alan Payne,<sup>e</sup> Simone Treiger Sredni,<sup>cf</sup> William R. Bishaj<sup>\*,bg</sup> and Hendra Gunosewoyo<sup>ib</sup> <sup>\*,a</sup>

⊕ Author affiliations

### Abstract

The omnipresent threat of tuberculosis (TB) and the scant treatment options thereof necessitate the development of new antitubercular agents, preferably working *via* a novel mechanism of action distinct from the current drugs. Various studies identified the mycobacterial membrane protein large 3 transporter (MmpL3) as the target of several classes of compounds, including the indole-2-carboxamides. Herein, several indoleamide analogues were rationally designed, synthesised, and evaluated for their antitubercular and antitumour activities. Compound **8g** displayed the highest activity (MIC = 0.32 μM) against the drug-sensitive (DS) *Mycobacterium tuberculosis* (*M. tb*) H37Rv strain. This compound also exhibited high selective activity towards *M. tb* over mammalian cells [IC<sub>50</sub> (Vero cells) = 40.9 μM, SI = 128], suggesting its minimal cytotoxicity. In addition, when docked into the MmpL3 active site, **8g** adopted a binding profile similar to the indoleamide ligand **ICA38**. A related compound **8f** showed dual antitubercular (MIC = 0.62 μM) and cytotoxic activities against paediatric glioblastoma multiforme (GBM) cell line KNS42 [IC<sub>50</sub> (viability) = 0.84 μM]. Compound **8f** also showed poor cytotoxic activity against healthy Vero cells (IC<sub>50</sub> = 39.9 μM). Compounds **9a** and **15**,

About

Cited by

Related

### Design, synthesis and evaluation of novel indole-2-carboxamides for growth inhibition of *Mycobacterium tuberculosis* and paediatric brain tumour cells

S. S. R. Alsayed, S. Lun, A. W. Bailey, A. Suri, C. Huang, M. Mocerino, A. Payne, S. T. Sredni, W. R. Bishaj and H. Gunosewoyo, *RSC Adv.*, 2021, **11**, 15497 DOI: 10.1039/D0RA10728J

This article is licensed under a [Creative Commons Attribution-NonCommercial 3.0 Unported Licence](#). You can use material from this article in other publications, without requesting further permission from the RSC, provided that the correct acknowledgement is given and it is not used for commercial purposes.

To request permission to reproduce material from this article in a commercial publication, please go to the [Copyright Clearance Center request page](#).

If you are an author contributing to an RSC publication, you do not need to request permission provided correct acknowledgement is given.

If you are the author of this article, you do not need to request permission to reproduce figures and diagrams provided correct acknowledgement is given. If you want to reproduce the whole article in a third-party commercial publication (excluding your thesis/dissertation for which permission is not required) please go to the [Copyright Clearance Center request page](#).

Read more about [how to correctly acknowledge RSC content](#).

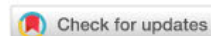
# **RSC Medicinal Chemistry**

**(Chapter 7, 2021 Article)**



From the journal:  
RSC Medicinal Chemistry

## Synthesis and antitumour evaluation of indole-2-carboxamides against paediatric brain cancer cells†



Shahinda S. R. Alsayed,<sup>a</sup> Amreena Suri,<sup>b</sup> Anders W. Bailey,<sup>b</sup> Samuel Lane,<sup>c</sup> Eryn L. Werry,<sup>cd</sup> Chiang-Ching Huang,<sup>e</sup> Li-Fang Yu,<sup>f</sup> Michael Kassiou,<sup>g</sup> Simone Treiger Sredni<sup>†bg</sup> and Hendra Gunosewoyo<sup>†\*a</sup>

Author affiliations

### Abstract

Paediatric glioblastomas are rapidly growing, devastating brain neoplasms with an invasive phenotype. Radiotherapy and chemotherapy, which are the current therapeutic adjuvant to surgical resection, are still associated with various toxicity profiles and only marginally improve the course of the disease and life expectancy. A considerable body of evidence supports the antitumour and apoptotic effects of certain cannabinoids, such as WIN55,212-2, against a wide spectrum of cancer cells, including gliomas. In fact, we previously highlighted the potent cytotoxic activity of the cannabinoid ligand **5** against glioblastoma KNS42 cells. Taken together, in this study, we designed, synthesised, and evaluated several indoles and indole bioisosteres for their antitumour activities. Compounds **8a**, **8c**, **8f**, **12c**, and **24d** demonstrated significant inhibitory activities against the viability ( $IC_{50} = 2.34\text{--}9.06\ \mu\text{M}$ ) and proliferation ( $IC_{50} = 2.88\text{--}9.85\ \mu\text{M}$ ) of paediatric glioblastoma KNS42 cells. All five compounds further retained their antitumour activities against two atypical teratoid/rhabdoid tumour (AT/RT) cell lines. When tested against a medulloblastoma DAOY cell line, only **8c**, **8f**, **12c**, and **24d** maintained their viability inhibitory activities. The viability assay against non-neoplastic human fibroblast HFF1 cells suggested that compounds **8a**, **8c**, **8f**, and **12c** act selectively towards the panel of paediatric brain tumour cells. In contrast, compound **24d** and WIN55,212-2 were highly toxic toward HFF1 cells. Due to their structural resemblance to known cannabimimetics, the most potent compounds were tested in cannabinoid 1

About

Cited by

Related

### Synthesis and antitumour evaluation of indole-2-carboxamides against paediatric brain cancer cells

S. S. R. Alsayed, A. Suri, A. W. Bailey, S. Lane, E. L. Werry, C. Huang, L. Yu, M. Kassiou, S. T. Sredni and H. Gunosewoyo, *RSC Med. Chem.*, 2021, Advance Article, DOI: 10.1039/D1MD00065A

To request permission to reproduce material from this article, please go to the [Copyright Clearance Center request page](#).

If you are an author contributing to an RSC publication, you do not need to request permission provided correct acknowledgement is given.

If you are the author of this article, you do not need to request permission to reproduce figures and diagrams provided correct acknowledgement is given. If you want to reproduce the whole article in a third-party publication (excluding your thesis/dissertation for which permission is not required) please go to the [Copyright Clearance Center request page](#).

Read more about [how to correctly acknowledge RSC content](#).